

# Experimental and Analytical Investigation of Blast Performance of Seismically Resistant Bridge Piers

by  
**Shuichi Fujikura and Michel Bruneau**



Technical Report MCEER-08-0028

December 8, 2008

## NOTICE

This report was prepared by the University at Buffalo, State University of New York as a result of research sponsored by MCEER through a contract from the Federal Highway Administration. Neither MCEER, associates of MCEER, its sponsors, the University at Buffalo, State University of New York, nor any person acting on their behalf:

- a. makes any warranty, express or implied, with respect to the use of any information, apparatus, method, or process disclosed in this report or that such use may not infringe upon privately owned rights; or
- b. assumes any liabilities of whatsoever kind with respect to the use of, or the damage resulting from the use of, any information, apparatus, method, or process disclosed in this report.

Any opinions, findings, and conclusions or recommendations expressed in this publication are those of the author(s) and do not necessarily reflect the views of MCEER or the Federal Highway Administration.

## Experimental and Analytical Investigation of Blast Performance of Seismically Resistant Bridge Piers

by

Shuichi Fujikura<sup>1</sup> and Michel Bruneau<sup>2</sup>

Publication Date: December 8, 2008

Submittal Date: November 12, 2008

Technical Report MCEER-08-0028

Task Number 094-EXT-1C

FHWA Contract Number DTFH61-98-C-00094

- 1 Graduate Student, Department of Civil, Structural and Environmental Engineering, University at Buffalo, State University of New York
- 2 Professor, Department of Civil, Structural and Environmental Engineering, University at Buffalo, State University of New York

MCEER

University at Buffalo, State University of New York

Red Jacket Quadrangle, Buffalo, NY 14261

Phone: (716) 645-3391; Fax (716) 645-3399

E-mail: [mceer@buffalo.edu](mailto:mceer@buffalo.edu); WWW Site: <http://mceer.buffalo.edu>

---



## Preface

The Multidisciplinary Center for Earthquake Engineering Research (MCEER) is a national center of excellence in advanced technology applications that is dedicated to the reduction of earthquake losses nationwide. Headquartered at the University at Buffalo, State University of New York, the Center was originally established by the National Science Foundation in 1986, as the National Center for Earthquake Engineering Research (NCEER).

Comprising a consortium of researchers from numerous disciplines and institutions throughout the United States, the Center's mission is to reduce earthquake losses through research and the application of advanced technologies that improve engineering, pre-earthquake planning and post-earthquake recovery strategies. Toward this end, the Center coordinates a nationwide program of multidisciplinary team research, education and outreach activities.

MCEER's research is conducted under the sponsorship of two major federal agencies, the National Science Foundation (NSF) and the Federal Highway Administration (FHWA), and the State of New York. Significant support is also derived from the Federal Emergency Management Agency (FEMA), other state governments, academic institutions, foreign governments and private industry.

The Center's Highway Project develops improved seismic design, evaluation, and retrofit methodologies and strategies for new and existing bridges and other highway structures, and for assessing the seismic performance of highway systems. The FHWA has sponsored three major contracts with MCEER under the Highway Project, two of which were initiated in 1992 and the third in 1998.

Of the two 1992 studies, one performed a series of tasks intended to improve seismic design practices for new highway bridges, tunnels, and retaining structures (MCEER Project 112). The other study focused on methodologies and approaches for assessing and improving the seismic performance of existing "typical" highway bridges and other highway system components including tunnels, retaining structures, slopes, culverts, and pavements (MCEER Project 106). These studies were conducted to:

- assess the seismic vulnerability of highway systems, structures, and components;
- develop concepts for retrofitting vulnerable highway structures and components;
- develop improved design and analysis methodologies for bridges, tunnels, and retaining structures, which include consideration of soil-structure interaction mechanisms and their influence on structural response; and
- develop, update, and recommend improved seismic design and performance criteria for new highway systems and structures.

The 1998 study, “Seismic Vulnerability of the Highway System” (FHWA Contract DTFH61-98-C-00094; known as MCEER Project 094), was initiated with the objective of performing studies to improve the seismic performance of bridge types not covered under Projects 106 or 112, and to provide extensions to system performance assessments for highway systems. Specific subjects covered under Project 094 include:

- development of formal loss estimation technologies and methodologies for highway systems;
- analysis, design, detailing, and retrofitting technologies for special bridges, including those with flexible superstructures (e.g., trusses), those supported by steel tower substructures, and cable-supported bridges (e.g., suspension and cable-stayed bridges);
- seismic response modification device technologies (e.g., hysteretic dampers, isolation bearings); and
- soil behavior, foundation behavior, and ground motion studies for large bridges.

In addition, Project 094 includes a series of special studies, addressing topics that range from non-destructive assessment of retrofitted bridge components to supporting studies intended to assist in educating the bridge engineering profession on the implementation of new seismic design and retrofitting strategies.

*This report focuses on the protection of highway bridges against earthquake and blast hazards. The results of a previously developed and experimentally validated multi-hazard bridge pier concept consisting of a multi-column pier bent with Concrete-Filled Steel Tube (CFST) columns are briefly presented (see MCEER-07-0005). The performance of the CFST columns is compared to the blast resistance of ductile reinforced concrete (RC) columns and non-ductile RC columns retrofitted with steel jackets, detailed in accordance to current seismic design codes and practices. This report describes the details of the design process and the experimental observations of the prototype bridge pier bent constructed using conventional and retrofitted seismic resistant RC columns. The results from blast experiments are compared with results obtained using simplified analysis methods. Nonlinear dynamic response history analyses are performed to simulate and better understand the behavior of CFST columns under blast loading. The tests on conventional and steel jacket retrofitted seismic resistant RC columns demonstrated the non-ductile behavior of the RC columns under blast loading and that the columns failed in direct shear at their base. Based on experimental and analytical observations, shape factors for the blast pressures acting on circular columns are established.*

## ABSTRACT

The issue of protecting infrastructure against multiple extreme events is gaining popularity in the field of civil engineering. This research focuses on the protection of highway bridges against two hazards, namely earthquakes and blasts. A similarity between seismic and blast events in relation to bridges is that they can both induce large inelastic deformations in key structural components. Since many bridges are (or will be) located in areas of moderate to high seismic activity, and because any bridge can be a potential target for terrorists, there is a need to develop structural systems capable of performing equally well under both events.

The authors previously presented the development and experimental validation of a multi-hazard bridge pier concept, and proposed a multi-column pier bent with concrete-filled steel tube (CFST) columns for this purpose (Fujikura et al. 2007, 2008). To compare with this first series of blast tests of CFST columns, this research investigates the blast resistance of commonly used bridge columns, namely seismically ductile reinforced concrete (RC) columns and non-ductile RC columns retrofitted with steel jackets to make them ductile, detailed in accordance to recent code of practice.

This report describes the design of the prototype bridge pier bent with these seismically resistant conventional columns under blast and seismic loading and the corresponding specimen design, experimental set-up, and experimental results. The results from the blast experiments are compared with the results from a simplified method of analysis considering an equivalent SDOF system having an elastic-perfectly-plastic behavior. Additionally, single degree of freedom (SDOF) and 2D nonlinear dynamic response-history analyses were used to simulate the behavior of CFST columns in the first series of the tests subjected to blast loading and to better understand their ultimate behavior.

The tested standard ductile RC and non-ductile RC columns retrofitted with steel jackets were not found to exhibit a ductile behavior under blast loading, but rather failed in shear at their base. Based on experimental and analytical observations, different values of shape a factor  $\beta$  that accounts for the reduction of the blast pressures acting on a circular column were established, as applicable for the different analytical methods considered.





## **ACKNOWLEDGMENTS**

The authors thank James C. Ray at the Engineer Research and Development Center in the Army Corps of Engineers for his help and assistance in the logistics of the experiments. Also acknowledged are the contributions of the staff of the Structural Engineering and Earthquake Simulation Laboratory at the University of Buffalo, Christopher Budden, Duane Kozlowski, Lou Moretta, Mark Pitman and Scot Weinreber for their assistance.

This research was conducted at the University at Buffalo (The State University of New York) and was supported by the Federal Highway Administration under contract number DTFH61-98-C-00094 to the Multidisciplinary Center for Earthquake Engineering Research. However, any opinions, findings, conclusions, and recommendations presented in this paper are those of the authors and do not necessarily reflect the views of the sponsors.



# TABLE OF CONTENTS

SECTION	TITLE	PAGE
<b>1:</b>	<b>INTRODUCTION</b>	<b>1</b>
1.1	Motivation	1
1.2	Scope of Research	3
1.3	Organization of This Report	4
<b>2:</b>	<b>LITERATURE REVIEW</b>	<b>7</b>
2.1	General	7
2.2	Seismic Design of Reinforced Concrete Column in Plastic Hinge	8
2.2.1	American Concrete Institute (ACI)	8
2.2.2	American Association State Highway and Transportation Officials (AASHTO)	9
2.2.3	California Department of Transportation (CALTRANS)	9
2.2.4	MCEER/ATC-49	10
2.3	Seismic Retrofit of Reinforced Concrete Column with Steel Jacket	11
2.3.1	Retrofit Measures for Reinforced Concrete Columns	11
2.3.2	Steel Jacketing	12
2.3.3	Research by Chai et al. (1991)	13
2.3.4	Research by Priestley et al. (1994a, 1994b)	14
2.4	Behavior of Reinforced Concrete subjected to Blast Load	16
2.4.1	Ductile Response	17
2.4.2	Brittle Response	19
2.4.3	Breaching and Spalling Resistance of Reinforced Concrete Element	21
2.5	Direct Shear Failure	22
2.5.1	General	22
2.5.2	Ultimate Capacity of Direct Shear under Static Loads	25
2.5.3	Ultimate Capacity of Direct Shear under Dynamic Loads	27
2.6	Structural Analysis Options under Blast Loading	29

## TABLE OF CONTENTS (CONT'D)

SECTION	TITLE	PAGE
2.6.1	Consideration of Blast Pressure.....	30
2.6.2	Interaction between Structure and Blast Loading.....	30
2.6.3	Discretization of Structure.....	31
2.6.4	Material and Geometric Nonlinearity.....	31
<b>3:</b>	<b>BLAST PERFORMANCE OF SEISMICALLY RESISTANT REINFORCED CONCRETE AND STEEL JACKETED BRIDGE PIERS.....</b>	<b>33</b>
3.1	Introduction.....	33
3.2	Experimental Design and Setup.....	34
3.2.1	General.....	34
3.2.2	Assumed Blast Scenario.....	35
3.2.3	Seismic Analysis and Design of Prototype Bridge Pier Bent.....	37
3.2.3.1	Prototype Bridge Structure.....	37
3.2.3.2	Analysis of Reinforced Concrete Section.....	37
3.2.3.3	Seismic Loading.....	42
3.2.3.4	Analysis of Bent Column for Seismic Loading.....	43
3.2.3.5	Design of Column Transverse Steel Reinforcement.....	45
3.2.3.6	Design Footing and Cap-beam.....	48
3.2.3.7	Design of Steel Jacketed Non-ductile RC Column.....	50
3.2.4	One-Fourth Scale Model Design.....	51
3.2.5	Specimen Materials.....	52
3.2.5.1	Concrete Properties.....	52
3.2.5.2	Reinforcing Steel and Steel Jacket Properties.....	53
3.2.6	Model Fabrication.....	58
3.2.7	Test Setup.....	62
3.3	Experimental Cases and Observations.....	66
3.3.1	General.....	66
3.3.2	Explosive Charge.....	66
3.3.3	Experimental Cases.....	66

## TABLE OF CONTENTS (CONT'D)

SECTION	TITLE	PAGE
3.3.4	Experimental Observations.....	69
3.3.4.1	Test 1 for Column RC1.....	69
3.3.4.2	Test 2 for Column RC2.....	70
3.3.4.3	Test 3 for Column SJ2.....	71
3.3.4.4	Test 4 for Column SJ1.....	72
3.3.5	Summary.....	73
3.4	Analytical Study.....	74
3.4.1	General.....	74
3.4.2	Moment-Curvature Analysis.....	74
3.4.3	Simple Plastic Analysis.....	76
3.4.4	Simplified Blast Analysis by Equivalent SDOF System.....	77
3.4.5	Direct Shear Resistance of Test Column.....	80
3.4.6	Breaching and Spalling Resistance.....	82
<b>4:</b>	<b>DYNAMIC ANALYSIS OF BRIDGE PIER SUBJECTED TO BLAST</b>	
	<b>LOADING.....</b>	<b>107</b>
4.1	Introduction.....	107
4.2	Summary of Bridge Pier Tests Subjected to Blast Loading.....	108
4.3	Selection of Analytical Methods.....	112
4.4	SDOF Dynamic Analysis.....	113
4.4.1	General.....	113
4.4.1	Program for SDOF Dynamic Analysis.....	114
4.4.2	Analytical Model.....	115
4.4.3	Applied Blast Loading.....	118
4.4.4	Methods for Solving Equation of Motion.....	119
4.4.5	Analytical Results.....	119
4.4.5.1	Effect of Damping and Load-mass Factor.....	119
4.4.5.2	Shape Factor $\beta$ .....	122
4.4.5.3	Structural Response.....	124

## TABLE OF CONTENTS (CONT'D)

SECTION	TITLE	PAGE
4.5	Fiber-based Analytical Model.....	131
4.5.1	General.....	131
4.5.2	Analytical Model and Solution Algorithm.....	132
4.5.3	Material Constitutive Models.....	134
4.5.3.1	Constitutive Model for Steel.....	135
4.5.3.2	Constitutive Model for Concrete.....	137
4.5.3.3	Tension Stiffening Model for Steel Bars.....	137
4.5.3.4	Strain Penetration Model for Steel Bars.....	138
4.5.4	Model Verification with Quasi-Static Tests.....	145
4.5.4.1	Overview of Experimental Studies.....	145
4.5.4.2	Analytical Model for Cyclic Loading Test Columns.....	147
4.5.4.3	Analytical Results and Comparison with Experimental Results.....	149
4.6	Fiber-based Dynamic Analysis.....	155
4.6.1	General.....	155
4.6.2	Analytical Model for Blast Loading Test Columns.....	157
4.6.3	Moment-Curvature Analysis for CFST Columns.....	159
4.6.4	Modal Analysis for CFST Columns.....	159
4.6.5	Applied Blast Loadings.....	163
4.6.6	Analytical Results.....	172
4.6.6.1	Shape Factor $\beta$ .....	172
4.6.6.2	Structural Response of CFST Columns.....	174
4.6.6.3	Structural Response of RC and Steel Jacketed RC Columns.....	185
4.7	Summary of Dynamic Analysis under Blast Loading.....	187
<b>5:</b>	<b>SUMMARY, CONCLUSIONS, AND RECOMMENDATIONS FOR FURTHER RESEARCH.....</b>	<b>191</b>
5.1	Summary.....	191
5.2	Conclusions.....	192
5.3	Recommendations for Further Research.....	193

## TABLE OF CONTENTS (CONT'D)

SECTION	TITLE	PAGE
6:	REFERENCES.....	195
APPENDIX A:	SECTION AND MATERIAL MODELS OF PROTOTYPE COLUMN FROM XTRACT.....	203
APPENDIX B:	SEISMIC ANALYSIS AND DESIGN OF PROTOTYPE BRIDGE BENT COLUMN.....	209
APPENDIX C:	DESIGN OF FOOTING AND CAP BEAM OF PROTOTYPE BRIDGE BENT.....	227
APPENDIX D:	DESIGN OF STEEL JACKETED RC COLUMN OF PROTOTYPE BRIDGE.....	239
APPENDIX E:	SHOP DRAWINGS OF PIER BENT SPECIMEN.....	245
APPENDIX F:	MODELS AND RESULTS OF MOMENT-CURVATURE ANALYSIS OF TEST COLUMNS FROM XTRACT.....	255
APPENDIX G:	SIMPLE PLASTIC ANALYSIS OF TEST COLUMNS.....	267
APPENDIX H:	SIMPLIFIED BLAST ANALYSES OF RC COLUMN TESTS.....	277
APPENDIX I:	CYLCIC ANALYSIS TEST SETUP AND HYSTERESIS LOOPS FOR FIBER-BASED MODEL VERIFICATION.....	283





## LIST OF FIGURES

FIGURE	TITLE	PAGE
2-1	Typical Steel Shell Retrofit (Buckle et al. 2006)	12
2-2	Test Setup and Column Details (Chai et al. 1991)	14
2-3	Test Setup and Reinforcement Details (Priestley et al. 1994a, 1994b)	15
2-4	Element Stirrup Reinforcement (USDA 1990)	17
2-5	Typical Laced Wall (USDA 1990)	18
2-6	Typical Resistance-deflection Curve for Concrete Element (adapted from USDA 1990)	19
2-7	Disengagement of Concrete Element Surface (USDA 1990)	20
2-8	Failure of Concrete Element under Blast Loading (USDA 1990)	21
2-9	Design Criteria for Breaching and Direct Spalling (UFC 2004)	22
2-10	Global and Local Roughness (adapted from Ali and White 1990)	24
2-11	Shear Friction Model (adapted from MacGregor and Wight 2005)	24
2-12	Shear Transfer Test Specimen (adapted from MacGregor and Wight 2005)	25
2-13	Comparison of Shear-friction Models with Test Data	27
2-14	Details of Test Specimens and Test Set-up (Hansen et al. 1961)	28
2-15	Details of Test Specimen (Chung 1978)	29
2-16	Discretization of Structure (Priestley et al. 1996)	32
3-1	Schematics of prototype bridge and assumed blast scenario	35
3-2	Blast Damage Threshold (FEMA 2003)	36
3-3	Elevation Details of Prototype Bridge Pier-bent	38
3-4	Reinforcement Details of Prototype Bridge Pier-bent	39
3-5	Stress-strain Model for Unconfined and Confined Concrete (Priestley et al. 1996)	41
3-6	Stress-strain Model for Section Analysis	41
3-7	Axial Force - Moment Interaction Curve for Prototype Bridge Column	42
3-8	Pseudo-acceleration Response Spectrum for Seismic Analysis and Design	43
3-9	General Layout of Experimental Specimen	51
3-10	Vacuum Furnace for Annealing	55
3-11	Stress-Strain Curve for D-1	55
3-12	Stress-Strain Curve for D-2	56
3-13	Stress-Strain Curve for D-3	56

## **LIST OF FIGURES (Continued)**

<b>FIGURE</b>	<b>TITLE</b>	<b>PAGE</b>
3-14	Stress-Strain Curve for D-4	57
3-15	Stress-Strain Curve for Steel Jacket	57
3-16	Reinforcement Details of Bent Pier Model	59
3-17	Reinforcement Details of Column Section	59
3-18	Reinforcement Details of Footing and Column	60
3-19	Reinforcement Details of Column – Footing Connection	60
3-20	Reinforcement Details of Column – Cap-beam Connection	61
3-21	Formwork for Column	61
3-22	Shipping Frame for Model	62
3-23	Test Setup and Reaction Frame Details	63
3-24	Test Setup from Front Diagonal View	64
3-25	Test Setup from Side View	64
3-26	Test Setup from Back Diagonal View	65
3-27	Reaction Frame	65
3-28	Explosive Charge Location	68
3-29	Sketch of Column RC1 after Test 1	84
3-30	Left Side View of Column RC1 (Test 1)	84
3-31	Front View of Column RC1 (Test 1)	84
3-32	Column RC1 at Bottom (Test 1)	85
3-33	Fracture Surface of Footing at Column RC1 (Test 1)	85
3-34	Fracture of Longitudinal Steel Bars at Footing (Test 1)	85
3-35	Right Side View of Column RC1 at Bottom (Test 1)	85
3-36	Left Side View of Column RC1 at Bottom (Test 1)	86
3-37	Front Diagonal View of Column RC1 around Charge Height	86
3-38	Left Side View of Column RC1 at Top (Test 1)	86
3-39	Right Side View of Column RC1 at Top (Test 1)	86
3-40	Front View of Column RC1 at Top (Test 1)	87
3-41	Fracture interface of Column RC1 at Top (Test 1)	87
3-42	Back Diagonal View of Column RC1 at Top (Test 1)	87
3-43	Sketch of Column RC2 after Test 2	88

## LIST OF FIGURES (Continued)

FIGURE	TITLE	PAGE
3-44	Front Diagonal View of Column RC2 (Test 2)	88
3-45	Back Diagonal View of Column RC2 (Test 2)	88
3-46	Front View of Column RC2 (Test 2)	89
3-47	Front Diagonal View of Column RC2 at Bottom (Test 2)	89
3-48	Right Side View of Column RC2 at Bottom (Test 2)	89
3-49	Left Side View of Column RC2 at Bottom after Cover Concrete Removal (Test 2)	89
3-50	Right Side View of Column RC2 at Bottom after Cover Concrete Removal (Test 2)	90
3-51	Right Diagonal Front View Column RC2 at Top (Test 2)	90
3-52	Left Diagonal Front View of Column RC2 at Top (Test 2)	90
3-53	Back View of Column RC2 at Top (Test 2)	90
3-54	Sketch of Column SJ2 after Test 3	91
3-55	Right Side View of Column SJ2 (Test 3)	91
3-56	Void at Column SJ2 after Test 3	91
3-57	Drift of Column SJ2 at Bottom (Test 3)	92
3-58	Front Diagonal View of Column SJ2 at Bottom (Test 3)	92
3-59	Fractures of Longitudinal Bars Column SJ2 at Bottom (Diagonally Front View, Test 3)	92
3-60	Back Diagonal View of Column SJ2 at Bottom (Test 3)	92
3-61	Close-in Back View of Column SJ2 at Bottom (Test 3)	93
3-62	Front View of Column SJ2 at Top (Test 3)	93
3-63	Left Side View of Column SJ2 at Top (Test 3)	93
3-64	Back View of Column SJ2 at Top (Test 3)	93
3-65	Cracks at Cap Beam of Column SJ2 (Test 3)	94
3-66	Sketch of Column SJ1 after Test 4	94
3-67	Left Side View of Column SJ1 (Test 4)	95
3-68	Drift of Column SJ1 at Bottom (Test 4)	95
3-69	Fracture of Longitudinal Steel Bars at Footing (Front Diagonal View, Test 4)	95
3-70	Cracking of Steel Tube at Bottom of Column SJ1 at Bottom (Front Diagonal View, Test 4)	95
3-71	Back Diagonal View of Column SJ1 at Bottom (Test 4)	96

## LIST OF FIGURES (Continued)

FIGURE	TITLE	PAGE
3-72	Back Diagonal View of Column SJ1 at Bottom (Test 4)	96
3-73	Front View of Column SJ1 at Top (Test 4)	96
3-74	Back View of Column SJ1 at Top (Test 4)	96
3-75	Moment-Curvature Relationship for RC column	97
3-76	Moment-Curvature Relationship for Steel Jacketed RC column at Middle Section	97
3-77	Moment-Curvature Relationship for Steel Jacketed RC column at bottom Section	98
3-78	Step-by-step Plastic Analysis of RC Column	99
3-79	History of Load versus Deflection at Load Point for RC Column	100
3-80	Step-by-step Plastic Analysis of Steel Jacketed RC Column	101
3-81	History of Load versus Deflection at Load Point for RC Column	102
3-82	Variation of Impulse and Peak Pressure along Height of Column for Column RC1 (Test 1) and SJ2 (Test 3)	102
3-83	Variation of Impulse and Peak Pressure along Height of Column for Column RC2 (Test 2) and SJ1 (Test 4)	103
3-84	RC Column under Bending Moment	103
3-85	Comparison of Shear Resistance with Shear Force at Base of RC Column	104
3-86	Comparison of Shear Resistance with Shear Force at Base of Steel Jacketed RC Column	104
3-87	Comparison of RC Column Damages and Pressure Distributions	105
3-88	Comparison of SJ Column Damages and Pressure Distributions	105
4-1	Comparison of Test Blast Parameters	110
4-2	Comparison of Tested Column Sections and Moment Capacities	110
4-3	Real and Equivalent SDOF System for SDOF Dynamic Analysis	115
4-4	Equivalent Pressure History	120
4-5	Analytical Results for Test 1-3 with $\beta = 0.472$ (C4 Column)	122
4-6	Analytical Results for Test 1-3 with $\beta = 0.566$ (C4 Column)	125
4-7	Analytical Results for Test 1-4 with $\beta = 0.540$ (C6 Column)	126
4-8	Analytical Results for Test 1-5 with $\beta = 0.521$ (C5 Column)	127
4-9	Analytical Results for Test 1-6 with $\beta = 0.558$ (C4 Column)	128
4-10	Analytical Results for Test 1-9 with $\beta = 0.524$ (C6 Column)	129

## **LIST OF FIGURES (Continued)**

<b>FIGURE</b>	<b>TITLE</b>	<b>PAGE</b>
4-11	Analytical Results for Test 1-10 with $\beta = 0.492$ (C5 Column)	130
4-12	Cross Sections for Fiber Element	133
4-13	Analytical Model for Cyclic Loading Test Specimen	134
4-14	Constitutive Model for Steel (Menegotto and Pinto 1973)	136
4-15	Shift of Yield Asymptote due to Isotropic Strain Hardening (Filippou et al. 1983)	137
4-16	Strain Penetration Model for Steel Bar (Zhao and Sritharan 2007)	140
4-17	Modified Chang-Mander Model for Concrete (adapted from Waugh 2007)	143
4-18	Modified Scott-Kent-Park Model for Concrete (adapted from Yassin 1994)	145
4-19	Analytical Model for CFST Column	148
4-20	Analytical Model for RC Column	148
4-21	Analytical Model for Steel Jacketed RC Column	149
4-22	Analytical Results for Cyclic Loading Test of CFST-34	151
4-23	Analytical Results for Cyclic Loading Test of CFST-42	152
4-24	Analytical Results for Cyclic Loading Test of RC-TP60	152
4-25	Analytical Results for Cyclic Loading Test of RC-Unit9	153
4-26	Analytical Results for Cyclic Loading Test of SJ-Unit4	153
4-27	Analytical Results for Cyclic Loading Test of SJ-CR2	154
4-28	Comparison of Analytical Results with Test Results of CFST Columns	154
4-29	Comparison of Analytical Results with Test Results of RC Columns	155
4-30	Comparison of Analytical Results with Test Results of Steel Jacketed RC Columns	155
4-31	Analytical Model for Blast Loading Tests	158
4-32	Comparison of Moment-Curvature Relationship for CFST C4 Column	160
4-33	Comparison of Moment-Curvature Relationship for CFST C5 Column	161
4-34	Comparison of Moment-Curvature Relationship for CFST C6 Column	161
4-35	Natural Mode Shapes of CFST Columns	162
4-36	Applied Blast Pressures of Test 1-3 (CFST C4 Column)	165
4-37	Applied Blast Pressures of Test 1-4 (CFST C6 Column)	166
4-38	Applied Blast Pressures of Test 1-5 (CFST C5 Column)	167
4-39	Applied Blast Pressures of Test 1-6 (CFST C4 Column)	168

## **LIST OF FIGURES (Continued)**

<b>FIGURE</b>	<b>TITLE</b>	<b>PAGE</b>
4-40	Applied Blast Pressures of Test 1-9 (CFST C6 Column) and Test 1-10 (CFST C5 Column)	169
4-41	Applied Blast Pressures of Test 2-1 (RC1 Column) and Test 2-3 (SJ2 Column)	170
4-42	Applied Blast Pressures of Test 2-2 (RC2 Column) and Test 2-4 (SJ1 Column)	171
4-43	Comparison of Analytical Results with Different Damping Ratio of Test 1-3 (CFST C4 Column)	174
4-44	Analytical Results of Test 1-3 (CFST C4 Column) subjected to Equivalent Uniform Pressures	179
4-45	Analytical Results of Test 1-4 (CFST C6 Column) subjected to Equivalent Uniform Pressures	180
4-46	Analytical Results of Test 1-5 (CFST C5 Column) subjected to Equivalent Uniform Pressures	180
4-47	Analytical Results of Test 1-3 (CFST C4 Column) subjected to Actual Pressures	181
4-48	Analytical Results of Test 1-4 (CFST C6 Column) subjected to Actual Pressures	182
4-49	Analytical Results of Test 1-5 (CFST C5 Column) subjected to Actual Pressures	182
4-50	Analytical Results of Test 1-6 (CFST C4 Column) subjected to Actual Pressures	183
4-51	Analytical Results of Test 1-9 (CFST C6 Column) subjected to Actual Pressures	184
4-52	Analytical Results of Test 1-10 (CFST C5 Column) subjected to Actual Pressures	184
4-53	Analytical Results of Test 2-2 (RC2 Column)	189
4-54	Displacement History of CFST C4 Column using Test 2-2 Blast Pressures (at $h = 0.55$ m)	189
4-55	Reaction Force History of Test 2-1 (RC1 Column at $h = 0.55$ m)	190
4-56	Reaction Force History of Test 2-4 (SJ1 Column at $h = 0.55$ m)	190
4-57	Reaction Force History of Test 2-3 (SJ2 Column at $h = 0.55$ m)	190

## LIST OF TABLES

TABLE	TITLE	PAGE
2-1	Design Variations of Test Specimens (Chai et al. 1991)	13
2-2	Design Variations of Test Specimens (Priestley et al. 1994a, 1994b)	16
2-3	Options for Blast Resistance Analysis	30
3-1	Summary of Seismic Analyses	45
3-2	Summary of Transverse Reinforcement for Confinement at Plastic Hinge Zone	48
3-3	Mix Design Formula for Model Concrete	52
3-4	Measured Concrete Properties	53
3-5	Reinforcing Steel Properties	54
3-6	Summary of Column Test Cases and Test Observations	68
3-7	Summary of Moment-Curvature Analyses	76
3-8	Summary of Results of Simplified Blast Analysis (RC Tests)	80
4-1	Summary of All Column Test Cases and Results	109
4-2	Comparison of Analytical Methods	112
4-3	Design Values for SDOF Dynamic Analysis	118
4-4	SDOF Dynamic Analysis Cases for CFST C4 Column of Test 1-3	121
4-5	Summary of Shape Factor from SDOF Dynamic Analysis	123
4-6	Summary of Maximum Response Values for SDOF Dynamic Analyses	131
4-7	Natural Period and Pressure Duration	131
4-8	Cyclic Loading Test Column Details	146
4-9	Material Properties of Cyclic Loading Test Columns	147
4-10	Modal Analysis Results of CFST Columns	162
4-11	Summary of Shape Factors from Fiber-based Dynamic Analyses of CFST Columns	172
4-12	Summary of Analytical Results from Fiber-based Dynamic Analyses of CFST Columns	175
4-13	Summary of Maximum Reaction Forces for RC and Steel Jacketed RC Columns	186
4-14	Summary of $\beta$ Values and Assumptions of Each Analytical Method	188





## NOTATIONS

$a_1$	Coefficient in Menegotto and Pinto model
$a_2$	Coefficient in Menegotto and Pinto model
$a_3$	Coefficient accounting for strain hardening in Menegotto and Pinto model
$a_4$	Coefficient accounting for strain hardening in Menegotto and Pinto model
$A_b$	Area longitudinal reinforcing bars
$A_{bh}$	Area of hoop or spiral reinforcing bars
$A_c$	(1) Core concrete area (2) area of concrete section resisting shear transfer
$A_c'$	Modified area of concrete section resisting shear transfer
$A_{cc}$	Core concrete area
$A_{ch}$	Cross-section area of structural member
$A_f$	Projected area normal to wind
$A_g$	(1) Peak ground acceleration (2) gross area of concrete section
$A_{sk}$	Area of skin reinforcement
$A_{vf}$	Area of shear-friction reinforcement
$A_v$	Shear area of concrete
$A_{vf}$	Area of shear-friction reinforcement across shear plane
$A_{vf}'$	Modified area of shear-friction reinforcement across shear plane
$b$	Strain hardening ratio
$B$	Cap-beam width
$B_f$	Footing width
$c$	(1) Damping coefficient (2) cohesion in shear-friction strength
$d_e$	Effective depth of concrete member
$D$	Column diameter
$D'$	Center to center diameter of longitudinal reinforcement
$D''$	Center to center sectional dimension of hoop or spiral reinforcing bars
$D_c$	Dynamic increase factor for concrete strength
$D_j$	Outside diameter of steel jacket
$D_{sy}$	Dynamic increase factor for steel yield strength
$e$	Eccentricity of axial load at footing
$E_c$	Secant elastic modulus of concrete

## NOTATIONS (Continued)

$E_s$	Elastic modulus of steel
$E_{\text{sec}}$	Secant modulus of elasticity
$EI_e$	Equivalent flexural stiffness
$f'_c$	Static compressive strengths of concrete
$f'_{cc}$	Compressive strengths of confined concrete
$f_{cr}$	Concrete cracking strength
$f'_{dc}$	Ultimate compressive strengths of concrete
$f_{dy}$	Dynamic yield stress of steel
$f_{du}$	Dynamic ultimate stress of steel
$f_l$	Effective lateral confining pressure
$f'_l$	Effective lateral confining pressure
$f_t$	Tensile strength of steel
$f_u$	Static ultimate stress of steel
$f_y$	Static yield stress of steel
$f_{yj}$	Yield strength of steel jacket
$f_{yt}$	Yield strength of transverse reinforcement
$H$	Column height
$h_x$	Maximum center-to-center horizontal spacing of crossties or hoop legs
$i$	Unit positive impulse
$i_{eq}$	Equivalent uniform impulse per unit area
$I$	Importance of the facility
$I_c$	Moment of inertia of core concrete section
$I_{cr}$	Moment of inertia of cracked concrete section
$I_D$	Equivalent moment of inertia of deck
$I_{eq}$	Equivalent uniform impulse per unit length
$I_s$	Moment of inertia of steel tube section
$k^*$	Generalized stiffness
$k_c$	Stiffness of column
$K$	Stiffness
$K_1$	Shear transfer stress of concrete
$K_e$	(1) Equivalent stiffness (2) confinement effectiveness coefficient

$K_E$	Equivalent elastic stiffness
$K_{eff}$	Total effective stiffness
$K_L$	(1) Load factor (2) total stiffness of column in longitudinal direction
$K_{LM}$	Load-mass factor
$K_{LMe}$	Load-mass factor for elastic range
$K_{LMp}$	Load-mass factor for plastic range
$K_M$	Mass factor
$K_P$	Stiffness of pier-bent
$K_S$	Stiffness factor
$KE$	Kinetic energy
$l_d$	Development length of longitudinal reinforcing bar
$L$	(1) Total height of column (2) Total span length
$L_f$	Footing length
$L_p$	Plastic hinge length
$m$	Unit mass
$m^*$	Generalized mass
$m_D$	Mass of a deck per unit length
$M$	Total mass
$M_e$	Equivalent total mass
$M_n$	Nominal moment capacity of column
$M_p$	Plastic moment capacity of column
$M_{pb}$	Plastic moment capacity at base of column
$M_{pm}$	Plastic moment capacity at mid of column
$p$	(1) External load per unit length (2) maximum pressure
$p_{eq}$	Equivalent peak pressure
$p_r$	Peak reflected pressure, reflected overpressure or peak positive normal reflected pressure
$p_s$	Peak overpressure
$P$	(1) Load (2) axial force
$P_e$	(1) Equivalent load (2) design axial load
$P_r$	(1) Reflected overpressure, peak positive normal reflected pressure (2) axial design strength
$r_e$	Yield resistance of column

$r_u$	Ultimate resistance of column
$R$	(1) Distance from explosion center (2) resistance of column (3) risk (4) Bauchinger effect coefficient
$R_0$	Coefficient in Menegotto and Pinto model
$R_e$	(1) Equivalent resistance of column (2) factor to control curve shape of strain penetration model
$R_u$	Strength per unit length of column
$s$	Spacing of hoop or spiral reinforcing bars
$s_0$	Minimum spacing of transverse reinforcement
$s_y$	Loaded-end slip of steel reinforcing bar at yield
$s_u$	Loaded-end slip of steel reinforcing bar at ultimate
$S_A$	Pseudo-acceleration response spectrum
$S_D$	Elastic displacement response of bridge
$t$	Thickness of steel tube, steel jacket
$t_0$	Duration of positive phase of blast pressure
$t_a$	Arrival time of blast wave
$t_b$	Minimum thickness to prevent breaching
$t_d$	Duration of positive phase of blast pressure
$t_j$	Steel jacket thickness
$t_m$	Time at which maximum deflection occurs
$t_s$	Minimum thickness to prevent direct spalling
$T$	Natural period of a bridge
$T_{eff}$	Effective natural period of a bridge
$U$	Strain energy
$U_{sf}$	Strain energy capacity of transverse reinforcement
$v_n$	Shear-friction strength
$V_c$	Tensile contribution of concrete to shear resistance
$V_e$	Elastic lateral force capacity of column
$V_n$	Nominal shear strength
$V_n'$	Modified direct shear resistance
$V_p$	Shear resistance by axial force strut action
$V_s$	Shear resistance by transverse reinforcement
$V_{sj}$	Shear enhancement due to steel jacket
$V_u$	Design shear force

$Z$	(1) Scaled distance (2) plastic modulus of C-channel
$W$	Explosive charge weight
$W_{int}$	Internal work
$W_p$	Explosive charge weight
$W_{super}$	Total weight of bridge superstructure
$WD$	Work done by load
$x$	Deflection
$\dot{x}$	Velocity
$\ddot{x}$	Acceleration
$x_0$	Maximum deflection
$\dot{x}_0$	Maximum velocity
$X_e$	Yield deflection of column
$X_E$	Equivalent maximum elastic deflection
$X_m$	Maximum deflection
$X_p$	(1) Horizontal distance between center of an explosive charge weight and a pier (2) Plastic deflection
$X_{test}$	Maximum residual deformation from test
$X_u$	Displacement capacity of column
$z$	Height of column
$Z$	(1) Scaled distance (2) plastic modulus of steel tube
$\beta$	Shape factor, pressure reduction factor
$\delta$	Normalized deflected shape of column
$\Delta_u$	Displacement demand
$\Delta_y$	Elastic displacement capacity of column
$\epsilon_c$	Concrete compression strain
$\epsilon_{cc}$	Strain at peak stress for confined concrete
$\epsilon_{max}$	Absolute maximum strain at instant of strain reversal
$\epsilon_t$	Strain of steel at tensile strength
$\epsilon_y$	Yield strain
$\epsilon_u$	Rupture strain
$\phi$	Resistance factor
$\phi_p$	Strength factor
$\theta$	Angle between column axis and principal tension cracking direction

$\theta_u$	Rotation capacity of column
$\lambda$	Coefficient for shear friction
$\Lambda$	Fixity factor
$\mu$	(1) Displacement ductility demand (2) friction coefficient
$\rho_s$	(1) Air density behind wavefront (2) volumetric spiral reinforcement ratio
$\rho_t$	Longitudinal reinforcement ratio
$\rho_v$	Reinforcement ratio across shear plane
$\sigma$	Compressive stress action on shear surface
$\sigma_{st}$	Stress shift in Menegotto and Pinto model accounting for strain hardening
$\psi$	Deformation shape

## ABBREVIATIONS

AASHTO	American Association of State Highway and Transportation Officials
BEL	Bridge Explosive Loading
CFST	Concrete-Filled Steel Tube
CALTRANS	California Department of Transportation
DIF	Dynamic Increase Factor
FEM	Finite Element Models
FHWA	Federal Highway Administration
FRP	Fiber-Reinforced Plastic
LRFD	Load and Resistance Factor Design
RC	Reinforced Concrete
SEESL	Structural Engineering and Earthquake Simulation Laboratory at the University at Buffalo
SDOF	Single Degree of Freedom
UB	University at Buffalo





# SECTION 1

## INTRODUCTION

### 1.1 Motivation

The United States has not suffered from sustained terrorist campaigns like in other countries (Jenkins 2001b). However, as seen in recent terrorist attacks in the United States such as the Oklahoma federal building bombing in 1995 and the September 11, 2001 attacks (9/11), the terrorist threat in the United States is real. The National Intelligence Council (NIC) forecasted that, at least for the period from 2008 to 2010, the US Homeland will face a persistent and evolving terrorist threat coming from Islamic terrorist groups and cells, especially al-Qa'ida which waged the 9/11 attacks (NIE 2007). NIC assesses that “al-Qa'ida's Homeland plotting is likely to focus on prominent political, economic, and infrastructure targets with the goal of producing mass casualties, visually dramatic destruction, significant economic aftershocks, and/or fear among the US population.”

Modern terrorists have targeted infrastructures, especially public transportation systems in order to achieve their goals because terrorists can easily and anonymously access the systems. Jenkins (1997, 2001a) chronologically compiled a list of worldwide terrorist attacks and major criminal assaults on surface transportation from 1920 to 2000. He reported that nearly 900 terrorist attacks and other significant criminal incidents related to public surface transportation systems occurred, most of them in the 30 years from 1970 to 2000 (Jenkins 2001b). No terrorist attack has yet struck bridges, tunnels and roads in the United States, however terrorist threats have been received against the four California suspension bridges, including the Golden Gate Bridge in 2001 (Williamson EB and Winget DG 2005), and the Brooklyn Bridge in 1993, 1997 and 2003 (Jenkins 2001b, FBI 2007).

While the focus of these threats has been on large landmark bridges due to their symbolic nature, the destruction of regular bridges along routes that are key lifelines to specific regional economies is also foreseeable due to the significant disruption these attacks can create and the

possibly simpler logistics in their planning. Historically, bridges have been targets of war and terrorism because loss of a bridge can have a massive impact on transportation mobility of troops and a detrimental effect to large populations. Following the aftermath of 9/11, government leaders, infrastructure owners and the engineering community have recognized that the nation's highway system has vulnerabilities and that collapse of a critical bridge could result in tremendous casualties and enormous economic loss, which resulted in the publication of a number of documents addressing this concern (see, for instance, FHWA 2003).

Beyond terrorist focused issues alone, bridges are exposed to multiple other hazards. To better integrate these diverse threats with conflicting demands on structural systems, there has been a growing trend in the engineering community to find integrated solutions for the design of infrastructures across various hazards, namely multi-hazard engineering. Multi-hazard engineering has recently emerged as a new consideration and the community has made an effort to clarify and establish multihazard engineering principles (see, for instance Multi-Hazard Symposium 2007). Multi-hazard engineering is defined here as the search for a single design concept which can satisfactorily fulfill the demands of multiple hazards. The properties that might be desirable to resist one hazard may have detrimental effects to resist other hazards. Therefore, multi-hazard engineering addresses problems of infrastructures from the system perspective by establishing the optimized solutions that can provide protections against multiple hazards.

The authors previously presented the development and experimental validation of a multi-hazard bridge pier concept, i.e., a bridge pier system capable of providing an adequate level of protection against collapse under both seismic and blast loading (Fujikura et al. 2007, 2008). The proposed concept was a multi-column pier bent with concrete-filled steel tube (CFST) columns that could provide ductile behavior up to 7 % drift under seismic excitations and approximately 20 % under blast loading (Marson and Bruneau 2004, Fujikura et al. 2007). The columns turned out to be effective for blast loadings because breaching and spalling of concrete are prevented in CFST columns.

While CFST columns perform excellently in a multi-hazard perspective, they have not been commonly used in bridge engineering practice (although they are sometimes used by some state

departments of transportation, such as Alaska DOT). Questions arose as to whether conventional columns designed to perform satisfactory under seismic excitations would possess adequate blast resistance. If they did, there would be no need to change current practice for the ductile detailing of bridge columns. Reinforced concrete (RC) has been widely used for bridge columns. Seismic detailing requirements for RC columns that can behave in a ductile manner during earthquake are provided by various documents, such as those published by the American Association of State Highway and Transportation Officials (AASHTO) and the California Department of Transportation (Caltrans). Furthermore, in many parts of the United States, particularly in California, reinforcement detailing requirements in effect prior to the 1971 San Fernando earthquake resulted in RC columns that exhibited non-ductile behavior during earthquakes. Many methods have been used to retrofit such non-ductile columns. One of the most popular methods is steel jacketing which has been commonly used on the west coast of the United States. A column retrofitted with a steel jacket visually resembles a CFST column, but is typically discontinuous at the column top and base in order to avoid undesirable overload of the adjacent members (i.e., footing or cap beam) due to composite action that would significantly increase the flexural strength of the column (Buckle et al. 2006).

Therefore, the objective of the research presented here was to investigate the blast resistance of commonly used bridge columns, namely seismically ductile RC columns and non-ductile RC columns retrofitted with steel jackets to make them ductile, detailed in accordance to recent code of practice. This second series of test also complements the first series of CFST columns testing under blast loading by Fujikura et al. (2007, 2008).

## **1.2 Scope of Research**

The research conducted and reported herein consisted of the following steps:

- Design a prototype bridge pier bent with ductile RC columns and one with non-ductile RC columns retrofitted with steel jacket, subjected to seismic load.
- Design a one-fourth scale model with RC and steel jacketed RC columns based on the prototype pier bent.
- Set up experimental blast parameters assuming the damage level of the column by using simplified method of analysis.

- Perform blast testing on two RC columns and two steel jacketed RC columns.
- Compare the results of damage between those columns and CFST columns that were tested previously.
- Compare the results of testing with predictions made using the simplified method of analysis.
- Assess the direct shear resistance of those columns and the shear force demands based on simple plastic analysis.
- Develop and evaluate dynamic analysis methods using a SDOF system model.
- Develop and verify a fiber-based finite element model using quasi-static cyclic loading data.
- Investigate the overall behavior of the tested specimens using a developed fiber-based finite element model.

### **1.3 Organization of This Report**

Following this introduction, Section 2 contains a review of seismic detailing requirements for ductile RC column in accordance with the American Concrete Institute (ACI), AASHTO, Caltrans and MCEER/ATC-49, and a review of the seismic retrofit technique of non-ductile RC columns using steel jackets. Then, research on the structural response of RC members under blast load and the direct shear failure of RC members are reviewed. Analysis options under blast loading are also described. Section 3 presents the seismic design of a conventional bridge pier bent with ductile RC columns and non-ductile RC columns retrofitted with steel jackets. A second series of blast testing program using these RC columns and steel jacketed RC columns is provided. The results of the tests are compared with the simplified method of blast analysis and the design equations for direct shear resistance of those columns. In Section 4, the analytical tools using a SDOF system model and a fiber-based finite element model are developed and evaluated through comparison with the maximum residual displacements obtained from the experiments. Finally, a summary, conclusions, and recommendations for further research for the development of multi-hazard resistant bridge columns are presented in Section 5.

Note that for security reasons, some key details of this blast-related study are withheld from this report. More specifically, the numerical values of some key quantities are not provided. Instead,

results are presented in terms of parameters. The values of all of these parameters will be listed in a special Appendix, which will be made available to selected individuals.



## **SECTION 2**

### **LITERATURE REVIEW**

#### **2.1 General**

As presented in the previous section, the purpose of this study is to research the blast resistance of commonly used bridge columns, detailed in accordance with recent seismic codes.

Accordingly, this section focuses on reviewing recent seismic design provisions for reinforced concrete columns and behavior of reinforced concrete members subjected to blast loading.

Recent earthquakes such as the 1989 Loma Prieta, 1994 Northridge and 1995 Kobe earthquakes revealed the importance of concrete confinement in RC columns, which can be typically achieved by providing adequate transverse reinforcement. Failures in columns with unconfined concrete have typically resulted in the collapse of bridges. Different methods and reinforcement details are available in various design codes to achieve adequate confinement of concrete. At the same time, various methods for retrofitting non-ductile RC bridge columns have been proposed in the literature for increasing their confinement and improving their ductility (Buckle et al. 2006). Steel jacketing is one of such retrofitting techniques widely used in many parts of the United States, particularly in California.

The behavior of RC members, especially bridge columns, subjected to blast loading is of particular interest in this research project. There exist no comprehensive design guidelines and specifications for bridges under impulsive blast loading, but the structural behavior of RC members has been experimentally investigated and well documented for mission-critical structures such as army facilities and petrochemical facilities (see for instance USDA 1990 and ASCE 1997). In addition to general behavior of RC members under blast loading, knowledge also exists regarding the need to consider the risk of direct shear failure as part of the blast effects design process (Conrath 1999).

In this section, various code-specified design requirements for the transverse reinforcement of RC columns in plastic hinge regions are reviewed. Then, seismic retrofit methods for RC columns are described, including steel jacketing as one common retrofit technique. After that, structural response of RC members under blast loading is presented followed by a review of direct shear failure. Finally, structural analysis options under blast loading are described.

## **2.2 Seismic Design of Reinforced Concrete Column in Plastic Hinge**

For a bridge to achieve satisfactory seismic performance, its columns should be designed and detailed such that they can undergo large cyclic inelastic deformations without degradation in strength and stiffness. *Ductility* is the ability of structural elements to sustain these plastic deformations. A non-ductile column may collapse during a severe earthquake as a result of losing its strength, whereas a ductile column can dissipate seismic energy through inelastic deformations. Well detailed column reinforcement, especially in the plastic hinge region, is essential to achieve the ductility of RC column. Such reinforcement can be detailed to increase flexural strength of concrete, but most importantly needs to be detailed to prevent premature buckling of the longitudinal bars and shear failure of the column. The 1989 Loma Prieta, 1994 Northridge and 1995 Kobe earthquakes provided many opportunities to witness the columns with inadequate transverse reinforcement that failed and triggered collapse of bridges.

In the various design codes and specifications, different methods and details are available to design transverse reinforcement to achieve concrete confinement and column ductility. A summary of the seismic design of plastic hinge region for circular columns is presented in the following sections.

### **2.2.1 American Concrete Institute (ACI)**

The *building code requirements for structural concrete and commentary* (ACI 2004) contains the code requirements for structural concrete buildings, is not applicable to bridges. However, it is widely used for designing concrete members. The ACI design provisions specify the detailing of transverse reinforcement such as to achieve performance in which core concrete of the column would remain to provide the lateral load-carrying capacity for the column in spite of the covered



concrete spalling off. The ACI provisions specify the minimum volumetric spiral reinforcement ratio,  $\rho_s$ , shall be the greater of

$$\rho_s = 0.45 \left( \frac{A_g}{A_{ch}} - 1 \right) \frac{f'_c}{f_{yt}} \quad (2-1)$$

and

$$\rho_s = 0.12 \frac{f'_c}{f_{yt}} \quad (2-2)$$

where  $A_g$ ,  $A_{ch}$ ,  $f'_c$  and  $f_{yt}$  are gross area of concrete section, cross-section area of a structural member measured outside-to-outside of transverse reinforcement, specified compressive strength of concrete and specified yield strength of transverse reinforcement, respectively. Equation 2-2 usually governs for columns with large diameter. The minimum spacing of transverse reinforcement is specified to be the smaller of one-quarter of the minimum member dimension, six times the diameter of the longitudinal reinforcement, and  $s_o$ , where  $s_o$  is defined by:

$$s_o = 4 + \left( \frac{14 - h_x}{3} \right) \leq 6 \text{ (in)} \quad (2-3)$$

where  $h_x$  is the maximum center-to-center horizontal spacing of crossties or hoop legs on all faces of the column. Note that  $s_o$  need not be taken less than 4 in (102 mm).

### 2.2.2 American Association State Highway and Transportation Officials (AASHTO)

The *AASHTO LRFD Bridge Design Specifications* (AASHTO 2004) provide the same equations as those in ACI for selection of the minimum volumetric ratio of spiral reinforcement, namely those presented in Equations 2-1 and 2-2, with the difference that it specifies the ratio,  $\rho_s$ , shall satisfy either equations and not necessarily both. Another difference is that the spacing of lateral reinforcement for confinement is not to exceed one-quarter of the minimum member dimension or 100 mm center-to center.

### 2.2.3 California Department of Transportation (CALTRANS)

The *CALTRANS Bridge Design Specifications* (CALTRANS 2003) specify the use of Equation 2-1 for the minimum volumetric ratio,  $\rho_s$ , of spiral reinforcement outside of potential plastic hinge region. In potential plastic hinge zone,  $\rho_s$  is limited by the following equations:

$$\rho_s = 0.45 \left( \frac{A_g}{A_c} - 1 \right) \frac{f'_c}{f_y} \left( 0.5 + \frac{1.25 P_e}{f'_c A_g} \right) \quad (2-4)$$

for columns less than or equal to 3 feet (914 mm) in diameter (or least dimension for non-circular columns), or

$$\rho_s = 0.12 \frac{f'_c}{f_y} \left( 0.5 + \frac{1.25 P_e}{f'_c A_g} \right) \quad (2-5)$$

for columns larger than 3 feet (914 mm) in diameter (or least dimension), where  $A_g$ ,  $A_c$ ,  $f'_c$ ,  $f_y$  and  $P_e$  are gross area of section, area of core of spirally reinforced compression member measured to the outside diameter of the spiral, specified compressive strength of concrete, specified yield strength of reinforcement and design axial load due to gravity and seismic loading, respectively. The confinement equations of 2-4 and 2-5 account for the effect of axial load.

The maximum spacing limit of transverse reinforcement for seismic design is specified in the CALTRANS *Seismic Design Criteria* (CALTRANS 2006) to be the smallest of one-fifth of the least dimension of the cross-section, six times the nominal diameter of the longitudinal reinforcement, and 8 in (220 mm).

#### 2.2.4 MCEER/ATC-49

MCEER/ATC-49 (2003a, 2003b) summarized and presented in the format of Guide Specifications the knowledge and results of research programs conducted over two decades prior to its issuance. Originally it was intended to be incorporated into the AASHTO LRFD Bridge Design Specifications. However, due to the complexity of the provisions, the provisions were adopted by AASHTO as a Guide Specification. According to this document, the volumetric ratio of spiral reinforcement at plastic hinges,  $\rho_s$ , shall not be less than:

$$\rho_s = 0.008 \frac{f'_c}{U_{sf}} \left[ 12 \left( \frac{P_e}{f'_c A_g} + \rho_t \frac{f_y}{f'_c} \right)^2 \left( \frac{A_g}{A_{cc}} \right)^2 - 1 \right] \quad (2-6)$$

where  $f'_c$ ,  $f_y$ ,  $A_g$  and  $P_e$  were defined previously, and  $A_{cc}$ ,  $\rho_t$  and  $U_{sf}$  are area of column core concrete measured to the centerline of the perimeter spiral, ratio of longitudinal reinforcement area to gross area of section and strain energy capacity of the transverse reinforcement (= 110

MPa), respectively. Equation 2-6 was developed by Dutta and Mander (1998) who experimentally demonstrated that the equation worked well for both regular mild steel spirals and high strength steel wire. The maximum spacing of lateral reinforcement for confinement is six times the diameter of the longitudinal reinforcement.

## **2.3 Seismic Retrofit of Reinforced Concrete Column with Steel Jacket**

### **2.3.1 Retrofit Measures for Reinforced Concrete Columns**

Following the substantial damage to bridge structures due to earthquakes in California, CALTRANS developed a comprehensive seismic retrofit program for its bridges implemented over a few decades. The first phase of its program, started following the 1971 San Fernando Earthquake, was to install restrainers across expansion joints of a large number of bridges because the greatest risk to those structures was assessed as unseating of superstructure during earthquakes. The first phase had been practically completed by the time of Whittier Earthquake (1987), Loma Prieta Earthquake (1989) and Northridge Earthquake (1994). These later earthquakes happened before the entire seismic retrofit program was completed. While the seismic restrainers performed well, damage to bridge piers and emphasized the need to retrofit non-ductile reinforced concrete columns. Therefore, following these earthquakes, CALTRANS started the second phase of its retrofit program to improve the safety of older bridge columns (Chai et al. 1991). Chai et al. (1991) categorized the structural inadequacies of the pre-1971 bridge column design as inadequate flexural strength, inadequate flexural ductility, undependable flexural capacity, inadequate shear strength, footing failures and joint failure.

The *Seismic Retrofitting Manual for Highway Structures* (Buckle et al. 2006) introduced methods of retrofitting RC columns including complete or partial replacement, addition of supplemental columns, shear or flexural strengthening and improvement of column ductility. Ductility improvement is the most popular of these methods and any of the following techniques can be applied to achieve the objective: steel jacketing, active confinement by prestressing wire, active or passive confinement by a composite fiber/epoxy jacket, and reinforced concrete jacketing. Of these techniques, the most common retrofit implementation has been steel jacketing and composite fiber/epoxy jacketing.

### 2.3.2 Steel Jacketing

Figures 2-1 (a) and (b) from Buckle et al. (2006) schematically show steel jacketing retrofit techniques for circular column and rectangular column, respectively, per the method recommended by CALTRANS (CALTRANS 1996). For circular columns, two rolled steel plate half-shells are placed around a column, typically with clearance of 13 to 25 mm (0.5 to 1 in) between the existing column and the jacket. This gap between the jacket and the column is then filled with a pure cement grout. Note that steel jacketing stops typically at 50 mm (2 in) before top and bottom of the column. These vertical gaps are left in place in order to avoid increasing the strength of the column, which is the way to control the maximum demand on the adjacent structural elements (i.e., footing or cap beam) when flexural plastic hinges develop the strength of the column. For rectangular columns, as shown in Figure 2-1 (b), an oval jacket is recommended by CALTRANS (CALTRANS 1996) since retrofitting with rectangular jackets does not provide enough confining action against concrete expansion as a result of bending. In this case, concrete using small sized aggregate can be grouted because of the larger gap between the original column and the steel jacket.

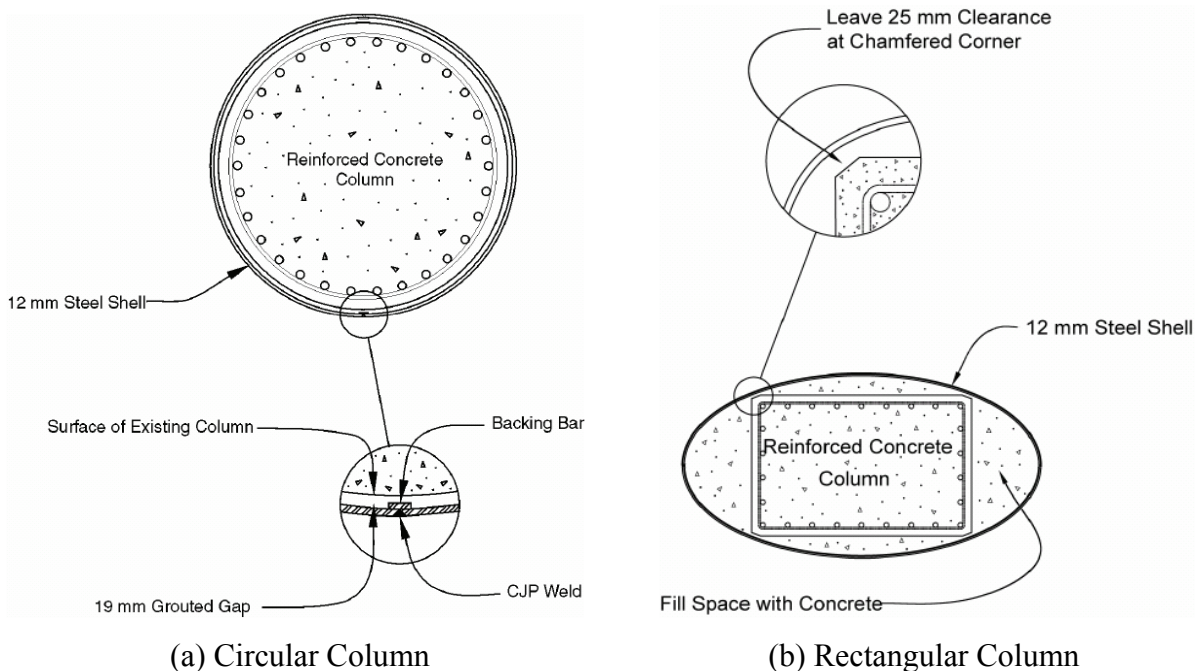


**Figure 2-1 Typical Steel Shell Retrofit (Buckle et al. 2006)**

### 2.3.3 Research by Chai et al. (1991)

Chai et al. (1991) experimentally investigated retrofitting techniques of bridge columns using a steel jacket for enhancing flexural ductility in the potential plastic hinge region. Six column models with diameter of 610 mm (24 in) and 3.657 m (12 ft) height were tested under lateral cyclic loading and constant axial load of 1779 kN (400 kips). The various design details for seven specimens tested by Chai et al. are presented in Table 2-1. Figures 2-2 (a) and (b) show the test setup and the reinforcement details of columns, respectively. The columns were 0.4 scale of a prototype bridge column with diameter of 1524 mm (60 in). The 4.76 mm (3/16 in) thick steel jacket provided a volumetric confinement ratio of 3.1 %. The columns were partially retrofitted with a steel jacket over part of their length at the base of the specimens around the plastic hinge region. The length of jackets was selected to be 1219 mm (48 in) such that the moment demand above the jacket did not exceed 75 % of the capacity of the non-retrofitted RC section.

**Table 2-1 Design Variations of Test Specimens (Chai et al. 1991)**

Test unit	Column and footing details		Remarks
1	20d <sub>s</sub> lap for longitudinal bars without steel jacket	Weak footing	Reference
2	20d <sub>s</sub> lap for longitudinal bars with steel jacket	Weak footing	Full retrofit
3	Continuous column bars without steel jacket	Strong footing	Reference
4	Continuous column bars with steel jacket	Strong footing	Full retrofit
5	20d <sub>s</sub> lap for longitudinal bars, ¼ in. styrofoam wrap	Strong footing	Partial retrofit
6	20d <sub>s</sub> lap for longitudinal bars with steel jacket	Strong footing	Full retrofit
1-R	20d <sub>s</sub> lap for longitudinal bars, repaired by steel jacket	Weak footing, 300 kips prestress	Repair

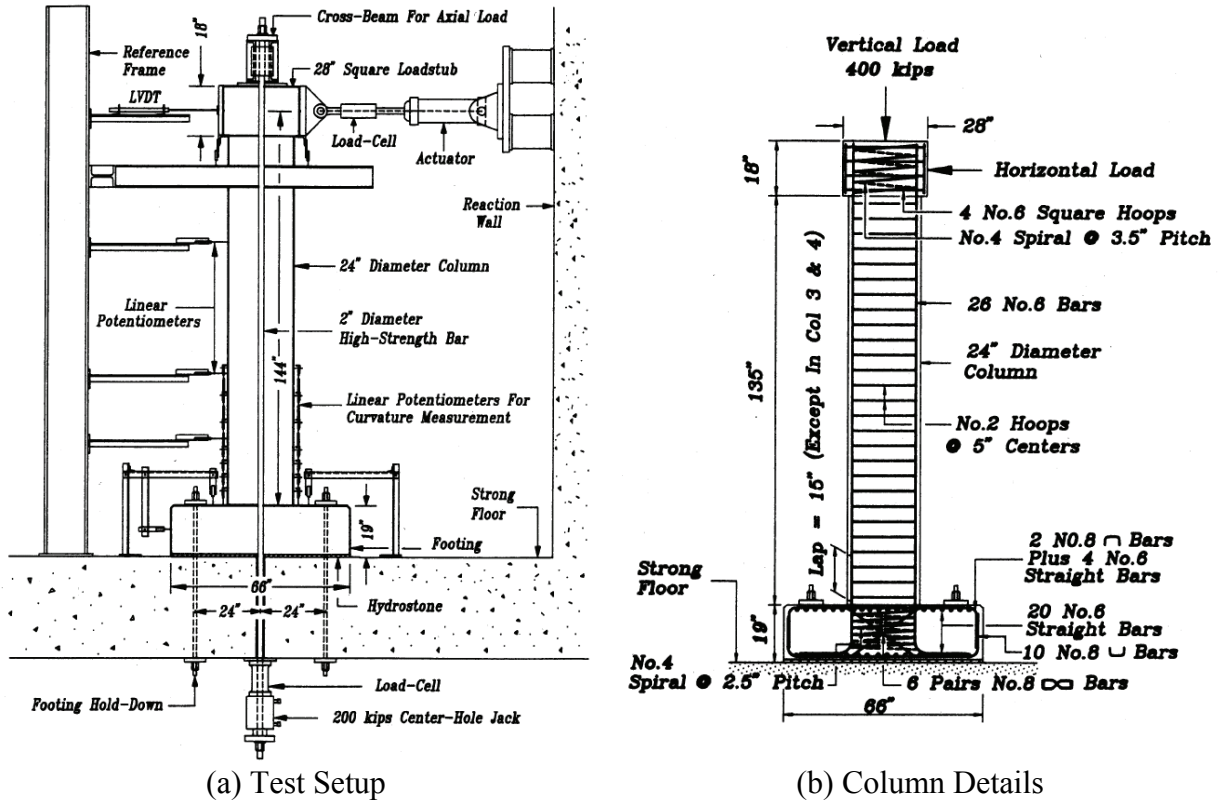


Figure 2-2 Test Setup and Column Details (Chai et al. 1991)

Columns retrofitted with a steel jacket exhibited a ductile behavior with stable hysteresis curves up to a ductility ratio of  $\mu = 7$  (drift ratio of 5.3 %), while the as-built column failed at ductility ratio of  $\mu = 1.5$  caused by spalling off the cover concrete in the lapped splice region near the base. Steel jacketing was also found by this test program to be effective to prevent bond failures of the lapped splices of longitudinal reinforcement from footing. The column stiffness with a steel jacket was increased by about 10 to 15 %.

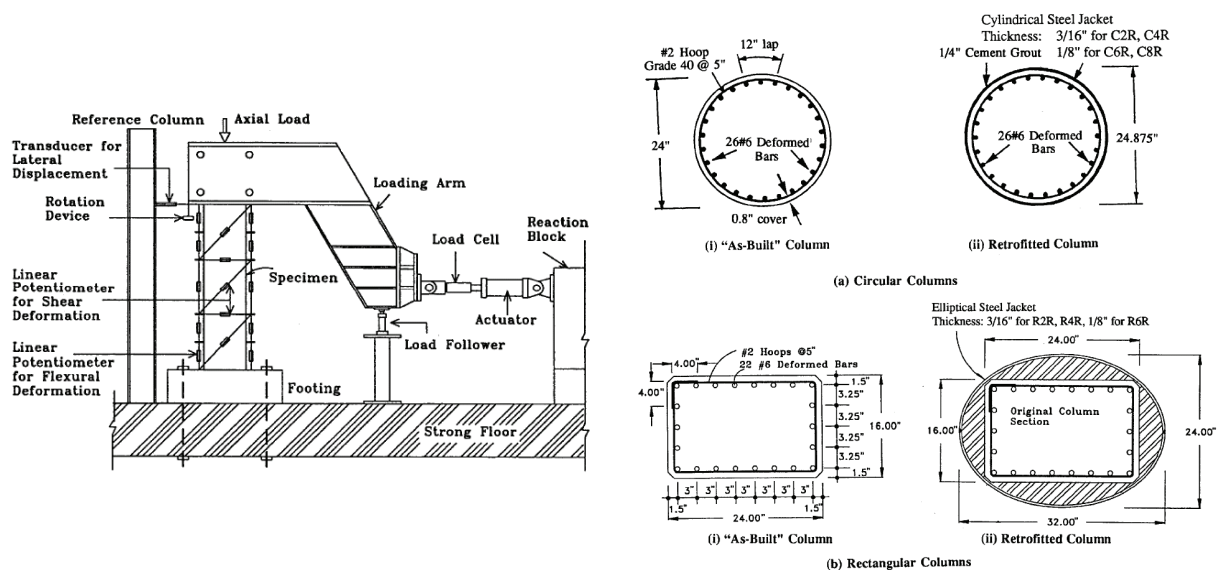
### 2.3.4 Research by Priestley et al. (1994a, 1994b)

Priestley et al. (1994a, 1994b) conducted theoretical and experimental investigation of retrofitting techniques of bridge columns using a full-height steel jacket focusing on improvement of the shear strength. An equation for shear strength enhancement by circular steel jackets was proposed by considering the jacket as continued independent hoops. By modeling behavior using a truss mechanism, the shear enhancement  $V_{sj}$  for circular columns is calculated by the following equation:

$$V_{sj} = \frac{\pi t_j^2 f_{yj} (D_j - t_j) \cot \theta}{2 t_j} = 0.865 \pi t_j f_{yj} (D_j - t_j) \quad (2-7)$$

where  $t_j$  is the jacket thickness,  $D_j$  is outside diameter of the steel jacket,  $f_{yj}$  is the yield strength of the steel jacket and  $\theta$  is the angle between the column axis and the principal tension cracking direction. Note that, based on experimental results,  $\theta$  is assumed to be 30 deg in Equation 2-7.

Using the test setup shown in Figure 2-3 (a), eight circular and six rectangular column specimens, which were 0.4 scale of a prototype bridge, were tested under lateral cyclic loading and constant axial loads of 591.6 kN (133 kips) or 1779.2 kN (400 kips) corresponding to axial load ratios of 0.06 or 0.18. The various design details for fourteen specimens tested by Priestley et al. are presented in Table 2-2. The aspect ratio of the columns was either 2 or 1.5 in order to model squat bridge columns that were susceptible to shear failure (rather than flexural failure). Figure 2-3 (b) shows the reinforcement details for columns. The steel jacket thickness was either 4.76 mm (3/16 in) or 3.18 mm (1/8 in).



(a) Test Setup

(b) Reinforcement Details

**Figure 2-3 Test Setup and Reinforcement Details (Priestley et al. 1994a, 1994b)**

**Table 2-2 Design Variations of Test Specimens (Priestley et al. 1994a, 1994b)**

Test unit	Aspect ratio, $M/VD$	Axial load $P$ , kips	$f'_c$ , ksi	$Pf'_c/A_g$	Longitudinal reinforcing bar (26#6) $f_{yt}$ , ksi	Transverse reinforcing bar (#2 hoops) $f_{yh}$ , ksi	Steel jacket details	$V_{if}$ , kips	$\frac{V_{shear}}{\mu \leq 2}$ , kips	$\frac{V_{shear}}{\mu \geq 4}$ , kips
(a) Circular columns										
C1A	2.0	133	4.5	0.065	47	52	—	119	139.6	83.7
C2R	2.0	133	4.93	0.059	47	52	$f_{jy} = 50.4$ ksi $t_j = 3/16$ in.	127	774.3	718.4
C3A	2.0	400	5.0	0.177	47	47	—	151	197.6	138.7
C4R	2.0	400	5.1	0.173	47	47	$f_{jy} = 50.4$ ksi $t_j = 3/16$ in.	165	832.3	773.4
C5A	2.0	133	5.2	0.056	68	47	—	171	142	85.9
C6R	2.0	133	5.8	0.051	68	47	$f_{jy} = 41.5$ ksi $t_j = 1/8$ in.	175	489	432.9
C7A	1.5	133	4.45	0.066	68	47	—	222	148	92.7
C8R	1.5	133	4.52	0.065	68	47	$f_{jy} = 41.5$ ksi $t_j = 1/8$ in.	226	495	439.7
(b) Rectangular columns										
R1A	2.0	114	5.5	0.054	47	52	—	118	143.0	90.6
R2R	2.0	114	5.6	0.053	47	52	$f_{jy} = 50.4$ ksi $t_j = 3/16$ in.	123	1021	968.6
R3A	2.0	114	5.0	0.059	68	47	—	160	130.0	80.1
R4R	2.0	114	5.2	0.057	68	47	$f_{jy} = 50.4$ ksi $t_j = 3/16$ in.	169	1008	958.1
R5A	1.5	114	4.7	0.063	68	47	—	213	134.1	85.4
R6R	1.5	114	4.8	0.062	68	47	$f_{jy} = 41.5$ ksi $t_j = 1/8$ in.	226	614.5	565.4

Note: A = as-built; R = retrofitted.  
1 kip = 4.5 kN; 1 ksi = 6.9 MPa; 1 in. = 25.4 mm.

The as-built circular and rectangular columns failed in shear with limited ductility. Columns retrofitted with a steel jacket exhibited ductile behavior with ductility ratios greater than or equal to  $\mu = 8$  (drift ratio of 4 %). Retrofitting with jackets was shown to prevent rapid degradation of strength and stiffness. The elastic stiffness of the columns with a steel jacket was increased by about 30 to 64 % for circular and rectangular columns, respectively. The test program indicated that full-height steel jacketing was effective to enhance shear resistance and flexural displacement capacity of shear critical RC columns.

## 2.4 Behavior of Reinforced Concrete subjected to Blast Load

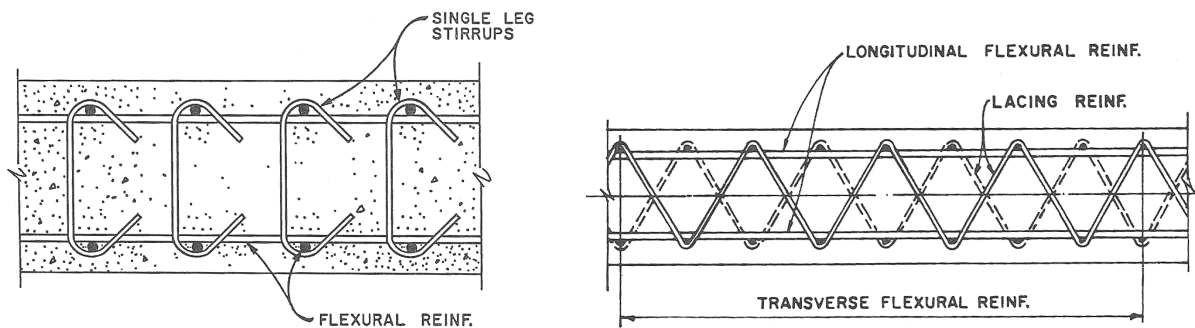
Three aspects related to the performance of reinforced concrete elements under blast loading are reviewed in the following. These are the issues related to ductile response and those related to brittle response, and a design criterion to prevent breaching and direct spalling of reinforced concrete slabs.



### 2.4.1 Ductile Response

Ductile behavior is the key to ensure seismic performance of structures. The blast engineering community has equally recognized the need for ductile design to ensure satisfactory blast performance. Ductile structures or structural elements are desirable because they can displace into the inelastic range without excessive degradation of stiffness and strength, and absorb large amounts of strain energy prior to their collapse.

To resist close-in blast loads and allow the large deformations to achieve ductile response, USDA (1990) suggested using lacing reinforcements as shown in Figure 2-4 (b), whereas the conventional shear reinforcement is single leg stirrup as shown in Figure 2-4 (a). In close-in blast loading, a structural element typically undergoes extremely high-pressure concentrations which can create local failure. The lacing reinforcements are effective to resist this pressure because they enhance the confinement of concrete and the displacement ductility and restrain the buckling of longitudinal bars. For reference, the implementation of this lacing reinforcement is shown in Figure 2-5 in a typical laced wall for barriers as an example. For far-field blast load, the applied blast loading is fairly distributed as uniform load and the deformations due to this uniform load are relatively small. Therefore, USDA (1990) indicates that conventional reinforcement, such as single leg stirrups (Figure 2-4 (a)), is sufficient to resist such loading and lacing reinforcement is not necessary.



(a) Single Leg Stirrups

(b) Lacing Reinforcement

**Figure 2-4 Element Stirrup Reinforcement (USDA 1990)**

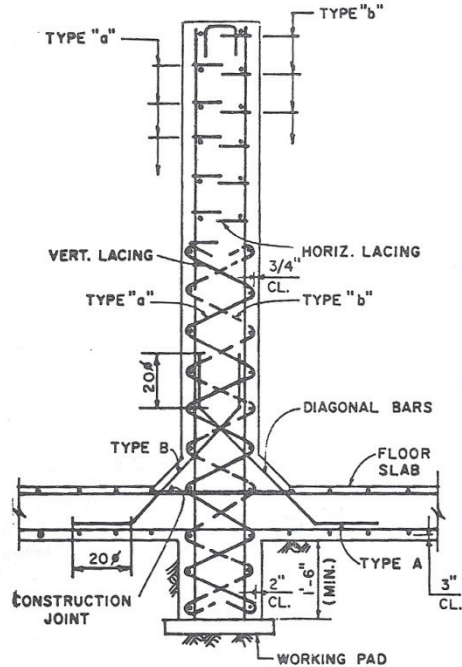


**Figure 2-5 Typical Laced Wall (USDA 1990)**

Figure 2-6 adapted from USDA (1990) schematically shows the flexural ductile response curve of concrete elements. This figure also shows brittle shear response. The rotation limit values at the support of concrete element designed under blast loading are presented in this figure to approximately relate deflection of the element to structural damage, such as yield, failure of compression concrete, and bending of strain hardening. Selection of transverse reinforcement is also presented to achieve these support rotations. Namely, the concrete element without shear reinforcement, with single leg stirrups, and with lacing reinforcement would be able to achieve the support rotations of 2 degree, 4 degree and 12 degree, respectively.

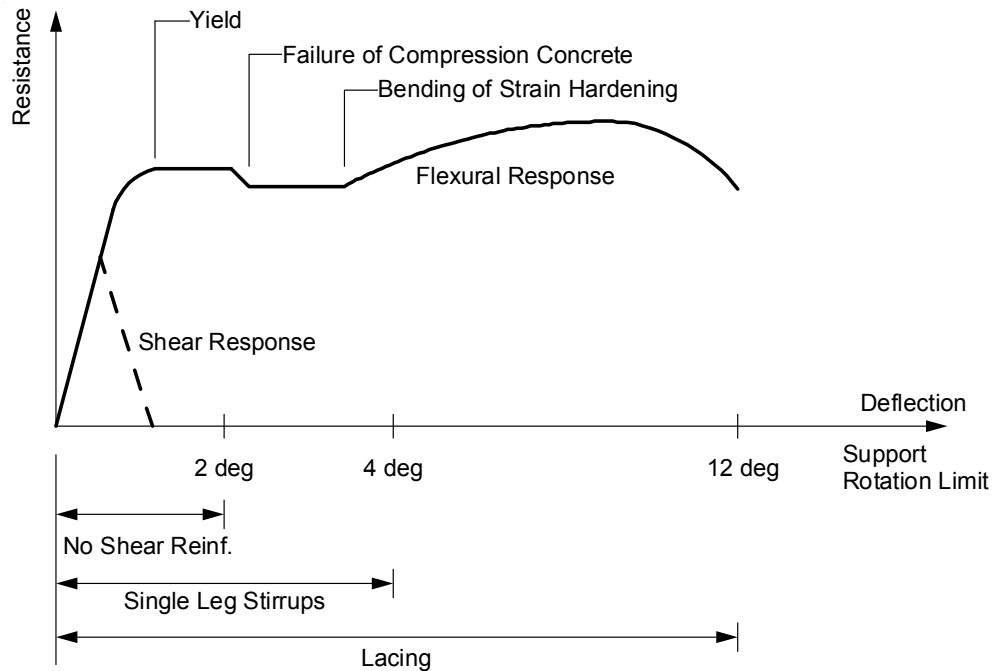


**Figure 2-6 Typical Resistance-deflection Curve for Concrete Element (adapted from USDA 1990)**

### 2.4.2 Brittle Response

Many types of structural elements are unable to exhibit the desirable ductile behavior that can help resisting blast loads. These structural elements typically fail in a number of brittle ways which are discussed in the following. The collapse of whole structures can be triggered by the original local failure of a few structural components. Four types of brittle modes of response associated with short-duration high dynamic loads are discussed in the following, namely direct spalling, scabbing, breaching and post-failure fragmentation. Direct shear failure is also regarded as brittle structural failure, and is addressed in detail in the following section.

Both direct spalling and scabbing are phenomenon of dynamic disengagement of the concrete element surface, but they are used in different situations. Figures 2-7 (a) and (b) show experimental results of direct spalled element and scabbed element, respectively. “Direct spalling” of a concrete element is caused by a tension failure normal to the free surface of the element (USDA 1990). When a shock front wave strikes a concrete element, a compression stress wave passes through the element. Once it reaches the rear face, the compression stress wave is reflected as a tension stress wave and then, this tension stress causes disengagement of

the concrete surface. Therefore, direct spalling is observed in the rear free surface. “Scabbing” is caused by large deflections and observed in the end stage of the ductile flexural mode of a reinforced concrete element. Large strains due to the large deflections induce severe cracking and/or crushing of the free surface of the concrete element. Note that Conrath et al. (1999) defined “scabbing” differently, stating that scabbing is local damage of a front surface when a shock front strikes the concrete structure.

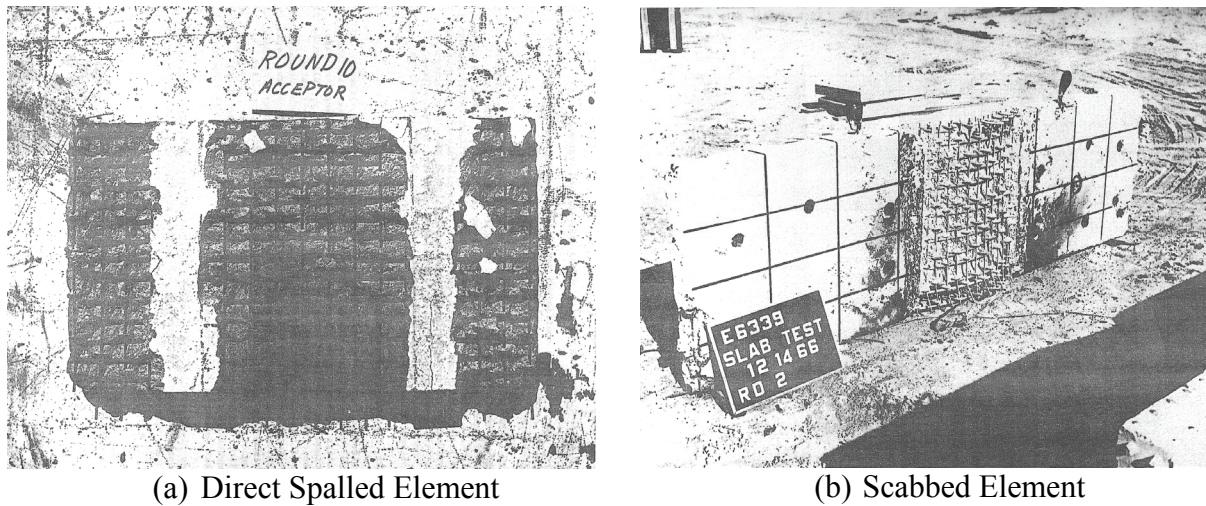


**Figure 2-7 Disengagement of Concrete Element Surface (USDA 1990)**

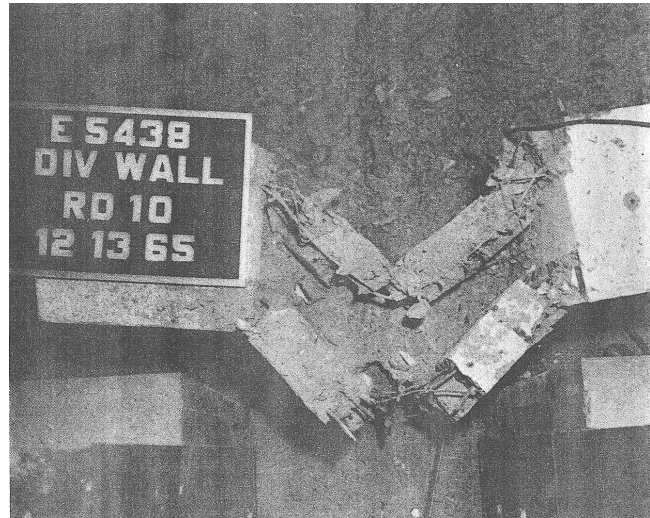
The full thickness of a concrete member can be punched through when the member is subjected to high explosive loading. This failure is called “Breaching.” Breaching is the local failure typically observed in reinforced concrete slabs subjected to close-in blast loading.

“Post-failure concrete fragments” are formed when a reinforced concrete element is extremely overloaded by blast pressures (USDA 1990). These fragments are displaced at high velocities from the original structure. Post-failure concrete fragments are the results of an element collapse; therefore the structural element is damaged heavily in this brittle mode. The lacing reinforcement previously shown in Figure 2-4 (b) is one of the effective ways to reduce this structural damage associated with post-failure concrete fragments subjected to severe blast pressures. Figures 2-8 (a) and (b) show the blast test results of concrete element without and with laced reinforcement, respectively (USDA 1990). The unlaced specimen disintegrated with

the dispersion of concrete fragments, while the concrete element with laced reinforcement exhibited less damage and the material between the plastic hinges remained intact.



(a) Unlaced Element



(b) Laced Element

**Figure 2-8 Failure of Concrete Element under Blast Loading (USDA 1990)**

### 2.4.3 Breaching and Spalling Resistance of Reinforced Concrete Element

UFC (2004) includes a design criterion to prevent breaching and direct spalling of reinforced concrete slabs. UFC specifies design performance objectives expressed in terms of desired damage category broken down into minor damage (cracking), spalling and breaching as shown in Figure 2-9 (a). Equations to determine the minimum thickness of RC slabs need to prevent these types of damage. The minimum thickness to prevent breaching,  $t_b$  (in), is given by:

$$t_b = 4.120 \left( \frac{R}{W^{1/3}} \right)^{-0.40} W^{1/3} \quad (2-8)$$

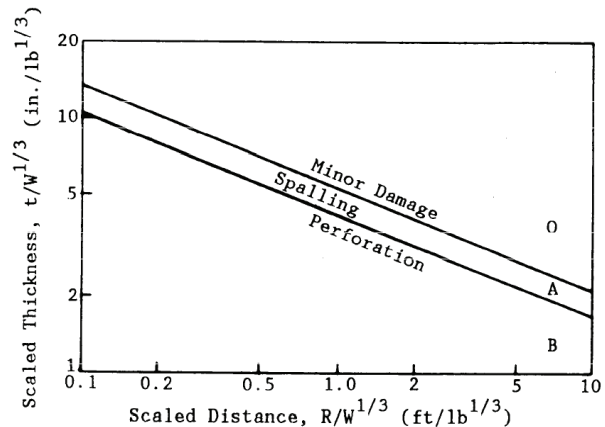
where  $R$  is the minimum distance from center of explosive to outside face of RC slab (ft) and  $W$  is the design explosive weight (lb TNT equivalent). The minimum thickness to prevent direct spalling,  $t_s$  (in), is determined from:

$$t_s = 5.309 \left( \frac{R}{W^{1/3}} \right)^{-0.40} W^{1/3} \quad (2-9)$$

These equations are plotted in Figure 2-9 (b). The difference between Equations 2-8 and 2-9 lies in the coefficient of 4.120 and 5.309 used for breaching and direct spalling, respectively.

Accordingly, the required minimum thickness for spalling is about 1.3 times larger than the one for breaching. According to Equations 2-8 and 2-9, for instance, when  $R$  is 3.0 m (9.84 ft) and  $W$  is 300 kg (661 lb), the required RC slab thicknesses  $t_b$  and  $t_s$  would be 869 mm (34.2 in) and 1118 mm (44.0 in), respectively.

Distance of Explosion from Wall	Characteristic Damages	Desired Damage Category
	No relevant damage, cracks, or small crater	<b>O</b> <b>MINOR</b>
	Crater deflections and cracks	
	Spalling on back	<b>A</b> <b>SPALLING</b>
	Heavy spalling on back	
	Perforation (BREACHING)	<b>B</b> <b>BREACHING</b>
	Heavy perforation (BREACHING)	



(a) Damage Categories

(b) Threshold of damage category

**Figure 2-9 Design Criteria for Breaching and Direct Spalling (UFC 2004)**

## 2.5 Direct Shear Failure

### 2.5.1 General

The possibility of direct shear failure needs to be considered in blast design since this mode of response can be critical in many instances. It is often the result of high shear inertia forces which do not exist in structural members subjected to static or slow dynamic loads (Conrath et al. 1999). However, direct shear failure (also called “shear-friction” in ACI (2004)) is examined in some cases when designing structural members under static loading (ACI 2004). This type of

failure can occur on an interface between different members or parts of members that can slide on the interface. Especially, direct shear failure needs be considered on an interface between concrete parts cast at different times and on an interface between different materials like concrete and steel. This failure is different from the shear failure in bridge columns typically observed in the event of an earthquake. In the latter case, the column without enough transverse reinforcement fails in shear with diagonal cracks.

ACI (2004) provides a design equation to prevent direct shear failure for structural members subjected to static loads. It suggests that this type of failure be considered in a number of conditions such as an interface between concretes cast at different times and an interface between different materials like concrete and steel. ACI (2004) cited direct shear as “shear-friction.”

The factors influencing the shear friction capacity can be categorized into global and local roughness, reinforcement crossing the interface, pressure applied normal to the interface and concrete strength (Ali and White 1999). As shown in Figure 2-10, global roughness is related to the overall path of the fracture surface of the concrete member, and local roughness relates to the localized irregular surface formed on the global roughness. Figure 2-11 schematically shows the forces developed along the direct shear fracture surface of a RC member subjected to a shear force. Since the parts on both side of the direct shear interface move laterally relative to one another, the steel reinforcement across the interface becomes in tension and tries to elongate. These tension forces in the reinforcement are equilibrated by the compression force developed along the crack interface as shown in Figure 2-11 (b). The compressive stress produces friction between the crack surfaces along with the local and global roughness on the surfaces. The reinforcement crossing the crack surface also provides dowel action to resist the shear forces as shown in Figure 2-11 (a).

The so-called push-off specimen, as shown in Figure 2-12, is most commonly used to investigate shear friction. According to the results from this type of experiments (for example, Hofbeck et al. 1969; and Mattock and Hawkins 1972), the shear-friction strength can be represented by:

$$v_n = c + \mu\sigma \quad (2-10)$$

where  $c$  is a cohesion term,  $\mu$  is the coefficient of friction and  $\sigma$  is the compressive stress acting on the shear surface (MacGregor and Wight 2005).

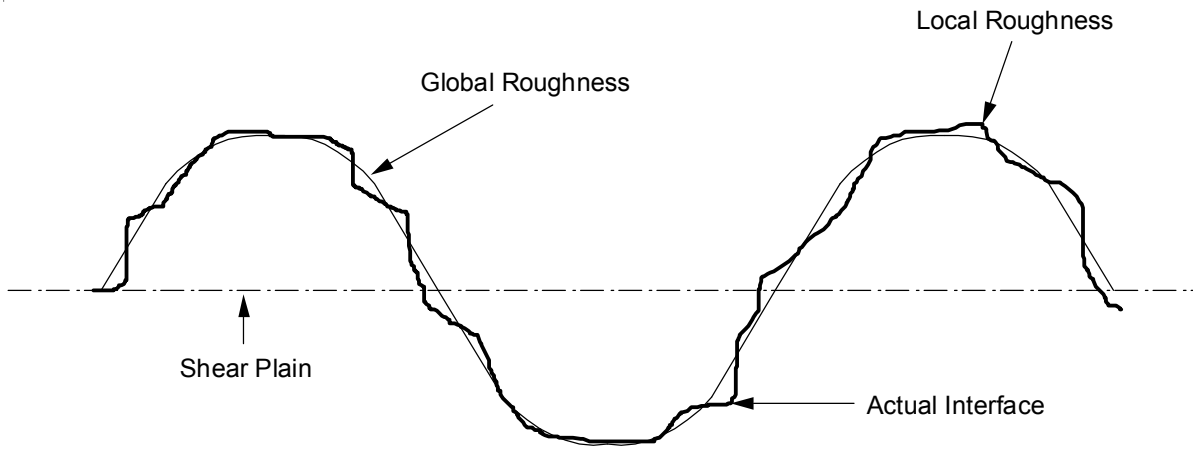
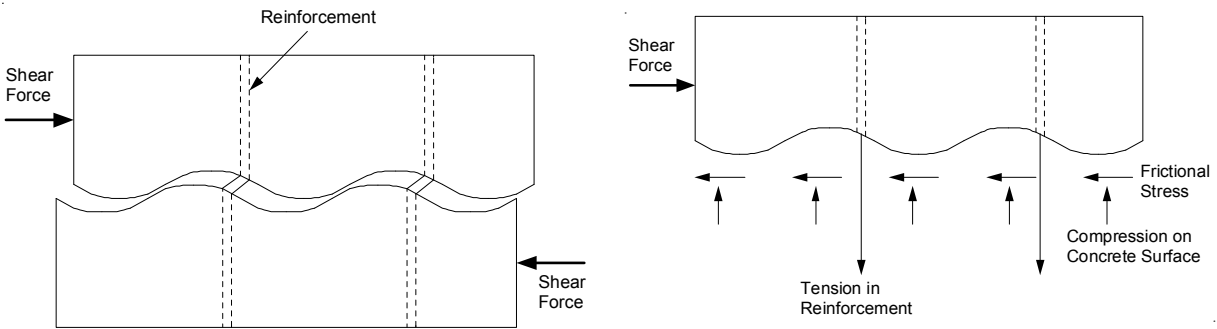


**Figure 2-10 Global and Local Roughness (adapted from Ali and White 1990)**



(a) Form of Horizontal Shear Crack

(b) Force Development

**Figure 2-11 Shear Friction Model (adapted from MacGregor and Wight 2005)**



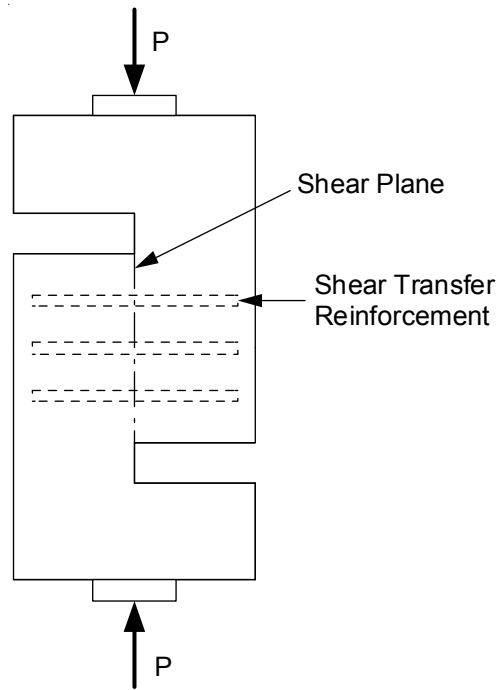


**Figure 2-12 Shear Transfer Test Specimen (adapted from MacGregor and Wight 2005)**

### 2.5.2 Ultimate Capacity of Direct Shear under Static Loads

ACI (2004) Section 11.7 provides design rules to estimate the shear-friction strength. The nominal shear strength,  $V_n$ , is calculated by:

$$V_n = A_{vf} f_y \mu \quad (2-11)$$

where  $A_{vf}$  is the area of shear-friction reinforcement across shear plane,  $f_y$  is the yield strength of reinforcement, and  $\mu$  is coefficient of friction. The coefficient  $\mu$  depends on the surface of the shear interface under consideration and is taken as  $1.4\lambda$  for concrete placed monolithically,  $1.0\lambda$  for concrete placed against hardened concrete with intentionally roughened surface, and  $0.6\lambda$  for concrete placed against hardened concrete not roughened intentionally, where  $\lambda = 1.0$  for normal weight concrete, 0.85 for sand-lightweight concrete, and 0.75 for all lightweight concrete. Equation 2-11 is based on the shear-friction model which assumes the shear resistance on the surface of the shear interface comes only from friction by ignoring the effect of cohesion.

ACI (2004) Commentary R11.7.3 provides another equation to estimate the shear-friction strength as an alternative method, which is a “modified shear-friction method.” This method has been proposed by Hofbeck et al. (1969) and Mattock and Hawkins (1972). They reported a series of push-off tests on specimens with initial cracks and without cracks along a shear plane, and suggested that the nominal shear strength,  $V_n$ , is given by:

$$V_n = 0.8A_{vf}f_y + A_cK_1 \quad (2-12)$$

where  $A_c$  is the area of the concrete section resisting shear transfer, and  $K_1 = 400$  psi (2.8 MPa) for normal weight concrete, 200 psi (1.4 MPa) for all-lightweight concrete, and 250 psi (1.7 MPa) for sand-lightweight concrete. These values of  $K_1$  can be used for both monolithically cast concrete and concrete cast against hardened concrete with a rough surface (ACI 2004). The first term in Equation 2-12 represents the shear transferred by friction with the coefficient of friction taken as 0.8. The second term represents the shear transfer resistance due to cohesion, which is the sum of the shearing of crack surface roughness and the dowel action of the reinforcement.

To compare the various shear-friction models with test results, Figure 2-13 was developed. In this figure, the solid lines represent the upper limit of shear-friction resistance from the shear-friction model given by Equation 2-11, and the dashed line represents the one from the modified shear-friction model given by Equation 2-12. Solid circles and open circles in this figure are respectively the test results for the uncracked and cracked push-off specimens by Hofbeck et al. (1969). In this figure, the shear stress,  $v_n$ , (instead of shear force) is plotted against  $\rho_v f_y$  where  $\rho_v$  is the reinforcement ratio across the shear plane. The upper limit of ACI shear-friction model comes from Section 11.7.5 that the nominal shear strength,  $V_n$ , shall not be taken greater than the smaller of  $0.2f'_cA_c$  and  $800A_c$  (lb). Therefore, the limit was taken as 800 psi (5.52 MPa) in this figure. The ACI shear-friction model gives a conservative prediction of shear strength, while the ACI modified shear-friction model fits the experimental results quite well.

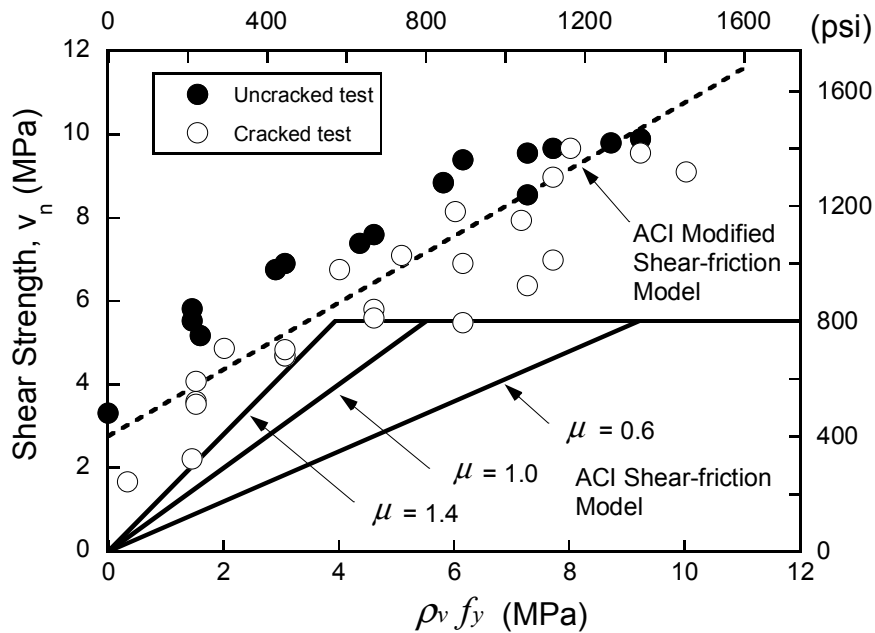


**Figure 2-13 Comparison of Shear-friction Models with Test Data**

### 2.5.3 Ultimate Capacity of Direct Shear under Dynamic Loads

Direct shear resistance under dynamic loading is of particular interest in this section. However, for security reasons, it is difficult to find public domain data on the direct shear resistance of reinforced concrete elements subjected to impulsive or blast loading. Ross (1983) reported at least two known studies on direct shear resistance of such elements. One is a series of shear key tests by Hansen et al. (1961) and the other of a series of push-off element tests by Chung (1978). Note that the tests by Hansen et al. (1961) were not direct shear tests but concrete shear key tests. However, it could provide useful information to compare the static and dynamic shear resistance of concrete elements.

Hansen et al. (1961) conducted a series of static and dynamic tests on three types of concrete shear keys; plain concrete, plain concrete under compressive stressed and concrete reinforced by dowel reinforcement embedded diagonally. The objective of this study was to find out the ultimate shear strength of concrete shear keys that were at the time required in buildings subjected to static loading and dynamic loading from a nuclear weapon. Details of these

specimens and test setup are shown in Figure 2-14. The static load duration for the test program was about 10 to 15 minutes. The dynamic loads applied were roughly of triangular shape with the peak load reached in 25 to 40 milliseconds and a total duration of 2250 to 2750 milliseconds. The shear stress rate was in the order of 200 to 400 N/mm<sup>2</sup>/sec with these load speeds. The tests showed that the dynamic shear strength of concrete elements was greater than the static strength, however the shear failure mode appeared to be similar between static and dynamic loading. The measured DIF of these shear key resistances were 1.15 for plain concrete, 1.54 for plain concrete with compressive stress of 1.0 MPa (150 psi), 1.70 for plain concrete with compressive stress of 2.1 MPa (300 psi) and 1.28 for concrete with dowels. The compressive stress and the dowel reinforcements contributed to increase the shear resistance under impulsive loading.

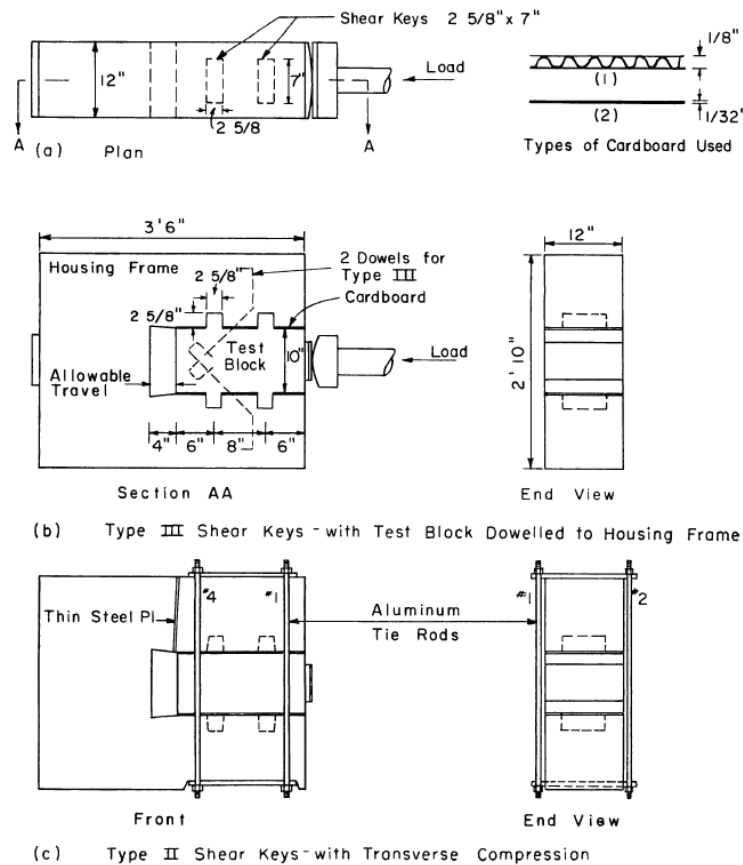


**Figure 2-14 Details of Test Specimens and Test Set-up (Hansen et al. 1961)**

Chung (1978) tested 48 concrete push-off specimens with and without dowel reinforcements across the shear plane as shown in Figure 2-15 under static and dynamic loadings. The objective

of this test program was to investigate the shear resistance of concrete joints under dynamic load and the effects of repeated loading on the dynamic strength of the joints. The hatched part of the specimen in Figure 2-15 was casted first, followed by unhatched part after hardening of the first casted segment, therefore creating a construction joint across the shear plain of the specimen. The peak load was reached in roughly 0.8 milliseconds. The total load duration was 1.5 milliseconds. This load speed was equivalent to a shear stress rate of  $12,000 \text{ N/mm}^2/\text{sec}$ . The dynamic shear strength of the concrete joint was higher than the static shear strength. The test results showed that the DIF of direct shear resistance was, respectively, 1.8 and 2.0 for with and without dowel reinforcements.

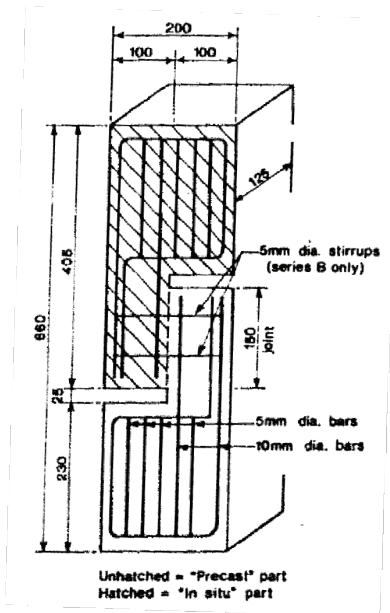


Figure 2-15 Details of Test Specimen (Chung 1978)

## 2.6 Structural Analysis Options under Blast Loading

There is a variety of analytical methods available to compute structural response of structures subjected to blast loading. These blast analytical methods range from a simplified analytical method using a SDOF system, as presented previously, to a finite element model (FEM) that replicates the detailed structural elements and materials and that accounts for the actual blast pressure histories acting to the structure. Table 2-3 summarizes some of the analytical options available on compute the response of structures subjected to blast loading. Winget et al. (2005)

provided a good overview of various analytical options by comparing their advantages and disadvantages. In this subsection, these structural analysis options are briefly reviewed.

**Table 2-3 Options for Blast Resistance Analysis**

---

1. Consideration of Blast Pressure
(a) Equivalent Static Analysis   (b) Dynamic Analysis
2. Interaction between Structure and Blast Loading
(a) Coupled Analysis   (b) Uncoupled Analysis
3. Discretization of Structure
(a) SDOF Model   (b) MDOF 2D or 3D Beam Model   (c) MDOF FEM
4. Material Nonlinearity
(a) Elastic Model   (b) Inelastic Model
5. Geometric Nonlinearity
(a) Linear Model   (b) Nonlinear Model

---

### **2.6.1 Consideration of Blast Pressure**

When calculating structural behavior under blast loading, one of the issues to resolve is how to consider the blast pressure into the analysis. As part of this determination, it would be possible to approach this blast loading either statically or dynamically. Static analysis was commonly used in the past, but is not recommended anymore in most cases. This method is typically called “equivalent static analysis” or “equivalent wind analysis.” In this method, a blast load is simply applied as a static load. However, it is difficult to specify an equivalent static blast load that can accurately replicate all the effects of a dynamic blast loading. This method was used for cases in which the target structure was located far from the blast source, the blast loading treating as a wind gust loading. This method had serious shortcomings. As a result, dynamic analysis is the recommended procedure commonly used in blast resistant. (ASCE 1997)

### **2.6.2 Interaction between Structure and Blast Loading**

In blast dynamic analysis, one issue is whether interaction between the structure and blast loading should be considered (Winget et al. 2005). A coupled analysis takes this interaction into account, and the applied blast loads and the structural response affect each other. This analytical

method predicts the structural response accurately, however it requires large amount of computations and advanced computational techniques because they are analyzed at the same time on the same platform. On the other hand, in an uncoupled analysis, the blast pressures and the structural responses are calculated separately. As such, the uncoupled analysis requires much less effort and time than the coupled analysis. Although the coupled analysis is the more accurate analytical method, the uncoupled analysis typically provides reasonable and conservative results. Accordingly, uncoupled analysis is commonly used in practical design of the structures under dynamic loading. (Winget et al. 2005)

### **2.6.3 Discretization of Structure**

Modeling is to formulate the geometry of a structure mathematically. This mathematical model is discretized by partitioning the structure into a mesh of elements (Cook et al. 2002). This discretization ranges from a SDOF lumped-mass model to a multi-degree of freedom (MDOF) FEM model. Figure 2-16 schematically shows this discretization for a bridge structure as an example. As previously shown in the simplified blast analysis, although the SDOF model cannot provide the detailed response of the structure, it is sufficient to calculate the response at one particular point of the structure, which is the maximum deflection point in most cases. This SDOF model is widely used in the blast resistant design practice because it is simple and provides reasonable predictions. However, this SDOF model does not capture the structural behaviors of the higher-order modes which are likely to develop in the structure under blast loading due to high frequency modes caused by the short duration of blast pressures (Winget et al. 2005). To account for these higher-order modes, it is necessary for the structures to be modeled by the higher degree of freedom models, such as MDOF 2D or 3D beam models and MDOF finite element models.

### **2.6.4 Material and Geometric Nonlinearity**

Structures subjected to blast loadings are typically expected to experience large inelastic deformations. The material nonlinearity can be considered in the stress-strain relationship using a simplified model, such as a bi-linear curve, or an accurate model representing the actual material behavior. If the deformations of the structure are large, geometric nonlinearity should also be included, which is achieved by considering equilibrium in the deformed structural

geometry. Also, the acting direction of the loads may need to be updated when pressures act on a membrane, such as a thin plate, because direction of the pressure changes as the membrane stretches and deforms. (Cook et al. 2002)

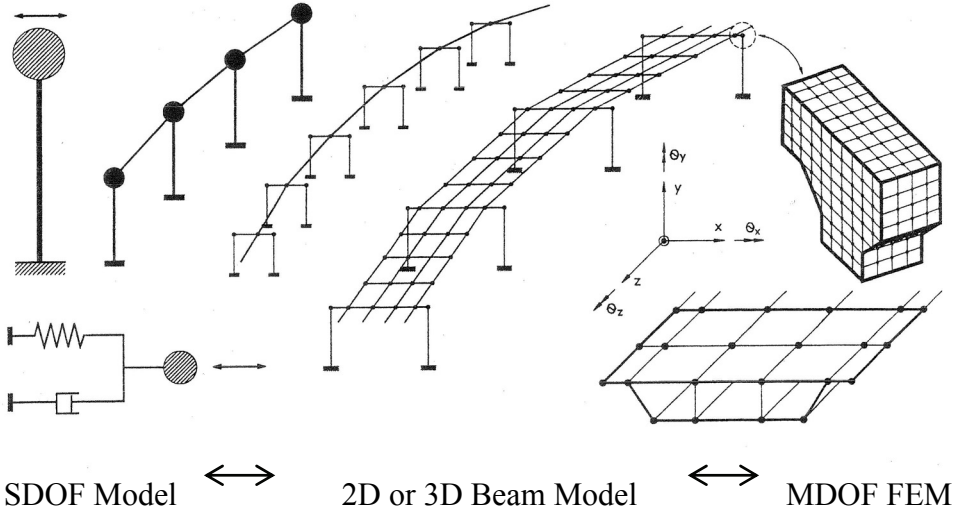


**Figure 2-16 Discretization of Structure (Priestley et al. 1996)**



# **SECTION 3**

## **BLAST PERFORMANCE OF SEISMICALLY RESISTANT REINFORCED CONCRETE AND STEEL JACKETED BRIDGE PIERS**

### **3.1 Introduction**

The authors previously presented the development and experimental validation of a multi-hazard bridge pier concept, i.e., a bridge pier system capable of providing an adequate level of protection against collapse under both seismic and blast loading (Fujikura et al. 2007, 2008). The proposed concept was a multi-column pier-bent with concrete-filled steel tube (CFST) columns that could provide ductile behavior up to 7 % drift under seismic excitations (Marson and Bruneau 2004) and up to 20 % under blast loading. The columns turned out to be effective for blast loadings because breaching and spalling of concrete are prevented to occur in CFST columns.

While CFST columns perform excellently in a multi-hazard perspective, they have not been commonly used in bridge engineering practice (although they are sometimes used by some state departments of transportation, such as Alaska DOT). Questions arose as to whether conventional columns designed to perform satisfactory under seismic excitations would possess adequate blast resistance. If they would, there would be little incentive to change current practice for ductile detailing of bridge columns to resist blast loadings. Therefore, the objective of the research presented here is to experimentally investigate the blast resistance of commonly used bridge columns detailed in accordance to recent seismic design codes. Ductile reinforced concrete (RC) columns and non-ductile RC columns retrofitted with steel jackets are selected as representative commonly used bridge columns. As such, this second series of test program complements the first series of CFST column tests under blast loading (Fujikura et al. 2007, 2008).

Following this section introduction, the seismic design of a prototype bridge pier bent and the design of a corresponding one-fourth scale model are presented along with details of the assumed

blast scenario. Next, experimental observations are summarized. Finally, the comparison of analytical studies and test results is presented, including a moment-curvature analysis, a simple plastic analysis and a simplified blast analysis using an equivalent SDOF system. Also, direct shear resistance of RC column, breaching, and spalling resistance are discussed.

## **3.2 Experimental Design and Setup**

### **3.2.1 General**

This section describes the design of the prototype and specimen of bridge pier as well as the setup used for testing for a multi-column bent. As described in Section 1, the objective of this project is to investigate whether conventional seismic designed bridge piers inherently provide satisfactory blast performance. These conventional types of bridge piers considered here are seismically designed ductile reinforced concrete piers as well as non-ductile reinforced concrete piers retrofitted with steel jackets being confirmed satisfactory seismic performance.

For the purpose of this project, first, to verify whether the seismically ductile systems can provide satisfactory blast resistance, a credible blast scenario is assumed as described in the following subsection. Secondly, seismic design of prototype bridge pier is conducted using response spectrum analysis. Detailing is accomplished in accordance with the recent design codes. Then, this prototype bridge is scaled down to one-fourth test specimen of bridge pier bent. Finally, measured properties of materials used in the specimen fabrication are presented followed by details of specimen, fabrication and experimental setup.

Test specimens were fabricated in the Structural Engineering and Earthquake Simulation Laboratory (SEESL) at the University at Buffalo (UB) and shipped to the U.S. Army Corps of Engineers Research Facility in Vicksburg, Mississippi where the blast tests were performed. Due to constraints in the maximum possible blast charge weight that could be used at the test site and specimen cost considerations, test specimen dimensions were set to be 1/4 scale of the prototype bridge piers. The specimens consist of two identical RC columns and two identical steel jacketed RC columns, connected to a cap-beam and a footing.

### 3.2.2 Assumed Blast Scenario

There are many possible courses of action by which terrorists might attempt to destroy a bridge structure, such as by detonation of hand-placed explosives, vehicle bomb, and collisions using large vehicles. In this study, the terrorist action considered consists of detonating explosives located inside a car vehicle placed below the deck at a close distance to the pier. This scenario is schematically illustrated in Figure 3-1. The horizontal distance  $X_p$  between the center of an explosive charge and the pier, referred to as either the blast distance or standoff distance, was selected based on assessing a credible threat for typical highway bridges (the exact value is not indicated here for security reasons). The vertical distance between the center of an explosive charge and the ground was set equal to 1 m (3.3 ft) based simply on the geometry of typical car vehicles.

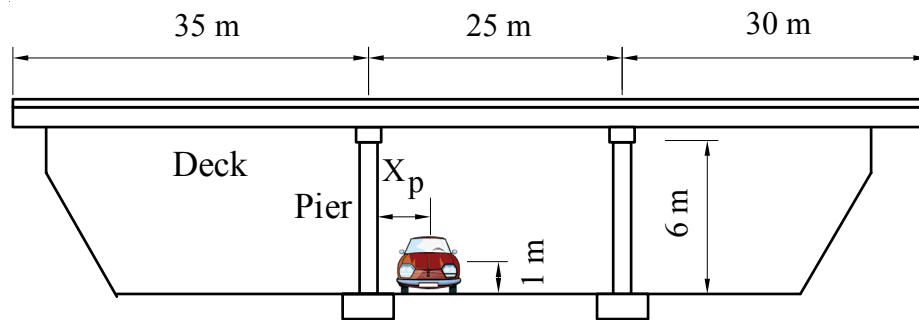


**Figure 3-1 Schematics of prototype bridge and assumed blast scenario**

Because of its very nature, it is virtually impossible to accurately predict the explosive charge weight to be used in a terrorist attack. However, reasonable estimates can be made by taking into account of some characteristics of terrorist actions. For instance, there is a relationship between the size of the vehicle used to carry explosives and the maximum possible charge weight, especially when taking into account how explosives will be hidden to avoid detection by simple visual inspection (Williamson and Winget 2005). Also, while high-tech explosives are expensive and difficult to handle (especially in large quantities), fertilizer-based explosives can be fabricated relatively easily using commercially available ingredients, which make them much more likely to be used. The explosive charge weight adopted in this study, referred to as  $W_p$ , was set based on these and other considerations, and was found to be very similar to the blast

weights predicted in FHWA (2003) for terrorist actions using car vehicles (shown in Figure 3-2). Incidentally, Figure 3-2 provides not only the connection between vehicle types and weapon yields but also the damage threshold of building components and windows associated with stand-off distance and size of bomb. For example, if an automobile loaded with 300 lbs-TNT (136 kg-TNT) is used for terrorist actions, a stand-off distance of about 24 ft (8.4 m) is at least required to prevent the concrete columns fail.

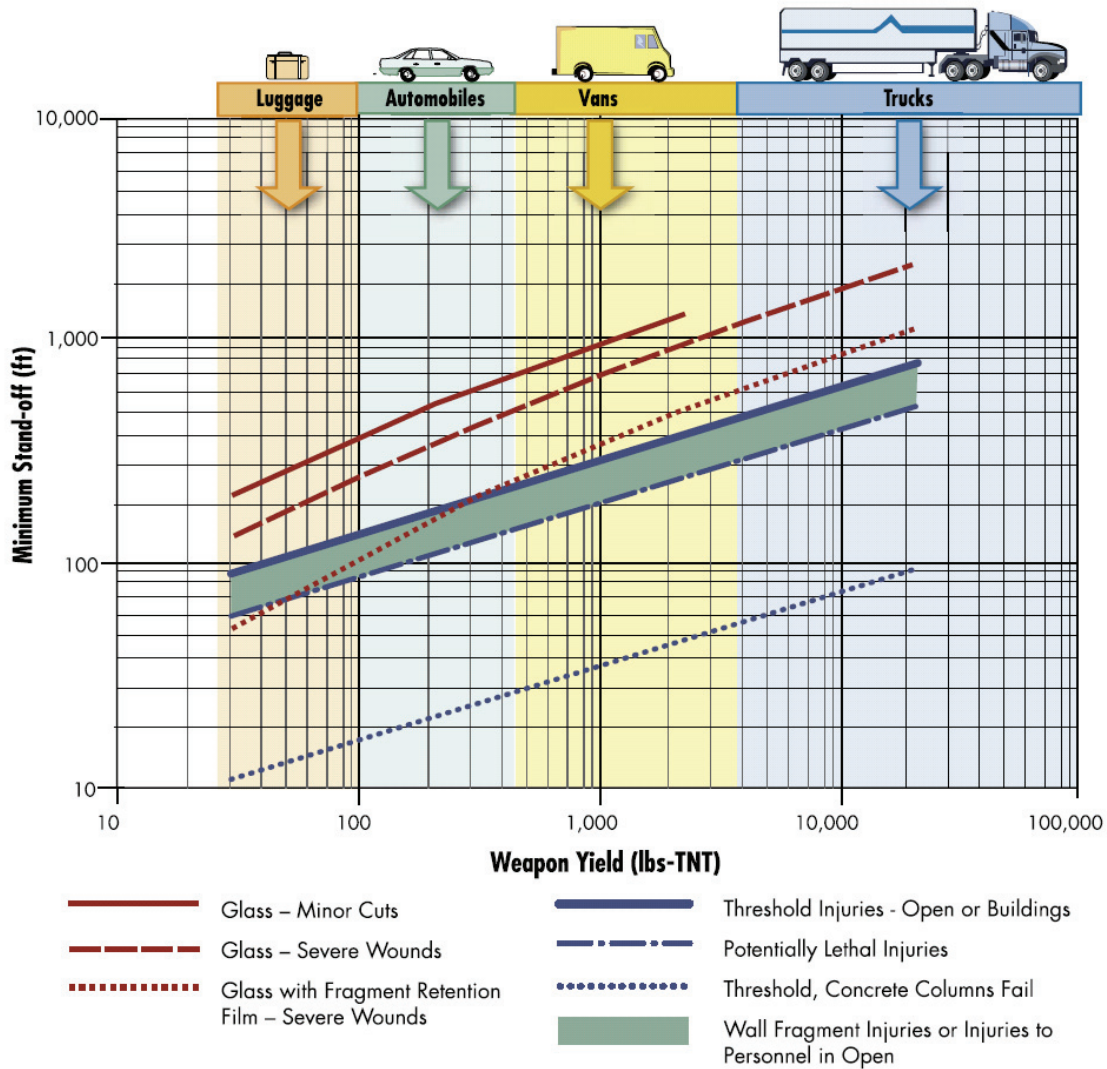


**Figure 3-2 Blast Damage Threshold (FEMA 2003)**

### 3.2.3 Seismic Analysis and Design of Prototype Bridge Pier Bent

Three different design codes or guidelines for bridges, namely AASHTO (2004), MCEER/ATC-49(2003a) and CALTRANS (2003, 2006), are used for the designed of the prototype bridge pier bent, and this bent is designed mainly by AASHTO. As discussed in the previous literature review, MCEER/ATC-49 has reflected the results of recent research programs. To calculate the shear resistance of the columns, MCEER/ATC-49 considers the contribution of shear resistance from transverse reinforcement, strut action and concrete tensile strength, while AASHTO does not consider the strut action in these three contributions. In the following design, MCEER/ATC-49 was used to calculate the shear resistance of the reinforced concrete columns to consider the updated research achievement. Detailing in the plastic hinge region of the columns is very important in this project to achieve the ductile behavior of the column. Accordingly, the transverse reinforcement in this plastic hinge region is designed by comparing the three different design specifications; AASHTO, MCEER/ATC-49, and CALTRANS.

#### 3.2.3.1 Prototype Bridge Structure

The prototype bridge chosen in this study is part of a typical 3-span continuous highway bridge described in Dicleli and Bruneau (1996). The span lengths are 35 m, 25 m and 30 m (total length  $L = 90$  m) as schematically shown in Figure 3-1. The width of the deck is 16 m, the equivalent cross-section area of the deck is  $0.592 \text{ m}^2$ , the equivalent moment of inertia of the deck (with respect to a vertical axis passing through the centroid) is  $I_D = 13.9 \text{ m}^4$ , the mass of the deck per unit length is  $m_D = 12.56 \text{ tons/m}$ , and the height of the columns is  $H = 6$  m. The total gravity load on each pier is assumed equal to 4098 kN. A multi-column pier bent with three columns is selected to compare with the first test series of CFST columns subjected to blast loading (Fujikura et al. 2007, 2008). Figures 3-3 and 3-4 show the designed elevation and reinforcement details of prototype pier bent, respectively. The design process is presented in the following subsections in detail.

#### 3.2.3.2 Analysis of Reinforced Concrete Section

In the analysis, the specified concrete compressive strength,  $f'_c$ , and longitudinal and transverse steel yield stress,  $f_y$ , were 27.6 MPa (4 ksi) and 414 MPa (60ksi), respectively. A column diameter of 813 mm (32 in) was selected such as to achieve an axial load level would be about

10 % of  $A_g f'_c$  ; the actual resulting axial load level,  $P/A_g f'_c$ , was 11 %. The column was reinforced with 16 – D19 (#6) longitudinal bars, resulting in a longitudinal reinforcement ratio,  $\rho_l$ , of 0.9 %. The clear cover of concrete was set to be 51 mm (2 in).

An axial force-moment interaction curve was calculated using XTRACT (2007) for the design of columns. XTRACT is commercial software for cross sectional analysis, such as moment curvature analysis and axial force moment interaction analysis. The Mander model (Mander et al. 1988; Priestley et al. 1996) was selected for the constitutive relationship of unconfined and

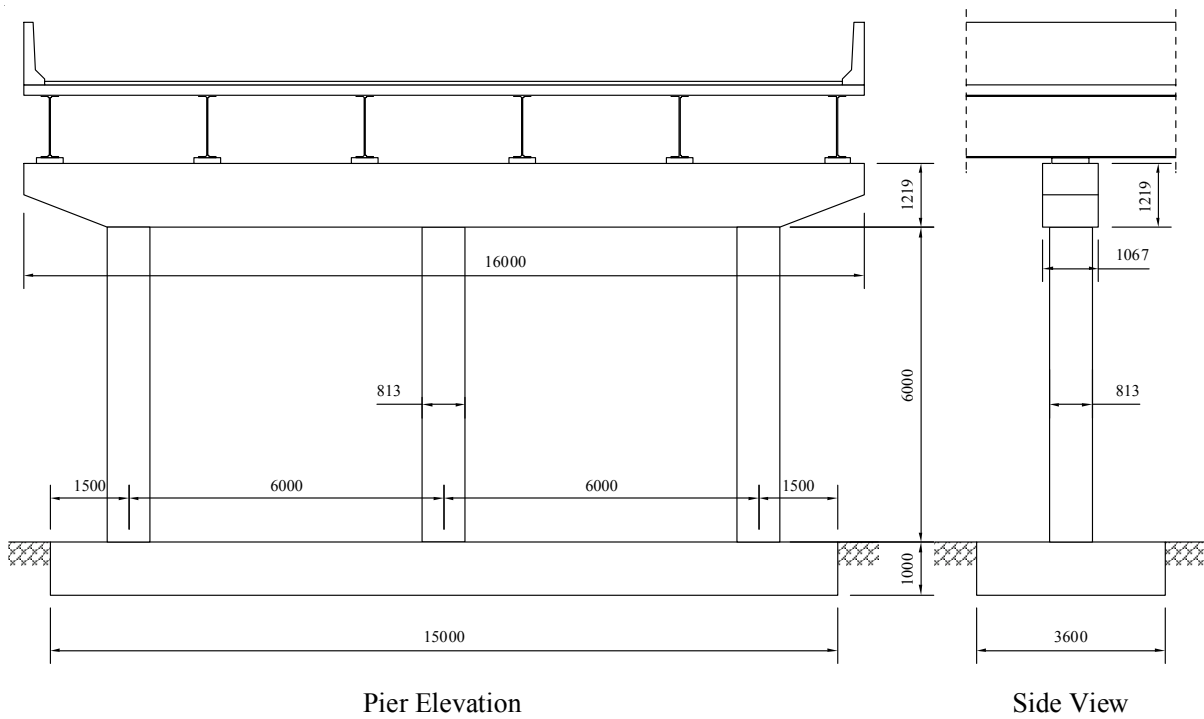


**Figure 3-3 Elevation Details of Prototype Bridge Pier-bent**

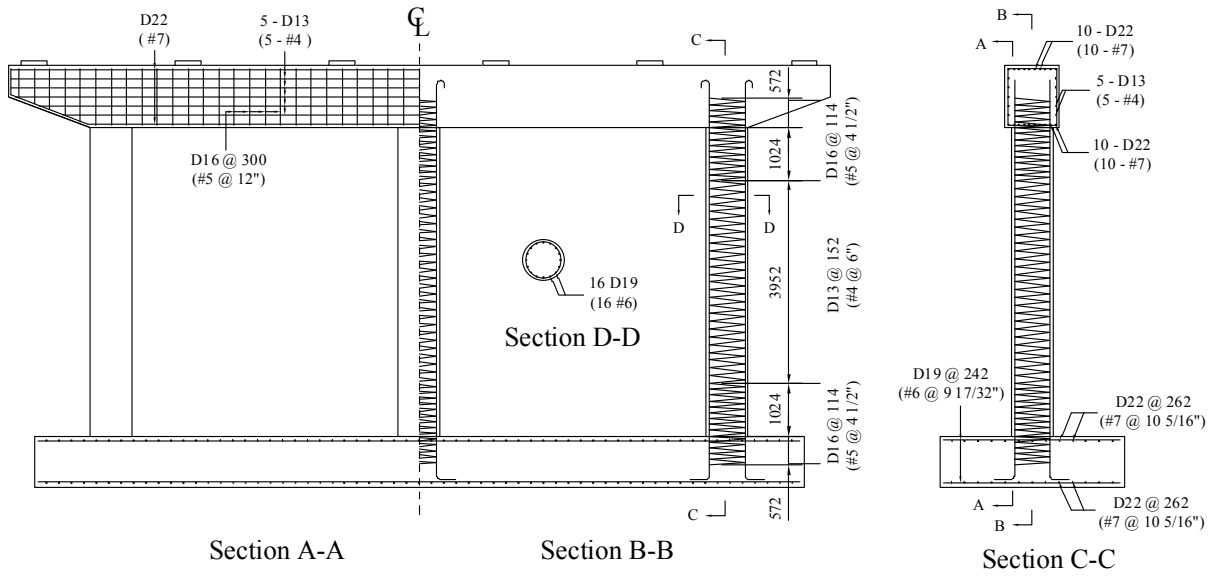


**Figure 3-4 Reinforcement Details of Prototype Bridge Pier-bent**

confined concrete. This model is schematically shown in Figure 3-5. In this model, the maximum strength of confined concrete,  $f'_{cc}$ , is related to the effective lateral confining pressure,  $f'_l$ . The stress-strain relationship of concrete (compressive stress,  $f_c$ , and strain,  $\epsilon_c$ ) is defined by the following equations:

$$f_c = \frac{f'_{cc} x r}{r - 1 + x'} \quad (3-1)$$

where

$$f'_{cc} = f'_c \left( 2.254 \sqrt{1 + \frac{7.94 f'_l}{f'_c}} - \frac{2 f'_l}{f'_c} - 1.254 \right) \quad (3-2)$$

$$x = \frac{\epsilon_c}{\epsilon_{cc}} \quad (3-3)$$

$$\epsilon_{cc} = 0.002 \left[ 1 + 5 \left( \frac{f'_{cc}}{f'_c} - 1 \right) \right] \quad (3-4)$$

$$r = \frac{E_c}{E_c - E_{sec}} \quad (3-5)$$

$$E_{sec} = \frac{f'_{cc}}{\epsilon_{cc}} \quad (3-6)$$

The elastic modulus of concrete,  $E_c$ , calculated as per ACI for normal weight concrete, is:

$$E_c = 57000\sqrt{f'_c} \text{ (psi)} \quad (3-7)$$

The effective lateral confining pressure,  $f'_l$ , is given by:

$$f'_l = K_e f_l = K_e \left( \frac{2f_{yh}A_{sp}}{D's_h} \right) \quad (3-8)$$

where  $f_l$  is the maximum effective lateral pressure, and  $f_{yh}$ ,  $A_{sp}$ ,  $D'$  and  $s_h$  are the yield strength, area, diameter and longitudinal spacing of spirals or hoops, respectively.  $K_e$  is typically taken as 0.95 for circular sections, 0.75 for rectangular sections and 0.6 for rectangular wall sections.

The stress-strain relationship for both confined and unconfined concrete used in this calculation is shown in Figure 3-6 (a). In the confined concrete model, D16 (#5) transverse spiral reinforcement was used at a spacing of 114 mm (4.5 in). These spiral details were determined from the seismic design presented in the following subsection. The maximum strength of confined concrete,  $f'_{cc}$ , was 38.8 MPa (5.619 ksi) at the strain,  $\epsilon_{cc}$ , of 0.00605. The crushing strain was assumed at 0.015. For the unconfined concrete, the effective lateral confining pressure was set to be  $f'_l = 0$ . After the unconfined concrete reached its crushing strain, the stress-strain model assumed straight line stress degradation up to the complete spalling. The crushing and spalling strain of the unconfined concrete were assumed to be 0.004 and 0.006, respectively.

The stress-strain relationship for longitudinal steel bars was idealized using a bi-linear elasto-perfectly plastic behavior with yield stress of 414 MPa (60ksi) and elastic modulus of 200,000 MPa (29,000 ksi), as shown in Figure 3-6 (b). The fracture strain of steel was set to be 0.03. The details of section and material models are provided in Appendix A. Finally, axial force-moment interaction curve for the prototype bridge column, as shown in Figure 3-7, was obtained by setting the limit strain of core concrete as the strain at maximum strength,  $\epsilon_{cc}$ , of 0.00605.



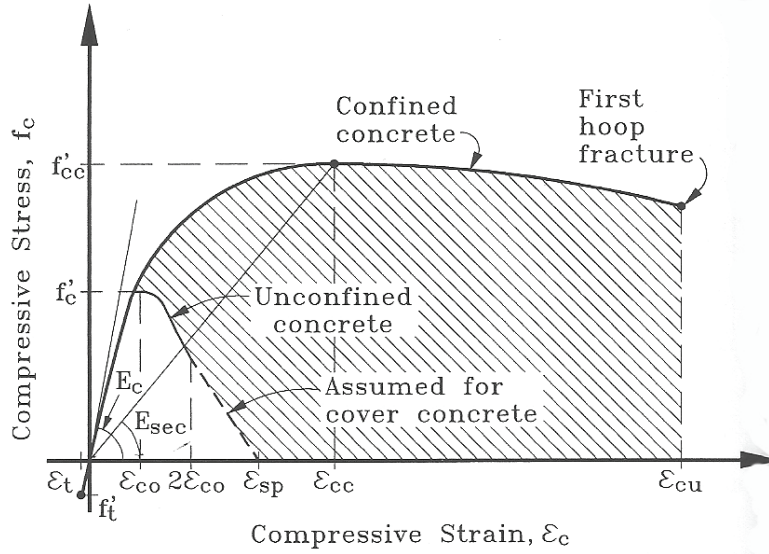


**Figure 3-5 Stress-strain Model for Unconfined and Confined Concrete (Priestley et al. 1996)**

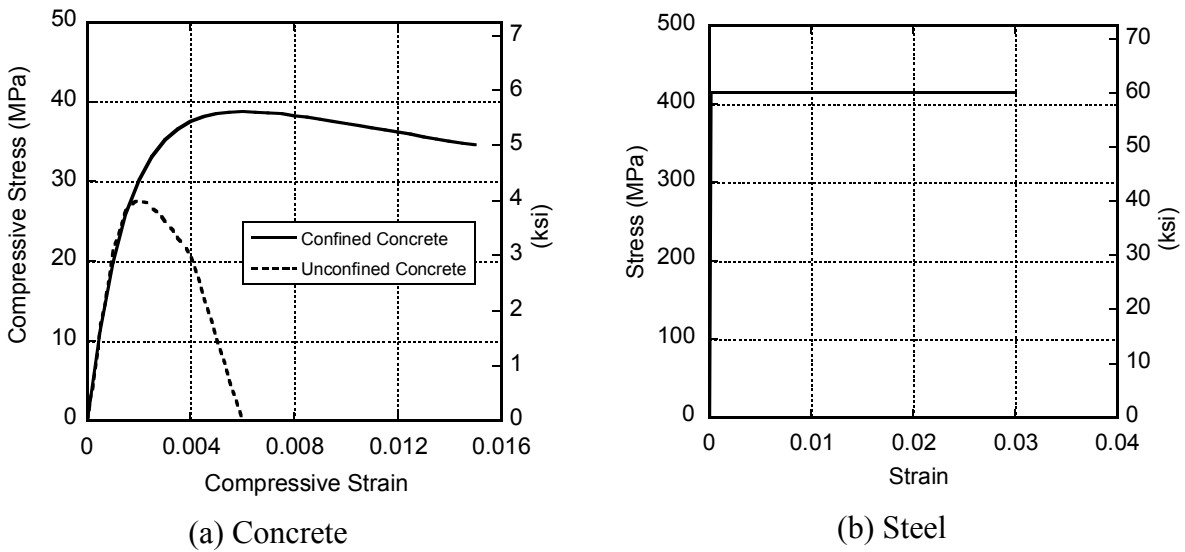


**Figure 3-6 Stress-strain Model for Section Analysis**

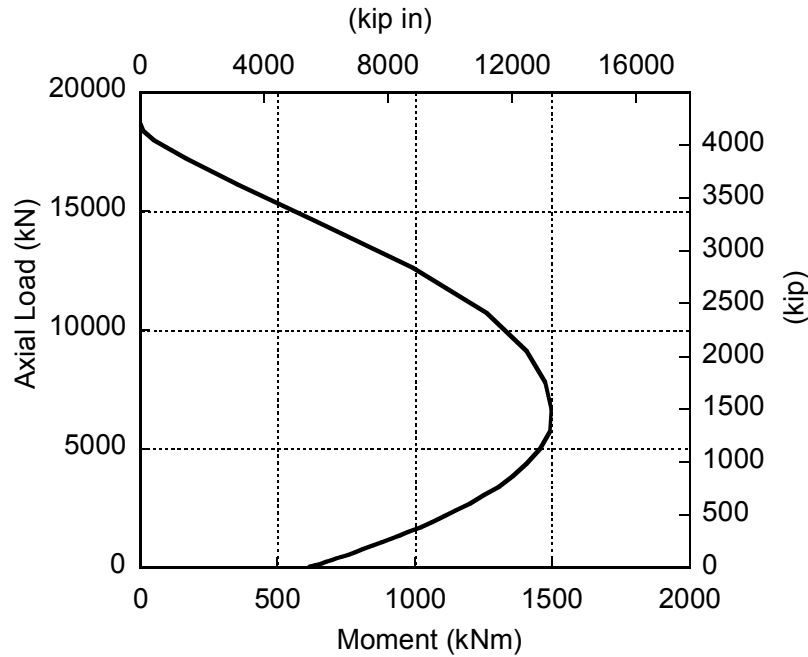


**Figure 3-7 Axial Force - Moment Interaction Curve for Prototype Bridge Column**

### 3.2.3.3 Seismic Loading

The prototype bridge structure described in the former subsection is assumed to be located in an area of moderate seismic activity. For analysis and design purposes, it is assumed that the corresponding pseudo-acceleration ( $S_A$ ) response spectrum is given by:

$$S_A = \min \left\{ (1 + 18.75 T) A_g, 2.50 A_g, \frac{A_g}{T} \right\} \quad (3-9)$$

where  $A_g$  (peak ground acceleration) is assumed equal to 0.3 g, and  $T$  denotes the bridge's natural period. The shape of the response spectrum defined by Equation 3-9 (shown in Figure 3-8) is typical of rock or very stiff soil foundations. Equation 3-9 is similar (but not identical) to the one implemented in the *AASHTO LRFD Bridge Design Specifications* (AASHTO 2004), the difference being that here, the short period range of the spectra is not taken as constant but rather varies as a function of  $T$ , and that the long period range varies as a function of  $1/T$  instead of the more conservative  $1/T^{2/3}$  in ASSHTO.

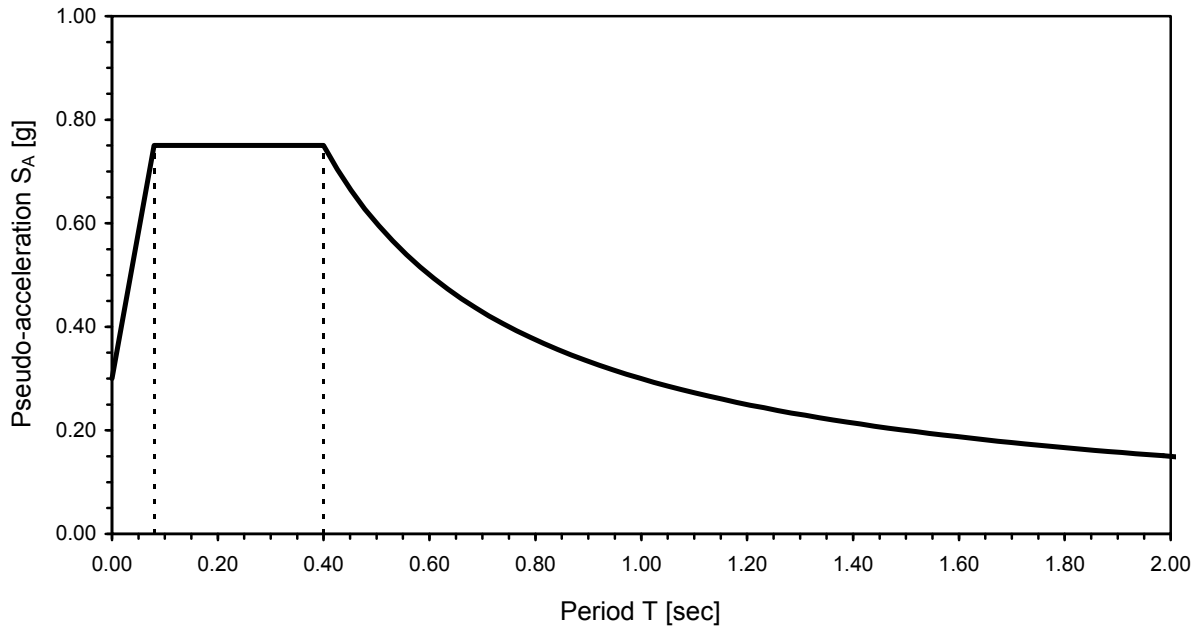


**Figure 3-8 Pseudo-acceleration Response Spectrum for Seismic Analysis and Design**

### 3.2.3.4 Analysis of Bent Column for Seismic Loading

The analyses of bent columns for seismic loading were made independently in the longitudinal and transverse directions. In each direction, conservatively assuming that the bearings supporting the end spans at the abutments do not restrain displacements, stiffness and strength are only provided by the piers. The inertia forces from the superstructure are assumed to be equally carried by two pier bents. Calculation details are presented in Appendix B along with design of the columns.

The prototype bridge has two pier bents, and each pier bent consists of three RC columns fixed at the foundation. The boundary conditions of the columns at the top is pinned in the longitudinal direction and fixed in the transverse direction. The stiffness of each column is given by:

$$k_c = \frac{3E_c I_{cr}}{H^3} \quad (\text{for longitudinal direction}) \quad (3-10)$$

$$k_c = \frac{12E_c I_{cr}}{H^3} \quad (\text{for transverse direction}) \quad (3-11)$$

where  $H$  is the height of column,  $E_c$  is the elastic modulus of concrete given by Equation 3-7 and  $I_{cr}$  is the moment of inertia of cracked section.  $I_{cr}$  is calculated assuming the moment of inertia of cracked section is taken as one-half of that of the gross section and given by:

$$I_{cr} = \frac{\pi}{64} \cdot \frac{D^4}{2} \quad (3-12)$$

where  $D$  is the column diameter. The total effective stiffness of the whole bridge,  $K_{eff}$ , and the effective natural period are calculated by:

$$K_{eff} = \sum k_c \quad (3-13)$$

$$T_{eff} = 2\pi \sqrt{\frac{W_{super}}{K_{eff} \cdot g}} \quad (3-14)$$

where the summation in Equation 3-13 is over all columns of the bridge,  $W_{super}$  is the total weight of bridge superstructure and  $g$  is the acceleration due to gravity. The elastic lateral force capacity of each column,  $V_e$ , is given by:

$$V_e = \frac{M_n}{H} \quad (\text{for longitudinal direction}) \quad (3-15)$$

$$V_e = \frac{2M_n}{H} \quad (\text{for transverse direction}) \quad (3-16)$$

where  $M_n$  is the nominal moment capacity of column which is obtained from the axial force - moment interaction corresponding to the axial load. The yield displacement of each column,  $\Delta_y$ , is given by:

$$\Delta_y = \frac{V_e}{k_c} \quad (3-17)$$

The maximum displacement response of the bridge is given by:

$$\Delta_{max} = \frac{T_{eff}^2 S_A(T_{eff})}{4\pi^2} \quad (3-18)$$

Equation 3-18 is derived under the assumption of “equal displacement rule.” This assumption is applicable when natural period of structure in the constant-velocity and displacement region of the spectrum in which the period is larger than about 0.5 sec (Chopra 2000).

Results of seismic analyses are summarized in Table 3-1. The natural period in each direction was in the range of the assumption of “equal displacement rule.” Calculated expected ductility demands in the longitudinal and transverse direction were 2.22 and 3.39, respectively. The calculations show that the reinforced concrete bent column with diameter of 813 mm (32 in) and 16-D19 (#6) longitudinal bars provided satisfactory performance for the considered seismic loading.

### 3.2.3.5 Design of Column Transverse Steel Reinforcement

Ductile energy dissipating elements in the bridge are the columns. Non-ductile failure of the columns such as shear failure need be avoided to achieve this ductile energy dissipation through inelastic flexural response of the columns. The rest of the structure has to be designed to remain elastic for the forces developed when the columns yield. This is consistent with capacity design principals where the members that are not part of the primary energy dissipating system are made strong enough to resist the forces coming from the failure of the primary energy dissipating members. To ensure the columns not to fail in shear prior to the full development of ductile flexural failure, the flexural capacity of the columns have to be magnified by overstrength factor accounting for the increase in strength that can be developed by strain hardening due to large strains. This overstrength factor was taken as 1.5 to calculate the shear demand in each column,

**Table 3-1 Summary of Seismic Analyses**

Design Direction	$k_c$ [kN/m]	T [sec]	$V_e$ [kN]	$\Delta_y$ [mm]	$\Delta_{max}$ [mm]	$\mu = \frac{\Delta_{max}}{\Delta_y}$
Longitudinal	2,328	1.79	140	60	133	2.22
Transverse	14,792	1.00	331	22	75	3.39

$V_u$  (MCEER/ATC-49 2003a). Calculation details are presented in Appendix B.

The design shear force,  $V_u$ , should satisfy with the following equation from MCEER/ATC-49 (2003a):

$$V_u \leq \phi(V_s + V_p + V_c) \quad (3-19)$$

where  $\phi$  is the resistance factor (= 0.90),  $V_s$  is the shear resistance carried by transverse reinforcement,  $V_p$  is the contribution of shear resistance from the strut action of column axial force, and  $V_c$  is the tensile contribution of concrete to shear resistance. The shear resistance by transverse reinforcement,  $V_s$ , for circular columns is calculated by:

$$V_s = \frac{\pi}{2} \frac{A_{bh}}{s} f_{yh} D'' \cot \theta \quad (3-20)$$

where  $A_{bh}$ ,  $s$ ,  $f_{yh}$  and  $D''$  are respectively the area, center-to-center spacing, yield stress and center-to-center sectional dimension of hoop or spiral reinforcing bars, and  $\theta$  is the principal crack angle or plane.  $\theta$  is given as follows:

$$\tan \theta = \left( \frac{1.6 \rho_v A_v}{\Lambda \rho_t A_g} \right) \geq \tan \alpha \quad (3-21)$$

where  $\rho_v$  and  $\rho_t$  are the transverse and longitudinal reinforcement ratio,  $A_g$  is the gross area of column,  $A_v$  is the shear area of concrete which may be taken as  $0.8A_g$  for a circular section,  $\Lambda$  is fixity factor (1.0 for fixed-free or fixed-pinned, and 2.0 for fixed-fixed), and  $\alpha$  is the geometric aspect ratio angle given by:

$$\tan \alpha = \frac{D'}{L} \quad (3-22)$$

where  $D'$  is the center-to-center diameter of longitudinal reinforcement and  $L$  is the column height. Equation 3-21 proposed by Kim and Mander (1999) is an analytical expression derived from an energy minimization of shear-flexure deflections and was validated by experimental observations. The contribution by arch action,  $V_p$ , is given by:

$$V_p = \frac{\Lambda}{2} P_e \tan \alpha \quad (3-23)$$

where  $P_e$  is the compressive axial force including seismic effects. The tensile contribution of concrete,  $V_c$ , can be calculated by the following equations:

$$V_c = 0.05 \sqrt{f'_c} A_v \quad (\text{Plastic hinge zone}) \quad (3-24 \text{ a})$$

$$V_c = 0.17 \sqrt{f'_c} A_v \quad (\text{Outside of plastic hinge zone}) \quad (3-24 \text{ b})$$

where  $f'_c$  is concrete strength (MPa). Finally, the amount of column transverse reinforcement is determined from Equations 3-19 and 3-20.

As discussed in the preceding literature review section, design codes typically prescribe minimum volumetric spiral reinforcement ratio and details for confinement in the plastic hinge zone. The transverse reinforcement in this plastic hinge zone is designed by comparing the three different bridge specifications; AASHTO, MCEER/ATC-49, and CALTRANS. There are two requirements to decide the minimum volumetric spiral reinforcement ratio in each specification. One is to determine its ratio,  $\rho_s$ , using the equation given, and the other one is to calculate its ratio,  $\rho_s$ , from the requirements for the minimum spacing of transverse reinforcement. The details have been presented in the literature review. Table 3-2 summarizes the minimum volumetric ratio in plastic hinge region in accordance with these two requirements for each specification. As shown in Table 3-2, the maximum spacing limit of spiral by CALTRANS and MCEER/ATC-49 gives the maximum amount of transverse reinforcement ratio of 0.98 %, which is based on six times the nominal diameter of longitudinal reinforcement. Therefore, in plastic hinge region, D16 (#5) was used for transverse spiral reinforcement at spacing of 114 mm (4.5 in). The plastic hinge region need be specified to be provided this transverse reinforcement. The length of this plastic hinge zone,  $L_p$ , was calculated in accordance with AASHTO (2004) to be:

$$L_p = \max\left(D, \frac{H}{6}, 18(in)\right) \quad (3-25)$$

where  $D$  and  $H$  are the column diameter (813 mm (32 in)) and height of the column (6 m (236 in)). Accordingly, the resulting plastic hinge length,  $L_p$ , was 1.0 m (39 in).

The connection between the column and its cap beam and footing needs to be reinforced such that the column flexural capacity can fully develop. AASHTO (2004) specifies that the development length for all longitudinal steel shall be 1.25 times  $l_d$  given by:

$$l_d = \frac{0.02 A_b f_y}{\sqrt{f'_c}} \quad (\text{for D36 bar or smaller}) \quad (3-26)$$

where  $A_b$  and  $f_y$  are the longitudinal reinforcing bar area ( $\text{mm}^2$ ) and the specified yield strength (MPa), respectively, and  $f'_c$  is the specified compressive concrete strength (MPa). The spiral reinforcement of the column must be extended into the pier cap and footing for a distance not less than one-half the column diameter or 380 mm (15 in) (AASHTO 2004). Accordingly, the longitudinal bars and spirals extended into the cap beam and footing for a distance more than specified distances as shown in Figure 3-4.

**Table 3-2 Summary of Transverse Reinforcement for Confinement at Plastic Hinge Zone**

	AASHTO	CALTRANS	ATC-49
$\rho_s = 0.45 \left( \frac{A_g}{A_c} - 1 \right) \frac{f'_c}{f_{yt}}$	0.92 %	0.92 %	N/A
$\rho_s = 0.45 \left( \frac{A_g}{A_c} - 1 \right) \frac{f'_c}{f_{yt}} \left( 0.5 + \frac{1.25 P_e}{f'_c A_g} \right)$	N/A	0.62 %	N/A
$\rho_s = 0.12 \frac{f'_c}{f_{yt}}$	0.80 %	N/A	N/A
$\rho_s = 0.008 \frac{f'_c}{U_{sf}} \left[ 12 \left( \frac{P_e}{f'_c A_g} + \rho_t \frac{f_y}{f'_c} \right)^2 \left( \frac{A_g}{A_{cc}} \right)^2 - 1 \right]$	N/A	N/A	0.10 %
Maximum Spacing	#5@8" (203 mm)	#5@6 · d <sub>b</sub> =4.5" (114 mm)	#5@6 · d <sub>b</sub> =4.5" (114 mm)
$\rho_s$	0.55 %	<b>0.98 %</b>	<b>0.98 %</b>

### 3.2.3.6 Design Footing and Cap-beam

The footing and cap-beam were designed to be capacity protected as well as the shear force design of the column as presented previously. This was considered through overstrength factor of 1.5. Calculation details are presented in Appendix C. This calculation was mainly followed by the design example in the *Design Examples, Recommended LRFD Guidelines for the Seismic Design of Highway Bridges* (MCEER/ATC-49 2003b).

The footing was designed for overturning, soil bearing capacity and sliding in both longitudinal and transverse directions. In order to limit the uplift of the footing to 50 percent of the footing



base, the eccentricity,  $e$ , of the axial load,  $P$ , that produces the overturning moment,  $M$ , must be less than one-third of the length,  $L_f$ , of the footing. Namely,

$$e = \frac{M}{P} < \frac{L_f}{3} \quad (3-27)$$

The maximum contact stress,  $q$ , at the edge of the footing, used to check if the soil bearing capacity is adequate to resist the applied loads, was calculated by:

$$q = \frac{2P}{3B_f \left( \frac{L_f}{2} - e \right)} \quad (3-28)$$

where  $B_f$  is the width of the footing. Equation 3-28 was derived assuming a triangular linear variation of the stress distribution under the footing. The ultimate sliding resistance was calculated based on the assumption that the footing rested on a competent rock whose coefficient of friction might be taken as 0.8. As shown in Figure 3-3, the resisting length, width and height of the footing were 3.6 m (11 ft 10 in), 15.0 m (49 ft 3 in) and 1.0 m (39 in), respectively. The footing reinforcement was designed to resist the moment and shear force capacity of the column, resulting in D19 bars spaced at 242 mm (#6 at 9 17/32 in) in the longitudinal direction and D22 bars spaced at 262 mm (#7 at 10 5/16 in) in the transverse direction, as shown in Figure 3-4.

The 1067 mm (42 in) by 1219 mm (48 in) cap-beam was also designed to resist the moment and shear force capacity of the column. Ten D22 (#7) longitudinal bars were provided in the cap-beam to provide flexural strength and D16 (#5) stirrups spaced at 300 mm (12") center-to-center were provided to resist the shear force, as shown in Figure 3-4. Although no longitudinal reinforcement in the cap-beam web is required to resist the moment and shear force, some reinforcement need to be provided in the web to control the cracking due to the creep and shrinkage. AASHTO (2004) requires longitudinal skin reinforcement for this purpose if the effective depth,  $d_e$  (mm), of nonprestressed or partially prestressed concrete members is more than 900 mm. The area of skin reinforcement,  $A_{sk}$  (mm<sup>2</sup>/mm), shall be given by:

$$A_{sk} \geq 0.001(d_e - 760) \quad (3-29)$$

The maximum spacing of the skin reinforcement shall be smaller of  $d_e/6$  and 300 mm. Accordingly, five D13 (#4) bars were provided on each side of the cap-beam web as skin reinforcement.

### 3.2.3.7 Design of Steel Jacketed Non-ductile RC Column

The second type of seismic designed columns is the non-ductile RC column retrofitted with a steel jacket. As indicated earlier, this steel jacketing is effective to enhance the ductility of non-ductile reinforced concrete columns by adding a steel shell that provides the confinement of the concrete. This steel jacketing allows the plastic hinges developed at the top and bottom where these plastic hinges would normally be impossible to form for the non-ductile columns without enough transverse reinforcement inside of the columns. For the purpose of this project, therefore, a non-ductile RC column was designed to enhance the seismic performance using a steel jack in accordance with the design procedure developed by Chai et al. (Buckle et al. 2006).

The same diameter and same amount of longitudinal bars used in the ductile RC column were selected for steel jacketed RC column, namely 813 mm (32 in) and 16-D19 (#6) longitudinal bars, respectively. Then, the transverse reinforcement was designed to resist the shear force. The D13 (#4) transverse reinforcement provided, spaced at 210 mm (8 1/4 in), resulted in a transverse reinforcement ratio of 0.35 %.

Then, this non-ductile RC column was retrofitted using steel jacket in accordance with the design procedure developed by Chai et al. (Buckle et al. 2006) as described in literature review. Detail calculations for the transverse reinforcement and steel jacket are presented in Appendix D. For a circular column, the required steel jacket thickness,  $t$ , could be obtained from equilibrium of stresses action on a half-column section by the following equation:

$$t \geq \frac{f_l D}{2f_s} \quad (3-30)$$

where  $f_l$  is the confinement stress,  $D$  is the diameter of column and  $f_s$  is the stress induced in the steel jacket (Buckle et al. 2006). A clearance of 13 mm (1/2 in) was provided between the existing column and the jacket. The confinement stress,  $f_l$ , was taken as 2.07 MPa (300 psi), which is the value used in this design methods developed by Chai et al. (1991). The stress induced in the steel jacket,  $f_s$ , was taken as 200 MPa (29 ksi) that is the stress at a strain of 0.001 calculated using a elastic modulus equal to 200 GPa (29,000 ksi). The resulting thickness of steel jacket was 4.3 mm (3/16”).

### 3.2.4 One-Fourth Scale Model Design

The design of the prototype bridge pier bent with either RC columns or steel jacketed RC columns was presented in the previous section. Using geometric similitude, a one-fourth (1/4) scale model was designed and constructed to accommodate the constraints in the maximum possible explosive weight that could be used at the test site and considerations for construction cost (as mentioned earlier).

For convenience, the bridge bent with two different kinds of the columns was used in this project. Recognizing that all columns in the real bridge bent would be identical, for the purpose of the experimental convenience and due to the budget constraints, it was deemed adequate to test each of the columns in this bent successively as if they were a part of the regular bent. The general layout of the bent of experimental specimens is shown in Figure 3-9. The bent consists of two identical RC columns (RC1 and RC2) and two identical steel jacketed RC columns (SJ1 and SJ2), connected to a cap-beam and a footing. Note that the prototype bridge pier bent has three columns while the specimen had four columns. This was intended to provide as many columns as possible in one bent, while at the same time providing some distance between the columns needed to avoid the blast effects from a test on one column to impact the other column tests. The preliminary calculation indicated that the spacing between these columns was large enough to preclude the damage to an adjacent column by a test on a target specimen.

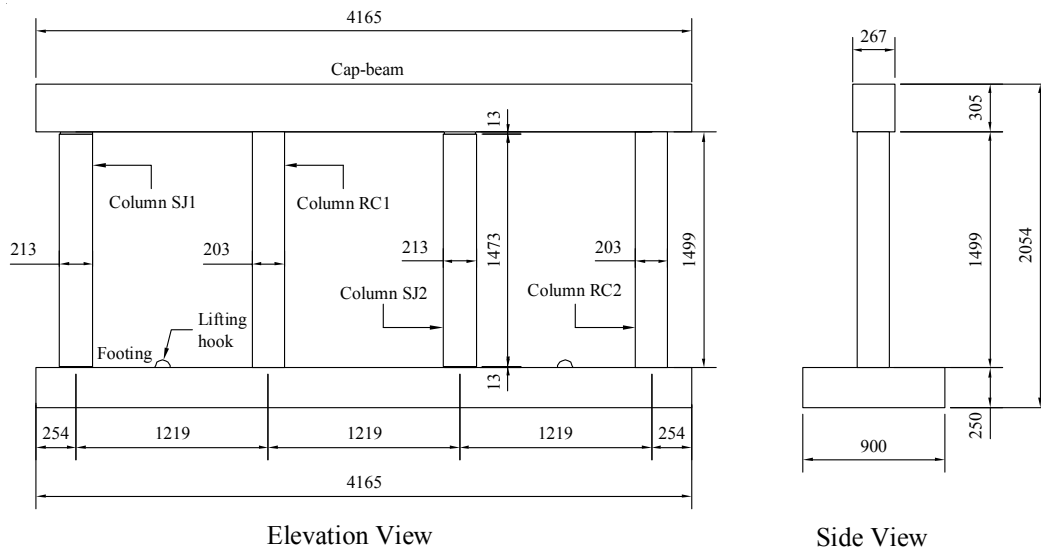


**Figure 3-9 General Layout of Experimental Specimen**

### 3.2.5 Specimen Materials

#### 3.2.5.1 Concrete Properties

The concrete was ready mixed and supplied by a local concrete batching plant. A design mix was formulated by the plant for a 28 day target compressive strength of 4 ksi (27.6 MPa), slump of 4.5 in (114 mm) and maximum size of coarse aggregate of 1/2 in (13 mm). The concrete was poured in two stages; first to do the footing and second to do the columns and cap-beam. At the concrete joints between the footing and the columns, the surface of the joints was cleaned and laitance was removed according to the ACI code requirement (ACI 2004). The mix design formula for 1<sup>st</sup> and 2<sup>nd</sup> batch concrete is shown in Table 3-3.

**Table 3-3 Mix Design Formula for Model Concrete**

Material	1 <sup>st</sup> Batch (1.5 cubic yard) Footing	2 <sup>nd</sup> Batch (2.75 cubic yard) Columns and Cap- beam
Type I Cement	2712 lb	4687 lb
Concrete Sand	4848 lb	8651 lb
No.1 Crushed Stone	908 lb	1684 lb
Water	16.9 gal.	62.1 gal.
Super-plasticizer	56.0 oz	84.1 oz
Micro-air	5.1 oz	11.2 oz

The compressive strength of the concrete was obtained from compression tests of concrete cylinders of 4 in (102 mm) diameter and 8 in (203 mm) height. The cylinder specimens were moist cured near the pier bent model. Sets of three cylinders were tested at seven days, twenty eight days and six days after the blast tests (corresponding to sixty one days and forty one days for the 1<sup>st</sup> and 2<sup>nd</sup> batch, respectively). Concrete slump and average compressive strength results are presented in Table 3-4.

**Table 3-4 Measured Concrete Properties**

Concrete Location	Slump	Compressive Strength		
		7 days	28 days	6 days after blast tests
Footing (1 <sup>st</sup> Batch)	102 mm (4 in)	28.9 MPa (4.187 ksi)	40.8 MPa (5.912 ksi)	41.5 MPa (6.024 ksi)
Columns and Cap-beam (2 <sup>nd</sup> Batch)	127 mm (5 in)	22.8 MPa (3.303 ksi)	28.9 MPa (4.193 ksi)	32.1 MPa (4.650 ksi)

### 3.2.5.2 Reinforcing Steel and Steel Jacket Properties

In the design of the prototype bridge, D13 (#4), D16 (#5), D19 (#6) and D22 (#7) deformed reinforcing bars with specified yield strength of 414 MPa (60 ksi) were used, with cross-sectional areas of 126.7 mm<sup>2</sup> (0.20 in<sup>2</sup>), 198.6 mm<sup>2</sup> (0.31 in<sup>2</sup>), 286.5 mm<sup>2</sup> (0.44 in<sup>2</sup>) and 387.2 mm<sup>2</sup> (0.60 in<sup>2</sup>), respectively. According to geometric similitude at one-quarter scale, D-1, D-2, D-3 and D-4 deformed steel wires were used to respectively model the D13, D16, D19 and D22 of the prototype bridge. These steel wire properties are shown in Table 3-5.

These are cold-worked deformed steel wires intended for use as reinforcement in concrete construction. Their properties are specified by ASTM A496 specified (ASTM 2005b). ASTM A496 requires tensile properties of 515 MPa (75 ksi) and 585 MPa (85 ksi) for yield strength and tensile strength based on nominal area of wire, respectively. The wires are available in sizes D-1 to D-45 whose number indicates the nominal cross-sectional areas of the wires in in<sup>2</sup>. The steel wires typically have high strength with no plateau and low ductility. Therefore, the steel wires used in the specimens were heat treated (annealed) to achieve properties similar to those of commercial steel reinforcing bars with design yield strength of 414 MPa (60 ksi). This was done for the D-1, D-2 and D-3 wires used to fabricate the column reinforcement. Heat treatment of the reinforcement used in the cap beam and footing was not accomplished since these structural elements were designed remain undamaged during this experimental program and were not the focus of this research. The wires were annealed in a vacuum furnaces produced by Ipsen, Inc. as shown in Figure 3-10 at a local heat treating company. The steel bars were placed in the vacuum

furnace at room temperature, heated to 1135 °F for 60 minutes, cooled to room temperature, and removed. The final annealing scheme that provided the desired properties was achieved through trial and error. First annealing attempt at a temperature of 1100 °F lowered the yield strength of D-3 from 607 MPa (88 ksi) to 538 MPa (78 ksi). To get the yield strength closer to the target strength of 414 MPa (60 ksi), a second annealing attempt was made with a different set of wires, for which temperature was set to be 1200 °F, but in this case yield strength was lowered to 390 MPa (40 ksi). Therefore, a final annealing attempt was made at a temperature of 1135 °F (interpolating 1100 °F and 1200 °F). Representative stress-strain relationships for the D-1 to D-3 wires used in the specimens are shown in Figures 3-11 through 3-13, respectively, from tensile tests on both the original and annealed wires. Figure 3-14 shows a representative stress-strain relationship of the original D-4. Mean coupon test results for the annealed wires are presented in Table 3-5.

**Table 3-5 Reinforcing Steel Properties**

Bar	Diameter mm (in)	Area mm <sup>2</sup> (in <sup>2</sup> )	Yield Stress MPa (ksi)	Ultimate Stress MPa (ksi)	Ultimate Strain	Elastic Modulus MPa (ksi)
D-1	2.87 (0.113)	6.45 (0.01)	380 (55.12)	454 (64.57)	0.145	194,289 (28,172)
D-2	4.04 (0.159)	12.90 (0.02)	314 (45.49)	426 (61.72)	0.154	193,269 (28,024)
D-3	4.95 (0.195)	19.35 (0.03)	501 (72.58)	561 (81.38)	0.090	195,007 (28,276)
D-4	5.72 (0.225)	25.81 (0.04)	N/A	N/A	N/A	N/A

The steel plate for the steel jacket was a cold-rolled commercial steel sheet with no mandatory mechanical properties specified by ASTM 1008 CS steel. Typical yield strength and elongation are specified to be between 140 and 275 MPa (20 and 40 ksi), and more than 30% in 50 mm (2 in), respectively (ASTM 2005c). Coupons for tension testing complying with ASTM A370 (ASTM 2005a) were fabricated from the plate material. Specified plate thickness for the plate used was 1.2mm (Gauge 18, 0.0478 in). The measured thickness of the plate was 1.13 mm (0.0445”). Representative stress-strain relationship is presented in Figure 3-15. The mean

values of measured yield strength, ultimate strength, ultimate strain and Young's modulus were 254 MPa (36.85 ksi), 352 MPa (51.06 ksi), 0.184 and 207,216 MPa (30,046 ksi), respectively.



**Figure 3-10 Vacuum Furnace for Annealing**

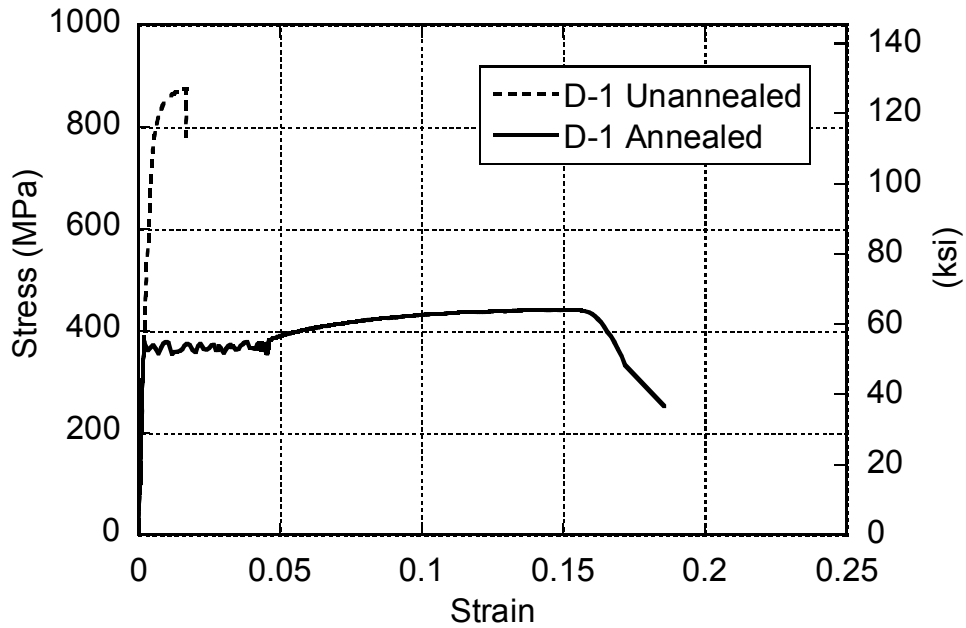


**Figure 3-11 Stress-Strain Curve for D-1**

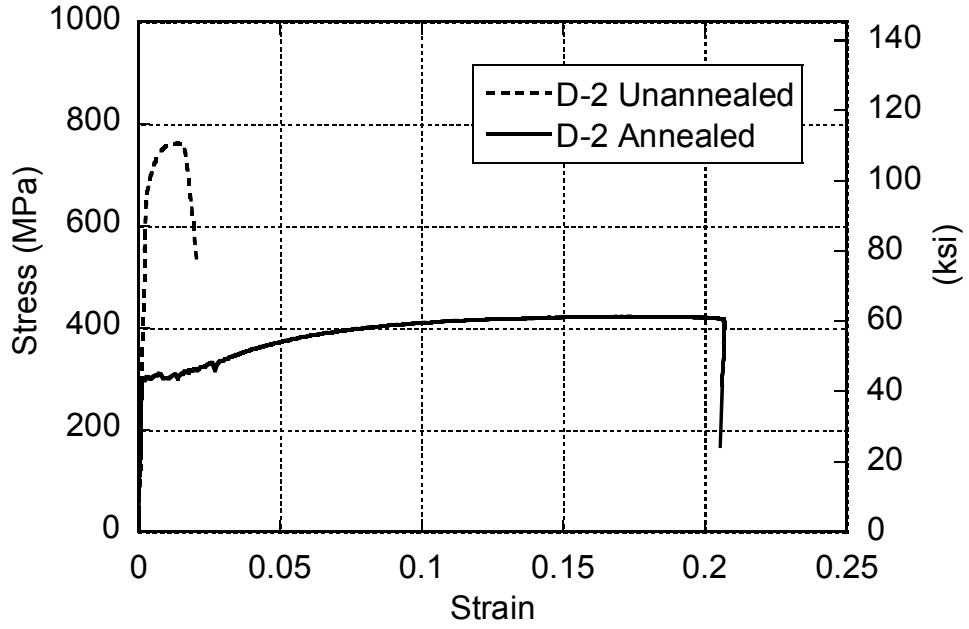


**Figure 3-12 Stress-Strain Curve for D-2**

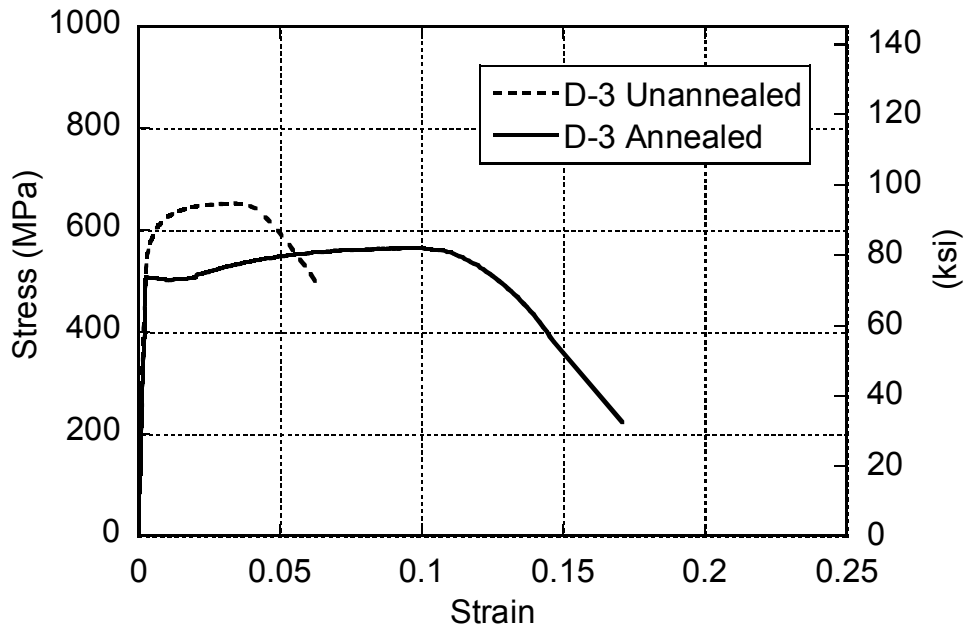


**Figure 3-13 Stress-Strain Curve for D-3**



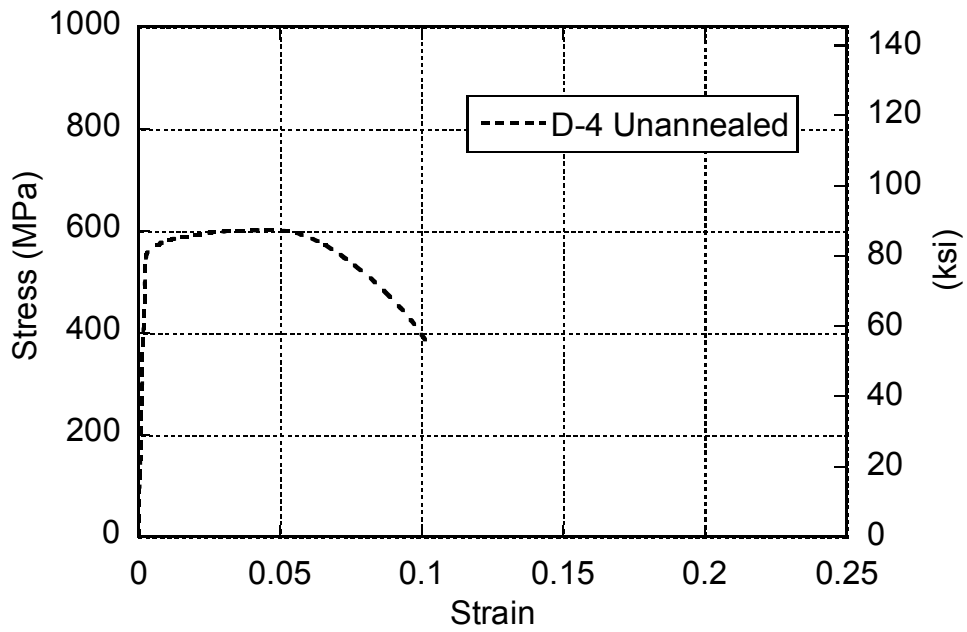


**Figure 3-14 Stress-Strain Curve for D-4**

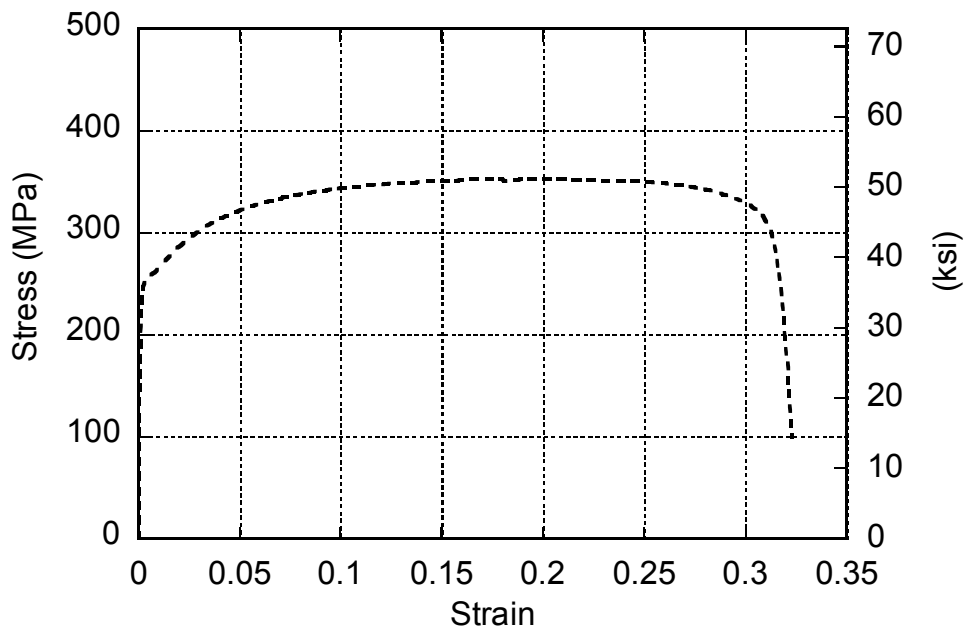


**Figure 3-15 Stress-Strain Curve for Steel Jacket**

### 3.2.6 Model Fabrication

The test specimens were fabricated in the Structural Engineering and Earthquake Simulation Laboratory (SEESL) at the University at Buffalo (UB). Reinforcement details of the bent pier and cross sections of the RC columns and steel jacketed RC columns are shown in Figure 3-16 and Figure 3-17, respectively. Shop drawings of the specimens are presented in Appendix E.

First, the footing cage reinforcement and column reinforcement up to mid-height of the column were fabricated, as shown in Figure 3-18 (a). Then, the rest of the column reinforcement was assembled after casting the footing concrete, as shown in Figure 3-18 (b). As shown in Figure 3-16, the spirals in the RC columns were extended into the footing and cap-beam as explained earlier, but the ones in the steel jacketed RC columns were stopped at the top and bottom of the column because this reinforcement of the steel jacketed RC columns was detailed in accordance with the pre-1971 design code. Figures 3-19 (a) and (b) show the column-to-footing connection of RC column and steel jacketed RC column, respectively, and Figures 3-20 (a) and (b) show the column-to-cap beam connection of the RC column and steel jacketed RC column, respectively. Figures 3-21 (a) and (b) show the formwork for the RC column and steel jacketed RC column, respectively. Round cardboard forms (Sonotube) with inside diameter of 203 mm (8 in) were used for RC columns. For steel jacketed RC columns, steel jackets with outer diameter of 213 mm (8 3/8 in) were used as formworks. To create the required gap of 13 mm (1/2 in) at the top and bottom of the steel jacketed RC column (as specified by CALTRANS (1996)), 13 mm (1/2 in) thick plywood pieces having a 203 mm (8 in) diameter hole were inserted between the steel jacket and the footing and cap-beam. Then, the cap-beam reinforcement cage was assembled. Finally, concrete was casted into the four columns and the cap-beam at the same time. As mentioned earlier, at the concrete joints between the footing and the columns, the surface of the joints was cleaned and laitance was removed according to the ACI code requirement (ACI 2004).

The model pier bent was shipped from the University at Buffalo to the facility of the U.S. Army Corps of Engineers Research Facility in Vicksburg, Mississippi, where tests were performed. Shipping frames, as shown in Figure 3-22, were fabricated to crate the specimen and avoid damage (especially to the columns) during shipping.

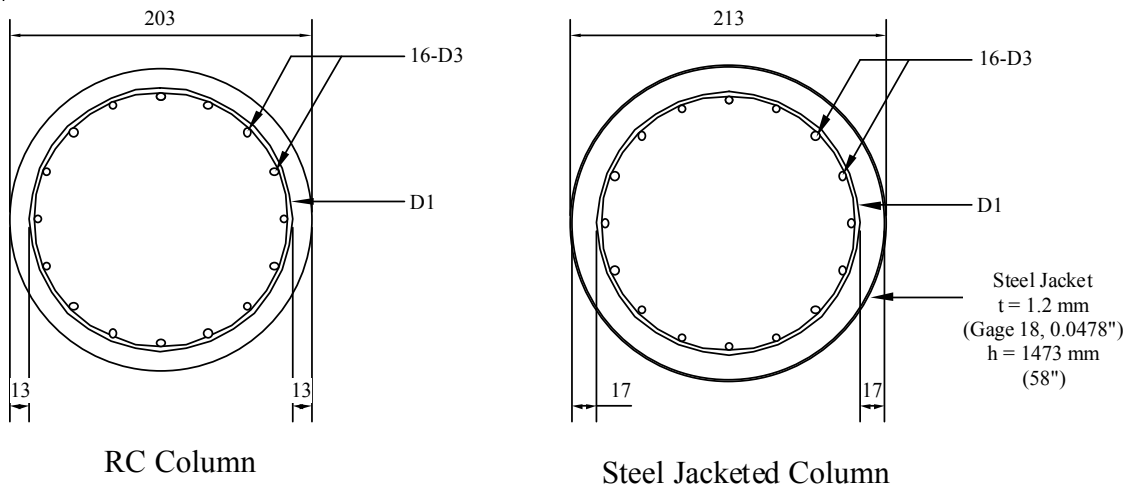
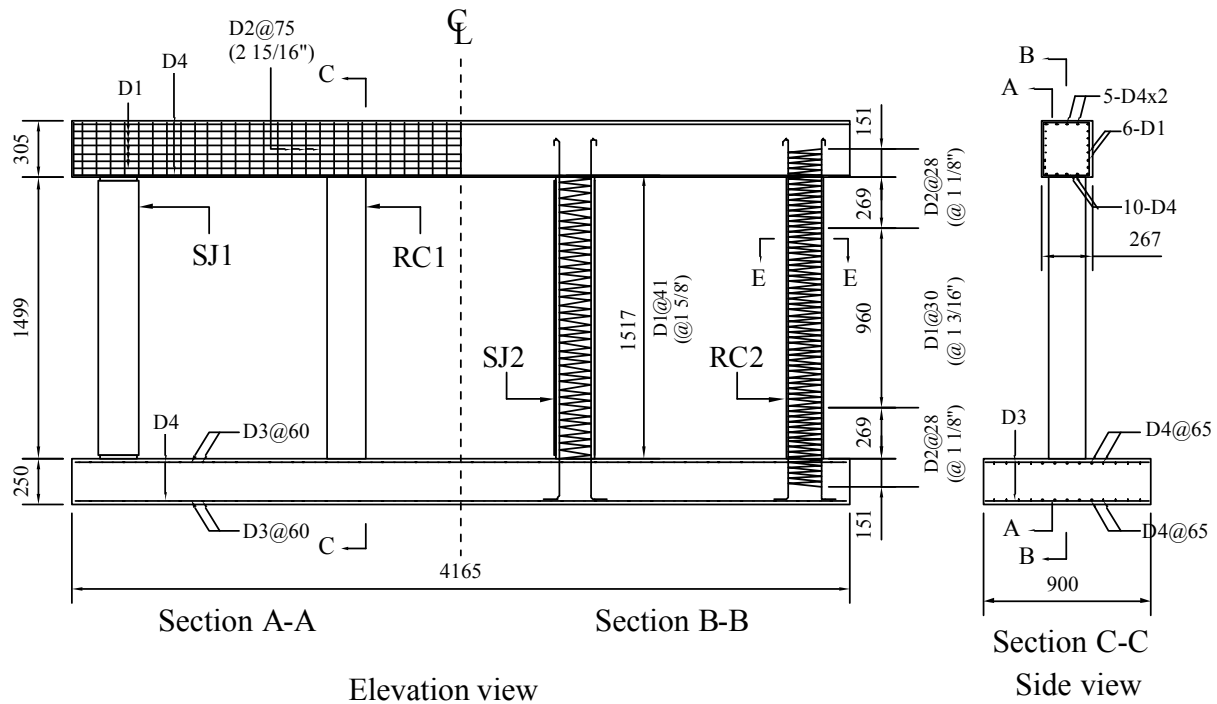
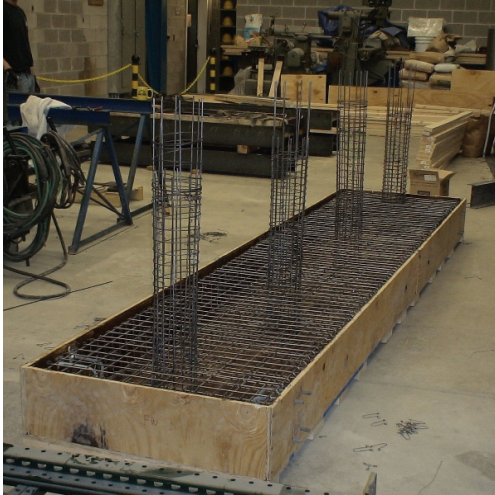


**Figure 3-17 Reinforcement Details of Column Section**



(a) Footing Reinforcement

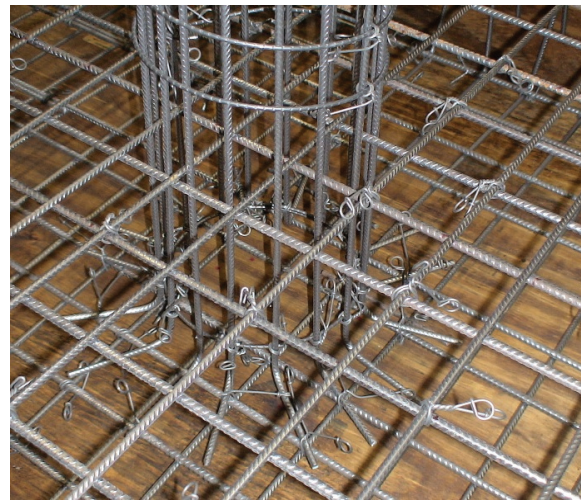


(b) Column Reinforcement after casting footing concrete

**Figure 3-18 Reinforcement Details of Footing and Column**



(a) RC Column (RC1 and RC2)



(b) SJ Column (SJ1 and SJ2)

**Figure 3-19 Reinforcement Details of Column – Footing Connection**



(a) RC Column (RC1 and RC2)

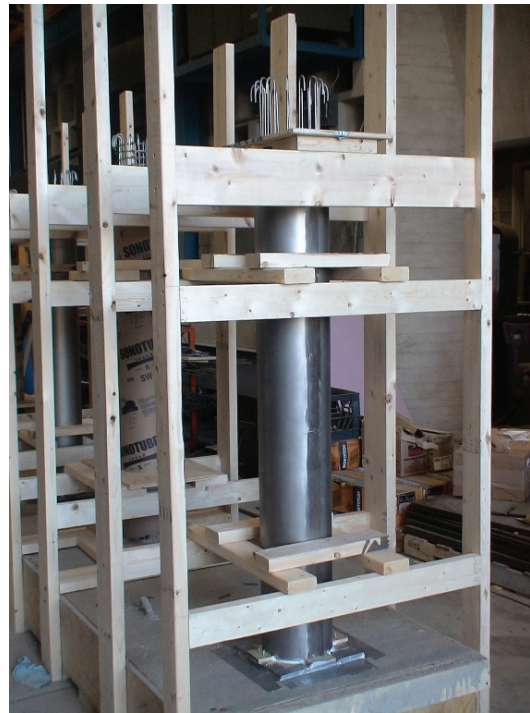


(b) SJ Column (SJ1 and SJ2)

**Figure 3-20 Reinforcement Details of Column – Cap-beam Connection**



(a) RC Column (RC1 and RC2)



(b) SJ Column (SJ1 and SJ2)

**Figure 3-21 Formwork for Column**



**Figure 3-22 Shipping Frame for Model**

### **3.2.7 Test Setup**

A series of tests were performed at the U.S. Army Corps of Engineers Research Facility in Vicksburg, Mississippi. Figure 3-23 illustrates side and plan views of the test setup. There was a reaction frame between two test models, namely the pier bent with two RC columns and two steel jacketed RC columns considered in this project, and a steel plate shear wall (SPSW) model tested as part of another project beyond the scope of this research. The experimental setup is shown in Figures 3-24 to 3-26 from front diagonal, side, and back diagonal views, respectively. The model was placed by casting concrete around the footing, as shown in these figures. Note that the cap-beam was not fixed to the reaction frames as it was intended to allow rotations at that location, to replicate actual boundary conditions in bridges. Figure 3-27 shows the photo of the reaction frame at the cap-beam from the back diagonal view.

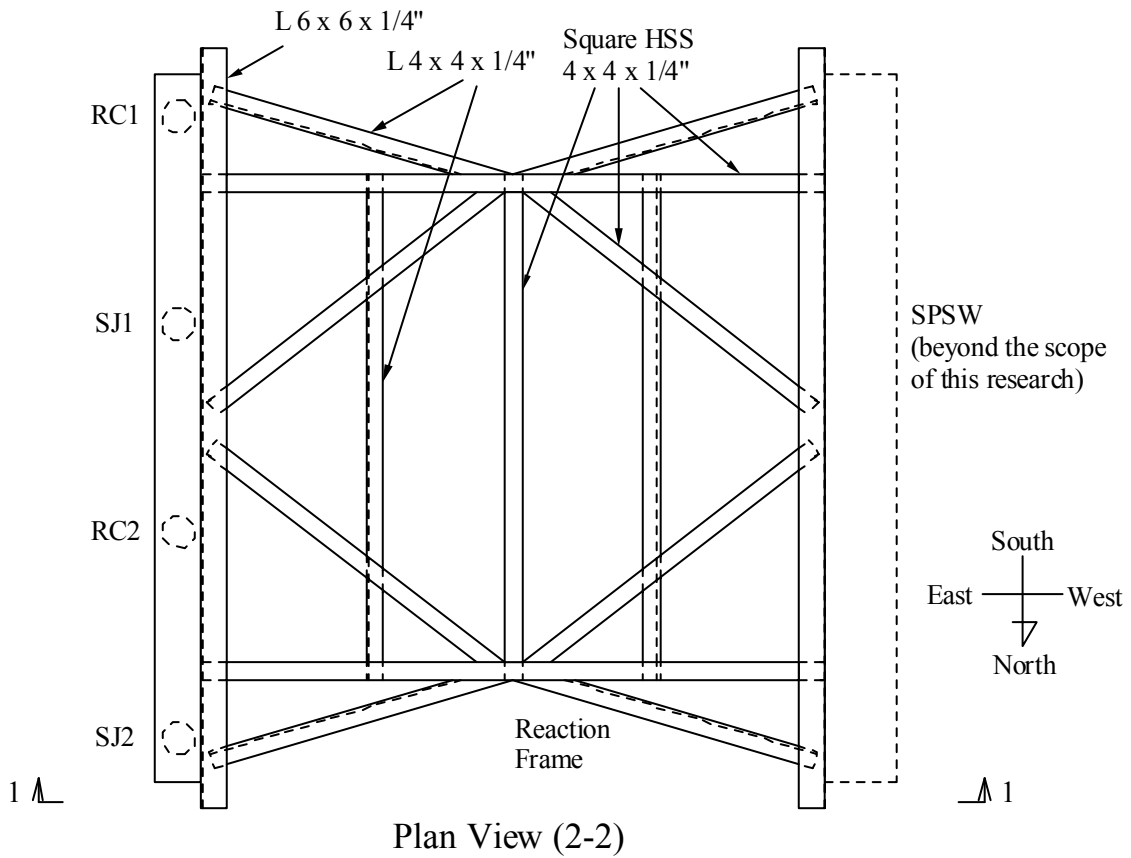
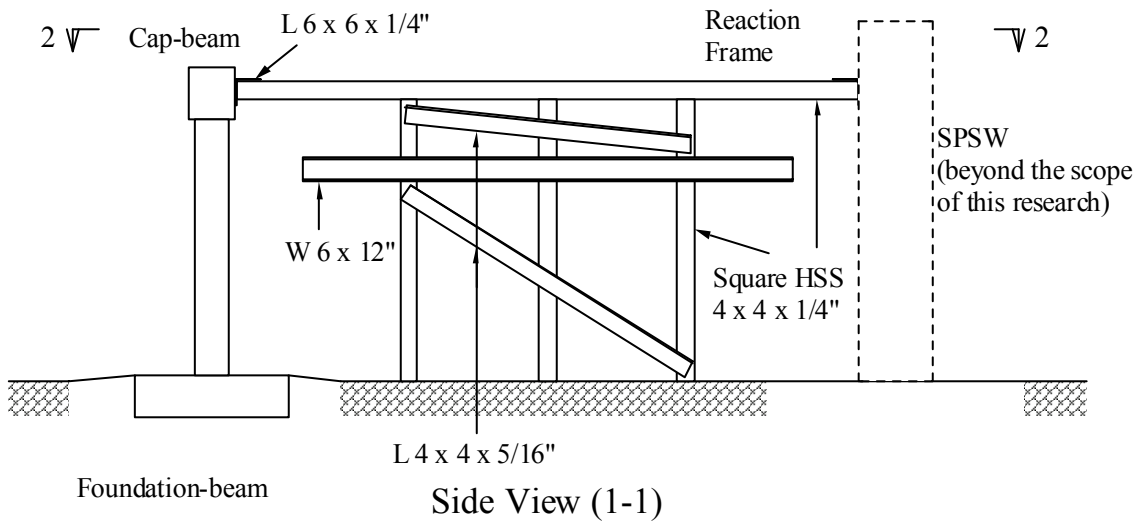


**Figure 3-23 Test Setup and Reaction Frame Details**

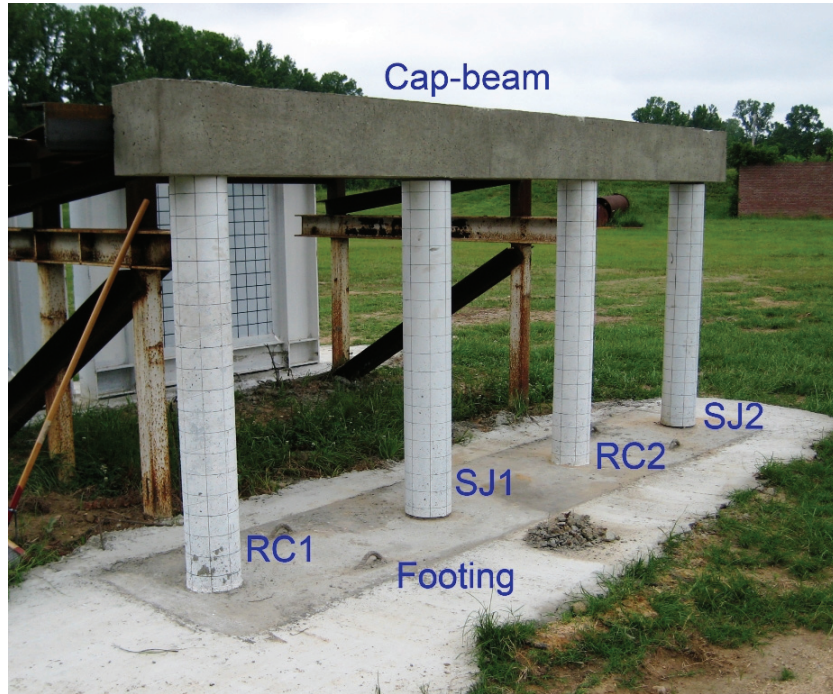


**Figure 3-24 Test Setup from Front Diagonal View**

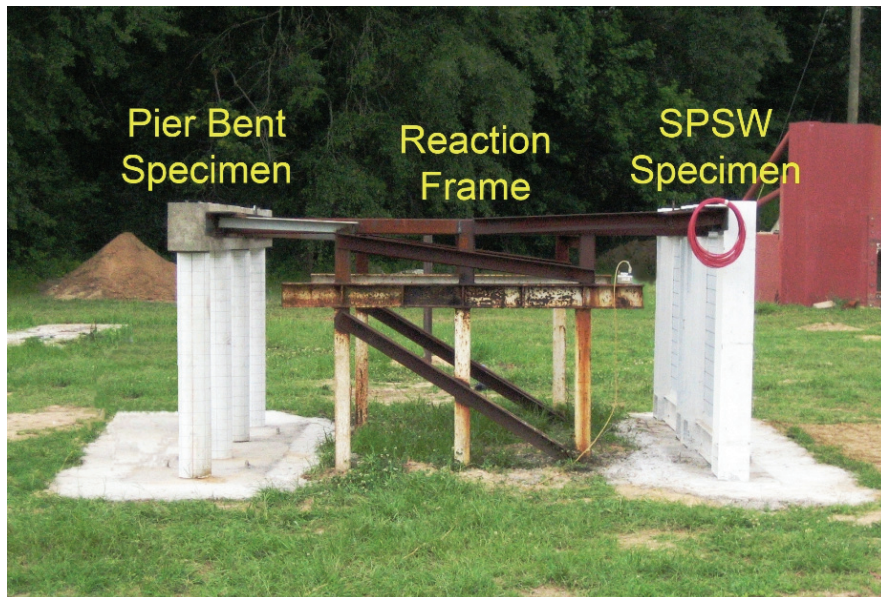


**Figure 3-25 Test Setup from Side View**





**Figure 3-26 Test Setup from Back Diagonal View**



**Figure 3-27 Reaction Frame**

### 3.3 Experimental Cases and Observations

#### 3.3.1 General

This section presents a description of the explosive charge used in the tests, the experimental cases, and the experimental observations made after the series of blast tests on two RC columns and two steel jacked RC columns. The tests were performed at the U.S. Army Corps of Engineers Research Facility in Vicksburg, Mississippi. Due to constraints in the maximum possible blast charge weight that could be used at the test site, test specimen dimensions were set to be 1/4 scale of the prototype bridge piers as mentioned in a previous section.

#### 3.3.2 Explosive Charge

Nitromethane was used for the explosive charges. Nitromethane with the chemical formula  $\text{CH}_3\text{NO}_2$  is widely used as a solvent in a variety of industrial applications such as a cleaning solvent and a reaction medium. The actual charge mass is conventionally converted into a TNT equivalent mass, and the conversion factor is 1.1. For instance, a 10 kg charge of nitromethane converts to 11 kg of TNT. In addition, 2% of sensitizer was added to aid initiation of the detonation. Figure 3-28 schematically shows the explosive charge location with respect to the specimen. The charge was included in a plastic cylindrical vessel with a diameter of 241 mm (9 1/2 inches). The charge weight is denoted as  $w$ , and the height of the charge,  $h$ , within the container varies depending on the charge volume. The standoff distance,  $x$ , is horizontal distance between the center of the explosive charge and the closest point of the column to the charge. The charge height is taken as the vertical distance from ground to the center of the charge.

#### 3.3.3 Experimental Cases

Summary of the column test cases is presented in Table 3-6 along with the description of test observations. Exact values of charge weights and standoff distances are not presented for security reasons; instead these values were normalized by the parameters of  $X$  and  $W$ , respectively. Three parameters were considered in deciding test conditions: height of charge,  $z$ , standoff distance,  $x$ , and weight of charge,  $w$ . Height was chosen to be 0.25 m representative of the height for the assumed blast scenario, which was 1 m for the prototype bridge. Scale distances,  $Z$ , given by:

$$Z = \frac{x}{W^{1/3}} \quad (3-31)$$

are also provided for each test case to compare with the case of the assumed terrorist attack scenario for the prototype bridge. Note that the smaller scale distances create larger pressure and impulse. The maximum blast charge was limited to  $W$  due to the constraints at the test site. Due to this constraint of maximum blast charge weight, the target deformation of the columns was achieved by changing the standoff distances.

The target deformations of the columns were set equal to 4 degree and 2 degree of rotational angle at the base of the column for Test 1 and Test 2, respectively. These deformation limits were chosen based on recommended design limits by Mays and Smith (1995) for reinforced concrete beams and slabs. The support rotations of 2 degree and 4 degree correspond to minor damage and extensive plastic hinging of the column, respectively. In this context, minor damage means that personnel and equipment should be protected against fragments coming from damage of the structural members.

These rotational angles at the bottom of the column were obtained by assuming that the maximum deformation of the column occurred at the height of explosion, i.e. 0.25 m from the ground. This maximum deformation was calculated by simplified analysis using an equivalent SDOF system and energy conservation. The details of this simplified analysis will be presented in Section 3.4 of the analytical study. The standoff distances and charge weights of Tests 3 and 4 on steel jacketed RC columns were selected to be the ones for Tests 1 and 2 on RC columns, respectively.

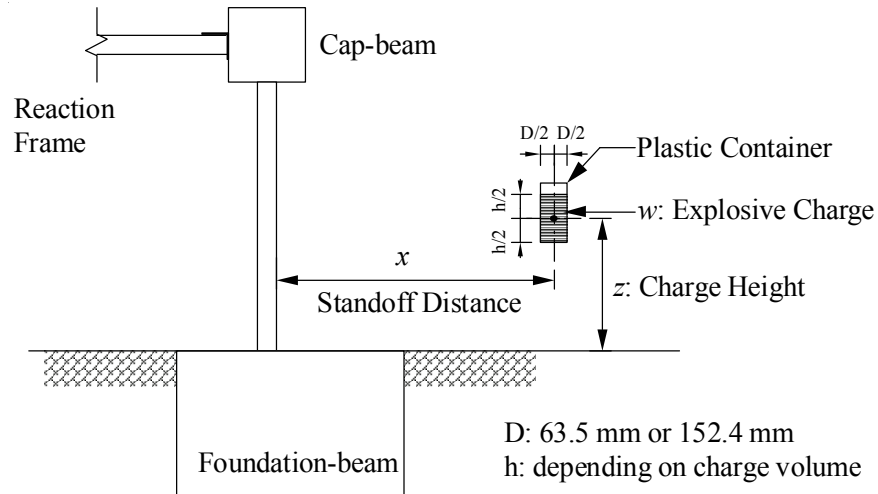


**Figure 3-28 Explosive Charge Location**

**Table 3-6 Summary of Column Test Cases and Test Observations**

Test Num.	Column	Objective	Charge Weight	Standoff Distance	Charge Height (m)	Scaled Distance ( $X/W^{0.333}$ )	Test Observations
Prototype	---	---	---	---	---	3.74	---
Test 1	RC1	$\theta = 4$ deg Collapse	W	2.16 X	0.250	2.16	Shear failure at bottom
Test 2	RC2	$\theta = 2$ deg Minor Damage	W	3.25 X	0.250	3.25	Onset of shear failure at bottom
Test 3	SJ2	Same as Test 1	W	2.16 X	0.250	2.16	Shear failure at bottom
Test 4	SJ1	Same as Test 2	W	3.25 X	0.250	3.25	Shear failure at bottom

### 3.3.4 Experimental Observations

#### 3.3.4.1 Test 1 for Column RC1

Column RC1 was tested using an explosion of charge weight  $W$  at a standoff distance of  $2.16X$  and height of 0.25 m, intended to induce 4 degree of total elastic and plastic rotational angle at the bottom of the column. Figure 3-29 illustrates the deformation and damage of the column after Test 1, showing left, blast, right and back side views as defined in this figure. Column RC1 did not to exhibit a ductile behavior under blast loading, but rather failed in shear at the base of the column. Figures 3-30 and 3-31 are the left side view and front view of the column after the test, respectively. As shown in Figure 3-30 by lines showing the original position of the specimen, the column was tilted towards the back side, rotating around a point at the top of the column after the column sheared off at the bottom.

Original position of the column at the footing is shown in Figure 3-32, and Figure 3-33 shows a close-up picture of the fracture surface at the footing. This surface was the construction joint. However, as described in the subsection on model fabrication, laitance was removed from the surface of the footing before casting column concrete. The fracture surfaces of longitudinal bars coming out from the footing are shown in Figure 3-34. The bottom part of the column was blown off as shown in Figures 3-35 and 3-36. The front face of the column was damaged more heavily than the back face because of the blast pressures acting on the front face. Many small pits were observed on the front side of the column around the blast charge height as shown in Figure 3-37.

Figures 3-38 and 3-39 show the top of the column from left and right side views. A 40 mm (1 9/16 in) gap between the cap beam and the column was observed on the front side of the column, and the width of a second crack positioned at 72 mm (2 13/16 in) from the top of the column on the front side was 3 mm (1/8 in), as shown in Figures 3-38. Figure 3-40 shows the top of the column from a front view, and Figure 3-41 is a close-up picture of the gap at the top of the column. Ten longitudinal bars were fractured out of total sixteen bars at that location. As shown in Figure 3-42, the cover concrete spalled off on the back of the column to the height of 90 mm (3 17/32 in) from the top of the column due to the large deformation of the column, but no

damage was observed in the core concrete because of the confinement by transverse reinforcement in this plastic hinge region.

The progression of damage for this Column RC1 could be explained as follows, based on observations on the condition of the column after the test. First, plastic hinges were deemed to form at the bottom of the column and at the height of the explosion, and possibly at the top of the column as well. Evidence of forming plastic hinging around the explosion height could be seen in some cracks observed on the back side of the column as shown in Figure 3-29. This figure also shows that the part of the column from the bottom up to a height of about 838 mm (33 in) from that point had a slight curvature outward to the back side, which agrees with the moment that would develop under this assumption. Then, while these plastic hinges were developing or after these hinges formed, the column could have been sheared off at its base because the shear force that developed there exceeded the direct shear strength at that location. Finally, blast pressures acting on the column and/or inertia forces developed in the column masses pushed the cantilever column supported from the top to rotate towards the back side. As a result, a negative moment developed at the top of the column, leading to fracture of the steel bars on the tension side at the top of the column and the spalling off the cover concrete on the compression side, as shown in Figures 3-40 and 3-42, respectively. Accordingly, cracks were also observed on the blast side from mid-height to the top of the column. Figure 3-29 shows that the part of the column from the top down to a height of about 838 mm (33 in) from the base had slight curvature inward to the back side due to this negative moment developed at the top.

#### **3.3.4.2 Test 2 for Column RC2**

Column RC2 was tested using an explosion of charge weight  $W$  at a standoff distance of  $3.25 X$  and height of 0.25 m, intended to induce 2 degree of total elastic and plastic rotational angle at the bottom of the column. Figure 3-43 illustrates the deformation and damage of the column after Test 2, showing left, blast, right and back side views. The concrete spalling was observed around the bottom of the column. The column deformed towards the back side, as shown in Figure 3-43 (a), and a maximum deformation of 16 mm (5/8 in) was observed around one third of the height from the base of the column. This figure also shows that the column had a slight curvature outward to the back side. Figures 3-44 to 3-46 show the column after Test 2 from

front diagonal, back diagonal and front views. Note that these pictures were taken after the rubble was removed from the bottom part of the column.

Figures 3-47 and 3-48 show the bottom of the column from front diagonal and right side views, respectively, before the rubble was removed. The cover concrete on the front face was still loosely in place in the column, although this material had almost fallen apart from the column, whereas the one in the back face was completely disengaged from the column. This disengagement is called “direct spalling” of concrete in the literature reviewing the structural response of reinforced concrete structures subjected to blast load, as described in literature review. A compression stress wave, created by blast pressures in the front face, traveled through the column and reflected on the rear column face as a tension stress wave. As a result of this tension stress, the direct spalling of the cover concrete occurred. Figures 3-49 and 3-50 respectively show the bottom of the column from left and right side views after the rubble was removed. The cover concrete spalled off up to a height of 117 mm (4 5/8 in) from the bottom of the column. The shear deformations at the bottom part of the column can be observed by comparing against the longitudinal reinforcement vertical solid line in Figure 3-49. Therefore, Column RC2 was deemed to exhibit the onset of direct shear failure at the bottom of the column.

Figures 3-51 to 3-53 show the top of the column from right diagonal front, left diagonal front, and back side views, respectively. A gap of 4 mm (5/32 in) observed between the cap beam and the top of the column on its front side, as shown in Figure 3-51, was again attributed to the negative moment that developed at the top of the column. As shown in Figure 3-53, the cracks were not observed at the top of the column on the back side since this part was in compression.

#### **3.3.4.3 Test 3 for Column SJ2**

Column SJ2 was tested using an explosion of charge weight  $W$  at a standoff distance of  $2.16 X$  and height of 0.25 m, which are the same blast parameters as Test 1 for Column RC1. Figure 3-54 illustrates the deformation and damage of the column after Test 3, showing left, blast, right and back side views. Column SJ2 did not exhibit a ductile behavior subjected to blast loading, but rather failed in shear at the base of the column as observed in Test 1 for Column RC1. Figure 3-55 shows the column after Test 3 from a right side view. As shown in this figure by

lines showing the original position of the specimen, the column was tilted towards the back, rotating around a point at the top of the column after the column sheared off at the bottom. The steel jacketed column remained straight and no structural damage was observed along this column. Figure 3-56 shows a dent of 14 mm (9/16 in) deep observed after the test, which had not been seen before the test. Since this occurred 0.3 m above the height of the blast charge, it was attributed to the possible presence of an air pocket inside the steel shell due to lack of vibration during casting the concrete. This was not investigated further since this local imperfection has no impact on the results.

A lateral displacement of the bottom of the column at the footing of about 78 mm (3 1/16 in) was measured, as shown in Figure 3-57. Figure 3-58 shows the bottom of the column from a front diagonal view. Figure 3-59 is a close-up picture of the footing from a front diagonal view. The fracture of longitudinal bars coming out from the footing can be seen in this picture. All the longitudinal bars at the bottom of the column were observed to be fractured. The bottom part of the column from a back view is shown in Figure 3-60 and a close-up picture of the bottom part of the column from the same view is shown in Figure 3-61. The fracture of the longitudinal bars and the crushing of concrete inside the steel jacket at the bottom part of the column can be seen in these photos.

Figures 3-62 to 3-64 show the top of the column from front, side and back views. Because of the negative moment developed at the top of the column, a 6 mm (1/4 in) gap between the cap beam and the column was observed on the front side, as shown in Figure 3-62, but no gap or crack was observed there on the back side, as shown in Figure 3-64. Diagonal cracks were observed on the bottom face of the cap beam developed from the column, as shown in Figure 3-65.

#### **3.3.4.4 Test 4 for Column SJ1**

Column SJ1 was tested using an explosion of charge weight  $W$  at a standoff distance of  $3.25 X$  and height of 0.25 m, which are the same blast parameters as Test 2 for Column RC2. Figure 3-66 illustrates the deformation and damage of the column after Test 4, showing left, blast, right and back side views. As in Test 3 for Column SJ2, Column SJ1 failed in shear at the column base. As shown in Figure 3-67 by lines showing the original position of the specimen, the



column was tilted towards the back side rotating around a point at the top of the column after the column sheared off at the bottom. The steel jacketed column remained straight and no structural damage was observed along the column as observed in Test 3 for Column SJ1.

The lateral displacement at the base of the column at the footing was 83 mm (3 1/4 in), as shown in Figure 3-68. The deformed shapes of the two steel jacketed columns, namely Column SJ1 and SJ2, were almost the same. All the longitudinal bars at the base of Column SJ1 were also fractured. Figure 3-69 from front diagonal view shows the fractured longitudinal bars coming out from the footing. A crack was observed along the welding seam of the steel tube on the back side of the column base, as shown in Figure 3-70. Figures 3-71 and 3-72 show the bottom of the column from back diagonal view. The column was sheared off from the footing surface at the concrete joint. However, there was no crushing of concrete observed inside the steel jacket at the column base on the back side. Making a comparison of this damage of the column base on the back face with the one of Column RC2 of Test 2, in which blast parameters were the same, here the concrete inside the steel jacket had not been damaged whereas the cover concrete of the RC column was disengaged as previously shown in Figures 3-49 and 3-50 due to direct spalling. From this comparison, it can be concluded that steel jacketing is effective to protect against direct spalling of the concrete, even though it is ineffective to prevent the observed direct shear failure.

Figures 3-73 to 3-74 show the top of the column from front and back views. Because of the negative moment developed at the top of the column, a 6 mm (1/4 in) gap between the cap beam and the column was observed on the front side, as shown in Figure 3-73. There were also some cracks between the cap beam and the column top on the back side, as shown in Figure 3-74, but these cracks closed at the center on the back side.

### **3.3.5 Summary**

The standard ductile RC and non-ductile RC columns retrofitted with steel jackets were not found to exhibit a ductile behavior under blast loading, but rather failed in shear at the base, contrary to the CFST columns which were shown to be effective to resist blast loadings in previous experiments. The steel jacketed columns, although visually resembling the CFST columns, are significantly different in construction due to the presence of gaps at the column top

and base purposely intended to prevent composite actions at the ends of the column. These gaps also produced a discontinuity of shear resistance at these locations, which resulted in the observed direct shear failure. However, steel jacketing was effective to prevent direct spalling of concrete.

### **3.4 Analytical Study**

#### **3.4.1 General**

This section compares the experimental results of the columns with the analytical results. First, moment-curvature analysis was conducted to calculate the structural properties of the columns, namely the plastic moment capacity and the flexural stiffness. These structural properties were required in the following simple plastic analyses and simplified blast analyses. Second, simple plastic analyses were conducted to calculate ultimate lateral load capacity of the columns and reactions. After that, simplified blast analyses were conducted to compare with the deformation and damage of the columns. Then, a modified calculation method for direct shear strength was proposed by considering moment-direct shear interaction, and this strength was compared with the reaction forces calculated by the simple plastic analyses. Finally, comparisons of breaching and spalling of RC members between the column test results and the design equations are presented.

#### **3.4.2 Moment-Curvature Analysis**

The following simplified blast analysis and simple plastic analysis require the plastic moment capacity and flexural stiffness of the column. Therefore, moment-curvature relationships were calculated using XTRACT for the test specimens. Three sections were calculated, namely a section at plastic hinge zone of the RC columns and two sections at the base and middle of the steel jacketed RC columns. For the steel jacketed RC columns, cross-section analysis did not consider the contribution of the jacket at the base section because the steel jacket was not provided at that location due to the gap between the footing and the column. Presence of the steel jacket was considered at the cross-section at mid-height of the column. The moment-curvature relationships were developed based on a plane section analysis assuming that a plane section remained plane when subjected to bending moment. In this plane section analysis, strain distribution on the section was assumed to remain linear.

These analyses were conducted using the strength values obtained from the compression tests of concrete cylinders and the tensile tests of reinforcement bars and steel plates from which the steel jackets were fabricated. For the analyses, concrete strength,  $f'_c$ , was taken as equal to 32.1 MPa (4.65 ksi). Young's modulus,  $E_c$ , was calculated by Equation 3-7 as per ACI (2004). Yield strength and Young's modulus of D-3 steel wire used as reinforcement (as described in Section 3.2.5.2) were equal to 501 MPa (72.58 ksi) and 195,007 MPa (28,276 ksi), respectively. Yield strength and Young's modulus of the steel jacket were equal to 254 MPa (36.85 ksi) and 207,216 MPa (30,046 ksi), respectively. The above concrete strength and yield stress of steel were multiplied by 1.25 and 1.2, respectively, to account for strength magnification at large strain rates under impulsive conditions (Mays and Smith 1995). The Mander model presented in Section 3.2.3.2 was used for the constitutive relationship of unconfined and confined concrete. The stress-strain relationships for longitudinal bars and steel jacket were idealized using a bi-linear elasto-perfectly plastic behavior. The details of section and material models are provided in Appendix F.

Figures 3-75 to 3-77 present the results of moment-curvature analyses for the RC column section, and for the steel jacketed RC column at base and middle sections, respectively. Solid lines represent the results of these analyses and dashed lines represent the corresponding bi-linear elasto-perfectly plastic curves used in the subsequent simple analyses. To simplify the moment-curvature relationships, these bi-linear curves were obtained such that the energy under the moment-curvature relationships of both curves was equal when reaching an ultimate curvature displacement. The section properties obtained from the cross-section analyses are summarized in Table 3-7. The details of how these results were obtained are provided in Appendix F.

**Table 3-7 Summary of Moment-Curvature Analyses**

Section	Effective Yield Curvature 1/m (1/in)	Effective Yield Moment kN-m (kip-in)	Effective Flexural Stiffness kN-m <sup>2</sup> (kip-in <sup>2</sup> )	Ultimate Curvature 1/m (1/in)
RC	0.030 (0.0008)	14.0 (124.0)	463.8 (161,600)	0.628 (0.0159)
SJ at bottom	0.020 (0.0005)	34.5 (305.0)	1698.2 (591,700)	0.508 (0.0129)
SJ at middle	0.032 (0.0008)	15.2 (134.6)	455.8 (158,800)	0.585 (0.0149)

### 3.4.3 Simple Plastic Analysis

Simple plastic analyses were conducted to calculate the ultimate lateral load capacity and reactions of the RC column and the steel jacketed RC column. A simple plastic analysis is suitable to calculate ultimate global structural capacities based on simple calculations. In this analysis, a rigid-perfectly plastic hinge model is assumed with a zero-length plastic hinge. The details of this analysis are presented in text books (such as in Bruneau et al. 1998). The step-by-step method of analysis was selected. This analytical method follows the structural behavior step-by-step, from the initial elastic stage up to collapse, through plastic hinging formations. The blast pressure was assumed to load the column as a point load acting at the height of the blast charge. Standard solutions presented in *LFRD Manual of Steel Construction* (AISC 2001) were used to calculate moment diagrams and deflections of the columns because the target structure was simply a beam fixed at both ends subjected to a concentrated load.

Figure 3-78 illustrates for the analyzed RC column, the incremental moment diagram and total moment diagram for each analysis step. In Step 1, the point load was increased until the plastic moment capacity,  $M_p$ , of 14.0 kN-m (124.0 kip-in) previously calculated by moment curvature analysis was reached at the base of the column. In Step 2, a modified structure fixed at the top and supported at the bottom was used to calculate the incremental load that produced for the additional load at which a plastic hinge at the height of the blast charge. Finally, in Step 3, a

cantilever fixed at the top was analyzed until the top of the column reached the plastic moment capacity. In these analyses, reactions at both top and base of the column and deflections at the load point were also calculated in each step and are plotted in Figure 3-79. Solid line with solid squares, dashed line with solid circles, and broken line with open circles represent, respectively, the applied load at the explosion height and reaction force at the base and the top of the column. As shown in this graph, much higher reaction force was developed at the base than the top because the load was applied close to the base. The maximum resulting reaction forces at the base and top were 112.1 kN (25.2 kip) and 22.4 kN (5.0 kip), respectively. The detailed calculations are presented in Appendix G.

Figure 3-80 illustrates the simple plastic analysis results of the steel jacket RC column obtained following the same step-by-step procedure. In this analysis, the plastic moment capacity at both top and base was taken as  $M_{pb}$  of 15.2 kN-m (134.6 kip-in) which was calculated from the reinforced concrete section without a steel jacket, and the one at the explosion height was taken as  $M_{pm}$  of 34.5 kN-m (305.0 kip-in) which was calculated from the steel jacketed reinforced concrete section acting as a composite section. The first plastic hinge formed at the base (as for the RC column), but the second plastic hinge formed at the top because the plastic moment capacity at the explosion height was more than twice the one at both top and base. The last plastic hinge formed at the height of the blast charge. Reactions at both top and base of the column and deflection at the load point were also calculated and are plotted in Figure 3-81. This graph shows that proportionally much higher reaction force developed at the base than at the top compared to the RC column. The maximum resulting reaction forces at the base and top were 198.7 kN (44.7 kip) and 39.7 kN (8.9 kip), respectively. The detailed calculations are presented in Appendix G.

#### **3.4.4 Simplified Blast Analysis by Equivalent SDOF System**

The blast parameters used in the experiments were determined based on the calculated maximum deformations of the columns. These maximum deformations were obtained by simplified analysis using an equivalent SDOF system and energy conservation (see Fujikura et al. 2007 for details). Essentially, this method considers an equivalent SDOF system having an elastic-

perfectly-plastic behavior, and assumes that all the energy imparted to the system by the blast loading is converted into internal strain energy.

Under these conditions, the maximum deformation due to impulsive-type blast loading,  $X_m$ , is given by:

$$X_m = \frac{1}{2} \left( \frac{I_{eq}^2}{K_{LM} m R_u} + X_E \right) \quad (3-32)$$

where  $I_{eq}$  is the equivalent uniform impulse per unit length,  $K_{LM}$  is the load-mass factor,  $m$  is the mass per unit length of the column,  $R_u$  is the strength per unit length of the column and  $X_E$  is the displacement at the onset of plastic behavior. In this analysis,  $I_{eq}$  was calculated by:

$$I_{eq} = \beta D i_{eq} \quad (3-33)$$

where  $i_{eq}$  is the equivalent uniform impulse per unit area,  $D$  is the column diameter and  $\beta$  is the factor to account for the reduction of pressures on the circular column due to its circular shape. This factor  $\beta$  could be taken as 0.45. This value of 0.45 was obtained from previous blast test results of CFST columns by comparing the observed maximum deformations with the results predicted by this simplified analysis.

The quantity of this equivalent uniform impulse per unit area,  $i_{eq}$ , in Equation 3-33 was calculated by:

$$i_{eq} = \frac{\int_0^H i(z) \delta(z) dz}{\int_0^H \delta(z) dz} \quad (3-34)$$

where  $i(z)$  indicates the variation of impulse per unit area along the height of the column and  $\delta(z)$  is the normalized deflected shape of the column. In this analysis,  $i(z)$  was taken as the envelop of maximum impulse (per unit area) at any time along the height of the column. Values of  $i(z)$  were calculated using the program Bridge Explosive Loading (BEL 2004). BEL generates airblast pressures considering reflections of the blast wave on the deck and on the ground. The resulting values of  $i(z)$  are qualitatively shown in Figure 3-82 for Test 1 and Test 3 and in Figure 3-83 for Test 2 and Test 4 along with the envelop of maximum pressure along the height of the columns. Assuming that the in-span hinge develops at the height of the blast charge

and both top and base of the column, the normalized deflected shape,  $\delta(z)$ , for inelastic deformations after plastic hinging is given as a system of rigid-link members between those plastic hinges.

For the boundary conditions and this deflected shape, the load-mass factor is  $K_{LM} = 0.66$  and  $r_u$  is given by  $r_u = 28.8M_p/L^2$  where  $L$  is the height of the column, and  $M_p$  is the plastic moment capacity of the column calculated by XTRACT as presented previously. Finally,  $X_E$  is given by  $X_E = r_u/K_e$  where  $K_e$ , the unit elastic stiffness of the equivalent SDOF system, is given by  $K_e = 307EI_e/L^4$ . The flexural stiffness of the column,  $EI_e$ , was also calculated by XTRACT. Detail calculations of these simplified blast analyses are presented in Appendix H.

The results of these simplified analyses of Column RC1 for Test 1 and Column RC2 for Test 2 are summarized in Table 3-8. The maximum deformation (total elastic and plastic deformation) and plastic rotation at bottom respectively resulted in 19.2 mm and 4.4 deg for Test 1 and 9.5 mm and 2.2 deg for Test 2. The objective of Test 1 and Test 2 were respectively to induce extensive plastic rotation of the column base and minor damage to the column base as presented in Section 3.3.3 about the test cases. Although Column RC1 after Test 1 exhibited some level of inelastic flexural deformations, the magnitude of plastic rotation that happened before direct shear failure can not be reliably calculated for a lack of the reference point at the base of the column. From the measured deformations of Column RC2 after Test 2, the plastic rotation at the base of this column was 2.5 deg (0.043 rad) calculated from the experimental maximum deformation of 16 mm at a height of 370 mm from the base. This experimentally obtained rotation was larger than the prediction of 2.2 deg calculated by the simplified analysis because the bottom part of the column itself also deformed in shear, which was not considered in this analysis, occurred in the experiment.

**Table 3-8 Summary of Results of Simplified Blast Analysis (RC Tests)**

Test Num. and Column	Equivalent Uniform Impulse MPa-msec (psi-msec)	Ultimate resistance kN/m (kip/in)	Yield Deformation mm (in)	Maximum Deformation mm (in)	Plastic Rotation at Bottom $\theta$
Test 1 RC1	6.07 (880.7)	180 (1.03)	6.4 (1/4)	19.2 (3/4)	4.4
Test 2 RC2	3.81 (552.0)	180 (1.03)	6.4 (1/4)	9.5 (3/8)	2.2

### 3.4.5 Direct Shear Resistance of Test Column

Direct shear resistance of the test columns was compared with the reaction forces calculated by simple plastic analyses in the previous subsection. The literature related to the ultimate capacity of direct shear subjected to static loads was reviewed and presented in literature review, but no equations were found in the public domain literature to quantify its resistance under dynamic loads. Consequently, the direct shear resistance of test specimens was calculated using Equation 2-12 developed for static loads. The effect of dynamic loading was considered by incorporating the strain rate effect on material properties into this equation through dynamic increase factors. By considering the dynamic increase factors, Equation 2-12 is modified to become:

$$V_n = 0.8A_{vf}f_yD_{sy} + A_cK_1D_c \quad (3-35)$$

where  $D_{sy}$  and  $D_c$  are, respectively, the dynamic increase factors for yield stress of steel and for concrete strength.  $D_{sy}$  and  $D_c$  were taken as 1.2 and 1.25, respectively (Mays and Smith 1995).

Because the RC column section and the steel jacketed RC column section at the base of the columns had the same configuration and materials, they were calculated to have the same direct shear resistance as given by Equation 3-35. For  $A_{vf} = 309.6 \text{ mm}^2$ ,  $f_y = 501 \text{ MPa}$ ,  $A_c = 32365 \text{ mm}^2$  and  $K_1 = 2.8 \text{ MPa}$ , the direct shear resistance,  $V_n$ , of the tested columns is 262.2 kN (58.9 kip). This resistance is larger than the maximum reaction forces at the bottom of the columns calculated by the simple plastic analyses presented in Section 3.4.3, namely 112.1 kN and 238.4 kN for the RC column and the steel jacketed RC column, respectively. This calculation



indicated that those columns would not fail in direct shear at the base. However three of the test columns were found to fail in direct shear at their base during the experiments.

To explain the direct shear behavior observed in the tests, it was decided to investigate the possible reduction of direct shear strength in a plastic hinge region. When a large bending moment is applied at the reinforced concrete section, cracking occurs in the tension zone of the concrete section. At that point, flexure is resisted by the compression zone of the section and the steel reinforcement in the tension zone of the section. Direct shear resistance given by Equation 2-48 is the sum of the cohesion and friction resistance along the direct shear interface. In this calculation, the parts on both sides of the direct shear interface fully contact each other. However, on the cracked section under bending moment, the compression zone of the section is deemed to only contact along that section. This is particularly the case in regions of plastic hinging. Therefore, because, as observed experimentally and from simple plastic analyses, a plastic moment was developed at the base of the column, the above is considered to develop a moment-direct shear interaction. For this model, only the part of the section in compression is assumed to be able to resist the shear force since direct shear resistance is deemed unable to develop when two surfaces do not contact each other.

Figure 3-84 schematically shows a reinforced concrete section subjected to a bending moment used to formulate the moment-direct shear interaction model. This model is based on plane section analysis assuming that plane section remained plane when subjected to bending, consistently with all earlier moment-curvature analyses. The part of the section hatched in Figure 3-84 is in compression. By replacing  $A_{yf}$  and  $A_c$  in Equation 3-35 with  $A_{yf}'$  and  $A_c'$ , respectively, the modified direct shear resistance,  $V_n'$ , is given by:

$$V_n' = 0.8A_{yf}'f_yD_{sy} + A_c'K_1D_c \quad (3-36)$$

where  $A_{yf}'$  and  $A_c'$  are the area of longitudinal reinforcement and concrete in compression zone as shown in Figure 3-84. The position of neutral axis needs to be determined to calculate this compression zone. This neutral axis position was calculated by moment-curvature analysis as described in the previous subsection.

Figures 3-85 and 3-86 compare the new direct shear resistance at the base of the columns calculated per the above modified procedure with the shear force developed at the base of RC columns and steel jacketed RC columns, respectively, varying as a function of the moment developed at the base. These direct shear resistance were calculated by Equation 3-36, and the shear forces were obtained from the simple plastic analyses. A solid curve with open circles and a dashed line represent the direct shear resistance and the shear force developed, respectively, in these figures. For both columns, as the moment increases, the direct shear resistance decreases due to the shift of the neutral axis position towards the outer compression fiber. Obviously, a larger shear force demand develops at the column base as the moment increases due to the increase of the applied load. The intersection of these curves is the point where the shear force is equal to the direct shear resistance. This point occurs at a shear force of 63.0 kN (14.2 kip) and a corresponding moment of 11.8 kN-m (104.5 kip-in) for the RC column, and a shear force of 63.6 kN (14.3 kip) and the moment of 11.9 kN-m (105.5 kip-in) for the steel jacketed RC column. Figures 3-85 and 3-86 also show that direct shear failure was deemed to occur in both columns before the first plastic hinge develops at the base of the columns. According to these results, it appears that this moment-direct shear interaction model correctly allows capturing the experimentally observed behavior. Note that this moment-direct shear interaction model is to be compared with static shear force developed from the simple plastic mechanism.

### **3.4.6 Breaching and Spalling Resistance**

Breaching and spalling of the bottom part of the column were observed at the RC columns in Test 1 and Test 2, respectively. Therefore, the required thickness to prevent breaching and spalling were calculated for Test 1 and Test 2 to compare with the test specimens according to the design equations presented in the literature review section. The minimum thickness to prevent breaching,  $t_b$ , and spalling,  $t_s$ , are given by Equations 2-8 and 2-9, respectively. Note that these equations were derived from test data for reinforced concrete slabs.

Figure 3-28 compares the damage of Column RC1 and RC2 with their envelopes of maximum pressure distributions calculated by BEL. The higher pressures act around the bottom of the columns because of the reflection of the pressures on the ground. The maximum pressures in these envelopes were 160.7 MPa (23.3 ksi) in Test 1 and 82.1 MPa (11.9 ksi) in Test 2. The

minimum thickness of RC slabs is calculated using the blast standoff distance and charge weight by Equations 2-8 and 2-9. These equations are based on the airburst blast, and the reflection of pressure on the ground is not considered in these equations. Therefore, to consider this pressure magnification due to the reflection of the pressures on the ground, the blast standoff distance and explosive charge weight need to be adjusted to calculate the minimum thickness required when subjected to the high pressure reflected on the ground. These parameters were calculated back from the maximum pressures by using the public domain computer program AT-Blast (ARA 2004).

Using this approach, the required thickness to prevent breaching and spalling for Test 1 were calculated to be 358 mm (14.1 in) and 461 mm (18.2 in), respectively. For Test 2, the resulting required thickness was 304 mm (12.0 in) and 392 mm (15.4 in) for breaching and spalling, respectively. These thickness values were larger than the column diameter of 203 mm (8 in). Therefore, these calculations indicated that RC slabs with a thickness of 203 mm would undergo breaching when subjected to the blast pressures used in both tests. According to the experimental results, breaching was observed in Test 1, but spalling was observed in Test 2 instead of breaching as shown in Figure 3-43. Therefore, these equations based on RC slabs could be too conservative to quantify the breaching and spalling resistance of reinforced concrete circular columns. Also, these equations are possibly not applicable to seismically detailed ductile reinforced concrete columns since the RC slabs, for which these equations have been derived, are not typically detailed well with similarly closely spaced reinforcement. Note that no equation was found in the public domain literature to quantify the breaching and spalling resistance of circular shape reinforced concrete columns.

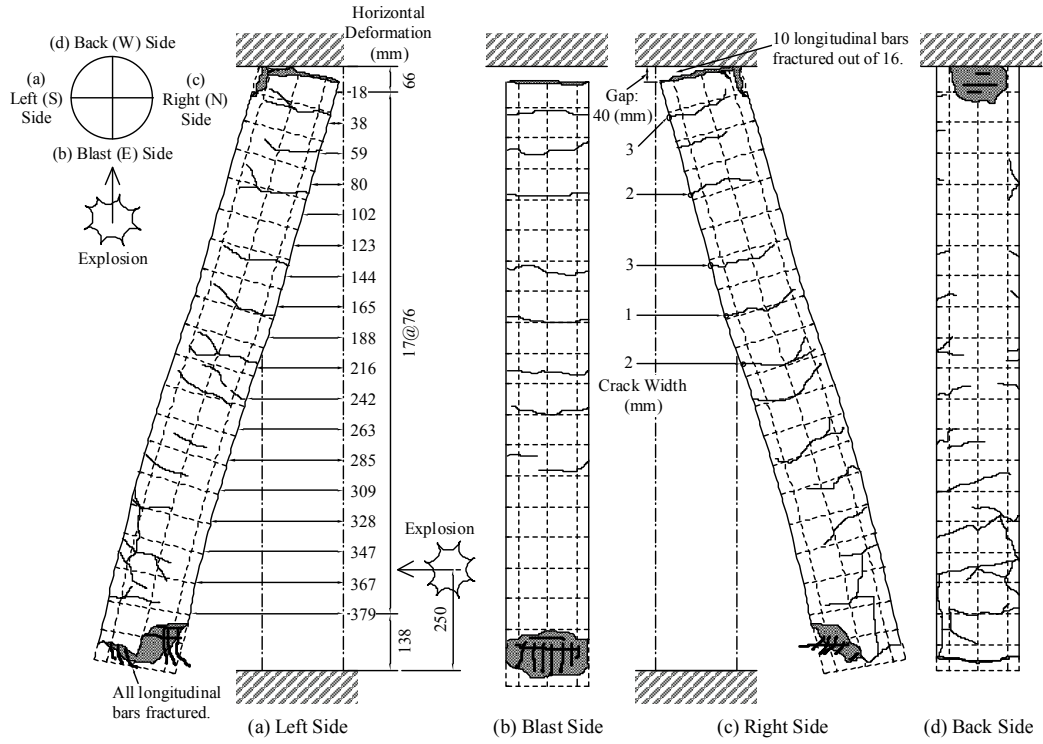


**Figure 3-29 Sketch of Column RC1 after Test 1**

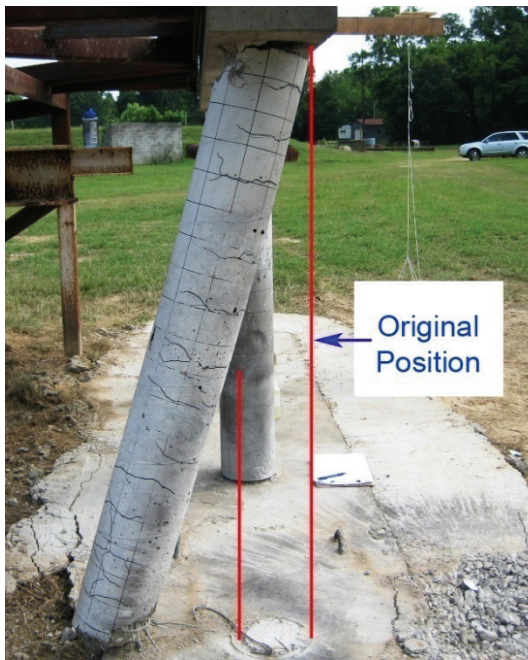


**Figure 3-30 Left Side View of Column RC1 (Test 1)**



**Figure 3-31 Front View of Column RC1 (Test 1)**



**Figure 3-32 Column RC1 at Bottom (Test 1)**



**Figure 3-33 Fracture Surface of Footing at Column RC1 (Test 1)**



**Figure 3-34 Fracture of Longitudinal Steel Bars at Footing (Test 1)**

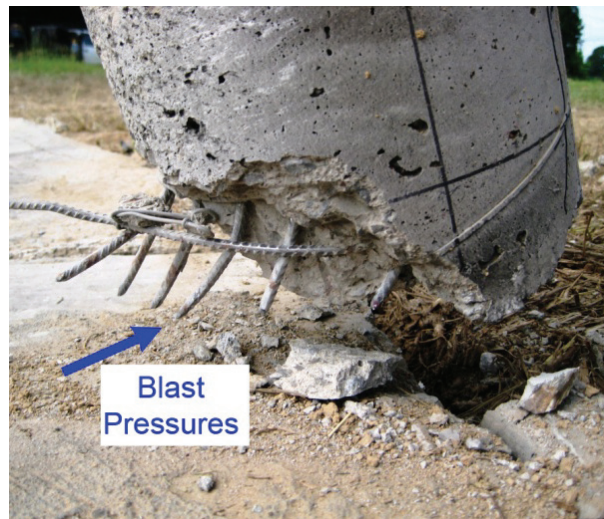


**Figure 3-35 Right Side View of Column RC1 at Bottom (Test 1)**

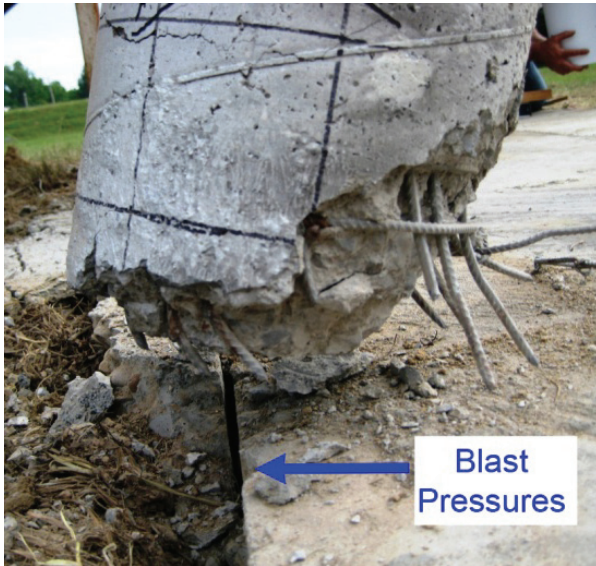


**Figure 3-36 Left Side View of Column RC1 at Bottom (Test 1)**

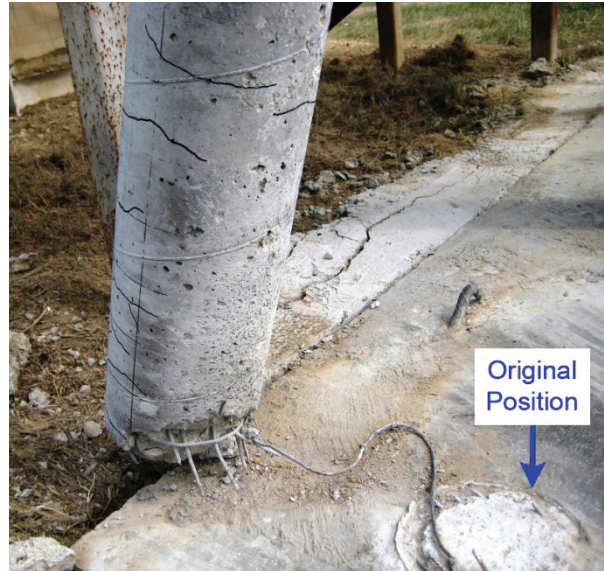


**Figure 3-37 Front Diagonal View of Column RC1 around Charge Height**

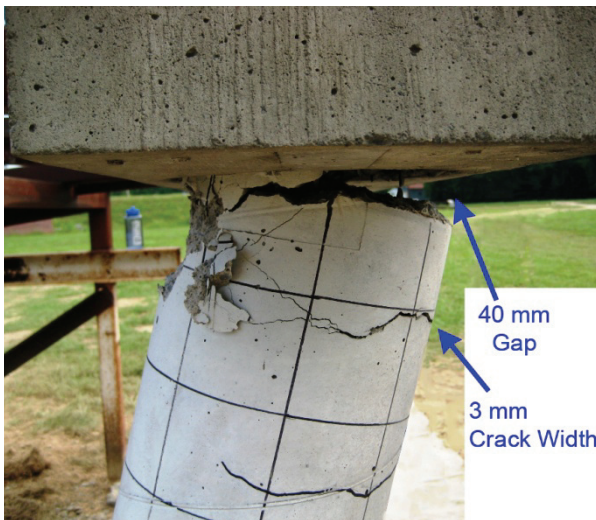


**Figure 3-38 Left Side View of Column RC1 at Top (Test 1)**



**Figure 3-39 Right Side View of Column RC1 at Top (Test 1)**



**Figure 3-40 Front View of Column RC1 at Top (Test 1)**



**Figure 3-41 Fracture interface of Column RC1 at Top (Test 1)**



**Figure 3-42 Back Diagonal View of Column RC1 at Top (Test 1)**

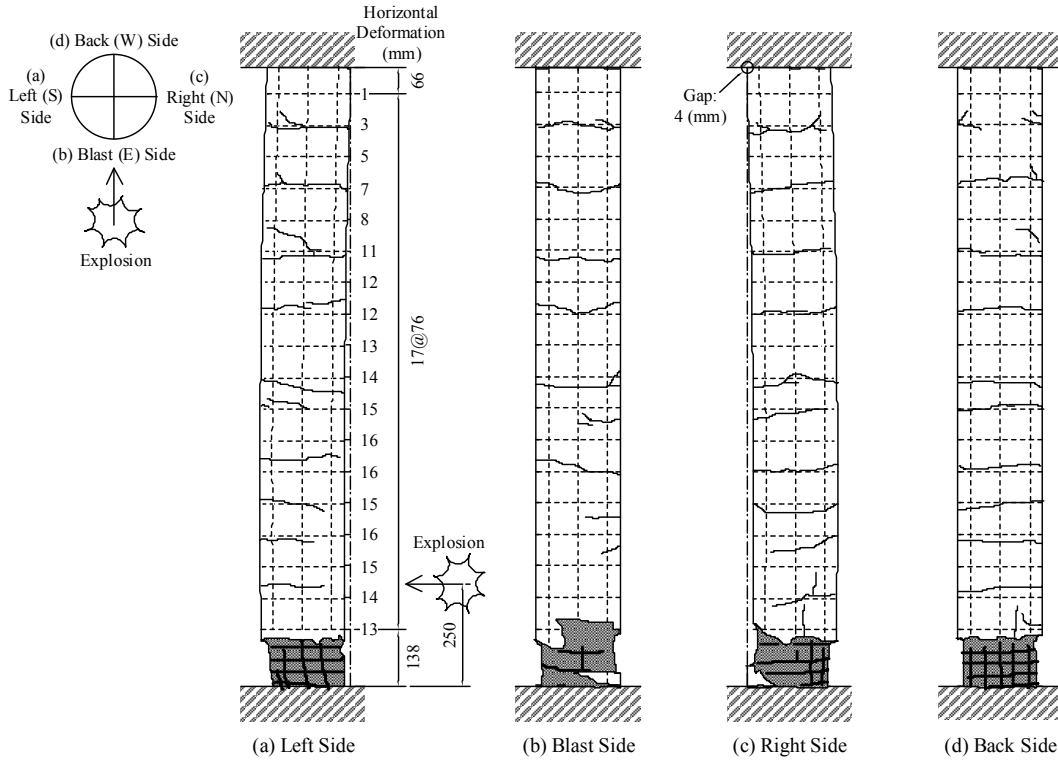


**Figure 3-43 Sketch of Column RC2 after Test 2**



**Figure 3-44 Front Diagonal View of Column RC2 (Test 2)**



**Figure 3-45 Back Diagonal View of Column RC2 (Test 2)**





**Figure 3-46 Front View of Column RC2 (Test 2)**



**Figure 3-47 Front Diagonal View of Column RC2 at Bottom (Test 2)**



**Figure 3-48 Right Side View of Column RC2 at Bottom (Test 2)**

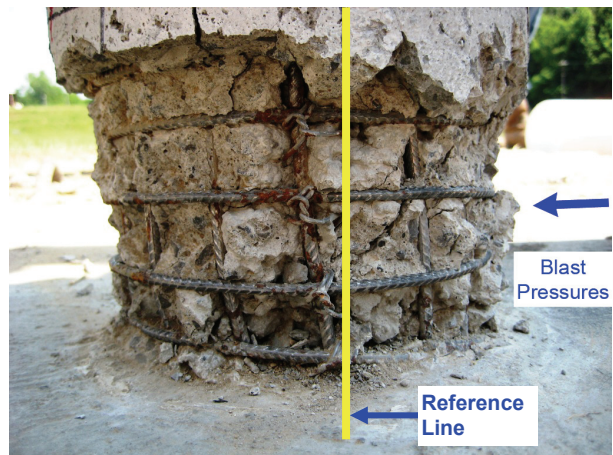


**Figure 3-49 Left Side View of Column RC2 at Bottom after Cover Concrete Removal (Test 2)**

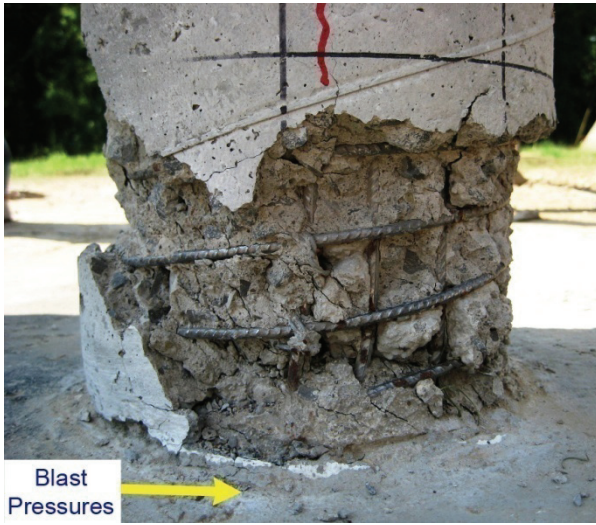


**Figure 3-50 Right Side View of Column RC2 at Bottom after Cover Concrete Removal (Test 2)**

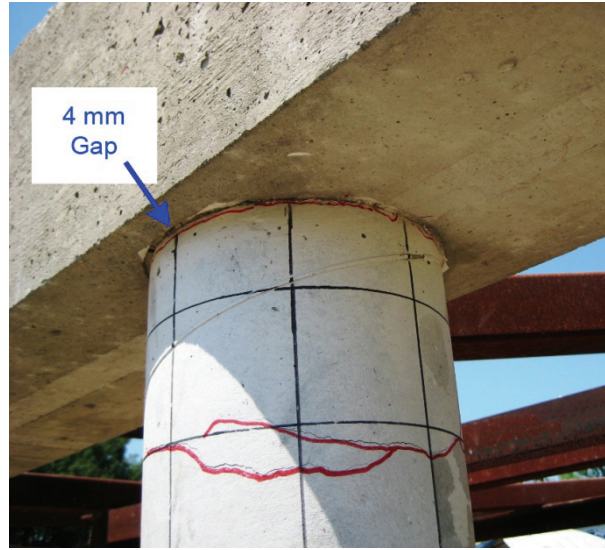


**Figure 3-51 Right Diagonal Front View Column RC2 at Top (Test 2)**



**Figure 3-52 Left Diagonal Front View of Column RC2 at Top (Test 2)**



**Figure 3-53 Back View of Column RC2 at Top (Test 2)**

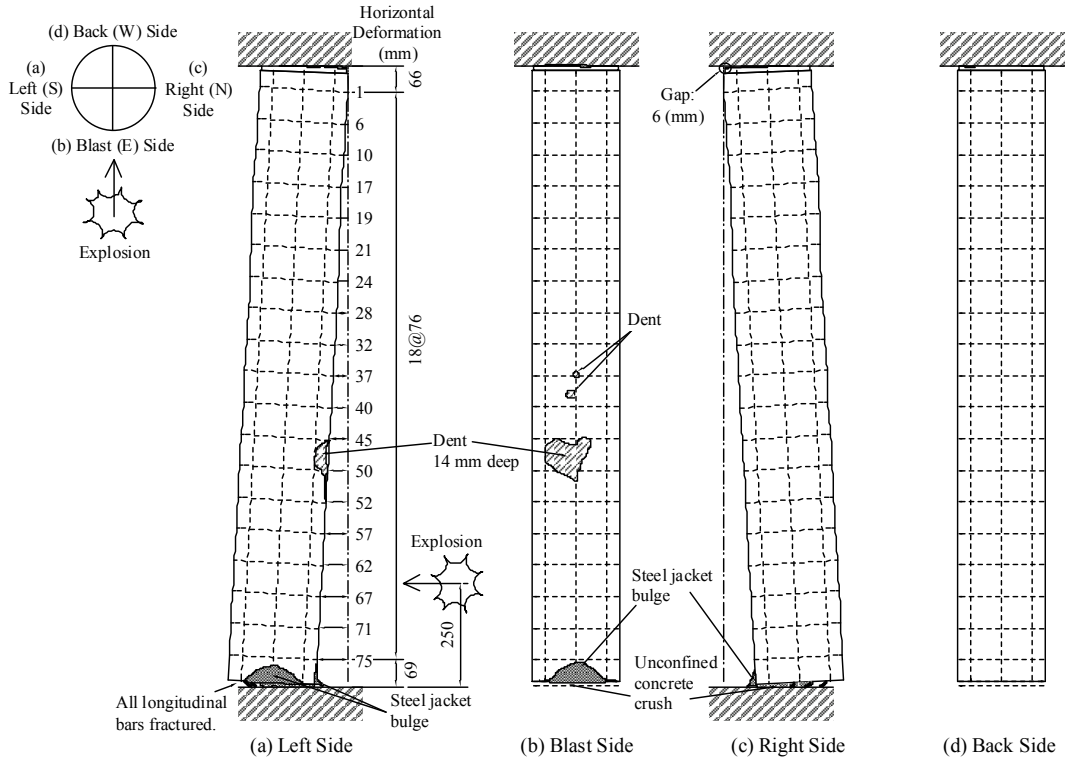


**Figure 3-54 Sketch of Column SJ2 after Test 3**

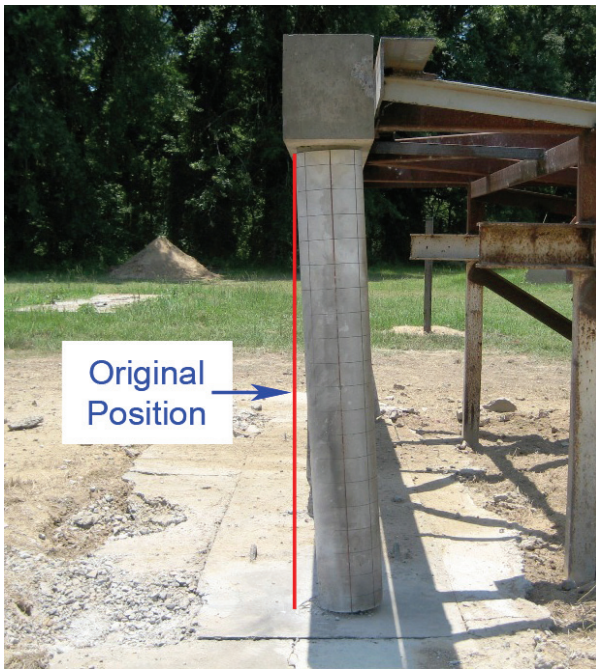


**Figure 3-55 Right Side View of Column SJ2 (Test 3)**



**Figure 3-56 Void at Column SJ2 after Test 3**

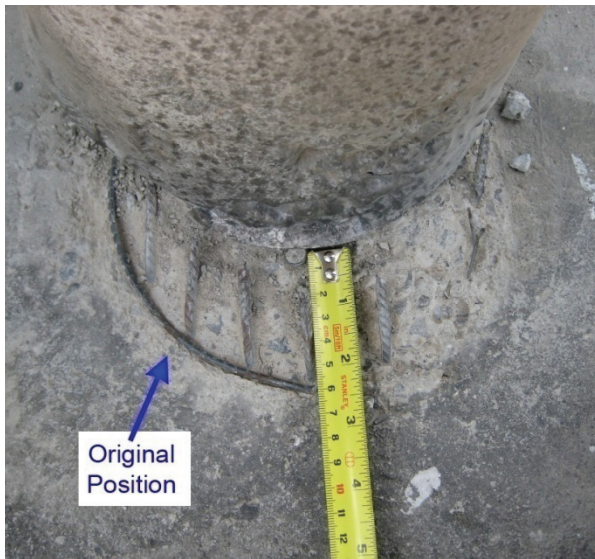


**Figure 3-57 Drift of Column SJ2 at Bottom (Test 3)**



**Figure 3-58 Front Diagonal View of Column SJ2 at Bottom (Test 3)**



**Figure 3-59 Fractures of Longitudinal Bars Column SJ2 at Bottom (Diagonally Front View, Test 3)**



**Figure 3-60 Back Diagonal View of Column SJ2 at Bottom (Test 3)**



**Figure 3-61 Close-in Back View of Column SJ2 at Bottom (Test 3)**

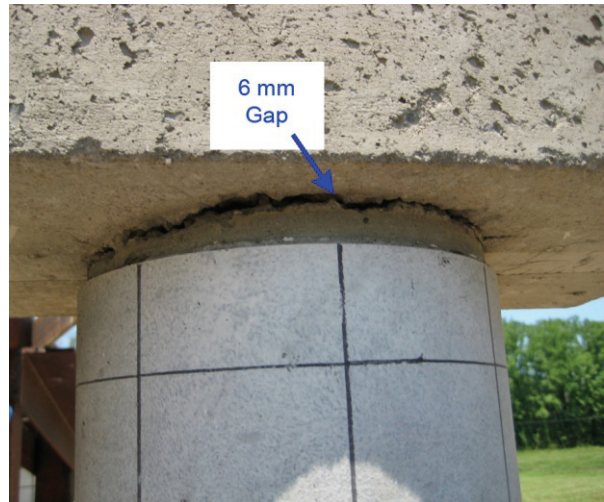


**Figure 3-62 Front View of Column SJ2 at Top (Test 3)**



**Figure 3-63 Left Side View of Column SJ2 at Top (Test 3)**



**Figure 3-64 Back View of Column SJ2 at Top (Test 3)**



**Figure 3-65 Cracks at Cap Beam of Column SJ2 (Test 3)**

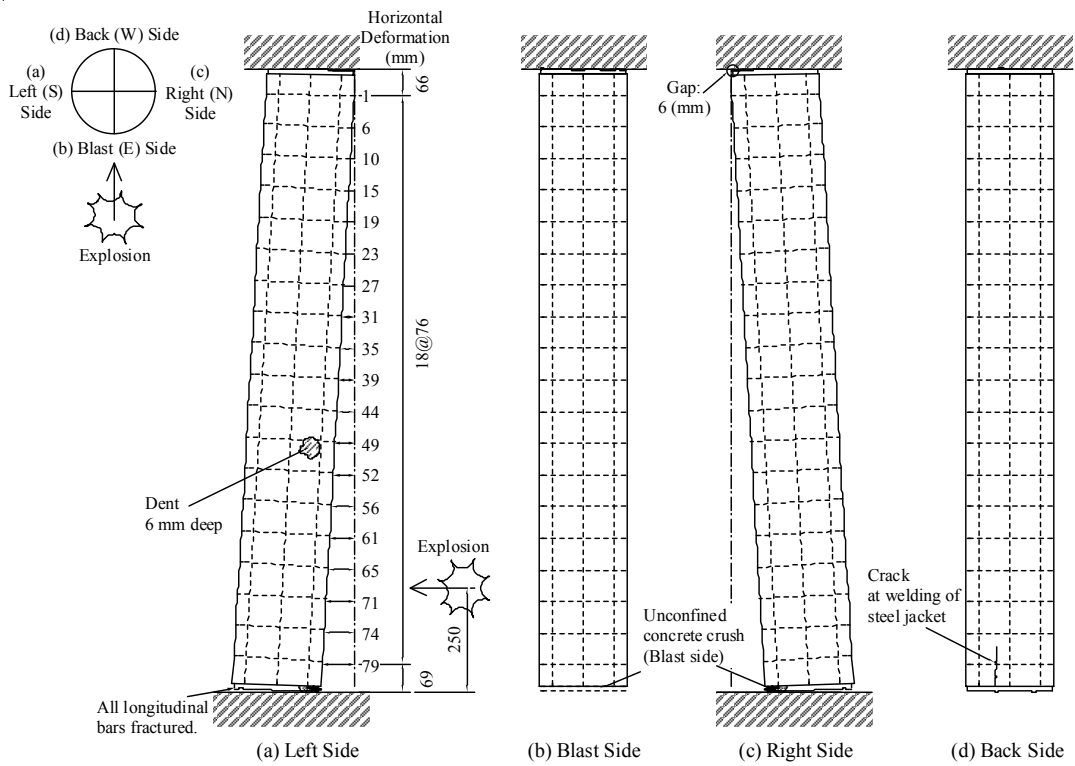


**Figure 3-66 Sketch of Column SJ1 after Test 4**



**Figure 3-67 Left Side View of Column SJ1 (Test 4)**



**Figure 3-68 Drift of Column SJ1 at Bottom (Test 4)**



**Figure 3-69 Fracture of Longitudinal Steel Bars at Footing (Front Diagonal View, Test 4)**

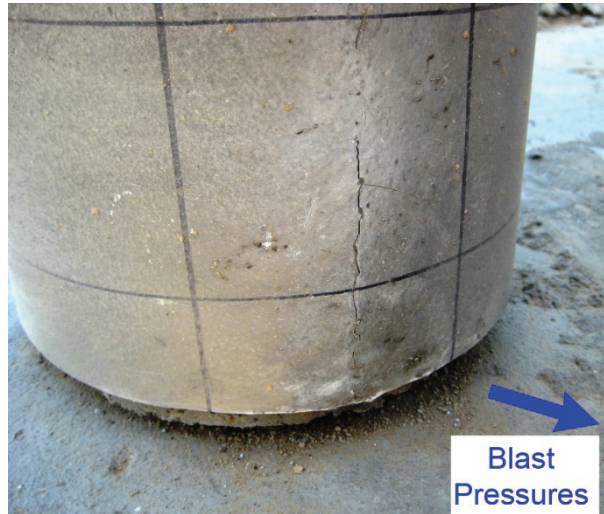


**Figure 3-70 Cracking of Steel Tube at Bottom of Column SJ1 at Bottom (Front Diagonal View, Test 4)**



**Figure 3-71 Back Diagonal View of Column SJ1 at Bottom (Test 4)**



**Figure 3-72 Back Diagonal View of Column SJ1 at Bottom (Test 4)**

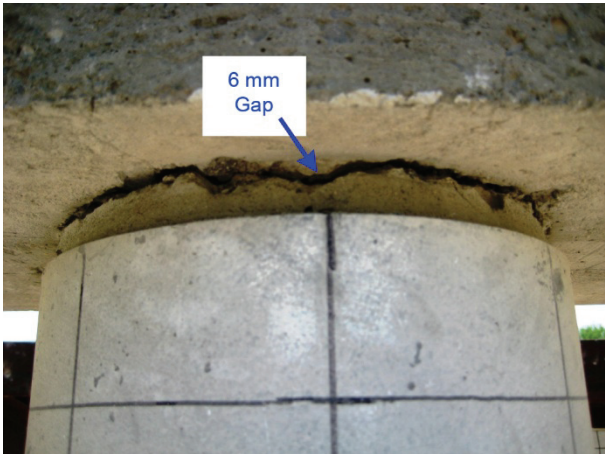


**Figure 3-73 Front View of Column SJ1 at Top (Test 4)**



**Figure 3-74 Back View of Column SJ1 at Top (Test 4)**



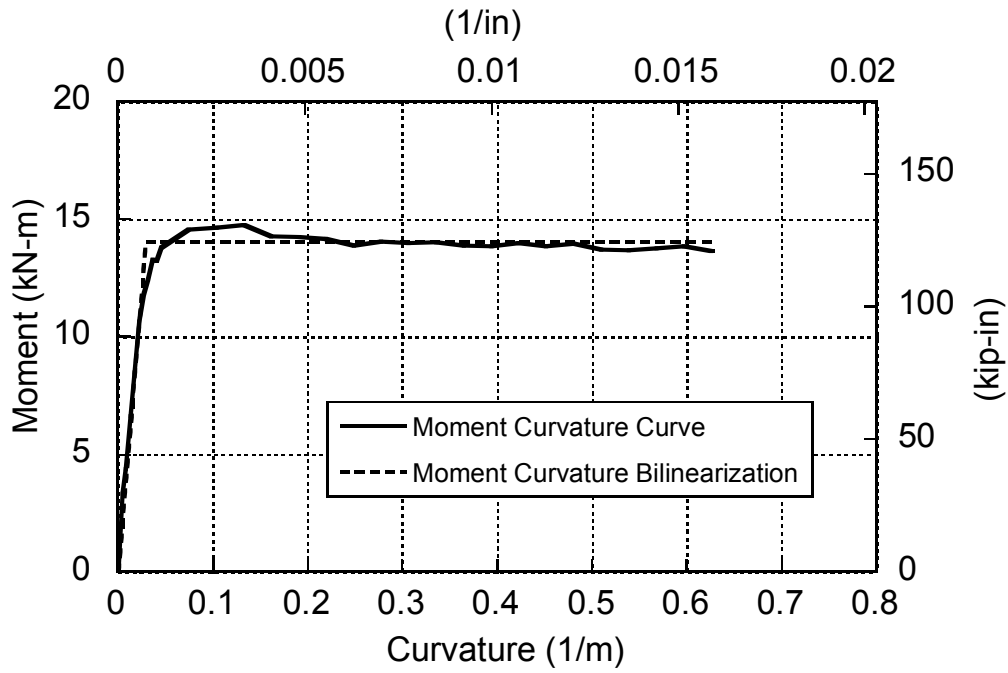


**Figure 3-75 Moment-Curvature Relationship for RC column**

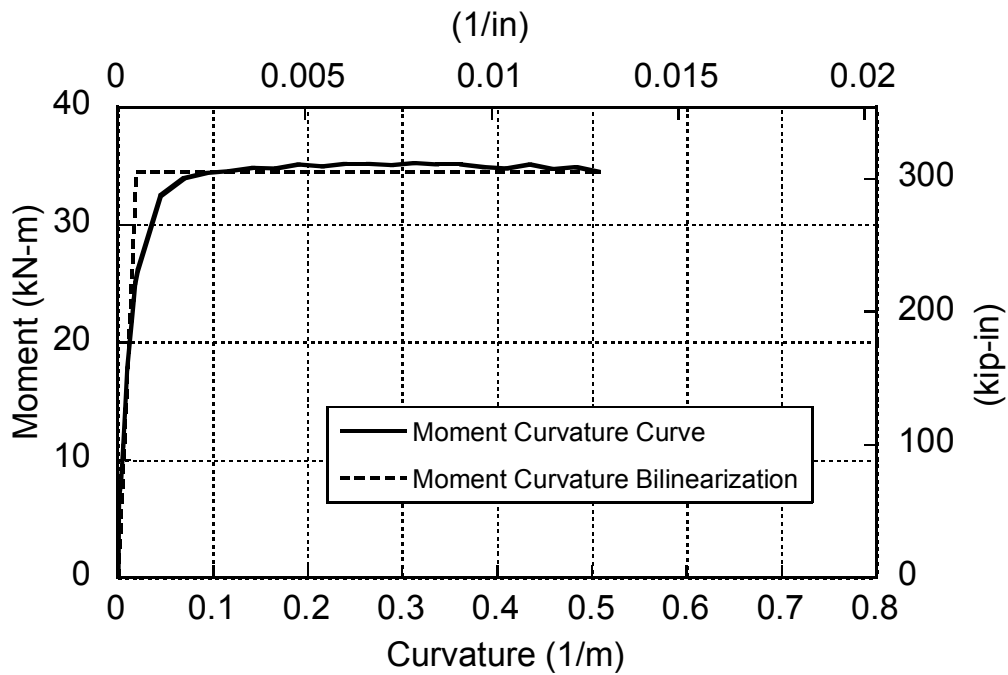


**Figure 3-76 Moment-Curvature Relationship for Steel Jacketed RC column at Middle Section**

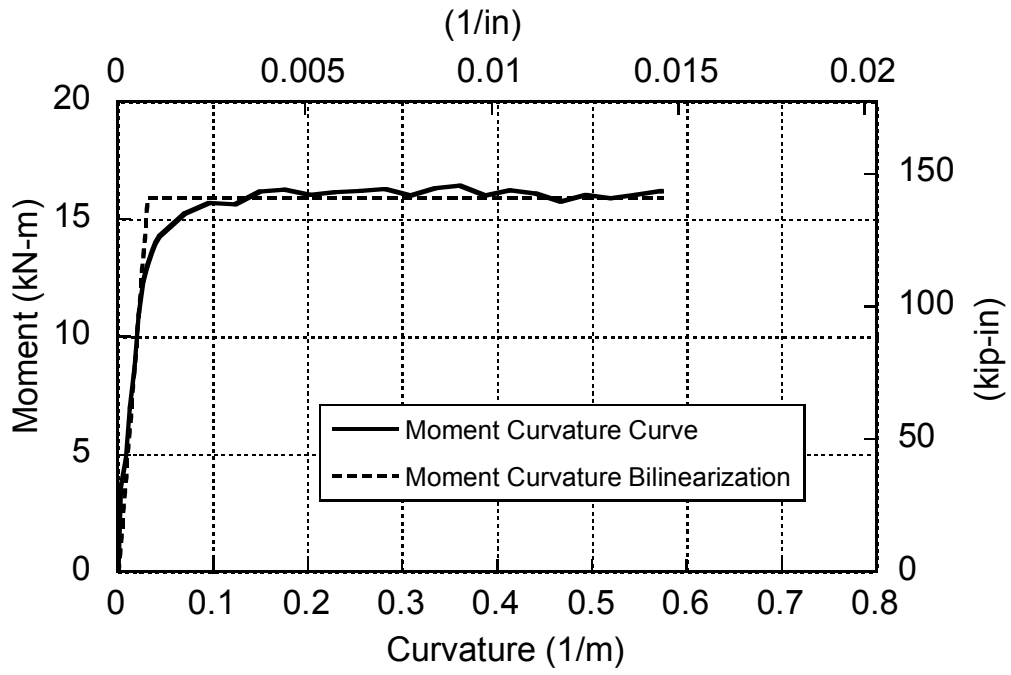


**Figure 3-77 Moment-Curvature Relationship for Steel Jacketed RC column at bottom Section**

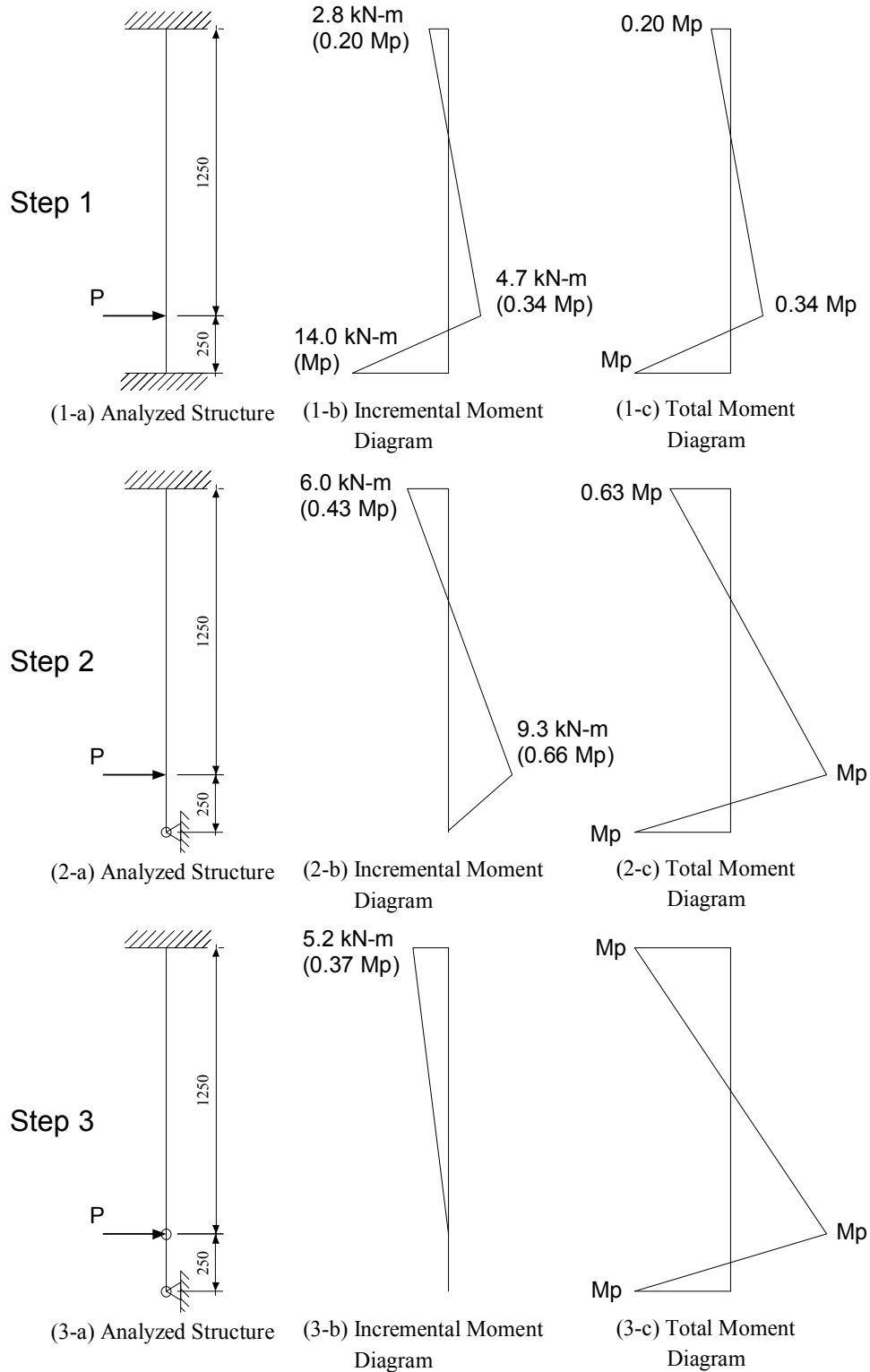


**Figure 3-78 Step-by-step Plastic Analysis of RC Column**

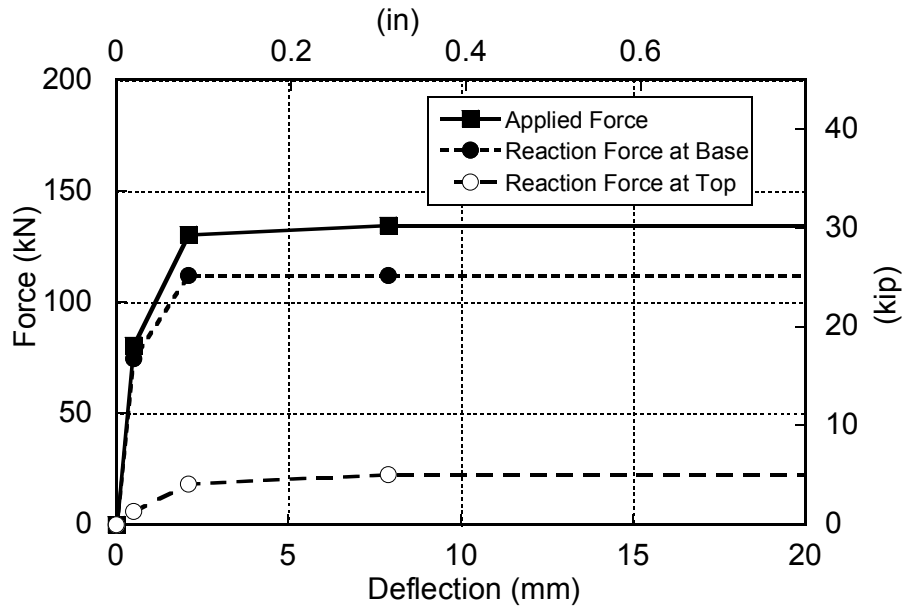


**Figure 3-79 History of Load versus Deflection at Load Point for RC Column**

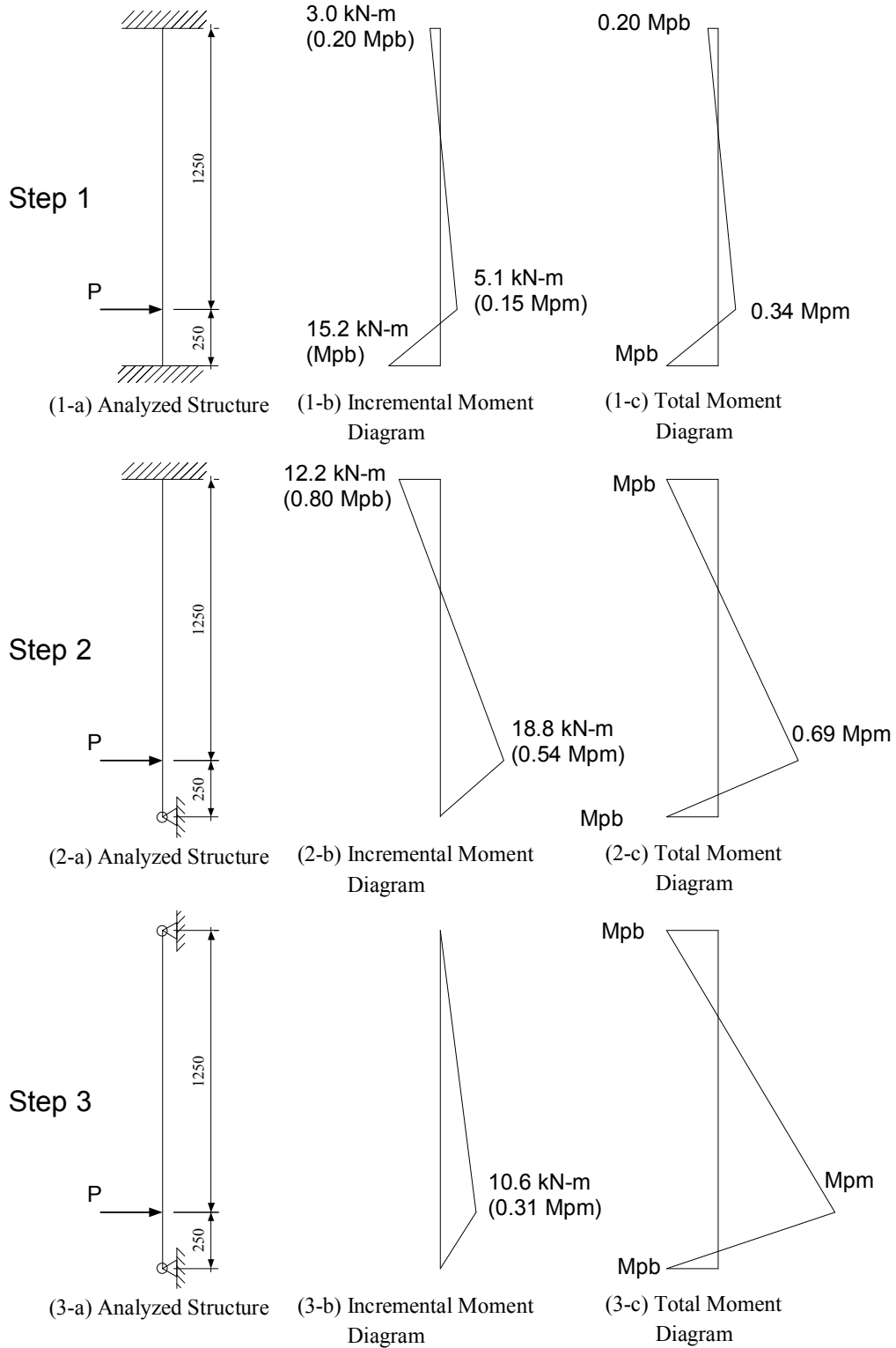


**Figure 3-80 Step-by-step Plastic Analysis of Steel Jacketed RC Column**

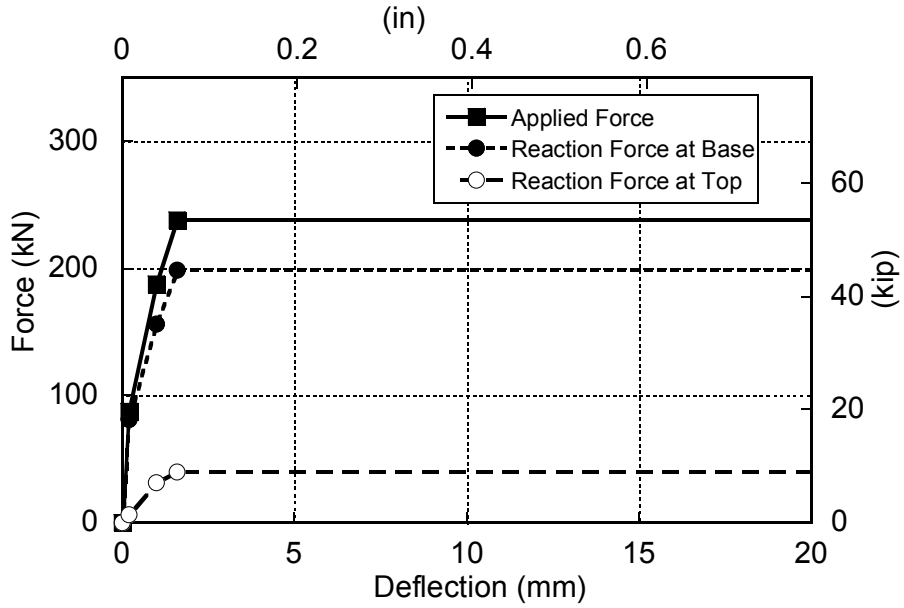


**Figure 3-81 History of Load versus Deflection at Load Point for RC Column**

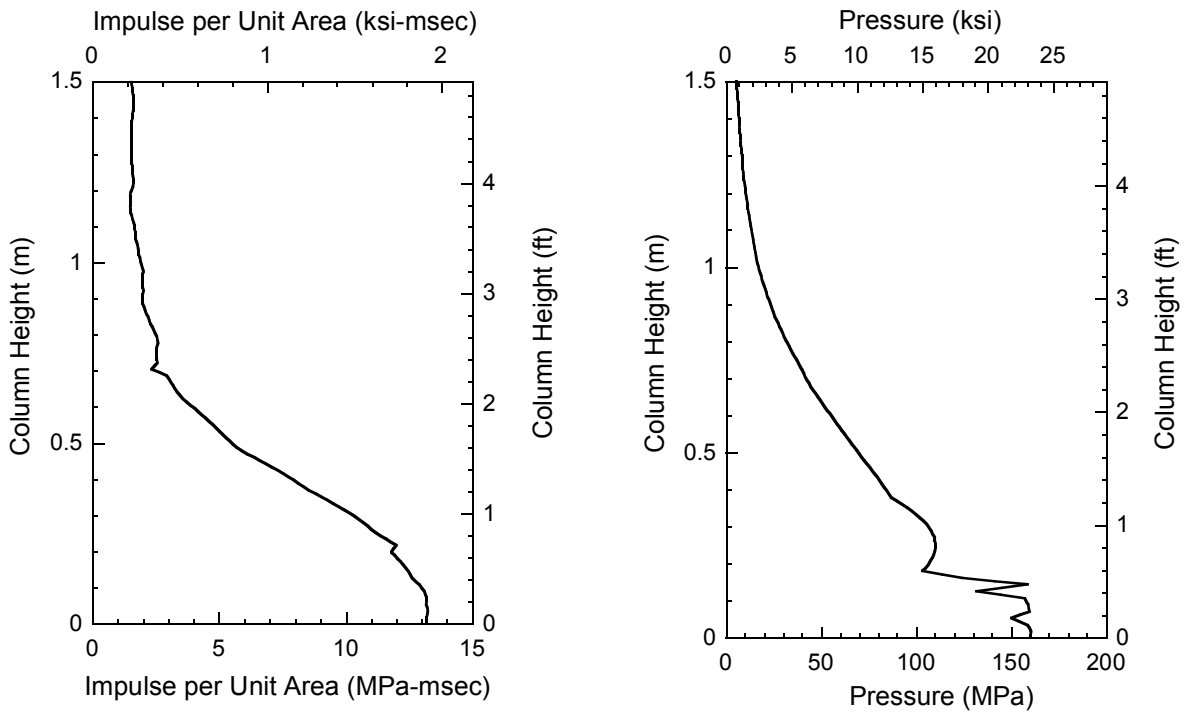


**Figure 3-82 Variation of Impulse and Peak Pressure along Height of Column for Column RC1 (Test 1) and SJ2 (Test 3)**

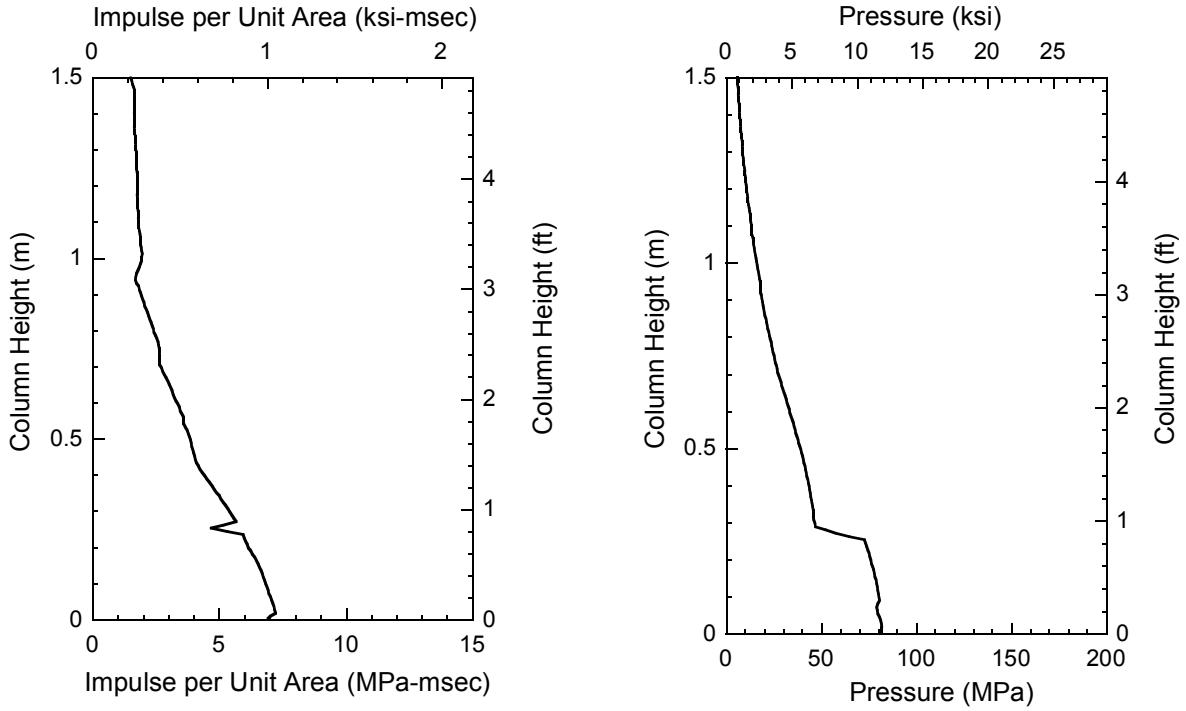


**Figure 3-83** Variation of Impulse and Peak Pressure along Height of Column for Column RC2 (Test 2) and SJ1 (Test 4)

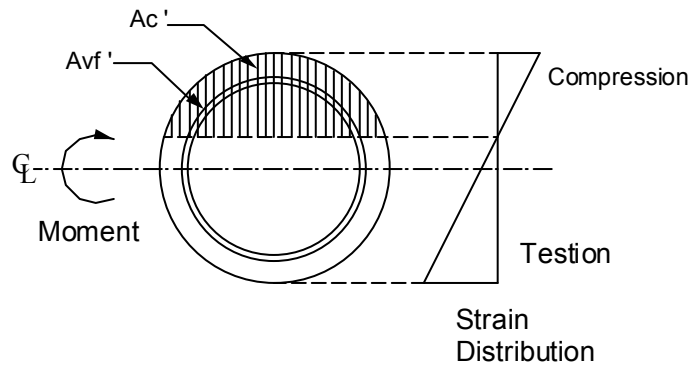


**Figure 3-84** RC Column under Bending Moment

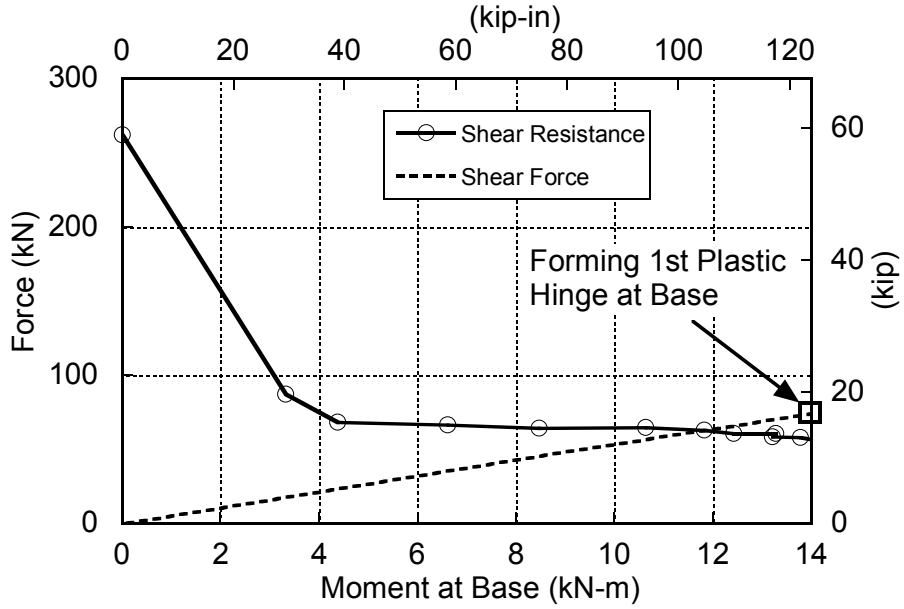


**Figure 3-85 Comparison of Shear Resistance with Shear Force at Base of RC Column**

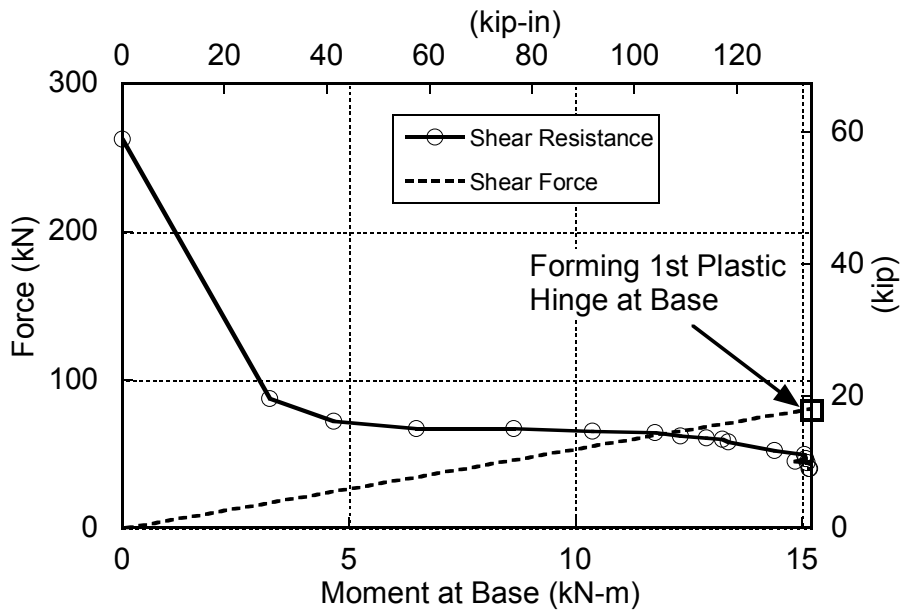
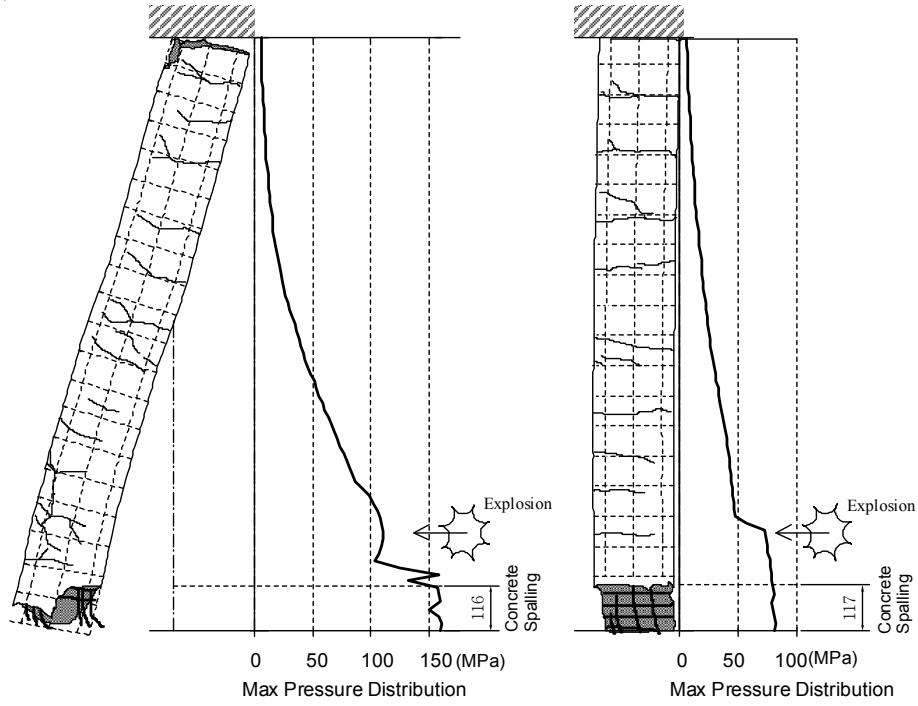


**Figure 3-86 Comparison of Shear Resistance with Shear Force at Base of Steel Jacketed RC Column**

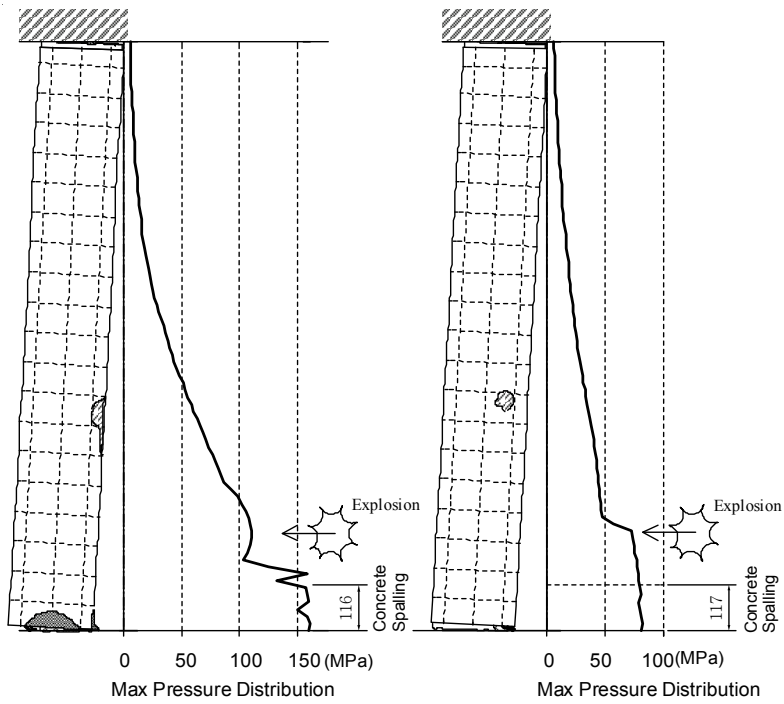




(a) Column RC1, Test 1

(b) Column RC2, Test 2

**Figure 3-87 Comparison of RC Column Damages and Pressure Distributions**



(a) Column SJ2, Test 3

(b) Column SJ1, Test 4

**Figure 3-88 Comparison of SJ Column Damages and Pressure Distributions**



## **SECTION 4**

# **DYNAMIC ANALYSIS OF BRIDGE PIER SUBJECTED TO BLAST LOADING**

### **4.1 Introduction**

Two series of blast tests on three different types of bridge columns showed that the performance of the proposed system of multi-column bent with CFST columns was superior to that of comparable seismically ductile RC columns and steel jacketed non-ductile RC columns. In fact, the seismically ductile RC columns and steel jacketed non-ductile RC columns failed to perform in a ductile manner when subjected to blast loading. Therefore, the rest of this report mainly focuses on analysis methods to capture the ductile response of the proposed CFST bridge pier columns subjected to blast loading. However, for the sake of obtaining shear forces for direct shear, an alternative analytical method is performed for the RC columns and steel jacketed RC columns.

As presented in the literature review, there is a variety of analytical methods available to compute the response of structures subjected to blast loading ranging from a simplified analytical method using a SDOF system to a finite element model (FEM). The objectives of the dynamic analyses conducted here are to develop the design tools to calculate the blast response of circular shaped bridge columns, and to understand the behavior of these bridge columns subjected to blast loading. For these purposes, in this research project, three different analytical methods have been adopted to replicate the behavior of the tested bridge columns subjected to blast loading, namely simplified analysis, SDOF dynamic analysis, and fiber-based dynamic analysis. The first analytical method, simplified analysis, was presented and was compared with the test results of CFST columns (Fujikura et al. 2007, 2008) and of RC columns and steel jacketed RC columns in Section 3.4.4. Here, the results obtained using the other two blast analysis methods, namely SDOF dynamic analysis, and fiber-based dynamic analysis, are compared with the experimental results.

The shape factor  $\beta$ , which is meant to represent the effect of the shape of the column in reducing the applied blast pressure, is unavoidably affected by some assumptions used in the simplified analytical model. So, if a more sophisticated analysis model is used and some of these assumptions are removed, it would be incorrect to use the same  $\beta$  value as developed for the simplified method. Therefore, the factor  $\beta$  needs to be reevaluated if more sophisticated analysis methods are used to eliminate some of these assumptions.

Following this section introduction, the experimental results for the two series of blast tests on three different types of columns are summarized before presenting the blast dynamic analyses. Then, the three analytical methods used in this research are compared. Next, the SDOF dynamic analysis is presented. After that, fiber-based analytical model is discussed, along with verification of this fiber-based analytical model based on quasi-static cyclic loading tests done by various researchers, and then the dynamic analysis results obtained using this fiber-based model are presented. Finally, results obtained using the three different analysis methods are summarized.

## **4.2 Summary of Bridge Pier Tests Subjected to Blast Loading**

This subsection summarizes the experimental results of two series of blast tests to the three different types of columns previously tested, because this information will be used in the subsequent blast dynamic analyses using SDOF model and fiber-base model presented later. Recall that, in the first series of blast tests, a multi-hazard bridge pier system, namely a pier bent with CFST columns, was proposed and its behavior was experimentally investigated when subjected to blast loading (Fujikura et al. 2007, 2008). Also, in Section 3, two types of seismically designed conventional bridge pier columns were investigated, namely ductile RC columns and non-ductile RC columns retrofitted with steel jackets, Table 4-1 summarizes the blast parameters and test results of all those test cases. The side view of these blast situations of these detonations to the column is schematically illustrated in Figure 4-1.

**Table 4-1 Summary of All Column Test Cases and Results**

		Blast Parameters				Test Results		
Test Num	Column	Charge Weight	Standoff Distance	Scaled Distance $\frac{X}{W^{1/3}}$	Height (m)	Residual Displ. (mm)	Experimental Observations	
Prototype		---	---	3.74	1.0	N/A	N/A	
1 <sup>st</sup> Series	1-1	CFST C4	0.1 W	3 X	6.46	0.25	0	No Damage
	1-2	CFST C4	0.55 W	3 X	3.66	0.75	0	No Damage
	1-3	CFST C4	W	2 X	2.00		30	Flexural
	1-4	CFST C6		1.1 X	1.10		46	Flexural
	1-5	CFST C5		1.3 X	1.30	76	Flexural	
	1-6	CFST C4		1.6 X	1.60	0.25	24	Flexural
	1-7	CFST C4		0.6 X	0.60		395	Flexural (Steel Fracture)
	1-9	CFST C6		0.8 X	0.80		45	Flexural
	1-10	CFST C5		0.8 X	0.80		100	Flexural (Steel Fracture)
	2 <sup>nd</sup> Series	2-1		RC1		2.16 X	2.16	N/A
2-2		RC2			3.25 X	3.25	N/A	Onset of Direct Shear
2-3		SJ2			2.16 X	2.16	N/A	Direct Shear
2-4		SJ1		3.25 X	3.25	N/A	Direct Shear	

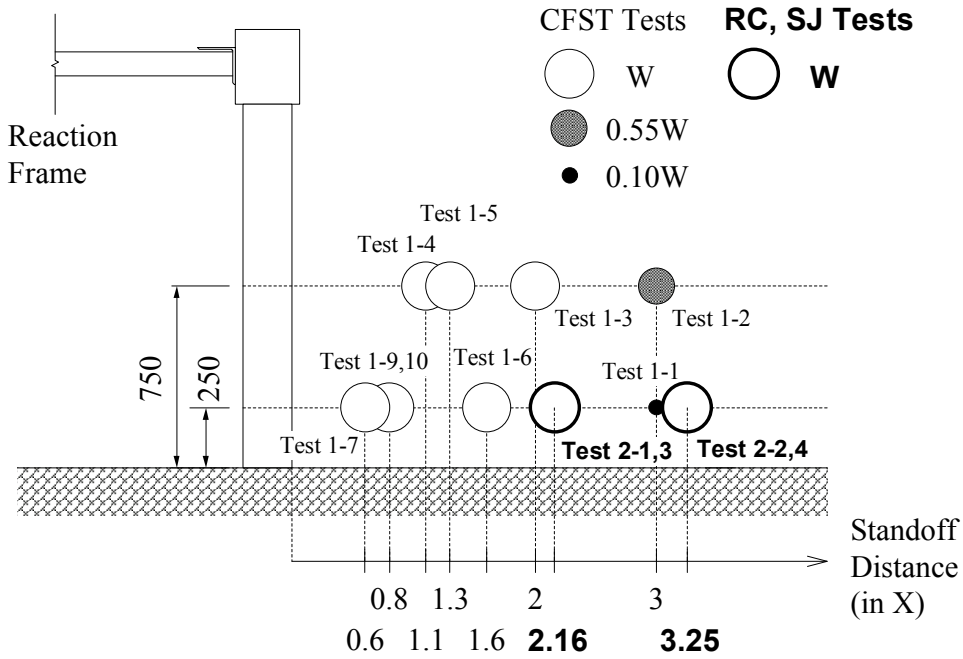


**Figure 4-1 Comparison of Test Blast Parameters**

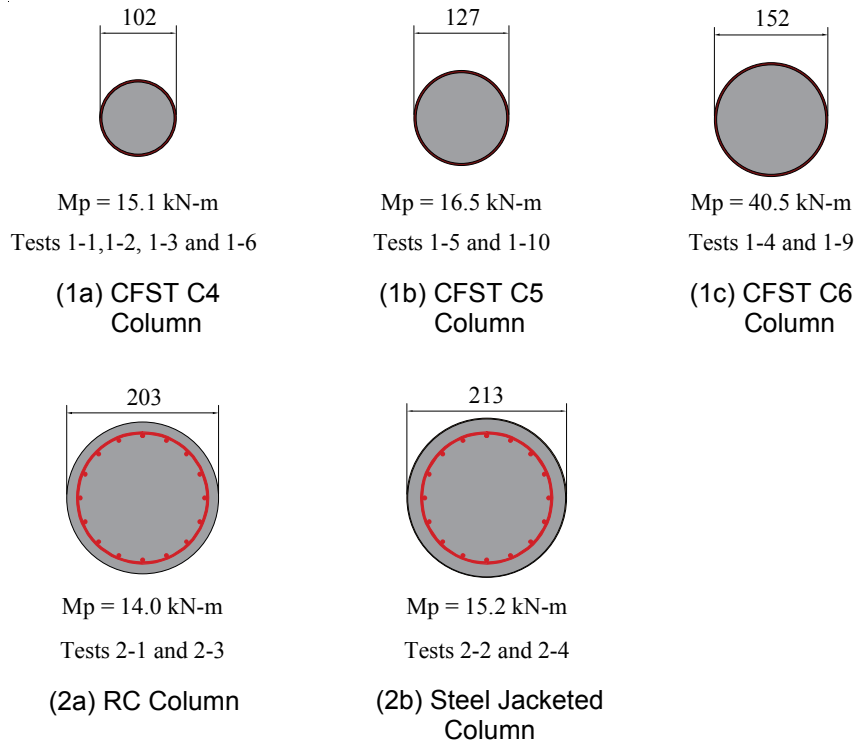


**Figure 4-2 Comparison of Tested Column Sections and Moment Capacities**

Figure 4-2 compares the cross-section and moment capacity of the tested CFST C4, C5 C6 columns, RC column and steel jacketed column. The moment capacity of CFST columns was calculated using the Bruneau and Marson (2004) equations, and that of RC column and steel jacketed RC column was obtained from the moment-curvature analyses presented in Section 3.4.2. As shown in Figure 4-2, the moment capacity of the CFST C4 column is comparable to that of the RC column and steel jacketed column. Being all ductile members of nearly identical strength, these three columns would be expected to perform equally well when subjected to seismic loading. Note that these columns are detailed to resist the shear force due to flexural hinging at the ends of the column. That would develop due to the earthquake loading. As shown in Table 4-1, the standoff distance of Test 1-6 for CFST C4 column is closer than that of Test 2-1 for RC1 column and Test 2-3 for SJ2 column. Although CFST C4 column was subjected to the larger blast pressures due to the closer standoff distance, it exhibited a ductile behavior under the blast loading while both RC1 column and SJ2 column failed in shear at their bases. From this observation, even though CFST, RC and steel jacketed RC columns perform equally well under seismic loading, only the CFST column would perform well under blast loading. This is attributed to the inadequate direct shear resistance at the base of the RC and steel jacketed RC column.

While the above is useful in quantifying the relative performance of these structural systems, it is instructive to review each of column types would have performed for the terrorist attack scenario assumed in this research (Sections 3.2.2). The basis of comparison for the experimental results with the prototype is achieved through the use of scaled distance concept. The scaled distance of the prototype is 3.74 (in  $X/W^{1/3}$ ) as shown Table 4-1, which is calculated from the charge weight and standoff distance of the terrorist attack scenario assumed in Sections 3.2.2. Since no damage was observed to CFST C4 column in Test 1-2 whose scale distance of 3.66 is smaller than that of the assumed blast scenario, this indicates the CFST columns would perform well to resist the assumed terrorist attack. Recall that the CFST column was originally designed assuming the  $\beta$  valued of 0.85 and expected the ductility of 7% which did not occur because the actual  $\beta$  valued for this type of column discovered to be 0.45 using the simplified analyses. From Test 2-3 which has the scale distance of 3.25, direct spalling of the cover concrete at the bottom of RC2 column and the shear deformation at this location were observed. Therefore,

when subjected to the assumed terrorist attack with slightly larger scale distance of 3.74, a seismically designed ductile reinforced concrete column would exhibit at most the minor damage of spalling cover concrete. Since SJ1 column failed in direct shear at the base of the column in Test 2-4 with a 3.25 scaled distance, steel jacketed reinforced concrete column would be expected to fail in shear at the base when subjected to the assumed terrorist attack with a slightly larger scale distance of 3.74. However, the assumed attack scenario. For other scenarios in which the explosive charge would be increased, it is clear from Figure 4-1 that the RC column (Test 2-1) and steel jacketed RC column (Test 2-3) would fail in shear at the base, but the CFST column (Test 1-6) would provide the greater robustness against the larger explosive charge.

### 4.3 Selection of Analytical Methods

As presented previously, three different analytical methods were adopted in this research, namely simplified analysis, SDOF dynamic analysis, and fiber-based dynamic analysis. Table 4-2

**Table 4-2 Comparison of Analytical Methods**

	Simplified Analysis	SDOF Dynamic Analysis	Fiber-based Dynamic Analysis
1. Analytical Procedure	Dynamic (Impulse)	Dynamic (Pressure-History)	Dynamic (Pressure-History)
2. Interaction between Structure and Blast Loading	Uncoupled	Uncoupled	Uncoupled
3. Descretization of Structure	SDOF	SDOF	MDOF 2D Fiber-Based
4. Material Nonlinearity	Inelastic	Inelastic	Inelastic
5. Geometric Nonlinearity	Nonlinear	Nonlinear	Nonlinear

compares these analytical methods in terms of the analytical options presented in Section 2.6.



The common options between these three analytical methods are that: (a) they are dynamic analysis, (b) the structure and the blast loading are uncoupled, (c) material nonlinearity is considered, and (d) geometric nonlinearity is not considered. The uncoupled analysis is chosen because this analysis is commonly used in the practical design of structures under dynamic loading and provides reasonable results, as discussed in literature review. The material nonlinearity should be included here because all materials behaved in the inelastic range under the blast pressures considered in this research. The blast experimental program shown in the previous sections was done without axial forces in the columns. Therefore, the geometric nonlinearity is not considered in the analysis because the moment magnification (namely  $P-\delta$  effect) associated with large deformation and axial force is small and negligible in these tests.

Between these analyses, the dynamic load is applied differently, and the structure is discretized differently. As presented previously, the simplified analysis uses the concept of equivalent impulse to calculate the maximum deformation assuming that all the energy imparted to the system by the blast loading is converted into internal strain energy. This analytical method provides acceptable results when the blast pressure duration is much shorter than the natural period of the structure (i.e. impulsive loading condition). The SDOF dynamic analyses and fiber-based dynamic analyses are conducted using the equivalent uniform pressure-history and the actual pressure-history, respectively, generated by the program Bridge Explosive Loading (BEL 2004). As for the discretization of the structure, the simplified analysis and the SDOF dynamic analysis use the same SDOF lumped-mass system (equivalent SDOF system) whereas the columns are modeled by the 2D fiber-based beam model in the fiber-based dynamic analysis.

## **4.4 SDOF Dynamic Analysis**

### **4.4.1 General**

Experimentally obtained maximum residual deformations of the tested columns were compared with the ones that could be calculated using the SDOF dynamic response history analyses. These analyses were conducted for the six test cases of CFST columns for which residual plastic deformations were obtained. The strength values obtained from the compression tests of concrete cylinders and the tensile tests for steel were considered in these analyses. The concrete strength and yield stress of steel were multiplied by 1.25 and 1.2, respectively, to account for

strength magnification at large strain rates under impulsive conditions (Mays and Smith 1995). The SDOF dynamic analyses were not conducted for the test RC columns and steel jacketed RC columns because the flexural residual deformations to be compared with the analytical results were not significant from these columns due to the shear failures of the column base.

The simplified analysis method used neglected the damping term because one cycle of structural response develops under blast loading and because the simplified analysis can not take the damping effect into account. Here, since response time-history analyses are performed, it is a small effort to include the damping effect. Accordingly, the damping is considered in the analyses to verify the impact of this phenomenon.

#### **4.4.1 Program for SDOF Dynamic Analysis**

There are a few programs available to perform a SDOF dynamic analysis for structures subjected to blast loading. The program SPAn32 (USACE-OD 2002), developed by the U.S. Army Corps of Engineers, is commonly used for this purpose subjected to blast loading in the blast engineering community. However, the distribution of this program is limited to the U.S. government agencies and their contractors. NONLIN (1996) is a public domain SDOF dynamic program, originally developed for seismic response time-history analysis of SDOF system that has an option to apply dynamic blast forces, and has been sometimes referenced in the literature. However, here, the program Single-Degree-of-Freedom Blast Effects Design Spreadsheets (SBEDS) version 3.1 (USACE-PDC 2007), which is a product of the U.S. Army Corps of Engineers, was used because its distribution is unlimited for public use and this program is tailored for blast engineering design rather than earthquake engineering design.

SBEDS is typically used to design structural components subjected to blast loading. Using an equivalent SDOF system, and running on an Excel workbook platform, SBEDS has pre-determined options for the analysis of ten common structural components, including a steel plate, a reinforced concrete slab, reinforced masonry and wood panel, with various support conditions. This program follows two design guidelines, namely TM 5-1300 *Structures to Resist the Effects of Accidental Explosions* (USDA 1990) and UFC 3-340-01 *Design and Analysis of Hardened Structures to Conventional Weapons Effects* (UFC 2002), as applicable. SBEDS generates a

uniform distributed pressure from a hemispherical surface burst explosion for a specified charge weight and standoff distance. A user defined pressure-history can also be incorporated in the analysis. (USACE-PDC 2006)

#### 4.4.2 Analytical Model

In the SDOF dynamic analysis conducted below, the test columns were represented by an equivalent SDOF system that was also used for the simplified blast analysis. This is schematically illustrated in Figure 4-3. The viscous damping was not considered in the simplified blast analysis, but it was considered in this SDOF dynamic analysis as shown in Figure 4-3. The equation of motion for an equivalent SDOF system shown in Figure 4-3 is given by:

$$M_e \ddot{x} + C_e \dot{x} + K_e x = P_e(t) \quad (4-1)$$

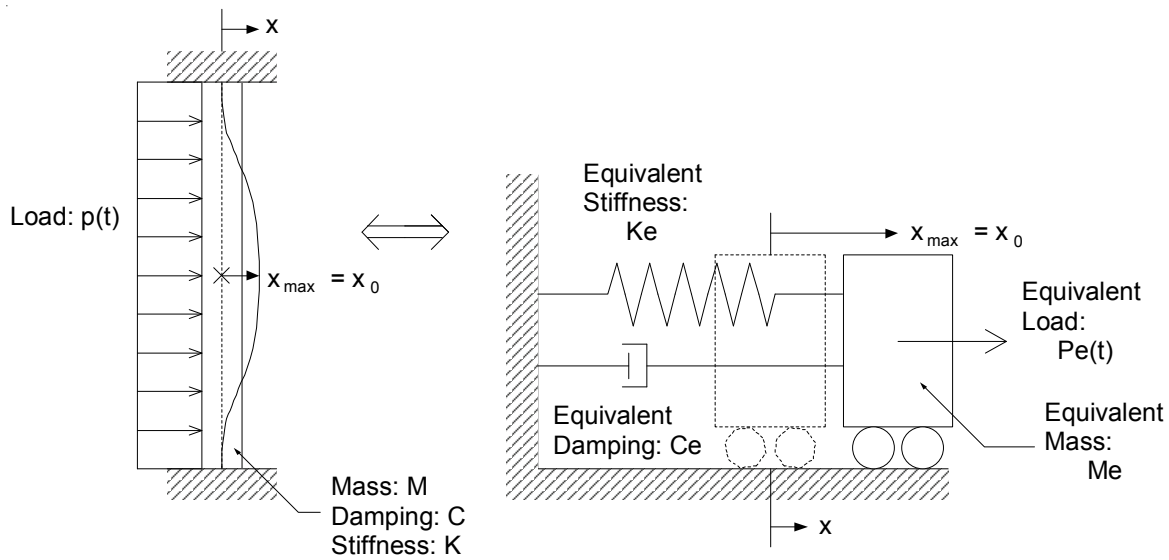


**Figure 4-3 Real and Equivalent SDOF System for SDOF Dynamic Analysis**

Using transformation factors which are the mass factor  $K_M$ , the viscous damping factor  $K_D$ , the stiffness factor  $K_S$ , and the load factor  $K_L$ , Equation 4-1 is rewritten in terms of the real structural system as:

$$K_M M \ddot{x} + K_D C \dot{x} + K_S K x = K_L P(t) \quad (4-2)$$

By setting  $K_L = K_S$  and  $K_L = K_D$  and using the load-mass factor,  $K_{LM}$ , Equation 4-2 is simplified to:

$$K_{LM}M\ddot{x} + C\dot{x} + Kx = P(t) \quad (4-3)$$

In this process, since the resistance of an element which comes from the stiffness in the internal force tending to restore the structure to its original position, the load factor  $K_L$  can be set equal to the stiffness factor  $K_S$ . For expediency, the equation of motion of the real structural system is written as a SDOF system that only depends on the load-mass factor,  $K_{LM}$ , therefore, it is implied that  $K_L = K_D$  in Equation 4-3. This is not necessarily correct mathematically, but it is the approach that has been used in SBEDS. (USACE-PDC 2006)

The load-mass factor,  $K_{LM}$ , depends on boundary conditions and loading conditions.

Furthermore, for the same given boundary condition and loading condition, the load-mass factor,  $K_{LM}$ , for the specific structure can take different values depending on whether the structure behaves in the elastic, elasto-plastic, or plastic ranges as presented in Table 2-4. This is because virtual work developed in the element depends on the element deformation shapes which are different in each range. A fixed-fixed boundary condition and a uniformly distributed load were chosen for the experimental columns. These are the boundary conditions that are representative of what happened in the experiments due to the torsional resistance of the cap beam. For this fixed-fixed boundary condition and a uniformly distributed load, the corresponding values of the load-mass factor,  $K_{LM}$ , are 0.77, 0.78 and 0.66 for response in the elastic, elasto-plastic, and plastic ranges, respectively.

The simplified analysis requires the idealized bi-linear resistance-displacement function,  $R_e(x)$ , also called an equivalent resistance function (see details in Fujikura et al. 2007). Even though the dynamic SDOF analyses conducted with SBEDS can handle a tri-linear resistance curve (as well as more complex ones), for the sake of comparing the dynamic analysis results with the simplified analysis results, it was decided to use the same equivalent resistance-displacement function,  $R_e(x)$ . In the equivalent resistance-deflection function,  $R_e(x)$ , for the one span fixed-fixed supported column, since the program SBEDS can assign different load-mass factors to

different ranges, the load-mass factor,  $K_{LM}$ , of 0.775 was taken as the average value of elastic and elasto-plastic range, and 0.66 for plastic range. Although one could investigate the effect of using the tri-linear curve instead of the bi-linear curve, the average value of  $K_{LM}$  is not expected to have the significant impact to the response because  $K_{LM}$  is 0.77 and 0.78 over the initial and second stiffness range, respectively. On the other hand, in the simplified blast analysis, the value of 0.66 was used for the load-mass factor because only one value could be considered in that analysis and the test columns deformed in large plastic deformations. For comparison purposes, the following analyses will investigate the influence of this load-mass factor on the responses.

The ultimate resistance of the column,  $r_u$ , is calculated assuming that plastic hinges form at the top and base of the column as well as at the explosion height, and is given by  $r_u = 12M_p/L^2$  for mid-height explosion cases and by  $r_u = 28.8M_p/L^2$  for low-height explosion cases for which the charge is at 0.25 m high.  $M_p$  is the plastic moment capacity of the column, which was calculated using the Bruneau and Marson (2004) equations. The resulting plastic moment,  $M_p$ , of the column specimens was 15.1 kN-m, 16.5 kN-m and 40.5 kN-m for CFST C4, C5 and C6 Columns, respectively. The equivalent maximum elastic deformation  $X_E$  is given by  $X_E = r_u/K_e$  where  $K_e$ , the unit elastic stiffness of the equivalent SDOF system, is given by  $K_e = 307EI_e/L^4$  (Mays and Smith 1995). The flexural stiffness of the column,  $EI_e$ , was calculated using the equation introduced in the Eurocode 4 (1994) because the AISC Provisions (AISC 1999) do not provide an equation for  $EI_e$  (Bruneau and Marson 2004). The design values used for the SBEDS analyses are summarized in Table 4-3 along with the explosion parameters considered. Note that these values are presented in unit per area because the program requires the per unit area values rather than for the element as a whole.

**Table 4-3 Design Values for SDOF Dynamic Analysis**

Test Num.	Column	Explosive Parameters			Mass per Unit Area (kg/m <sup>2</sup> )	Stiffness per Unit Area (kPa/mm)	Resistance per Unit Area (kPa)
		w	x	z (m)			
Test 1-3	C4	W	2 X	0.75	243.7	192.2	1062.0
Test 1-4	C6		1.1 X		340.0	538.9	1892.2
Test 1-5	C5		1.3 X		291.9	322.6	924.9
Test 1-6	C4		1.6 X	0.25	243.7	192.2	1911.1
Test 1-9	C6		0.6 X		340.0	538.9	3404.7
Test 1-10	C5		0.8 X		291.9	322.6	1664.5

#### 4.4.3 Applied Blast Loading

The blast pressures acting on the column vary with time and locations along the column. In the simplified analysis, a single value of the equivalent uniform impulse was needed to calculate the maximum response of the column modeled as SDOF system. Accordingly, an equivalent uniform impulse was used to take the blast pressures into account, and the envelope of the maximum impulse was used to calculate the equivalent uniform impulse as presented in Equation 3-34.

In the SDOF dynamic analysis, the equivalent uniform pressure at a given time is applied to the structural model following a time history step-by-step analysis. This equivalent uniform pressure at time of  $t$ ,  $p_{eq}(t)$ , is given by:

$$p_{eq}(t) = \frac{\int_0^H p(z,t) \delta(z) dz}{\int_0^H \delta(z) dz} \quad (4-4)$$

where  $p(z,t)$  is the pressure distribution along the height of the column at time  $t$ , and  $\delta(z)$  is the normalized deflected shape of the column. The values of  $p(z,t)$  were calculated using the Bridge Explosive Loading program (BEL 2004) which was used for the simplified analyses as

well. The normalized deflected shape,  $\delta(z)$ , was taken as inelastic deformations after plastic hinging. The shape was defined by rigid-link members between plastic hinges assuming that an in-span hinge develops at the height of the blast charge and that other hinges form at both the top and base of the column. The resulting equivalent pressure histories,  $p_{eq}(t)$ , for the six test cases of CFST columns are shown in Figure 4-4. The time increment of each step in these pressure histories is 0.01 msec.

#### **4.4.4 Methods for Solving Equation of Motion**

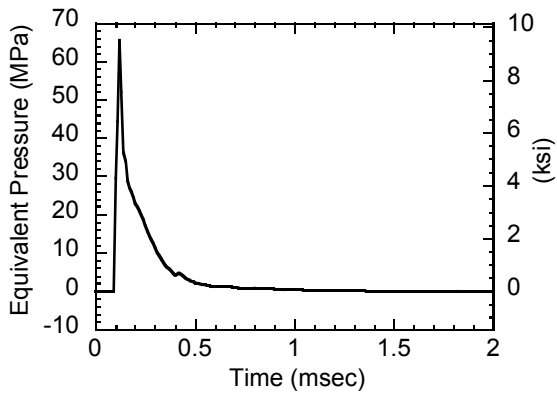
To calculate the maximum response of the equivalent SDOF system, Equation 4-3 needs to be solved. The program SBEDS uses the constant velocity method to solve this equation (USACE-PDC 2006). There are more accurate methods for the numerical integration of the equations of motion such as Newmark-beta method (USACE-PDC 2006), but this constant velocity method is simple and stable, and suitable for the workbook based software. However, it is necessary to use a small time step to obtain an accurate solution using the constant velocity method.

Biggs (1964) suggests that the time step interval in the constant velocity method should not be larger than one-tenth of the natural period of the structural system to obtain sufficiently accurate results for practical purposes. The comparison of selected analytical results obtained using the Newmark-beta method showed that the program SBEDS provided solutions within a 2% difference if using the recommended small time step (USACE-PDC 2006).

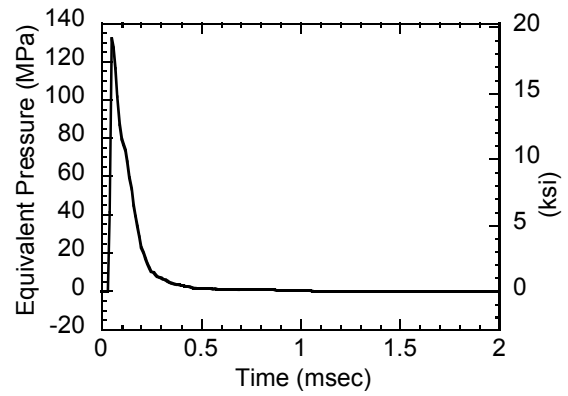
#### **4.4.5 Analytical Results**

##### **4.4.5.1 Effect of Damping and Load-mass Factor**

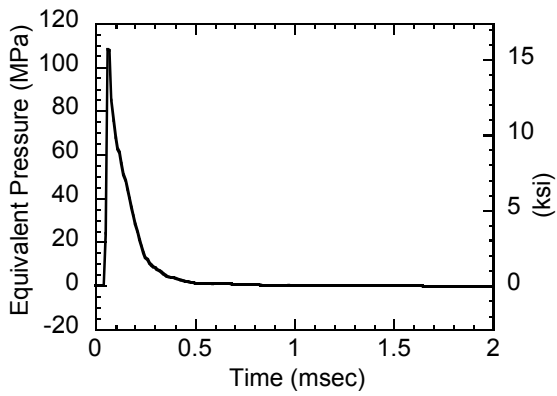
For the sake of comparison, this subsection investigates the sensitivity of the load-mass factor,  $K_{LM}$  and the damping effect on the structural response. To do this, only one case of the CFST column was considered, which was the CFST C4 column of Test 1-3. In the simplified analysis procedure, the damping effect was not considered and the load-mass factor,  $K_{LM}$ , was assumed to be 0.66. By comparison, the SDOF dynamic analysis here considers both a damping of 0% and 5%. Since the program SBEDS can account for the different load-mass factors to different ranges, the load-mass factor of 0.775 and 0.66 was used for the elastic and plastic range, respectively as presented in Section 4.4.2.



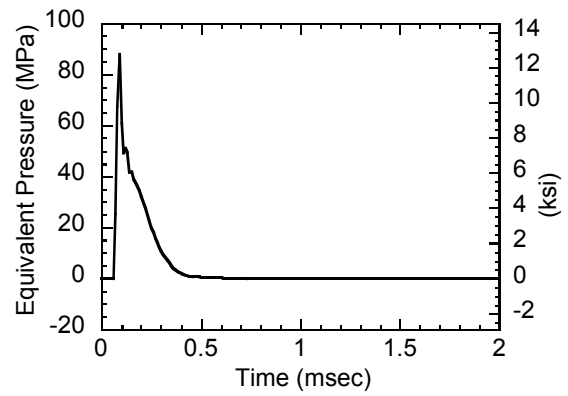
(a) Test 1-3, B1-C4 Column



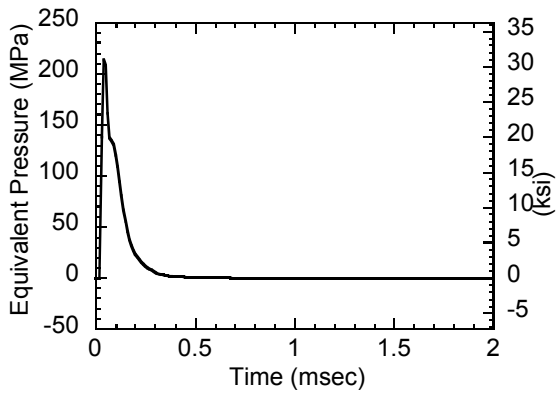
(b) Test 1-4, B1-C6 Column



(c) Test 1-5, B1-C5 Column



(d) Test 1-6, B2-C4 Column



(e) Test 1-9, B2-C6 Column  
and Test 1-10, B2-C5 Column

**Figure 4-4 Equivalent Pressure History**

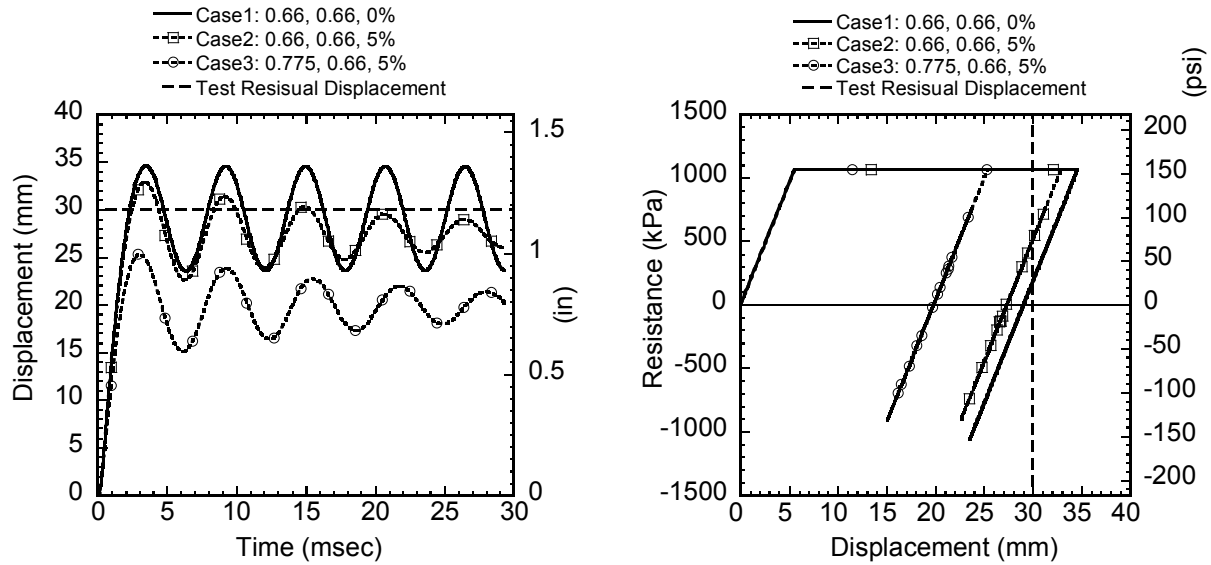


To compare the SDOF dynamic analyses with the simplified analyses and to compare three different set of assumptions of the SDOF dynamic analyses, three different cases are analyzed as shown in Table 4-4.  $K_{LMe}$  and  $K_{LMp}$  in Table 4-4 are respectively the load-mass factors for the elastic and plastic range. Case 1 considers the same load-mass factors and damping ratio as those considered in the simplified analysis, namely  $K_{LMe} = K_{LMp} = 0.66$  and no damping. Case 2 is identical to Case 1 except that it considers the damping ratio of 5%. Case 3 considers the load-mass factors that vary over the different ranges of structural response where  $K_{LMe}$  and  $K_{LMp}$  are 0.775 and 0.66, respectively. The shape factor  $\beta$  of 0.472 used in these analyses was the resulting value from the simplified analysis for this particular column case as presented in Table 3-8.

**Table 4-4 SDOF Dynamic Analysis Cases for CFST C4 Column of Test 1-3**

	Case 1	Case 2	Case 3
$K_{LMe}$	0.66	0.66	0.775
$K_{LMp}$	0.66	0.66	0.66
Damping Ratio (%)	0	5	5

The analytical results of the displacement history and resistance-displacement relationship obtained for each of the three cases considered are shown in Figure 4-5 (a) and (b), respectively. Note that the resistance in Figure 4-5 (b) is expressed in a unit of pressure (kPa) because the program considers the structure per unit area. The vertical dashed line at 30 mm in these figures shows the maximum residual displacement obtained in the experiment. The displacement when resistance equals zero (after the structure has been loaded and unloaded) in Figure 4-5 (b) is the residual plastic displacement which should be equal to the experimentally obtained residual displacement of 30 mm in this case.



(a) Displacement History

(b) Resistance-Displacement Relationship

**Figure 4-5 Analytical Results for Test 1-3 with  $\beta=0.472$  (C4 Column)**

By comparing displacement history curves of Case 1 and Case 2 in Figure 4-5 (a), it can be seen that considering the damping effect does have a small effect of approximately 5% less on the maximum deformation reached. However, considering the damping shows the progressive attenuation of the amplitude of vibrations. More importantly, by comparing displacement history curves of Case 2 and Case 3 in Figure 4-5 (a), using the two values of load-mass factor,  $K_{LM}$  reduces the maximum displacement amplitude significantly, by 23%. Therefore this factor has a more significant impact on the maximum displacement. These trends on the effect of the damping and the load-mass factor can also be seen in the residual displacement as shown in Figure 4-5 (b).

#### 4.4.5.2 Shape Factor $\beta$

To match the analytical residual displacements with the experimental results, the shape factor  $\beta$  was calibrated for the six test CFST columns here. Table 4-5 summarizes the resulting shape factors  $\beta$  for those six cases, including the ones obtained from the simplified analyses. Since in Tests 3, 4 and 5 the blast charges were located at mid-height of the column and in Tests 6, 8 and 10 they were located at low-height of the column, the factors  $\beta$  were averaged differently for

these two sets of three cases. It is observed from Table 4-5 that the value of  $\beta$  is typically 4% less at low-height tests than at mid-height tests. The height of the explosion does not have a huge impact on the value of  $\beta$ , therefore the average values of  $\beta$  for all columns are shown at the bottom of this table. The average  $\beta$  factor calculated for all columns considered was 0.453, 0.463, 0.521 and 0.534 for Cases 1, 2, 3 and 4, respectively. Note that the shape factors obtained for the simplified analysis and for Case 1 compare within 1%. This means that the simplified analysis based on energy conservation calculates the same structural response as the SDOF dynamic analysis under the same conditions of load-mass factor (i.e.  $K_{LM} = 0.66$ ) and the damping ratio (i.e. 0%).

**Table 4-5 Summary of Shape Factor from SDOF Dynamic Analysis**

Test Num.	Simplified Analysis		SDOF Dynamic Analysis							
	$K_{LMe}=0.66$ $K_{LMp}=0.66$ 0% Damping		Case 1		Case 2		Case 3		Case 4	
			$K_{LMe}=0.66$ $K_{LMp}=0.66$ 0% Damping		$K_{LMe}=0.66$ $K_{LMp}=0.66$ 5% Damping		$K_{LMe}=0.775$ $K_{LMp}=0.66$ 0% Damping		$K_{LMe}=0.775$ $K_{LMp}=0.66$ 5% Damping	
			$\beta$	Ave	$\beta$	Ave	$\beta$	Ave	$\beta$	Ave
1-3	0.472	0.459	0.479	0.463	0.492	0.472	0.552	0.532	0.566	0.542
1-4	0.458		0.461		0.469		0.531		0.540	
1-5	0.447		0.450		0.456		0.514		0.521	
1-6	0.465	0.441	0.466	0.442	0.483	0.453	0.538	0.510	0.558	0.525
1-9	0.440		0.442		0.452		0.508		0.524	
1-10	0.417		0.418		0.424		0.485		0.492	
Ave.		0.450		0.453		0.463		0.521		0.534

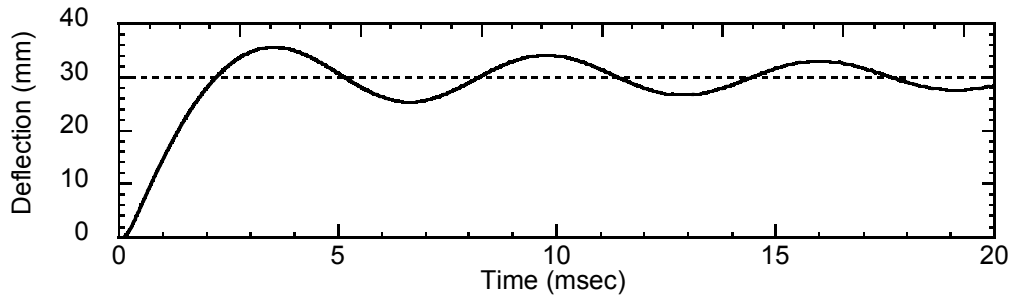
Using a 5% damping factor slightly reduces structural response and thus slightly increases the factor  $\beta$  required to obtain the same residual deformation, which can be observed by comparing the shape factor obtained for Cases 1 and 2, and Cases 3 and 4. The difference is within 3%.

The increase of  $\beta$  value is larger for Cases 3 and 4. In Cases 3 and 4, using the load-mass factor in the elastic range,  $K_{LMe}$ , of 0.775, in addition to that over the plastic range of 0.66, increases the shape factor by about 15% over that for Cases 1 and 2, respectively. The resulting value of  $\beta$  for this type of circular columns is 0.534 (i.e. mean value of 0.543 and standard deviation of 0.027 from the six samples considered) for SDOF dynamic analysis using 5% damping and the different load-mass factors corresponding to the different structural ranges. Note that the larger the shape factor, the larger the blast pressures that the structure can resist.

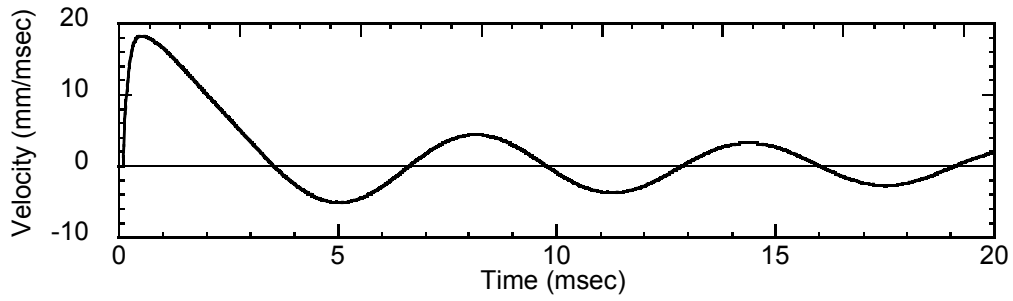
#### 4.4.5.3 Structural Response

The structural responses of six CFST test cases shown in Table 4-5 are presented in Figures 4-6 to 4-11, to verify that the analytical residual displacements using the shape factor  $\beta$  shown in Table 4-5 match the experimental residual displacements and to illustrate the structural response of SDOF dynamic analyses using these  $\beta$  values. In each analytical case, (a) displacement history, (b) velocity history, (c) acceleration history, and (d) resistance displacement relationship are presented. The dashed lines in the figures of (a) displacement history and (d) resistance displacement relationship represent the plastic residual displacements obtained from the experiments. Table 4-6 summarizes the maximum acceleration, velocity and displacement response, and the corresponding time when those responses occurred after the blast pressure began to be applied to the structure, along with the pressure duration of the positive phase.

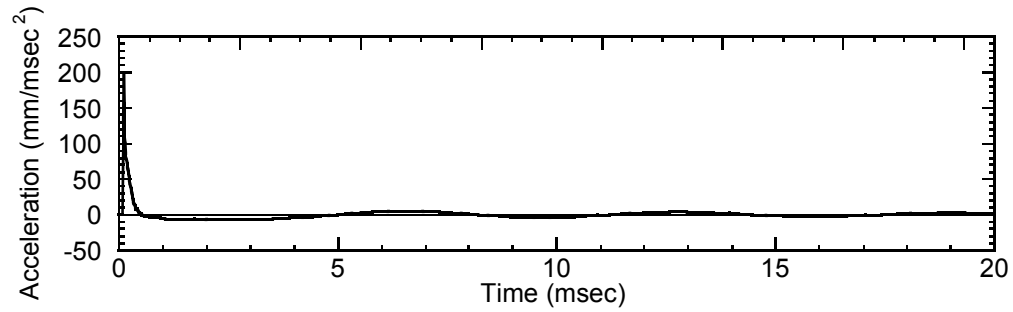
As shown in Table 4-6, accelerations reach their maximum values shortly after the blast pressure is applied. Table 4-6 also shows that the displacements reach their maximum values much later after the end of the applied blast pressure. This is typically the case when the blast pressure duration is much shorter than the natural period of the structure (i.e. impulsive loading case). To illustrate that this is indeed the case here, Table 4-7 shows the relationship between the duration of the positive phase of the blast pressure history and the natural period of the structure. The ratios  $t_d/T_n$  in the range of 1/30 to 1/45 confirm that these test cases are indeed the impulsive loading cases because the blast pressure duration is much shorter than the natural period of the structure.



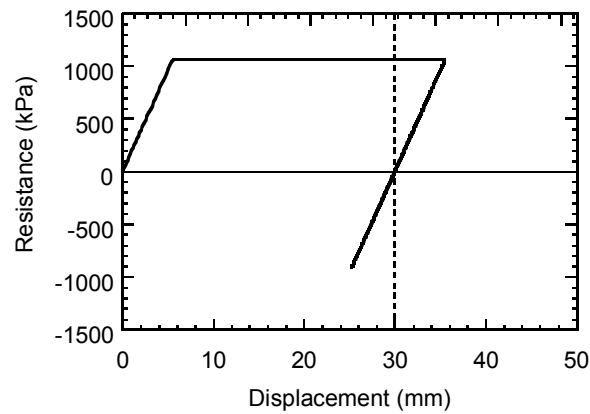
(a) Displacement History



(b) Velocity History

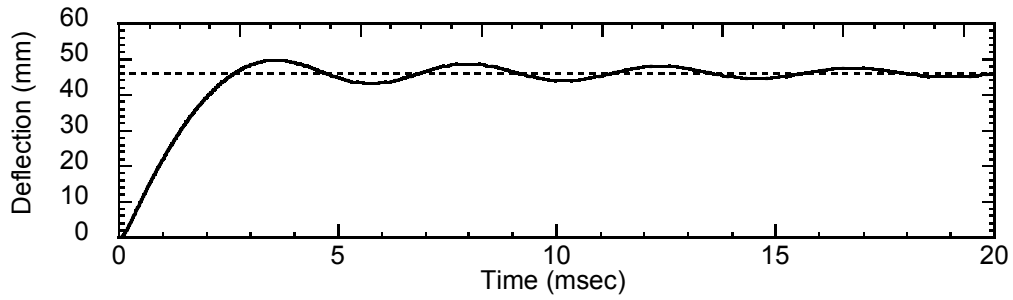


(c) Acceleration History

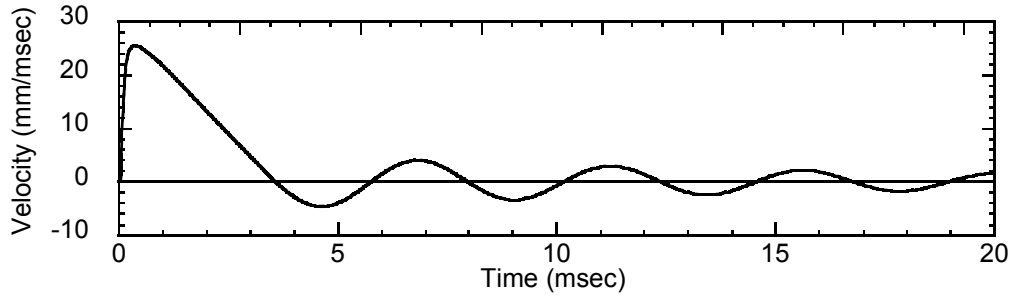


(d) Resistance Displacement Relationship

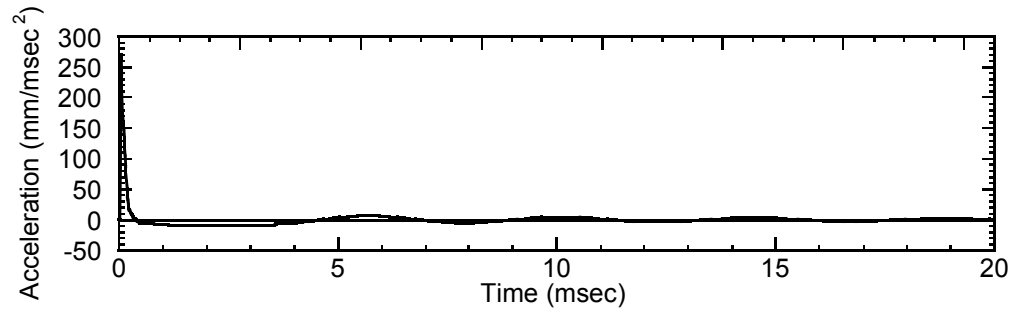
**Figure 4-6 Analytical Results for Test 1-3 with  $\beta=0.566$  (C4 Column)**



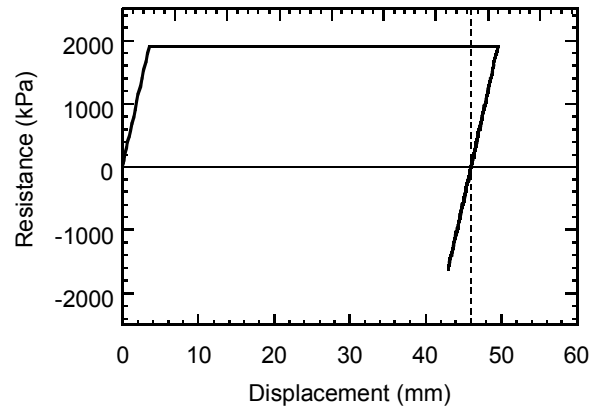
(a) Displacement History



(b) Velocity History

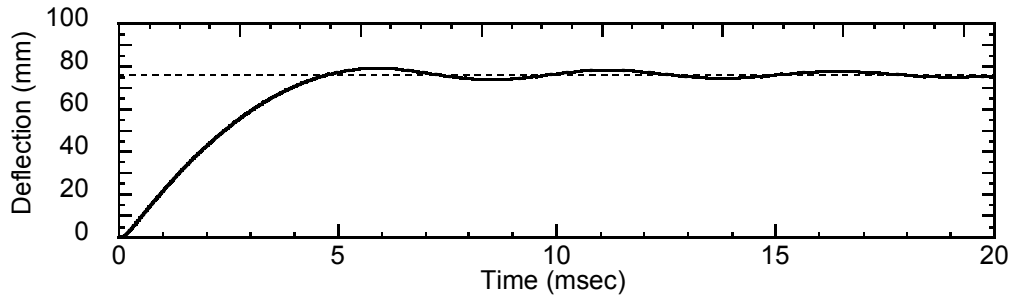


(c) Acceleration History

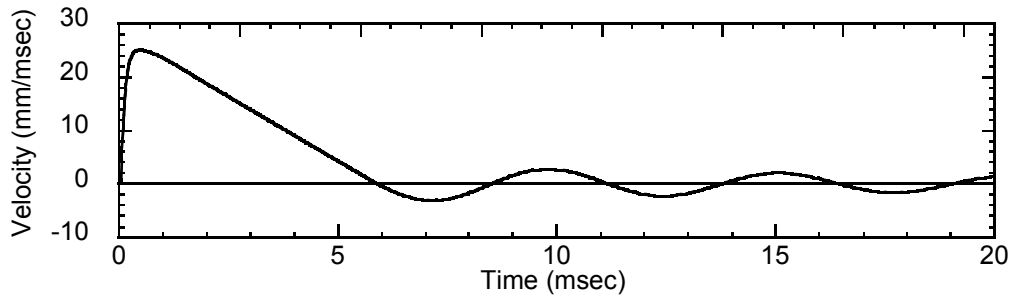


(d) Resistance Displacement Relationship

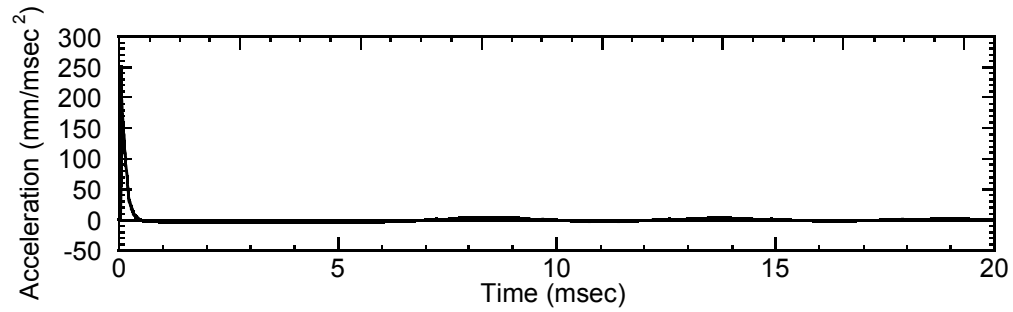
**Figure 4-7 Analytical Results for Test 1-4 with  $\beta=0.540$  (C6 Column)**



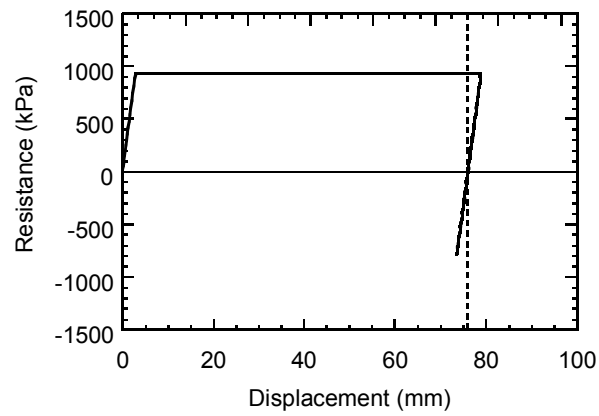
(a) Displacement History



(b) Velocity History

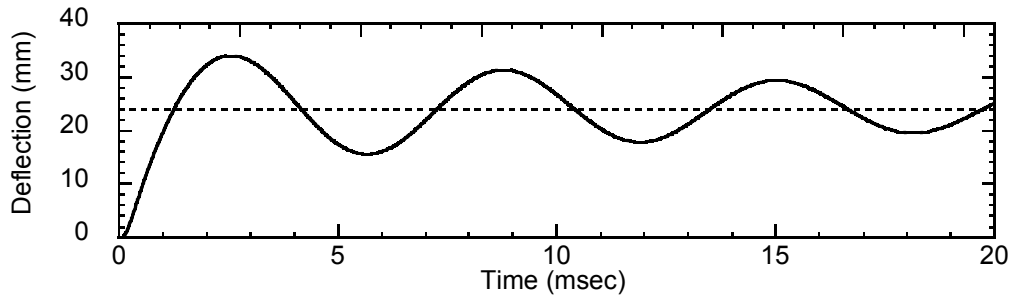


(c) Acceleration History

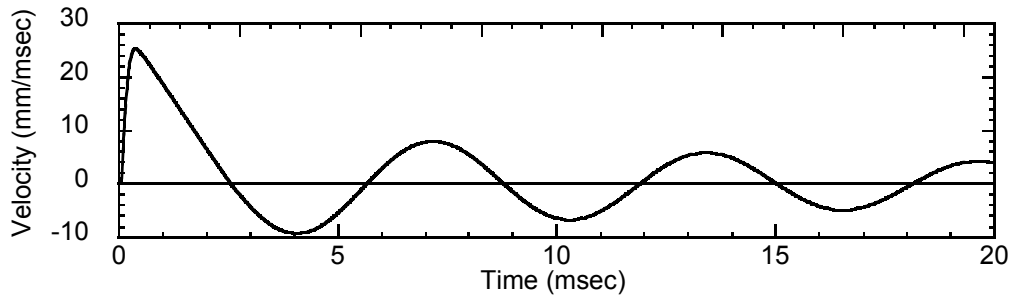


(d) Resistance Displacement Relationship

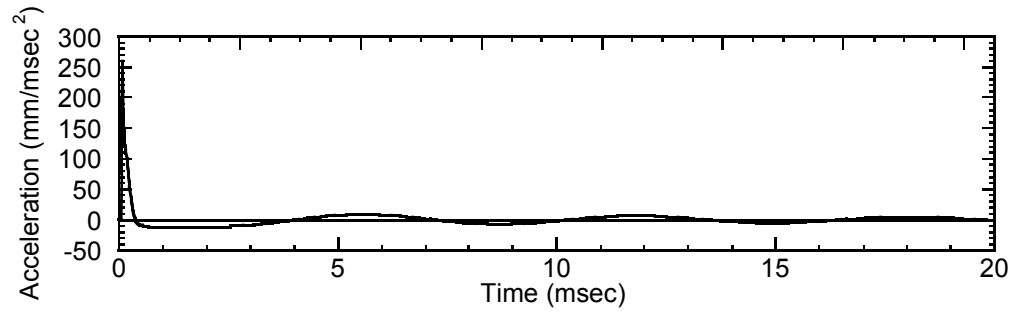
**Figure 4-8 Analytical Results for Test 1-5 with  $\beta=0.521$  (C5 Column)**



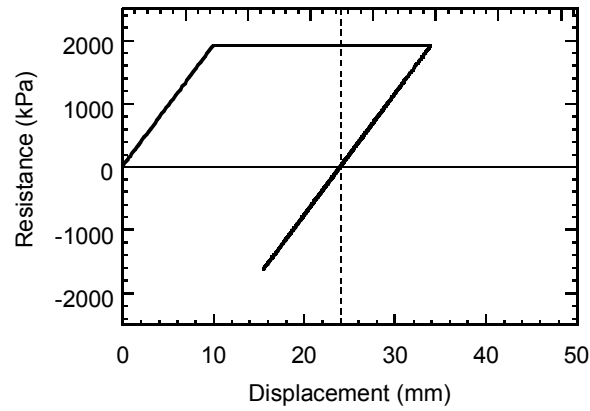
(a) Displacement History



(b) Velocity History



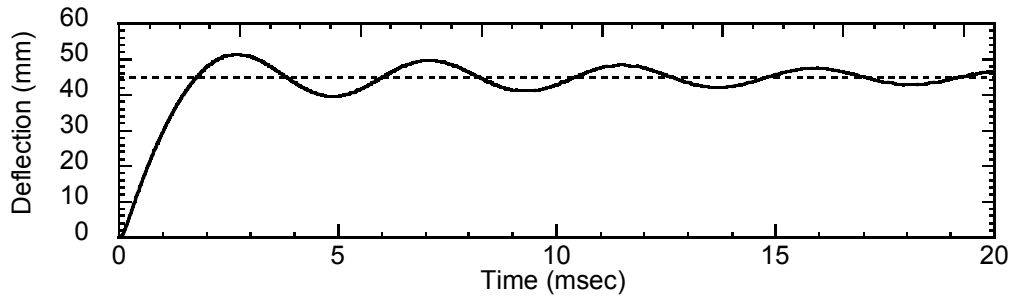
(c) Acceleration History



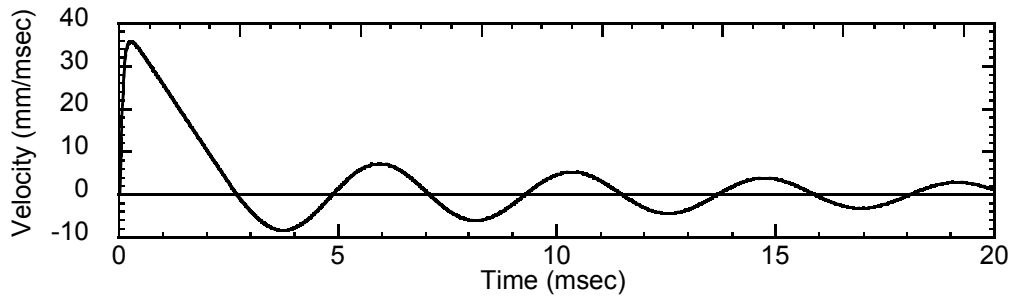
(d) Resistance Displacement Relationship

**Figure 4-9 Analytical Results for Test 1-6 with  $\beta=0.558$  (C4 Column)**

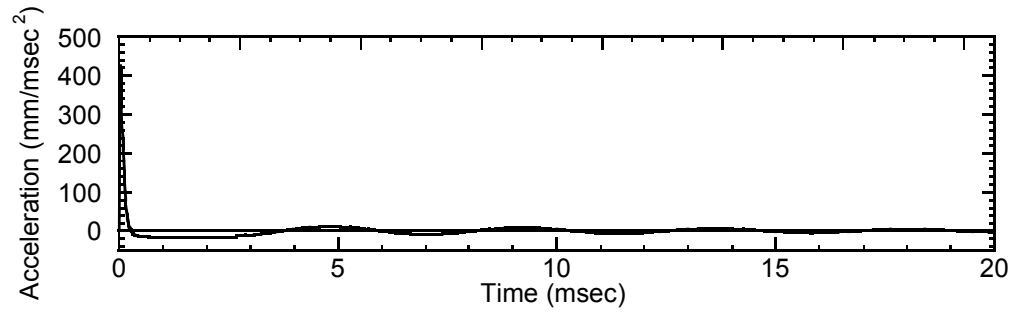




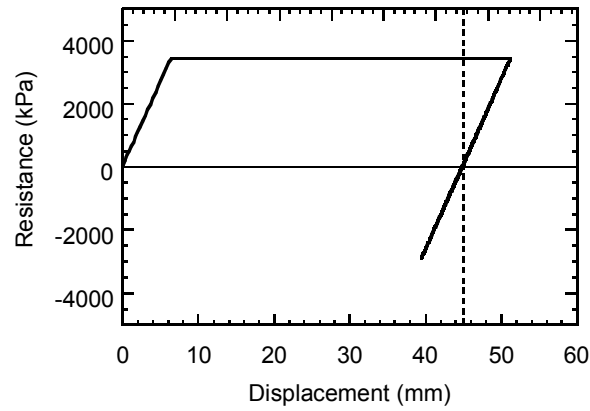
(a) Displacement History



(b) Velocity History

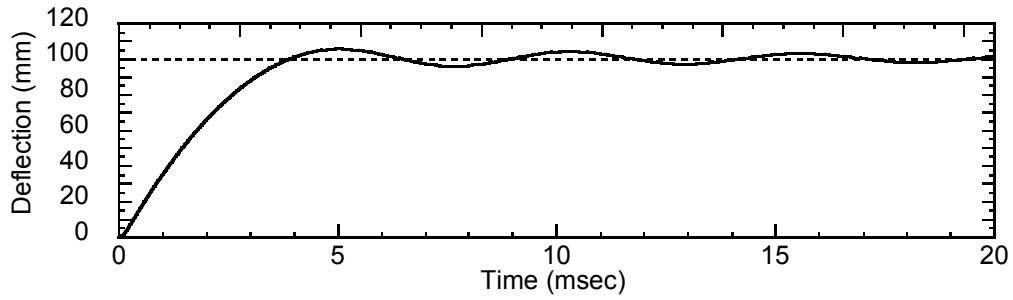


(c) Acceleration History

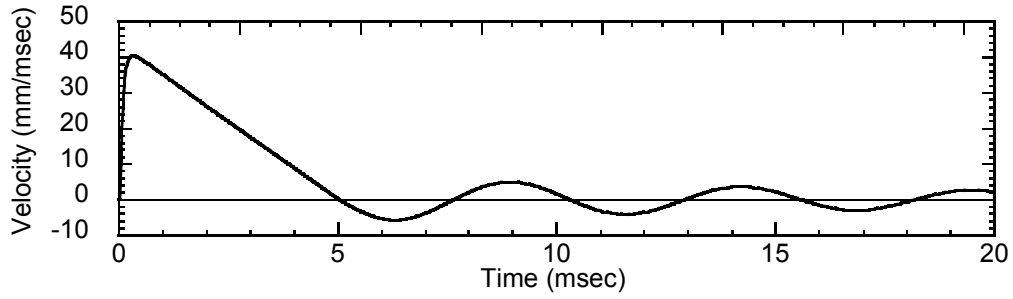


(d) Resistance Displacement Relationship

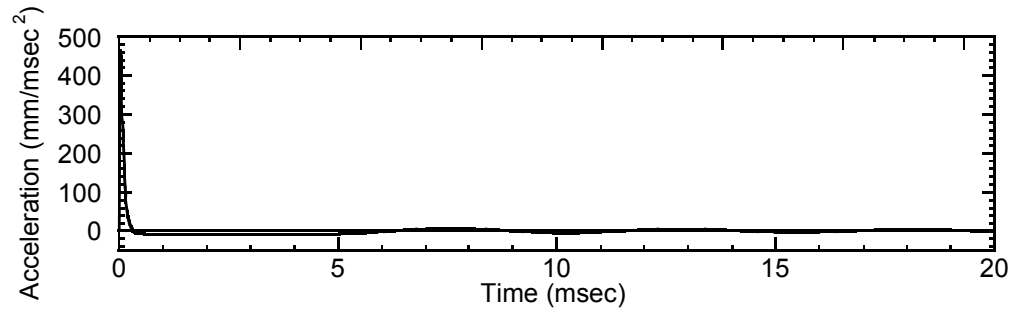
**Figure 4-10 Analytical Results for Test 1-9 with  $\beta=0.524$  (C6 Column)**



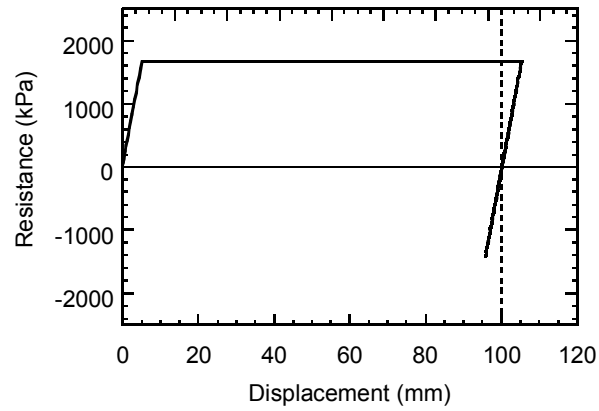
(a) Displacement History



(b) Velocity History



(c) Acceleration History



(d) Resistance Displacement Relationship

Figure 4-11 Analytical Results for Test 1-10 with  $\beta=0.492$  (C5 Column)

**Table 4-6 Summary of Maximum Response Values for SDOF Dynamic Analyses**

Test Num.	Col.	Pressure	Acceleration		Velocity		Displacement	
		Duration (msec)	Acc. (mm/msec <sup>2</sup> )	Time (msec)	Vel. (mm/msec)	Time (msec)	Displ. (mm)	Time (msec)
Test 1-3	C4	0.16	196.1	0.02	18.5	0.42	35.5	3.43
Test 1-4	C6	0.13	270.8	0.01	25.5	0.34	49.6	3.53
Test 1-5	C5	0.12	249.1	0.01	25.1	0.42	78.9	5.84
Test 1-6	C4	0.14	259.3	0.02	25.2	0.31	33.9	2.48
Test 1-9	C6	0.14	424.4	0.01	35.8	0.26	51.2	2.66
Test 1-10	C5	0.14	463.6	0.01	40.4	0.29	105.5	5.00

**Table 4-7 Natural Period and Pressure Duration**

Test Num.	Column	Natural Period $T_n$ (msec)	Pressure Duration $t_d$ (msec)	$t_d/T_n$
Test 1-3	C4	6.2	0.16	1/38.8
Test 1-4	C6	4.4	0.13	1/33.8
Test 1-5	C5	5.3	0.12	1/44.2
Test 1-6	C4	6.2	0.14	1/44.3
Test 1-9	C6	4.4	0.14	1/31.4
Test 1-10	C5	5.3	0.14	1/37.9

## 4.5 Fiber-based Analytical Model

### 4.5.1 General

The behavior of the three different types of bridge columns tested previously, namely CFST columns, RC columns and steel jacketed RC columns, needs to be analyzed using an advanced

analytical model to understand their behavior when subjected to blast loading. A fiber-based model was used for this purpose. The first step of a fiber-based model analysis is calibration of the model for the hysteretic behavior of materials under consideration for the three types of the bridge pier columns considered here. This is required to correctly set the parameters describing the model. Ideally this calibration should be accomplished using experimental results obtained from blast loading. However, the experimental data of these three type columns subjected to blast loading is not available for this purpose. Therefore, here, quasi-static cyclic loading test data is used instead to verify the developed analytical model itself.

Although an advanced finite element models (FEM) using solid elements or shell elements might be appropriate for capturing the localized behavior of the structural elements such as beam-column connections, frame models using a fiber-based beam-column model are more computationally effective to accurately capture the non-linear dynamic response analysis of structures (Spacone et al. 1996a, 1996b). In the fiber-based model, the member section is divided into fibers in which the unidirectional stress-strain relationships of the materials are assigned to represent the section characteristic. Note that the fiber-based model assumes that plane section remains plane and the section is normal to the longitudinal axis when the element deforms. The open-source computational program OpenSees (2007) was used to perform the fiber-based analyses in this research.

Following this subsection introduction, analytical model and solution algorithm used are discussed. Then, the details of the uniaxial constitutive models in this research are presented. Finally, the fiber-based analytical model is calibrated and verified by comparing with the quasi-static cyclic loading test data of CFST columns, RC columns and steel jacketed RC columns.

#### **4.5.2 Analytical Model and Solution Algorithm**

Figure 4-12 schematically shows the analytical model sections for (a) CFST columns, (b) RC columns and (c) steel jacketed RC columns. The sections are divided into fibers for which the different materials, as shown in Figure 4-12, are assigned different unidirectional stress-strain relationships. Core concrete and cover concrete are modeled by 256 confined concrete and 32 unconfined concrete relationships, respectively. Each rebar is modeled by one element. Steel

tube and steel jacket are modeled as 64 discretize steel bar fibers. Note that CFST column did not have the reinforcing steel bars inside of core concrete.

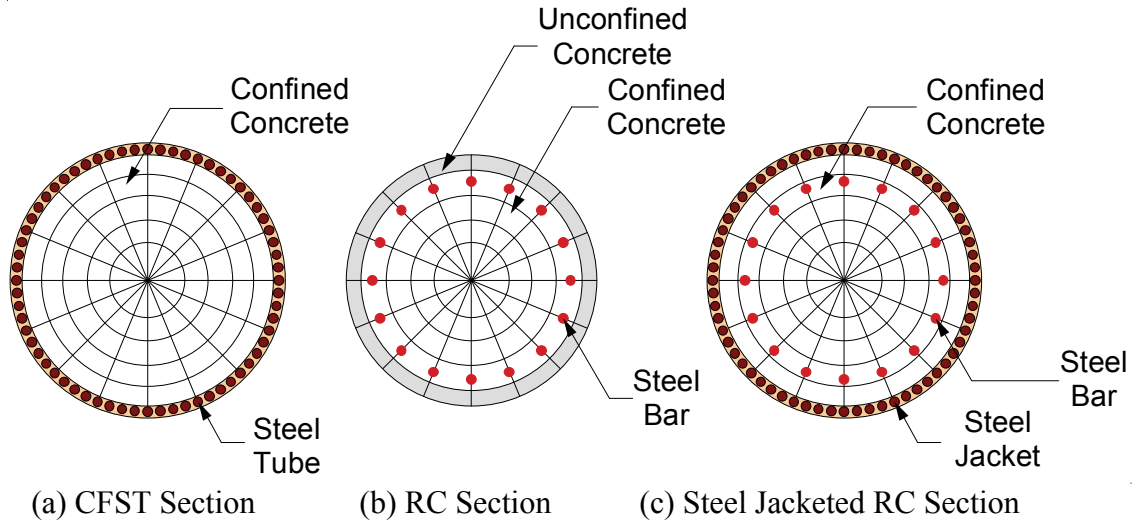


**Figure 4-12 Cross Sections for Fiber Element**

Figure 4-13 schematically shows the analytical models of the piers used for the quasi-static calibration tests using two-dimensional discrete frame models. This figure considers lateral load applied at the top of the column for a cantilever fixed at the base. The base of the RC column and steel jacketed RC column are modeled using zero-length section element to model strain penetration at this section. The strain penetration is the localized inelastic deformation occurring at the member end regions due to bar slips typically observed during the cyclic loading tests and also subjected to earthquake loading (Zhao and Sritharan 2007). A special inelastic element is introduced at that zero-length section element to model this behavior of reinforcing bars. Note that this strain penetration was not modeled for the blast test columns because these localized inelastic deformations at the member end regions were not observed in the experimental observations.

To solve the nonlinear equilibrium equation, the Krylov-Newton algorithm provided by OpenSees (2007) was used. Krylov-Newton algorithm is an iterative incremental solver based on the modified Newton method with Krylov subspace acceleration to calculate the next time

step. This algorithm gives relatively faster and more robust convergence in general. (Charlson and Miller 1998)

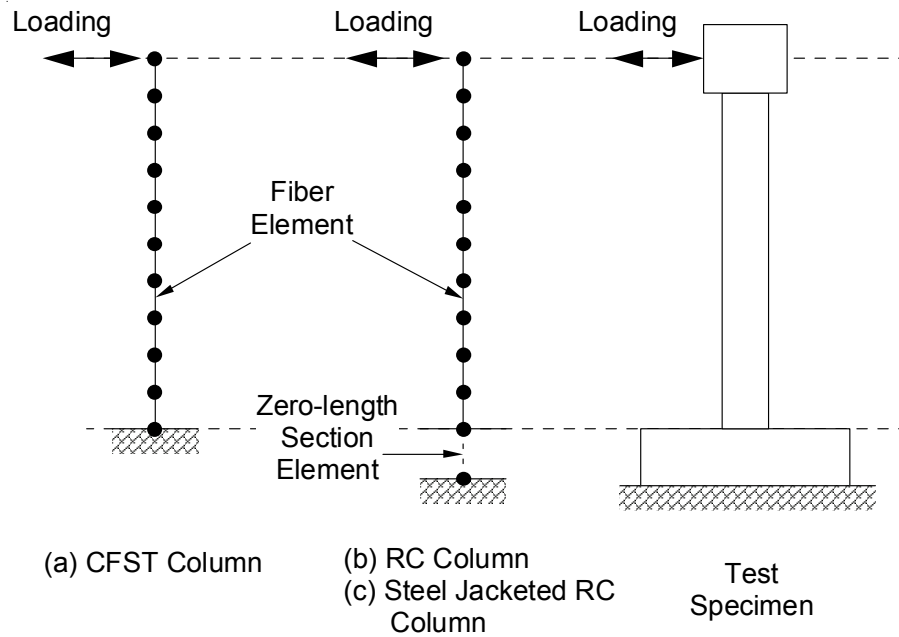


**Figure 4-13 Analytical Model for Cyclic Loading Test Specimen**

### 4.5.3 Material Constitutive Models

A variety of unidirectional stress-strain relationships is available for steel and concrete to replicate the behavior of reinforced concrete elements. Selection of the constitutive model is the key to simulate structural response accurately. Research on the analysis of reinforced concrete structures (e.g. Orakcal and Wallace 2006a, Zhao and Sritharan 2007 to name a few) has showed that using fiber models implemented with appropriate constitutive relations for concrete and reinforcing steel can accurately predict the nonlinear behavior of the structures when compared with the experimental results. The following subsections describe the details of the uniaxial constitutive models for concrete and steel adopted in this research. The tension stiffening model for steel bars in the RC members and the strain penetration model occurring along longitudinal steel bars at the connection intersection are also described.

#### 4.5.3.1 Constitutive Model for Steel

To represent the uniaxial constitutive model for reinforcing steel bars, steel jackets, and steel tubes of CFST columns, the Menegotto-Pinto model (Menegotto and Pinto 1973) was used. This model considers the hysteretic behavior of steel and account for Bauschinger effect. Isotropic strain hardening is expected to occur during crack closure in a reinforced concrete member (Filippou et al. 1983). To account for this effect, the modified Menegotto-Pinto model by Filippou et al. (1983) is implemented in the reinforcing steel bars of the reinforced concrete members considered here.

The stress-strain ( $\sigma - \varepsilon$ ) relationship of Menegotto-Pinto model is schematically shown in Figure 4-14. The points  $(\varepsilon_r, \sigma_r)$  and  $(\varepsilon_0, \sigma_0)$  in Figure 4-14 are, respectively, the reversal point and the intersection of two asymptotes which are the elastic asymptote with stiffness of  $E_0$  and the yield asymptote with stiffness of  $E_1$ . The point  $(\varepsilon_r', \sigma_r')$  is the previous reversal point. The model is represented by:

$$\sigma^* = b\varepsilon^* + \frac{(1-b)\varepsilon^*}{(1+\varepsilon^{*R})^{\frac{1}{R}}} \quad (4-5)$$

where

$$\varepsilon^* = \frac{\varepsilon - \varepsilon_r}{\varepsilon_0 - \varepsilon_r} \quad (4-6)$$

$$\sigma^* = \frac{\sigma - \sigma_r}{\sigma_0 - \sigma_r} \quad (4-7)$$

$$b = \frac{E_1}{E_0} \quad (4-8)$$

$b$  is the strain hardening ratio, and  $R$  is the Bauchinger effect coefficient given by:

$$R = R_0 - \frac{a_1 \xi}{a_2 + \xi} \quad (4-9)$$

where

$$\xi = \left| \frac{\varepsilon_0 - \varepsilon_r'}{\varepsilon_y} \right| \quad (4-10)$$

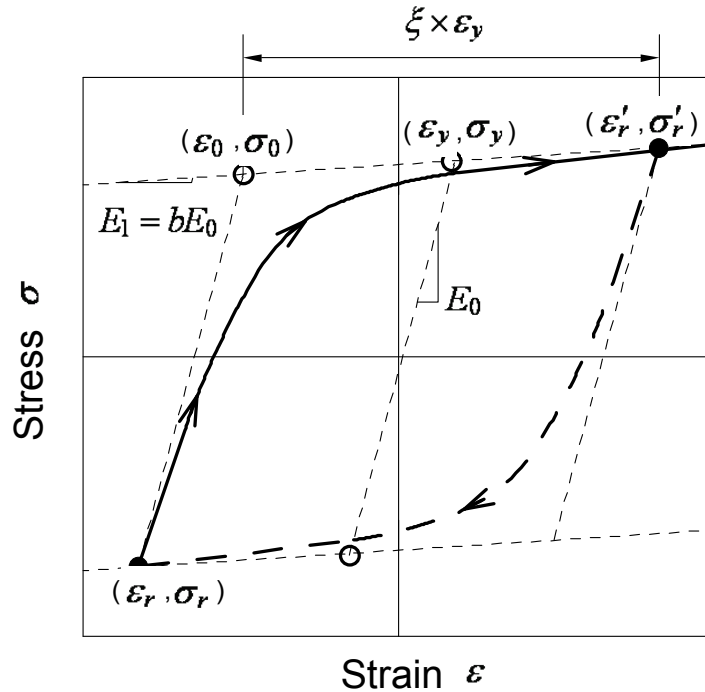


**Figure 4-14 Constitutive Model for Steel (Menegotto and Pinto 1973)**

$R_0 = 20$ ,  $a_1 = 18.5$  and  $a_2 = 0.15$  are the values recommended by Menegotto and Pinto experimentally for reinforcing bars.

Filippou et al. (1983) proposed a modified Menegotto-Pinto model for the reinforcing steel bars in reinforced concrete members to account for isotropic strain hardening. As schematically shown in Figure 4-15, this isotropic strain hardening effect is simply considered by shifting the yield asymptote by  $\sigma_{st}$ .  $\sigma_{st}$  is given by:

$$\sigma_{st} = a_3 \left( \frac{\varepsilon_{\max}}{\varepsilon_y} - a_4 \right) \sigma_y \quad (4-11)$$

where  $\varepsilon_{\max}$  is the absolute maximum strain at the instant of strain reversal,  $\varepsilon_y$  and  $\sigma_y$  are yield strain and stress, respectively, and  $a_3$  and  $a_4$  are parameters to be determined experimentally.

Filippou et al recommended using values of  $a_3 = 0.01$  and  $a_4 = 7$ .



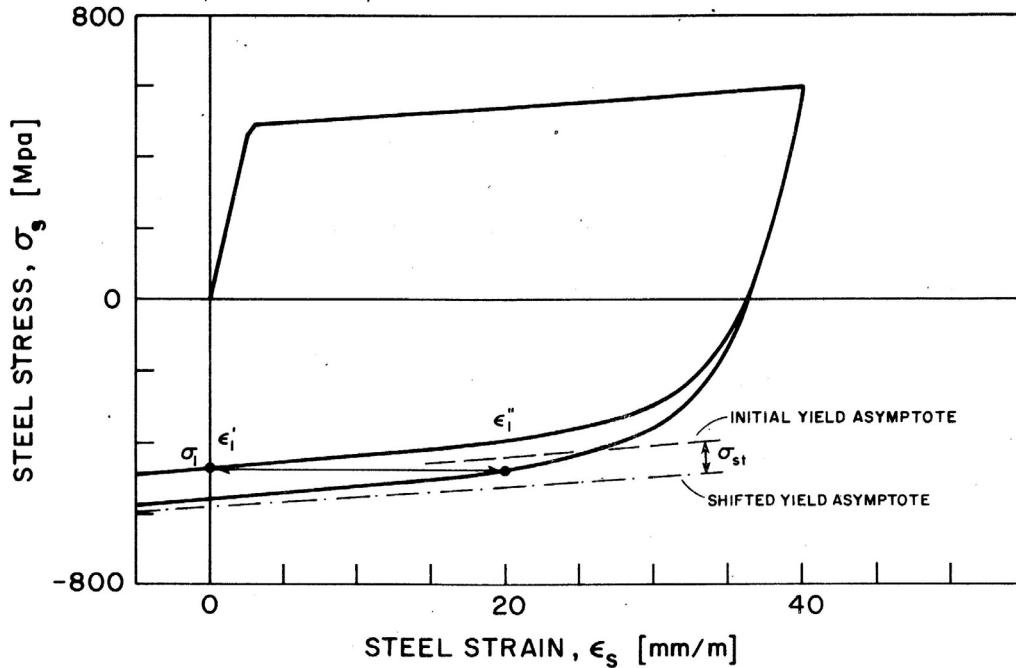


**Figure 4-15 Shift of Yield Asymptote due to Isotropic Strain Hardening (Filippou et al. 1983)**

#### 4.5.3.2 Constitutive Model for Concrete

As shown in Figure 4-12, core concrete of RC columns, and concrete of CFST columns and steel jacketed RC columns are modeled by confined concrete, and cover concrete of RC column was modeled by unconfined concrete. The uniaxial hysteretic constitutive relationship of modified Chang-Mander model (Waugh 2007) was adopted for both unconfined and confined concrete except for the core concrete of the zero-length section element (see Figure 4-13). This is because large deformation needs to be accommodated at this location (the zero-length section element) in the analysis due to the strain penetration of longitudinal steel bars at the base of the column. For this purpose, modified Scott-Kent-Park model (Yassin 1994) was used in the core concrete of the zero-length section element.

#### 4.5.3.3 Tension Stiffening Model for Steel Bars

The stress-strain relationship of steel bars embedded in concrete is different from that of bare bars (as typically tested to determine their material properties), because steel bars in concrete are stiffened by concrete (called “tension stiffening”). When a reinforced concrete member is

subjected to a uniaxial tension force, cracks develop in the member between the forces. Since the cracked and uncracked parts of the reinforced concrete member resist the longitudinal tension force, the stresses and strains vary along the member.

Belarbi and Hsu (1994) proposed the stress-strain constitutive model for a mild steel bar embedded in a reinforced concrete member by averaging the stress and the strain of steel bars along the member, based on comprehensive reinforced concrete panel tests subjected to uniaxial stresses. It was found that the average yield stress of steel bars in concrete was lower than that of bare bars. The following bilinear model was proposed for the average stress-strain ( $f_s - \epsilon_s$ ) constitutive model of mild steel bars embedded in concrete:

$$f_s = E_s \epsilon_s \quad f_s \leq (0.93 - 2B) f_y \quad (4-12)$$

$$f_s = (0.91 - 2B) f_y + (0.02 + 0.25B) E_s \epsilon_s \quad f_s > (0.93 - 2B) f_y \quad (4-13)$$

with

$$B = \frac{1}{\rho} \left( \frac{f_{cr}}{f_y} \right)^{1.5} \quad (4-14)$$

where  $f_y$  and  $E_s$  are the yield strength and modulus of elasticity of bare steel bars, respectively, and  $f_{cr}$  is the concrete cracking strength.

Note that this tension stiffening model provides a backbone envelop curve of constitutive stress-strain curve. Therefore, the hysteresis constitutive model for reinforcing steel bars was determined such that the backbone envelope of the curve was decided by this tension stiffening model and the hysteresis rules within that envelope followed the Menegotto-Pinto model as presented in Section 4.5.3.1.

#### 4.5.3.4 Strain Penetration Model for Steel Bars

As previously discussed in Section 4.5.2, large deformations typically develops at the base of a column due to the strain penetration of longitudinal steel bars during cyclic loading tests and also as such during to earthquakes. For this purpose, the zero-length section element was used at this location as shown in Figure 4-13. Zhao and Sritharan (2007) proposed a hysteretic stress-slip

model for reinforcing bars that can be implemented in fiber-based analysis using the zero-length section element.

The proposed hysteretic stress-slip model ( $\sigma - s$ ) is shown in Figure 4-16. The backbone envelope curve has two regions, namely a straight line for the elastic region and a curvilinear part for the post-yield region, as shown in Figure 4-16 (a). The post-yield curve is represented by:

$$\tilde{\sigma} = \frac{\frac{\tilde{s}}{\mu - \tilde{s}}}{\left[ \left( \frac{1}{\mu b} \right)^{R_e} + \left( \frac{\tilde{s}}{\mu - \tilde{s}} \right)^{R_e} \right]^{\frac{1}{R_e}}} \quad (4-15)$$

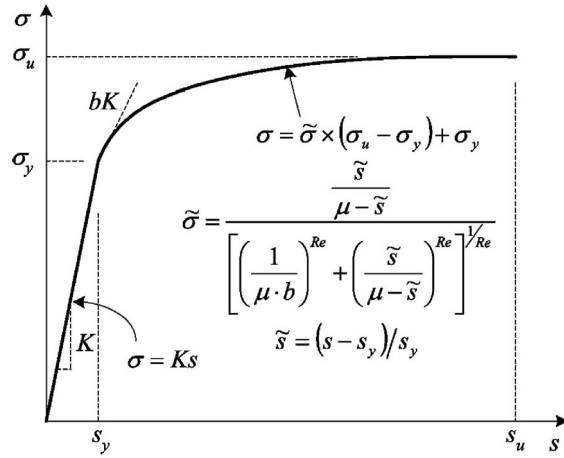
with

$$\tilde{\sigma} = \frac{\sigma - f_y}{f_u - f_y} \quad (4-16)$$

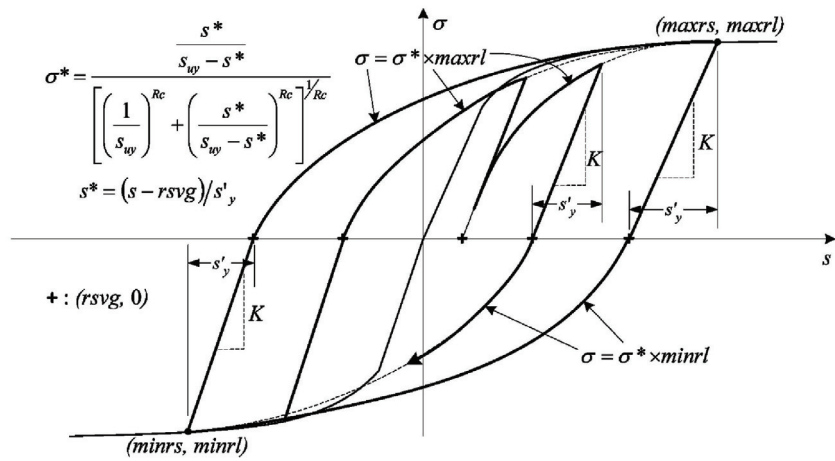
$$\tilde{s} = \frac{s - s_y}{s_y} \quad (4-17)$$

$$\mu = \frac{s_u - s_y}{s_y} \quad (4-18)$$

where  $b$  is the stiffness reduction factor,  $R_e$  is a factor to control the shape of the curve (taken as 1.01 by Zhao and Sritharan),  $f_y$  and  $f_u$  are respectively the yield and ultimate strengths of the steel reinforcing bar, and  $s_y$  and  $s_u$  are the corresponding loaded-end slips. From the experimental database, they also found that  $s_u = 30 \sim 40 s_y$  and  $b = 0.3 \sim 0.5$  would be appropriate in their proposed model. As shown in Figure 4-16 (b), the unloading path follows a straight line with the elastic slope until the stress becomes zero. The reloading path follows the same shape as the post-yield envelop curve.



(a) Envelope Curve



(b) Hysteresis Curve

**Figure 4-16 Strain Penetration Model for Steel Bar (Zhao and Sritharan 2007)**

**4.5.3.4.1 Modified Chang-Mander Model (Waugh 2007)**

The Chang-Mander model (Chang and Mander 1994) is a uniaxial hysteretic constitutive model for unconfined and confined concrete, which was developed using statistical regression analysis for an extensive experimental database of cyclic compression tests from a number of researchers. Waugh (2007) simplified this Chang-Mander model to increase its computational efficiency and the numerical stability. The modified model is schematically shown in Figure 4-17. Three simplifications of the Cheng-Mander model were made for this purpose. First, the original

model uses a power function for its unloading and reloading paths, but these power function curves are simplified into tri-linear curves. Second, the original model represented in dashed line in Figure 4-17 shifts the tension envelop by  $\varepsilon_0$  (as shown in Figure 4-17), but the modified model does not shift the tension envelop. Lastly, when the curve rejoins the backbone envelope after unloading and reloading, increases in additional strain transition smoothly in the original model, but this is not modeled in the modified model. Compressive and tensile stress-strain backbone envelope curves for unconfined and confined concrete are presented as follows.

The compressive stress-strain ( $f_c - \varepsilon_c$ ) backbone envelope curve for unconfined concrete of the Cheng-Mander model is given by:

$$y = \frac{nx}{1 + \left(n - \frac{r}{r-1}\right)x + \frac{x^r}{r-1}} \quad (4-19)$$

where  $y = f_c/f'_c$ ,  $x = \varepsilon_c/\varepsilon'_c$ ,  $f'_c$  is the maximum compressive strength (MPa),  $\varepsilon'_c$  is the corresponding strain, and  $n$  and  $r$  are parameters to control the curve shape. The parameter  $n$  is given by:

$$n = \frac{E_c \varepsilon'_c}{f'_c} \quad (4-20)$$

where  $E_c$  is initial modulus of elasticity. Based on experimental results, the recommended values for parameters  $E_c$ ,  $\varepsilon'_c$ , and  $r$  to define the compressive envelope are:

$$E_c = 8200 f'_c \text{ (MPa)} \quad (4-21)$$

$$\varepsilon'_c = \frac{(f'_c)^{\frac{1}{4}}}{28} \quad (4-22)$$

$$r = \frac{f'_c}{5.2} - 1.9 \text{ (MPa)} \quad (4-23)$$

The tension stress-strain backbone envelope curve for unconfined concrete is in the same shape as that of the compression envelope. The recommended tensile strength,  $f_t$ , and the corresponding strain  $\varepsilon_t$  (see Figure 4-17) are:

$$f_t = 0.62 \sqrt{f'_c} \text{ (MPa)} \quad (4-24)$$

$$\varepsilon_t = \frac{2f_t}{E_c} \quad (4-25)$$

A compressive stress-strain ( $f_c - \varepsilon_c$ ) backbone envelope curve for confined concrete is given by the same equation as that for unconfined concrete (i.e. Equation 4-19). In this case,  $y = f_c / f'_{cc}$  and  $x = \varepsilon_c / \varepsilon'_{cc}$  where  $f'_{cc}$  is the maximum compressive strength of confined concrete (MPa) and  $\varepsilon'_{cc}$  is the corresponding strain. The maximum compressive strength,  $f'_{cc}$ , is given by:

$$f'_{cc} = f'_c (1 + k_1 \bar{x}) \quad (4-26)$$

with

$$k_1 = A \left( 0.1 + \frac{0.9}{1 + B\bar{x}} \right) \quad (4-27)$$

$$\bar{x} = \frac{f'_{l1} + f'_{l2}}{2f'_c} \quad (4-28)$$

$$A = 0.68886 - (0.6069 + 17.275r) e^{-4.989r} \quad (4-29)$$

$$B = \frac{4.5}{\frac{5}{A} (0.9849 + 0.6306 e^{-3.8939r}) - 0.1} - 5 \quad (4-30)$$

$$r = \frac{f'_{l1}}{f'_{l2}} \quad f'_{l2} \geq f'_{l1} \quad (4-31)$$

where  $f'_{l1}$  and  $f'_{l2}$  are lateral confinement pressure in each direction (and where  $f'_{l1} = f'_{l2} = f'_l$  for circular column). The strain at peak stress,  $\varepsilon'_{cc}$ , is given by:

$$\varepsilon'_{cc} = \varepsilon'_c (1 + k_2 \bar{x}) \quad (4-32)$$

with  $k_2 = 5k_1$ .

The effective lateral confining pressure,  $f'_l$ , of a reinforced concrete column is given by:

$$f'_l = K_e f_l = K_e \left( \frac{2f_{yh} A_{sp}}{D' s_h} \right) \quad (4-33)$$

where  $f_l$  is the maximum effective lateral pressure, and  $f_{yh}$ ,  $A_{sp}$ ,  $D'$  and  $s_h$  are the yield strength, area, diameter and longitudinal spacing of spirals or hoops, respectively.  $K_e$  is typically taken as 0.95 for circular sections, 0.75 for rectangular sections, and 0.6 for rectangular

wall sections. Note that the above equation for the effective lateral confining pressure is used here for RC columns, but is not used for CFST columns and steel jacketed RC columns. This is because Bruneau and Marson (2004) have shown that using the confined concrete strength of CFST columns significantly overestimate their capacity. Therefore, here, the effective confinement stress,  $f'_l$ , was taken as 2.07 MPa (300 psi), which is the value used in this design methods of a steel jacketed RC column developed by Chai et al. (1991).

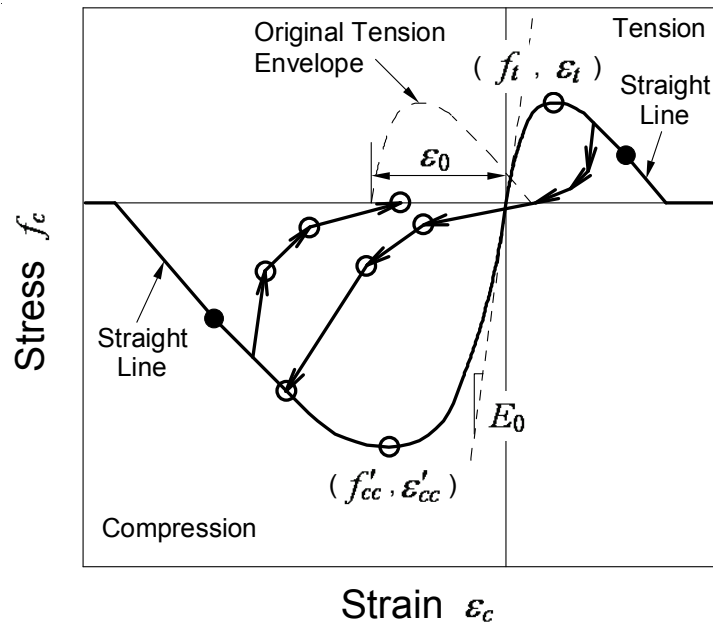


**Figure 4-17 Modified Chang-Mander Model for Concrete (adapted from Waugh 2007)**

#### 4.5.3.4.2 Modified Scott-Kent-Park Model by Yassin et al. (1994)

The modified Scott-Kent-Park model (Yassin 1994) was used in the core concrete of the zero-length section element to accommodate the large deformation there. Orakcal et al. (2006b) provided a good description of this model. Yassin (1994) proposed the hysteretic unloading and reloading rules using the Scott-Kent-Park model strain-stress relationship model for confined concrete (Scott et al. 1982).

The modified Scott-Kent-Park Model is schematically shown in Figure 4-18. There are three regions in this backbone envelope curve, namely an ascending curve (OA), a descending straight a horizontal (AB), and constant straight curve (BC), which are given by:

$$f_c = Kf'_c \left[ 2 \left( \frac{\epsilon_c}{\epsilon_0} \right) - \left( \frac{\epsilon_c}{\epsilon_0} \right)^2 \right] \quad \epsilon_c \leq \epsilon_0 \text{ (OA)} \quad (4-34)$$

$$f_c = Kf'_c [1 - Z(\epsilon_c - \epsilon_0)] \quad \epsilon_0 < \epsilon_c \leq \epsilon_{\alpha 0} \text{ (AB)} \quad (4-35)$$

$$f_c = \alpha Kf'_c \quad \epsilon_c > \epsilon_{\alpha 0} \text{ (BC)} \quad (4-36)$$

where

$$\epsilon_0 = 0.002K \quad (4-37)$$

$$K = 1 + \frac{\rho_s f_{yh}}{f'_c} \quad (4-38)$$

$$Z = \frac{0.5}{\frac{3 + 0.29f'_c}{145f'_c - 100} + 0.75\rho_s \sqrt{\frac{h'}{s_h}} - \epsilon_0} \quad (4-39)$$

In these equations,  $\epsilon_0$  is the concrete strain at maximum stress of  $Kf'_c$ ,  $\epsilon_{\alpha 0}$  is the strain when the horizontal straight curve segment starts (at point B in Figure 4-18),  $K$  is the factor accounting for the strength increase in maximum stress due to confinement (at point A in Figure 4-18),  $Z$  is the slope of strain softening (along AB in Figure 4-18),  $f'_c$  and  $f_{yh}$  are, respectively, the concrete compressive strength (MPa) and the transverse reinforcement yield strength (MPa),  $\rho_s$  is the volumetric ratio of transverse reinforcement,  $h'$  is the width of core concrete, and  $s_h$  is the spacing of stirrups of hoop. Also,  $\alpha$  is a factor to determine the magnitude of the strength in region BC in Figure 4-18. Scott et al. (1982) suggested  $\alpha = 0.2$ , but  $\alpha = 0.6$  was used to accommodate the large deformation in the zero-length section element at the base of the column in this research.



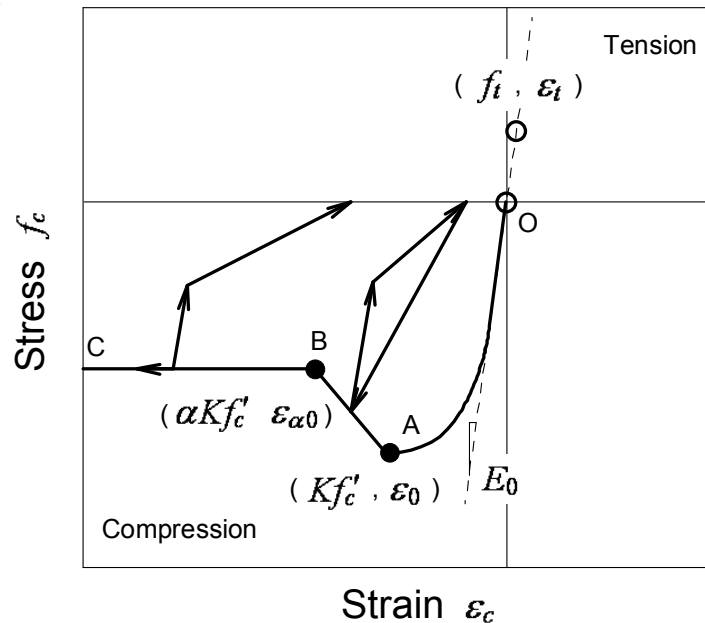


**Figure 4-18 Modified Scott-Kent-Park Model for Concrete (adapted from Yassin 1994)**

#### 4.5.4 Model Verification with Quasi-Static Tests

As discussed in the beginning of this subsection, the purpose of this analytical study is to simulate the blast response of three different types of the bridge pier columns, namely CFST columns, RC columns and steel jacketed RC columns, using fiber-based analysis model as presented above. As a first step, for the sake of verifying the fiber-based model itself, correlation studies were conducted for the quasi-static cyclic loading tests of the three different type columns. The analytically predicted behavior of these columns was compared with the experimentally obtained one. Accordingly, two different columns for each type of column tested by various researchers were used for each CFST column, RC column and steel jacketed RC column, and the details of these columns are provided in the following.

##### 4.5.4.1 Overview of Experimental Studies

Two different columns for each column type were selected, namely the two CFST column specimens CFST-34 and CFST-42 tested by Marson and Bruneau (2004), the two RC column specimens RC-TP60 and RC-Unit9 tested by Matsukawa et al. (2002) and Ghee et al. (1989),

respectively, and the two steel jacketed RC column specimens SJ-Unit4 and SJ-CR2 tested by Chai et al. (1991) and Priestley et al. (1994a, 1994b), respectively. All these six columns were tested under cyclic loading to investigate the seismic performance of each type of columns.

Details and material properties of each test column are shown in Table 4-8 and Table 4-9, respectively. All columns were fixed at their base and free at their top where loads were applied, except for the SJ-CR2 Column. In the case of the SJ-CR2 Column, the base of the column was fixed and rotation of the top of the column was constrained. “Effective height” in Table 4-8 is defined as the distance between the bottom of the column and the center of the loading actuator. In Table 4-9,  $f'_c$  is the concrete strength,  $f_y$ ,  $f_{yh}$  and  $f_{yj}$  are, respectively, the yield strength of longitudinal reinforcement steel, transverse reinforcement steel, and steel tube or steel jacket. The details of specimen and the hysteresis loops experimentally obtained are presented in Appendix I. These hysteresis loops from the experiments are compared with those of analytical results later.

**Table 4-8      Cyclic Loading Test Column Details**

	Column Type	Effective Height (mm)	Column Diameter (mm)	Axial Force (kN)	Boundary Condition
CFST-34	CFST Column	2200	323.9	1920	Fix-Free
CFST-42		2200	406.4	1920	Fix-Free
RC-TP60	RC Column	1350	400.0	180	Fix-Free
RC-Unit9		1000	400.0	751.5	Fix-Free
SJ-Unit4	Steel Jacketed Column	3658	632.2	1779	Fix-Free
SJ-CR2		2438	632.2	591.6	Fix-Fix (Rotation)

**Table 4-9 Material Properties of Cyclic Loading Test Columns**

	Column Type	Longitudinal Steel Ratio (%)	Transverse Steel Ratio (%)	$f'_c$ (MPa)	$f_y$ (MPa)	$f_{yh}$ (MPa)	$f_{yj}$ (MPa)
CFST-34	CFST Column	9.05	N/A	40	N/A	N/A	415
CFST-42		9.13	N/A	35	N/A	N/A	505
RC-TP60	RC Column	2.02	0.745	27.8	377	374	N/A
RC-Unit9		3.20	1.02	29.9	448	372	N/A
SJ-Unit4	Steel Jacketed Column	2.53	0.174	38.1	315	352	324
SJ-CR2		2.53	0.18	34.0	324	359	348

#### 4.5.4.2 Analytical Model for Cyclic Loading Test Columns

The six columns were modeled by two-dimensional discrete models using beam-column elements as previously described in Section 4.5.2. Figures 4-19 to 4-21 show the individual analytical models for the CFST columns, RC columns, and steel jacketed RC columns, respectively, along with the assignment of fiber sections to the elements. CFST columns were modeled using the CFST sections shown in Figure 4-12 (a), and RC columns were modeled using the RC sections shown in Figure 4-12 (b). In steel jacketed RC columns, assuming the bond stress between the steel jacket and grout developed at a length of half of the column diameter from the edge of the jacket, the contribution of the steel jacket to the flexural resistance of the column was not considered over these length, but confinement effect by the steel jacket (SJ Confined in Figure 4-21 (a)) was considered. Therefore, the label quote as “SJ Section” in Figure 4-21 means that steel jackets increase the flexural strength as well as increasing the confinement of the reinforced concrete section. The label quote as “RC Section (SJ Confined)” in Figure 4-21 means that the reinforced concrete section is confined, but the steel jackets do not increase the flexural strength of the section. Note that in Figure 4-21 (a) for that particular column, the steel jacket extended only for limited height from the bottom of the column upward as opposed to the SJ-CR2 Column in Figure 4-21 (b) for which the steel jacket spanned the entire height of the column. The rotation of the top of the SJ-CR2 Column was constrained as shown

in Figure 4-21 (b). The zero-length element was used in both RC columns and steel jacketed RC columns to implement the strain penetration model.

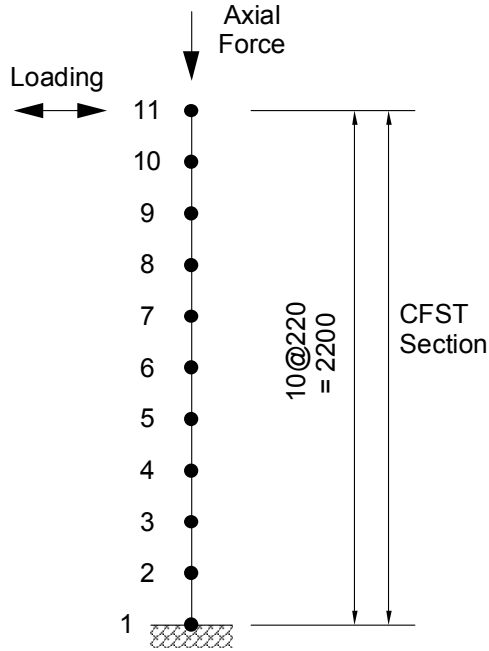


**Figure 4-19 Analytical Model for CFST Column**

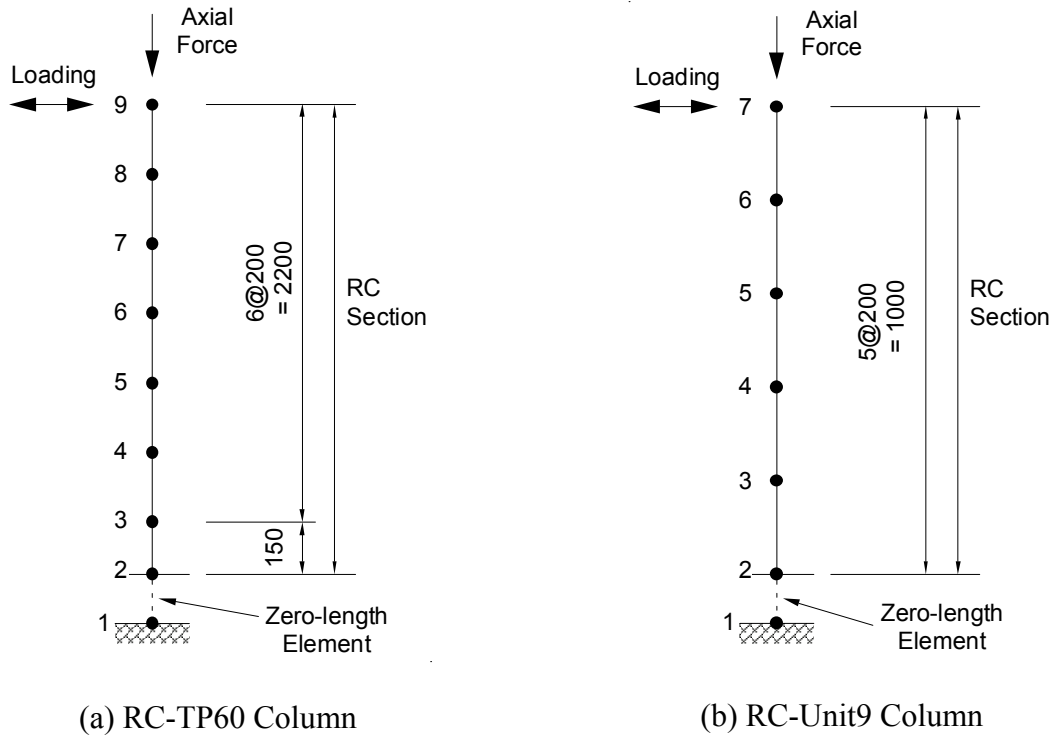
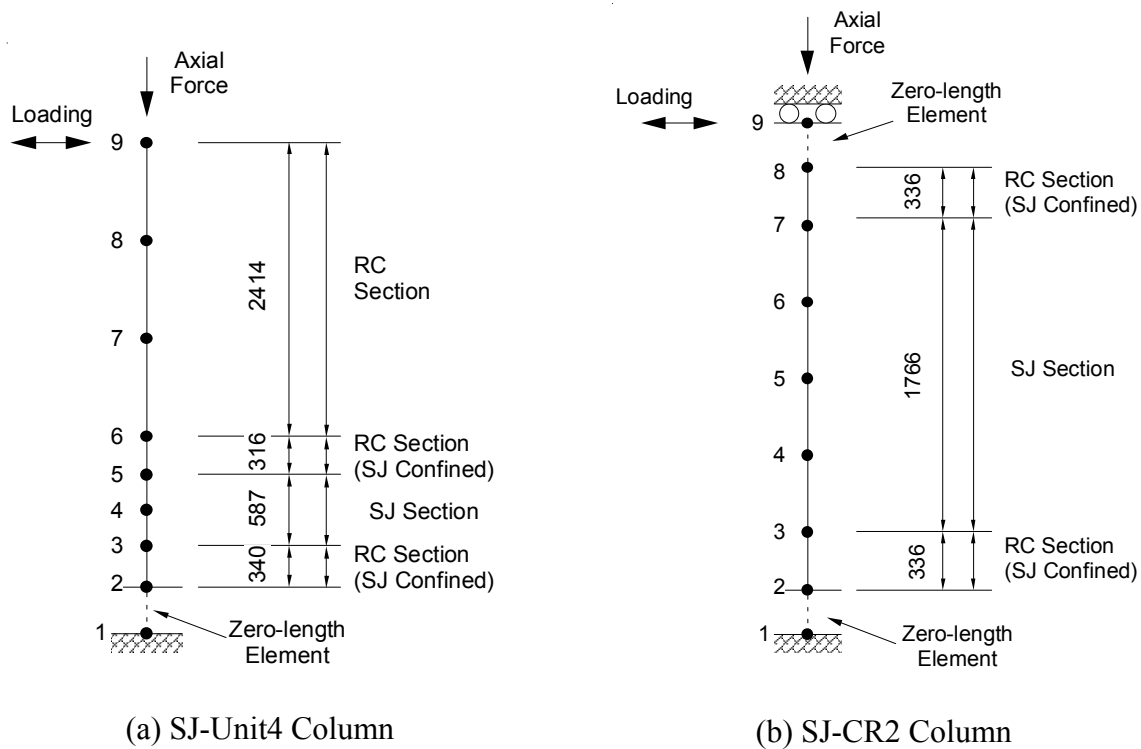


**Figure 4-20 Analytical Model for RC Column**



(a) SJ-Unit4 Column (b) SJ-CR2 Column  
**Figure 4-21 Analytical Model for Steel Jacketed RC Column**

#### 4.5.4.3 Analytical Results and Comparison with Experimental Results

Figures 4-22 (a) through 4-27 (a) compare the experimentally obtained hysteresis loops with the analytical results computed using the fiber-based model for the column and material properties outlined in the prior subsections for the same six columns. Figures 4-22 (a) and 4-23 (a) compare the base moment-displacement hysteresis loops, and Figures 4-24 (a) through 4-27 (a) compare the lateral force-displacement hysteresis loops (because that is how they were presented in the original publications). In Figures 4-22 to 4-27, the analytical stress-strain relationships of (b) the core concrete at the compression edge and (c) the steel tube or steel bar at the tension edge, are also presented. Note that in many of the experiments multiple cycles of loadings were applied to each specified value of displacements (sometimes up to 3 or 5 cycles depending on the experiment), but here only one cycle of loading was applied in the numerical analyses conducted. The experimental hysteresis loops of CFST-34 and CFST-42, and SJ-CR2 were plotted based on the graphs presented in Marson and Bruneau (2004) and Priestley et al. (1994b), respectively. The experimental hysteresis loops of RC-TP60, and RC-Unit9 and SJ-Unit4 were obtained from

the Kawashima Lab Test Database (Tokyo Tech 2008) and the PEER Structural Performance Database (PEER 2008), respectively. Here, it is observed in Figures 4-22 (a) through 4-27 (a) that the analytically obtained hysteretic behaviors capture well the experimentally obtained ones at least for the first cycle of displacement at the same displacement amplitude.

To further evaluate effectiveness of the analytical results in replicating the experimentally obtained hysteresis loops, (a) the maximum base moment or lateral force at each cycle and (b) the residual displacement at each cycle, are compared with those obtained from the test results for the CFST columns, RC columns and steel jacketed RC columns in Figures 4-28 to 4-30, respectively. The results on the figures show the ratio of the analytical results to the experimental results versus the maximum drift at each cycle.

Figure 4-28 shows that the maximum base moment of CFST columns was predicted within 10% accuracy when the drift is larger than 2%. The accuracy was substantially less for those values at lower magnitude of drift. The difference between the analytical and experimental results was significantly larger for the residual displacements although at larger drift in excess of 1% in positive direction and 4% in negative direction the accuracy is still within 10%. This provided confidence in the analytical model particularly given for the blast analyses, presented in subsequence subsection, for which the specimens were subjected to significantly larger than 2% drift.

As shown in Figure 4-29(a), the difference in maximum lateral force of RC columns between the analyses and experiments are within 20%. The residual displacement of RC-TP60 was predicted very well, but the analytical residual displacement of RC-Unit9 was larger than experimental one by more than 20% as shown in Figure 4-29(b). Note that the data between -1.5% and 1.0 % was not available in these cases.

Figure 4-30 shows that the maximum lateral force of steel jacketed RC columns was predicted within 10% accuracy when the drift is larger than 1.5%. The accuracy was substantially less for those values at lower magnitude of drift. The difference between the analytical and experimental

results was significantly larger for the residual displacements although at larger drift in excess of 1.5 % in positive direction and 3% in negative direction the accuracy is still within 20%.

Overall, for all the types of columns considered, the analyses conducted in this section demonstrate that the fiber-based model is able to capture reasonably well the maximum lateral forces that can be developed in the specimen as well as their residual displacements for the magnitude of inelastic deformation typically expected to develop in blast loading situations.

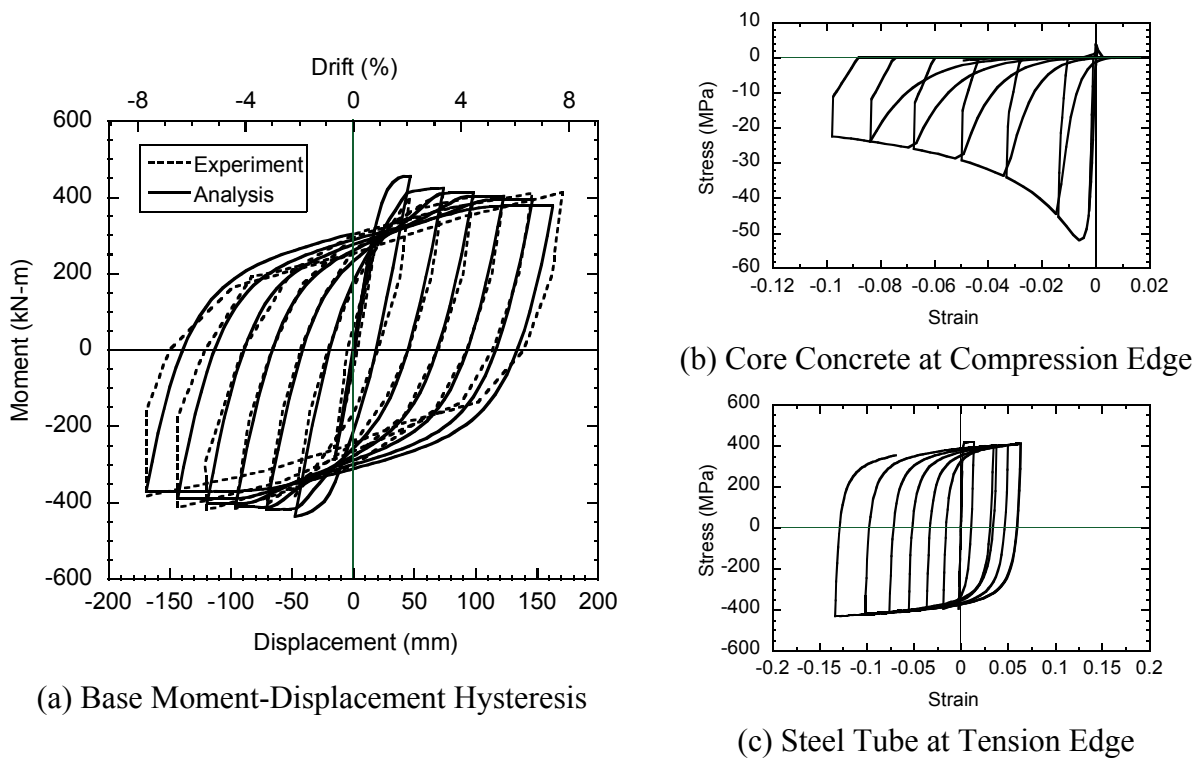
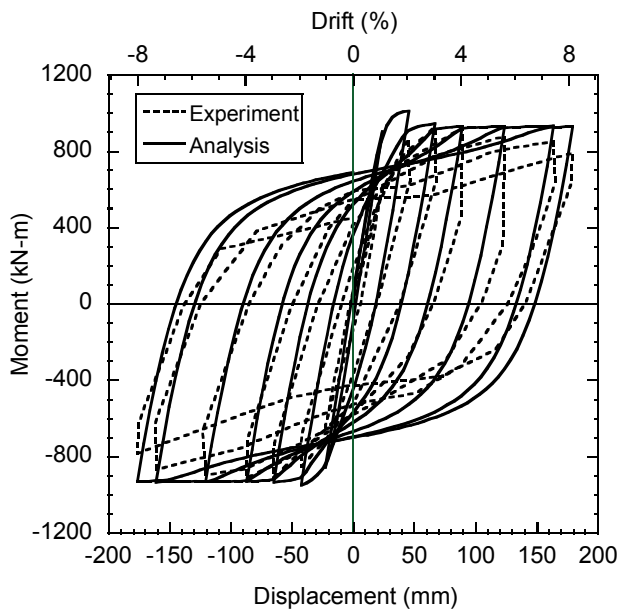
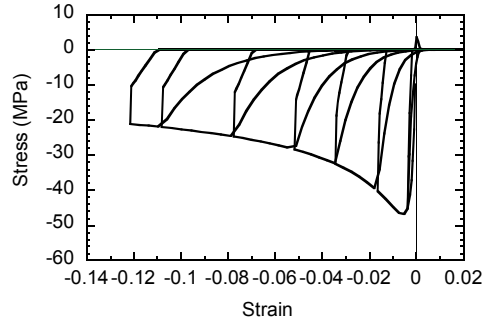


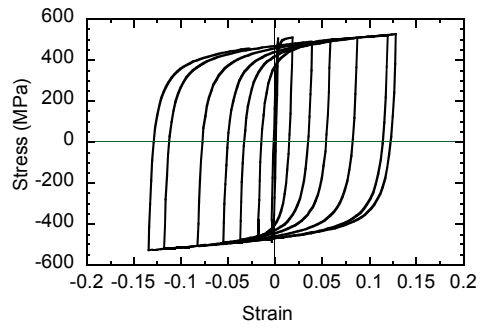
**Figure 4-22 Analytical Results for Cyclic Loading Test of CFST-34**



(a) Base Moment-Displacement Hysteresis

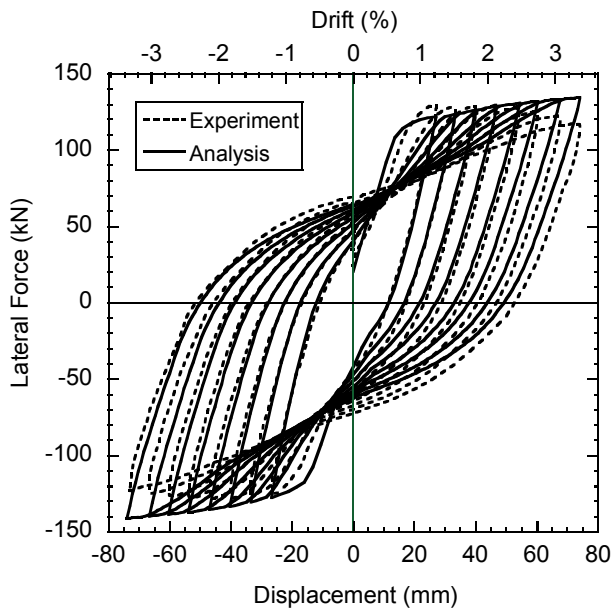


(b) Core Concrete at Compression Edge

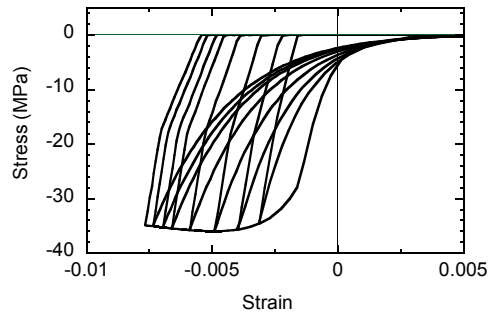


(c) Steel Tube at Tension Edge

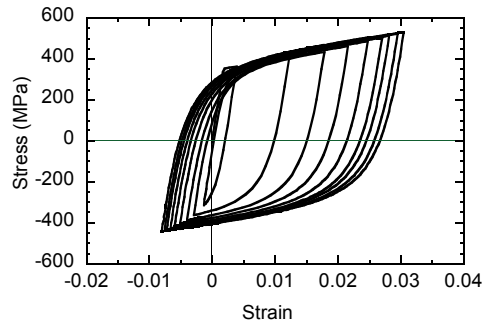
**Figure 4-23 Analytical Results for Cyclic Loading Test of CFST-42**



(a) Lateral Force-Displacement Hysteresis



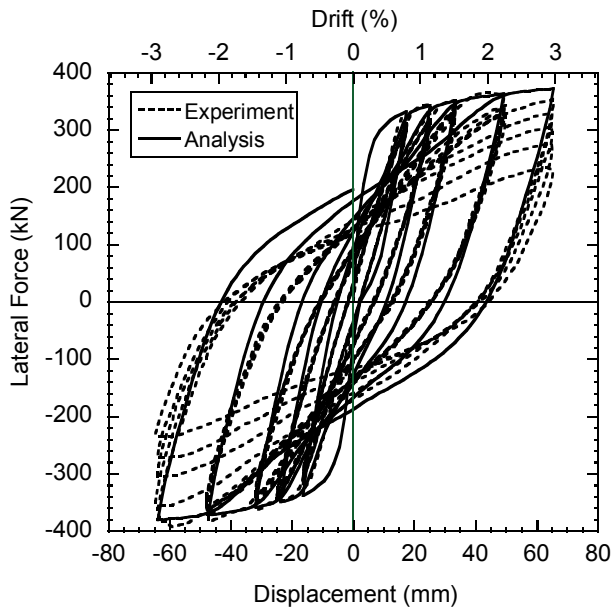
(b) Core Concrete at Compression Edge



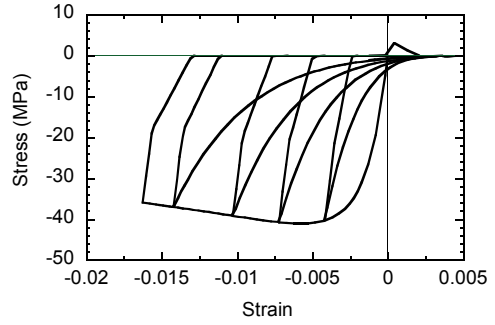
(c) Steel Bar at Tension Edge

**Figure 4-24 Analytical Results for Cyclic Loading Test of RC-TP60**

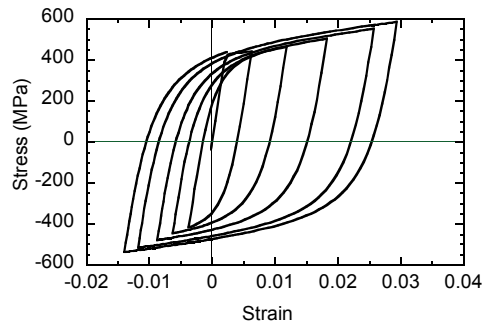




(a) Lateral Force-Displacement Hysteresis

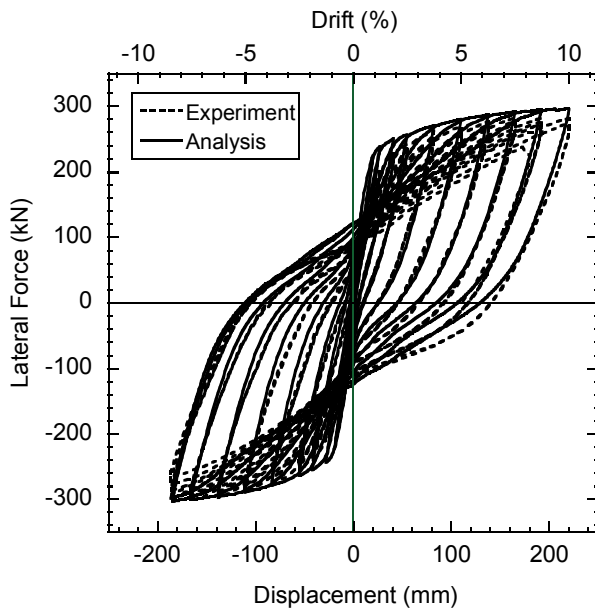


(b) Core Concrete at Compression Edge

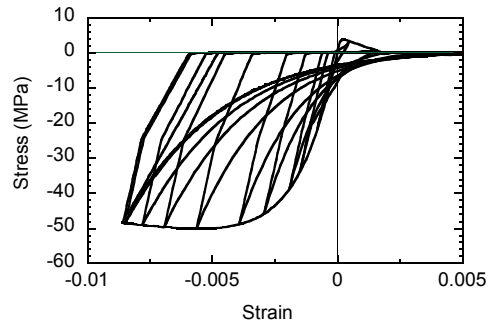


(c) Steel Bar at Tension Edge

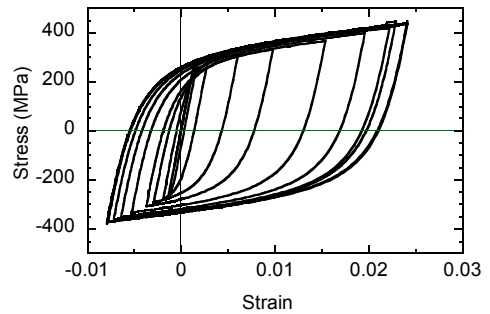
**Figure 4-25 Analytical Results for Cyclic Loading Test of RC-Unit9**



(a) Lateral Force-Displacement Hysteresis

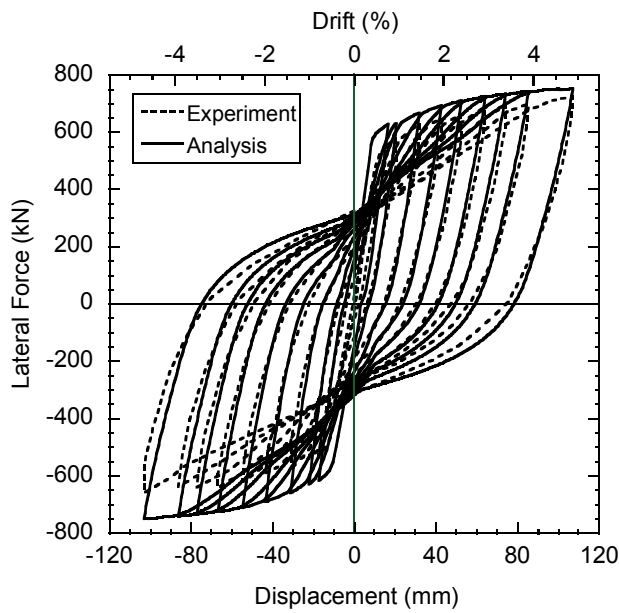


(b) Core Concrete at Compression Edge

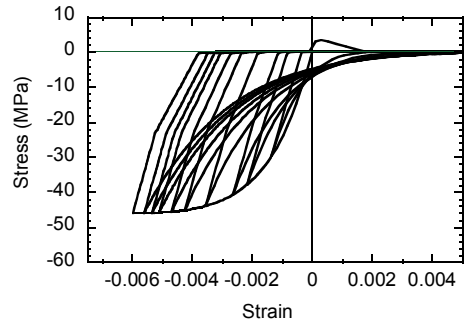


(c) Steel Bar at Tension Edge

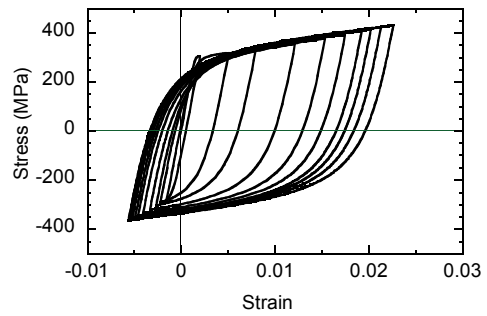
**Figure 4-26 Analytical Results for Cyclic Loading Test of SJ-Unit4**



(a) Lateral Force-Displacement Hysteresis

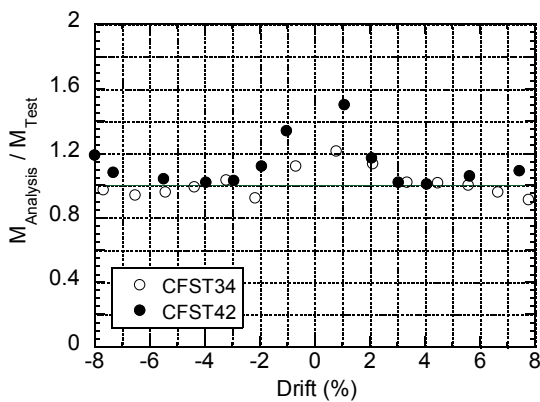


(b) Core Concrete at Compression Edge

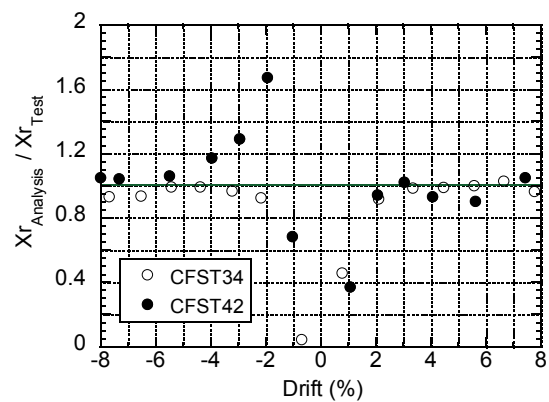


(c) Steel Bar at Tension Edge

**Figure 4-27 Analytical Results for Cyclic Loading Test of SJ-CR2**

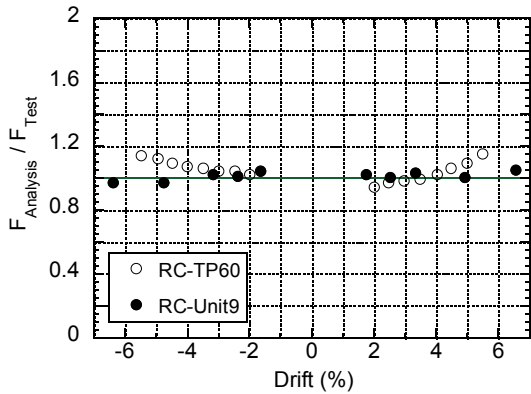


(a) Maximum Base Moment at Each Cycle

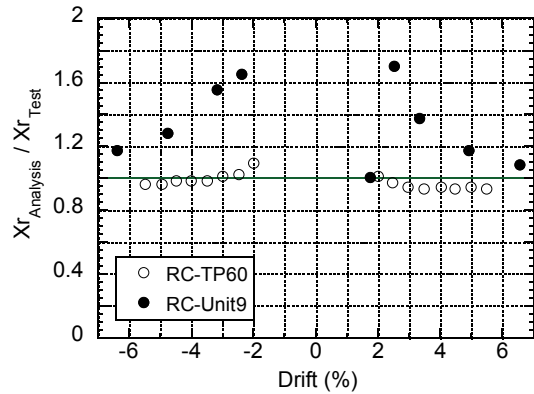


(b) Residual Displacement at Each Cycle

**Figure 4-28 Comparison of Analytical Results with Test Results of CFST Columns**

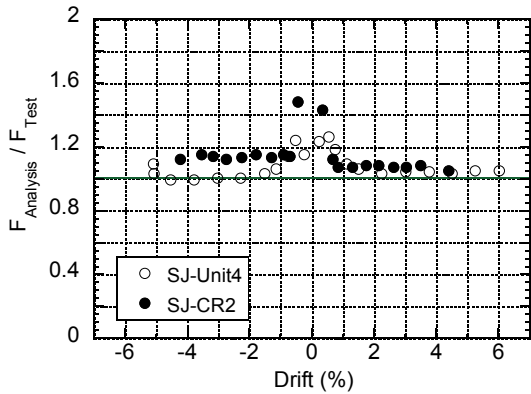


(a) Maximum Lateral Force at Each Cycle

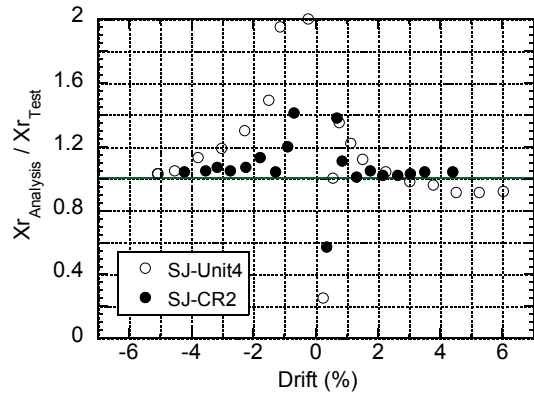


(b) Residual Displacement at Each Cycle

**Figure 4-29 Comparison of Analytical Results with Test Results of RC Columns**



(a) Maximum Lateral Force at Each Cycle



(b) Residual Displacement at Each Cycle

**Figure 4-30 Comparison of Analytical Results with Test Results of Steel Jacketed RC Columns**

## 4.6 Fiber-based Dynamic Analysis

### 4.6.1 General

The purpose of fiber-based dynamic analyses presented here is hopefully to better capture full response history of the column when subjected to blast loading, and also to revisit the shape factor  $\beta$  derived previously from the simplified analyses and the SDOF dynamic analyses. As

discussed in Section 4.1, the shape factor  $\beta$  accounting for the reduction of blast pressures unavoidably is affected by some assumptions built in the analytical model and method applied. Some of these assumptions are dynamic increase factors used in the material model, moment-curvature relationship used in the structural model, and viscous damping ratio.

Section 4.5 demonstrated that the fiber-based analytical method using the appropriate uniaxial constitutive model for concrete and steel was able to capture reasonably well the maximum lateral forces and residual displacement developed in the cyclically tested validation specimen selected. Thus, here, this validated model is used to investigate in more details the behavior and response of three different types of columns tested previously, namely CFST columns, RC columns and steel jacketed RC columns when subjected to blast loading.

Flexural residual displacements obtained from the blast tests of CFST bridge columns (that exhibited a ductile behavior) were selected as the comparison basis to assess the accuracy of the analytical results obtained from the fiber-based model. Note that the flexural residual deformations of the tested RC columns and steel jacketed RC columns were not significant due to the shear failures of the column base. Therefore, as a first step, maximum residual deformations of the tested CFST columns were compared with the ones that could be calculated using the fiber-based analytical model. From there, the procedures to determine the factor  $\beta$  follow what was done in Section 4.4 for the SDOF dynamic response history analyses.

By using the value of the factor  $\beta$  calibrated by the fiber-based model analyses for CFST columns, the tested RC columns and steel jacketed RC columns were then analyzed using the fiber-based model. Since the fiber-based analysis used in this research cannot capture the direct shear failure which was actually observed in these column tests, the purpose of these fiber-based analyses of the RC columns and steel jacketed RC columns are to calculate the shear force at the column base (i.e. reaction force) to compare with the direct shear resistance of the columns.

In the following subsection, analytical models used for fiber-based analyses are discussed. Then, moment-curvature analyses and modal analyses for CFST columns are presented. After the description of how the applied blast loads are modeled in the analyses, analytical results of the

fiber-based based dynamic analyses are presented for the three different types of test columns, namely CFST columns, RC columns and steel jacketed RC columns.

#### **4.6.2 Analytical Model for Blast Loading Test Columns**

The three different types of columns tested previously, namely CFST columns, RC columns and steel jacketed RC columns, subjected to blast loading, were modeled using two-dimensional discrete frame models as presented in Section 4.5. Figure 4-31 schematically shows a two-dimensional discrete frame model analyzed and the type of cross-section assigned to the elements for each column type (using the properties described in Section 4.5.2), along with two different profile of applied blast loading. The model has 17 nodes, from Node 1 to Node 17, and 16 elements, from Elem 1 (Node 1 to Node 2) to Elem 16 (Node 16 to Node 17). The columns were fixed at the bottom (Node 1) and the rotation and horizontal translation of the column top (Node 17) was constrained to apply the axial force coming from the cap beam. The applied axial forces were taken as 5.81 kN (1.31 kip) for the CFST columns and 2.00 kN (0.45 kip) for both the RC columns and steel jacketed RC columns. The discrete lumped mass was assigned to the nodes of Node 2 to Node16 as inertias to resist the blast loads. The gravity load corresponding to these masses was applied as a uniformly distributed load along a column height. Note that the strain penetration model used in the quasi-static cyclic loading test specimens was not modeled for these blast test columns because these localized inelastic deformations were not observed in specimens.

As shown in Figure 4-31, the CFST sections shown in Figure 4-12 (a) were assigned to the CFST columns, and the RC sections shown in Figure 4-12 (b) were assigned to the RC columns. The labels stating “PH Confined” and “OPH Confined” in Figure 4-31 (b) means that the reinforced concrete sections are confined according to the actual transverse reinforcement ratios in the plastic hinge (PH) region and outside of the plastic hinge (OPH) region, respectively. In the steel jacketed RC columns, assuming that the bond stress between the steel jacket and grout developed at a length of about half of the column diameter from the edge of the jacket, the contribution of the steel jacket to the flexural resistance of the column was not considered over these length, but confinement effect by the steel jacket was considered (as for the analytical model of the cyclic loading test steel jacketed RC columns presented in Section 4.5.4.2).

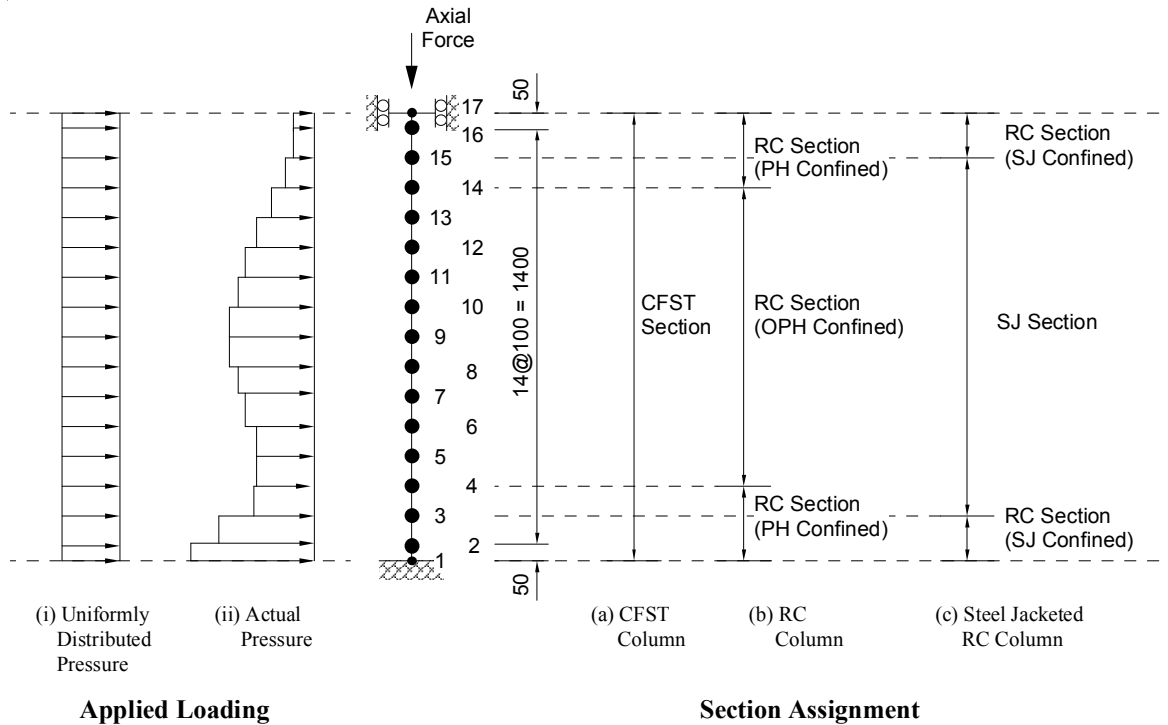


**Figure 4-31 Analytical Model for Blast Loading Tests**

The Menegotto-Pinto model (Menegotto and Pinto 1973) was used to represent the uniaxial constitutive model for steel jackets and steel tubes of the CFST columns. The reinforcing steel bars were modeled using a tension stiffening model by Belarbi and Hsu (1994) to provide a backbone envelope curve of constitutive stress-strain relationship and using the modified Menegotto-Pinto model (Filippou et al. 1983) with isotropic strain hardening effect to determine hysteresis rules within that envelope. The modified Chang-Mander model (Vaughan 2007) was used to model the uniaxial constitutive model for unconfined and confined concrete. The details of these material constitutive models were presented previously in Section 4.5.3.

The strength values obtained from the compression tests of concrete cylinders and the tensile tests for steel were considered in the analyses. The concrete strength and yield stress of steel were multiplied by 1.25 and 1.2, respectively, to account for strength magnification at large strain rates under impulsive conditions (Mays and Smith 1995).

To account for the damping effect of the structure, Rayleigh damping was used. A damping ratio was assumed to be 5% for the first and third modes. The Krylov-Newton algorithm (see Section 4.5.2) provided by OpenSees (2007) was used to solve the nonlinear equilibrium equation. The time increment of each step in the applied pressure histories was 0.01 msec, and the time step of analyses was 0.0025 msec.

#### **4.6.3 Moment-Curvature Analysis for CFST Columns**

The moment-curvature relationship calculated using the fiber-based model, in which the appropriate material stress-strain relationships were used, was compared with that used for the simplified analysis and SDOF dynamic analysis. The moment-curvature relationship is one of the analytical assumptions to affect the value of factor  $\beta$ . Both simplified analysis presented in Section 3.4 and SDOF dynamic analysis presented in Section 4.4 used the same simplified elasto-perfectly plastic moment-curvature relationship based on simple calculations. Figures 4-32 to 4-34 respectively compare the moment-curvature curves of CFST C4, C5, and C6 columns from the fiber-based model with the simplified moment-curvature curves (obtained using the Bruneau and Marson (2004) equations for  $M_p$  and effective stiffness). The resulting maximum moment capacity calculated using the fiber-based model was 15.57, 18.50, and 43.05 kN-m for the CFST C4, C5, and C6 columns, respectively. These values are, respectively, 3, 12, and 6% higher than those obtained by the simple calculations. The differences are attributed to the strain hardening effect of the steel tubes modeled in the fiber-based calculations whereas this effect was not considered in the simple calculations. These differences are small, and it shows that the previous assumptions are reasonable. Therefore, it will be possible to compare results obtained from the fiber-based model with those obtained from the simplified model.

#### **4.6.4 Modal Analysis for CFST Columns**

Modal analyses were performed for the three CFST columns (C4, C5, and C6 columns) to investigate their vibration properties, namely natural periods and mode shapes. Table 4-10 presents the modal analysis results of natural periods and effective masses for Mode 1 through 7. These are based on the initial stiffness of the columns. The natural periods of the first mode, which has the highest effective mass of 69%, are 5.13, 4.18, and 3.65 for CFST C4, C5, and C6 columns, respectively. Because of the fix-fix boundary conditions of the columns, the effective

masses of the anti-symmetric Modes 2, 4, and 6 are zero. Therefore, these even modes do not contribute the structural responses. The natural mode shapes of Mode 1, 3, 5, and 7 for the three CFST columns are shown in Figure 4-35. First, the mode shapes were normalized such that maximum displacements become unity, and then these normalized mode shapes were multiplied by their corresponding effective masses. The resulting normalized mode shapes of same modes for these different columns are almost identical.

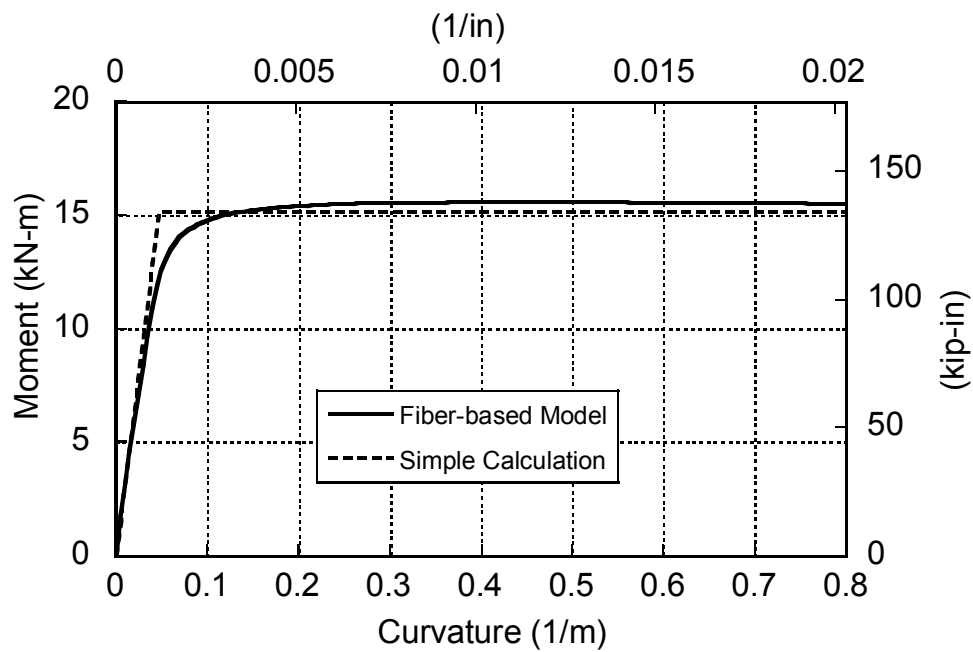


**Figure 4-32 Comparison of Moment-Curvature Relationship for CFST C4 Column**



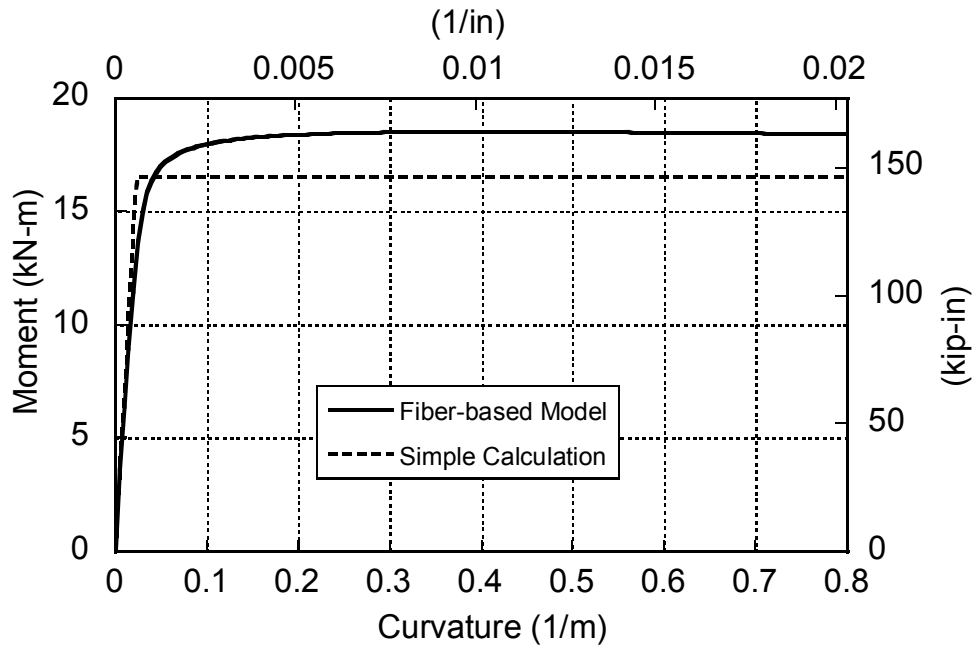


Figure 4-33 Comparison of Moment-Curvature Relationship for CFST C5 Column

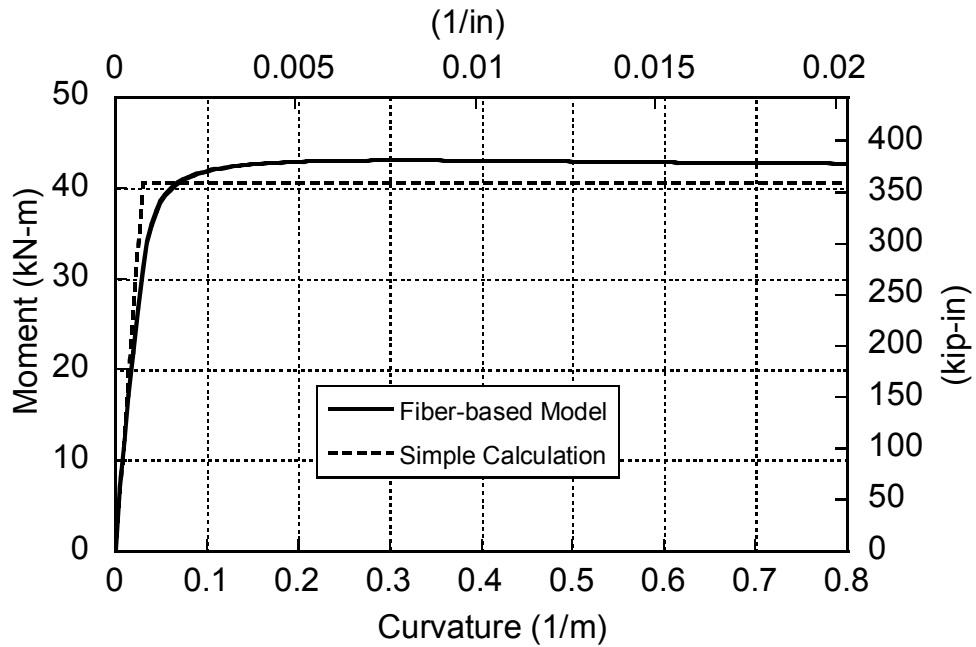
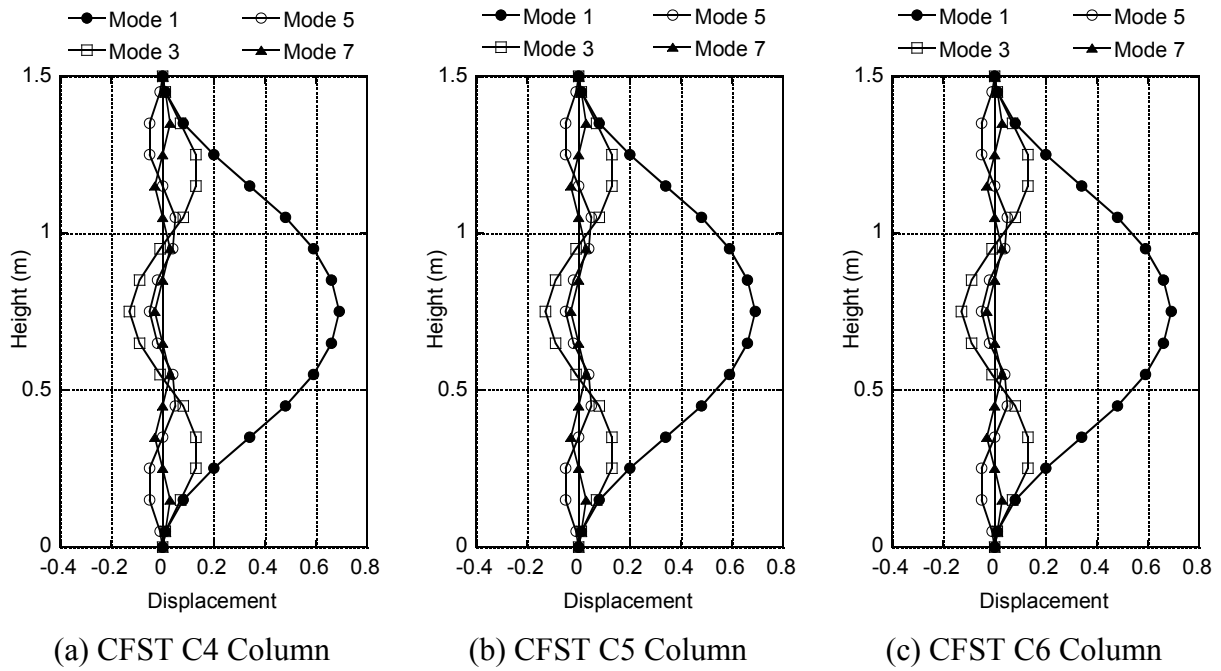


Figure 4-34 Comparison of Moment-Curvature Relationship for CFST C6 Column



**Figure 4-35 Natural Mode Shapes of CFST Columns**

**Table 4-10 Modal Analysis Results of CFST Columns**

Mode	CFST C4 Column		CFST C5 Column		CFST C6 Column	
	Natural Period (msec)	Effective Mass (%)	Natural Period (msec)	Effective Mass (%)	Natural Period (msec)	Effective Mass (%)
1	5.13	69.0	4.18	69.0	3.65	69.0
2	1.86	0.0	1.52	0.0	1.32	0.0
3	0.95	13.2	0.77	13.2	0.67	13.2
4	0.57	0.0	0.47	0.0	0.41	0.0
5	0.38	5.4	0.31	5.4	0.27	5.4
6	0.28	0.0	0.23	0.0	0.20	0.0
7	0.21	2.9	0.17	2.9	0.15	2.9

#### 4.6.5 Applied Blast Loadings

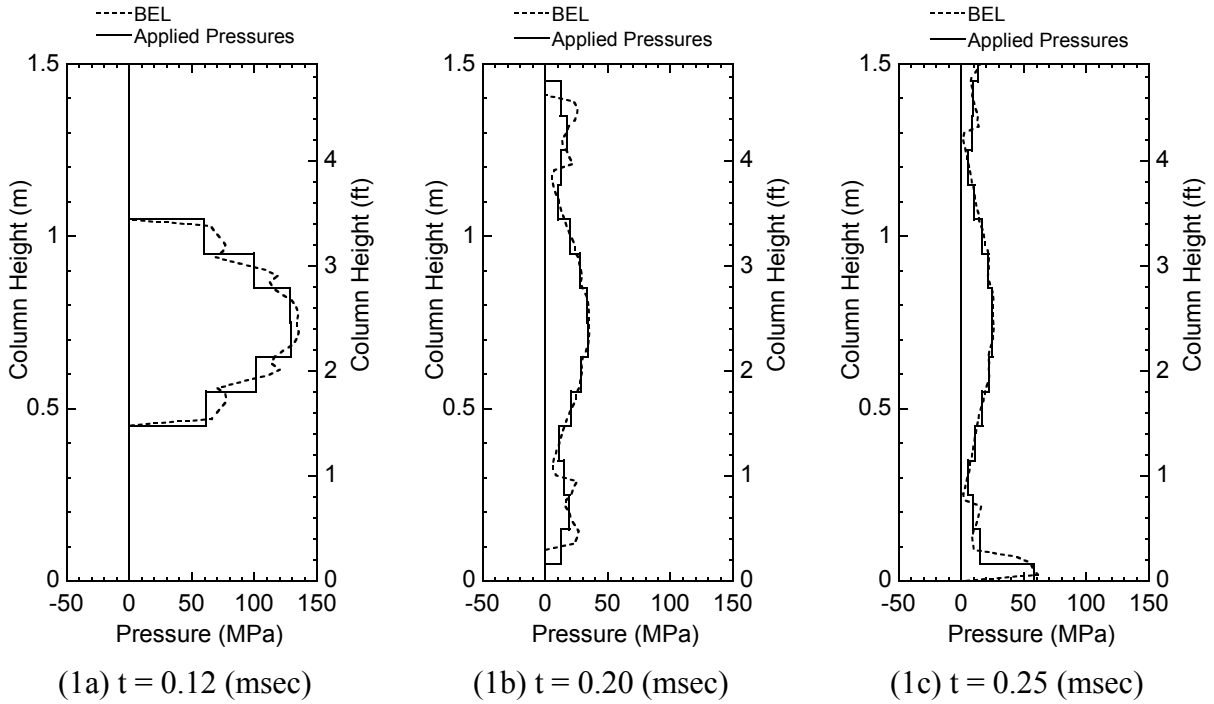
As shown in Figure 4-31, there were two profiles of blast loadings applied in the blast pressure history analyses. One is (i) the uniformly distributed equivalent pressures, and the other is (ii) the actual pressure distribution (obtained as described later). The uniformly distributed equivalent pressures were selected to compare with the SDOF dynamic analyses which also used uniformly distributed equivalent pressures. The analyses using the uniformly distributed pressures also provide some preliminary basic understanding of the column response subjected to blast. The equivalent pressure histories used here are identical to those used in the SDOF dynamic analyses presented in Figure 4-4. The analyses conducted using uniformly distributed equivalent pressures were only performed for the three test cases with mid-height explosion, namely Test 1-3 of CFST C4 Column, Test 1-4 of CFST C6 Column, and Test 1-5 of CFST C5 Column, because the pressures actually applied to these columns during the tests were closer to symmetrically loading to the structure and are suited for modeling using uniformly distributed loads due to this symmetry.

The analyses conducted using actual pressure profiles were done by calculating these profiles using Bridge Explosive Loading program (BEL 2004). The blast pressures along the height of column were obtained at 84 data points along the height of the column, and these pressures were averaged within each member (approximately five pressure points with each member). Figures 4-36 to 4-42 show the resulting applied blast pressures for Tests 1-3, 1-4, 1-5, 1-6, 1-9 and 1-10, 2-1 and 2-3, and 2-2 and 2-4, respectively. These figures present (1) comparison of blast pressure distributions along the height at three selected different times from BEL with those applied in the analyses, and (2) applied pressure histories for two selected elements which are Elem 1 and 8, and Elem 1 and 3 for the mid-height and low-height explosion cases, respectively. Note that the times in these figures start at the initiation of the explosions.

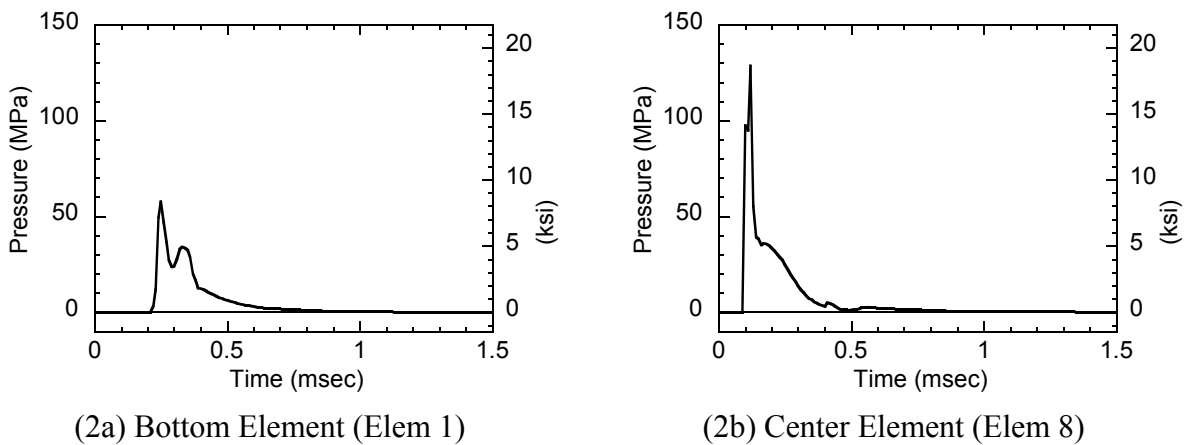
Figure 4-36(1) shows by comparing the pressure distribution obtained from BEL with those averaged as indicated before that the resolution of the pressure distributions is satisfactory. It also illustrates that the symmetric distribution of pressures is applied to the column as shown in Figures 4-36(1a) and (1b) until the pressures are reflected on the ground and act on the elements around the bottom of the column. The pressures reflected on the ground are observed in the

bottom element (Elem 1) in Figure 4-36(1c). The maximum blast pressure applied to the center element is 2.3 times higher than that applied to the bottom element in this case as shown in Figures 4-36(2a) and (2b). The trends described above are also observed in the mid-height explosion cases of Test 1-4 and Test 1-5 as shown in Figure 4-37 and Figure 4-38, respectively.

For the cases with low-height explosions, the applied blast pressures of Tests 1-6, 1-9, 1-10, 2-1, 2-3, 2-2 and 2-4 are presented in Figures 4-39 to 4-42 (sometimes grouped together). Because the explosions are closer to the ground surface, the higher pressures are applied to the lower height of the column, due to the Mack reflection, than highest pressures of the mid-height explosion cases. For example, the values of maximum pressures of Tests 2-1 and 2-3 is 151.7 MPa developed at mid-height element whereas that of Test 1-3 is 128.7 MPa developed at the base element, even though the standoff distance of Test 1-3 ( $x = 2X$ ) is closer than those of Tests 2-1 and 2-3 ( $x = 2.16X$ ). The maximum pressures were calculated at the base of the column due to the Mack reflection except for Tests 1-9 and 1-10. This is because the standoff distances of these cases ( $x = 0.8X$ ) were so close that the Mack mechanism did not form between the explosive charge and the column. Therefore, the maximum pressures were not computed at the base of the column, but at the height of the explosion in these test cases.

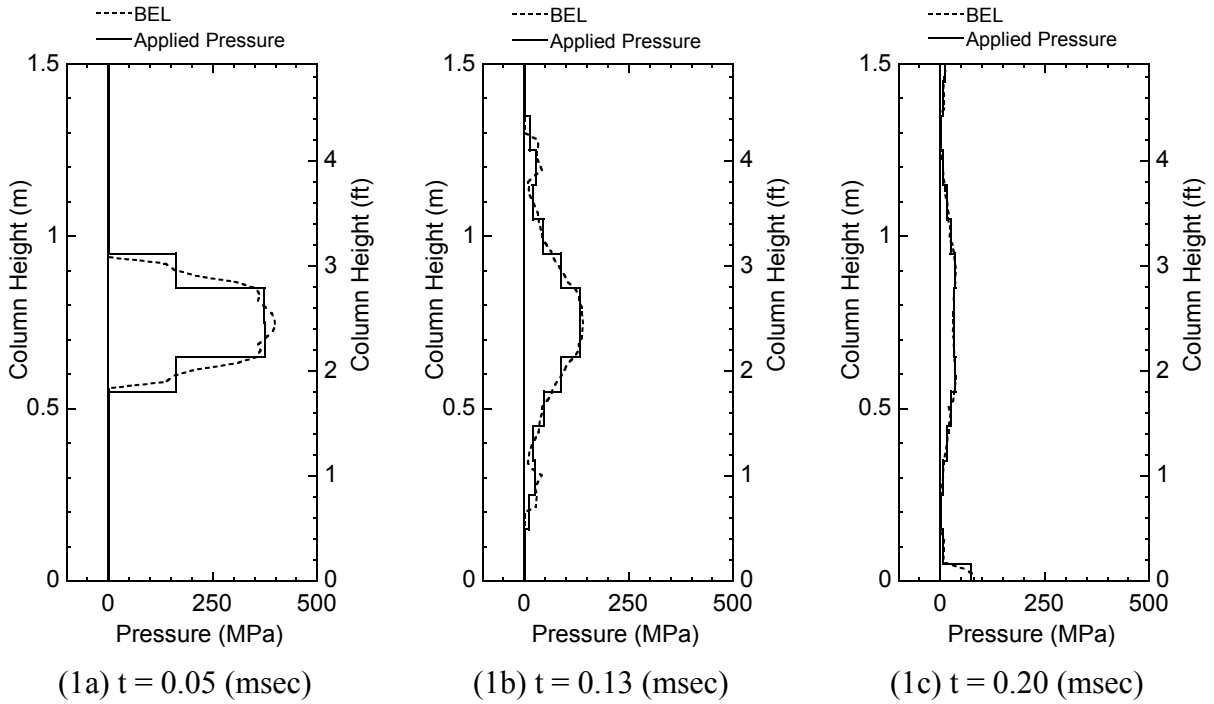


(1) Comparison of Pressure Distributions

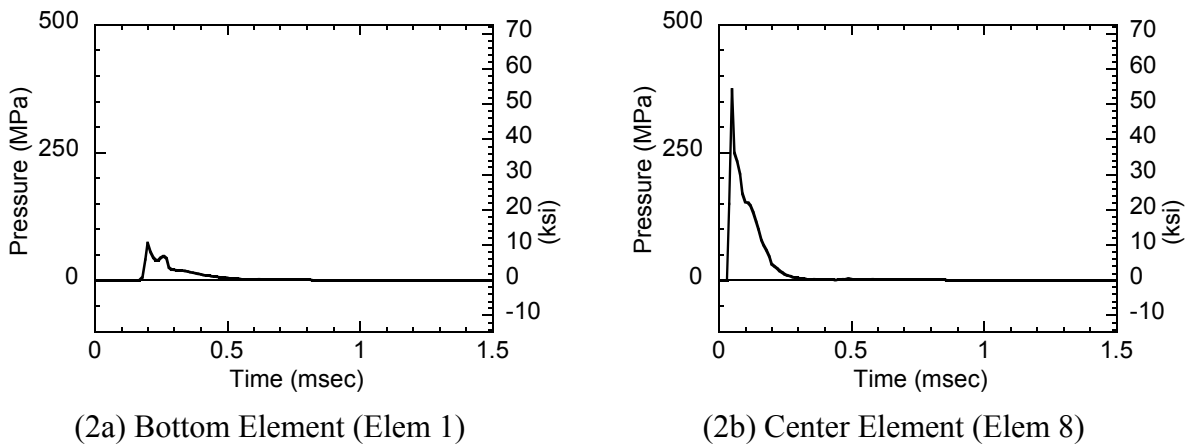


(2) Applied Pressure Histories

**Figure 4-36 Applied Blast Pressures of Test 1-3 (CFST C4 Column)**

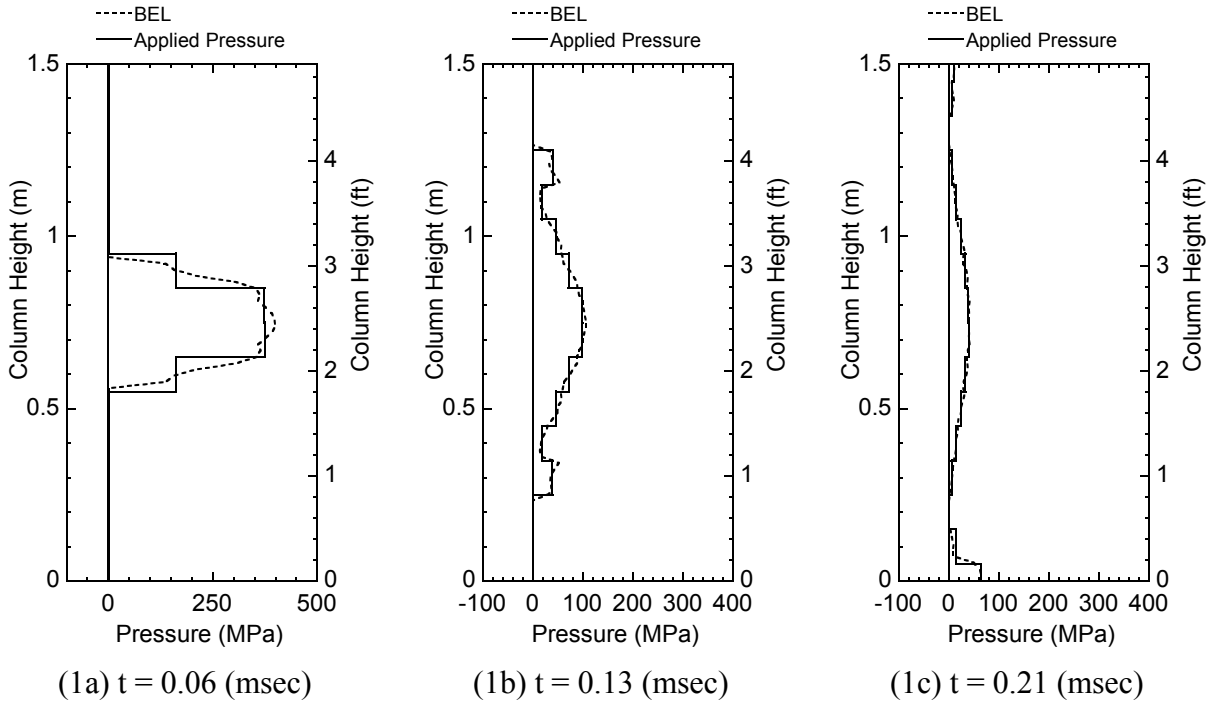


(1) Comparison of Pressure Distributions

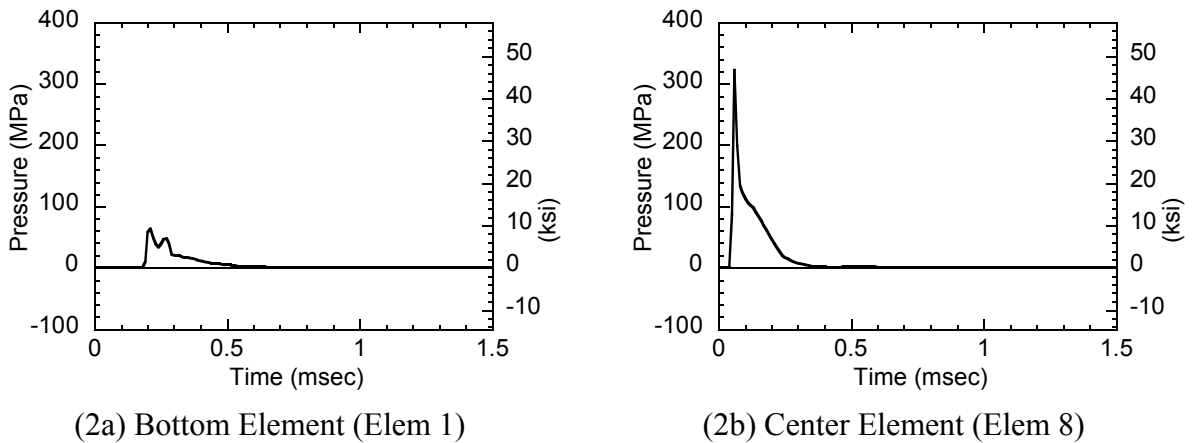


(2) Applied Pressure Histories

**Figure 4-37 Applied Blast Pressures of Test 1-4 (CFST C6 Column)**

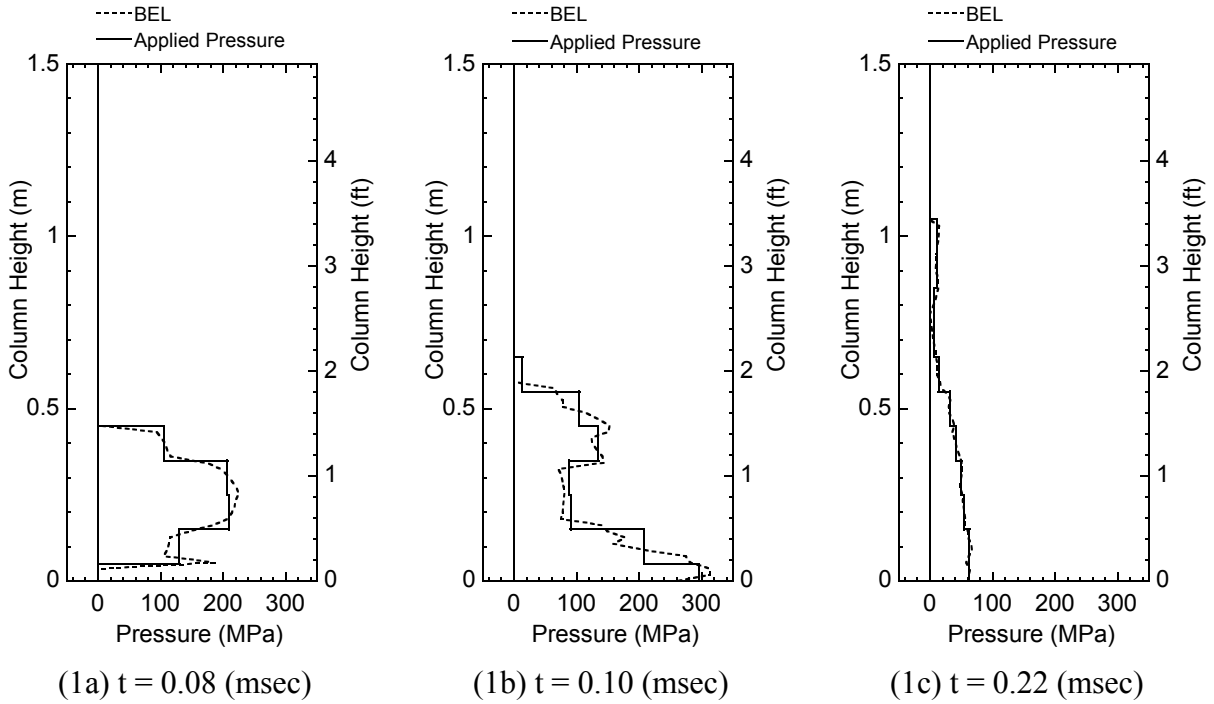


(1) Comparison of Pressure Distributions

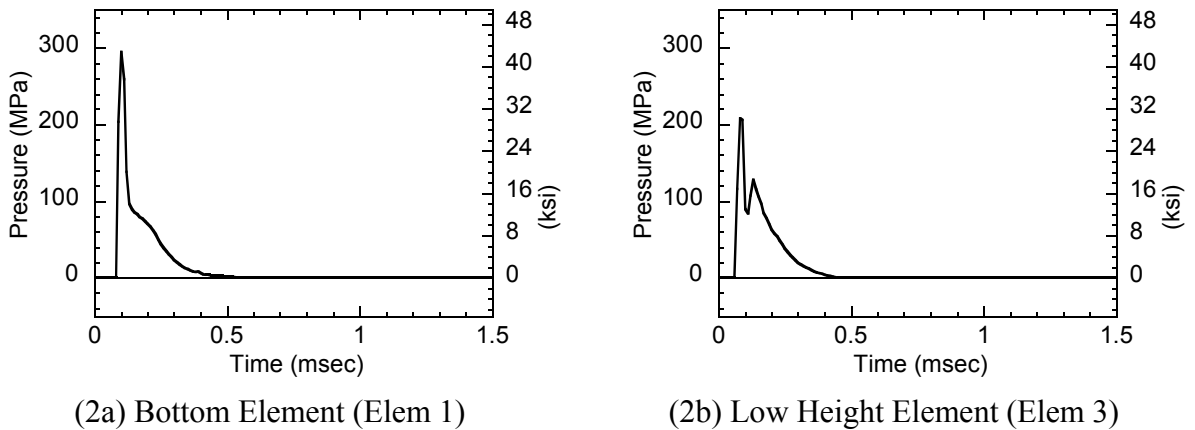


(2) Applied Pressure Histories

**Figure 4-38 Applied Blast Pressures of Test 1-5 (CFST C5 Column)**



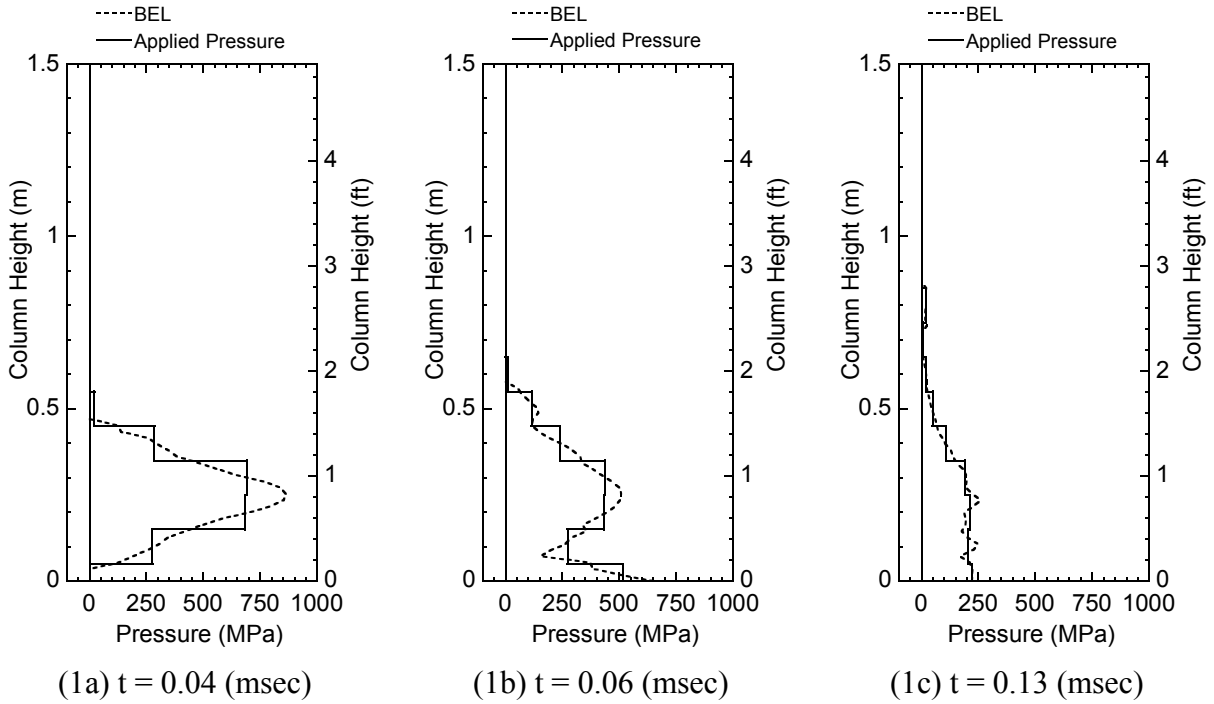
(1) Comparison of Pressure Distributions



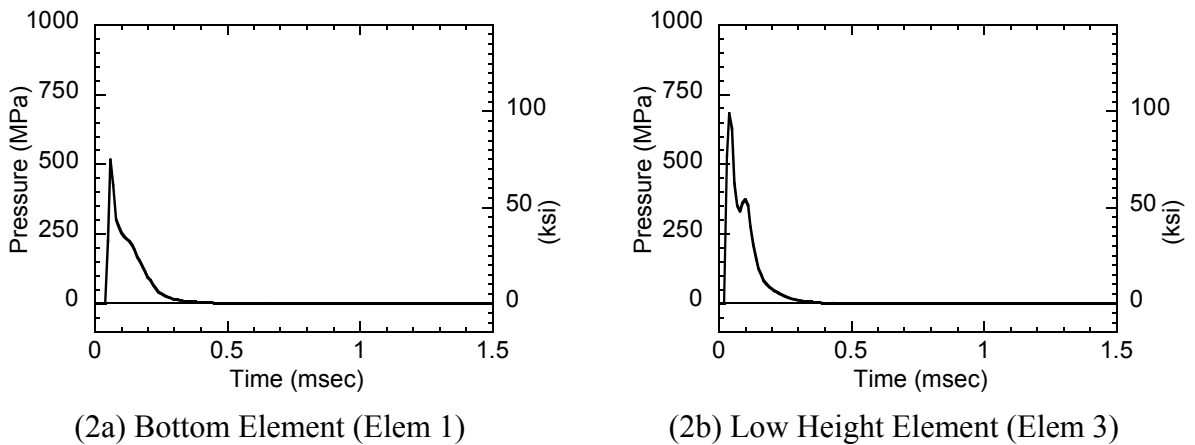
(2) Applied Pressure Histories

**Figure 4-39 Applied Blast Pressures of Test 1-6 (CFST C4 Column)**



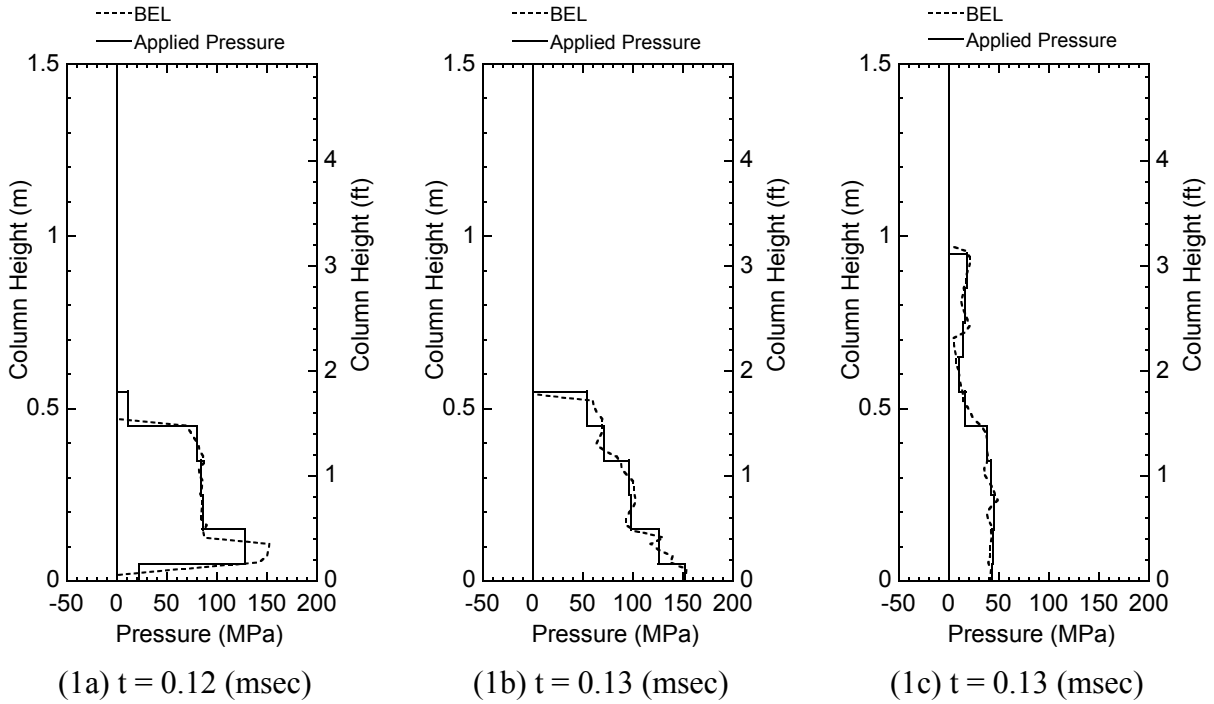


(1) Comparison of Pressure Distributions

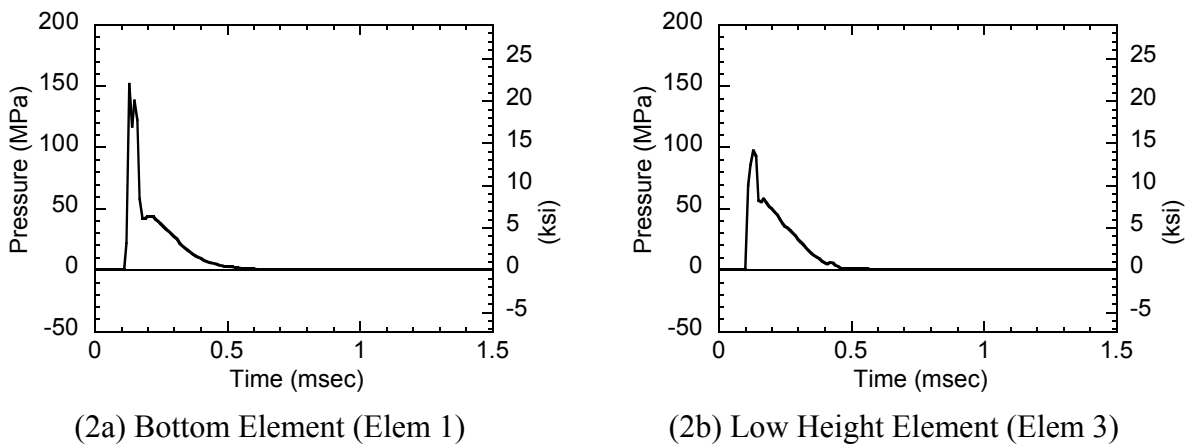


(2) Applied Pressure Histories

**Figure 4-40 Applied Blast Pressures of Test 1-9 (CFST C6 Column) and Test 1-10 (CFST C5 Column)**

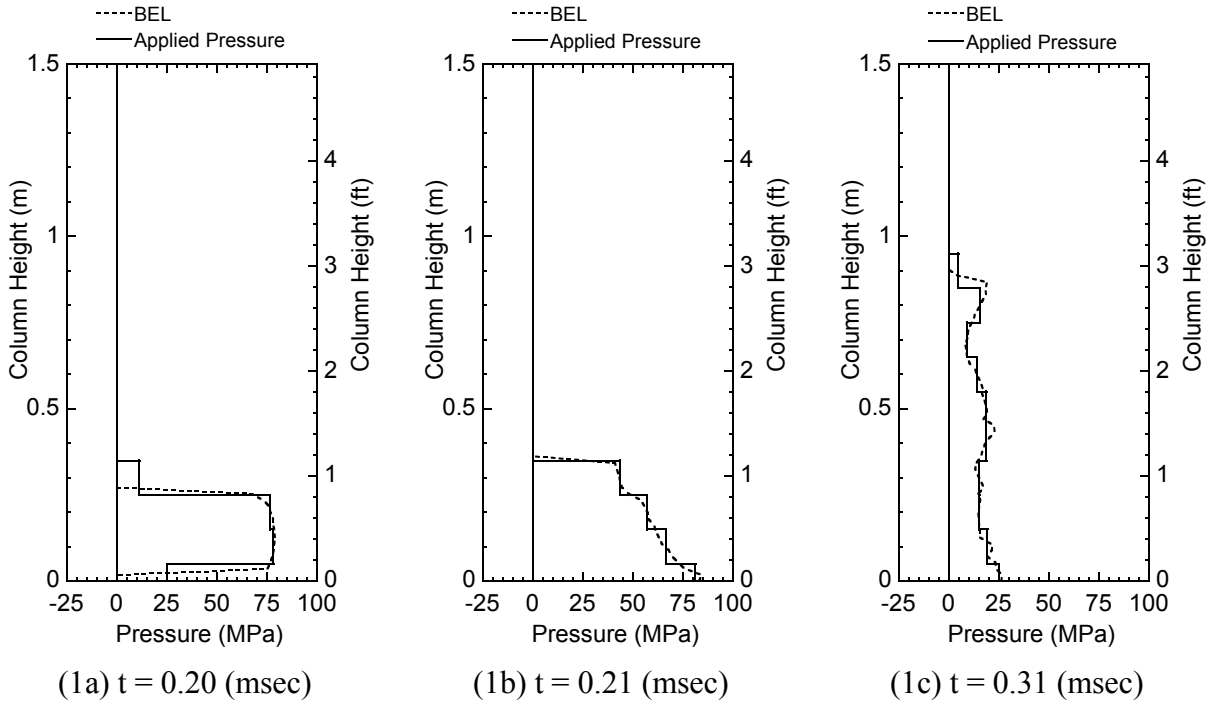


(1) Comparison of Pressure Distributions

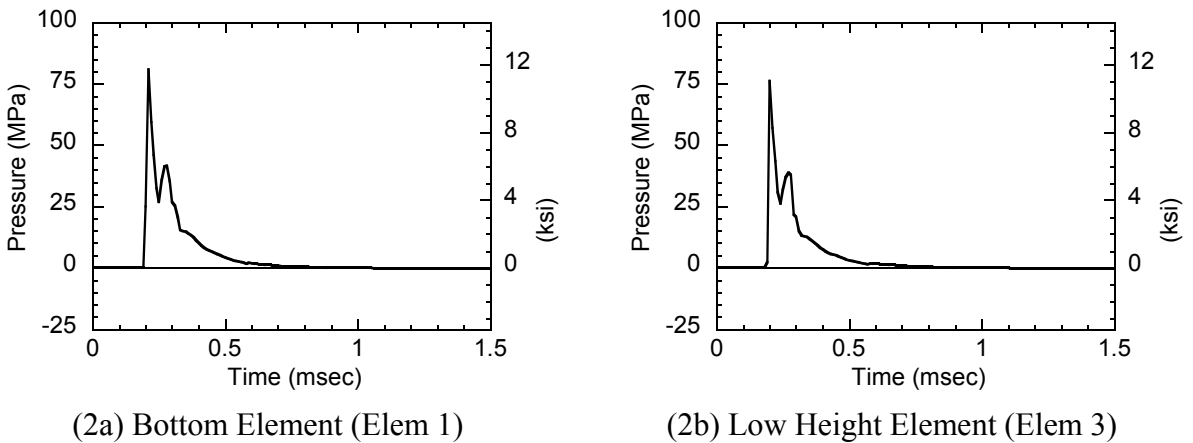


(2) Applied Pressure Histories

**Figure 4-41 Applied Blast Pressures of Test 2-1 (RC1 Column) and Test 2-3 (SJ2 Column)**



(1) Comparison of Pressure Distributions



(2) Applied Pressure Histories

**Figure 4-22 Applied Blast Pressures of Test 2-2 (RC2 Column) and Test 2-4 (SJ1 Column)**

## 4.6.6 Analytical Results

### 4.6.6.1 Shape Factor $\beta$

The shape factor  $\beta$  was calibrated for the six tested CFST columns, as well as the simplified analyses (Fujikura et al. 2007, 2008) and SDOF dynamic analyses (Section 4.4.5.2), to match the analytical results obtained using the fiber-based analyses with the experimental results. Table 4-11 summarizes the resulting shape factor  $\beta$  for the six tested CFST columns. As described in Section 4.6.5, there were two profiles of blast loadings applied, namely the uniformly distributed equivalent pressures and the actual pressure distributions. For comparison purposes, the resulting values of  $\beta$  obtained from the analyses with 0.5% damping ratio, in addition to 5% damping ratio, are also presented in Table 4-11 to investigate the sensitivity of the damping effect on the values of  $\beta$ . Because the analyses with 0% Rayleigh damping ratio did not converge, a small damping ratio of 0.5% was selected for this purpose.

**Table 4-11 Summary of Shape Factors from Fiber-based Dynamic Analyses of CFST Columns**

Test Num.	Col.	Test Displ. (mm)	Equivalent Pressures				Actual Pressures	
			0.5 % Damping		5 % Damping		5 % Damping	
			$\beta$	Ave. $\beta$	$\beta$	Ave. $\beta$	$\beta$	Ave. $\beta$
1-3	C4	30	0.564	0.547	0.630	0.643	0.670	0.665
1-4	C6	46	0.544		0.637		0.652	
1-5	C5	76	0.534		0.662		0.672	
1-6	C4	24	N/A	N/A	N/A	N/A	0.606	0.561
1-9	C5	45	N/A		N/A		0.550	
1-10	C6	100	N/A		N/A		0.528	
Ave.				N/A		N/A		0.613

The average  $\beta$  value of 0.547 obtained using the uniformly distributed equivalent pressures and fiber-based model with 0.5% damping ratio are comparable to the one of 0.532 from the SDOF

dynamic analyses with 0% damping ratio using the two different load-mass factors corresponding to the different structural ranges (i.e. Case 3 in Table 4-5). The difference between these two  $\beta$  values is within 3%, which is attributed to the difference of their moment-curvature relationship as presented in Section 4.6.3.

The  $\beta$  value increases significantly, by about 18%, for the fiber-based model with the increase of the damping ratio from 0.5% to 5% in the equivalent pressure profiles as shown in Table 4-11. By contrast, the increase of the damping ratio from 0% to 5% did not affect the  $\beta$  value significantly in the SDOF dynamic analyses as presented in Section 4.4.5.2. This is because the fiber-based analysis can take the higher modes of vibrations into account and uses the Rayleigh damping here. To investigate this, Figure 4-43 compares the displacement history at the column mid-height and the reaction force history at the column base corresponding to 0.5% and 5% damping ratios for the Test 1-3 case. Note that the average  $\beta$  factors of 0.564 for 0.5% damping and 0.630 for 5% damping were determined by matching the residual displacements obtained analytically with those obtained from the experiments as shown in Figure 4-43(a). As shown in Figure 4-43(b), the resulting reaction force at the base of the column using 0.5% damping ratio fluctuates at a higher frequency (i.e. at short periods in the range of 0.1 to 0.2 msec) whereas the reaction history curve using 5% damping ratio is relatively smoother and has less effects of higher frequency modes. The origin of the high frequency modes that develop during response to the blast loadings will be explained in the subsequent subsection. Since the 5% Rayleigh damping was used based on the first and third modes of vibrations, the high frequency modes above the 3<sup>rd</sup> mode were less significant in this case. Therefore, the Rayleigh damping for the fiber-based model has an effect, and can significantly reduce the structural response when subjected to the blast loading.

Beyond the above, it is also observed in Table 4-11 that using the actual pressure profiles slightly increases the average  $\beta$  value by 4% over using the uniformly distributed equivalent pressures for the mid-height explosion cases. When using actual pressure profiles, the average  $\beta$  value for the low-height explosion cases is 15% smaller than that for the mid-height explosion cases, while this difference was only 3% for the SDOF dynamic analyses (in Table 4-5). This could be

partly attributed to the reflected pressures on the ground computed by BEL. The BEL assumes that the pressure reflects on the ground perfectly, but this was not the case in the experiments. Accordingly, the reflected pressures applied to the column close to the ground could be overestimated, resulting in the lower values of  $\beta$  for the low-height explosion cases. In the SDOF dynamic analyses, this possible overestimation of the reflected pressures can be reduced in the process of calculating the equivalent pressures given by Equation 4-4 because of the normalized deflected shape of the column assumed in the calculation.

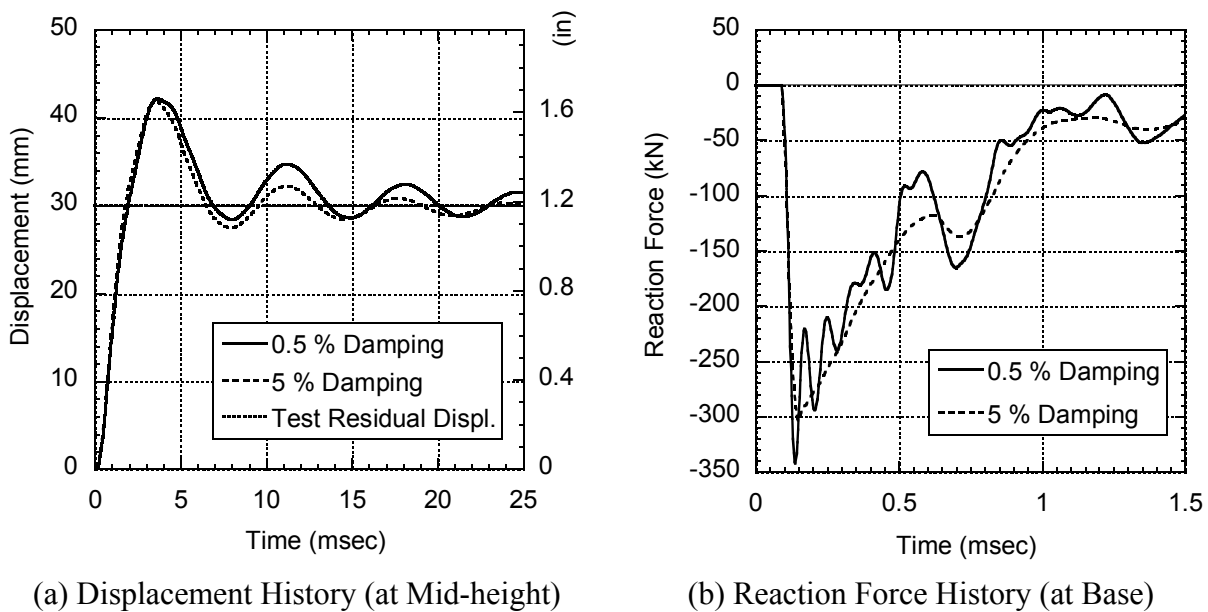


**Figure 4-43 Comparison of Analytical Results with Different Damping Ratio of Test 1-3 (CFST C4 Column)**

#### 4.6.6.2 Structural Response of CFST Columns

In order to verify that the analytical residual displacements obtained using the shape factor  $\beta$  presented in Table 4-11 would match the experimental ones, and to illustrate the structural response using these factors, the structural responses of six tested CFST columns computed using a fiber-based model with 5% damping ratio are presented in Figures 4-44 to 4-52. The resulting maximum displacements and maximum reaction forces at the base and top of the

column are summarized in Table 4-12. Note that the maximum displacements obtained from the SDOF dynamic analyses are also presented in Table 4-12.

**Table 4-12 Summary of Analytical Results from Fiber-based Dynamic Analyses of CFST Columns**

Test Num.	Col.	Maximum Displacement			Maximum Reaction Force			
		SDOF Dynamic Analysis	Equivalent Pressures	Actual Pressures	Equivalent Pressures		Actual Pressures	
		mm	mm	mm	Base kN	Top kN	Base kN	Top kN
1-3	C4	35.5	41.8	43.5	-303.8	-303.8	-280.2	-97.9
1-4	C6	49.6	57.8	57.8	-1106.4	-1106.4	-306.1	321.9
1-5	C5	78.9	86.4	86.0	-643.2	-643.2	-322.7	-115.8
1-6	C4	33.9	N/A	36.9	N/A	N/A	-855.0	-101.0
1-9	C6	51.2	N/A	55.7	N/A	N/A	-2074.0	-326.7
1-10	C5	105.5	N/A	108.3	N/A	N/A	-1157.3	-149.5

#### 4.6.6.2.1 Mid-height Explosion and Equivalent Pressure Cases

Figures 4-44 to 4-46 present the analytical results of Tests 1-3, 1-4 and 1-5, respectively, for the mid-height explosion cases when subjected to the uniformly distributed equivalent pressures. Figure 4-44(1) presents acceleration, velocity, and displacement distributions along the height of the column at three selected different times ( $t = 0.12, 0.60, \text{ and } 1.04$  msec). The time of 0.12 msec is shortly after the blast loadings were applied and largest accelerations were observed: at that time almost no deformations are observed along the column. The times of 0.60 and 1.04 msec, are arbitrarily selected to show the high frequency modes in the acceleration shapes similar to the mode shapes of the third mode and fifth mode, respectively, as shown in Figure 4-35. These high frequency mode effects are summed in both the velocity and displacement shapes.

In Figure 4-44(2), the maximum displacement of 41.8 mm is observed at time of 4.02 msec, much later than the end of the applied blast pressure (the blast pressure starts at the time of 0.10 msec, and the pressure duration is 0.16 msec as shown in Table 4-7). This maximum displacement is larger than that of SDOF dynamic analysis shown in Table 4-12 by 18%. The reaction forces at the base and top of the column are identical due to the symmetry of the column and the blast pressure profiles applied as shown in Figure 4-44(3). The maximum reaction forces of -303.8 kN are observed at time of 0.15 msec that occurs before the end of the applied blast pressure. In Figure 4-44(3), there are some localized fluctuations of the reaction forces in the overall reaction force history curve. This is again attributed to the high frequency modes of vibrations. For instance, the acceleration shape at time of 0.60 msec in Figure 4-44(1a) causes the localized fluctuation of the reaction forces observed around time of 0.60 msec in Figure 4-44(3). This localized fluctuation of the reaction force is observed more significantly in the analytical results with small damping ratio as presented in Figure 4-43(b).

The stress-strain relationships of core concrete and steel tube in Figure 4-44(4) show that these fiber materials experience less cyclic loading than typically the case under earthquake loadings. However, these curves show that the response following the point of maximum displacement is not purely linear elastic and that rather the stiffness of the structure is less at that point than the initial stiffness. The trends described above are also observed in the other mid-height explosion cases of Test 1-4 and Test 1-5 under equivalent pressures as shown in Figures 4-45 and 4-46.

#### **4.6.6.2.2 Mid-height Explosion and Actual Pressure Cases**

Figures 4-47 to 4-49 present the analytical results of Tests 1-3, 1-4 and 1-5, respectively, for the mid-height explosion cases when subjected to the actual pressure profiles. Figure 4-47(1) presents acceleration, velocity, and displacement distributions along the height of the column at three selected different times ( $t = 0.12, 0.38, \text{ and } 0.62$  msec). At time of 0.12 msec, the masses around mid-height only are subjected to the accelerations and velocities because the blast pressures are only applied to around mid-height of the column as presented in Figure 4-36(1a). The times of 0.38 and 0.62 msec are arbitrarily selected to show the acceleration and velocity distributions. These distributions are not symmetric because the reflected pressures on the



ground are applied around low-height of the column as shown in Figure 4-36(1c). The high frequency modes are also observed in the acceleration distribution at times of 0.38 and 0.62 msec.

Displacement history at mid-height (in Figure 4-47(2)), and stress-strain relationship of core concrete and steel tube (in Figure 4-47(4)) are similar to those observed in the analytical results of equivalent pressure case (in Figure 4-44). As shown in Figure 4-36(3), the reaction forces at the base and top of the column are identical up to 0.23 msec, but after that, the magnitude of the reaction force at the bottom increases significantly due to the reflected pressures on the ground applied around low-height of the column as shown in Figure 4-36(1c).

The trends described above are also observed in the other mid-height explosion cases of Test 1-4 and Test 1-5 under actual pressure profiles as shown in Figures 4-48 and 4-49. Table 4-12 shows that the maximum displacements obtained from actual pressures are comparable to those from equivalent pressures, and that the maximum reaction forces obtained from actual pressures are overall smaller than those from equivalent pressures.

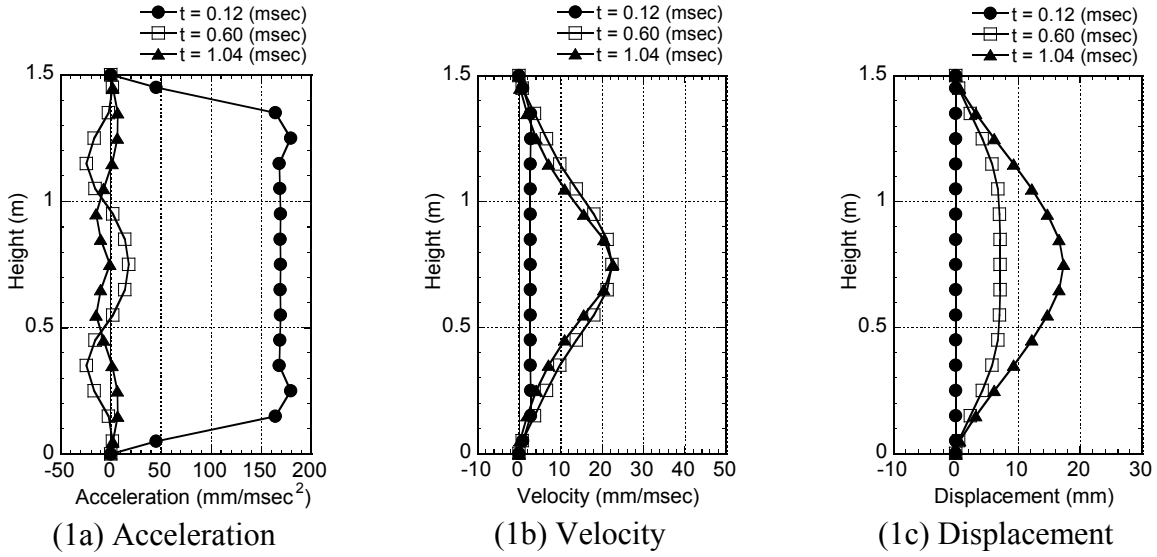
#### **4.6.6.2.3 Low-height Explosion and Actual Pressure Cases**

Figures 4-50 to 4-52 present the analytical results of Tests 1-6, 1-9 and 1-10, respectively, for low-height explosion cases ( $h = 0.25$  m) when subjected to the actual pressure profiles. Figure 4-50(1) presents acceleration, velocity, and displacement distributions along the height of the column at three selected different times ( $t = 0.09, 2.25,$  and  $5.25$  msec). At time of 0.09 msec, the masses around low-height only are subjected to the accelerations and velocities because the blast pressures are only applied to around mid-height of the column as presented in Figure 4-39(1a). As shown in Figure 4-50(2), the maximum displacement at height of 0.35 m is observed at time of 2.25 msec, and after that, another peak displacement is observed at time of 5.52 msec. This phenomenon can be explained either by recognizing contributions of the higher mode effects or by thinking about it in terms of traveling wave effects. First, the maximum velocity around low-height of the column occurs at time of 0.09 msec. Then, by traveling wave effects, the masses above that point are pulled outwards up to time of 2.25 msec to create the second velocity distribution shown in Figure 4-50(1b). Under the effect of the traveling impulse,

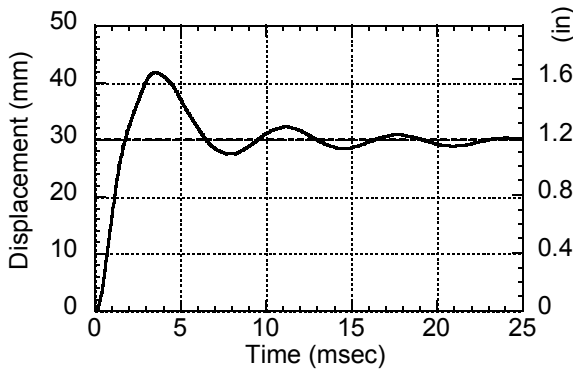
another maximum displacement occurs at time of 5.25 msec per the deflected shape shown in Figure 4-50(1c).

There is a significant difference of maximum reaction forces developed at the base and top of the column as shown in Figure 4-50(3). The maximum reaction forces observed are -855.0 kN and -101.0 kN at the base and top, respectively as shown in Table 4-12. This is because the higher pressures are applied to around lower-height of the column due to the Mach reflection of the blast pressures on the ground as presented in Figure 4-39(1).

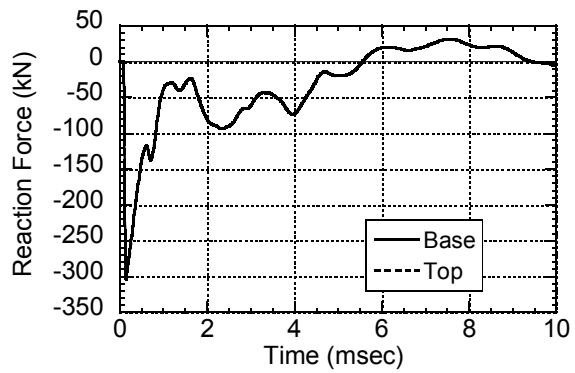
The trends described above are also observed in the other low-height explosion cases of Test 1-9 and Test 1-10 under actual pressure profiles as shown in Figures 4-51 and 4-52. Figures 4-51(4) and 4-52(4) show the large strains developed both in the core concrete fiber at compression edge and in the steel tube at tension edge. Maximum strains of 0.84 and 1.38 are developed in the steel tube of Test 1-9 and Test 1-10, respectively. These values are much larger than their fracture strain of about 0.25 in CFST C6 column (Test 1-9) and 0.4 in CFST C5 column (Test 1-10) obtained from the coupon tests of their steel tubes. The blast test observations presented in Section 3.4.4 showed that the steel tube of CFST C5 column (Test 1-10) fractured at the base of the column, but that of CFST C6 column (Test 1-9) did not fracture. Although the model was not developed to investigate why CFST C6 column did not fracture even though its analytically obtained strain suggests otherwise, it is speculated that the strain at the base of the steel tube might have been less than the predicted strain by the analytical model on account of unbounding of the steel tube in the concrete foundation allowing the strains to propagate below the foundation.



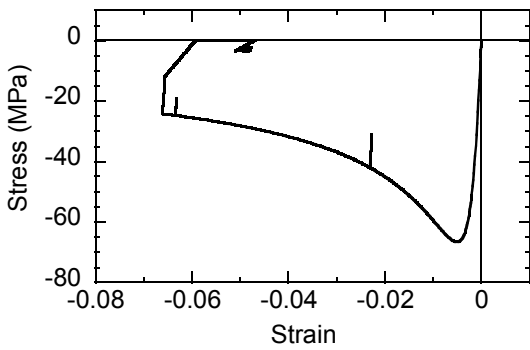
(1) Structural Response Distributions along Height



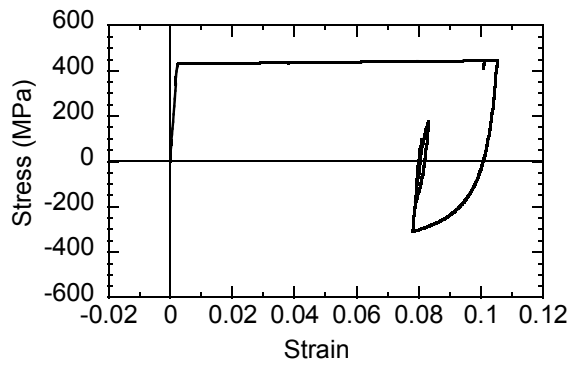
(2) Displacement History (at Mid-height)



(3) Reaction Force History



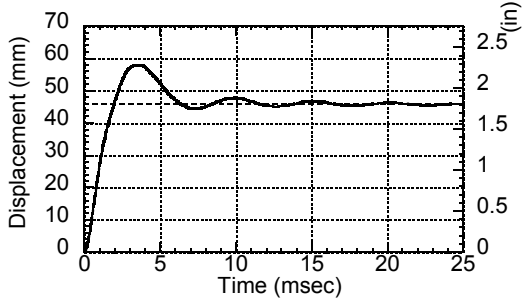
(4a) Core Concrete at Compression Edge



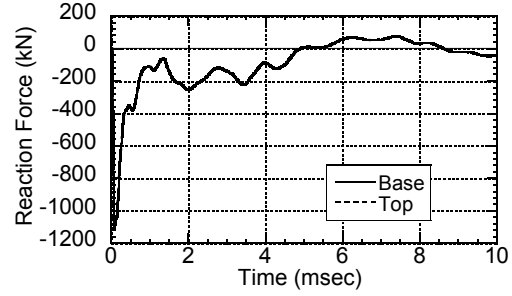
(4b) Steel Tube at Tension Edge

(4) Stress-Strain Relationships

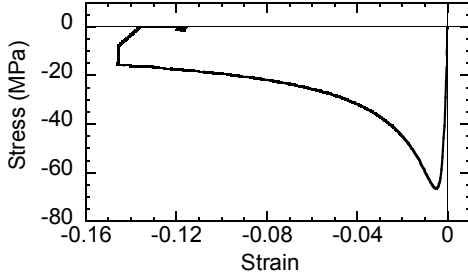
**Figure 4-44 Analytical Results of Test 1-3 (CFST C4 Column) subjected to Equivalent Uniform Pressures**



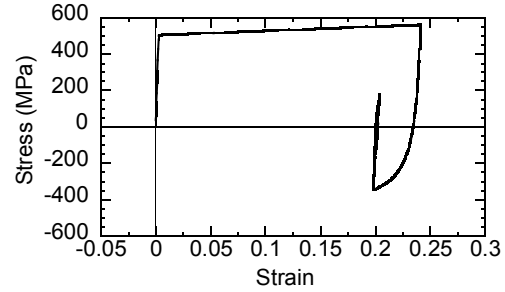
(1) Displacement History (at Mid-height)



(2) Reaction Force History



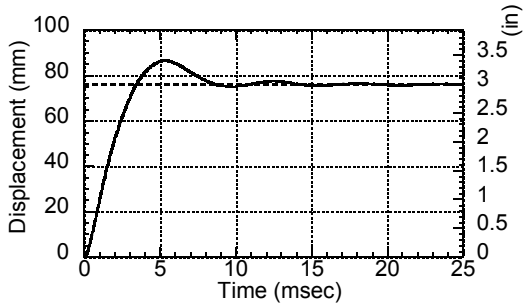
(3a) Core Concrete at Compression Edge



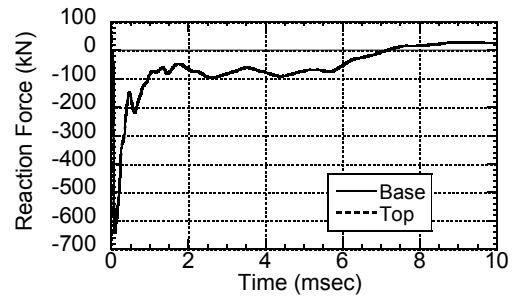
(3b) Steel Tube at Tension Edge

(3) Stress-Strain Relationships

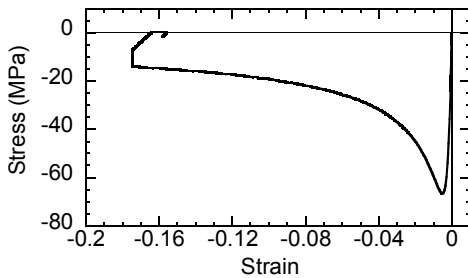
**Figure 4-45 Analytical Results of Test 1-4 (CFST C6 Column) subjected to Equivalent Uniform Pressures**



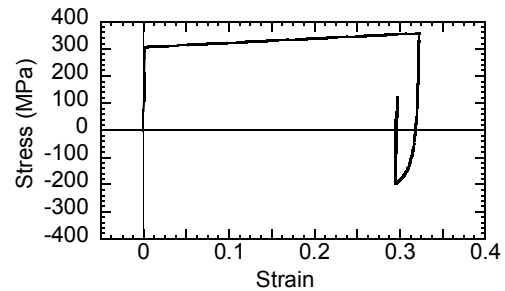
(1) Displacement History (at Mid-height)



(2) Reaction Force History



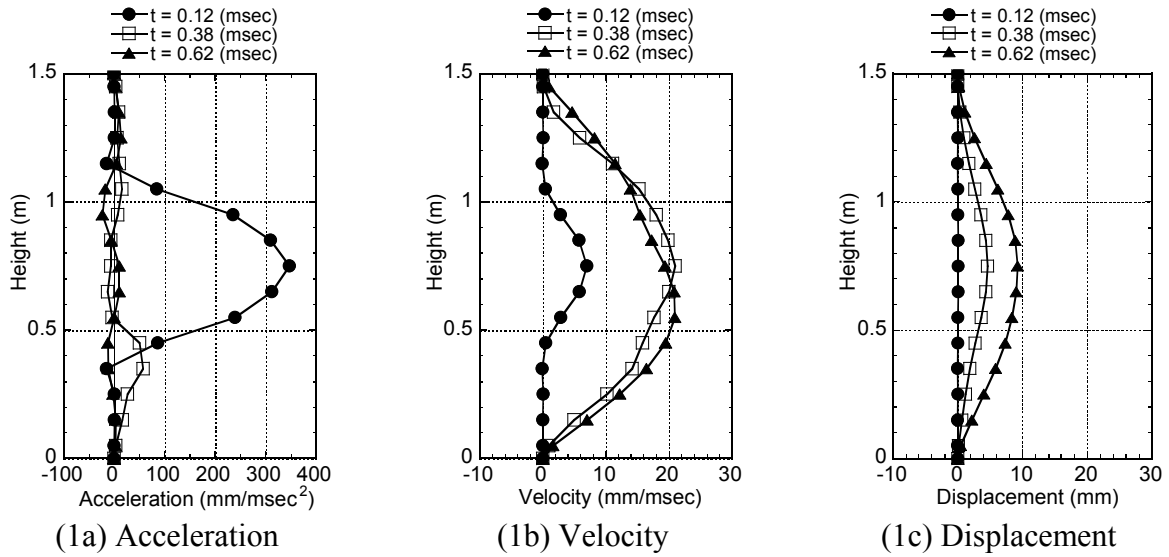
(3a) Core Concrete at Compression Edge



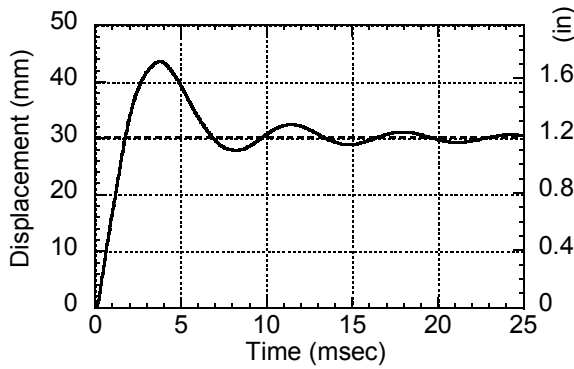
(3b) Steel Tube at Tension Edge

(3) Stress-Strain Relationships

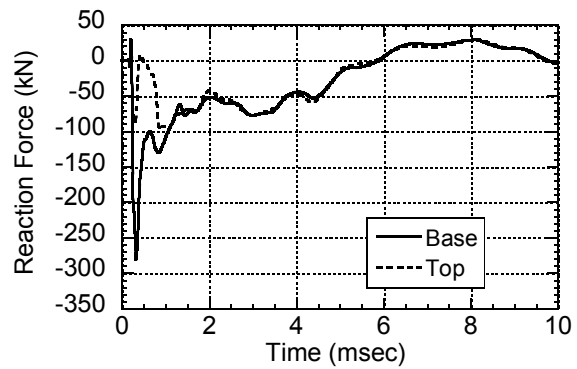
**Figure 4-46 Analytical Results of Test 1-5 (CFST C5 Column) subjected to Equivalent Uniform Pressures**



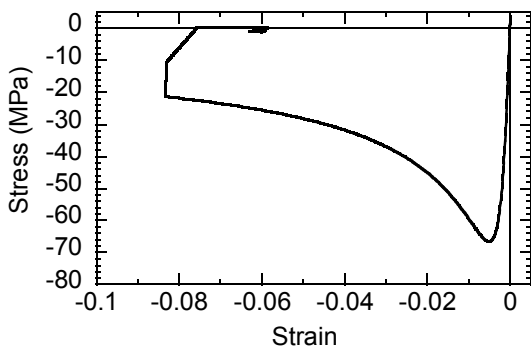
(1) Structural Response Distributions along Height



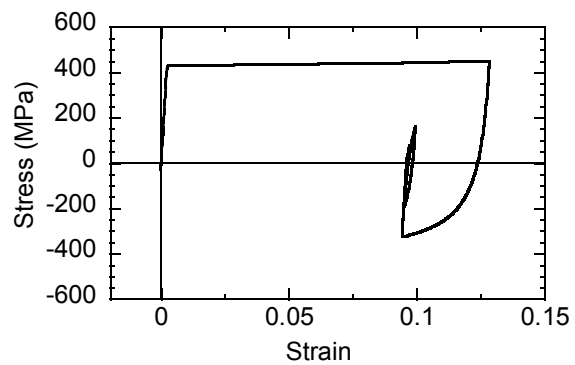
(2) Displacement History (at Mid-height)



(3) Reaction Force History



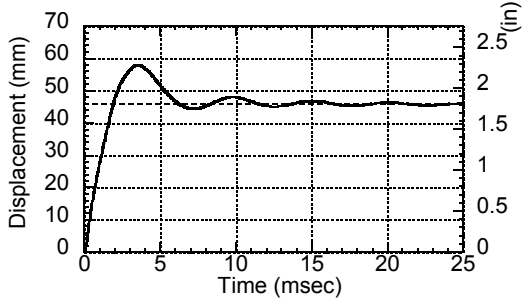
(4a) Core Concrete at Compression Edge



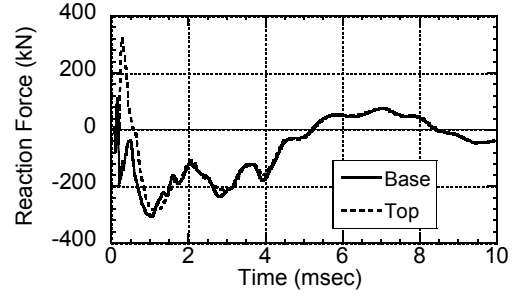
(4b) Steel Tube at Tension Edge

(4) Stress-Strain Relationships

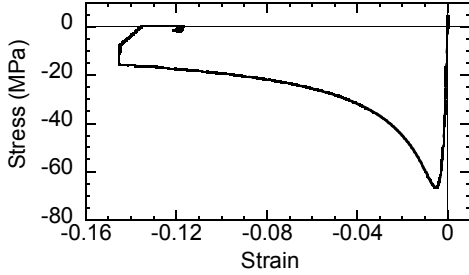
**Figure 4-47 Analytical Results of Test 1-3 (CFST C4 Column) subjected to Actual Pressures**



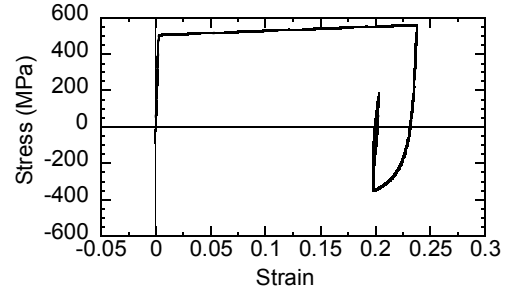
(1) Displacement History (at Mid-height)



(2) Reaction Force History



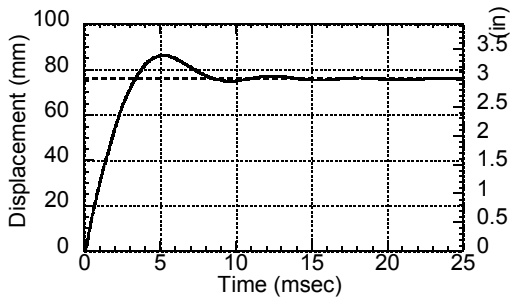
(3a) Core Concrete at Compression Edge



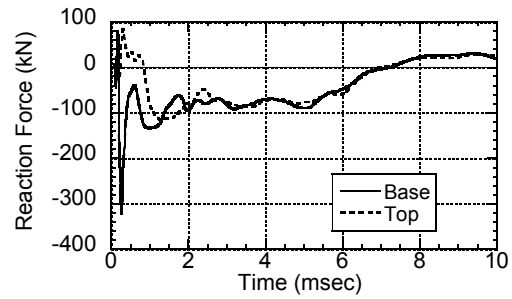
(3b) Steel Tube at Tension Edge

(3) Stress-Strain Relationships

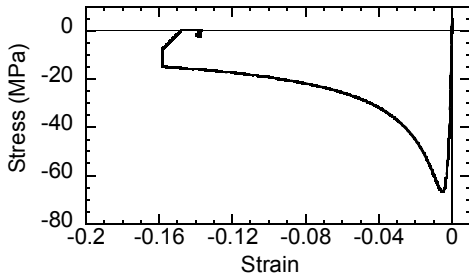
**Figure 4-48 Analytical Results of Test 1-4 (CFST C6 Column) subjected to Actual Pressures**



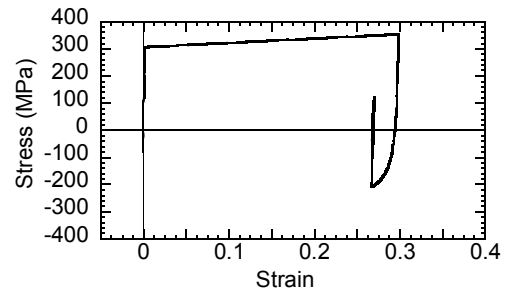
(1) Displacement History (at Mid-height)



(2) Reaction Force History



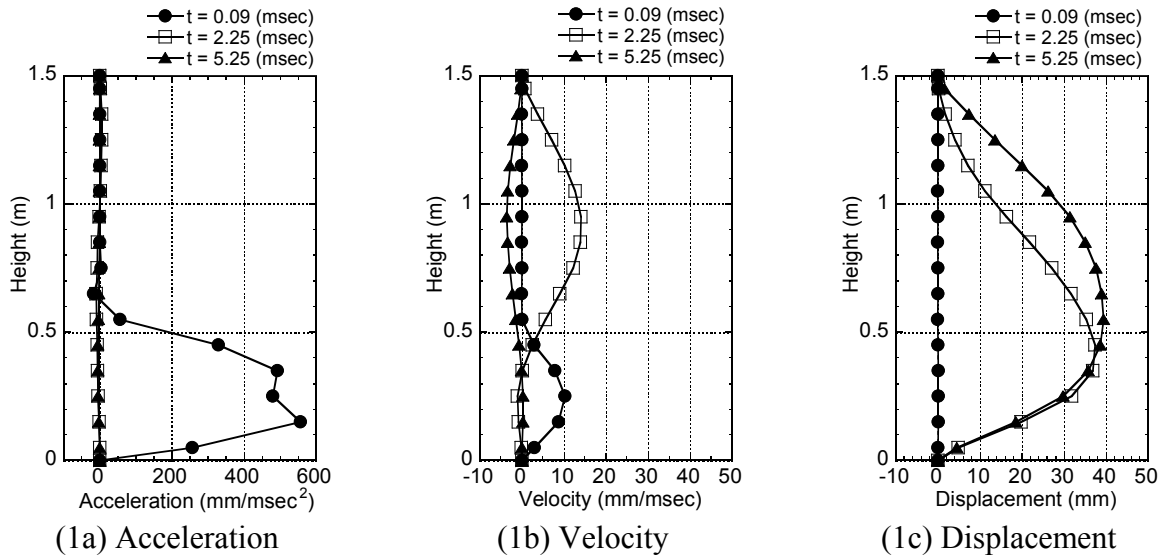
(3a) Core Concrete at Compression Edge



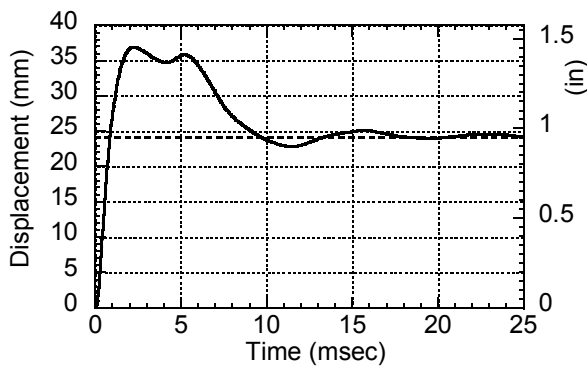
(3b) Steel Tube at Tension Edge

(3) Stress-Strain Relationships

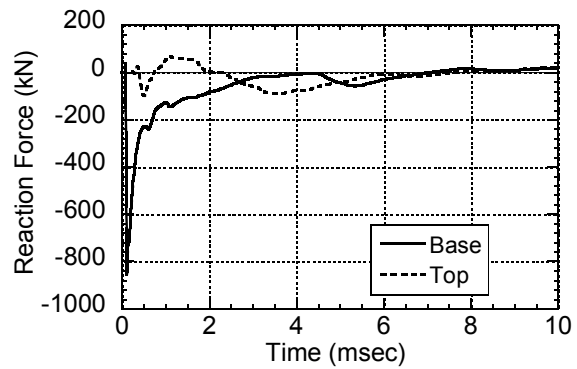
**Figure 4-49 Analytical Results of Test 1-5 (CFST C5 Column) subjected to Actual Pressures**



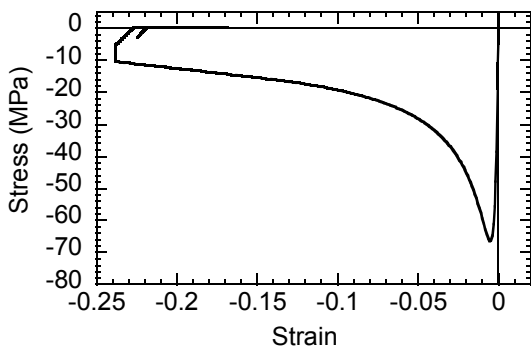
(1) Structural Response Distributions along Height



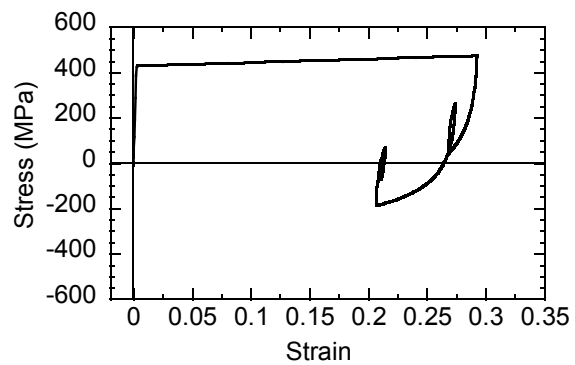
(2) Displacement History (H = 0.35 m)



(3) Reaction Force History



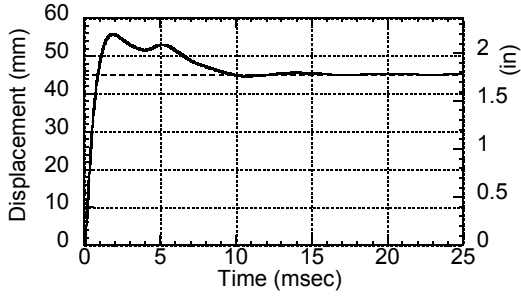
(4a) Core Concrete at Compression Edge



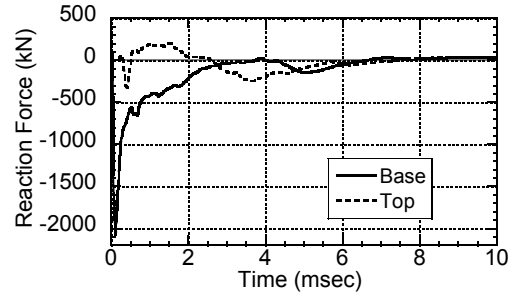
(4b) Steel Tube at Tension Edge

(4) Stress-Strain Relationships

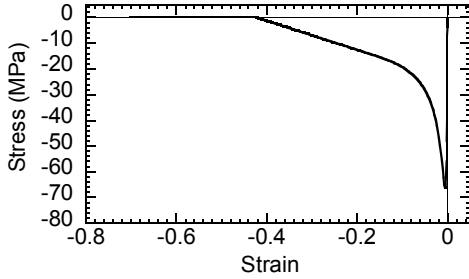
**Figure 4-50 Analytical Results of Test 1-6 (CFST C4 Column) subjected to Actual Pressures**



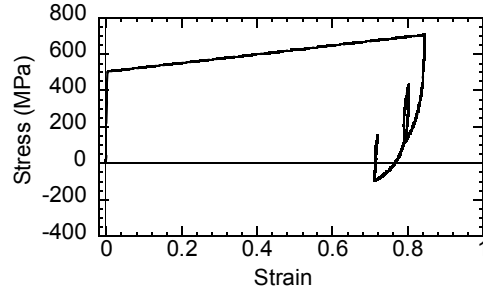
(1) Displacement History (H = 0.25 m)



(2) Reaction Force History



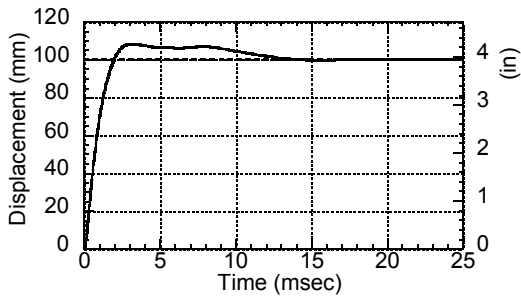
(3a) Core Concrete at Compression Edge



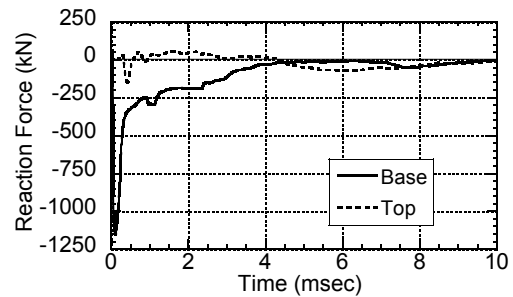
(3b) Steel Tube at Tension Edge

(3) Stress-Strain Relationships

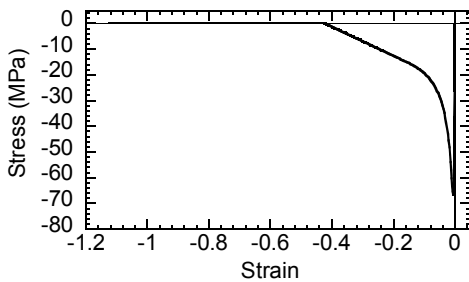
**Figure 4-51 Analytical Results of Test 1-9 (CFST C6 Column) subjected to Actual Pressures**



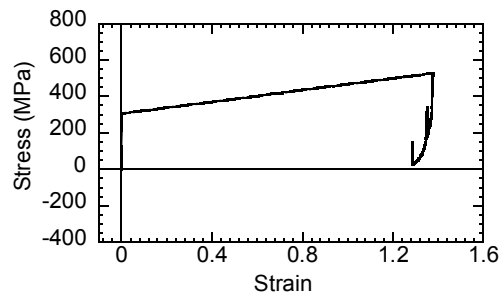
(1) Displacement History (at Mid-height)



(2) Reaction Force History



(3a) Core Concrete at Compression Edge



(3b) Steel Tube at Tension Edge

(3) Stress-Strain Relationships

**Figure 4-52 Analytical Results of Test 1-10 (CFST C5 Column) subjected to Actual Pressures**



#### 4.6.6.3 Structural Response of RC and Steel Jacketed RC Columns

The second series of tested columns, namely RC columns and steel jacketed RC columns, subjected to blast loading, were analyzed using a fiber-based analytical model. Two identical RC columns (RC1 and RC2) and two identical steel jacketed RC columns (SJ1 and SJ2) were tested, and their test cases and test observations were summarized in Table 4-1. As presented in Section 3.3.4, RC1 column and both SJ1 and SJ2 column failed in direct shear at their bases, and RC2 column did not fail in direct shear, but was deemed to exhibit the onset of direct shear at the same location. Therefore, the purpose of the fiber-based analyses was to compute the maximum reaction forces developed at the base of the columns. Displacement history and stress-strain relationships of concrete and steel reinforcement are also investigated for RC2 column which did not fail in direct shear.

The shape factor  $\beta$  was taken as 0.561 that was obtained from the previous fiber-based analytical results of CFST columns for the low-height explosions (Section 4.6.6.1). The damping ratio of 5% was considered using Rayleigh damping for the first and third modes.

Figure 4-53 presents displacement history, reaction force history, and stress-strain relationship of core concrete at compression edge and steel bar at tension edge for Test 2-2 of RC2 column. The displacement history was computed at the height of 0.55 m where the analytically obtained maximum flexural residual displacement of the column is observed. Figure 4-53(1) shows that after reaching the maximum displacement of 8.5 mm, the column at this point displaces back to -1.7 mm. This negative displacement was not observed in the analytical displacement histories of the six CFST columns presented in Section 4.6.6.2. This is because the pressures applied to CFST columns were much higher than these applied to this RC2 column, thus the residual displacements were so large that the columns did not displace in negative phase. For comparison purposes only, CFST C4 column was re-analyzed using the same blast pressure profile as that for Test 2-2 of RC2 column. As presented in Figure 4-54, the same trend is observed in the displacement history curve as that for Test 2-2 of RC2 column shown in Figure 4-53(1). Note that the fact that displacement history swings back to the negative displacement range is a minor point overall. The residual displacement nonetheless remains positive displacement. As shown in Figure 4-53(2), the maximum reaction force at the base is -594.9 kN.

Figures 4-55 to 4-57 show reaction force histories at the base and top of each column up to 1.0 msec for Test 2-1, Test 2-4, and Test 2-3, respectively. The maximum reaction forces at the base of the column observed in these figures and Figure 4-53(2) are summarized in Table 4-13 along with those calculated from simple plastic analyses presented in Section 3.4.3. Note that because the maximum reaction forces obtained from the simple plastic analyses are calculated using the moment capacity of the column sections, reaction forces for a given columns remain the same regardless of the blast charge weight and standoff distance because the flexural plastic mechanism fully develops and limits the maximum shear in the column assumed statically applied loads. By contrast, the maximum reaction forces at the base obtained using the fiber-based dynamic analyses are significantly larger than those from the simple plastic analyses, and are larger when standoff distances are closer with same charge weight. This is because the dynamic fiber-based analysis allows considering dynamic equilibrium that accounts for the large blast pressures and the inertia force before the plastic mechanism develops. The maximum reaction forces of steel jacketed RC columns from the fiber-based dynamic analyses are larger than those of RC columns by 12% and 6% for the standoff distance of 2.16X and 3.25X, respectively. These differences are not as large as that of 77% from the simple plastic analysis results.

**Table 4-13 Summary of Maximum Reaction Forces for RC and Steel Jacketed RC Columns**

Test Num.	Col.	Charge Weight	Standoff Distance	Maximum Reaction Force at Base	
				Fiber-based Analysis	Simple Plastic Analysis
				kN	kN
2-1	RC1	W	2.16 X	-931.7	-112.1
2-2	SJ2			-1042.0	-198.7
2-3	RC2	W	3.25 X	-594.9	-112.1
2-4	SJ1			-632.5	-198.7

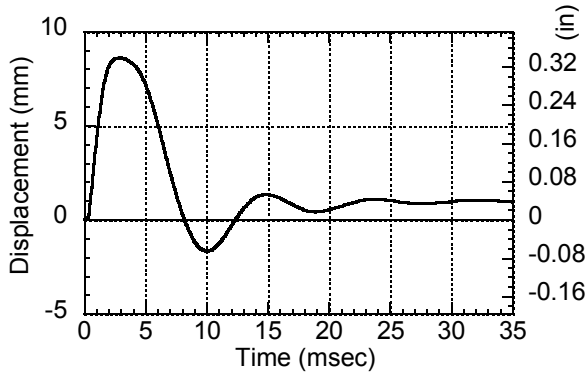
Note that the reaction forces from the fiber-based dynamic analyses provided in Table 4-12 for CFST columns and in Table 4-13 for RC and steel jacketed RC columns are all valuable but cannot be compared with the direct shear strength calculated earlier. These forces are only applied in a small amount of time, as impulses. The fact that they exceed the direct shear capacity does not necessarily mean that direct shear failure will develop because it takes a finite amount of time for direct shear failure to initiate and propagate. Direct shear resistances that have been used earlier could be compared with the forces obtained from the statically applied load. Dynamic shear force likely exceeds the value calculated per Equation 3-36. This remains to be determined from future research, and as such the reaction forces obtained from the dynamic fiber-based analysis models cannot be compared with direct shear resistance at this time.

#### **4.7 Summary of Dynamic Analysis under Blast Loading**

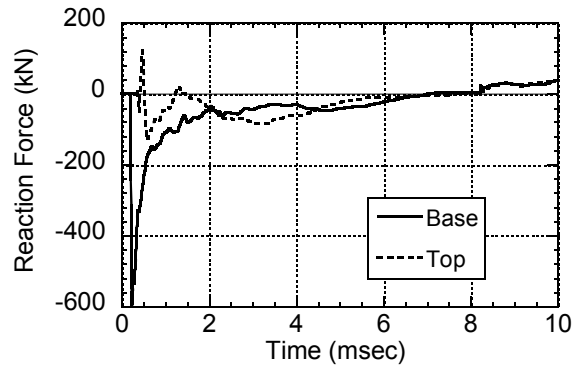
In this project, three different analytical methods have been adopted to replicate the behavior of bridge tested columns subjected to blast loading, namely simplified analysis, SDOF dynamic analysis, and fiber-based dynamic analysis. In this section, the later two analysis methods were investigated in depth and the results obtained compared together as well as against those obtained from the simplified analysis method. The important objective of these series of analyses was to determine the shape factor  $\beta$  to account for the reduction of the blast pressures applied to the column. This shape factor is principally intended to account for the reduction of the blast pressures due to the circular shape of the column; however, in fact this factor  $\beta$  unavoidably is affected by some of assumptions built in the analytical model and method applied. Therefore, it is important to use the value of  $\beta$  that corresponds to the assumptions and conditions used for each analytical method. These are summarized in Table 4-14 along with the resulting  $\beta$  values for each analytical method.

**Table 4-14 Summary of  $\beta$  Values and Assumptions of Each Analytical Method**

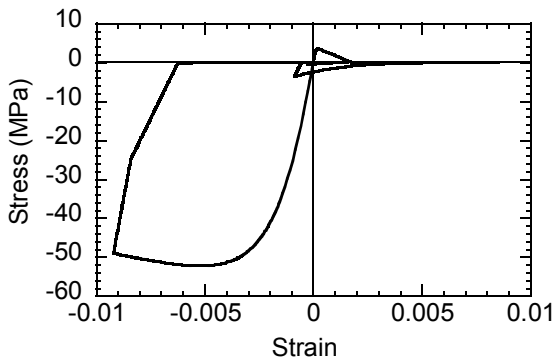
	Assumptions and Conditions	Simplified Analysis	SDOF Dynamic Analysis	Fiber-based Dynamic Analysis
$\beta$ Value	Mid-height	0.459	0.542	0.665
	Low-height	0.441	0.525	0.561
	All Ave.	0.450	0.534	0.613
Modeling Considerations	Column Shape	Circular Shape		
	Dynamic Increase Factor	Concrete Strength: 1.25 Steel Yield Stress: 1.20		
	Strain Hardening of Steel	Not Considered		Considered
	Discretization	SDOF Model		2D Fiber-based Model
	Load-mass Factor	$K_{LMe} = 0.66$ $K_{LMp} = 0.66$	$K_{LMe} = 0.775$ $K_{LMp} = 0.66$	No Need
	Damping	Neglected	5% Viscous Damping	5% Rayleigh Damping
Blast Loading Considerations	Physical Quantity	Energy	Pressure	
	Applied Loading	Equivalent Impulse	Uniform Equivalent Pressure History	Actual Pressure Profile History
	Clearing Effect	Not Considered		



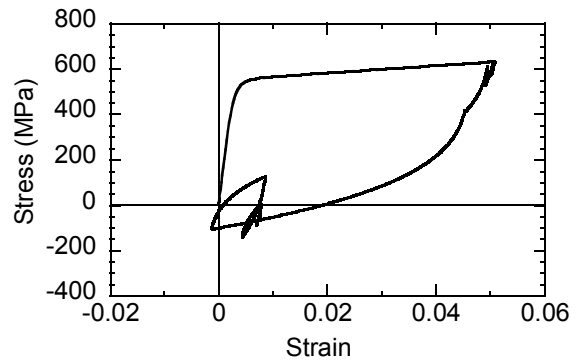
(1) Displacement History (at H = 0.55 m)



(2) Reaction Force History



(3a) Core Concrete at Compression Edge



(3b) Steel Bar at Tension Edge

(3) Stress-Strain Relationships

**Figure 4-53 Analytical Results of Test 2-2 (RC2 Column)**

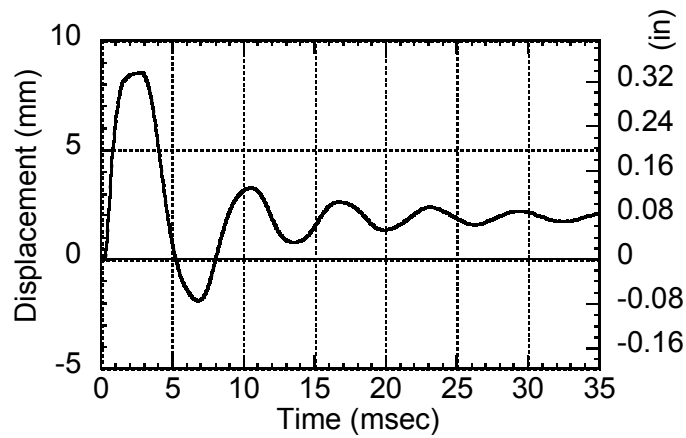


**Figure 4-54 Displacement History of CFST C4 Column using Test 2-2 Blast Pressures (at h = 0.55 m)**

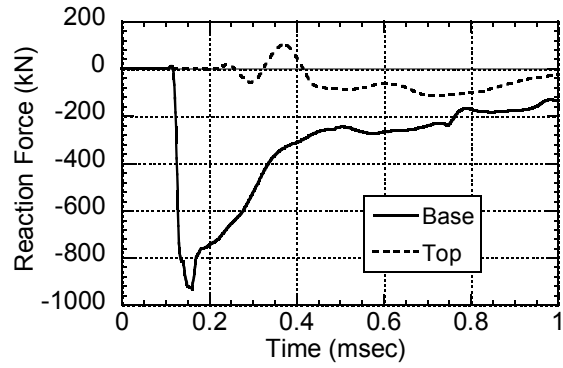


**Figure 4-55** Reaction Force History of Test 2-1 (RC1 Column at  $h = 0.55$  m)

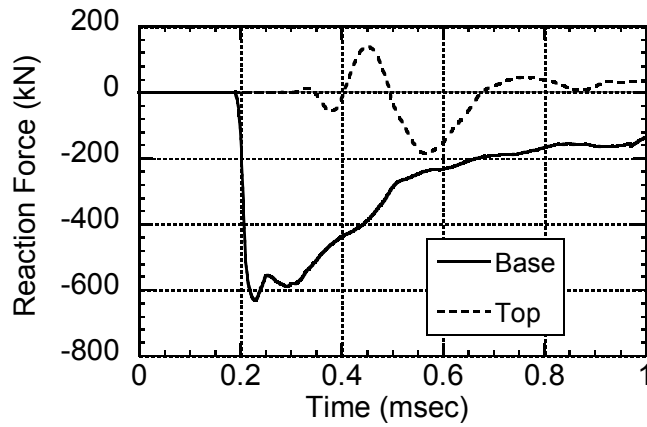


**Figure 4-56** Reaction Force History of Test 2-4 (SJ1 Column at  $h = 0.55$  m)

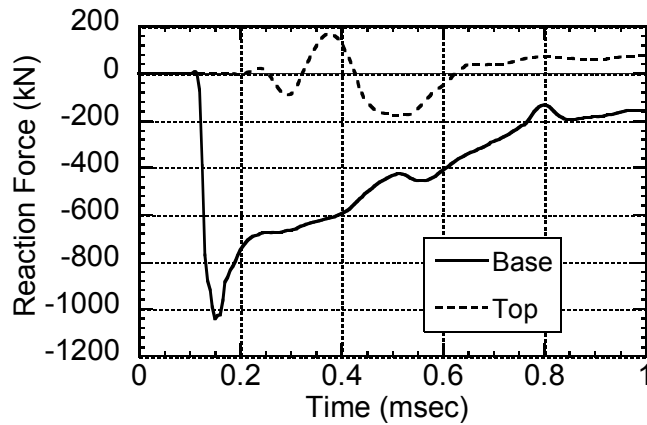


**Figure 4-57** Reaction Force History of Test 2-3 (SJ2 Column at  $h = 0.55$  m)

## **SECTION 5**

# **SUMMARY, CONCLUSIONS, AND RECOMMENDATIONS FOR FURTHER RESEARCH**

### **5.1 Summary**

In this research, the blast resistance of two commonly used seismically designed bridge pier systems with ductile reinforced concrete (RC) columns and non-ductile RC column retrofitted with steel jackets has been investigated experimentally and analytically to complement the first series of CFST columns testing under blast loading by Fujikura et al. (2007, 2008). A fiber-based finite element model was developed and the overall behavior of the tested specimens was investigated using this developed fiber-based finite element model.

The seismic designs of prototype bridge pier with these two types of commonly used columns were conducted using response spectrum analysis with the same response spectrum as the CFST columns. Detailing was accomplished in accordance with the recent seismic design code requirements to achieve concrete confinement and column ductility.

Blast testing was conducted at the U.S. Army Corps of Engineers Research Facility for a one-fourth scale multi-column bent specimen having two RC columns and two steel jacketed RC columns. The one-fourth scale specimen was designed based on the seismically designed prototype bridge columns and using geometric similitude. The test blast parameters were determined using the simplified analysis method using the calibrated value of  $\beta$  obtained from earlier test results on CFST columns. The tested RC columns and steel jacketed RC columns did not exhibit ductile behavior under blast loading, and failed in direct shear at the base.

Simple plastic analyses were conducted to calculate the reaction shear forces at the base of the RC columns and steel jacketed RC columns. The resulting reaction shear forces at the base of these columns were not found to be larger than the direct shear strengths calculated using conventional equations, but these reaction shear forces were found to exceed the direct shear

strength obtained using a moment-direct shear interaction model that was developed and proposed here to calculate the direct shear strength on cross-sections simultaneously subjected to large moments – which confirmed the experimentally observed behavior.

SDOF dynamic analyses considering an equivalent SDOF system were performed for the CFST column tests using an equivalent pressure history. The sensitivity of the load-mass factor required in an equivalent SDOF system, as well as the effect of damping on structural response, was investigated. The shape factor  $\beta$  was reevaluated for SDOF dynamic analysis, and it was found that the resulting factor appropriate to be used in conjunction with this particular analysis method was equal to 0.534 is used in conjunction with a value of 5% viscous damping and two different load-mass factors corresponding to the elastic and inelastic stages of structural response.

Fiber-based analytical models were developed for the CFST column, RC column and steel jacketed column and verified using the quasi-static cyclic loading tests done by various researchers. Then, using these fiber-based analytical models, response history analyses subjected to actual blast pressure profile were conducted for the tested CFST columns to investigate their behavior and to calibrate the shape factor  $\beta$  corresponding to this particular analytical method. The resulting  $\beta$  values were 0.665 for mid-height explosions and 0.561 for low-height explosions using 5% Rayleigh damping. Using these calibrated  $\beta$  values, dynamic analyses were also conducted for the RC columns and steel jacketed columns using the fiber-based structural models.

## 5.2 Conclusions

Two seismically designed conventional bridge pier systems with ductile RC columns and with non-ductile steel jacketed RC columns have been investigated experimentally and analytically when subjected to blast loading. A multi-hazard bridge pier system with CFST columns conducted in the first series of the tests has also been investigated analytically. The key conclusions from this research are as follows:

1. The standard ductile RC and non-ductile RC columns retrofitted with steel jackets were not found to exhibit a ductile behavior under blast loading, and failed in shear at their



base. The steel jacketed columns, although visually resembling the CFST columns, are significantly different in construction due to the presence of gaps between the ends of the steel jacket and the footing and pier cap, purposely intended to prevent composite actions at the ends of the column. These gaps also produced a discontinuity of shear resistance at these locations, which resulted in the observed direct shear failure. However, steel jacketing was effective to prevent direct spalling of concrete.

2. This study has allowed establishing the different values of  $\beta$  that account for the reduction in blast pressures applied to the circular column, as appropriate for the different analytical methods considered. The assumptions and conditions that affect the values of  $\beta$  have been presented in Table 4-14.
3. A moment-direct shear interaction model to calculate the direct shear resistance of RC sections was proposed to account for the reduction of direct shear resistance on cross-sections simultaneously subjected to large moments. This model explained the direct shear failure observed in the RC and steel jacketed RC columns when compared with the reaction force calculated using simple plastic analysis.
4. It was found that the structural response obtained using SDOF dynamic analysis is sensitive to the load-mass factors needed to model structural components as an equivalent SDOF system. Appropriate load-mass factors should be used corresponding to the elastic and inelastic ranges of structural response during time history analysis.
5. Analyses using fiber-based models showed that high frequency modes of vibration have some influence on the structural response when subjected to blast loading. It was also found that using Rayleigh damping with the fiber-based model can significantly reduce the structural response under blast loading due to the high frequency mode effects.

### **5.3 Recommendations for Further Research**

The following recommendations for further research are provided based on the observations and results from this research to further develop the multi-hazard resistant highway bridge pier:

1. The mechanism of dynamic direct shear resistance of RC sections and CFST sections under impulsive loading should be investigated. Models to assess the dynamic direct shear strength of these sections need to be developed to compare with the shear force predicted by the analyses using fiber-based models under blast loading.
2. The influence of axial force on the behavior of columns under blast loading should be investigated. The blast tests on columns presented here were done without the axial force typically applied in actual bridge columns. This effect was investigated analytically using P-delta analysis for the CFST column cases (Fujikura et al. 2007, 2008), but it needs to be validated experimentally. In the RC and steel jacketed RC columns, the existence of axial force in the column could increase the direct shear strength at the base.
3. The uniaxial constitutive models for confined and unconfined concrete, and steel when subjected to impulsive loading should be investigated to model the uniaxial material behavior in analyses using fiber-element models. In this research, the uniaxial constitutive models under the quasi-static loading were adopted by simply multiplying strength by the dynamic increase factors.
4. Detailed 3-D finite element models could be developed for the tested columns to further investigate their behavior, such as for the development of the direct shear failure at the base of the columns.
5. Future research should investigate means and methods to prevent direct shear failure at the base of reinforced concrete columns and steel jacketed reinforced concrete columns. One such strategy might be to introduce circular shear collars at the base of the columns that would transfer shear forces to the foundation by bearing directly on the columns..

## SECTION 6

### REFERENCES

- AASHTO (2004). *AASHTO LRFD Bridge Design Specifications (SI Units, 3<sup>rd</sup> Edition)*, American Association of State Highway and Transportation Officials, Washington, D.C.
- ACI (2004). *Building code requirements for structural concrete (ACI 318-05) and commentary (ACI 318R-05)*, American Concrete Institute, ACI Committee 318, Farmington Hills, MI.
- AISC (1999). *LRFD Specifications for Structural Steel Buildings*, American Institute of Steel Construction, Chicago, IL.
- AISC (2001). *LRFD Manual of Steel Construction*, American Institute of Steel Construction, Chicago, IL (3<sup>rd</sup> edition).
- Ali, M.A. and White, R.N. (1999). “Enhanced Contact Model for Shear Friction of Normal and High-Strength Concrete.” *ACI Structural Journal*, 96-S38, 348-362.
- ARA (2004). *Anti-Terrorist Blast (AT-Blast) version 2.1*, Applied Research Associates, Albuquerque, NM.
- ASCE (1997). *Design of Blast Resistant Buildings in Petrochemical Facilities*, Task Committee on Blast Resistant Design of the Petrochemical Committee, American Society of Civil Engineers, New York, NY.
- ASTM (2005a), “Standard Test Methods and Definitions for Mechanical Testing of Steel Products”, A 370-03a, American Society for Testing and Materials, Philadelphia, PA.
- ASTM (2005b), “Standard Specification for Steel Wire, Deformed, for Concrete Reinforcement”, A 496-02, American Society for Testing and Materials, Philadelphia, PA.
- ASTM (2005c), “Standard Specification for Steel, Sheet, Cold-Rolled, Carbon, Structural, High-Strength Low-Alloy and High-Strength Low-Alloy with Improved Formability”, A 1000/A 1008M-04b, American Society for Testing and Materials, Philadelphia, PA.

- BEL. (2004). *Bridge Explosive Loading (BEL) version 1.1.0.3*. US Army Corps of Engineers' Engineer Research and Development Center, Vicksburg, MS. (distribution limited to U.S. Government agencies and their contractors).
- Belarbi, A. and Hsu, T.T.C. (1994). "Constitutive Laws of Concrete in Tension and Reinforcing Bars Stiffened by Concrete." *ACI Structural Journal*, 91-S46, 465-474.
- Biggs, J. (1964), *Introduction to Structural Dynamics*, McGraw Hill, New York
- Bruneau, M., Uang, C.M. and Whittaker, A. (1998). *Ductile Design of Steel Structures*, McGraw-Hill.
- Bruneau, M. and Marson, J. (2004). "Seismic design of concrete-filled circular steel bridge piers", *Journal of Bridge Engineering*, 9(1), 24-34.
- Buckle, I.G., Friedland, I, Mander, J., Martin, G., Nutt, R. and Power, M. (2006). "Seismic Retrofitting Manual for Highway Structures: Part 1 – Bridges", MCEER-06-SP10, MCEER.
- CALTRANS. (1996). *Earthquake Retrofit Guidelines for Bridges*, Memo to Designers 20-4, California Department of Transportation, Sacramento, CA.
- CALTRANS. (2003). *Bridge Design Specifications*, September, Sacramento, CA.
- CALTRANS. (2006). *Seismic Design Criteria*, Version 1.4, Sacramento, CA.
- Chai, Y.H., Priestley, M.J.N. and Seible, F. (1991). "Seismic Retrofit of Circular Bridge Columns for Enhanced Flexural Performance." *ACI Structural Journal*, V.88, No.5 Sep.-Oct., 572-583.
- Chang, G.A. and Mander, J.B. (1994). *Seismic Energy Based Fatigue Damage Analysis of Bridge Columns: Part I – Evaluation of Seismic Capacity*, Technical Report NCEER-94-0006, NCEER, State University of New York at Buffalo, Buffalo, NY.
- Charlson, N.N. and Miller, K. (1998). "Design and Application of A Gradient-Weighted Moving Finite Element Code I: In One Dimension." *SIAM Journal of Scientific Computing*, vol. 19, No.3, pp.728-765, Society for Industrial and Applied Mathematics.

- Chopra, A.K. (2000). *Dynamics of Structures*, 2<sup>nd</sup> Edition, Prentice Hall, NJ.
- Chung, H.W. (1978). "Shear Strength of Concrete Joints under Dynamic Loads." *Journal of the Concrete Society*, 12(3), 27-29.
- Conrath, E.J., Krauthammer, T., Marchand, K.A. and Mlakar, P.F. (1999). *Structural Design for Physical Security: State of the Practice*, ASCE, Reston, Va.
- Cook, R.D., Malkus, D.S., Plesha, M.E. and Witt, R.J. (2002). *Concepts and Applications of Finite Element Analysis*, 4<sup>th</sup> Edition, John Wiley & Sons, NJ.
- Dicleli M, Bruneau M (1996). "Quantitative approach to rapid seismic evaluation of slab-on-girder steel highway bridges." *Journal of Structural Engineering*, 122(10), 1160-1168.
- Dutta, A. and Mander, J.B. (1998). "Capacity Design and Fatigue Analysis of Confined Concrete Columns", Technical Report MCEER-98-0007, Multidisciplinary Center for Earthquake Engineering Research, State University of New York at Buffalo, Buffalo, NY.
- Eurocode 4. (1994). "Design of composite steel and concrete structures." Commission of the European Communities, Brussels.
- FBI. (2007). "Terrorism 2002-2005." Federal Bureau of Investigation, U.S. Department of Justice.
- FHWA. (2003). *Recommendations for bridge and tunnel security*. Prepared by the Blue Ribbon Panel on Bridge and Tunnel Security, Federal Highway Administration, Washington, D.C.
- Filippou, F.C, Popov, E.P. and Bertero, V.V. (1983). *Effects of bond deterioration on hysteretic behavior of reinforced concrete joints*. EERC Report No. UCB/EERC-83/19. Earthquake Engineering Research Center. University of California, Berkley. California.
- Fujikura, S., Bruneau, M., Lopez-Garcia, D. (2007). "Experimental Investigation of Blast Performance of Seismically Resistant Concrete-Filled Steel Tube Bridge Piers", Technical Report MCEER-07-0005, MCEER, University at Buffalo, Buffalo, NY.

- Fujikura, S., Bruneau, M. and Lopez-Garcia, D. (2008) "Experimental Investigation of Multihazard Resistant Bridge Piers having Concrete-Filled Steel Tube under Blast Loading", *Journal of Bridge Engineering*, 13(6), 586-594.
- Ghee, A.B., Priestley, M.J.N. and Paulay, T. (1989). "Seismic Shear Strength of Circular Reinforced Concrete." *ACI Structural Journal*, Vol.86, No.1, Jan.-Feb., 45-59.
- Hansen, R.J., Nawy, E.G. and Shah, J.M., (1961). "Response of Concrete Shear Keys to Dynamic Loading." *Journal of The ACI*, 57(65), 1475-1490.
- Hofbeck, J.A., Ibrahim, A.H and Mattock, A.H. (1969). "Shear Transfer in Reinforced Concrete." *ACI Journal*, 66(2), 119-128.
- Jenkins, B.M. (1997). *Protecting Public Surface Transportation Systems and Patrons from Terrorism Activities*. MTI Report 97-04, Mineta Transportation Institute, San Jose, CA
- Jenkins, B.M. (2001a). *Protecting Public Surface Transportation Systems and Patrons from Terrorism Activities*. MTI Report 97-04, Mineta Transportation Institute, San Jose, CA
- Jenkins, B.M. (2001b). "Protecting Public Surface Transportation Against Terrorism and Serious Crime: Continuing Research on Best Security Practices." *MTI Report 01-07*, Mineta Transportation Institute, San Jose, CA
- Kim, J-H. and Mander, J.B. (1999). *Truss Modeling of Reinforced Concrete Shear-Flexure Behavior*, Technical Report MCEER-99-0005, Multidisciplinary Center for Earthquake Engineering Research, State University of New York at Buffalo, Buffalo, NY.
- Mander, J.B., Priestley, M.J.N. and R. Park (1988). "Theoretical Stress-Strain Model for Confined Concrete Columns." *Journal of Structural Engineering*, ASCE, Vol. 114, No. 8, 1804-1826.
- MacGregor, J.G. and Wight, J.K. (2005). *Reinforced Concrete Mechanics and Design Fourth Edition*, Prentice, NJ.
- Marson, J. and Bruneau, M. (2004). "Cyclic testing of concrete-filled circular steel bridge piers having encased fixed-based detail." *Journal of Bridge Engineering*, ASCE, 9(1), 14-23.

- Matsukawa, R, A. Kawashima, K., Sakai, J. and Shoji, G. (2002). "Effect of Lateral Confinement by Spirals on Seismic Performance of Circular Reinforced Concrete Bridge Piers." *Journal of Structural Engineering*, Vol. 48A, pp. 715-723, Japan Society of Civil Engineers. (in Japanese)
- Mattock, A.H. and Hawkins, N.M. (1972). "Shear Transfer in Reinforced Concrete-Recent Research." *PCI Journal*, 17(2), 55-75.
- Mays, G.C. and Smith, P.D. (1995): *Blast effects on buildings*. Telford, London, UK.
- MCEER/ATC-49. (2003a). *Recommended LRFD Guidelines for the Seismic Design of Highway Bridges, Part I: Specifications and II: Commentary and Appendices*, ATC and MCEER.
- MCEER/ATC-49. (2003b). *Design Examples, Recommended LRFD Guidelines for the Seismic Design of Highway Bridges*, ATC and MCEER.
- Menegotto, M. and Pinto, E. (1973). "Method of analysis for cyclically loaded reinforced concrete plane frames including changes in geometry and non-elastic behavior of elements under combined normal force and bending." *Proceedings of IABSE Symposium*. Lisbon, Portugal.
- Multi-Hazard Symposium. (2007). Symposium on Emerging Developments in Multi-Hazard Engineering, Architectural Engineering Institute and MCEER, McGraw Hill Conference Center, New York City, September 18, 2007.  
<<http://mceer.buffalo.edu/meetings/aei/default.asp>> (January 18, 2008).
- NIE. (2007). "The Terrorist Threat to the US Homeland", *National Intelligence Estimate*, National Intelligence Council.
- NONLIN version 6.01. (1996). Advanced Structural Concepts, Golden, Colo.
- OpenSees. (2007). *Open System for Earthquake Engineering Simulation ver 1.7.5*, Pacific Earthquake Engineering Research Center, University of California, Berkeley, CA.
- Orakcal, K. and Wallace, J.W. (2006a). "Flexural Modeling of Reinforced Concrete Walls-Experimental Verification." *ACI Structural Journal*, 103-S21, 196-206.

- Orakcal, K., Massone, L.M. and Wallace, J.W. (2006b). *Analytical Modeling of Reinforced Concrete Walls for Predicting Flexural and Coupled-Shear-Flexural Responses*. PEER Report 2006/07. Pacific Earthquake Engineering Research Center. University of California, Berkeley, California.
- PEER (2008). "PEER Structural Performance Database." Pacific Earthquake Engineering Research Center, <<http://nisee.berkeley.edu/spd/>> (May 1, 2008).
- Priestley, M.J.N., Seible, F., Xiao, Y. and Verma, R. (1994a). "Steel Jacket Retrofitting of Reinforced Concrete Bridge Columns for Enhanced Shear Strength – Part 1: Theoretical Considerations and Test Design." *ACI Structural Journal*, V.91, No.4 Jul.-Aug., 394-405.
- Priestley, M.J.N., Seible, F., Xiao, Y. and Verma, R. (1994b). "Steel Jacket Retrofitting of Reinforced Concrete Bridge Columns for Enhanced Shear Strength – Part 2: Test Results and Comparison with Theory." *ACI Structural Journal*, V.91, No.5 Sep.-Oct., 537-551.
- Priestley, M.J.N., Seible, F. and Calvi, G.M. (1996). *Seismic Design and Retrofit of Bridges*, Wiley, New York, NY.
- Ross, T.J. (1983). *Direct Shear Failure in Reinforced Concrete Beams under Impulsive Loading*, Technical Report AFWL-TR-83-84, Air Force Weapons Laboratory, Kirtland Air Force Base, NM.
- Scott, B.D., Park, R. and Priestley, M.J.N. (1982). "Stress-strain Behavior of Concrete Confined by Overlapping Hoops at Low and High Strain Rate." *Journal of ACI*, 79(1), 13-27.
- Spacone, E., Filippou, F.C. and Taucer, F.F.(1996a). "Fiber Beam-Column Model for Non-Linear Analysis of R/C Frames: Part I. Formulation." *Earthquake Engineering and Structural Dynamics*, Vol. 25, 711-725.
- Spacone, E., Filippou, F.C. and Taucer, F.F.(1996b). "Fiber Beam-Column Model for Non-Linear Analysis of R/C Frames: Part II. Applications." *Earthquake Engineering and Structural Dynamics*, Vol. 25, 711-725.
- Tokyo Tech (2008). "Kawashima Lab Test Database." Kawashima Earthquake Engineering Laboratory, Tokyo Institute of Technology, <<http://seismic.cv.titech.ac.jp/en/titdata/>> (May 1, 2008).



- UFC. (2002). *Design and Analysis of Hardened Structures to Conventional Weapons Effects*. Unified Facilities Criteria UFC 3-340-01, Department of Defense, USA. (distribution limited to U.S. Government agencies and their contractors)
- UFC. (2004). *Basic Guidelines for Chemical Hardening of New Military Facilities*. Unified Facilities Criteria UFC 3-340-13, Department of Defense, USA.
- USACE-OD. (2002). *SPAn32 version 1.2.7.2*. U.S. Army Corps of Engineers Omaha District, Omaha, Neb. (distribution limited to U.S. Government agencies and their contractors).
- USACE-PDC. (2006). *User's Guide for the Single-Degree-of-Freedom Blast Effects Design Spreadsheets (SBEDS)*, U.S. Army Corps of Engineers Protective Design Center, Omaha, Neb.
- USACE-PDC. (2007). *Single-Degree-of-Freedom Blast Effects Design Spreadsheets (SBEDS) version 3.1*, U.S. Army Corps of Engineers Protective Design Center, Omaha, Neb.
- USDA. (1990). *Structures to Resist the Effects of Accidental Explosions*. Technical Manual TM 5-1300, US Department of the Army, Washington, DC.
- Waugh J. (2007). Personal correspondence with writer. Department of Civil, Construction and Environmental Engineering, Iowa State University.
- Williamson, E.B. and Winget, D.G. (2005). "Risk management and design of critical bridges for terrorist attacks." *Journal of Bridge Engineering*, 10(1), 96-106.
- Winget DG, Marchand KA and Williamson EB (2005). "Analysis and design of critical bridges subjected to blast loads." *Journal of Structural Engineering*, 131(8), 1243-1255.
- XTRACT (2007). *XTRACT Educational Version ver. 3.0.8*, TRC/Imbsen Software Systems, Rancho Cordova, CA.
- Yassin, M.H.M. (1994). *Nonlinear Analysis of Prestressed Concrete Structures under Monotonic and Cyclic Loads*. Dissertation. University of California, Berkeley. California.
- Zhao, J and Sritharan, S. (2007). "Modeling of Strain Penetration Effects in Fiber-Based Analysis of Reinforced Concrete Structures." *ACI Structural Journal*, 104-S14, 133-141.



**APPENDIX A**  
**SECTION AND MATERIAL MODELS OF PROTOTYPE**  
**COLUMN FROM XTRACT**

Axial force - moment interaction curve was calculated using XTRACT (2007) for the design of the prototype bridge bent column. This appendix provides the details of section and material models. The stress-strain relationships for confined and unconfined concrete and steel bars are presented.

# XTRACT Section Report - Educational

For use only in an academic or research setting

Section Name: Section1

Imbsen & Associates, Inc. (Educational u

UB

3/13/2008

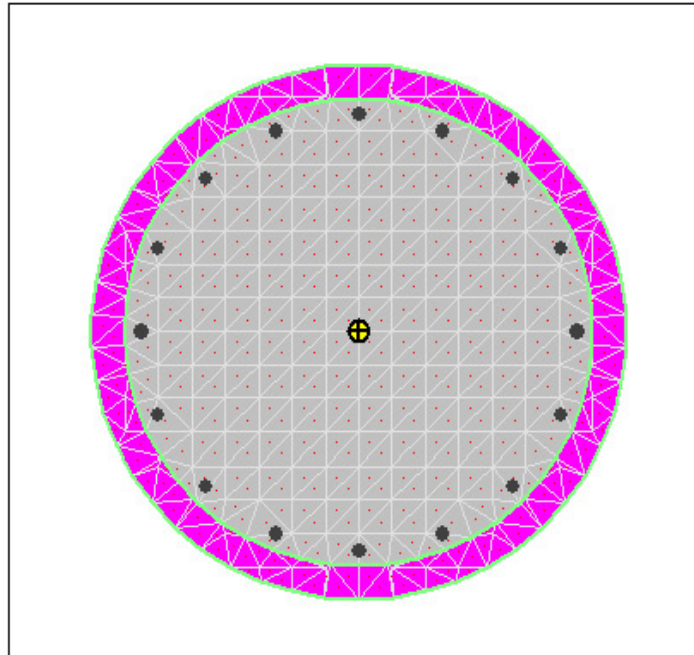
Multihazard

1

Page \_\_ of \_\_

## Section Details:

X Centroid:	- .2574E-6 in
Y Centroid:	- .8267E-16 in
Section Area:	802.1 in <sup>2</sup>
EI gross about X:	1.99E+8 kip-in <sup>2</sup>
EI gross about Y:	1.99E+8 kip-in <sup>2</sup>
I trans(Confined1) about X:	55.25E+3 in <sup>4</sup>
I trans(Confined1) about Y:	55.24E+3 in <sup>4</sup>
Reinforcing Bar Area:	7.069 in <sup>2</sup>
Percent Longitudinal Steel:	.8813 %
Overall Width:	31.94 in
Overall Height:	32.00 in
Number of Fibers:	494
Number of Bars:	16
Number of Materials:	3



## Material Types and Names:

Unconfined Concrete:	■ Unconfined1
Confined Concrete:	■ Confined1
Strain Hardening Steel:	■ Steel

## Comments:

User Comments

# XTRACT Material Report - Educational

Imbsen & Associates, Inc. (Educational u

UB

3/13/2008

Multihazard

1

Page \_\_ of \_\_

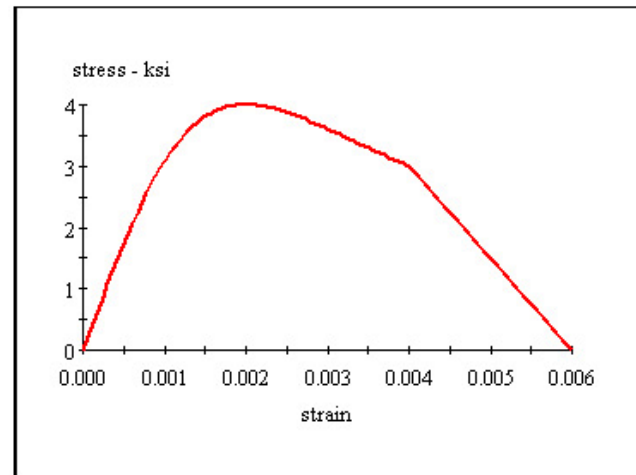
For use only in an academic or research setting

Material Name: Unconfined1

Material Type: Unconfined Concrete

## Input Parameters:

Tension Strength: 0 ksi  
 28 Day Strength: 4.000 ksi  
 Post Crushing Strength: 0 ksi  
 Tension Strain Capacity: 0 Ten  
 Spalling Strain: 6.000E-3 Comp  
 Failure Strain: 1.0000 Comp  
 Elastic Modulus: 3605 ksi  
 Secant Modulus: 2000 ksi



## Model Details:

For Strain -  $\varepsilon < 2 \cdot \varepsilon_t$   $f_c = 0$

For Strain -  $\varepsilon < 0$   $f_c = \varepsilon \cdot E_c$

For Strain -  $\varepsilon < \varepsilon_{cu}$   $f_c = \frac{f_c \cdot x \cdot r}{r - 1 + x^r}$

For Strain -  $\varepsilon < \varepsilon_{sp}$   $f_c = f_{cu} + (f_{cp} - f_{cu}) \cdot \frac{(\varepsilon - \varepsilon_{cu})}{(\varepsilon_{sp} - \varepsilon_{cu})}$

$$x = \frac{\varepsilon}{\varepsilon_{cc}}$$

$$r = \frac{E_c}{E_c - E_{sec}}$$

$$E_{sec} = \frac{f_c}{\varepsilon_{cc}}$$

$\varepsilon$  = Concrete Strain

$f_c$  = Concrete Stress

$E_c$  = Elastic Modulus

$E_{sec}$  = Secant Modulus

$\varepsilon_t$  = Tension Strain Capacity

$\varepsilon_{cu}$  = Ultimate Concrete Strain

$\varepsilon_{cc}$  = Strain at Peak Stress = .002

$\varepsilon_{sp}$  = Spalling Strain

$f_c$  = 28 Day Compressive Strength

$f_{cu}$  = Stress at  $\varepsilon_{cu}$

$f_{cp}$  = Post Spalling Strength

## Material Color States:

- Tension strain after tension capacity
- Tension strain before tension capacity
- Initial state
- Compression before crushing strain
- Compression before end of spalling
- Compression after spalling

## Reference:

Mander, J.B., Priestley, M. J. N., "Observed Stress-Strain Behavior of Confined Concrete", Journal of Structural Engineering ASCE, Vol. 114, No. 8, August 1988, pp. 1827-1849

# XTRACT Material Report - Educational

Imbsen & Associates, Inc. (Educational u

For use only in an academic or research setting

UB

3/13/2008

Material Name: Confined1

Multihazard

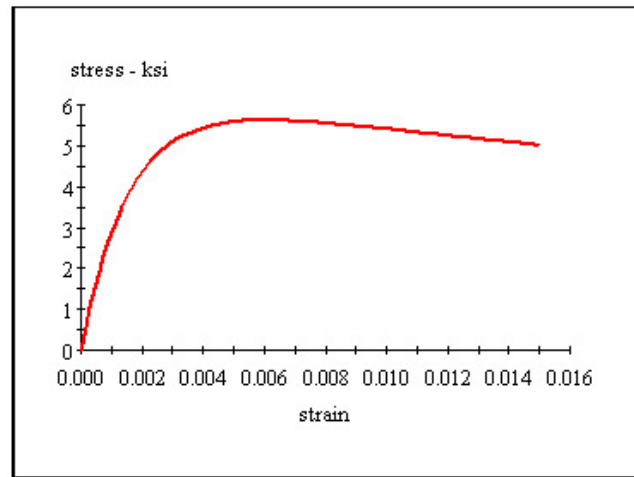
Material Type: Confined Concrete

1

Page \_\_ of \_\_

## Input Parameters:

Tension Strength: 0 ksi  
 28 Day Strength: 4.000 ksi  
 Confined Concrete Strength: 5.619 ksi  
 Tension Strain Capacity: 0 Ten  
 Strain at Peak Stress: 6.048E-3  
 Crushing Strain: 15.00E-3 Comp  
 Elastic Modulus: 3605 ksi  
 Secant Modulus: 929.1 ksi



## Model Details:

For Strain -  $\varepsilon < 2 \cdot \varepsilon_t$        $f_c = 0$   
 For Strain -  $\varepsilon < 0$                $f_c = \varepsilon \cdot E_c$   
 For Strain -  $\varepsilon < \varepsilon_{cu}$            $f_c = \frac{f_{cc} \cdot x \cdot r}{r - 1 + x^r}$

$$x = \frac{\varepsilon}{\varepsilon_{cc}}$$

$$\varepsilon_{cc} = .002 \cdot \left[ 1 + 5 \cdot \left( \frac{f_{cc}}{f_c} - 1 \right) \right]$$

$$r = \frac{E_c}{E_c - E_{sec}}$$

$$E_{sec} = \frac{f_{cc}}{\varepsilon_{cc}}$$

$\varepsilon$  = Concrete Strain

$f_c$  = Concrete Stress

$E_c$  = Elastic Modulus

$\varepsilon_t$  = Tension Strain Capacity

$\varepsilon_{cu}$  = Ultimate Concrete Strain

$\varepsilon_{cc}$  = Strain at Peak Stress

$f_c$  = 28 Day Compressive Strength

$f_{cc}$  = Confined Concrete Strength

## Material Color States:

- Tension strain after tension capacity
- Tension strain before tension capacity
- Initial state
- Compression before crushing strain

## Reference:

Mander, J.B., Priestley, M. J. N., "Observed Stress-Strain Behavior of Confined Concrete", Journal of Structural Engineering ASCE, Vol. 114, No. 8, August 1988, pp. 1827-1849

# XTRACT Material Report - Educational

For use only in an academic or research setting

Material Name: Steel1

Material Type: Strain Hardening Steel

Imbsen & Associates, Inc. (Educational u

UB

3/13/2008

Multihazard

1

Page \_\_ of \_\_

## Input Parameters:

Yield Stress: 60.00 ksi  
Fracture Stress: 60.00 ksi  
Yield Strain: 2.069E-3  
Strain at Strain Hardening: .1000  
Failure Strain: .3000  
Elastic Modulus: 29.00E+3 ksi  
Additional Information: Symetric Tension and Comp.

## Model Details:

For Strain -  $\varepsilon < \varepsilon_y$   $f_s = E \cdot \varepsilon$

For Strain -  $\varepsilon < \varepsilon_{sh}$   $f_s = f_y$

For Strain -  $\varepsilon < \varepsilon_{su}$   $f_s = f_u - (f_u - f_y) \cdot \left( \frac{\varepsilon_{su} - \varepsilon}{\varepsilon_{su} - \varepsilon_{sh}} \right)^2$

$\varepsilon$  = Steel Strain

$f_s$  = Steel Stress

$f_y$  = Yield Stress

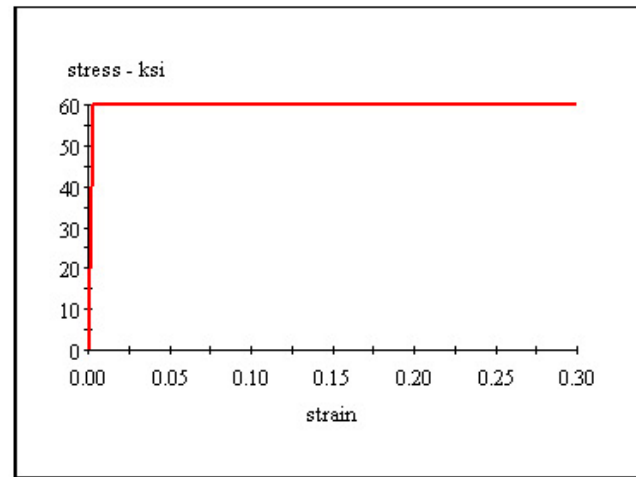
$f_u$  = Fracture Stress

$\varepsilon_y$  = Yield Strain

$\varepsilon_{sh}$  = Strain at Strain Hardening

$\varepsilon_{su}$  = Failure Strain

E = Elastic Modulus



## Material Color States:

- Tension force after onset of strain hardening
- Tension force after yield
- Initial state
- Compression force after yield
- Compression force after onset of strain hardening





## **APPENDIX B**

### **SEISMIC ANALYSIS AND DESIGN OF PROTOTYPE BRIDGE BENT COLUMN**

This appendix provides details on the analysis and design of prototype bridge bent columns. Response spectrum analysis was executed for the prototype bridge. The pier bent was designed according to the recent design code. A column diameter of 813 mm (32 in) is selected and the column was reinforced with 16 – D19 (#6) longitudinal bars. Calculated expected ductility demands in the longitudinal and transverse direction were 2.22 and 3.39, respectively. Transverse spiral reinforcement was provided with D16 (#5) at spacing of 114 mm (4.5 in) in plastic hinge region and D13 (#4) at spacing of 152 mm (6 in) outside of plastic hinge region.

## Appendix B

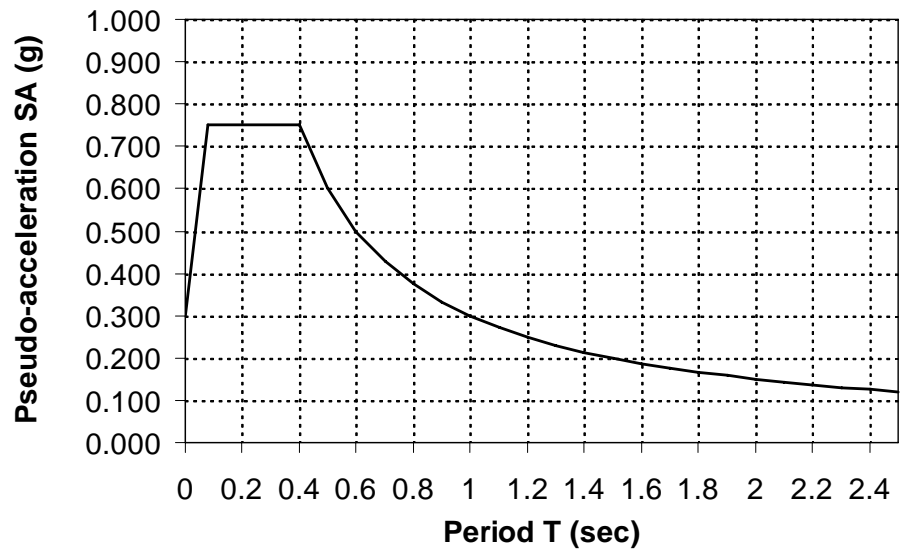
### --- RC Column of Prototype Bridge Design ---

D = 32 in, L. Bar = 16 #6, T. Bar = #4@4.5 in  
 $f'_c = 4 \text{ ksi}$

#### DESIGN STEP 1 \_ Design Earthquake Response Spectra

$$F_a := 1.0 \quad S_s := 0.75$$

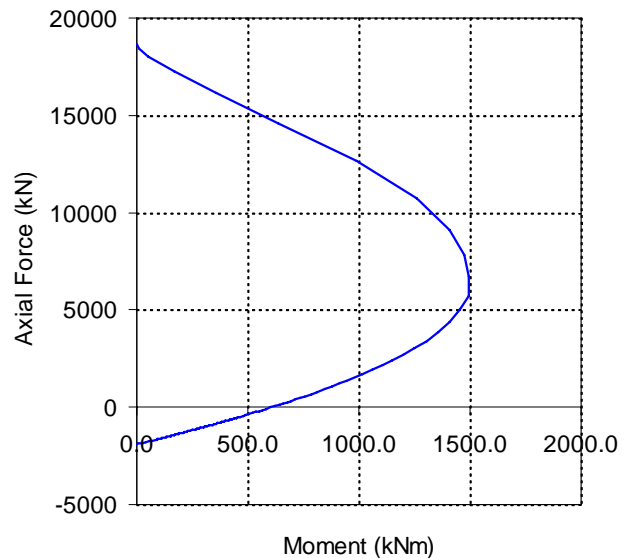
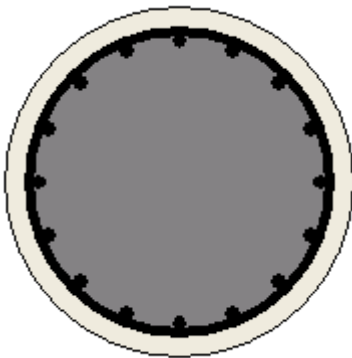
$$F_v := 1.0 \quad S_1 := 0.30$$



#### DESIGN STEP 2 \_ Section Properties

From XTRACT

D = 32 inches, Logitudinal bar 16#6



## Appendix B

### DESIGN STEP 3 \_ Determine Elastic Seismic Forces and Displacements

#### Design Step 3.1 \_ Longitudinal Direction

##### Effective Weights

Total superstructure weight,  $W_{\text{super}}$ :

$L := 90\text{m}$       Length of bridge

$$w_{\text{super}} := 123.21 \frac{\text{kN}}{\text{m}}$$

$$W_{\text{super}} := w_{\text{super}} \cdot L$$

$$W_{\text{super}} = 11089 \text{ kN}$$

Vertical load,  $P_{\text{pier}}$ :

$$P_{\text{pier}} := 4090 \cdot \text{kN}$$

Dead load of column,  $P_{\text{col}}$ :

$$D_{\text{col}} := 32 \cdot \text{in} \quad D_{\text{col}} = 813 \text{ mm}$$

$$H_{\text{clr}} := 6 \cdot \text{m}$$

$$P_{\text{col}} := \frac{\pi}{4} \cdot D_{\text{col}}^2 \cdot 24 \cdot \frac{\text{kN}}{\text{m}^3} \cdot H_{\text{clr}} \quad P_{\text{col}} = 74.7 \text{ kN}$$

Weight of cap beam,  $P_{\text{cap\_bm}}$ :

$$P_{\text{cap\_bm}} := (42 \cdot \text{in}) \cdot (48 \cdot \text{in}) \cdot (15 \cdot \text{m}) \cdot 24 \cdot \frac{\text{kN}}{\text{m}^3} \quad P_{\text{cap\_bm}} = 468 \text{ kN}$$

Total dead load at bottom of column,  $P_{\text{col\_dl}}$ :

$n := 3$       Number of columns per pier

$$P_{\text{col\_dl}} := \frac{P_{\text{pier}}}{n} + \frac{P_{\text{cap\_bm}}}{n} + P_{\text{col}} \quad P_{\text{col\_dl}} = 1594 \text{ kN}$$

Total dead load at top of column,  $P_{\text{col\_dltop}}$ :

Number of columns per pier

$$P_{\text{col\_dltop}} := \frac{P_{\text{pier}}}{n} + \frac{P_{\text{cap\_bm}}}{n} \quad P_{\text{col\_dltop}} = 1519 \text{ kN}$$

## Appendix B

### Yield Displacement

$$P := P_{col\_dltop} \quad P = 1519 \text{ kN}$$

$$M_{x1} := 978.2 \text{ kN}\cdot\text{m} \quad P_{x1} := 1522.6 \text{ kN}$$

$$M_{x2} := 944.1 \text{ kN}\cdot\text{m} \quad P_{x2} := 1367.3 \text{ kN}$$

$$\rightarrow M := \frac{P - P_{x2}}{P_{x1} - P_{x2}} \cdot (M_{x1} - M_{x2}) + M_{x2} \quad M = 977 \text{ kN}\cdot\text{m} \quad M_n := M \quad \text{From P-M Curve}$$

$$M_n = 977 \text{ m kN} \quad \text{Nominal moment at top of column}$$

$$H := 7.0 \cdot \text{m} \quad \text{Height to bearing from foundation}$$

$$f'_c := 4000 \cdot \text{psi}$$

$$E_c := 57000 \cdot \text{psi}^{0.5} \cdot \sqrt{f'_c} \quad E_c = 3605 \text{ ksi} \quad E_c = 24856 \text{ MPa}$$

$$I_{cr} := \frac{\pi}{64} \cdot \frac{D_{col}^4}{2} \quad \text{Cracked section taken as one-half gross section.}$$

$$\Delta_y := \frac{M_n \cdot H^2}{3 \cdot E_c \cdot I_{cr}} \quad \Delta_y = 60 \text{ mm} \quad \Delta_y = 0.20 \text{ ft}$$

### Effective Period

$$H_{clr} = 6.00 \text{ m}$$

$$K_{eff} := 2 \cdot n \cdot \frac{3 \cdot E_c \cdot I_{cr}}{H^3} \quad K_{eff} = 13973 \frac{\text{kN}}{\text{m}}$$

$$T_{eff} := 2\pi \sqrt{\frac{W_{super}}{K_{eff} \cdot g}} \quad T_{eff} = 1.79 \text{ s}$$

### Required Lateral Strength

Required lateral strength of column,  $V_{up}$ :

$$V_{up} := \frac{M_n}{H} \quad V_{up} = 140 \text{ kN}$$

$$\Sigma V_{up} := 2 \cdot n \cdot V_{up} \quad \Sigma V_{up} = 838 \text{ kN}$$

## Appendix B

Seismic coefficient,  $C_s$

$$C_s := \frac{\Sigma V_{up}}{W_{super}} \quad C_s = 0.08$$

### Maximum Deformation

$$S_a := \frac{F_v \cdot S_1}{T_{eff}} \cdot sec \quad S_a = 0.168$$

$$V_{EQ} := S_a \cdot W_{super} \quad V_{EQ} = 1861 \text{ kN}$$

$$\Delta_{max} := \frac{V_{EQ}}{K_{eff}} \quad \Delta_{max} = 133 \text{ mm}$$

$$\mu := \frac{\Delta_{max}}{\Delta_y} \quad \mu = 2.22$$

$$\theta_p := \frac{\Delta_{max}}{H} \quad \theta_p = 0.019 \quad \theta_p = 1.9\% \quad \text{Plastic Rotation}$$

## Appendix B

### ***Design Step 3.2 \_ Transverse Direction***

#### **Effective Weights**

Same as longitudinal direction.

#### **Yield Displacement**

$$M_n = 977 \text{ kN}\cdot\text{m}$$

$$\Delta_y := \frac{2 \cdot M_n \cdot H_{clr}^2}{12 \cdot E_c \cdot I_{cr}} \quad \Delta_y = 22 \text{ mm}$$

#### **Effective Period**

$$H_{clr} = 6.00 \text{ m}$$

$$K_{eff} := 2 \cdot n \cdot \frac{6 \cdot E_c \cdot I_{cr}}{H_{clr}^3} \quad K_{eff} = 44376 \frac{\text{kN}}{\text{m}}$$

$$T_{eff} := 2\pi \sqrt{\frac{W_{super}}{K_{eff} \cdot g}} \quad T_{eff} = 1.00 \text{ s}$$

#### **Required Lateral Strength**

First iteration:

$$V_{up} := \frac{2 \cdot M_n}{H_{clr}} \quad V_{up} = 326 \text{ kN}$$

$$V_{up1} := V_{up} \quad V_{up2} := V_{up} \quad V_{up3} := V_{up}$$

$$M_{n1} := M_n \quad M_{n2} := M_n \quad M_{n3} := M_n$$

$$H_{cg\_bot} := 7.0 \cdot \text{m} \quad \text{Height from cg of superstructure to bottom of column}$$

$$H_{cg\_top} := 1.0 \cdot \text{m} \quad \text{Height from cg of superstructure to top of column}$$

$$\Delta P_{\_bot} := \frac{(V_{up1} + V_{up2} + V_{up3}) \cdot H_{cg\_bot} - (M_{n1} + M_{n2} + M_{n3})}{12 \cdot \text{m}}$$

$$\Delta P_{\_bot} = 326 \text{ kN} \quad \text{Increment on outer columns}$$

$$P_1 := P_{col\_dl} + \Delta P_{\_bot} \quad P_1 = 1920 \text{ kN} \quad \text{Outer column}$$

$$P_2 := P_{col\_dl} \quad P_2 = 1594 \text{ kN} \quad \text{Inner column}$$

## Appendix B

$$P_3 := P_{col\_dl} - \Delta P_{bot} \quad P_3 = 1268 \text{ kN} \quad \text{Outer column}$$

Second iteration:

From the column interaction diagram:

$$P := P_1 \quad P = 1920 \text{ kN}$$

$$M_{x1} := 1061.3 \cdot \text{kN}\cdot\text{m} \quad P_{x1} := 1922.9 \text{ kN}$$

$$M_{x2} := 1017.5 \cdot \text{kN}\cdot\text{m} \quad P_{x2} := 1707.6 \text{ kN}$$

$$\rightarrow M := \frac{P - P_{x2}}{P_{x1} - P_{x2}} \cdot (M_{x1} - M_{x2}) + M_{x2} \quad M = 1061 \text{ kN}\cdot\text{m} \quad M_{n1} := M \quad \text{From P-M Curve}$$

$$P := P_2 \quad P = 1594 \text{ kN}$$

$$M_{x1} := 1017.5 \cdot \text{kN}\cdot\text{m} \quad P_{x1} := 1707.6 \text{ kN}$$

$$M_{x2} := 978.2 \cdot \text{kN}\cdot\text{m} \quad P_{x2} := 1522.6 \text{ kN}$$

$$\rightarrow M := \frac{P - P_{x2}}{P_{x1} - P_{x2}} \cdot (M_{x1} - M_{x2}) + M_{x2} \quad M = 993 \text{ kN}\cdot\text{m} \quad M_{n2} := M \quad \text{From P-M Curve}$$

$$P := P_3 \quad P = 1268 \text{ kN}$$

$$M_{x1} := 944.1 \cdot \text{kN}\cdot\text{m} \quad P_{x1} := 1367.3 \text{ kN}$$

$$M_{x2} := 912.8 \cdot \text{kN}\cdot\text{m} \quad P_{x2} := 1228.5 \text{ kN}$$

$$\rightarrow M := \frac{P - P_{x2}}{P_{x1} - P_{x2}} \cdot (M_{x1} - M_{x2}) + M_{x2} \quad M = 922 \text{ kN}\cdot\text{m} \quad M_{n3} := M \quad \text{From P-M Curve}$$

$$M_{n1} = 1061 \text{ kN}\cdot\text{m} \quad V_{up1} := \frac{2M_{n1}}{H_{clr}}$$

$$M_{n2} = 993 \text{ kN}\cdot\text{m} \quad V_{up2} := \frac{2M_{n2}}{H_{clr}}$$

$$M_{n3} = 922 \text{ kN}\cdot\text{m} \quad V_{up3} := \frac{2M_{n3}}{H_{clr}}$$

$$\Delta P_{bot} := \frac{(V_{up1} + V_{up2} + V_{up3}) \cdot H_{cg\_bot} - (M_{n1} + M_{n2} + M_{n3})}{12 \cdot \text{m}}$$

$$\Delta P_{bot} = 331 \text{ kN} \quad \text{Increment on outer columns at bottom}$$

## Appendix B

$$V_{bent} := V_{up1} + V_{up2} + V_{up3} \quad V_{bent} = 992 \text{ kN}$$

$$\frac{V_{bent}}{3 \cdot V_{up}} = 1.01 \quad \text{Converge}$$

$$\Delta P_{top} := \frac{-(V_{up1} + V_{up2} + V_{up3}) \cdot H_{cg\_top} + (M_{n1} + M_{n2} + M_{n3})}{12 \cdot m}$$

$$\Delta P_{top} = 165 \text{ kN} \quad \text{Increment on outer columns at top}$$

Seismic coefficient,  $C_s$

$$C_s := \frac{2 \cdot V_{bent}}{W_{super}} \quad C_s = 0.18$$

### Maximum Deformation

$$S_a := \frac{F_v \cdot S_1}{T_{eff}} \cdot sec \quad S_a = 0.299$$

$$V_{EQ} := S_a \cdot W_{super} \quad V_{EQ} = 3317 \text{ kN}$$

$$\Delta_{max} := \frac{V_{EQ}}{K_{eff}} \quad \Delta_{max} = 75 \text{ mm}$$

$$\mu := \frac{\Delta_{max}}{\Delta_y} \quad \mu = 3.39$$

$$\theta_p := \frac{\Delta_{max}}{H} \quad \theta_p = 0.011 \quad \theta_p = 1.1\% \quad \text{Plastic Rotation}$$



## Appendix B

### DESIGN STEP 4 \_ Determine Transverse Steel in Columns

#### Required Shear Strength by Transverse Steel for $P_{max}$ Column

$c := 2 \cdot \text{in}$	Clear cover
$d_t := \frac{6}{8} \cdot \text{in}$	Diameter of longitudinal reinforcement
$d_v := \frac{4}{8} \cdot \text{in}$	Diameter of transverse reinforcement
$D := 32 \cdot \text{in}$	Column diameter
$D' := D - 2 \cdot d_v - d_t - 2 \cdot c$	Circle diameter of longitudinal reinforcement
	$D' = 667 \text{ mm} \quad D' = 26.25 \text{ in}$
$D'' := D - 2 \cdot c$	Circle diameter of transverse reinforcement
	$D'' = 711 \text{ mm} \quad D'' = 28.00 \text{ in}$
$H_{clr} = 6.00 \text{ m}$	
$\alpha := \frac{D'}{H_{clr}}$	$\alpha = 6.37 \text{ deg}$
$f'_c = 27.6 \text{ MPa}$	

Inside potential plastic hinge zones:

$$P_{col\_top} := P_{col\_dltop} + \Delta P_{top}$$

$$P := P_{col\_top} \quad P = 1685 \text{ kN}$$

$$M_{x1} := 1017.5 \cdot \text{kN} \cdot \text{m} \quad P_{x1} := 1707.6 \text{ kN}$$

$$M_{x2} := 978.2 \cdot \text{kN} \cdot \text{m} \quad P_{x2} := 1522.6 \text{ kN}$$

$$\rightarrow M := \frac{P - P_{x2}}{P_{x1} - P_{x2}} \cdot (M_{x1} - M_{x2}) + M_{x2} \quad M = 1013 \text{ kN} \cdot \text{m} \quad M_{p\_top} := M \quad \text{From P-M Curve}$$

$$M_{p\_top} = 1013 \text{ m kN}$$

$$P_{col\_bot} := P_{col\_dl} + \Delta P_{bot} \quad P_{col\_bot} = 1925 \text{ kN}$$

$$P := P_{col\_bot} \quad P = 1925 \text{ kN}$$

$$M_{x1} := 1106.7 \cdot \text{kN} \cdot \text{m} \quad P_{x1} := 2169.3 \text{ kN}$$

$$M_{x2} := 1061.3 \cdot \text{kN} \cdot \text{m} \quad P_{x2} := 1922.9 \text{ kN}$$

## Appendix B

$$\rightarrow M := \frac{P - P_{x2}}{P_{x1} - P_{x2}} \cdot (M_{x1} - M_{x2}) + M_{x2} \quad M = 1062 \text{ kN}\cdot\text{m} \quad M_{p\_bot} := M \quad \text{From P-M Curve}$$

$$M_{p\_bot} = 1062 \text{ kN}\cdot\text{m}$$

Suppose the overstrength factor, OS, to 1.5.

$$OS := 1.5$$

$$P_e := P_{col\_dl} + OS \cdot \Delta P_{bot}$$

$$P_e = 2090 \text{ kN}$$

$$M_{p\_top} := OS \cdot M_{p\_top}$$

$$M_{p\_top} = 1519 \text{ kN}\cdot\text{m}$$

$$M_{p\_bot} := OS \cdot M_{p\_bot}$$

$$M_{p\_bot} = 1592 \text{ kN}\cdot\text{m}$$

$$V_u := \frac{M_{p\_top} + M_{p\_bot}}{H_{clr}}$$

$$V_u = 519 \text{ kN}$$

Shear resistance in the end regions:

$$A_g := \frac{\pi \cdot D^2}{4} \quad A_g = 0.5189 \text{ m}^2$$

Cross-sectional area of column

$$A_c := \frac{\pi \cdot D_{c1}^2}{4} \quad A_c = 0.40 \text{ m}^2$$

Cross-sectional area of column core

$$A_v := 0.8 \cdot A_g \quad A_v = 0.42 \text{ m}^2$$

Shear area of concrete

$$V_c := 0.05 \cdot \sqrt{f'_c} \cdot A_v \cdot MPa^{0.5} \quad V_c = 109 \text{ kN}$$

Contribution of concrete

$$\Lambda := 2$$

Fixity Factor: 2 for Fix-Fix

$$V_p := \frac{\Lambda \cdot P_e \cdot \tan(\alpha)}{2} \quad V_p = 233 \text{ kN}$$

Contribution of arch action

$$\phi := 0.90$$

Strength reduction factor for shear

$$V_s := \frac{V_u}{\phi} - V_c - V_p \quad V_{s1} := V_s \quad V_{s1} = 234 \text{ kN}$$

Contribution of truss action

### Required Shear Strength by Transverse Steel for $P_{min}$ Column

Inside potential plastic hinge zones:

$$P_{col\_top} := P_{col\_dltop} - \Delta P_{top}$$

$$P := P_{col\_top} \quad P = 1354 \text{ kN}$$

## Appendix B

$$M_{x1} := 944.1 \cdot \text{kN}\cdot\text{m} \quad P_{x1} := 1367.3 \text{ kN}$$

$$M_{x2} := 912.8 \cdot \text{kN}\cdot\text{m} \quad P_{x2} := 1228.5 \text{ kN}$$

$$\rightarrow M := \frac{P - P_{x2}}{P_{x1} - P_{x2}} \cdot (M_{x1} - M_{x2}) + M_{x2} \quad M = 941 \text{ kN}\cdot\text{m} \quad M_{p\_top} := M \quad \text{From P-M Curve}$$

$$M_{p\_top} = 941 \text{ m kN}$$

$$P_{col\_bot} := P_{col\_dl} - \Delta P_{bot}$$

$$P := P_{col\_bot} \quad P = 1263 \text{ kN}$$

$$M_{x1} := 912.8 \cdot \text{kN}\cdot\text{m} \quad P_{x1} := 1228.5 \text{ kN}$$

$$M_{x2} := 879.9 \cdot \text{kN}\cdot\text{m} \quad P_{x2} := 1084.4 \text{ kN}$$

$$\rightarrow M := \frac{P - P_{x2}}{P_{x1} - P_{x2}} \cdot (M_{x1} - M_{x2}) + M_{x2} \quad M = 921 \text{ kN}\cdot\text{m} \quad M_{p\_bot} := M \quad \text{From P-M Curve}$$

$$M_{p\_bot} = 921 \text{ kN}\cdot\text{m}$$

Suppose the overstrength factor, OS, to 1.5.

$$OS := 1.5$$

$$P_e := P_{col\_dl} - OS \cdot \Delta P_{bot} \quad P_e = 1098 \text{ kN}$$

$$M_{p\_top} := OS \cdot M_{p\_top} \quad M_{p\_top} = 1412 \text{ kN}\cdot\text{m}$$

$$M_{p\_bot} := OS \cdot M_{p\_bot} \quad M_{p\_bot} = 1381 \text{ kN}\cdot\text{m}$$

$$V_u := \frac{M_{p\_top} + M_{p\_bot}}{H_{clr}} \quad V_u = 465 \text{ kN}$$

Shear resistance in the end regions:

$$V_c := 0.05 \cdot \sqrt{f'_c} \cdot A_v \cdot MPa^{0.5} \quad V_c = 109 \text{ kN} \quad \text{Contribution of concrete}$$

$$\Lambda := 2 \quad \text{Fixity Factor: 2 for Fix-Fix}$$

$$V_p := \frac{\Lambda \cdot P_e \cdot \tan(\alpha)}{2} \quad V_p = 123 \text{ kN} \quad \text{Contribution of arch action}$$

$$\phi := 0.90 \quad \text{Strength reduction factor for shear}$$

## Appendix B

$$V_s := \frac{V_u}{\phi} - V_c - V_p \quad V_{s2} := V_s \quad V_{s2} = 286 \text{ kN} \quad \text{Contribution of truss action}$$

### Transverse Reinforcement for Confinement at Plastic Hinges

$$V_s := \max(V_{s1}, V_{s2}) \quad V_s = 286 \text{ kN}$$

Suppose  $s := 20 \cdot \text{in}$  and  $A_{bh} := 0.20 \cdot \text{in}^2$  (#4)

$$\rho_v := \frac{2 \cdot A_{bh}}{s \cdot D''} \quad \rho_v = 0.0007 \quad \rho_v = 0.07\%$$

$$A_t := 16 \cdot 0.44 \cdot \text{in}^2$$

$$\rho_t := \frac{A_t}{A_g} \quad \rho_t = 0.009 \quad \rho_t = 0.9\%$$

$$\theta := \text{atan} \left[ \left( \frac{1.6 \cdot \rho_v \cdot A_v}{\Lambda \cdot \rho_t \cdot A_g} \right)^{0.25} \right] \quad \theta = 25.5 \text{ deg}$$

$$\tan(\theta) = 0.48 > \tan(\alpha) = 0.11 \quad \text{---> use } \tan(\theta)$$

For a circular section:

$$f_{yh} := 60 \cdot \text{ksi} \quad \text{Yield strength of spiral}$$

$$A_{bhr} := \left( \frac{2}{\pi} \right) \cdot \left( \frac{V_s \cdot s}{f_{yh} \cdot D''} \right) \left( \frac{1}{\cot(\theta)} \right) \quad A_{bhr} = 0.233 \text{ in}^2 < A_{bh} = 0.20 \text{ in}^2 \quad \text{OK}$$

Outside the plastic hinge zone:

$$V_c := 0.17 \cdot \sqrt{f'_c} \cdot A_v \cdot \text{MPa}^{0.5} \quad V_c = 371 \text{ kN} \quad \text{Contribution of concrete}$$

Therefore, the spiral spacing can be much greater than the one in plastic hinge zone.

Note that according to LRFD Article 5.10.6.2, the spiral spacing for a compression member shall not exceed 6 inches.

--->  $s := 6 \cdot \text{in}$  and  $A_{bh} := 0.20 \cdot \text{in}^2$  (#4)

$$\rho_s := \frac{4 \cdot A_{bh}}{s \cdot D''} \quad \rho_s = 0.48\% \quad \text{Provided}$$

### Transverse Reinforcement for Confinement at Plastic Hinges by LRFD

## Appendix B

Extent of plastic hinge region,  $L_p$ :

$$D = 32.00 \text{ in} \quad \text{Column diameter}$$

$$H_{clr} = 6.00 \text{ m} \quad \text{Column height}$$

$$L_p := \max\left(D, \frac{H_{clr}}{6}, 18 \cdot \text{in}\right) \quad L_p = 1.00 \text{ m} \quad L_p = 39 \text{ in} \quad \text{LRFD Article 5.10.11.4.1 c}$$

Minimum reinforcement from LRFD Article 5.10.11.4.1 d:

$$f'_c = 4000 \text{ psi} \quad f'_c = 27.6 \text{ MPa}$$

$$f_y := 60 \cdot \text{ksi} \quad f_y = 413.7 \text{ MPa}$$

$$\rho_{s\_min1} := 0.12 \cdot \frac{f'_c}{f_y} \quad \rho_{s\_min1} = 0.008$$

Minimum reinforcement from LRFD Article 5.7.4.6:

$$A_g = 804.25 \text{ in}^2$$

$$A_c = 615.75 \text{ in}^2$$

$$f_{yh} = 60.00 \text{ ksi} \quad f_{yh} = 413.7 \text{ MPa}$$

$$\rho_{s\_min2} := 0.45 \cdot \left(\frac{A_g}{A_c} - 1\right) \cdot \frac{f'_c}{f_{yh}} \quad \rho_{s\_min2} = 0.0092$$

$$\rho_{s\_min} := \max(\rho_{s\_min1}, \rho_{s\_min2}) \quad \rho_{s\_min} = 0.0092$$

Suppose  $s := 4.5 \cdot \text{in}$  and  $A_{bh} := 0.31 \cdot \text{in}^2$  (#5)

$$\rho_s := \frac{4 \cdot A_{bh}}{s \cdot D''} \quad \rho_s = 0.0098 > \rho_{s\_min} = 0.0092$$

$$\rho_s = 0.98 \% \quad \text{Provided}$$

--- Steel Jacketing Design of Prototype Bridge ---

**DESIGN STEP 1 \_ As-built Column Transverse Reinforcement**

**Required Shear Strength by Transverse Steel for  $P_{max}$  Column**

$c := 2 \cdot \text{in}$	Clear cover
$d_t := \frac{6}{8} \cdot \text{in}$	Diameter of longitudinal reinforcement
$d_v := \frac{4}{8} \cdot \text{in}$	Diameter of transverse reinforcement
$D := 32 \cdot \text{in}$	Column diameter
$D' := D - 2 \cdot d_v - d_t - 2 \cdot c$	Circle diameter of longitudinal reinforcement
	$D' = 667 \text{ mm} \quad D' = 26.25 \text{ in}$
$D'' := D - 2 \cdot c$	Circle diameter of transverse reinforcement
	$D'' = 711 \text{ mm} \quad D'' = 28.00 \text{ in}$
$H_{clr} = 6.00 \text{ m}$	
$\alpha := \frac{D'}{H_{clr}}$	$\alpha = 6.37 \text{ deg}$
$f'_c = 27.6 \text{ MPa}$	

Inside potential plastic hinge zones:

$P_{col\_top} := P_{col\_dltop} + \Delta P_{top}$	
$P := P_{col\_top}$	$P = 1685 \text{ kN}$
$M_{x1} := 1017.5 \cdot \text{kN} \cdot \text{m}$	$P_{x1} := 1707.6 \text{ kN}$
$M_{x2} := 978.2 \cdot \text{kN} \cdot \text{m}$	$P_{x2} := 1522.6 \text{ kN}$
$\text{---> } M := \frac{P - P_{x2}}{P_{x1} - P_{x2}} \cdot (M_{x1} - M_{x2}) + M_{x2} \quad M = 1013 \text{ kN} \cdot \text{m} \quad M_{p\_top} := M \quad \text{From P-M Curve}$	
$M_{p\_top} = 1013 \text{ m kN}$	
$P_{col\_bot} := P_{col\_dl} + \Delta P_{bot}$	$P_{col\_bot} = 1925 \text{ kN}$

## Appendix B

$$P := P_{col\_bot} \quad P = 1925 \text{ kN}$$

$$M_{x1} := 1061.3 \cdot \text{kN} \cdot \text{m} \quad P_{x1} := 2169.3 \text{ kN}$$

$$M_{x2} := 1017.5 \cdot \text{kN} \cdot \text{m} \quad P_{x2} := 1707.6 \text{ kN}$$

$$\rightarrow M := \frac{P - P_{x2}}{P_{x1} - P_{x2}} \cdot (M_{x1} - M_{x2}) + M_{x2} \quad M = 1038 \text{ kN} \cdot \text{m} \quad M_{p\_bot} := M \quad \text{From P-M Curve}$$

$$M_{p\_bot} = 1038 \text{ kN} \cdot \text{m}$$

Suppose the overstrength factor, OS, to 1.0.

$$OS := 1.0$$

$$P_e := P_{col\_dl} + OS \cdot \Delta P_{bot}$$

$$P_e = 1925 \text{ kN}$$

$$M_{p\_top} := OS \cdot M_{p\_top}$$

$$M_{p\_top} = 1013 \text{ kN} \cdot \text{m}$$

$$M_{p\_bot} := OS \cdot M_{p\_bot}$$

$$M_{p\_bot} = 1038 \text{ kN} \cdot \text{m}$$

$$V_u := \frac{M_{p\_top} + M_{p\_bot}}{H_{clr}}$$

$$V_u = 342 \text{ kN}$$

Shear resistance in the end regions:

$$A_g := \frac{\pi \cdot D^2}{4}$$

$$A_g = 0.5189 \text{ m}^2$$

Cross-sectional area of column

$$A_c := \frac{\pi \cdot D''^2}{4}$$

$$A_c = 0.40 \text{ m}^2$$

Cross-sectional area of column

$$A_v := 0.8 \cdot A_g$$

$$A_v = 0.42 \text{ m}^2$$

Shear area of concrete

$$V_c := 0.05 \cdot \sqrt{f'_c} \cdot A_v \cdot \text{MPa}^{0.5}$$

$$V_c = 109 \text{ kN}$$

Contribution of concrete

$$\phi := 0.90$$

Strength reduction factor for shear

$$V_s := \frac{V_u}{\phi} - V_c$$

$$V_{s1} := V_s$$

$$V_{s1} = 271 \text{ kN}$$

Contribution of truss action

### Required Shear Strength by Transverse Steel for $P_{min}$ Column

Inside potential plastic hinge zones:

$$P_{col\_top} := P_{col\_dltop} - \Delta P_{top}$$

$$P := P_{col\_top}$$

$$P = 1354 \text{ kN}$$

## Appendix B

$$M_{x1} := 944.1 \cdot \text{kN} \cdot \text{m} \quad P_{x1} := 1367.3 \text{ kN}$$

$$M_{x2} := 912.8 \cdot \text{kN} \cdot \text{m} \quad P_{x2} := 1228.5 \text{ kN}$$

$$\rightarrow M := \frac{P - P_{x2}}{P_{x1} - P_{x2}} \cdot (M_{x1} - M_{x2}) + M_{x2} \quad M = 941 \text{ kN} \cdot \text{m} \quad M_{p\_top} := M \quad \text{From P-M Curve}$$

$$M_{p\_top} = 941 \text{ m kN}$$

$$P_{col\_bot} := P_{col\_dl} - \Delta P_{bot}$$

$$P := P_{col\_bot} \quad P = 1263 \text{ kN}$$

$$M_{x1} := 944.1 \cdot \text{kN} \cdot \text{m} \quad P_{x1} := 1367.3 \text{ kN}$$

$$M_{x2} := 912.8 \cdot \text{kN} \cdot \text{m} \quad P_{x2} := 1228.5 \text{ kN}$$

$$\rightarrow M := \frac{P - P_{x2}}{P_{x1} - P_{x2}} \cdot (M_{x1} - M_{x2}) + M_{x2} \quad M = 921 \text{ kN} \cdot \text{m} \quad M_{p\_bot} := M \quad \text{From P-M Curve}$$

$$M_{p\_bot} = 921 \text{ kN} \cdot \text{m}$$

Suppose the overstrength factor, OS, to 1.5.

$$OS := 1.0$$

$$P_e := P_{col\_dl} - OS \cdot \Delta P_{bot} \quad P_e = 1263 \text{ kN}$$

$$M_{p\_top} := OS \cdot M_{p\_top} \quad M_{p\_top} = 941 \text{ kN} \cdot \text{m}$$

$$M_{p\_bot} := OS \cdot M_{p\_bot} \quad M_{p\_bot} = 921 \text{ kN} \cdot \text{m}$$

$$V_u := \frac{M_{p\_top} + M_{p\_bot}}{H_{clr}} \quad V_u = 310 \text{ kN}$$

Shear resistance in the end regions:

$$V_c := 0.05 \cdot \sqrt{f'_c} \cdot A_v \cdot \text{MPa}^{0.5} \quad V_c = 109 \text{ kN} \quad \text{Contribution of concrete}$$

$$\phi := 0.90 \quad \text{Strength reduction factor for shear}$$

$$V_s := \frac{V_u}{\phi} - V_c \quad V_{s2} := V_s \quad V_{s2} = 236 \text{ kN} \quad \text{Contribution of truss action}$$

### Transverse Reinforcement for Confinement at Plastic Hinges

$$V_s := \max(V_{s1}, V_{s2}) \quad V_s = 271 \text{ kN}$$



## Appendix B

Suppose  $s := 8.25 \cdot \text{in}$

$$A_t := 16 \cdot 0.44 \cdot \text{in}^2$$

$$\rho_t := \frac{A_t}{A_g} \quad \rho_t = 0.009 \quad \rho_t = 0.9\% \quad \text{Longitudinal reinforcement ratio}$$

$$\theta := 45 \cdot \text{deg}$$

$$f_{yh} := 60 \cdot \text{ksi} \quad \text{Yield strength of spiral}$$

$$A_{bhr} := \left( \frac{2}{\pi} \right) \cdot \left( \frac{V_s \cdot s}{f_{yh} \cdot D''} \right) \cdot \left( \frac{1}{\cot(\theta)} \right) \quad A_{bhr} = 0.190 \text{ in}^2 \quad \text{-----} \rightarrow \quad A_{bh} := 0.20 \cdot \text{in}^2 \quad (\#4)$$

$$\rho_s := \frac{4 \cdot A_{bhr}}{s \cdot D''} \quad \rho_s = 0.0033 \quad \rho_s = 0.33\% \quad \text{Required}$$

$$\rho_s := \frac{4 \cdot A_{bh}}{s \cdot D''} \quad \rho_s = 0.0035 \quad \rho_s = 0.35\% \quad \text{Provided}$$

### DESIGN STEP 2 \_ Steel Jacketing Design

#### Required Steel thickness, $t_j$ for Confinement

$$f_s := 200 \cdot \text{MPa} \quad \text{Stress induced in the jacket}$$

At strain of 0.001 when  $E_s = 200,000 \text{ MPa}$

$$f_l := 2.07 \cdot \text{MPa} \quad \text{Required confinement stress}$$

This assumption is from Chai et al., 1991

Suppose  $x_c := 0.25 \cdot \text{in}$  Clearance

$$D_j := D + 2 \cdot x_c \quad D_j = 826 \text{ mm} \quad D_j = 32.5 \text{ in} \quad \text{Outside diameter of steel jacket}$$

$$t_j := \frac{f_l \cdot D_j}{2 \cdot f_s} \quad t_j = 4.3 \text{ mm} \quad t_j = 0.17 \text{ in}$$

#### Check steel thickness, $t_j$ for Shear

$$V_s = 271 \text{ kN} \quad \text{Required shear strength}$$

$$t_j = 4.3 \text{ mm}$$

## Appendix B

$$f_{yj} := 42 \cdot \text{ksi} \quad f_{yj} = 290 \text{ MPa}$$

$$\theta := 30 \cdot \text{deg}$$

Shear strength enhancement by steel jacket,  $V_{sj}$ :

$$V_{sj} := \frac{\pi}{2} \cdot t_j \cdot f_{yj} \cdot (D_j - t_j) \cdot \cot(\theta) \quad V_{sj} = 2764 \text{ kN} > V_s = 271 \text{ kN} \quad \text{OK}$$

## **APPENDIX C**

### **DESIGN OF FOOTING AND CAP BEAM OF PROTOTYPE BRIDGE BENT**

This appendix provides details on the design of the footing and cap beam for the prototype bridge pier bent. The footing and cap-beam were designed to be capacity protected as well as the shear force design of the column as presented previously. This was considered through overstrength factor of 1.5. The resisting length, width and height of the footing were 3.6 m (11 ft 10 in), 15.0 m (49 ft 3 in) and 1.0 m (39 in), respectively. The footing reinforcement was designed to resist the moment and shear force capacity of the column, resulting in D19 bars spaced at 242 mm (#6 at 9 17/32 in) in the longitudinal direction and D22 bars spaced at 262 mm (#7 at 10 5/16 in) in the transverse direction. For 1067 mm (42 in) by 1219 mm (48 in) cap-beam, ten D22 (#7) longitudinal bars were provided to resist the moment and D16 (#5) stirrups spaced at 300 mm (12") center-to-center were provided to resist the shear force.

--- Prototype Footing and Cap-beam Design ---

Column: D = 32 in, L. Bar = 16 #6, T. Bar = #4@6 in  
 $f'_c = 4 \text{ ksi}$

**DESIGN STEP 1 \_ Footing Design in Longitudinal Direction**

**Design Step 1.1 \_ Forces**

$B_f := 15.0 \cdot \text{m}$  Width of footing

$D_f := 1.0 \cdot \text{m}$  Depth of footing

$L_f := 3.6 \cdot \text{m}$  Length of footing

$V_{ftg} := B_f \cdot D_f \cdot L_f$   $V_{ftg} = 54.00 \text{ m}^3$  Volume of footing

Foundation weight:

$P_{ftg} := V_{ftg} \cdot 2.350 \cdot \frac{\text{kN}}{\text{m}^3}$   $P_{ftg} = 127 \text{ kN}$

Axial Force:

$P_{col\_dl} := 1594 \cdot \text{kN}$  Dead load a top of a column

$n := 3$  Number of columns per pier

$P := P_{col\_dl} \cdot n + P_{ftg}$   $P = 4909 \text{ kN}$

$P := 1.25 \cdot P$   $P = 6136 \text{ kN}$  Load factor (1.25 for DC)

Design moment and shear forces:

$OS := 1.5$  Overstrength factor

$M_n := 1055 \cdot \text{kN} \cdot \text{m}$

$M_{OT} := OS \cdot M_n \cdot n$   $M_{OT} = 4748 \text{ kN} \cdot \text{m}$

$H := 6 \cdot \text{m}$

$V_{OT} := \frac{M_{OT}}{H}$   $V_{OT} = 791 \text{ kN}$

## Appendix C

$$M_V := V_{OT} \cdot D_f \qquad M_V = 791 \text{ kN}\cdot\text{m}$$

Design moment for overturning check:

$$M_{weak} := M_{OT} + M_V \qquad M_{weak} = 5539 \text{ kN}\cdot\text{m} \qquad M_{weak} = 4085 \text{ ft}\cdot\text{kip}$$

Design shear forced for sliding check:

$$V_{weak} := \frac{M_{OT}}{H} \qquad V_{weak} = 791 \text{ kN} \qquad V_{weak} = 178 \text{ kip}$$

### **Design Step 1.2 \_ Check foundation for overturning**

$$L_f = 3.60 \text{ m}$$

$$e := \frac{M_{weak}}{P} \qquad e = 0.90 \text{ m} \quad < \quad \frac{L_f}{3} = 1.20 \text{ m} \quad \text{Eccentricity limit} \quad \text{OK}$$

### **Design Step 1.3 \_ Check soil bearing capacity**

$$B_f = 15.00 \text{ m} \qquad \text{Width of footing}$$

$$q := \frac{2 \cdot P}{3 \cdot B_f \cdot \left( \frac{L_f}{2} - e \right)} \qquad \text{Maximum contact stress at edge footing}$$

$$q = 0.30 \text{ MPa} \quad < \quad 0.38 \text{ MPa (Coarse to midium sand) LRFD 10.6.2.3.1}$$

$$q = 44 \text{ psi}$$

### **Design Step 1.4 \_ Check foundation for sliding**

$$V_r := 0.8 \cdot P \qquad \text{Sliding resistance (0.8: concrete cast-in-place on sand, LRFD 10.5.5)}$$

$$V_r = 4909 \text{ kN} \quad > \quad V_{OT} = 791 \text{ kN} \quad \text{OK}$$

### **Design Step 1.5 \_ Design of footing reinforcement**

#### Design forces

Ultimate shear:

$$V_U := P \qquad V_U = 6136 \text{ kN} \qquad V_U = 1379 \text{ kip}$$

Ultimate moment:

$$M_U := M_{weak} \qquad M_U = 5539 \text{ kN}\cdot\text{m} \qquad M_U = 4085 \text{ kip}\cdot\text{ft}$$

## Appendix C

### Design for moment

Required longitudinal Bar:

$$\phi := 0.90 \quad f_y := 60 \cdot \text{ksi} \quad j := 0.925$$

$$c := 3 \cdot \text{in}$$

$$d_{bl} := \frac{6}{8} \cdot \text{in}$$

$$d := D_f - c - \frac{d_{bl}}{2} \quad d = 0.91 \text{ m} \quad d = 36.00 \text{ in}$$

$$A_{st} := \frac{M_u}{\phi \cdot f_y \cdot j \cdot d} \quad A_{st} = 27.27 \text{ in}^2$$

$$A_s := 0.44 \cdot \text{in}^2 \quad (\#6)$$

$$s := \frac{B_f \cdot A_s}{A_{st}} \quad s = 9.53 \text{ in} \quad s = 242 \text{ mm}$$

### Design for shear

$$f'_c := 4.0 \cdot \text{ksi} \quad f_y = 60.00 \text{ ksi}$$

$$a := \frac{A_{st} \cdot f_y}{0.85 \cdot f'_c \cdot B_f} \quad a = 20.69 \text{ mm} \quad \text{Depth of equivalent stress block}$$

$$d_v := d - \frac{a}{2} \quad d_v = 0.90 \text{ m} \quad \text{Effective depth}$$

$$\phi := 0.9$$

One-way shear:

$$\beta := 2.0$$

$$B_f = 15.00 \text{ m}$$

$$\phi V_{c1} := \phi \cdot 0.0316 \cdot \text{ksi}^{0.5} \cdot \beta \cdot \sqrt{f'_c} \cdot B_f \cdot d_v \quad \phi V_{c1} = 10635 \text{ kN} \quad \phi V_{c1} = 2391 \text{ kip}$$

$$\phi V_{c2} := \phi \cdot 0.25 \cdot f'_c \cdot B_f \cdot d_v \quad \phi V_{c2} = 84137 \text{ kN} \quad \phi V_{c2} = 18915 \text{ kip}$$

$$\phi V_c := \min(\phi V_{c1}, \phi V_{c2}) \quad \phi V_c = 10635 \text{ kN} > V_u = 6136 \text{ kN} \quad \text{OK}$$

Two-way shear:

## Appendix C

$\beta_c := 1$  For circular column

$d_v = 0.90 \text{ m}$

$D_{col} := 28 \cdot \text{in}$

$b_0 := 2\pi \cdot \left( \frac{D_{col}}{2} + \frac{d_v}{2} \right)$        $b_0 = 5.07 \text{ m}$        $b_0 = 200 \text{ in}$       Length of critical shear perimeter

$\phi V_{c1} := \phi \cdot \left( 0.063 + \frac{0.126}{\beta_c} \right) \cdot \text{ksi}^{0.5} \cdot \sqrt{f'_c} \cdot b_0 \cdot d_v$        $\phi V_{c1} = 10758 \text{ kN}$        $\phi V_{c1} = 2419 \text{ kip}$

$\phi V_{c2} := \phi \cdot 0.126 \cdot \text{ksi}^{0.5} \cdot \sqrt{f'_c} \cdot b_0 \cdot d_v$        $\phi V_{c2} = 7172 \text{ kN}$        $\phi V_{c2} = 1612 \text{ kip}$       Limit

$\phi V_c := \min(\phi V_{c1}, \phi V_{c2})$        $\phi V_c = 7172 \text{ kN}$        $>$        $V_u = 6136 \text{ kN}$       OK

### **Design Step 1.6 \_ Extention column steel into footing**

Extention of column steel into a footing is set to be  $1.25l_d$ .

$f_y = 414 \text{ MPa}$

$f'_c = 27.6 \text{ MPa}$

$A_b := 0.44 \cdot \text{in}^2$  (#6 : column longitudinal bars)

$l_d := \frac{1.25 \cdot A_b \cdot f_y}{\text{in} \cdot \text{ksi}^{0.5} \cdot \sqrt{f'_c}}$        $l_d = 419 \text{ mm}$        $l_d = 17 \text{ in}$

$l_d := 1.25 \cdot l_d$        $l_d = 524 \text{ mm}$        $l_d = 21 \text{ in}$

## Appendix C

### DESIGN STEP 2 \_ Footing Design in Transverse Direction

#### Design Step 2.1 \_ Forces

$B_f := 3.6 \cdot \text{m}$	Width of footing
$D_f = 1.00 \text{ m}$	Depth of footing
$L_f := 15.0 \cdot \text{m}$	Length of footing

From column design in transvers direction,

$$P_1 := 1926 \cdot \text{kN} \quad P_2 := 1594 \cdot \text{kN} \quad P_3 := 1263 \cdot \text{kN}$$

$$\Sigma P := P_1 + P_2 + P_3 \quad \Sigma P = 4783 \text{ kN}$$

$$V_{\text{bent}} := 1028 \cdot \text{kN}$$

$$\Sigma V_{\text{up}} := V_{\text{bent}} \quad \Sigma V_{\text{up}} = 1028 \text{ kN}$$

$$M_{n1} := 1091 \cdot \text{kN} \cdot \text{m} \quad M_{n2} := 1055 \cdot \text{kN} \cdot \text{m} \quad M_{n3} := 938 \cdot \text{kN} \cdot \text{m}$$

$$\Sigma M_n := M_{n1} + M_{n2} + M_{n3} \quad \Sigma M_n = 3084 \text{ kN} \cdot \text{m}$$

$$M_v := \Sigma V_{\text{up}} \cdot D_f \quad M_v = 1028 \text{ kN} \cdot \text{m}$$

$$M_{\Delta P} := 6 \cdot \text{m} \cdot P_1 + 0 \cdot \text{m} \cdot P_2 - 6 \cdot \text{m} \cdot P_3 \quad M_{\Delta P} = 3978 \text{ kN} \cdot \text{m}$$

Design moment:

$$OS := 1.5 \quad \text{Overstrength factor}$$

$$M_{\text{strong}} := OS \cdot (\Sigma M_n + M_v + M_{\Delta P}) \quad M_{\text{strong}} = 12135 \text{ kN} \cdot \text{m} \quad \text{Strong direction driving moment}$$

Design shear forces:

$$V_{\text{strong}} := OS \cdot \Sigma V_{\text{up}} \quad V_{\text{strong}} = 1542 \text{ kN} \quad \text{Shear in strong direction}$$

Axial forces:

$$P = 6136 \text{ kN} \quad \text{Factored axial force (1.25 for DC)}$$

#### Design Step 2.2 \_ Check foundation for overturning

$$L_f = 15.00 \text{ m}$$



## Appendix C

$$e := \frac{M_{\text{strong}}}{P} \quad e = 1.98 \text{ m} < \frac{L_f}{3} = 5.00 \text{ m} \quad \text{Eccentricity limit} \quad \text{OK}$$

### **Design Step 2.3 \_ Check soil bearing capacity**

$$B_f = 3.60 \text{ m} \quad \text{Width of footing}$$

$$q := \frac{2 \cdot P}{3 \cdot B_f \cdot \left( \frac{L_f}{2} - e \right)} \quad \text{Maximum contact stress at edge footing}$$

$$q = 0.21 \text{ MPa} < 0.38 \text{ MPa (Coarse to midium sand) LRFD 10.6.2.3.1}$$

$$q = 30 \text{ psi}$$

### **Design Step 2.4 \_ Check foundation for sliding**

$$V_r := 0.8 \cdot P \quad \text{Sliding resistance (0.8: concrete cast-in-place on sand, LRFD 10.5.5)}$$

$$V_r = 4909 \text{ kN} > V_{\text{strong}} = 1542 \text{ kN} \quad \text{OK}$$

### **Design Step 2.5 \_ Design of footing reinforcement**

#### Design forces

Ultimate shear:

$$V_u := P \quad V_u = 6136 \text{ kN} \quad V_u = 1379 \text{ kip}$$

Ultimate moment:

$$M_u := 0.5 \cdot \max(M_{n1}, M_{n2}, M_{n3}) \quad M_u = 1637 \text{ kN}\cdot\text{m} \quad M_u = 1207 \text{ kip}\cdot\text{ft}$$

#### Design for moment

Required longitudinal Bar:

$$\phi := 0.90 \quad f_y := 60 \cdot \text{ksi} \quad j := 0.925$$

$$c := 3 \cdot \text{in}$$

$$d_{bt} := \frac{7}{8} \cdot \text{in} \quad d_{bl} = 0.75 \text{ in}$$

$$d := D_f - c - d_{bl} - \frac{d_{bt}}{2} \quad d = 0.89 \text{ m} \quad d = 35.18 \text{ in}$$

$$A_{st} := \frac{M_u}{\phi \cdot f_y \cdot j \cdot d} \quad A_{st} = 8.24 \text{ in}^2$$

## Appendix C

$$A_s := 0.60 \cdot \text{in}^2 \quad (\#7)$$

$$s := \frac{B_f \cdot A_s}{A_{st}} \quad s = 10.32 \text{ in} \quad s = 262 \text{ mm}$$

### Design for shear

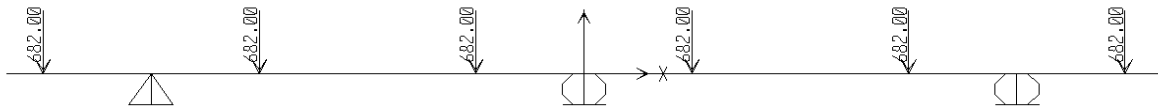
Same as longitudinal direction.

## Appendix C

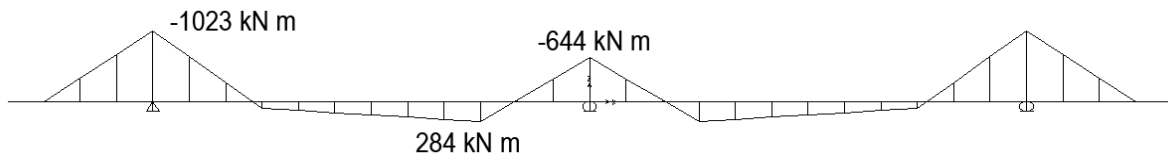
### DESIGN STEP 3 \_ Cap-beam Design

#### Design Step 3.1 \_ Forces

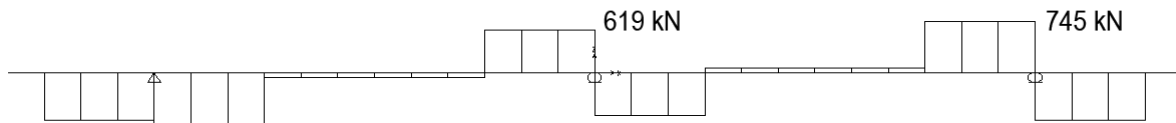
##### Design forces of dead load



Analysis model



Moment diagram



Shear diagram

$$M_{uu\_d} := 1023 \cdot \text{kN} \cdot \text{m} \quad \text{Maximum moment at column}$$

$$M_{ul\_d} := 284 \cdot \text{kN} \cdot \text{m} \quad \text{Maximum moment at span}$$

$$V_{u\_d} := 745 \cdot \text{kN} \quad \text{Maximum shear force}$$

Considering Load factor (1.25 for DC):

$$M_{uu\_d} := 1.25 \cdot M_{uu\_d} \quad M_{uu\_d} = 1279 \text{ kN} \cdot \text{m}$$

$$M_{ul\_d} := 1.25 \cdot M_{ul\_d} \quad M_{ul\_d} = 355 \text{ kN} \cdot \text{m}$$

$$V_{u\_d} := 1.25 \cdot V_{u\_d} \quad V_{u\_d} = 931 \text{ kN}$$

##### Design forces of earthquake load

$$M_{uu\_eq} := 1091 \cdot \text{kN} \cdot \text{m} \quad \text{Maximum moment at top (form transverse design of column)}$$

## Appendix C

$$M_{ul\_eq} := 1091 \cdot \text{kN}\cdot\text{m}$$

Maximum moment at bottom (form transverst design of column)

$$OS = 1.50$$

$$M_{uu\_eq} := OS \cdot M_{uu\_eq}$$

$$M_{uu\_eq} = 1637 \text{ kN}\cdot\text{m}$$

$$M_{ul\_eq} := OS \cdot M_{ul\_eq}$$

$$M_{ul\_eq} = 1637 \text{ kN}\cdot\text{m}$$

$$H := 6 \cdot \text{m}$$

$$V_{u\_eq} := \frac{M_{ul\_eq} + M_{uu\_eq}}{H}$$

$$V_{u\_eq} = 546 \text{ kN}$$

### Design forces

$$M_{uu} := \max(M_{uu\_d}, M_{uu\_eq})$$

$$M_{uu} = 1637 \text{ kN}\cdot\text{m}$$

$$M_{ul} := \max(M_{ul\_d}, M_{ul\_eq})$$

$$M_{ul} = 1637 \text{ kN}\cdot\text{m}$$

$$V_u := \max(V_{u\_d}, V_{u\_eq})$$

$$V_u = 931 \text{ kN}$$

### Capbeam dimension

$$B_c := 42 \cdot \text{in}$$

$$B_c = 1067 \text{ mm}$$

Width of cap-beam

$$D_c := 48 \cdot \text{in}$$

$$D_c = 1219 \text{ mm}$$

Depth of cap-beam

## ***Design Step 3.2 \_ Design of cap-beam reinforcement***

### Design for moment

Required longitudinal Bar:

$$M_u := M_{uu}$$

$$M_u = 1637 \text{ kN}\cdot\text{m}$$

$$\phi := 0.90$$

$$f_y := 60 \cdot \text{ksi}$$

$$j := 0.875$$

$$c := 2 \cdot \text{in}$$

$$d_{tr} := \frac{4}{8} \cdot \text{in}$$

(#4)

Transverse bar diameter

$$d_b := \frac{7}{8} \cdot \text{in}$$

(#7)

Longitudinal bar diameter

$$d := D_c - c - d_{tr} - \frac{d_b}{2}$$

$$d = 1.14 \text{ m}$$

$$d = 45.06 \text{ in}$$

## Appendix C

$$A_{st} := \frac{M_u}{\phi \cdot f_y \cdot j \cdot d} \quad A_{st} = 6.80 \text{ in}^2$$

$$A_s := 0.66 \cdot \text{in}^2 \quad (\#7)$$

$$s := \frac{B_c \cdot A_s}{A_{st}} \quad s = 4.07 \text{ in} \quad s = 104 \text{ mm}$$

### Design for shear

$$B_c = 1.07 \text{ m} \quad f'_c = 4.00 \text{ ksi}$$

$$d_v := d$$

$$\beta := 2.0$$

$$V_{c1} := 0.0316 \cdot \text{ksi}^{0.5} \cdot \beta \cdot \sqrt{f'_c} \cdot B_c \cdot d_v \quad V_{c1} = 1064 \text{ kN} \quad V_{c1} = 239 \text{ kip}$$

$$V_{c2} := 0.25 \cdot f'_c \cdot B_c \cdot d_v \quad V_{c2} = 8419 \text{ kN} \quad V_{c2} = 1893 \text{ kip}$$

$$V_c := \min(V_{c1}, V_{c2}) \quad V_c = 1064 \text{ kN}$$

$$V_u = 931 \text{ kN}$$

$$V_s := \frac{V_u}{\phi} - V_c \quad V_s = -29 \text{ kN}$$

$$A_s := 0.31 \cdot \text{in}^2 \quad (\#5)$$

$$\theta := 45 \text{ deg}$$

$$s := \frac{\pi}{2} \cdot \frac{f_y \cdot A_s \cdot d_v \cdot \cot(\theta)}{V_s} \quad s = -199.1 \text{ in} \quad \text{-----} \rightarrow \text{Transverse reinforcement is not required.}$$

Check minimum transverse reinforcement:

$$A_s := 0.31 \cdot \text{in}^2 \quad (\#5)$$

$$A_{v\_min} := 0.0316 \cdot \text{ksi}^{0.5} \cdot \sqrt{f'_c} \cdot B_c \cdot \frac{s}{f_y} \quad A_{v\_min} = -8.81 \text{ in}^2 > 2 \cdot A_s = 0.62 \text{ in}^2 \quad \text{NG}$$

Suppose  $s := 14 \cdot \text{in}$   $s = 356 \text{ mm}$

## Appendix C

$$A_{v\_min} := 0.0316 \cdot \text{ksi}^{0.5} \cdot \sqrt{f'_c} \cdot B_c \cdot \frac{s}{f_y} \quad A_{v\_min} = 0.619 \text{ in}^2 < 2 \cdot A_s = 0.62 \text{ in}^2 \quad \text{OK}$$

Note that according to LRFD Article 5.10.6.3, the spiral spacing for a compression member shall not exceed 300 mm.

$$\text{---> } s := 300 \cdot \text{mm} \text{ and } A_s = 0.31 \text{ in}^2 \quad (\#5)$$

### Design Step 3.3 \_ Skin reinforcement

$$d = 1145 \text{ mm}$$

$$A_{sk} := 0.001 \cdot (d - 760 \cdot \text{mm}) \quad A_{sk} = 0.38 \frac{\text{mm}^2}{\text{mm}} \quad A_{sk} = 0.18 \frac{\text{in}^2}{\text{ft}} \quad \text{LRFD Article 5.7.3.4}$$

$$A_{st} = 6.80 \text{ in}^2 \quad \text{Flexural tension reinforcement}$$

$$D_c = 1219 \text{ mm}$$

$$A_{skt} := A_{sk} \cdot D_c \quad A_{skt} = 0.73 \text{ in}^2 < \frac{A_{st}}{4} = 1.70 \text{ in}^2 \quad \text{OK} \quad \text{Limit}$$

$$A_s := 0.20 \cdot \text{in}^2 \quad (\#4)$$

$$s := \min\left(\frac{d}{6}, 300 \cdot \text{mm}\right) \quad s = 191 \text{ mm} \quad s = 7.5 \text{ in} \quad \text{Maximum spacing}$$

$$\frac{D_c - 2 \cdot c - d_b}{s} = 5.74 \quad \text{----->} \quad n := 4 \quad \text{Number of bars}$$

$$n \cdot A_s = 0.80 \text{ in}^2 > A_{skt} = 0.73 \text{ in}^2 \quad \text{OK}$$

### Design Step 3.4 \_ Extention column steel into cap-beam

Same as footing.

## **APPENDIX D**

### **DESIGN OF STEEL JACKETED RC COLUMN OF PROTOTYPE BRIDGE**

This appendix provides details on the design of steel jacketed RC columns of prototype bridge pier bent. The non-ductile RC column with diameter of 813 mm (32 in), 16-D19 (#6) longitudinal bars and transverse reinforcement ratio of 0.35 % was retrofitted with steel jacket with thickness of 4.3 mm (3/18 in). A clearance of 13 mm (1/2 in) was provided between the existing column and the jacket. This thickness of steel jacket was designed such that a steel jacket provided the confinement stress of 2.07 MPa.

--- Steel Jacketing Design of Prototype Bridge ---

DESIGN STEP 1 \_ As-built Column Transverse Reinforcement

Required Shear Strength by Transverse Steel for  $P_{max}$  Column

- $c := 2 \cdot \text{in}$  Clear cover
- $d_t := \frac{6}{8} \cdot \text{in}$  Diameter of longitudinal reinforcement
- $d_v := \frac{4}{8} \cdot \text{in}$  Diameter of transverse reinforcement
- $D := 32 \cdot \text{in}$  Column diameter
- $D' := D - 2 \cdot d_v - d_t - 2 \cdot c$  Circle diameter of longitudinal reinforcement  
 $D' = 667 \text{ mm}$        $D' = 26.25 \text{ in}$
- $D'' := D - 2 \cdot c$  Circle diameter of transverse reinforcement  
 $D'' = 711 \text{ mm}$        $D'' = 28.00 \text{ in}$
- $H_{clr} = 6.00 \text{ m}$
- $\alpha := \frac{D'}{H_{clr}}$        $\alpha = 6.37 \text{ deg}$
- $f'_c = 27.6 \text{ MPa}$

Inside potential plastic hinge zones:

$$P_{col\_top} := P_{col\_dltop} + \Delta P_{top}$$

$$P := P_{col\_top} \quad P = 1685 \text{ kN}$$

$$M_{x1} := 1017.5 \cdot \text{kN} \cdot \text{m} \quad P_{x1} := 1707.6 \text{ kN}$$

$$M_{x2} := 978.2 \cdot \text{kN} \cdot \text{m} \quad P_{x2} := 1522.6 \text{ kN}$$

$$\rightarrow M := \frac{P - P_{x2}}{P_{x1} - P_{x2}} \cdot (M_{x1} - M_{x2}) + M_{x2} \quad M = 1013 \text{ kN} \cdot \text{m} \quad M_{p\_top} := M \quad \text{From P-M Curve}$$

$$M_{p\_top} = 1013 \text{ m kN}$$

$$P_{col\_bot} := P_{col\_dl} + \Delta P_{bot} \quad P_{col\_bot} = 1925 \text{ kN}$$



## Appendix D

$$P := P_{col\_bot} \quad P = 1925 \text{ kN}$$

$$M_{x1} := 1061.3 \cdot \text{kN} \cdot \text{m} \quad P_{x1} := 2169.3 \text{ kN}$$

$$M_{x2} := 1017.5 \cdot \text{kN} \cdot \text{m} \quad P_{x2} := 1707.6 \text{ kN}$$

$$\rightarrow M := \frac{P - P_{x2}}{P_{x1} - P_{x2}} \cdot (M_{x1} - M_{x2}) + M_{x2} \quad M = 1038 \text{ kN} \cdot \text{m} \quad M_{p\_bot} := M \quad \text{From P-M Curve}$$

$$M_{p\_bot} = 1038 \text{ kN} \cdot \text{m}$$

Suppose the overstrength factor, OS, to 1.0.

$$OS := 1.0$$

$$P_e := P_{col\_dl} + OS \cdot \Delta P_{bot} \quad P_e = 1925 \text{ kN}$$

$$M_{p\_top} := OS \cdot M_{p\_top} \quad M_{p\_top} = 1013 \text{ kN} \cdot \text{m}$$

$$M_{p\_bot} := OS \cdot M_{p\_bot} \quad M_{p\_bot} = 1038 \text{ kN} \cdot \text{m}$$

$$V_u := \frac{M_{p\_top} + M_{p\_bot}}{H_{clr}} \quad V_u = 342 \text{ kN}$$

Shear resistance in the end regions:

$$A_g := \frac{\pi \cdot D^2}{4} \quad A_g = 0.5189 \text{ m}^2 \quad \text{Cross-sectional area of column}$$

$$A_c := \frac{\pi \cdot D''^2}{4} \quad A_c = 0.40 \text{ m}^2 \quad \text{Cross-sectional area of column}$$

$$A_v := 0.8 \cdot A_g \quad A_v = 0.42 \text{ m}^2 \quad \text{Shear area of concrete}$$

$$V_c := 0.05 \cdot \sqrt{f'_c} \cdot A_v \cdot \text{MPa}^{0.5} \quad V_c = 109 \text{ kN} \quad \text{Contribution of concrete}$$

$$\phi := 0.90 \quad \text{Strength reduction factor for shear}$$

$$V_s := \frac{V_u}{\phi} - V_c \quad V_{s1} := V_s \quad V_{s1} = 271 \text{ kN} \quad \text{Contribution of truss action}$$

### Required Shear Strength by Transverse Steel for $P_{min}$ Column

Inside potential plastic hinge zones:

$$P_{col\_top} := P_{col\_dltop} - \Delta P_{top}$$

$$P := P_{col\_top} \quad P = 1354 \text{ kN}$$

## Appendix D

$$M_{x1} := 944.1 \cdot \text{kN} \cdot \text{m} \quad P_{x1} := 1367.3 \text{ kN}$$

$$M_{x2} := 912.8 \cdot \text{kN} \cdot \text{m} \quad P_{x2} := 1228.5 \text{ kN}$$

$$\rightarrow M := \frac{P - P_{x2}}{P_{x1} - P_{x2}} \cdot (M_{x1} - M_{x2}) + M_{x2} \quad M = 941 \text{ kN} \cdot \text{m} \quad M_{p\_top} := M \quad \text{From P-M Curve}$$

$$M_{p\_top} = 941 \text{ m kN}$$

$$P_{col\_bot} := P_{col\_dl} - \Delta P_{bot}$$

$$P := P_{col\_bot} \quad P = 1263 \text{ kN}$$

$$M_{x1} := 944.1 \cdot \text{kN} \cdot \text{m} \quad P_{x1} := 1367.3 \text{ kN}$$

$$M_{x2} := 912.8 \cdot \text{kN} \cdot \text{m} \quad P_{x2} := 1228.5 \text{ kN}$$

$$\rightarrow M := \frac{P - P_{x2}}{P_{x1} - P_{x2}} \cdot (M_{x1} - M_{x2}) + M_{x2} \quad M = 921 \text{ kN} \cdot \text{m} \quad M_{p\_bot} := M \quad \text{From P-M Curve}$$

$$M_{p\_bot} = 921 \text{ kN} \cdot \text{m}$$

Suppose the overstrength factor, OS, to 1.0.

$$OS := 1.0$$

$$P_e := P_{col\_dl} - OS \cdot \Delta P_{bot} \quad P_e = 1263 \text{ kN}$$

$$M_{p\_top} := OS \cdot M_{p\_top} \quad M_{p\_top} = 941 \text{ kN} \cdot \text{m}$$

$$M_{p\_bot} := OS \cdot M_{p\_bot} \quad M_{p\_bot} = 921 \text{ kN} \cdot \text{m}$$

$$V_u := \frac{M_{p\_top} + M_{p\_bot}}{H_{clr}} \quad V_u = 310 \text{ kN}$$

Shear resistance in the end regions:

$$V_c := 0.05 \cdot \sqrt{f'_c} \cdot A_v \cdot \text{MPa}^{0.5} \quad V_c = 109 \text{ kN} \quad \text{Contribution of concrete}$$

$$\phi := 0.90 \quad \text{Strength reduction factor for shear}$$

$$V_s := \frac{V_u}{\phi} - V_c \quad V_{s2} := V_s \quad V_{s2} = 236 \text{ kN} \quad \text{Contribution of truss action}$$

### Transverse Reinforcement for Confinement at Plastic Hinges

$$V_s := \max(V_{s1}, V_{s2}) \quad V_s = 271 \text{ kN}$$

## Appendix D

Suppose  $s := 8.25 \cdot \text{in}$

$$A_t := 16 \cdot 0.44 \cdot \text{in}^2$$

$$\rho_t := \frac{A_t}{A_g} \quad \rho_t = 0.009 \quad \rho_t = 0.9\% \quad \text{Longitudinal reinforcement ratio}$$

$$\theta := 45 \cdot \text{deg}$$

$$f_{yh} := 60 \cdot \text{ksi} \quad \text{Yield strength of spiral}$$

$$A_{bhr} := \left( \frac{2}{\pi} \right) \cdot \left( \frac{V_s \cdot s}{f_{yh} \cdot D''} \right) \left( \frac{1}{\cot(\theta)} \right) \quad A_{bhr} = 0.190 \text{ in}^2 \quad \text{-----} \rightarrow \quad A_{bh} := 0.20 \cdot \text{in}^2 \quad (\#4)$$

$$\rho_s := \frac{4 \cdot A_{bhr}}{s \cdot D''} \quad \rho_s = 0.0033 \quad \rho_s = 0.33\% \quad \text{Required}$$

$$\rho_s := \frac{4 \cdot A_{bh}}{s \cdot D''} \quad \rho_s = 0.0035 \quad \rho_s = 0.35\% \quad \text{Provided}$$

### DESIGN STEP 2 \_ Steel Jacketing Design

#### Required Steel thickness, $t_j$ for Confinement

$$f_s := 200 \cdot \text{MPa} \quad \text{Stress induced in the jacket}$$

At strain of 0.001 when  $E_s = 200,000 \text{ MPa}$

$$f_l := 2.07 \cdot \text{MPa} \quad \text{Required confinement stress}$$

This assumption is from Chai et al., 1991

Suppose  $x_c := 0.5 \cdot \text{in}$  Clearance

$$D_j := D + 2 \cdot x_c \quad D_j = 838 \text{ mm} \quad D_j = 33.0 \text{ in} \quad \text{Outside diameter of steel jacket}$$

$$t_j := \frac{f_l \cdot D_j}{2 \cdot f_s} \quad t_j = 4.3 \text{ mm} \quad t_j = 0.17 \text{ in}$$

#### Check steel thickness, $t_j$ for Shear

$$V_s = 271 \text{ kN} \quad \text{Required shear strength}$$

$$t_j = 4.3 \text{ mm}$$

## Appendix D

$$f_{yj} := 42 \cdot \text{ksi} \quad f_{yj} = 290 \text{ MPa}$$

$$\theta := 30 \cdot \text{deg}$$

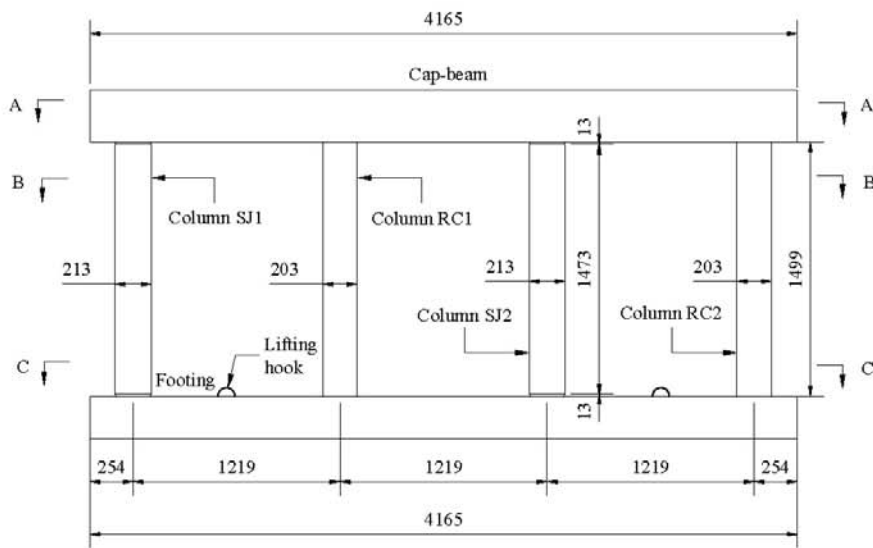
Shear strength enhancement by steel jacket,  $V_{sj}$ :

$$V_{sj} := \frac{\pi}{2} \cdot t_j \cdot f_{yj} \cdot (D_j - t_j) \cdot \cot(\theta) \quad V_{sj} = 2850 \text{ kN} > V_s = 271 \text{ kN} \quad \text{OK}$$

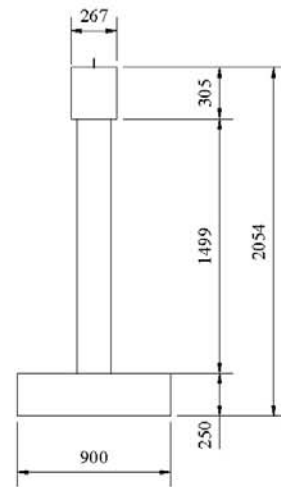
## **APPENDIX E**

### **SHOP DRAWINGS OF PIER BENT SPECIMEN**

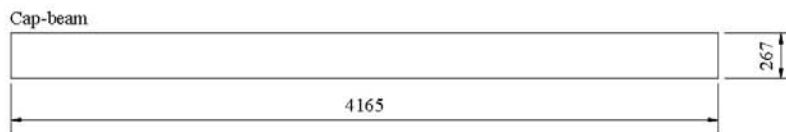
This appendix provides the shop drawings of pier bent specimen. The general layout, reinforcement details, formwork details and shipping frame details are presented.



Elevation View



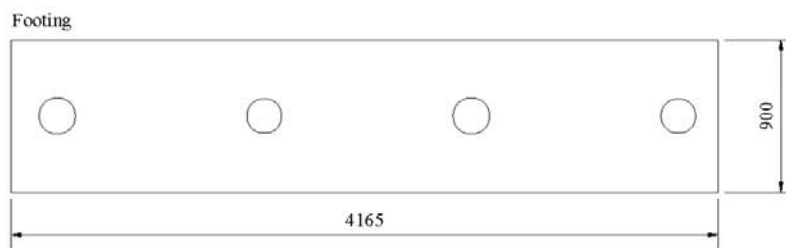
Side View



Plan View (A-A)



Plan View (B-B)



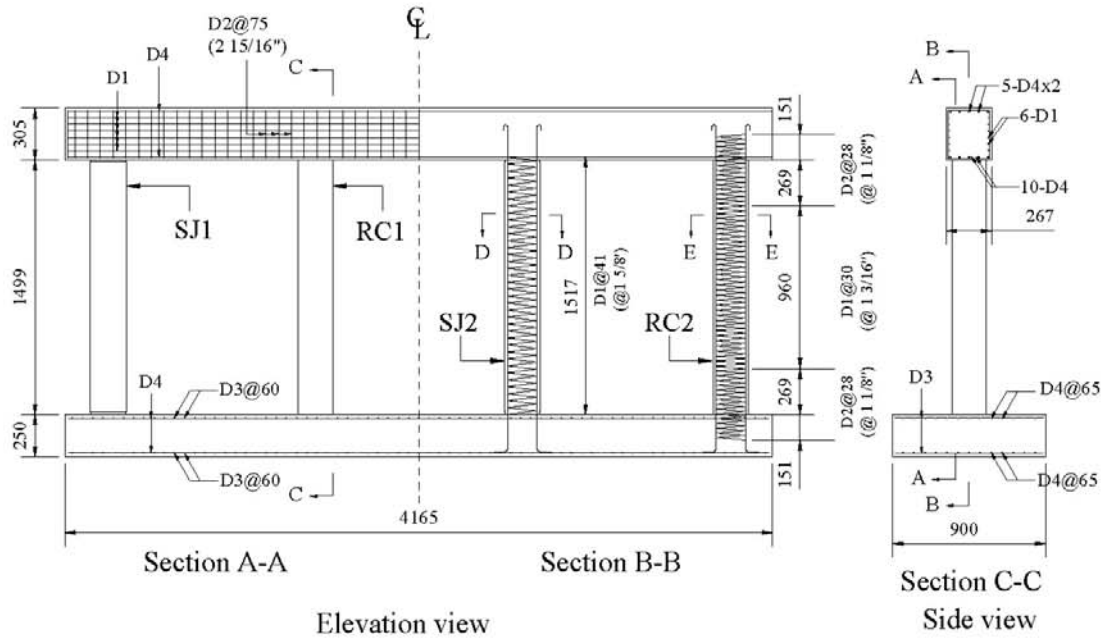
Plan View (C-C)

Scale: 1:40

Total Weight = 3.6 tf

Pier-bent Details (1/1)

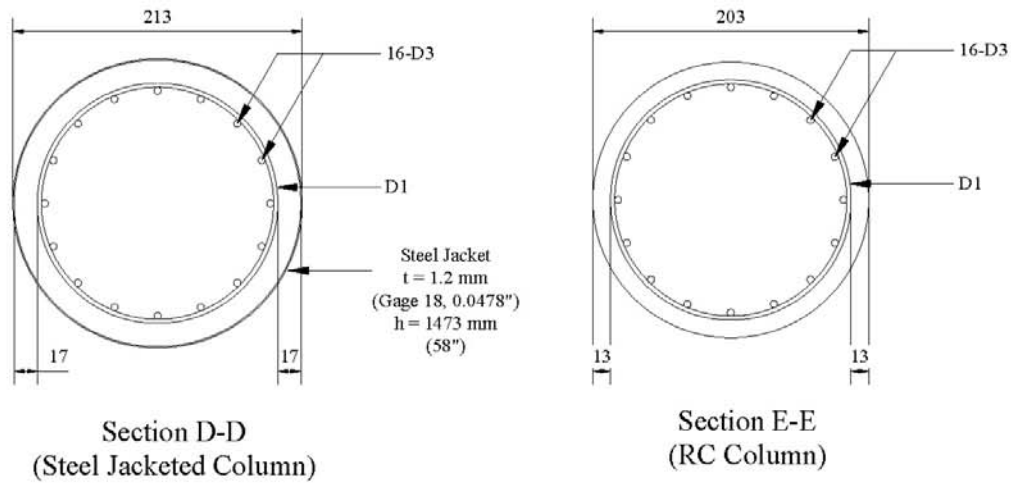
University at Buffalo			DRAWING No.
PROJECT: FHWA Highway Bridges	CONTENT:		1
BY: S. Fujikura	REV:	DATE: 03/14/07	SCALE: Indicated



Elevation view

Side view

Scale: 1:40



Section D-D  
(Steel Jacketed Column)

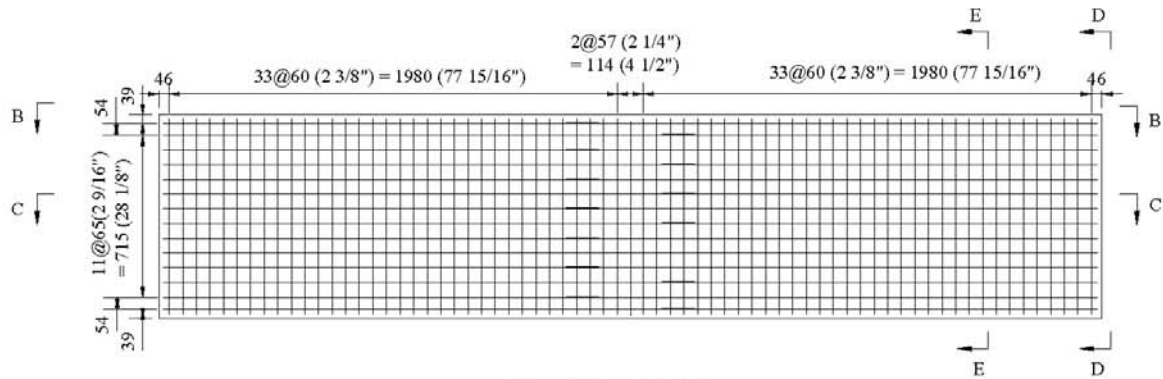
Section E-E  
(RC Column)

Scale: 1:5

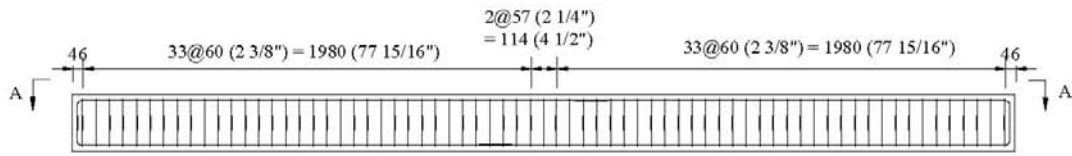
Reinforcement Details(1/1)

	Diameter in (mm)	Area in <sup>2</sup> (mm <sup>2</sup> )
D1	0.113 (2.87)	0.01 (6.45)
D2	0.159 (4.04)	0.02 (12.90)
D3	0.195 (4.95)	0.03 (19.35)
D4	0.225 (5.72)	0.04 (25.81)

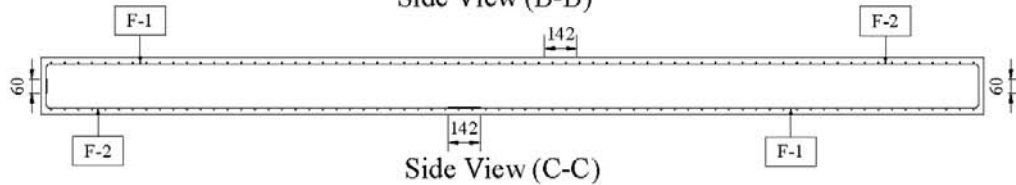
University at Buffalo			DRAWING No.
PROJECT: FHWA Highway Bridges	CONTENT:		2
BY: S. Fujikura	REV:	DATE: 02/17/07	SCALE: Indicated



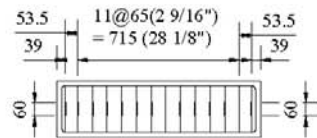
Plan View (A-A)



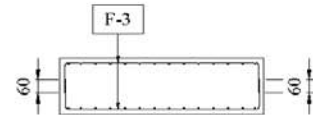
Side View (B-B)



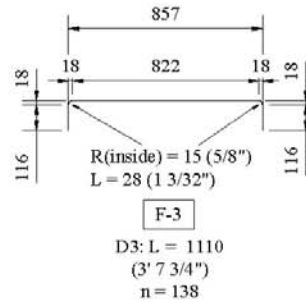
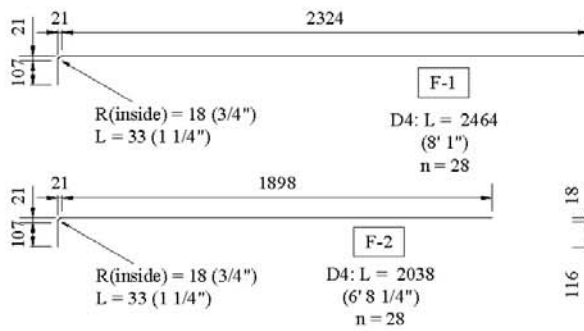
Side View (C-C)



Side View (D-D)



Side View (E-E)



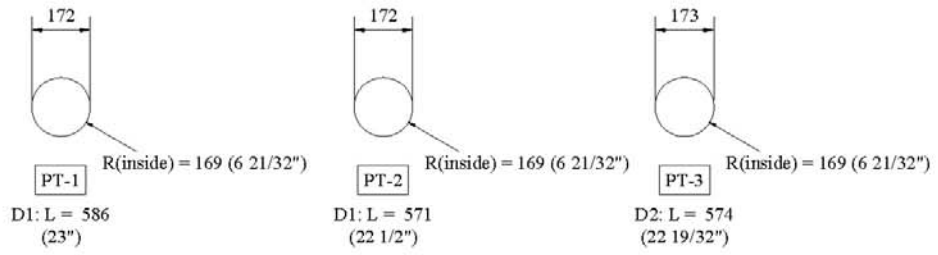
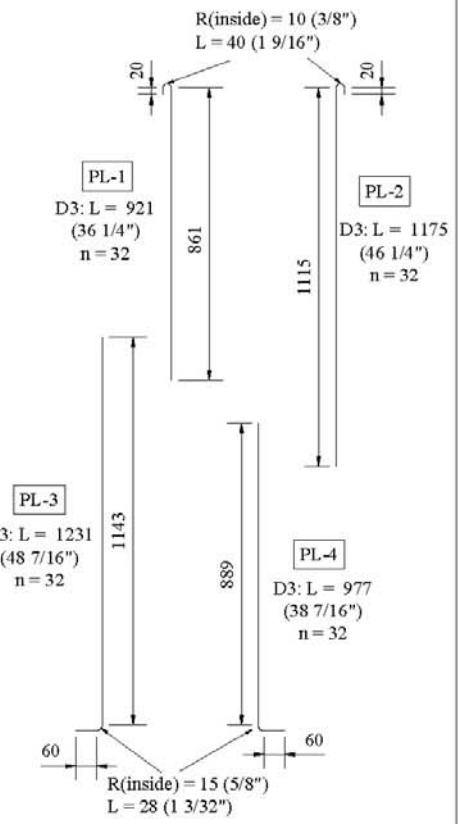
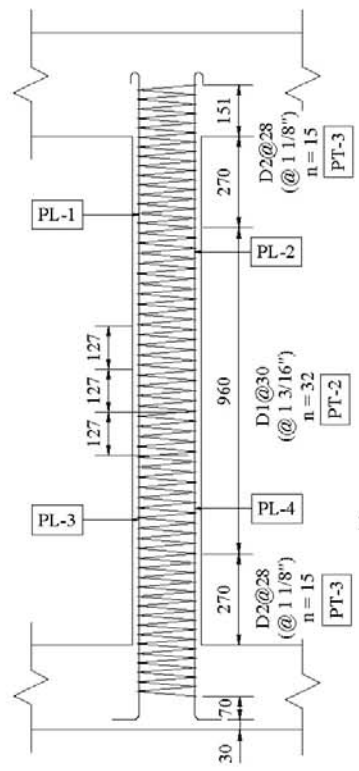
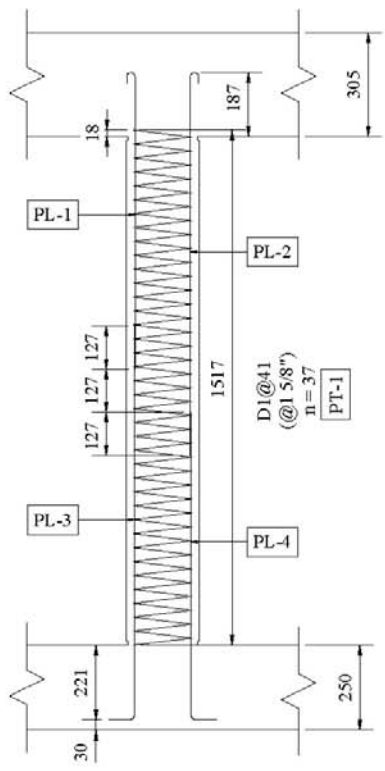
Shop Drawing

Scale: 1:30

Footing Reinforcement Details (1/1)

University at Buffalo		DRAWING No.	
PROJECT: FHWA Highway Bridges	CONTENT:	3	
BY: S. Fujikura	REV.:	DATE: 02/06/07	SCALE: Indicated

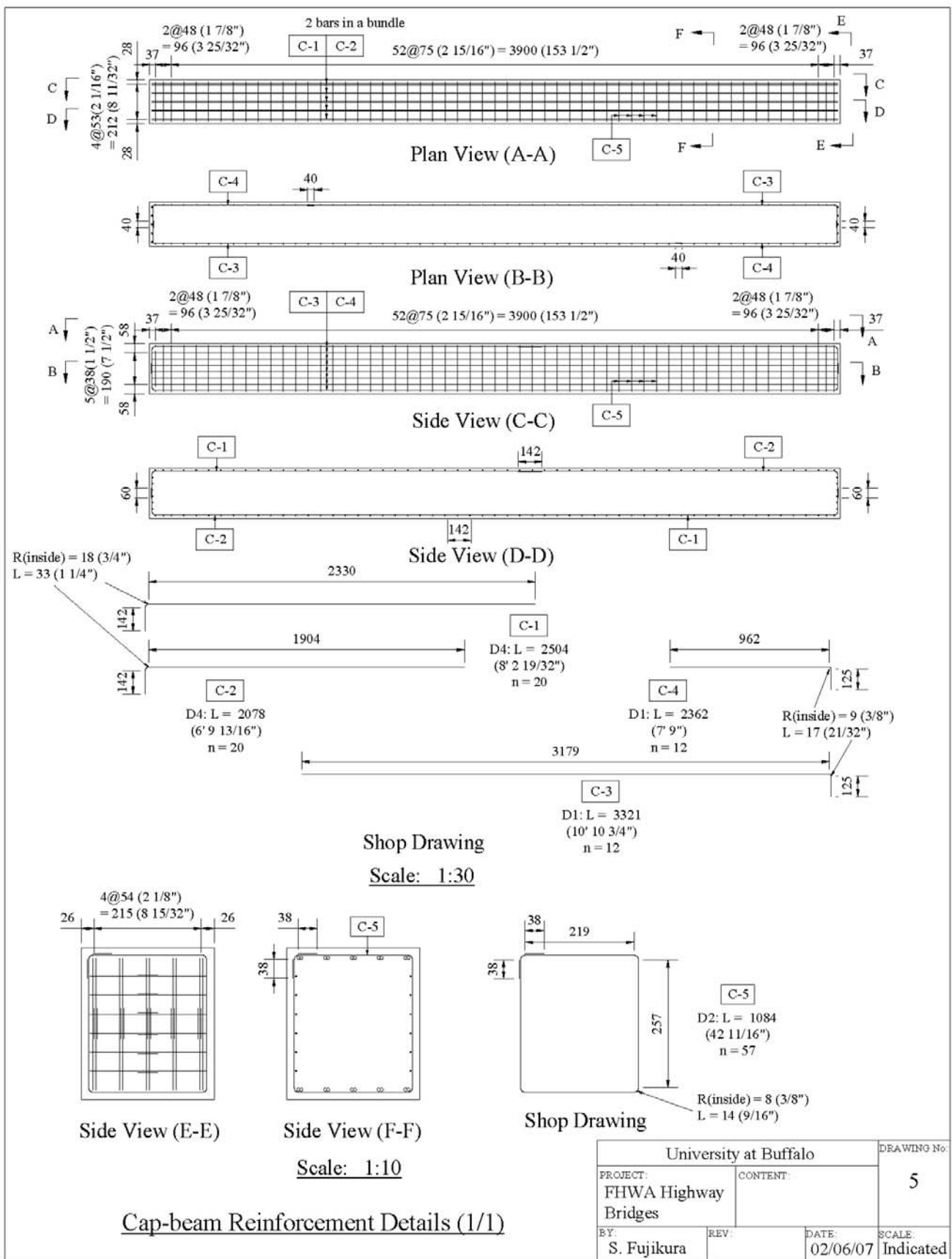


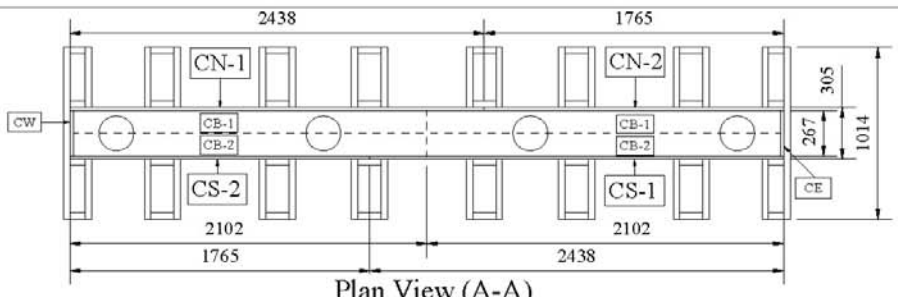


Column Reinforcement Details

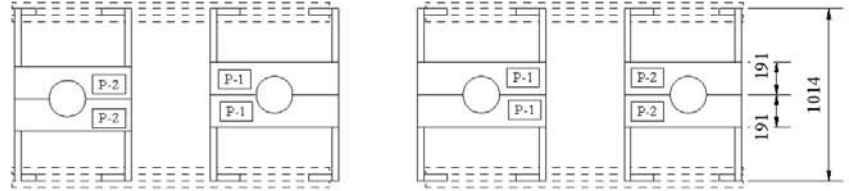
Scale: 1:20

University at Buffalo			DRAWING No.
PROJECT: FHWA Highway Bridges	CONTENT:		4
BY: S. Fujikura	REV:	DATE: 02/06/07	SCALE: Indicated

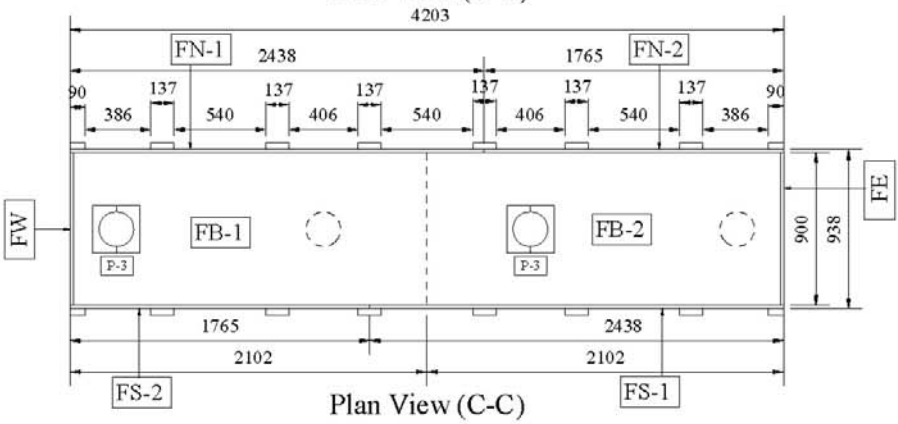




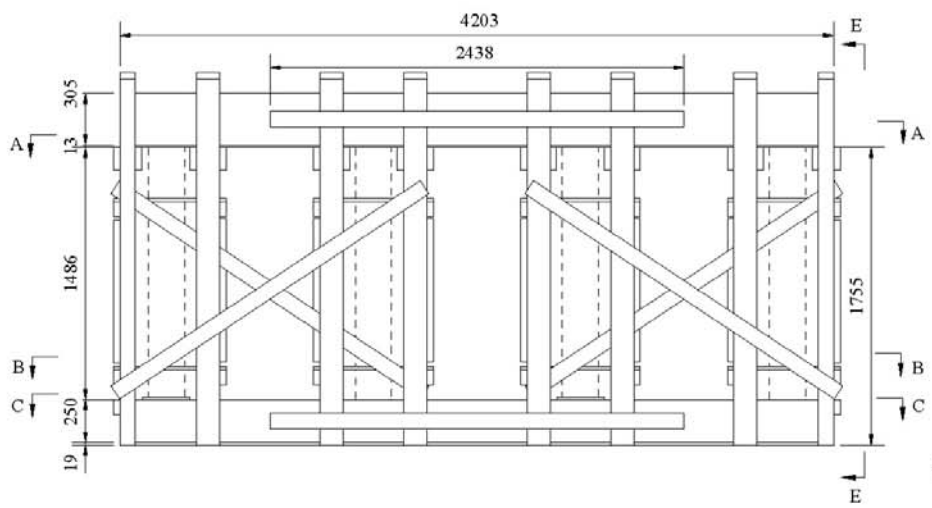
Plan View (A-A)



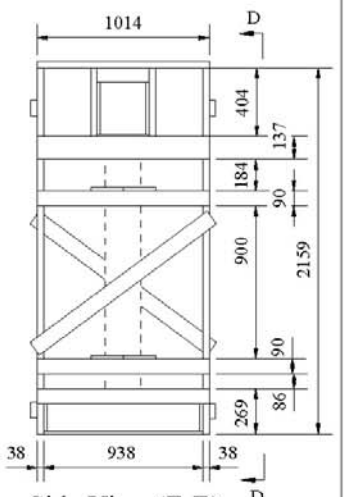
Plan View (B-B)



Plan View (C-C)



Side View (D-D)

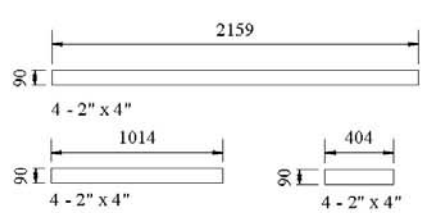
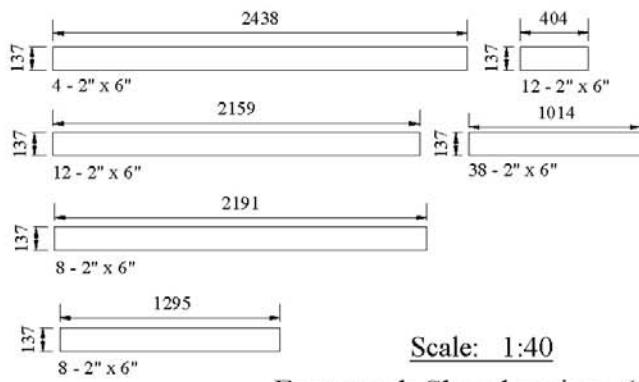
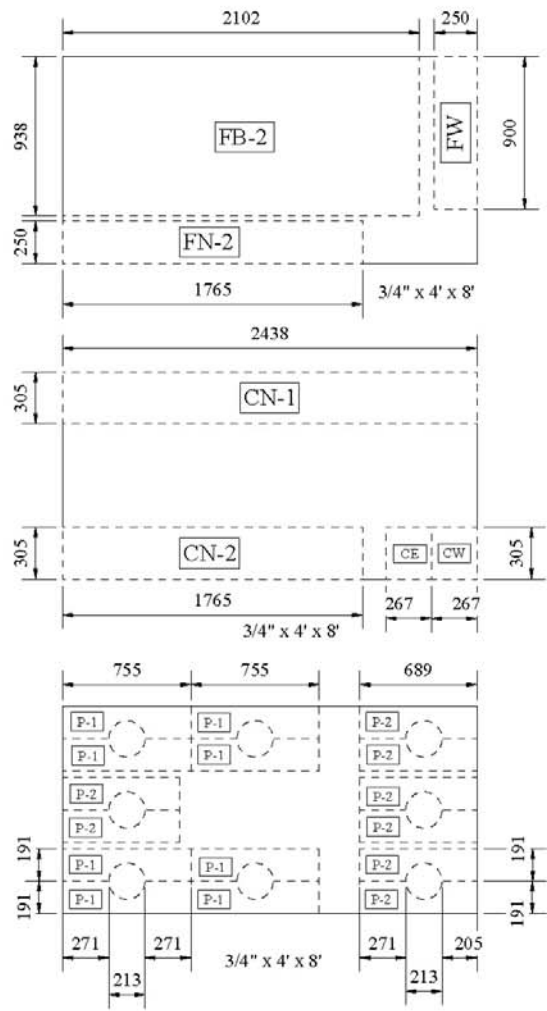
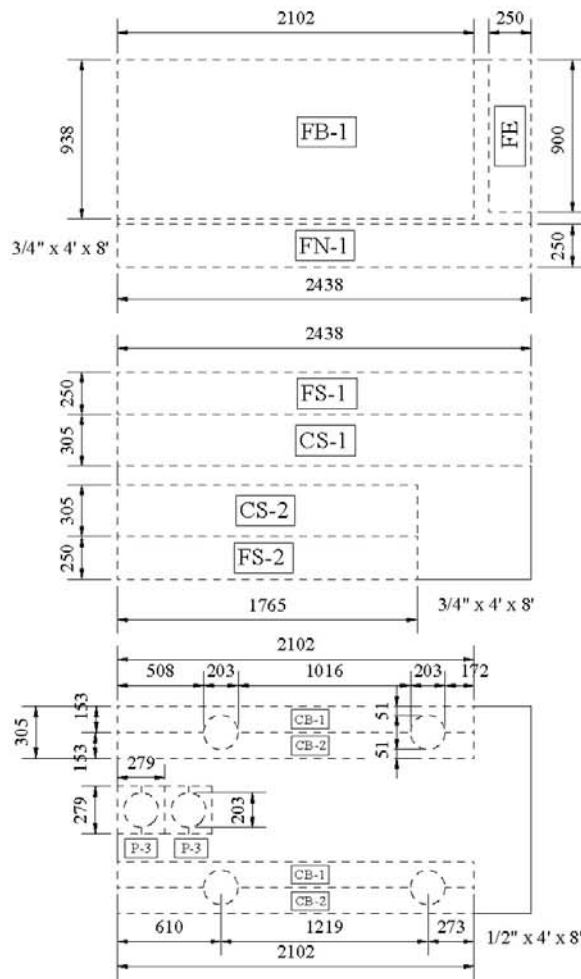


Side View (E-E)

Scale: 1:40

Formwork Details (1/1)

University at Buffalo		DRAWING No.	
PROJECT: FHWA Highway Bridges	CONTENT:	6	
BY: S. Fujikura	REV.	DATE: 02/27/07	SCALE: Indicated

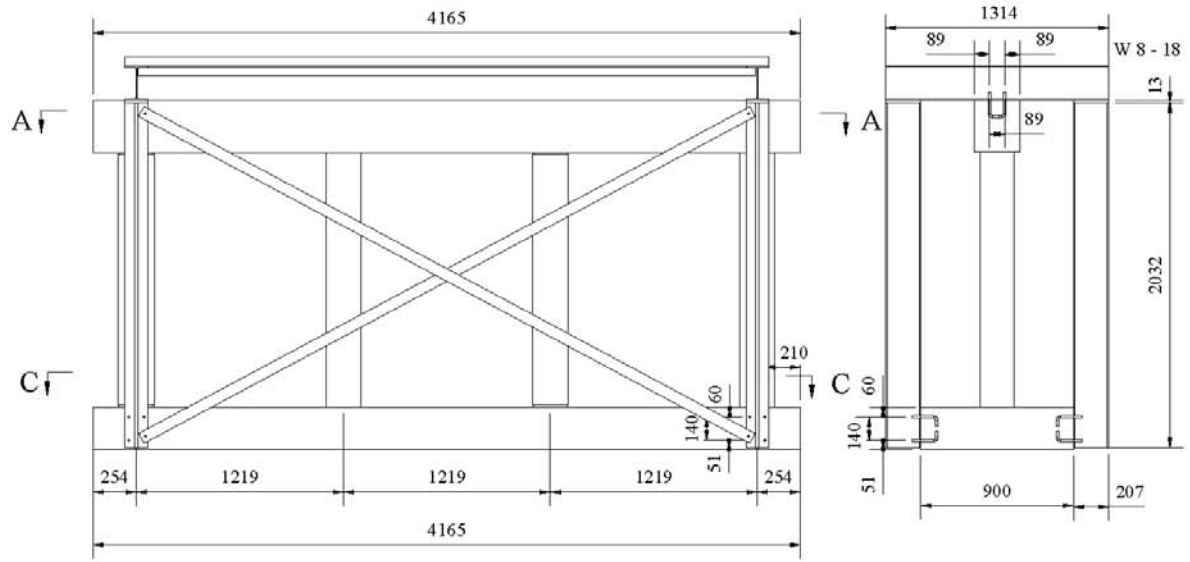


Scale: 1:40

Formwork Shopdrawings (1/1)

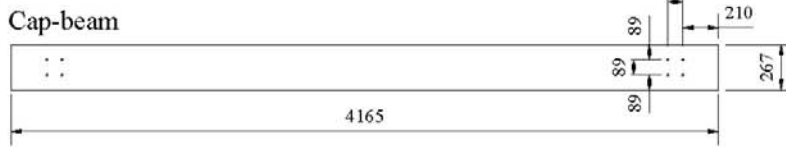
Material List		
- Wood	- Screw	- Hex bolt & nut
47 - 2" x 6" x 96"	1 5/8", 2", 2 1/2", 3"	24 - 1/2" x 4 1/2"
7 - 2" x 4" x 96"	- Chair	- Sonotube
5 - 3/4" x 4" x 8"	1/2" (Columns, Cap-beam)	2 - D = 8" x 58 1/2"
1 - 1/2" x 4" x 8"	3/4" (Footings)	

University at Buffalo		DRAWING No.	
PROJECT:	CONTENT:		7
FHWA Highway Bridges			
BY:	REV.	DATE:	SCALE:
S. Fujikura		02/27/07	Indicated

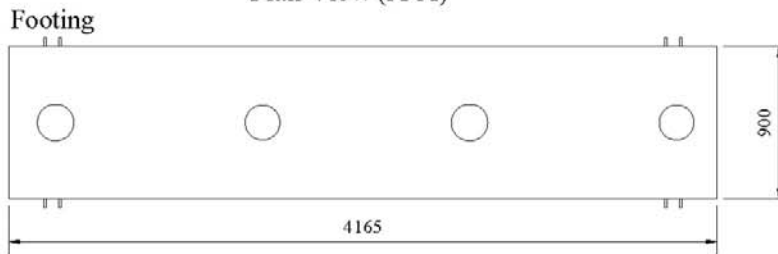


Elevation View

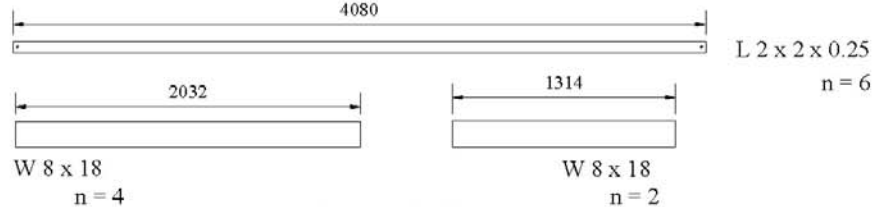
Side View



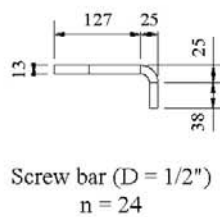
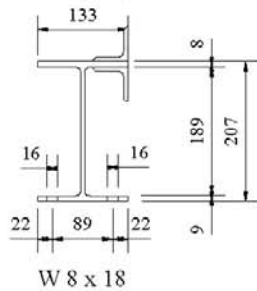
Plan View (A-A)



Plan View (C-C)



Scale: 1:40



Screw bar (D = 1/2")  
n = 24

Scale: 1:10

Shipping Frame Details (1/1)

University at Buffalo		DRAWING No.	
PROJECT: FHWA Highway Bridges	CONTENT:	8	
BY: S. Fujikura	REV:	DATE: 04/25/07	SCALE: Indicated



**APPENDIX F**

**MODELS AND RESULTS OF MOMENT-CURVATURE**

**ANALYSIS OF TEST COLUMNS FROM XTRACT**

Moment-curvature relationships were calculated using XTRACT (2007) for the test columns. This appendix provides the details of section and material models and analytical results. The stress-strain relationships for confined and unconfined concrete, steel bars and steel jacket are presented.

# XTRACT Material Report - Educational

For use only in an academic or research setting

Material Name: Unconfined1  
Material Type: Unconfined Concrete

S. Fujikura  
UB  
4/4/2008  
Multihazard  
RC1  
Page \_\_ of \_\_

## Input Parameters:

Tension Strength: -5710 ksi  
28 Day Strength: 5.813 ksi  
Post Crushing Strength: 0 ksi  
Tension Strain Capacity: .1314E-3 Comp  
Spalling Strain: 6.000E-3 Comp  
Failure Strain: 1.0000 Comp  
Elastic Modulus: 4346 ksi  
Secant Modulus: 2907 ksi

## Model Details:

For Strain -  $\varepsilon < 2 \cdot \varepsilon_t$   $f_c = 0$

For Strain -  $\varepsilon < 0$   $f_c = \varepsilon \cdot E_c$

For Strain -  $\varepsilon < \varepsilon_{cu}$   $f_c = \frac{f_c \cdot x \cdot r}{r - 1 + x^r}$

For Strain -  $\varepsilon < \varepsilon_{sp}$   $f_c = f_{cu} + (f_{cp} - f_{cu}) \cdot \frac{(\varepsilon - \varepsilon_{cu})}{(\varepsilon_{sp} - \varepsilon_{cu})}$

$$x = \frac{\varepsilon}{\varepsilon_{cc}}$$

$$r = \frac{E_c}{E_c - E_{sec}}$$

$$E_{sec} = \frac{f_c}{\varepsilon_{cc}}$$

$\varepsilon$  = Concrete Strain

$f_c$  = Concrete Stress

$E_c$  = Elastic Modulus

$E_{sec}$  = Secant Modulus

$\varepsilon_t$  = Tension Strain Capacity

$\varepsilon_{cu}$  = Ultimate Concrete Strain

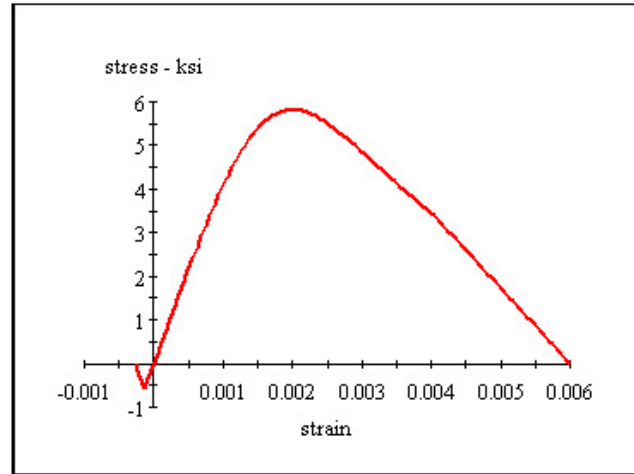
$\varepsilon_{cc}$  = Strain at Peak Stress = .002

$\varepsilon_{sp}$  = Spalling Strain

$f_c$  = 28 Day Compressive Strength

$f_{cu}$  = Stress at  $\varepsilon_{cu}$

$f_{cp}$  = Post Spalling Strength



## Material Color States:

- Tension strain after tension capacity
- Tension strain before tension capacity
- Initial state
- Compression before crushing strain
- Compression before end of spalling
- Compression after spalling

## Reference:

Mander, J.B., Priestley, M. J. N., "Observed Stress-Strain Behavior of Confined Concrete", Journal of Structural Engineering, ASCE, Vol. 114, No. 8, August 1988, pp. 1827-1849



# XTRACT Material Report - Educational

For use only in an academic or research setting

Material Name: Confined1  
Material Type: Confined Concrete

S. Fujikura  
UB  
4/4/2008  
Multihazard  
RC1  
Page \_\_ of \_\_

## Input Parameters:

Tension Strength: - .5710 ksi  
28 Day Strength: 5.813 ksi  
Confined Concrete Strength: 7.465 ksi  
Tension Strain Capacity: .1314E-3 Comp  
Strain at Peak Stress: 4.842E-3  
Crushing Strain: 20.00E-3 Comp  
Elastic Modulus: 4346 ksi  
Secant Modulus: 1542 ksi

## Model Details:

For Strain -  $\varepsilon < 2 \cdot \varepsilon_t$   $f_c = 0$   
For Strain -  $\varepsilon < 0$   $f_c = \varepsilon \cdot E_c$   
For Strain -  $\varepsilon < \varepsilon_{cu}$   $f_c = \frac{f_{cc} \cdot x \cdot r}{r - 1 + x^r}$

$$x = \frac{\varepsilon}{\varepsilon_{cc}}$$

$$\varepsilon_{cc} = .002 \cdot \left[ 1 + 5 \cdot \left( \frac{f_{cc}}{f_c} - 1 \right) \right]$$

$$r = \frac{E_c}{E_c - E_{sec}}$$

$$E_{sec} = \frac{f_{cc}}{\varepsilon_{cc}}$$

$\varepsilon$  = Concrete Strain

$f_c$  = Concrete Stress

$E_c$  = Elastic Modulus

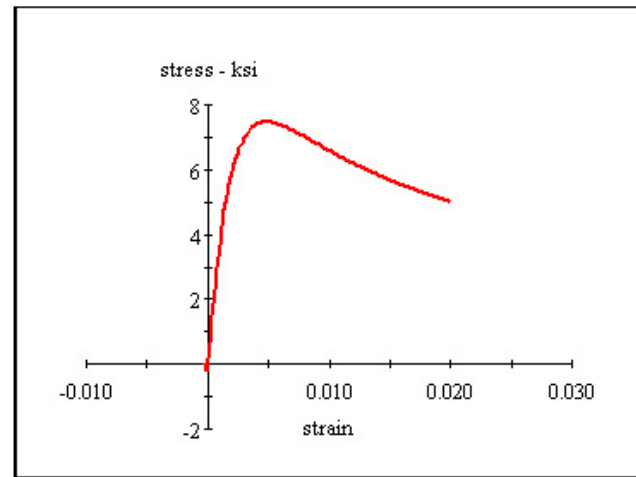
$\varepsilon_t$  = Tension Strain Capacity

$\varepsilon_{cu}$  = Ultimate Concrete Strain

$\varepsilon_{cc}$  = Strain at Peak Stress

$f_c$  = 28 Day Compressive Strength

$f_{cc}$  = Confined Concrete Strength



## Material Color States:

- Tension strain after tension capacity
- Tension strain before tension capacity
- Initial state
- Compression before crushing strain

## Reference:

Mander, J.B., Priestley, M. J. N., "Observed Stress-Strain Behavior of Confined Concrete", Journal of Structural Engineering ASCE, Vol. 114, No. 8, August 1988, pp. 1827-1849

# XTRACT Material Report - Educational

For use only in an academic or research setting

Material Name: Steel1

Material Type: Strain Hardening Steel

S. Fujikura

UB

4/4/2008

Multihazard

RC1

Page \_\_ of \_\_

## Input Parameters:

Yield Stress: 87.09 ksi  
Fracture Stress: 87.09 ksi  
Yield Strain: 3.080E-3  
Strain at Strain Hardening: 10.00E-3  
Failure Strain: 90.10E-3  
Elastic Modulus: 28.28E+3 ksi  
Additional Information: Symetric Tension and Comp.

## Model Details:

For Strain -  $\varepsilon < \varepsilon_y$   $f_s = E \cdot \varepsilon$

For Strain -  $\varepsilon < \varepsilon_{sh}$   $f_s = f_y$

For Strain -  $\varepsilon < \varepsilon_{su}$   $f_s = f_u - (f_u - f_y) \cdot \left( \frac{\varepsilon_{su} - \varepsilon}{\varepsilon_{su} - \varepsilon_{sh}} \right)^2$

$\varepsilon$  = Steel Strain

$f_s$  = Steel Stress

$f_y$  = Yield Stress

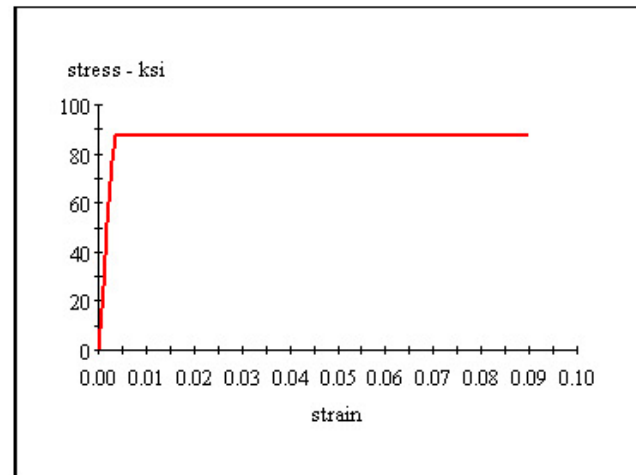
$f_u$  = Fracture Stress

$\varepsilon_y$  = Yield Strain

$\varepsilon_{sh}$  = Strain at Strain Hardening

$\varepsilon_{su}$  = Failure Strain

$E$  = Elastic Modulus



## Material Color States:

- Tension force after onset of strain hardening
- Tension force after yield
- Initial state
- Compression force after yield
- Compression force after onset of strain hardening

# XTRACT Material Report - Educational

For use only in an academic or research setting

Material Name: Steel2

Material Type: Strain Hardening Steel

S. Fujikura

UB

4/4/2008

Multihazard

RC1

Page \_\_ of \_\_

## Input Parameters:

Yield Stress: 44.22 ksi  
Fracture Stress: 44.22 ksi  
Yield Strain: 1.471E-3  
Strain at Strain Hardening: 7.000E-3  
Failure Strain: .1840  
Elastic Modulus: 30.07E+3 ksi  
Additional Information: Symetric Tension and Comp.

## Model Details:

For Strain -  $\varepsilon < \varepsilon_y$   $f_s = E \cdot \varepsilon$

For Strain -  $\varepsilon < \varepsilon_{sh}$   $f_s = f_y$

For Strain -  $\varepsilon < \varepsilon_{su}$   $f_s = f_u - (f_u - f_y) \cdot \left( \frac{\varepsilon_{su} - \varepsilon}{\varepsilon_{su} - \varepsilon_{sh}} \right)^2$

$\varepsilon$  = Steel Strain

$f_s$  = Steel Stress

$f_y$  = Yield Stress

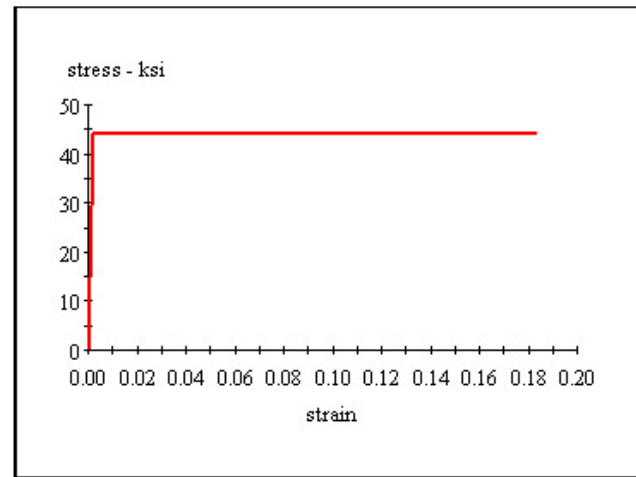
$f_u$  = Fracture Stress

$\varepsilon_y$  = Yield Strain

$\varepsilon_{sh}$  = Strain at Strain Hardening

$\varepsilon_{su}$  = Failure Strain

$E$  = Elastic Modulus



## Material Color States:

- Tension force after onset of strain hardening
- Tension force after yield
- Initial state
- Compression force after yield
- Compression force after onset of strain hardening

# XTRACT Material Report - Educational

For use only in an academic or research setting

Material Name: Confined2  
Material Type: Confined Concrete

S. Fujikura  
UB  
4/4/2008  
Multihazard  
RC1  
Page \_\_ of \_\_

## Input Parameters:

Tension Strength: - .5710 ksi  
28 Day Strength: 5.813 ksi  
Confined Concrete Strength: 7.612 ksi  
Tension Strain Capacity: .1314E-3 Comp  
Strain at Peak Stress: 5.095E-3  
Crushing Strain: 20.00E-3 Comp  
Elastic Modulus: 4346 ksi  
Secant Modulus: 1494 ksi

## Model Details:

For Strain -  $\varepsilon < 2 \cdot \varepsilon_t$   $f_c = 0$   
For Strain -  $\varepsilon < 0$   $f_c = \varepsilon \cdot E_c$   
For Strain -  $\varepsilon < \varepsilon_{cu}$   $f_c = \frac{f_{cc} \cdot x \cdot r}{r - 1 + x^r}$

$$x = \frac{\varepsilon}{\varepsilon_{cc}}$$

$$\varepsilon_{cc} = .002 \cdot \left[ 1 + 5 \cdot \left( \frac{f_{cc}}{f_c} - 1 \right) \right]$$

$$r = \frac{E_c}{E_c - E_{sec}}$$

$$E_{sec} = \frac{f_{cc}}{\varepsilon_{cc}}$$

$\varepsilon$  = Concrete Strain

$f_c$  = Concrete Stress

$E_c$  = Elastic Modulus

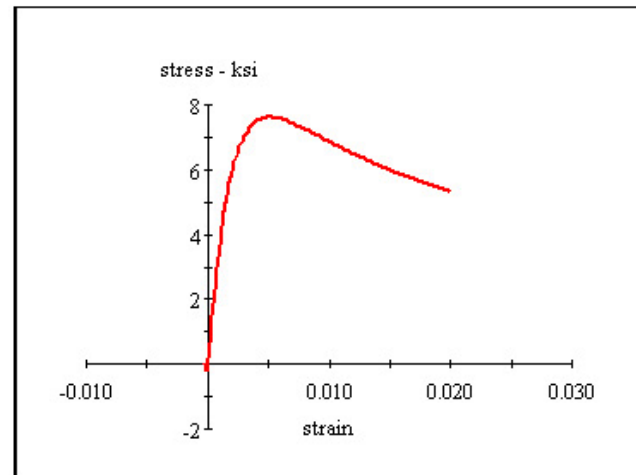
$\varepsilon_t$  = Tension Strain Capacity

$\varepsilon_{cu}$  = Ultimate Concrete Strain

$\varepsilon_{cc}$  = Strain at Peak Stress

$f_c$  = 28 Day Compressive Strength

$f_{cc}$  = Confined Concrete Strength



## Material Color States:

- Tension strain after tension capacity
- Tension strain before tension capacity
- Initial state
- Compression before crushing strain

## Reference:

Mander, J.B., Priestley, M. J. N., "Observed Stress-Strain Behavior of Confined Concrete", Journal of Structural Engineering ASCE, Vol. 114, No. 8, August 1988, pp. 1827-1849

# XTRACT Section Report - Educational

For use only in an academic or research setting

Section Name: RC

S. Fujikura

UB

4/4/2008

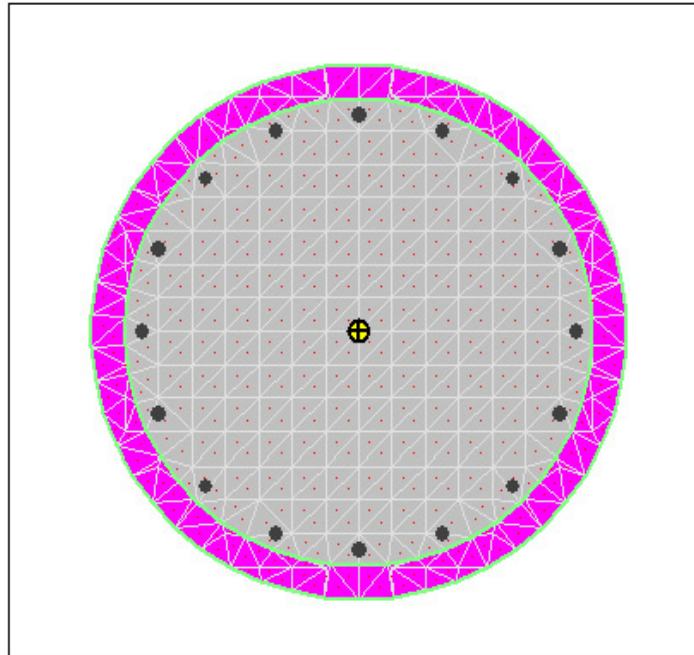
Multihazard

RC1

Page \_\_ of \_\_

## Section Details:

X Centroid:	-64.93E-9 in
Y Centroid:	-.2446E-15 in
Section Area:	50.13 in <sup>2</sup>
EI gross about X:	1.363E+6 kip-in <sup>2</sup>
EI gross about Y:	1.363E+6 kip-in <sup>2</sup>
I trans(Confined1) about X:	213.3 in <sup>4</sup>
I trans(Confined1) about Y:	213.3 in <sup>4</sup>
Reinforcing Bar Area:	.4800 in <sup>2</sup>
Percent Longitudinal Steel:	.9574 %
Overall Width:	7.984 in
Overall Height:	8.000 in
Number of Fibers:	494
Number of Bars:	16
Number of Materials:	3



## Material Types and Names:

Unconfined Concrete:	■ Unconfined1
Confined Concrete:	■ Confined1
Strain Hardening Steel:	■ Steel

## Comments:

User Comments

# XTRACT Section Report - Educational

For use only in an academic or research setting

Section Name: SJ Middle

S. Fujikura

UB

4/4/2008

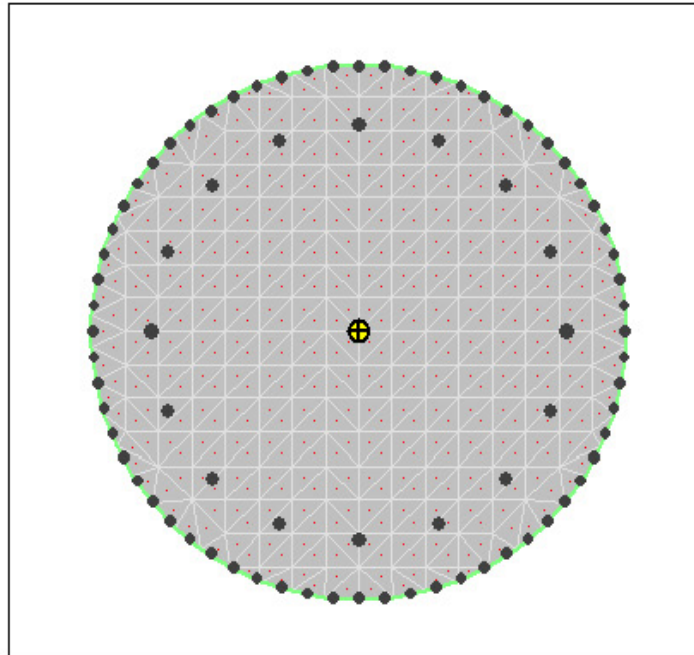
Multihazard

RC1

Page \_\_ of \_\_

## Section Details:

X Centroid:	.3657E-16 in
Y Centroid:	-.2359E-15 in
Section Area:	54.96 in <sup>2</sup>
EI gross about X:	1.363E+6 kip-in <sup>2</sup>
EI gross about Y:	1.363E+6 kip-in <sup>2</sup>
I trans(Confined2) about X:	313.6 in <sup>4</sup>
I trans(Confined2) about Y:	313.6 in <sup>4</sup>
Reinforcing Bar Area:	1.651 in <sup>2</sup>
Percent Longitudinal Steel:	3.005 %
Overall Width:	8.359 in
Overall Height:	8.376 in
Number of Fibers:	418
Number of Bars:	80
Number of Materials:	3



## Material Types and Names:

Strain Hardening Steel:	■ Steel1
Strain Hardening Steel:	■ Steel2
Confined Concrete:	■ Confined2

## Comments:

User Comments

# XTRACT Section Report - Educational

For use only in an academic or research setting

Section Name: SJ Bottom

S. Fujikura

UB

4/4/2008

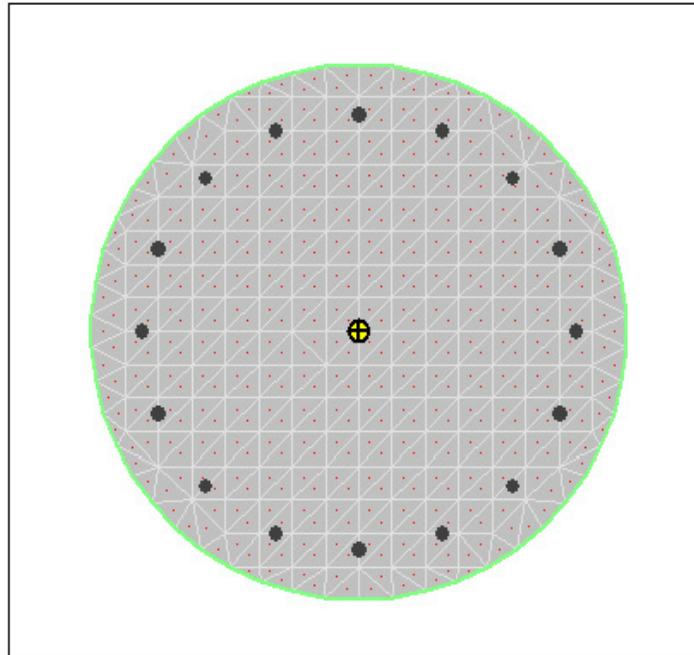
Multihazard

RC1

Page \_\_ of \_\_

## Section Details:

X Centroid:	- .2112E-15 in
Y Centroid:	- .2208E-15 in
Section Area:	50.13 in <sup>2</sup>
EI gross about X:	1.363E+6 kip-in <sup>2</sup>
EI gross about Y:	1.363E+6 kip-in <sup>2</sup>
I trans(Confined2) about X:	213.2 in <sup>4</sup>
I trans(Confined2) about Y:	213.2 in <sup>4</sup>
Reinforcing Bar Area:	.4800 in <sup>2</sup>
Percent Longitudinal Steel:	.9574 %
Overall Width:	7.984 in
Overall Height:	8.000 in
Number of Fibers:	418
Number of Bars:	32
Number of Materials:	2



## Material Types and Names:

Strain Hardening Steel:	■ Steel
Confined Concrete:	■ Confined2

## Comments:

User Comments

# XTRACT Analysis Report - Educational

For use only in an academic or research setting

Section Name: RC  
Loading Name: RC X  
Analysis Type: Moment Curvature

S. Fujikura  
UB  
4/4/2008  
Multihazard  
RC1  
Page \_\_ of \_\_

## Section Details:

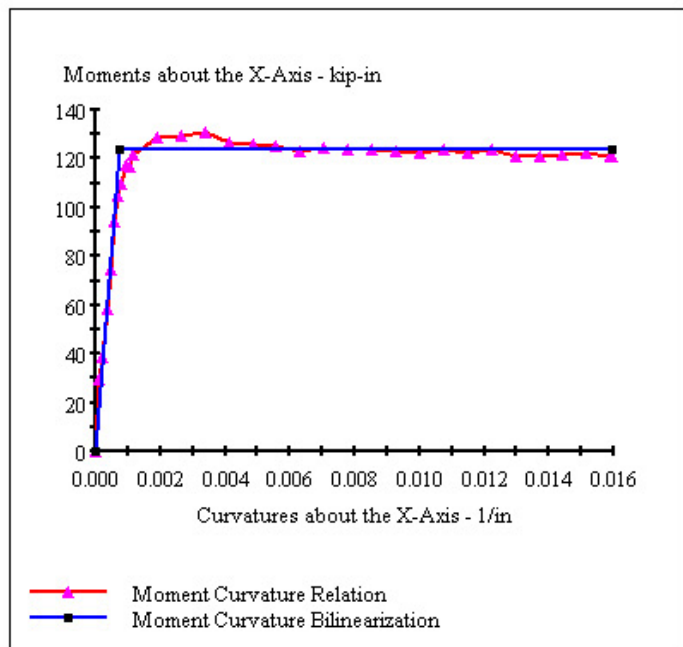
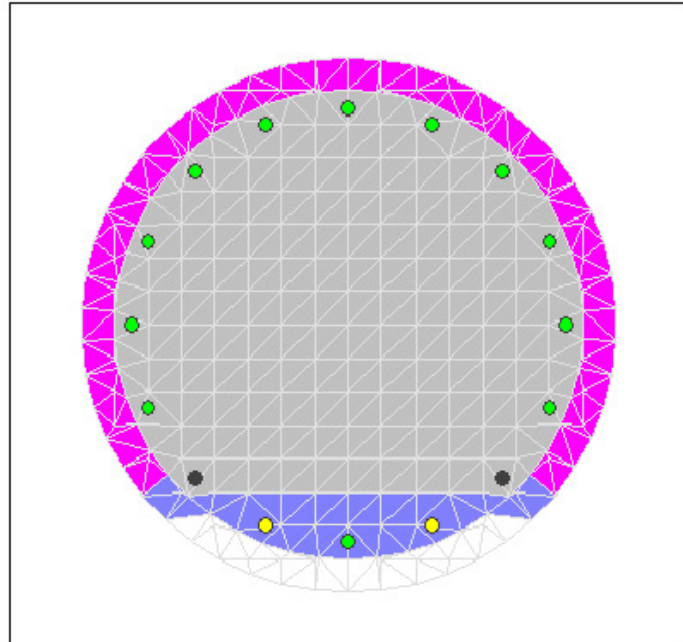
X Centroid: -64.93E-9 in  
Y Centroid: -.2446E-15 in  
Section Area: 50.13 in<sup>2</sup>

## Loading Details:

Incrementing Loads: Mxx Only  
Number of Points: 31  
Analysis Strategy: Displacement Control

## Analysis Results:

Failing Material: Steel  
Failure Strain: 90.10E-3 Tension  
Curvature at Initial Load: 0 1/in  
Curvature at First Yield: .5777E-3 1/in  
Ultimate Curvature: 15.94E-3 1/in  
Moment at First Yield: 93.37 kip-in  
Ultimate Moment: 120.8 kip-in  
Centroid Strain at Yield: 1.206E-3 Ten  
Centroid Strain at Ultimate: 38.39E-3 Ten  
N.A. at First Yield: 2.087 in  
N.A. at Ultimate: 2.409 in  
Energy per Length: 1.929 kips  
Effective Yield Curvature: .7670E-3 1/in  
Effective Yield Moment: 124.0 kip-in  
Over Strength Factor: .9743  
EI Effective: 161.6E+3 kip-in<sup>2</sup>  
Yield EI Effective: 0 kip-in<sup>2</sup>  
Bilinear Hardening Slope: 0 %  
Curvature Ductility: 20.78





# XTRACT Analysis Report - Educational

For use only in an academic or research setting

Section Name: SJ Middle  
Loading Name: SJ1 X  
Analysis Type: Moment Curvature

S. Fujikura  
UB  
4/4/2008  
Multihazard  
RC1  
Page \_\_ of \_\_

## Section Details:

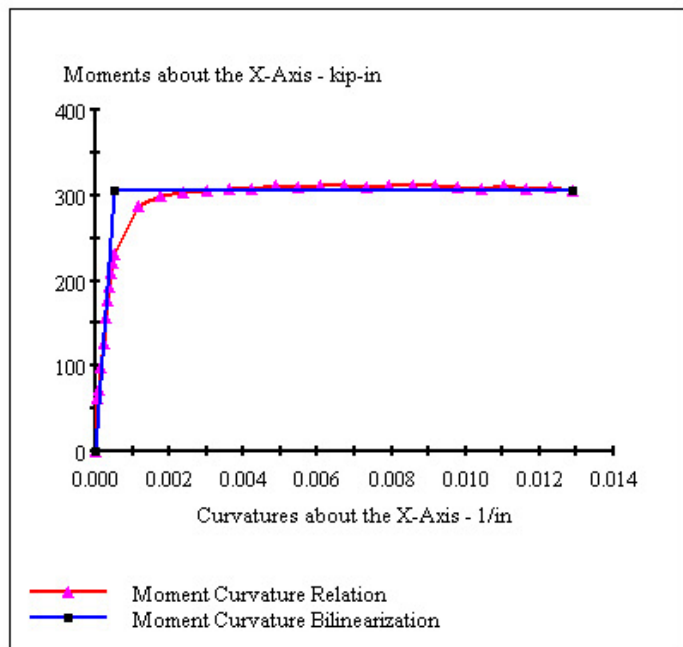
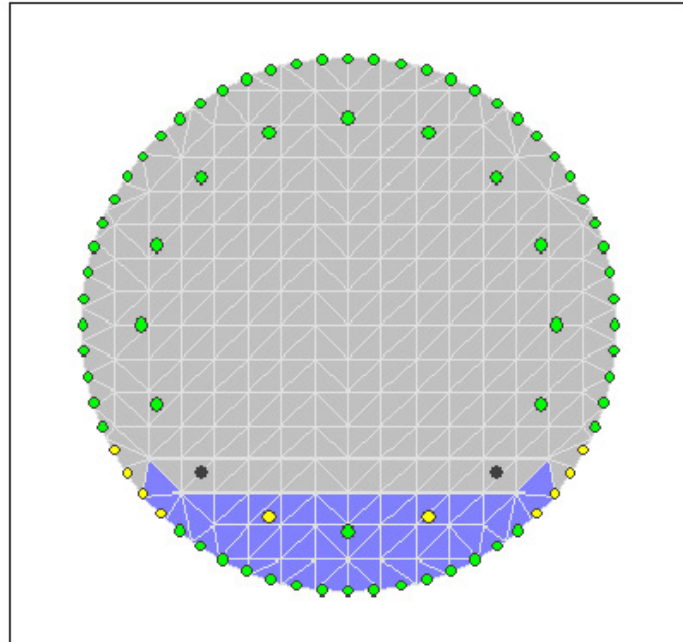
X Centroid: .3657E-16 in  
Y Centroid: -.2359E-15 in  
Section Area: 54.96 in<sup>2</sup>

## Loading Details:

Incrementing Loads: Mxx Only  
Number of Points: 31  
Analysis Strategy: Displacement Control

## Analysis Results:

Failing Material: Confined2  
Failure Strain: 20.00E-3 Compression  
Curvature at Initial Load: 0 1/in  
Curvature at First Yield: .2670E-3 1/in  
Ultimate Curvature: 12.91E-3 1/in  
Moment at First Yield: 158.0 kip-in  
Ultimate Moment: 305.3 kip-in  
Centroid Strain at Yield: .3584E-3 Ten  
Centroid Strain at Ultimate: 31.67E-3 Ten  
N.A. at First Yield: 1.342 in  
N.A. at Ultimate: 2.453 in  
Energy per Length: 3.858 kips  
Effective Yield Curvature: .5154E-3 1/in  
Effective Yield Moment: 305.0 kip-in  
Over Strength Factor: 1.001  
EI Effective: 591.7E+3 kip-in<sup>2</sup>  
Yield EI Effective: 0 kip-in<sup>2</sup>  
Bilinear Hardening Slope: 0 %  
Curvature Ductility: 25.05



# XTRACT Analysis Report - Educational

For use only in an academic or research setting

Section Name: SJ Bottom  
Loading Name: SJ2 X  
Analysis Type: Moment Curvature

S. Fujikura  
UB  
4/4/2008  
Multihazard  
RC1  
Page \_\_ of \_\_

## Section Details:

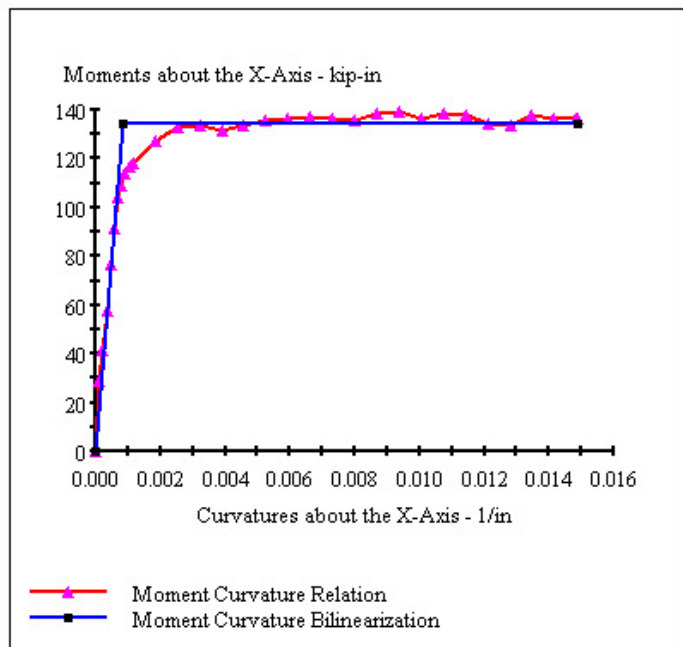
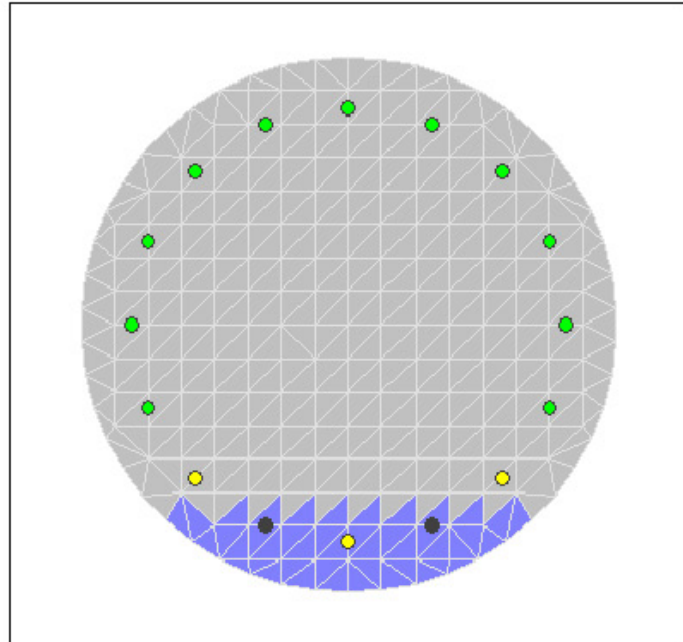
X Centroid: -2.112E-15 in  
Y Centroid: -2.208E-15 in  
Section Area: 50.13 in<sup>2</sup>

## Loading Details:

Incrementing Loads: Mxx Only  
Number of Points: 31  
Analysis Strategy: Displacement Control

## Analysis Results:

Failing Material: Steel  
Failure Strain: 90.10E-3 Tension  
Curvature at Initial Load: 0 1/in  
Curvature at First Yield: .5791E-3 1/in  
Ultimate Curvature: 14.87E-3 1/in  
Moment at First Yield: 91.93 kip-in  
Ultimate Moment: 136.5 kip-in  
Centroid Strain at Yield: 1.201E-3 Ten  
Centroid Strain at Ultimate: 41.87E-3 Ten  
N.A. at First Yield: 2.074 in  
N.A. at Ultimate: 2.816 in  
Energy per Length: 1.944 kips  
Effective Yield Curvature: .8477E-3 1/in  
Effective Yield Moment: 134.6 kip-in  
Over Strength Factor: 1.014  
EI Effective: 158.8E+3 kip-in<sup>2</sup>  
Yield EI Effective: 0 kip-in<sup>2</sup>  
Bilinear Hardening Slope: 0 %  
Curvature Ductility: 17.54



## **APPENDIX G**

### **SIMPLE PLASTIC ANALYSIS OF TEST COLUMNS**

This appendix provides details on the simple plastic analyses of the RC columns and steel jacketed RC columns. These plastic analyses were conducted to calculate ultimate lateral load capacity and reactions of these columns. The maximum resulting reaction forces at the base and top of the RC columns were 112.1 kN (25.2 kip) and 22.4 kN (5.0 kip), respectively. The maximum resulting reaction forces at the base and top of the steel jacketed RC columns were 198.7 kN (44.7 kip) and 39.7 kN (8.9 kip), respectively.

## Appendix G

### Simple Plastic Analysis

#### --- RC1 and RC2 Test Specimen --- (Applied Force at Blast Height)

**Units:**                      kip := 1000·lbf                      ksi :=  $\frac{\text{kip}}{\text{in}^2}$                       msec :=  $\frac{\text{sec}}{1000}$   
   kN := 1000·N                      MPa := 1000000·Pa

**Geometry:**    L := 1.5·m                      Height of Column:  
   a := 0.25·m                      Height of Load  
   b := L – a                      b = 1.250 m  
  
   EI :=  $161.6 \cdot 10^3 \cdot \text{kip} \cdot \text{in}^2$     EI = 463.8 kN·m<sup>2</sup>                      Flexural Stiffness \*1  
  
   Mp := 124.0·kip·in                      Mp = 14.0 kN·m                      Plastic Moment  
      Capacity of Column \*1

\*1 : Dinamic Increase Factors were considered for material.

## Appendix G

### Step 1: Forming 1st Plastic Hinge

Maximum Force

$$P_1 := \frac{M_p \cdot L^2}{a \cdot b^2} \quad P_1 = 80.7 \text{ kN} \quad \text{When base moment } (M_1) \text{ reaches } M_p$$

Reactions

$$R_{1\_1} := \frac{P_1 \cdot b^2}{L^3} \cdot (3 \cdot a + b) \quad R_{1\_1} = 74.7 \text{ kN} \quad \text{Reaction @ Bottom}$$

$$R_{2\_1} := \frac{P_1 \cdot a^2}{L^3} \cdot (a + 3 \cdot b) \quad R_{2\_1} = 6.0 \text{ kN} \quad \text{Reaction @ Top}$$

Moment

$$M_{1\_1} := -\frac{P_1 \cdot a \cdot b^2}{L^2} \quad M_{1\_1} = -14.0 \text{ kN} \cdot \text{m} \quad \text{Moment @ Bottom}$$

$$M_{2\_1} := -\frac{P_1 \cdot a^2 \cdot b}{L^2} \quad M_{2\_1} = -2.8 \text{ kN} \cdot \text{m} \quad \text{Moment @ Top}$$

$$M_{a\_1} := \frac{2 \cdot P_1 \cdot a^2 \cdot b^2}{L^3} \quad M_{a\_1} = 4.7 \text{ kN} \cdot \text{m} \quad \text{Moment @ Load Point}$$

Deflection

$$w_{a\_1} := \frac{P_1 \cdot a^3 \cdot b^3}{3 \cdot EI \cdot L^3} \quad w_{a\_1} = 0.5 \text{ mm} \quad \text{Deflection @ Load Point}$$

### Step 2: Forming 2nd Plastic Hinge

Maximum Force

$$P_{2a} := (M_p - M_{a\_1}) \cdot \frac{2 \cdot L^3}{a \cdot b^2} \cdot \frac{1}{a + 2 \cdot L} \quad P_{2a} = 49.7 \text{ kN} \quad \text{When } M_a \text{ reaches } M_p$$

$$P_{22} := -(-M_p - M_{2\_1}) \cdot \frac{2 \cdot L^2}{a \cdot b} \cdot \frac{1}{a + L} \quad P_{22} = 92.2 \text{ kN} \quad \text{When } M_2 \text{ reaches } M_p$$

$$P_2 := \min(P_{2a}, P_{22}) \quad P_2 = 49.7 \text{ kN} \quad \text{----> Plastic hinge forms at load point}$$

## Appendix G

### Reactions

$$R_{1\_2} := \frac{P_2 \cdot b^2}{2 \cdot L^3} \cdot (a + 2 \cdot L) \quad R_{1\_2} = 37.4 \text{ kN} \quad \text{Reaction @ Bottom}$$

$$R_{2\_2} := \frac{P_2 \cdot a}{2 \cdot L^3} (3 \cdot L^2 - a^2) \quad R_{2\_2} = 12.3 \text{ kN} \quad \text{Reaction @ Top}$$

### Moment

$$M_{2\_2} := -\frac{P_2 \cdot a \cdot b}{2 \cdot L^2} \cdot (a + L) \quad M_{2\_2} = -6.0 \text{ kN} \cdot \text{m} \quad \text{Moment @ Top}$$

$$M_{a\_2} := R_{1\_2} \cdot a \quad M_{a\_2} = 9.3 \text{ kN} \cdot \text{m} \quad \text{Moment @ Load Point}$$

### Deflection

$$w_{a\_2} := \frac{P_2 \cdot a^2 \cdot b^3}{12 \cdot EI \cdot L^3} \cdot (3 \cdot L + a) \quad w_{a\_2} = 1.5 \text{ mm} \quad \text{Deflection @ Load Point}$$

### Step 3: Forming Last Plastic Hinge

#### Maximum Force

$$P_3 := \frac{M_p + M_{2\_1} + M_{2\_2}}{b} \quad P_3 = 4.1 \text{ kN} \quad \text{When } M_2 \text{ reaches } M_p$$

#### Reactions

$$R_{2\_3} := P_3 \quad R_{2\_3} = 4.1 \text{ kN} \quad \text{Reaction @ Top}$$

#### Moment

$$M_{2\_3} := P_3 \cdot b \quad M_{2\_3} = 5.2 \text{ kN} \cdot \text{m} \quad \text{Moment @ Top}$$

#### Deflection

$$w_{a\_3} := \frac{P_3 \cdot b^3}{3 \cdot EI} \quad w_{a\_3} = 5.8 \text{ mm} \quad \text{Deflection @ Load Point}$$

## Appendix G

### Summary

#### Step 1:

$$\begin{aligned} P &:= P_1 & P_1 &= 80.7 \text{ kN} \\ R_1 &:= R_{1\_1} & R_1 &= 74.7 \text{ kN} \\ R_2 &:= R_{2\_1} & R_2 &= 6.0 \text{ kN} \\ w_a &:= w_{a\_1} & w_a &= 0.5 \text{ mm} \end{aligned}$$

#### Step 2:

$$\begin{aligned} P' &:= P_1 + P_2 & P' &= 130.4 \text{ kN} \\ R'_1 &:= R_{1\_1} + R_{1\_2} & R'_1 &= 112.1 \text{ kN} \\ R'_2 &:= R_{2\_1} + R_{2\_2} & R'_2 &= 18.3 \text{ kN} \\ w'_a &:= w_{a\_1} + w_{a\_2} & w'_a &= 2.1 \text{ mm} \end{aligned}$$

#### Step 3:

$$\begin{aligned} P'' &:= P_1 + P_2 + P_3 & P'' &= 134.5 \text{ kN} \\ R''_1 &:= R_{1\_1} + R_{1\_2} & R''_1 &= 112.1 \text{ kN} \\ R''_2 &:= R_{2\_1} + R_{2\_2} + R_{2\_3} & R''_2 &= 22.4 \text{ kN} \\ w''_a &:= w_{a\_1} + w_{a\_2} + w_{a\_3} & w''_a &= 7.9 \text{ mm} \end{aligned}$$

## Appendix G

### Simple Plastic Analysis

#### --- SJ1 and SJ2 Test Specimen --- (Applied Force at Blast Height)

**Units:**

	kip := 1000·lbf	ksi := $\frac{\text{kip}}{\text{in}^2}$	msec := $\frac{\text{sec}}{1000}$
	kN := 1000·N	MPa := 1000000·Pa	

**Geometry:**

L := 1.5·m	Height of Column:	
a := 0.25·m	Height of Load	
b := L – a	b = 1.250 m	
EI := 591.7·10 <sup>3</sup> ·kip·in <sup>2</sup>	EI = 1698.1 kN·m <sup>2</sup>	Flexural Stiffness *1 (Steel Jacketed Column)
M <sub>pB</sub> := 134.6·kip·in	M <sub>pB</sub> = 15.2 kN·m	Plastic Moment Capacity of Column at Base and Top *1
M <sub>pM</sub> := 305.0·kip·in	M <sub>pM</sub> = 34.5 kN·m	Plastic Moment Capacity of Column at Middle *1

\*1 : Dynamic Increase Factors were considered for material.



## Appendix G

### Step 1: Forming 1st Plastic Hinge

Maximum Force

$$P_1 := \frac{M_{pB} \cdot L^2}{a \cdot b^2} \quad P_1 = 87.6 \text{ kN} \quad \text{When base moment } (M_1) \text{ reaches } M_p$$

Reactions

$$R_{1\_1} := \frac{P_1 \cdot b^2}{L^3} \cdot (3 \cdot a + b) \quad R_{1\_1} = 81.1 \text{ kN} \quad \text{Reaction @ Bottom}$$

$$R_{2\_1} := \frac{P_1 \cdot a^2}{L^3} \cdot (a + 3 \cdot b) \quad R_{2\_1} = 6.5 \text{ kN} \quad \text{Reaction @ Top}$$

Moment

$$M_{1\_1} := -\frac{P_1 \cdot a \cdot b^2}{L^2} \quad M_{1\_1} = -15.2 \text{ kN} \cdot \text{m} \quad \text{Moment @ Bottom}$$

$$M_{2\_1} := -\frac{P_1 \cdot a^2 \cdot b}{L^2} \quad M_{2\_1} = -3.0 \text{ kN} \cdot \text{m} \quad \text{Moment @ Top}$$

$$M_{a\_1} := \frac{2 \cdot P_1 \cdot a^2 \cdot b^2}{L^3} \quad M_{a\_1} = 5.1 \text{ kN} \cdot \text{m} \quad \text{Moment @ Load Point}$$

Deflection

$$w_{a\_1} := \frac{P_1 \cdot a^3 \cdot b^3}{3 \cdot EI \cdot L^3} \quad w_{a\_1} = 0.2 \text{ mm} \quad \text{Deflection @ Load Point}$$

### Step 2: Forming 2nd Plastic Hinge

Maximum Force

$$P_{2a} := (M_{pM} - M_{a\_1}) \cdot \frac{2 \cdot L^3}{a \cdot b^2} \cdot \frac{1}{a + 2 \cdot L} \quad P_{2a} = 156.3 \text{ kN} \quad \text{When } M_a \text{ reaches } M_p$$

$$P_{22} := -(-M_{pB} - M_{2\_1}) \cdot \frac{2 \cdot L^2}{a \cdot b} \cdot \frac{1}{a + L} \quad P_{22} = 100.1 \text{ kN} \quad \text{When } M_2 \text{ reaches } M_p$$

$$P_2 := \min(P_{2a}, P_{22}) \quad P_2 = 100.1 \text{ kN} \quad \text{----> Plastic hinge forms at Top}$$

## Appendix G

### Reactions

$$R_{1\_2} := \frac{P_2 \cdot b^2}{2 \cdot L^3} \cdot (a + 2 \cdot L) \quad R_{1\_2} = 75.3 \text{ kN} \quad \text{Reaction @ Bottom}$$

$$R_{2\_2} := \frac{P_2 \cdot a}{2 \cdot L^3} (3 \cdot L^2 - a^2) \quad R_{2\_2} = 24.8 \text{ kN} \quad \text{Reaction @ Top}$$

### Moment

$$M_{2\_2} := -\frac{P_2 \cdot a \cdot b}{2 \cdot L^2} \cdot (a + L) \quad M_{2\_2} = -12.2 \text{ kN} \cdot \text{m} \quad \text{Moment @ Top}$$

$$M_{a\_2} := R_{1\_2} \cdot a \quad M_{a\_2} = 18.8 \text{ kN} \cdot \text{m} \quad \text{Moment @ Load Point}$$

### Deflection

$$w_{a\_2} := \frac{P_2 \cdot a^2 \cdot b^3}{12 \cdot EI \cdot L^3} \cdot (3 \cdot L + a) \quad w_{a\_2} = 0.8 \text{ mm} \quad \text{Deflection @ Load Point}$$

### Step 3: Forming Last Plastic Hinge

#### Maximum Force

$$P_3 := \frac{M_p M - M_{a\_1} - M_{a\_2}}{a \cdot b} \cdot L \quad P_3 = 50.7 \text{ kN} \quad \text{When } M_a \text{ reaches } M_p$$

### Reactions

$$R_{1\_3} := \frac{P_3 \cdot b}{L} \quad R_{1\_3} = 42.2 \text{ kN} \quad \text{Reaction @ Bottom}$$

$$R_{2\_3} := \frac{P_3 \cdot a}{L} \quad R_{2\_3} = 8.4 \text{ kN} \quad \text{Reaction @ Top}$$

### Moment

$$M_{a\_3} := \frac{P_3 \cdot a \cdot b}{L} \quad M_{a\_3} = 10.6 \text{ kN} \cdot \text{m} \quad \text{Moment @ Top}$$

### Deflection

$$w_{a\_3} := \frac{P_3 \cdot a^2 \cdot b^2}{3 \cdot EI \cdot L} \quad w_{a\_3} = 0.6 \text{ mm} \quad \text{Deflection @ Load Point}$$

## Appendix G

### Summary

#### Step 1:

$$P := P_1 \qquad P_1 = 87.6 \text{ kN}$$

$$R_1 := R_{1\_1} \qquad R_1 = 81.1 \text{ kN}$$

$$R_2 := R_{2\_1} \qquad R_2 = 6.5 \text{ kN}$$

$$w_a := w_{a\_1} \qquad w_a = 0.2 \text{ mm}$$

#### Step 2:

$$P' := P_1 + P_2 \qquad P' = 187.7 \text{ kN}$$

$$R'_1 := R_{1\_1} + R_{1\_2} \qquad R'_1 = 156.4 \text{ kN}$$

$$R'_2 := R_{2\_1} + R_{2\_2} \qquad R'_2 = 31.3 \text{ kN}$$

$$w'_a := w_{a\_1} + w_{a\_2} \qquad w'_a = 1.0 \text{ mm}$$

#### Step 3:

$$P'' := P_1 + P_2 + P_3 \qquad P'' = 238.4 \text{ kN}$$

$$R''_1 := R_{1\_1} + R_{1\_2} + R_{1\_3} \qquad R''_1 = 198.7 \text{ kN}$$

$$R''_2 := R_{2\_1} + R_{2\_2} + R_{2\_3} \qquad R''_2 = 39.7 \text{ kN}$$

$$w''_a := w_{a\_1} + w_{a\_2} + w_{a\_3} \qquad w''_a = 1.6 \text{ mm}$$



## **APPENDIX H**

### **SIMPLIFIED BLAST ANALYSES OF RC COLUMN TESTS**

This appendix provides details on the simplified analyses of the RC columns for Test 1 and Test 2 to calculate the maximum deformations of the columns under blast loading. The maximum deformations were obtained using an equivalent SDOF system and energy conservation. The maximum deformation and plastic rotation at base respectively resulted in 19.2 mm and 4.4 deg for Test 1 and 9.5 mm and 2.2 deg for Test 2.

## Appendix H

--- Test Specimen: Column RC1, Test 1 ---

w=W lb-TNT, x=2.16X, z=0.25m

### INELASTIC RESPONSE OF A RC COLUMN UNDER BLAST LOADING

<b>Geometry:</b>	Height of the column:	$L := 59\text{in}$
	Outside diameter of the column:	$D := 8\cdot\text{in}$
	Concrete cover:	$c := 0.5\cdot\text{in}$
	Diameter of longitudinal bar:	$d_l := 0.195\cdot\text{in}$
	Center to center diameter of perimeter hoop:	$D'' := D - 2\cdot c - d_l$ $D'' = 6.805\text{ in}$
	Area of section:	$A_c := \frac{D^2 \cdot \pi}{4}$ $A_c = 32429\text{ mm}^2$

Assumed boundary conditions: [fixed at the bottom](#), [fixed at the top](#).

**Blast load parameters:** (these parameters were obtained using BEL)

Height of charge:	$H := 0.25\cdot\text{m}$	$H = 0.820\text{ ft}$
Equivalent uniform pressure:	$p_r := 9280\cdot\text{psi}$	$p_r = 64.0\text{ MPa}$
Equivalent uniform impulse:	$i_r := 880.7\cdot\text{psi}\cdot\text{msec}$	$i_r = 6.07\text{ MPa}\cdot\text{msec}$
Time parameter:	$t_d := \frac{i_r \cdot 2}{p_r}$	$t_d = 0.19\text{ msec}$

## Appendix H

### Inelastic deformation of the column:

Moment curvature Analysis of RC column:  
(using XTRACT)

Plastic moment Capacity:  $M_p := 124.0 \cdot \text{kip} \cdot \text{in}$   $M_p = 14.01 \text{ kN} \cdot \text{m}$

Equivalent flexural stiffness:  $EI_e := 161600 \cdot \text{kip} \cdot \text{in}^2$   $EI_e = 464 \text{ kN} \cdot \text{m}^2$

Inelastic deformation:

Equivalent elastic stiffness per unit length:  $K_E := \frac{307 \cdot EI_e}{L^4}$   $K_E = 28229 \frac{\text{kN}}{\text{m}^2}$

Load - mass factor:  $K_{LM} := 0.66$

Mass per unit length:  $\text{mass} := A_c \cdot 2500 \cdot \frac{\text{kg}}{\text{m}^3}$   $\text{mass} = 81 \frac{\text{kg}}{\text{m}}$

Ultimate resistance per unit length:  $r_u := \frac{28.8 \cdot M_p}{L^2}$   $r_u = 180 \frac{\text{kN}}{\text{m}}$

Deflection at yielding:  $X_E := \frac{r_u}{K_E}$   $X_E = 6.4 \text{ mm}$

Shape factor of circular column:  $\beta := 0.450$

Impulse per unit length:  $i := \beta \cdot D \cdot i_r$

Inelastic deformation demand:  $X_d := \frac{i^2}{2 \cdot K_{LM} \cdot \text{mass} \cdot r_u} + \frac{X_E}{2}$   $X_d = 19.2 \text{ mm}$

$X_d - X_E = 12.9 \text{ mm}$

Plastic rotation:  $\theta := \text{atan}\left(\frac{X_d}{H}\right)$   $\theta = 0.077 \text{ rad}$   $\theta = 4.4 \text{ deg}$

## Appendix H

--- Test Specimen: Column RC2, Test 2 ---

w=W lb-TNT, x=3.25X, z=0.25m

### INELASTIC RESPONSE OF A RC COLUMN UNDER BLAST LOADING

<b>Geometry:</b>	Height of the column:	$L := 59\text{in}$
	Outside diameter of the column:	$D := 8\cdot\text{in}$
	Concrete cover:	$c := 0.5\cdot\text{in}$
	Diameter of longitudinal bar:	$d_l := 0.195\cdot\text{in}$
	Center to center diameter of perimeter hoop:	$D'' := D - 2\cdot c - d_l \quad D'' = 6.805\text{ in}$
	Area of section:	$A_c := \frac{D^2 \cdot \pi}{4} \quad A_c = 32429\text{ mm}^2$

Assumed boundary conditions: [fixed at the bottom](#), [fixed at the top](#).

**Blast load parameters:** (these parameters were obtained using BEL)

Height of charge:	$H := 0.25\cdot\text{m}$	
Equivalent uniform pressure:	$p_r := 5438\cdot\text{psi}$	$p_r = 37.5\text{ MPa}$
Equivalent uniform impulse:	$i_r := 552\cdot\text{psi}\cdot\text{msec}$	$i_r = 3.81\text{ MPa}\cdot\text{msec}$
Time parameter:	$t_d := \frac{i_r \cdot 2}{p_r}$	$t_d = 0.20\text{ msec}$



## Appendix H

### Inelastic deformation of the column:

Moment curvature Analysis of RC column:  
(using XTRACT)

Plastic moment Capacity:  $M_p := 124.0 \cdot \text{kip} \cdot \text{in}$   $M_p = 14.01 \text{ kN} \cdot \text{m}$

Equivalent flexural stiffness:  $EI_e := 161600 \cdot \text{kip} \cdot \text{in}^2$   $EI_e = 464 \text{ kN} \cdot \text{m}^2$

Inelastic deformation:

Equivalent elastic stiffness per unit length:  $K_E := \frac{307 \cdot EI_e}{L^4}$   $K_E = 28229 \frac{\text{kN}}{\text{m}^2}$

Load - mass factor:  $K_{LM} := 0.66$

Mass per unit length:  $\text{mass} := A_c \cdot 2500 \cdot \frac{\text{kg}}{\text{m}^3}$   $\text{mass} = 81 \frac{\text{kg}}{\text{m}}$

Ultimate resistance per unit length:  $r_u := \frac{28.8 \cdot M_p}{L^2}$   $r_u = 180 \frac{\text{kN}}{\text{m}}$

Deflection at yielding:  $X_E := \frac{r_u}{K_E}$   $X_E = 6.4 \text{ mm}$

Shape factor of circular column:  $\beta := 0.450$

Impulse per unit length:  $i := \beta \cdot D \cdot i_r$

Inelastic deformation demand:  $X_d := \frac{i^2}{2 \cdot K_{LM} \cdot \text{mass} \cdot r_u} + \frac{X_E}{2}$   $X_d = 9.5 \text{ mm}$

$X_d - X_E = 3.1 \text{ mm}$

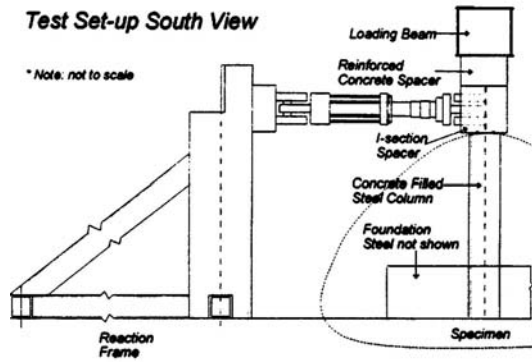
Plastic rotation:  $\theta := \text{atan}\left(\frac{X_d}{H}\right)$   $\theta = 0.038 \text{ rad}$   $\theta = 2.2 \text{ deg}$



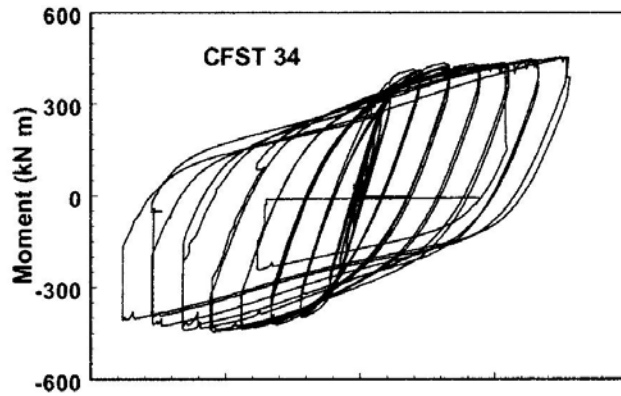
# **APPENDIX I**

## **CYLCIC ANALYSIS TEST SETUP AND HYSTERESIS LOOPS FOR FIBER-BASED MODEL VERIFICATION**

This appendix provides details on the cyclic analysis test setups and hysteresis loops for fiber-based analysis verification. Figures I-1 to I-6 show the test setups and the hysteresis loops experimentally obtained for CFST-34, CFST-42, RC-TP60, RC-Unit9, SJ-Unit4, and SJ-CR2 Column, respectively.

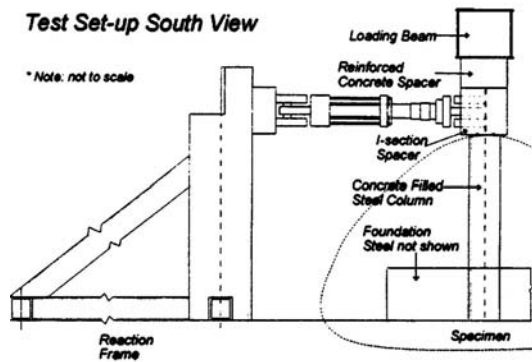


(a) Specimen

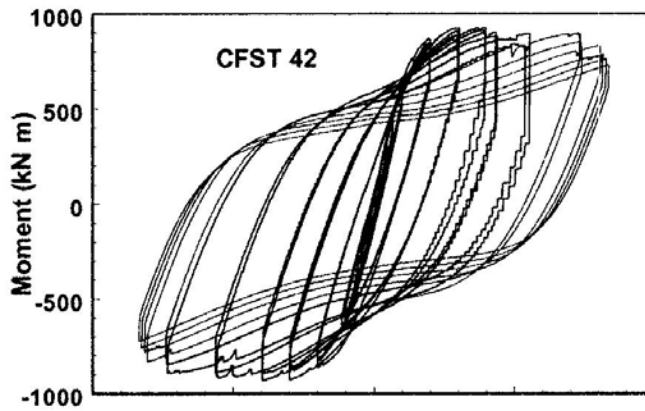


(b) Hysteresis Loops

**Figure I-1 Specimen and Hysteresis Loops for CFST-34 (Marson and Bruneau 2004)**



(a) Specimen



(b) Hysteresis Loops

**Figure I-2 Specimen and Hysteresis Loops for CFST-34 (Marson and Bruneau 2004)**

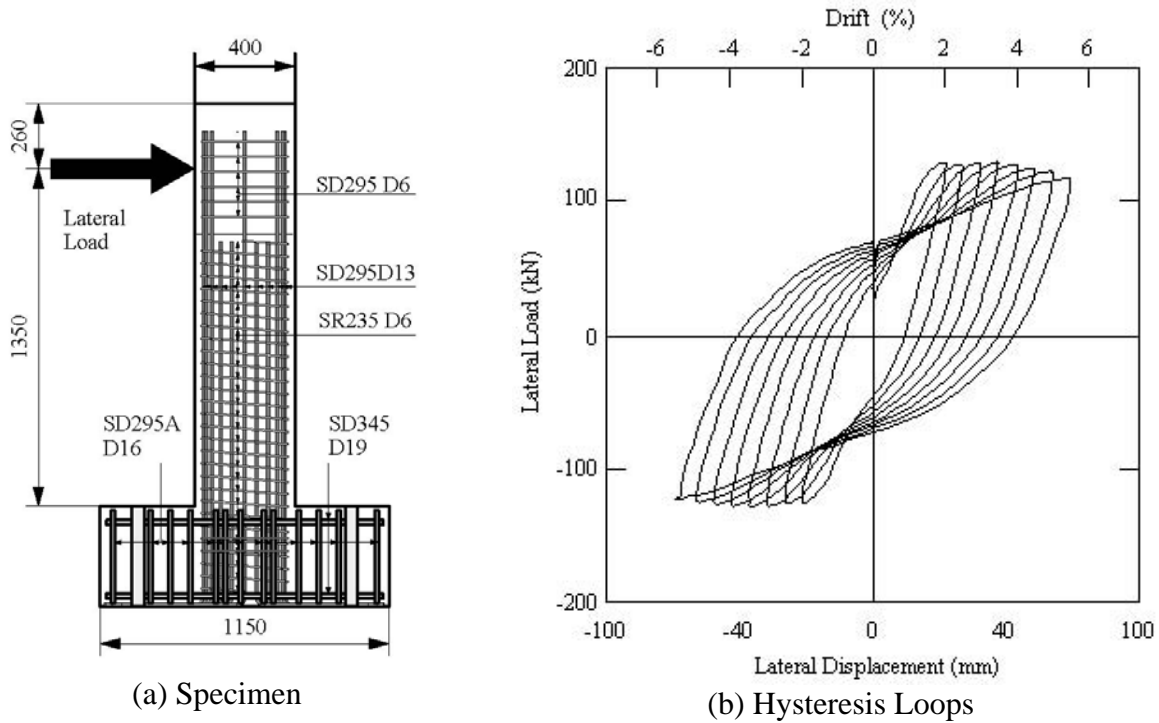


Figure I-3 Specimen and Hysteresis Loops for RC-TP60 (Matsukawa et al. 2002)

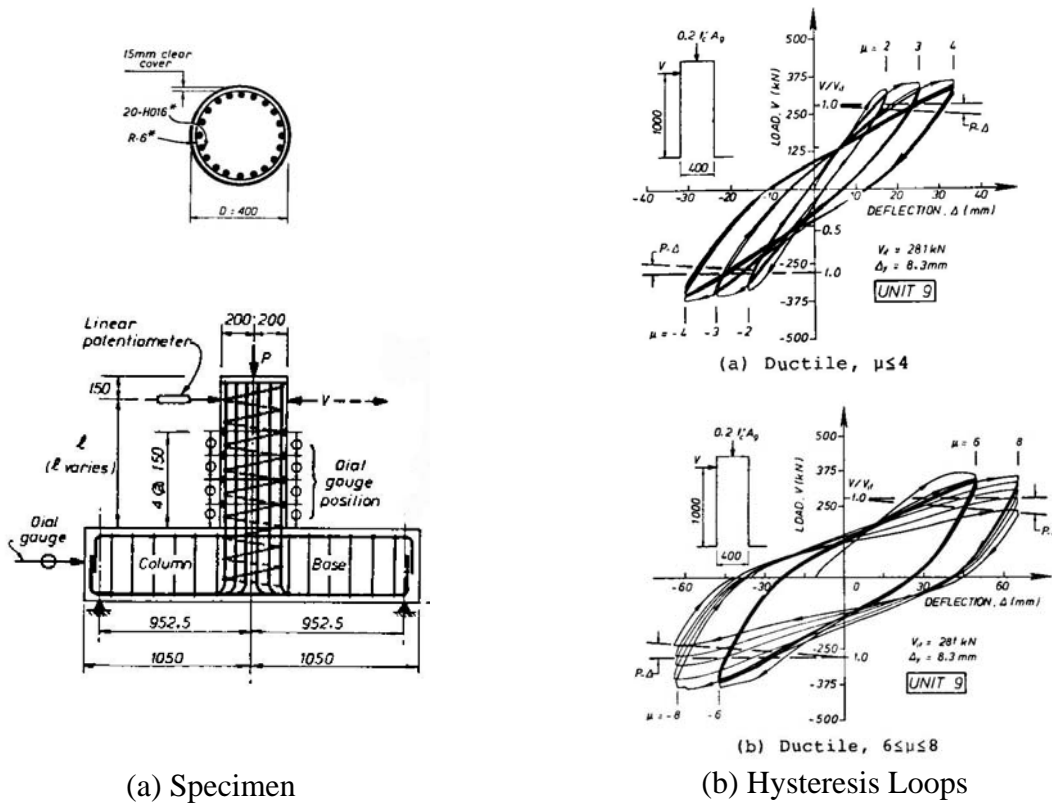
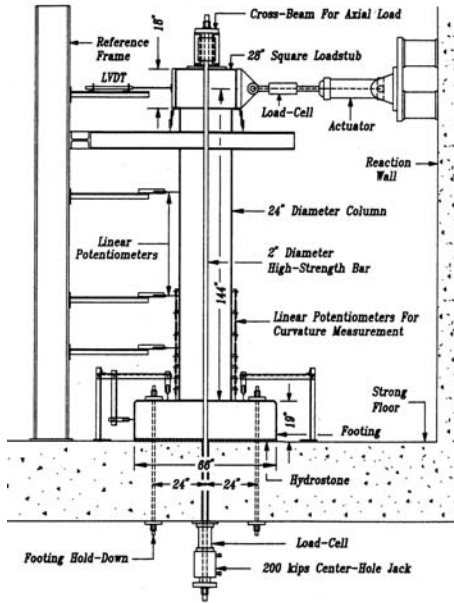
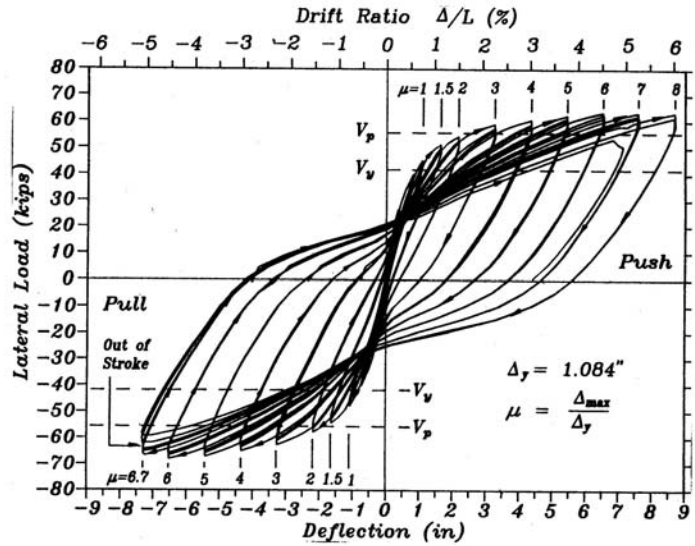


Figure I-4 Specimen and Hysteresis Loops for RC-Unit9 (Ghee et al. 1989)

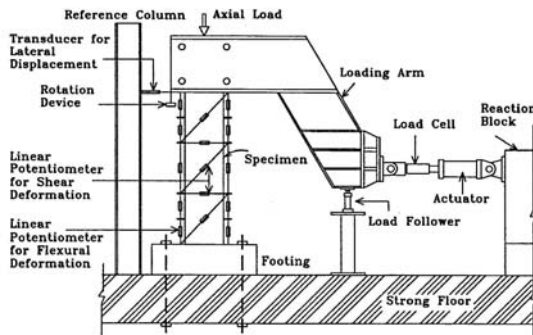


(a) Specimen

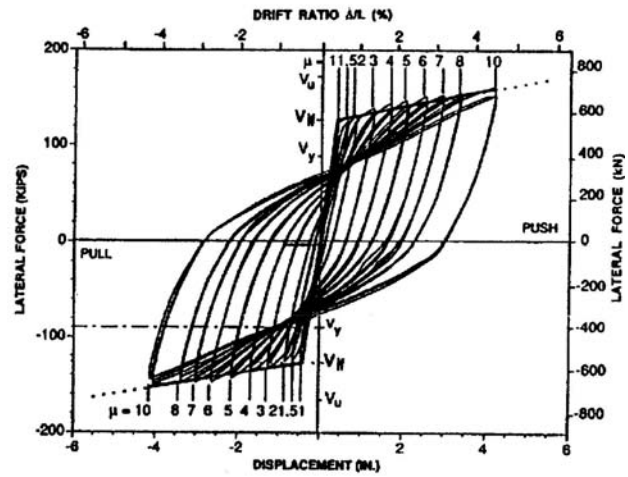


(b) Hysteresis Loops

Figure I-5 Specimen and Hysteresis Loops for SJ-Unit4 (Chai et al. 1991)



(a) Specimen



(b) Hysteresis Loops

Figure I-6 Specimen and Hysteresis Loops for SJ-CR2 (Priestley et al. 1994a, 1994b)

## MCEER Technical Reports

MCEER publishes technical reports on a variety of subjects written by authors funded through MCEER. These reports are available from both MCEER Publications and the National Technical Information Service (NTIS). Requests for reports should be directed to MCEER Publications, MCEER, University at Buffalo, State University of New York, Red Jacket Quadrangle, Buffalo, New York 14261. Reports can also be requested through NTIS, 5285 Port Royal Road, Springfield, Virginia 22161. NTIS accession numbers are shown in parenthesis, if available.

- NCEER-87-0001 "First-Year Program in Research, Education and Technology Transfer," 3/5/87, (PB88-134275, A04, MF-A01).
- NCEER-87-0002 "Experimental Evaluation of Instantaneous Optimal Algorithms for Structural Control," by R.C. Lin, T.T. Soong and A.M. Reinhorn, 4/20/87, (PB88-134341, A04, MF-A01).
- NCEER-87-0003 "Experimentation Using the Earthquake Simulation Facilities at University at Buffalo," by A.M. Reinhorn and R.L. Ketter, to be published.
- NCEER-87-0004 "The System Characteristics and Performance of a Shaking Table," by J.S. Hwang, K.C. Chang and G.C. Lee, 6/1/87, (PB88-134259, A03, MF-A01). This report is available only through NTIS (see address given above).
- NCEER-87-0005 "A Finite Element Formulation for Nonlinear Viscoplastic Material Using a Q Model," by O. Gyebe and G. Dasgupta, 11/2/87, (PB88-213764, A08, MF-A01).
- NCEER-87-0006 "Symbolic Manipulation Program (SMP) - Algebraic Codes for Two and Three Dimensional Finite Element Formulations," by X. Lee and G. Dasgupta, 11/9/87, (PB88-218522, A05, MF-A01).
- NCEER-87-0007 "Instantaneous Optimal Control Laws for Tall Buildings Under Seismic Excitations," by J.N. Yang, A. Akbarpour and P. Ghaemmaghami, 6/10/87, (PB88-134333, A06, MF-A01). This report is only available through NTIS (see address given above).
- NCEER-87-0008 "IDARC: Inelastic Damage Analysis of Reinforced Concrete Frame - Shear-Wall Structures," by Y.J. Park, A.M. Reinhorn and S.K. Kunnath, 7/20/87, (PB88-134325, A09, MF-A01). This report is only available through NTIS (see address given above).
- NCEER-87-0009 "Liquefaction Potential for New York State: A Preliminary Report on Sites in Manhattan and Buffalo," by M. Budhu, V. Vijayakumar, R.F. Giese and L. Baumgras, 8/31/87, (PB88-163704, A03, MF-A01). This report is available only through NTIS (see address given above).
- NCEER-87-0010 "Vertical and Torsional Vibration of Foundations in Inhomogeneous Media," by A.S. Veletsos and K.W. Dotson, 6/1/87, (PB88-134291, A03, MF-A01). This report is only available through NTIS (see address given above).
- NCEER-87-0011 "Seismic Probabilistic Risk Assessment and Seismic Margins Studies for Nuclear Power Plants," by Howard H.M. Hwang, 6/15/87, (PB88-134267, A03, MF-A01). This report is only available through NTIS (see address given above).
- NCEER-87-0012 "Parametric Studies of Frequency Response of Secondary Systems Under Ground-Acceleration Excitations," by Y. Yong and Y.K. Lin, 6/10/87, (PB88-134309, A03, MF-A01). This report is only available through NTIS (see address given above).
- NCEER-87-0013 "Frequency Response of Secondary Systems Under Seismic Excitation," by J.A. HoLung, J. Cai and Y.K. Lin, 7/31/87, (PB88-134317, A05, MF-A01). This report is only available through NTIS (see address given above).
- NCEER-87-0014 "Modelling Earthquake Ground Motions in Seismically Active Regions Using Parametric Time Series Methods," by G.W. Ellis and A.S. Cakmak, 8/25/87, (PB88-134283, A08, MF-A01). This report is only available through NTIS (see address given above).
- NCEER-87-0015 "Detection and Assessment of Seismic Structural Damage," by E. DiPasquale and A.S. Cakmak, 8/25/87, (PB88-163712, A05, MF-A01). This report is only available through NTIS (see address given above).

- NCEER-87-0016 "Pipeline Experiment at Parkfield, California," by J. Isenberg and E. Richardson, 9/15/87, (PB88-163720, A03, MF-A01). This report is available only through NTIS (see address given above).
- NCEER-87-0017 "Digital Simulation of Seismic Ground Motion," by M. Shinozuka, G. Deodatis and T. Harada, 8/31/87, (PB88-155197, A04, MF-A01). This report is available only through NTIS (see address given above).
- NCEER-87-0018 "Practical Considerations for Structural Control: System Uncertainty, System Time Delay and Truncation of Small Control Forces," J.N. Yang and A. Akbarpour, 8/10/87, (PB88-163738, A08, MF-A01). This report is only available through NTIS (see address given above).
- NCEER-87-0019 "Modal Analysis of Nonclassically Damped Structural Systems Using Canonical Transformation," by J.N. Yang, S. Sarkani and F.X. Long, 9/27/87, (PB88-187851, A04, MF-A01).
- NCEER-87-0020 "A Nonstationary Solution in Random Vibration Theory," by J.R. Red-Horse and P.D. Spanos, 11/3/87, (PB88-163746, A03, MF-A01).
- NCEER-87-0021 "Horizontal Impedances for Radially Inhomogeneous Viscoelastic Soil Layers," by A.S. Veletsos and K.W. Dotson, 10/15/87, (PB88-150859, A04, MF-A01).
- NCEER-87-0022 "Seismic Damage Assessment of Reinforced Concrete Members," by Y.S. Chung, C. Meyer and M. Shinozuka, 10/9/87, (PB88-150867, A05, MF-A01). This report is available only through NTIS (see address given above).
- NCEER-87-0023 "Active Structural Control in Civil Engineering," by T.T. Soong, 11/11/87, (PB88-187778, A03, MF-A01).
- NCEER-87-0024 "Vertical and Torsional Impedances for Radially Inhomogeneous Viscoelastic Soil Layers," by K.W. Dotson and A.S. Veletsos, 12/87, (PB88-187786, A03, MF-A01).
- NCEER-87-0025 "Proceedings from the Symposium on Seismic Hazards, Ground Motions, Soil-Liquefaction and Engineering Practice in Eastern North America," October 20-22, 1987, edited by K.H. Jacob, 12/87, (PB88-188115, A23, MF-A01). This report is available only through NTIS (see address given above).
- NCEER-87-0026 "Report on the Whittier-Narrows, California, Earthquake of October 1, 1987," by J. Pantelic and A. Reinhorn, 11/87, (PB88-187752, A03, MF-A01). This report is available only through NTIS (see address given above).
- NCEER-87-0027 "Design of a Modular Program for Transient Nonlinear Analysis of Large 3-D Building Structures," by S. Srivastav and J.F. Abel, 12/30/87, (PB88-187950, A05, MF-A01). This report is only available through NTIS (see address given above).
- NCEER-87-0028 "Second-Year Program in Research, Education and Technology Transfer," 3/8/88, (PB88-219480, A04, MF-A01).
- NCEER-88-0001 "Workshop on Seismic Computer Analysis and Design of Buildings With Interactive Graphics," by W. McGuire, J.F. Abel and C.H. Conley, 1/18/88, (PB88-187760, A03, MF-A01). This report is only available through NTIS (see address given above).
- NCEER-88-0002 "Optimal Control of Nonlinear Flexible Structures," by J.N. Yang, F.X. Long and D. Wong, 1/22/88, (PB88-213772, A06, MF-A01).
- NCEER-88-0003 "Substructuring Techniques in the Time Domain for Primary-Secondary Structural Systems," by G.D. Manolis and G. Juhn, 2/10/88, (PB88-213780, A04, MF-A01).
- NCEER-88-0004 "Iterative Seismic Analysis of Primary-Secondary Systems," by A. Singhal, L.D. Lutes and P.D. Spanos, 2/23/88, (PB88-213798, A04, MF-A01).
- NCEER-88-0005 "Stochastic Finite Element Expansion for Random Media," by P.D. Spanos and R. Ghanem, 3/14/88, (PB88-213806, A03, MF-A01).



- NCEER-88-0006 "Combining Structural Optimization and Structural Control," by F.Y. Cheng and C.P. Pantelides, 1/10/88, (PB88-213814, A05, MF-A01).
- NCEER-88-0007 "Seismic Performance Assessment of Code-Designed Structures," by H.H-M. Hwang, J-W. Jaw and H-J. Shau, 3/20/88, (PB88-219423, A04, MF-A01). This report is only available through NTIS (see address given above).
- NCEER-88-0008 "Reliability Analysis of Code-Designed Structures Under Natural Hazards," by H.H-M. Hwang, H. Ushiba and M. Shinozuka, 2/29/88, (PB88-229471, A07, MF-A01). This report is only available through NTIS (see address given above).
- NCEER-88-0009 "Seismic Fragility Analysis of Shear Wall Structures," by J-W Jaw and H.H-M. Hwang, 4/30/88, (PB89-102867, A04, MF-A01).
- NCEER-88-0010 "Base Isolation of a Multi-Story Building Under a Harmonic Ground Motion - A Comparison of Performances of Various Systems," by F-G Fan, G. Ahmadi and I.G. Tadjbakhsh, 5/18/88, (PB89-122238, A06, MF-A01). This report is only available through NTIS (see address given above).
- NCEER-88-0011 "Seismic Floor Response Spectra for a Combined System by Green's Functions," by F.M. Lavelle, L.A. Bergman and P.D. Spanos, 5/1/88, (PB89-102875, A03, MF-A01).
- NCEER-88-0012 "A New Solution Technique for Randomly Excited Hysteretic Structures," by G.Q. Cai and Y.K. Lin, 5/16/88, (PB89-102883, A03, MF-A01).
- NCEER-88-0013 "A Study of Radiation Damping and Soil-Structure Interaction Effects in the Centrifuge," by K. Weissman, supervised by J.H. Prevost, 5/24/88, (PB89-144703, A06, MF-A01).
- NCEER-88-0014 "Parameter Identification and Implementation of a Kinematic Plasticity Model for Frictional Soils," by J.H. Prevost and D.V. Griffiths, to be published.
- NCEER-88-0015 "Two- and Three- Dimensional Dynamic Finite Element Analyses of the Long Valley Dam," by D.V. Griffiths and J.H. Prevost, 6/17/88, (PB89-144711, A04, MF-A01).
- NCEER-88-0016 "Damage Assessment of Reinforced Concrete Structures in Eastern United States," by A.M. Reinhorn, M.J. Seidel, S.K. Kunnath and Y.J. Park, 6/15/88, (PB89-122220, A04, MF-A01). This report is only available through NTIS (see address given above).
- NCEER-88-0017 "Dynamic Compliance of Vertically Loaded Strip Foundations in Multilayered Viscoelastic Soils," by S. Ahmad and A.S.M. Israil, 6/17/88, (PB89-102891, A04, MF-A01).
- NCEER-88-0018 "An Experimental Study of Seismic Structural Response With Added Viscoelastic Dampers," by R.C. Lin, Z. Liang, T.T. Soong and R.H. Zhang, 6/30/88, (PB89-122212, A05, MF-A01). This report is available only through NTIS (see address given above).
- NCEER-88-0019 "Experimental Investigation of Primary - Secondary System Interaction," by G.D. Manolis, G. Juhn and A.M. Reinhorn, 5/27/88, (PB89-122204, A04, MF-A01).
- NCEER-88-0020 "A Response Spectrum Approach For Analysis of Nonclassically Damped Structures," by J.N. Yang, S. Sarkani and F.X. Long, 4/22/88, (PB89-102909, A04, MF-A01).
- NCEER-88-0021 "Seismic Interaction of Structures and Soils: Stochastic Approach," by A.S. Veletsos and A.M. Prasad, 7/21/88, (PB89-122196, A04, MF-A01). This report is only available through NTIS (see address given above).
- NCEER-88-0022 "Identification of the Serviceability Limit State and Detection of Seismic Structural Damage," by E. DiPasquale and A.S. Cakmak, 6/15/88, (PB89-122188, A05, MF-A01). This report is available only through NTIS (see address given above).
- NCEER-88-0023 "Multi-Hazard Risk Analysis: Case of a Simple Offshore Structure," by B.K. Bhartia and E.H. Vanmarcke, 7/21/88, (PB89-145213, A05, MF-A01).

- NCEER-88-0024 "Automated Seismic Design of Reinforced Concrete Buildings," by Y.S. Chung, C. Meyer and M. Shinozuka, 7/5/88, (PB89-122170, A06, MF-A01). This report is available only through NTIS (see address given above).
- NCEER-88-0025 "Experimental Study of Active Control of MDOF Structures Under Seismic Excitations," by L.L. Chung, R.C. Lin, T.T. Soong and A.M. Reinhorn, 7/10/88, (PB89-122600, A04, MF-A01).
- NCEER-88-0026 "Earthquake Simulation Tests of a Low-Rise Metal Structure," by J.S. Hwang, K.C. Chang, G.C. Lee and R.L. Ketter, 8/1/88, (PB89-102917, A04, MF-A01).
- NCEER-88-0027 "Systems Study of Urban Response and Reconstruction Due to Catastrophic Earthquakes," by F. Kozin and H.K. Zhou, 9/22/88, (PB90-162348, A04, MF-A01).
- NCEER-88-0028 "Seismic Fragility Analysis of Plane Frame Structures," by H.H-M. Hwang and Y.K. Low, 7/31/88, (PB89-131445, A06, MF-A01).
- NCEER-88-0029 "Response Analysis of Stochastic Structures," by A. Kardara, C. Bucher and M. Shinozuka, 9/22/88, (PB89-174429, A04, MF-A01).
- NCEER-88-0030 "Nonnormal Accelerations Due to Yielding in a Primary Structure," by D.C.K. Chen and L.D. Lutes, 9/19/88, (PB89-131437, A04, MF-A01).
- NCEER-88-0031 "Design Approaches for Soil-Structure Interaction," by A.S. Veletsos, A.M. Prasad and Y. Tang, 12/30/88, (PB89-174437, A03, MF-A01). This report is available only through NTIS (see address given above).
- NCEER-88-0032 "A Re-evaluation of Design Spectra for Seismic Damage Control," by C.J. Turkstra and A.G. Tallin, 11/7/88, (PB89-145221, A05, MF-A01).
- NCEER-88-0033 "The Behavior and Design of Noncontact Lap Splices Subjected to Repeated Inelastic Tensile Loading," by V.E. Sagan, P. Gergely and R.N. White, 12/8/88, (PB89-163737, A08, MF-A01).
- NCEER-88-0034 "Seismic Response of Pile Foundations," by S.M. Mamoon, P.K. Banerjee and S. Ahmad, 11/1/88, (PB89-145239, A04, MF-A01).
- NCEER-88-0035 "Modeling of R/C Building Structures With Flexible Floor Diaphragms (IDARC2)," by A.M. Reinhorn, S.K. Kunnath and N. Panahshahi, 9/7/88, (PB89-207153, A07, MF-A01).
- NCEER-88-0036 "Solution of the Dam-Reservoir Interaction Problem Using a Combination of FEM, BEM with Particular Integrals, Modal Analysis, and Substructuring," by C-S. Tsai, G.C. Lee and R.L. Ketter, 12/31/88, (PB89-207146, A04, MF-A01).
- NCEER-88-0037 "Optimal Placement of Actuators for Structural Control," by F.Y. Cheng and C.P. Pantelides, 8/15/88, (PB89-162846, A05, MF-A01).
- NCEER-88-0038 "Teflon Bearings in Aseismic Base Isolation: Experimental Studies and Mathematical Modeling," by A. Mokha, M.C. Constantinou and A.M. Reinhorn, 12/5/88, (PB89-218457, A10, MF-A01). This report is available only through NTIS (see address given above).
- NCEER-88-0039 "Seismic Behavior of Flat Slab High-Rise Buildings in the New York City Area," by P. Weidlinger and M. Ettouney, 10/15/88, (PB90-145681, A04, MF-A01).
- NCEER-88-0040 "Evaluation of the Earthquake Resistance of Existing Buildings in New York City," by P. Weidlinger and M. Ettouney, 10/15/88, to be published.
- NCEER-88-0041 "Small-Scale Modeling Techniques for Reinforced Concrete Structures Subjected to Seismic Loads," by W. Kim, A. El-Attar and R.N. White, 11/22/88, (PB89-189625, A05, MF-A01).
- NCEER-88-0042 "Modeling Strong Ground Motion from Multiple Event Earthquakes," by G.W. Ellis and A.S. Cakmak, 10/15/88, (PB89-174445, A03, MF-A01).

- NCEER-88-0043 "Nonstationary Models of Seismic Ground Acceleration," by M. Grigoriu, S.E. Ruiz and E. Rosenblueth, 7/15/88, (PB89-189617, A04, MF-A01).
- NCEER-88-0044 "SARCF User's Guide: Seismic Analysis of Reinforced Concrete Frames," by Y.S. Chung, C. Meyer and M. Shinozuka, 11/9/88, (PB89-174452, A08, MF-A01).
- NCEER-88-0045 "First Expert Panel Meeting on Disaster Research and Planning," edited by J. Pantelic and J. Stoyke, 9/15/88, (PB89-174460, A05, MF-A01).
- NCEER-88-0046 "Preliminary Studies of the Effect of Degrading Infill Walls on the Nonlinear Seismic Response of Steel Frames," by C.Z. Chrysostomou, P. Gergely and J.F. Abel, 12/19/88, (PB89-208383, A05, MF-A01).
- NCEER-88-0047 "Reinforced Concrete Frame Component Testing Facility - Design, Construction, Instrumentation and Operation," by S.P. Pessiki, C. Conley, T. Bond, P. Gergely and R.N. White, 12/16/88, (PB89-174478, A04, MF-A01).
- NCEER-89-0001 "Effects of Protective Cushion and Soil Compliancy on the Response of Equipment Within a Seismically Excited Building," by J.A. HoLung, 2/16/89, (PB89-207179, A04, MF-A01).
- NCEER-89-0002 "Statistical Evaluation of Response Modification Factors for Reinforced Concrete Structures," by H.H-M. Hwang and J-W. Jaw, 2/17/89, (PB89-207187, A05, MF-A01).
- NCEER-89-0003 "Hysteretic Columns Under Random Excitation," by G-Q. Cai and Y.K. Lin, 1/9/89, (PB89-196513, A03, MF-A01).
- NCEER-89-0004 "Experimental Study of 'Elephant Foot Bulge' Instability of Thin-Walled Metal Tanks," by Z-H. Jia and R.L. Ketter, 2/22/89, (PB89-207195, A03, MF-A01).
- NCEER-89-0005 "Experiment on Performance of Buried Pipelines Across San Andreas Fault," by J. Isenberg, E. Richardson and T.D. O'Rourke, 3/10/89, (PB89-218440, A04, MF-A01). This report is available only through NTIS (see address given above).
- NCEER-89-0006 "A Knowledge-Based Approach to Structural Design of Earthquake-Resistant Buildings," by M. Subramani, P. Gergely, C.H. Conley, J.F. Abel and A.H. Zaghaw, 1/15/89, (PB89-218465, A06, MF-A01).
- NCEER-89-0007 "Liquefaction Hazards and Their Effects on Buried Pipelines," by T.D. O'Rourke and P.A. Lane, 2/1/89, (PB89-218481, A09, MF-A01).
- NCEER-89-0008 "Fundamentals of System Identification in Structural Dynamics," by H. Imai, C-B. Yun, O. Maruyama and M. Shinozuka, 1/26/89, (PB89-207211, A04, MF-A01).
- NCEER-89-0009 "Effects of the 1985 Michoacan Earthquake on Water Systems and Other Buried Lifelines in Mexico," by A.G. Ayala and M.J. O'Rourke, 3/8/89, (PB89-207229, A06, MF-A01).
- NCEER-89-R010 "NCEER Bibliography of Earthquake Education Materials," by K.E.K. Ross, Second Revision, 9/1/89, (PB90-125352, A05, MF-A01). This report is replaced by NCEER-92-0018.
- NCEER-89-0011 "Inelastic Three-Dimensional Response Analysis of Reinforced Concrete Building Structures (IDARC-3D), Part I - Modeling," by S.K. Kunnath and A.M. Reinhorn, 4/17/89, (PB90-114612, A07, MF-A01). This report is available only through NTIS (see address given above).
- NCEER-89-0012 "Recommended Modifications to ATC-14," by C.D. Poland and J.O. Malley, 4/12/89, (PB90-108648, A15, MF-A01).
- NCEER-89-0013 "Repair and Strengthening of Beam-to-Column Connections Subjected to Earthquake Loading," by M. Corazao and A.J. Durrani, 2/28/89, (PB90-109885, A06, MF-A01).
- NCEER-89-0014 "Program EXKAL2 for Identification of Structural Dynamic Systems," by O. Maruyama, C-B. Yun, M. Hoshiya and M. Shinozuka, 5/19/89, (PB90-109877, A09, MF-A01).

- NCEER-89-0015 "Response of Frames With Bolted Semi-Rigid Connections, Part I - Experimental Study and Analytical Predictions," by P.J. DiCorso, A.M. Reinhorn, J.R. Dickerson, J.B. Radzinski and W.L. Harper, 6/1/89, to be published.
- NCEER-89-0016 "ARMA Monte Carlo Simulation in Probabilistic Structural Analysis," by P.D. Spanos and M.P. Mignolet, 7/10/89, (PB90-109893, A03, MF-A01).
- NCEER-89-P017 "Preliminary Proceedings from the Conference on Disaster Preparedness - The Place of Earthquake Education in Our Schools," Edited by K.E.K. Ross, 6/23/89, (PB90-108606, A03, MF-A01).
- NCEER-89-0017 "Proceedings from the Conference on Disaster Preparedness - The Place of Earthquake Education in Our Schools," Edited by K.E.K. Ross, 12/31/89, (PB90-207895, A012, MF-A02). This report is available only through NTIS (see address given above).
- NCEER-89-0018 "Multidimensional Models of Hysteretic Material Behavior for Vibration Analysis of Shape Memory Energy Absorbing Devices, by E.J. Graesser and F.A. Cozzarelli, 6/7/89, (PB90-164146, A04, MF-A01).
- NCEER-89-0019 "Nonlinear Dynamic Analysis of Three-Dimensional Base Isolated Structures (3D-BASIS)," by S. Nagarajaiah, A.M. Reinhorn and M.C. Constantinou, 8/3/89, (PB90-161936, A06, MF-A01). This report has been replaced by NCEER-93-0011.
- NCEER-89-0020 "Structural Control Considering Time-Rate of Control Forces and Control Rate Constraints," by F.Y. Cheng and C.P. Pantelides, 8/3/89, (PB90-120445, A04, MF-A01).
- NCEER-89-0021 "Subsurface Conditions of Memphis and Shelby County," by K.W. Ng, T-S. Chang and H-H.M. Hwang, 7/26/89, (PB90-120437, A03, MF-A01).
- NCEER-89-0022 "Seismic Wave Propagation Effects on Straight Jointed Buried Pipelines," by K. Elhmadi and M.J. O'Rourke, 8/24/89, (PB90-162322, A10, MF-A02).
- NCEER-89-0023 "Workshop on Serviceability Analysis of Water Delivery Systems," edited by M. Grigoriu, 3/6/89, (PB90-127424, A03, MF-A01).
- NCEER-89-0024 "Shaking Table Study of a 1/5 Scale Steel Frame Composed of Tapered Members," by K.C. Chang, J.S. Hwang and G.C. Lee, 9/18/89, (PB90-160169, A04, MF-A01).
- NCEER-89-0025 "DYNA1D: A Computer Program for Nonlinear Seismic Site Response Analysis - Technical Documentation," by Jean H. Prevost, 9/14/89, (PB90-161944, A07, MF-A01). This report is available only through NTIS (see address given above).
- NCEER-89-0026 "1:4 Scale Model Studies of Active Tendon Systems and Active Mass Dampers for Aseismic Protection," by A.M. Reinhorn, T.T. Soong, R.C. Lin, Y.P. Yang, Y. Fukao, H. Abe and M. Nakai, 9/15/89, (PB90-173246, A10, MF-A02). This report is available only through NTIS (see address given above).
- NCEER-89-0027 "Scattering of Waves by Inclusions in a Nonhomogeneous Elastic Half Space Solved by Boundary Element Methods," by P.K. Hadley, A. Askar and A.S. Cakmak, 6/15/89, (PB90-145699, A07, MF-A01).
- NCEER-89-0028 "Statistical Evaluation of Deflection Amplification Factors for Reinforced Concrete Structures," by H.H.M. Hwang, J-W. Jaw and A.L. Ch'ng, 8/31/89, (PB90-164633, A05, MF-A01).
- NCEER-89-0029 "Bedrock Accelerations in Memphis Area Due to Large New Madrid Earthquakes," by H.H.M. Hwang, C.H.S. Chen and G. Yu, 11/7/89, (PB90-162330, A04, MF-A01).
- NCEER-89-0030 "Seismic Behavior and Response Sensitivity of Secondary Structural Systems," by Y.Q. Chen and T.T. Soong, 10/23/89, (PB90-164658, A08, MF-A01).
- NCEER-89-0031 "Random Vibration and Reliability Analysis of Primary-Secondary Structural Systems," by Y. Ibrahim, M. Grigoriu and T.T. Soong, 11/10/89, (PB90-161951, A04, MF-A01).

- NCEER-89-0032 "Proceedings from the Second U.S. - Japan Workshop on Liquefaction, Large Ground Deformation and Their Effects on Lifelines, September 26-29, 1989," Edited by T.D. O'Rourke and M. Hamada, 12/1/89, (PB90-209388, A22, MF-A03).
- NCEER-89-0033 "Deterministic Model for Seismic Damage Evaluation of Reinforced Concrete Structures," by J.M. Bracci, A.M. Reinhorn, J.B. Mander and S.K. Kunnath, 9/27/89, (PB91-108803, A06, MF-A01).
- NCEER-89-0034 "On the Relation Between Local and Global Damage Indices," by E. DiPasquale and A.S. Cakmak, 8/15/89, (PB90-173865, A05, MF-A01).
- NCEER-89-0035 "Cyclic Undrained Behavior of Nonplastic and Low Plasticity Silts," by A.J. Walker and H.E. Stewart, 7/26/89, (PB90-183518, A10, MF-A01).
- NCEER-89-0036 "Liquefaction Potential of Surficial Deposits in the City of Buffalo, New York," by M. Budhu, R. Giese and L. Baumgrass, 1/17/89, (PB90-208455, A04, MF-A01).
- NCEER-89-0037 "A Deterministic Assessment of Effects of Ground Motion Incoherence," by A.S. Veletsos and Y. Tang, 7/15/89, (PB90-164294, A03, MF-A01).
- NCEER-89-0038 "Workshop on Ground Motion Parameters for Seismic Hazard Mapping," July 17-18, 1989, edited by R.V. Whitman, 12/1/89, (PB90-173923, A04, MF-A01).
- NCEER-89-0039 "Seismic Effects on Elevated Transit Lines of the New York City Transit Authority," by C.J. Costantino, C.A. Miller and E. Heymsfield, 12/26/89, (PB90-207887, A06, MF-A01).
- NCEER-89-0040 "Centrifugal Modeling of Dynamic Soil-Structure Interaction," by K. Weissman, Supervised by J.H. Prevost, 5/10/89, (PB90-207879, A07, MF-A01).
- NCEER-89-0041 "Linearized Identification of Buildings With Cores for Seismic Vulnerability Assessment," by I-K. Ho and A.E. Aktan, 11/1/89, (PB90-251943, A07, MF-A01).
- NCEER-90-0001 "Geotechnical and Lifeline Aspects of the October 17, 1989 Loma Prieta Earthquake in San Francisco," by T.D. O'Rourke, H.E. Stewart, F.T. Blackburn and T.S. Dickerman, 1/90, (PB90-208596, A05, MF-A01).
- NCEER-90-0002 "Nonnormal Secondary Response Due to Yielding in a Primary Structure," by D.C.K. Chen and L.D. Lutes, 2/28/90, (PB90-251976, A07, MF-A01).
- NCEER-90-0003 "Earthquake Education Materials for Grades K-12," by K.E.K. Ross, 4/16/90, (PB91-251984, A05, MF-A05). This report has been replaced by NCEER-92-0018.
- NCEER-90-0004 "Catalog of Strong Motion Stations in Eastern North America," by R.W. Busby, 4/3/90, (PB90-251984, A05, MF-A01).
- NCEER-90-0005 "NCEER Strong-Motion Data Base: A User Manual for the GeoBase Release (Version 1.0 for the Sun3)," by P. Friberg and K. Jacob, 3/31/90 (PB90-258062, A04, MF-A01).
- NCEER-90-0006 "Seismic Hazard Along a Crude Oil Pipeline in the Event of an 1811-1812 Type New Madrid Earthquake," by H.H.M. Hwang and C-H.S. Chen, 4/16/90, (PB90-258054, A04, MF-A01).
- NCEER-90-0007 "Site-Specific Response Spectra for Memphis Sheahan Pumping Station," by H.H.M. Hwang and C.S. Lee, 5/15/90, (PB91-108811, A05, MF-A01).
- NCEER-90-0008 "Pilot Study on Seismic Vulnerability of Crude Oil Transmission Systems," by T. Ariman, R. Dobry, M. Grigoriu, F. Kozin, M. O'Rourke, T. O'Rourke and M. Shinozuka, 5/25/90, (PB91-108837, A06, MF-A01).
- NCEER-90-0009 "A Program to Generate Site Dependent Time Histories: EQGEN," by G.W. Ellis, M. Srinivasan and A.S. Cakmak, 1/30/90, (PB91-108829, A04, MF-A01).
- NCEER-90-0010 "Active Isolation for Seismic Protection of Operating Rooms," by M.E. Talbott, Supervised by M. Shinozuka, 6/8/9, (PB91-110205, A05, MF-A01).

- NCEER-90-0011 "Program LINEARID for Identification of Linear Structural Dynamic Systems," by C-B. Yun and M. Shinozuka, 6/25/90, (PB91-110312, A08, MF-A01).
- NCEER-90-0012 "Two-Dimensional Two-Phase Elasto-Plastic Seismic Response of Earth Dams," by A.N. Yiagos, Supervised by J.H. Prevost, 6/20/90, (PB91-110197, A13, MF-A02).
- NCEER-90-0013 "Secondary Systems in Base-Isolated Structures: Experimental Investigation, Stochastic Response and Stochastic Sensitivity," by G.D. Manolis, G. Juhn, M.C. Constantinou and A.M. Reinhorn, 7/1/90, (PB91-110320, A08, MF-A01).
- NCEER-90-0014 "Seismic Behavior of Lightly-Reinforced Concrete Column and Beam-Column Joint Details," by S.P. Pessiki, C.H. Conley, P. Gergely and R.N. White, 8/22/90, (PB91-108795, A11, MF-A02).
- NCEER-90-0015 "Two Hybrid Control Systems for Building Structures Under Strong Earthquakes," by J.N. Yang and A. Daniellians, 6/29/90, (PB91-125393, A04, MF-A01).
- NCEER-90-0016 "Instantaneous Optimal Control with Acceleration and Velocity Feedback," by J.N. Yang and Z. Li, 6/29/90, (PB91-125401, A03, MF-A01).
- NCEER-90-0017 "Reconnaissance Report on the Northern Iran Earthquake of June 21, 1990," by M. Mehrain, 10/4/90, (PB91-125377, A03, MF-A01).
- NCEER-90-0018 "Evaluation of Liquefaction Potential in Memphis and Shelby County," by T.S. Chang, P.S. Tang, C.S. Lee and H. Hwang, 8/10/90, (PB91-125427, A09, MF-A01).
- NCEER-90-0019 "Experimental and Analytical Study of a Combined Sliding Disc Bearing and Helical Steel Spring Isolation System," by M.C. Constantinou, A.S. Mokha and A.M. Reinhorn, 10/4/90, (PB91-125385, A06, MF-A01). This report is available only through NTIS (see address given above).
- NCEER-90-0020 "Experimental Study and Analytical Prediction of Earthquake Response of a Sliding Isolation System with a Spherical Surface," by A.S. Mokha, M.C. Constantinou and A.M. Reinhorn, 10/11/90, (PB91-125419, A05, MF-A01).
- NCEER-90-0021 "Dynamic Interaction Factors for Floating Pile Groups," by G. Gazetas, K. Fan, A. Kaynia and E. Kausel, 9/10/90, (PB91-170381, A05, MF-A01).
- NCEER-90-0022 "Evaluation of Seismic Damage Indices for Reinforced Concrete Structures," by S. Rodriguez-Gomez and A.S. Cakmak, 9/30/90, PB91-171322, A06, MF-A01).
- NCEER-90-0023 "Study of Site Response at a Selected Memphis Site," by H. Desai, S. Ahmad, E.S. Gazetas and M.R. Oh, 10/11/90, (PB91-196857, A03, MF-A01).
- NCEER-90-0024 "A User's Guide to Strongmo: Version 1.0 of NCEER's Strong-Motion Data Access Tool for PCs and Terminals," by P.A. Friberg and C.A.T. Susch, 11/15/90, (PB91-171272, A03, MF-A01).
- NCEER-90-0025 "A Three-Dimensional Analytical Study of Spatial Variability of Seismic Ground Motions," by L-L. Hong and A.H.-S. Ang, 10/30/90, (PB91-170399, A09, MF-A01).
- NCEER-90-0026 "MUMOID User's Guide - A Program for the Identification of Modal Parameters," by S. Rodriguez-Gomez and E. DiPasquale, 9/30/90, (PB91-171298, A04, MF-A01).
- NCEER-90-0027 "SARCF-II User's Guide - Seismic Analysis of Reinforced Concrete Frames," by S. Rodriguez-Gomez, Y.S. Chung and C. Meyer, 9/30/90, (PB91-171280, A05, MF-A01).
- NCEER-90-0028 "Viscous Dampers: Testing, Modeling and Application in Vibration and Seismic Isolation," by N. Makris and M.C. Constantinou, 12/20/90 (PB91-190561, A06, MF-A01).
- NCEER-90-0029 "Soil Effects on Earthquake Ground Motions in the Memphis Area," by H. Hwang, C.S. Lee, K.W. Ng and T.S. Chang, 8/2/90, (PB91-190751, A05, MF-A01).

- NCEER-91-0001 "Proceedings from the Third Japan-U.S. Workshop on Earthquake Resistant Design of Lifeline Facilities and Countermeasures for Soil Liquefaction, December 17-19, 1990," edited by T.D. O'Rourke and M. Hamada, 2/1/91, (PB91-179259, A99, MF-A04).
- NCEER-91-0002 "Physical Space Solutions of Non-Proportionally Damped Systems," by M. Tong, Z. Liang and G.C. Lee, 1/15/91, (PB91-179242, A04, MF-A01).
- NCEER-91-0003 "Seismic Response of Single Piles and Pile Groups," by K. Fan and G. Gazetas, 1/10/91, (PB92-174994, A04, MF-A01).
- NCEER-91-0004 "Damping of Structures: Part 1 - Theory of Complex Damping," by Z. Liang and G. Lee, 10/10/91, (PB92-197235, A12, MF-A03).
- NCEER-91-0005 "3D-BASIS - Nonlinear Dynamic Analysis of Three Dimensional Base Isolated Structures: Part II," by S. Nagarajaiah, A.M. Reinhorn and M.C. Constantinou, 2/28/91, (PB91-190553, A07, MF-A01). This report has been replaced by NCEER-93-0011.
- NCEER-91-0006 "A Multidimensional Hysteretic Model for Plasticity Deforming Metals in Energy Absorbing Devices," by E.J. Graesser and F.A. Cozzarelli, 4/9/91, (PB92-108364, A04, MF-A01).
- NCEER-91-0007 "A Framework for Customizable Knowledge-Based Expert Systems with an Application to a KBES for Evaluating the Seismic Resistance of Existing Buildings," by E.G. Ibarra-Anaya and S.J. Fennes, 4/9/91, (PB91-210930, A08, MF-A01).
- NCEER-91-0008 "Nonlinear Analysis of Steel Frames with Semi-Rigid Connections Using the Capacity Spectrum Method," by G.G. Deierlein, S-H. Hsieh, Y-J. Shen and J.F. Abel, 7/2/91, (PB92-113828, A05, MF-A01).
- NCEER-91-0009 "Earthquake Education Materials for Grades K-12," by K.E.K. Ross, 4/30/91, (PB91-212142, A06, MF-A01). This report has been replaced by NCEER-92-0018.
- NCEER-91-0010 "Phase Wave Velocities and Displacement Phase Differences in a Harmonically Oscillating Pile," by N. Makris and G. Gazetas, 7/8/91, (PB92-108356, A04, MF-A01).
- NCEER-91-0011 "Dynamic Characteristics of a Full-Size Five-Story Steel Structure and a 2/5 Scale Model," by K.C. Chang, G.C. Yao, G.C. Lee, D.S. Hao and Y.C. Yeh," 7/2/91, (PB93-116648, A06, MF-A02).
- NCEER-91-0012 "Seismic Response of a 2/5 Scale Steel Structure with Added Viscoelastic Dampers," by K.C. Chang, T.T. Soong, S-T. Oh and M.L. Lai, 5/17/91, (PB92-110816, A05, MF-A01).
- NCEER-91-0013 "Earthquake Response of Retaining Walls; Full-Scale Testing and Computational Modeling," by S. Alampalli and A-W.M. Elgamel, 6/20/91, to be published.
- NCEER-91-0014 "3D-BASIS-M: Nonlinear Dynamic Analysis of Multiple Building Base Isolated Structures," by P.C. Tsopelas, S. Nagarajaiah, M.C. Constantinou and A.M. Reinhorn, 5/28/91, (PB92-113885, A09, MF-A02).
- NCEER-91-0015 "Evaluation of SEAOC Design Requirements for Sliding Isolated Structures," by D. Theodossiou and M.C. Constantinou, 6/10/91, (PB92-114602, A11, MF-A03).
- NCEER-91-0016 "Closed-Loop Modal Testing of a 27-Story Reinforced Concrete Flat Plate-Core Building," by H.R. Somaprasad, T. Toksoy, H. Yoshiyuki and A.E. Aktan, 7/15/91, (PB92-129980, A07, MF-A02).
- NCEER-91-0017 "Shake Table Test of a 1/6 Scale Two-Story Lightly Reinforced Concrete Building," by A.G. El-Attar, R.N. White and P. Gergely, 2/28/91, (PB92-222447, A06, MF-A02).
- NCEER-91-0018 "Shake Table Test of a 1/8 Scale Three-Story Lightly Reinforced Concrete Building," by A.G. El-Attar, R.N. White and P. Gergely, 2/28/91, (PB93-116630, A08, MF-A02).
- NCEER-91-0019 "Transfer Functions for Rigid Rectangular Foundations," by A.S. Veletsos, A.M. Prasad and W.H. Wu, 7/31/91, to be published.

- NCEER-91-0020 "Hybrid Control of Seismic-Excited Nonlinear and Inelastic Structural Systems," by J.N. Yang, Z. Li and A. Daniellians, 8/1/91, (PB92-143171, A06, MF-A02).
- NCEER-91-0021 "The NCEER-91 Earthquake Catalog: Improved Intensity-Based Magnitudes and Recurrence Relations for U.S. Earthquakes East of New Madrid," by L. Seeber and J.G. Armbruster, 8/28/91, (PB92-176742, A06, MF-A02).
- NCEER-91-0022 "Proceedings from the Implementation of Earthquake Planning and Education in Schools: The Need for Change - The Roles of the Changemakers," by K.E.K. Ross and F. Winslow, 7/23/91, (PB92-129998, A12, MF-A03).
- NCEER-91-0023 "A Study of Reliability-Based Criteria for Seismic Design of Reinforced Concrete Frame Buildings," by H.H.M. Hwang and H-M. Hsu, 8/10/91, (PB92-140235, A09, MF-A02).
- NCEER-91-0024 "Experimental Verification of a Number of Structural System Identification Algorithms," by R.G. Ghanem, H. Gavin and M. Shinozuka, 9/18/91, (PB92-176577, A18, MF-A04).
- NCEER-91-0025 "Probabilistic Evaluation of Liquefaction Potential," by H.H.M. Hwang and C.S. Lee, 11/25/91, (PB92-143429, A05, MF-A01).
- NCEER-91-0026 "Instantaneous Optimal Control for Linear, Nonlinear and Hysteretic Structures - Stable Controllers," by J.N. Yang and Z. Li, 11/15/91, (PB92-163807, A04, MF-A01).
- NCEER-91-0027 "Experimental and Theoretical Study of a Sliding Isolation System for Bridges," by M.C. Constantinou, A. Kartoum, A.M. Reinhorn and P. Bradford, 11/15/91, (PB92-176973, A10, MF-A03).
- NCEER-92-0001 "Case Studies of Liquefaction and Lifeline Performance During Past Earthquakes, Volume 1: Japanese Case Studies," Edited by M. Hamada and T. O'Rourke, 2/17/92, (PB92-197243, A18, MF-A04).
- NCEER-92-0002 "Case Studies of Liquefaction and Lifeline Performance During Past Earthquakes, Volume 2: United States Case Studies," Edited by T. O'Rourke and M. Hamada, 2/17/92, (PB92-197250, A20, MF-A04).
- NCEER-92-0003 "Issues in Earthquake Education," Edited by K. Ross, 2/3/92, (PB92-222389, A07, MF-A02).
- NCEER-92-0004 "Proceedings from the First U.S. - Japan Workshop on Earthquake Protective Systems for Bridges," Edited by I.G. Buckle, 2/4/92, (PB94-142239, A99, MF-A06).
- NCEER-92-0005 "Seismic Ground Motion from a Haskell-Type Source in a Multiple-Layered Half-Space," A.P. Theoharis, G. Deodatis and M. Shinozuka, 1/2/92, to be published.
- NCEER-92-0006 "Proceedings from the Site Effects Workshop," Edited by R. Whitman, 2/29/92, (PB92-197201, A04, MF-A01).
- NCEER-92-0007 "Engineering Evaluation of Permanent Ground Deformations Due to Seismically-Induced Liquefaction," by M.H. Baziar, R. Dobry and A-W.M. Elgamal, 3/24/92, (PB92-222421, A13, MF-A03).
- NCEER-92-0008 "A Procedure for the Seismic Evaluation of Buildings in the Central and Eastern United States," by C.D. Poland and J.O. Malley, 4/2/92, (PB92-222439, A20, MF-A04).
- NCEER-92-0009 "Experimental and Analytical Study of a Hybrid Isolation System Using Friction Controllable Sliding Bearings," by M.Q. Feng, S. Fujii and M. Shinozuka, 5/15/92, (PB93-150282, A06, MF-A02).
- NCEER-92-0010 "Seismic Resistance of Slab-Column Connections in Existing Non-Ductile Flat-Plate Buildings," by A.J. Durrani and Y. Du, 5/18/92, (PB93-116812, A06, MF-A02).
- NCEER-92-0011 "The Hysteretic and Dynamic Behavior of Brick Masonry Walls Upgraded by Ferrocement Coatings Under Cyclic Loading and Strong Simulated Ground Motion," by H. Lee and S.P. Pravel, 5/11/92, to be published.
- NCEER-92-0012 "Study of Wire Rope Systems for Seismic Protection of Equipment in Buildings," by G.F. Demetriades, M.C. Constantinou and A.M. Reinhorn, 5/20/92, (PB93-116655, A08, MF-A02).



- NCEER-92-0013 "Shape Memory Structural Dampers: Material Properties, Design and Seismic Testing," by P.R. Witting and F.A. Cozzarelli, 5/26/92, (PB93-116663, A05, MF-A01).
- NCEER-92-0014 "Longitudinal Permanent Ground Deformation Effects on Buried Continuous Pipelines," by M.J. O'Rourke, and C. Nordberg, 6/15/92, (PB93-116671, A08, MF-A02).
- NCEER-92-0015 "A Simulation Method for Stationary Gaussian Random Functions Based on the Sampling Theorem," by M. Grigoriu and S. Balopoulou, 6/11/92, (PB93-127496, A05, MF-A01).
- NCEER-92-0016 "Gravity-Load-Designed Reinforced Concrete Buildings: Seismic Evaluation of Existing Construction and Detailing Strategies for Improved Seismic Resistance," by G.W. Hoffmann, S.K. Kunnath, A.M. Reinhorn and J.B. Mander, 7/15/92, (PB94-142007, A08, MF-A02).
- NCEER-92-0017 "Observations on Water System and Pipeline Performance in the Limón Area of Costa Rica Due to the April 22, 1991 Earthquake," by M. O'Rourke and D. Ballantyne, 6/30/92, (PB93-126811, A06, MF-A02).
- NCEER-92-0018 "Fourth Edition of Earthquake Education Materials for Grades K-12," Edited by K.E.K. Ross, 8/10/92, (PB93-114023, A07, MF-A02).
- NCEER-92-0019 "Proceedings from the Fourth Japan-U.S. Workshop on Earthquake Resistant Design of Lifeline Facilities and Countermeasures for Soil Liquefaction," Edited by M. Hamada and T.D. O'Rourke, 8/12/92, (PB93-163939, A99, MF-E11).
- NCEER-92-0020 "Active Bracing System: A Full Scale Implementation of Active Control," by A.M. Reinhorn, T.T. Soong, R.C. Lin, M.A. Riley, Y.P. Wang, S. Aizawa and M. Higashino, 8/14/92, (PB93-127512, A06, MF-A02).
- NCEER-92-0021 "Empirical Analysis of Horizontal Ground Displacement Generated by Liquefaction-Induced Lateral Spreads," by S.F. Bartlett and T.L. Youd, 8/17/92, (PB93-188241, A06, MF-A02).
- NCEER-92-0022 "IDARC Version 3.0: Inelastic Damage Analysis of Reinforced Concrete Structures," by S.K. Kunnath, A.M. Reinhorn and R.F. Lobo, 8/31/92, (PB93-227502, A07, MF-A02).
- NCEER-92-0023 "A Semi-Empirical Analysis of Strong-Motion Peaks in Terms of Seismic Source, Propagation Path and Local Site Conditions, by M. Kamiyama, M.J. O'Rourke and R. Flores-Berrones, 9/9/92, (PB93-150266, A08, MF-A02).
- NCEER-92-0024 "Seismic Behavior of Reinforced Concrete Frame Structures with Nonductile Details, Part I: Summary of Experimental Findings of Full Scale Beam-Column Joint Tests," by A. Beres, R.N. White and P. Gergely, 9/30/92, (PB93-227783, A05, MF-A01).
- NCEER-92-0025 "Experimental Results of Repaired and Retrofitted Beam-Column Joint Tests in Lightly Reinforced Concrete Frame Buildings," by A. Beres, S. El-Borgi, R.N. White and P. Gergely, 10/29/92, (PB93-227791, A05, MF-A01).
- NCEER-92-0026 "A Generalization of Optimal Control Theory: Linear and Nonlinear Structures," by J.N. Yang, Z. Li and S. Vongchavalitkul, 11/2/92, (PB93-188621, A05, MF-A01).
- NCEER-92-0027 "Seismic Resistance of Reinforced Concrete Frame Structures Designed Only for Gravity Loads: Part I - Design and Properties of a One-Third Scale Model Structure," by J.M. Bracci, A.M. Reinhorn and J.B. Mander, 12/1/92, (PB94-104502, A08, MF-A02).
- NCEER-92-0028 "Seismic Resistance of Reinforced Concrete Frame Structures Designed Only for Gravity Loads: Part II - Experimental Performance of Subassemblages," by L.E. Aycaardi, J.B. Mander and A.M. Reinhorn, 12/1/92, (PB94-104510, A08, MF-A02).
- NCEER-92-0029 "Seismic Resistance of Reinforced Concrete Frame Structures Designed Only for Gravity Loads: Part III - Experimental Performance and Analytical Study of a Structural Model," by J.M. Bracci, A.M. Reinhorn and J.B. Mander, 12/1/92, (PB93-227528, A09, MF-A01).

- NCEER-92-0030 "Evaluation of Seismic Retrofit of Reinforced Concrete Frame Structures: Part I - Experimental Performance of Retrofitted Subassemblages," by D. Choudhuri, J.B. Mander and A.M. Reinhorn, 12/8/92, (PB93-198307, A07, MF-A02).
- NCEER-92-0031 "Evaluation of Seismic Retrofit of Reinforced Concrete Frame Structures: Part II - Experimental Performance and Analytical Study of a Retrofitted Structural Model," by J.M. Bracci, A.M. Reinhorn and J.B. Mander, 12/8/92, (PB93-198315, A09, MF-A03).
- NCEER-92-0032 "Experimental and Analytical Investigation of Seismic Response of Structures with Supplemental Fluid Viscous Dampers," by M.C. Constantinou and M.D. Symans, 12/21/92, (PB93-191435, A10, MF-A03). This report is available only through NTIS (see address given above).
- NCEER-92-0033 "Reconnaissance Report on the Cairo, Egypt Earthquake of October 12, 1992," by M. Khater, 12/23/92, (PB93-188621, A03, MF-A01).
- NCEER-92-0034 "Low-Level Dynamic Characteristics of Four Tall Flat-Plate Buildings in New York City," by H. Gavin, S. Yuan, J. Grossman, E. Pekelis and K. Jacob, 12/28/92, (PB93-188217, A07, MF-A02).
- NCEER-93-0001 "An Experimental Study on the Seismic Performance of Brick-Infilled Steel Frames With and Without Retrofit," by J.B. Mander, B. Nair, K. Wojtkowski and J. Ma, 1/29/93, (PB93-227510, A07, MF-A02).
- NCEER-93-0002 "Social Accounting for Disaster Preparedness and Recovery Planning," by S. Cole, E. Pantoja and V. Razak, 2/22/93, (PB94-142114, A12, MF-A03).
- NCEER-93-0003 "Assessment of 1991 NEHRP Provisions for Nonstructural Components and Recommended Revisions," by T.T. Soong, G. Chen, Z. Wu, R-H. Zhang and M. Grigoriu, 3/1/93, (PB93-188639, A06, MF-A02).
- NCEER-93-0004 "Evaluation of Static and Response Spectrum Analysis Procedures of SEAOC/UBC for Seismic Isolated Structures," by C.W. Winters and M.C. Constantinou, 3/23/93, (PB93-198299, A10, MF-A03).
- NCEER-93-0005 "Earthquakes in the Northeast - Are We Ignoring the Hazard? A Workshop on Earthquake Science and Safety for Educators," edited by K.E.K. Ross, 4/2/93, (PB94-103066, A09, MF-A02).
- NCEER-93-0006 "Inelastic Response of Reinforced Concrete Structures with Viscoelastic Braces," by R.F. Lobo, J.M. Bracci, K.L. Shen, A.M. Reinhorn and T.T. Soong, 4/5/93, (PB93-227486, A05, MF-A02).
- NCEER-93-0007 "Seismic Testing of Installation Methods for Computers and Data Processing Equipment," by K. Kosar, T.T. Soong, K.L. Shen, J.A. HoLung and Y.K. Lin, 4/12/93, (PB93-198299, A07, MF-A02).
- NCEER-93-0008 "Retrofit of Reinforced Concrete Frames Using Added Dampers," by A. Reinhorn, M. Constantinou and C. Li, to be published.
- NCEER-93-0009 "Seismic Behavior and Design Guidelines for Steel Frame Structures with Added Viscoelastic Dampers," by K.C. Chang, M.L. Lai, T.T. Soong, D.S. Hao and Y.C. Yeh, 5/1/93, (PB94-141959, A07, MF-A02).
- NCEER-93-0010 "Seismic Performance of Shear-Critical Reinforced Concrete Bridge Piers," by J.B. Mander, S.M. Waheed, M.T.A. Chaudhary and S.S. Chen, 5/12/93, (PB93-227494, A08, MF-A02).
- NCEER-93-0011 "3D-BASIS-TABS: Computer Program for Nonlinear Dynamic Analysis of Three Dimensional Base Isolated Structures," by S. Nagarajaiah, C. Li, A.M. Reinhorn and M.C. Constantinou, 8/2/93, (PB94-141819, A09, MF-A02).
- NCEER-93-0012 "Effects of Hydrocarbon Spills from an Oil Pipeline Break on Ground Water," by O.J. Helweg and H.H.M. Hwang, 8/3/93, (PB94-141942, A06, MF-A02).
- NCEER-93-0013 "Simplified Procedures for Seismic Design of Nonstructural Components and Assessment of Current Code Provisions," by M.P. Singh, L.E. Suarez, E.E. Matheu and G.O. Maldonado, 8/4/93, (PB94-141827, A09, MF-A02).
- NCEER-93-0014 "An Energy Approach to Seismic Analysis and Design of Secondary Systems," by G. Chen and T.T. Soong, 8/6/93, (PB94-142767, A11, MF-A03).

- NCEER-93-0015 "Proceedings from School Sites: Becoming Prepared for Earthquakes - Commemorating the Third Anniversary of the Loma Prieta Earthquake," Edited by F.E. Winslow and K.E.K. Ross, 8/16/93, (PB94-154275, A16, MF-A02).
- NCEER-93-0016 "Reconnaissance Report of Damage to Historic Monuments in Cairo, Egypt Following the October 12, 1992 Dahshur Earthquake," by D. Sykora, D. Look, G. Croci, E. Karaesmen and E. Karaesmen, 8/19/93, (PB94-142221, A08, MF-A02).
- NCEER-93-0017 "The Island of Guam Earthquake of August 8, 1993," by S.W. Swan and S.K. Harris, 9/30/93, (PB94-141843, A04, MF-A01).
- NCEER-93-0018 "Engineering Aspects of the October 12, 1992 Egyptian Earthquake," by A.W. Elgamal, M. Amer, K. Adalier and A. Abul-Fadl, 10/7/93, (PB94-141983, A05, MF-A01).
- NCEER-93-0019 "Development of an Earthquake Motion Simulator and its Application in Dynamic Centrifuge Testing," by I. Krstelj, Supervised by J.H. Prevost, 10/23/93, (PB94-181773, A-10, MF-A03).
- NCEER-93-0020 "NCEER-Taisei Corporation Research Program on Sliding Seismic Isolation Systems for Bridges: Experimental and Analytical Study of a Friction Pendulum System (FPS)," by M.C. Constantinou, P. Tsopelas, Y-S. Kim and S. Okamoto, 11/1/93, (PB94-142775, A08, MF-A02).
- NCEER-93-0021 "Finite Element Modeling of Elastomeric Seismic Isolation Bearings," by L.J. Billings, Supervised by R. Shepherd, 11/8/93, to be published.
- NCEER-93-0022 "Seismic Vulnerability of Equipment in Critical Facilities: Life-Safety and Operational Consequences," by K. Porter, G.S. Johnson, M.M. Zadeh, C. Scawthorn and S. Eder, 11/24/93, (PB94-181765, A16, MF-A03).
- NCEER-93-0023 "Hokkaido Nansei-oki, Japan Earthquake of July 12, 1993, by P.I. Yanev and C.R. Scawthorn, 12/23/93, (PB94-181500, A07, MF-A01).
- NCEER-94-0001 "An Evaluation of Seismic Serviceability of Water Supply Networks with Application to the San Francisco Auxiliary Water Supply System," by I. Markov, Supervised by M. Grigoriu and T. O'Rourke, 1/21/94, (PB94-204013, A07, MF-A02).
- NCEER-94-0002 "NCEER-Taisei Corporation Research Program on Sliding Seismic Isolation Systems for Bridges: Experimental and Analytical Study of Systems Consisting of Sliding Bearings, Rubber Restoring Force Devices and Fluid Dampers," Volumes I and II, by P. Tsopelas, S. Okamoto, M.C. Constantinou, D. Ozaki and S. Fujii, 2/4/94, (PB94-181740, A09, MF-A02 and PB94-181757, A12, MF-A03).
- NCEER-94-0003 "A Markov Model for Local and Global Damage Indices in Seismic Analysis," by S. Rahman and M. Grigoriu, 2/18/94, (PB94-206000, A12, MF-A03).
- NCEER-94-0004 "Proceedings from the NCEER Workshop on Seismic Response of Masonry Infills," edited by D.P. Abrams, 3/1/94, (PB94-180783, A07, MF-A02).
- NCEER-94-0005 "The Northridge, California Earthquake of January 17, 1994: General Reconnaissance Report," edited by J.D. Goltz, 3/11/94, (PB94-193943, A10, MF-A03).
- NCEER-94-0006 "Seismic Energy Based Fatigue Damage Analysis of Bridge Columns: Part I - Evaluation of Seismic Capacity," by G.A. Chang and J.B. Mander, 3/14/94, (PB94-219185, A11, MF-A03).
- NCEER-94-0007 "Seismic Isolation of Multi-Story Frame Structures Using Spherical Sliding Isolation Systems," by T.M. Al-Hussaini, V.A. Zayas and M.C. Constantinou, 3/17/94, (PB94-193745, A09, MF-A02).
- NCEER-94-0008 "The Northridge, California Earthquake of January 17, 1994: Performance of Highway Bridges," edited by I.G. Buckle, 3/24/94, (PB94-193851, A06, MF-A02).
- NCEER-94-0009 "Proceedings of the Third U.S.-Japan Workshop on Earthquake Protective Systems for Bridges," edited by I.G. Buckle and I. Friedland, 3/31/94, (PB94-195815, A99, MF-A06).

- NCEER-94-0010 "3D-BASIS-ME: Computer Program for Nonlinear Dynamic Analysis of Seismically Isolated Single and Multiple Structures and Liquid Storage Tanks," by P.C. Tsopelas, M.C. Constantinou and A.M. Reinhorn, 4/12/94, (PB94-204922, A09, MF-A02).
- NCEER-94-0011 "The Northridge, California Earthquake of January 17, 1994: Performance of Gas Transmission Pipelines," by T.D. O'Rourke and M.C. Palmer, 5/16/94, (PB94-204989, A05, MF-A01).
- NCEER-94-0012 "Feasibility Study of Replacement Procedures and Earthquake Performance Related to Gas Transmission Pipelines," by T.D. O'Rourke and M.C. Palmer, 5/25/94, (PB94-206638, A09, MF-A02).
- NCEER-94-0013 "Seismic Energy Based Fatigue Damage Analysis of Bridge Columns: Part II - Evaluation of Seismic Demand," by G.A. Chang and J.B. Mander, 6/1/94, (PB95-18106, A08, MF-A02).
- NCEER-94-0014 "NCEER-Taisei Corporation Research Program on Sliding Seismic Isolation Systems for Bridges: Experimental and Analytical Study of a System Consisting of Sliding Bearings and Fluid Restoring Force/Damping Devices," by P. Tsopelas and M.C. Constantinou, 6/13/94, (PB94-219144, A10, MF-A03).
- NCEER-94-0015 "Generation of Hazard-Consistent Fragility Curves for Seismic Loss Estimation Studies," by H. Hwang and J-R. Huo, 6/14/94, (PB95-181996, A09, MF-A02).
- NCEER-94-0016 "Seismic Study of Building Frames with Added Energy-Absorbing Devices," by W.S. Pong, C.S. Tsai and G.C. Lee, 6/20/94, (PB94-219136, A10, A03).
- NCEER-94-0017 "Sliding Mode Control for Seismic-Excited Linear and Nonlinear Civil Engineering Structures," by J. Yang, J. Wu, A. Agrawal and Z. Li, 6/21/94, (PB95-138483, A06, MF-A02).
- NCEER-94-0018 "3D-BASIS-TABS Version 2.0: Computer Program for Nonlinear Dynamic Analysis of Three Dimensional Base Isolated Structures," by A.M. Reinhorn, S. Nagarajaiah, M.C. Constantinou, P. Tsopelas and R. Li, 6/22/94, (PB95-182176, A08, MF-A02).
- NCEER-94-0019 "Proceedings of the International Workshop on Civil Infrastructure Systems: Application of Intelligent Systems and Advanced Materials on Bridge Systems," Edited by G.C. Lee and K.C. Chang, 7/18/94, (PB95-252474, A20, MF-A04).
- NCEER-94-0020 "Study of Seismic Isolation Systems for Computer Floors," by V. Lambrou and M.C. Constantinou, 7/19/94, (PB95-138533, A10, MF-A03).
- NCEER-94-0021 "Proceedings of the U.S.-Italian Workshop on Guidelines for Seismic Evaluation and Rehabilitation of Unreinforced Masonry Buildings," Edited by D.P. Abrams and G.M. Calvi, 7/20/94, (PB95-138749, A13, MF-A03).
- NCEER-94-0022 "NCEER-Taisei Corporation Research Program on Sliding Seismic Isolation Systems for Bridges: Experimental and Analytical Study of a System Consisting of Lubricated PTFE Sliding Bearings and Mild Steel Dampers," by P. Tsopelas and M.C. Constantinou, 7/22/94, (PB95-182184, A08, MF-A02).
- NCEER-94-0023 "Development of Reliability-Based Design Criteria for Buildings Under Seismic Load," by Y.K. Wen, H. Hwang and M. Shinozuka, 8/1/94, (PB95-211934, A08, MF-A02).
- NCEER-94-0024 "Experimental Verification of Acceleration Feedback Control Strategies for an Active Tendon System," by S.J. Dyke, B.F. Spencer, Jr., P. Quast, M.K. Sain, D.C. Kaspari, Jr. and T.T. Soong, 8/29/94, (PB95-212320, A05, MF-A01).
- NCEER-94-0025 "Seismic Retrofitting Manual for Highway Bridges," Edited by I.G. Buckle and I.F. Friedland, published by the Federal Highway Administration (PB95-212676, A15, MF-A03).
- NCEER-94-0026 "Proceedings from the Fifth U.S.-Japan Workshop on Earthquake Resistant Design of Lifeline Facilities and Countermeasures Against Soil Liquefaction," Edited by T.D. O'Rourke and M. Hamada, 11/7/94, (PB95-220802, A99, MF-E08).

- NCEER-95-0001 “Experimental and Analytical Investigation of Seismic Retrofit of Structures with Supplemental Damping: Part 1 - Fluid Viscous Damping Devices,” by A.M. Reinhorn, C. Li and M.C. Constantinou, 1/3/95, (PB95-266599, A09, MF-A02).
- NCEER-95-0002 “Experimental and Analytical Study of Low-Cycle Fatigue Behavior of Semi-Rigid Top-And-Seat Angle Connections,” by G. Pekcan, J.B. Mander and S.S. Chen, 1/5/95, (PB95-220042, A07, MF-A02).
- NCEER-95-0003 “NCEER-ATC Joint Study on Fragility of Buildings,” by T. Anagnos, C. Rojahn and A.S. Kiremidjian, 1/20/95, (PB95-220026, A06, MF-A02).
- NCEER-95-0004 “Nonlinear Control Algorithms for Peak Response Reduction,” by Z. Wu, T.T. Soong, V. Gattulli and R.C. Lin, 2/16/95, (PB95-220349, A05, MF-A01).
- NCEER-95-0005 “Pipeline Replacement Feasibility Study: A Methodology for Minimizing Seismic and Corrosion Risks to Underground Natural Gas Pipelines,” by R.T. Eguchi, H.A. Seligson and D.G. Honegger, 3/2/95, (PB95-252326, A06, MF-A02).
- NCEER-95-0006 “Evaluation of Seismic Performance of an 11-Story Frame Building During the 1994 Northridge Earthquake,” by F. Naeim, R. DiSulio, K. Benuska, A. Reinhorn and C. Li, to be published.
- NCEER-95-0007 “Prioritization of Bridges for Seismic Retrofitting,” by N. Basöz and A.S. Kiremidjian, 4/24/95, (PB95-252300, A08, MF-A02).
- NCEER-95-0008 “Method for Developing Motion Damage Relationships for Reinforced Concrete Frames,” by A. Singhal and A.S. Kiremidjian, 5/11/95, (PB95-266607, A06, MF-A02).
- NCEER-95-0009 “Experimental and Analytical Investigation of Seismic Retrofit of Structures with Supplemental Damping: Part II - Friction Devices,” by C. Li and A.M. Reinhorn, 7/6/95, (PB96-128087, A11, MF-A03).
- NCEER-95-0010 “Experimental Performance and Analytical Study of a Non-Ductile Reinforced Concrete Frame Structure Retrofitted with Elastomeric Spring Dampers,” by G. Pekcan, J.B. Mander and S.S. Chen, 7/14/95, (PB96-137161, A08, MF-A02).
- NCEER-95-0011 “Development and Experimental Study of Semi-Active Fluid Damping Devices for Seismic Protection of Structures,” by M.D. Symans and M.C. Constantinou, 8/3/95, (PB96-136940, A23, MF-A04).
- NCEER-95-0012 “Real-Time Structural Parameter Modification (RSPM): Development of Innervated Structures,” by Z. Liang, M. Tong and G.C. Lee, 4/11/95, (PB96-137153, A06, MF-A01).
- NCEER-95-0013 “Experimental and Analytical Investigation of Seismic Retrofit of Structures with Supplemental Damping: Part III - Viscous Damping Walls,” by A.M. Reinhorn and C. Li, 10/1/95, (PB96-176409, A11, MF-A03).
- NCEER-95-0014 “Seismic Fragility Analysis of Equipment and Structures in a Memphis Electric Substation,” by J-R. Huo and H.H.M. Hwang, 8/10/95, (PB96-128087, A09, MF-A02).
- NCEER-95-0015 “The Hanshin-Awaji Earthquake of January 17, 1995: Performance of Lifelines,” Edited by M. Shinozuka, 11/3/95, (PB96-176383, A15, MF-A03).
- NCEER-95-0016 “Highway Culvert Performance During Earthquakes,” by T.L. Youd and C.J. Beckman, available as NCEER-96-0015.
- NCEER-95-0017 “The Hanshin-Awaji Earthquake of January 17, 1995: Performance of Highway Bridges,” Edited by I.G. Buckle, 12/1/95, to be published.
- NCEER-95-0018 “Modeling of Masonry Infill Panels for Structural Analysis,” by A.M. Reinhorn, A. Madan, R.E. Valles, Y. Reichmann and J.B. Mander, 12/8/95, (PB97-110886, MF-A01, A06).
- NCEER-95-0019 “Optimal Polynomial Control for Linear and Nonlinear Structures,” by A.K. Agrawal and J.N. Yang, 12/11/95, (PB96-168737, A07, MF-A02).

- NCEER-95-0020 "Retrofit of Non-Ductile Reinforced Concrete Frames Using Friction Dampers," by R.S. Rao, P. Gergely and R.N. White, 12/22/95, (PB97-133508, A10, MF-A02).
- NCEER-95-0021 "Parametric Results for Seismic Response of Pile-Supported Bridge Bents," by G. Mylonakis, A. Nikolaou and G. Gazetas, 12/22/95, (PB97-100242, A12, MF-A03).
- NCEER-95-0022 "Kinematic Bending Moments in Seismically Stressed Piles," by A. Nikolaou, G. Mylonakis and G. Gazetas, 12/23/95, (PB97-113914, MF-A03, A13).
- NCEER-96-0001 "Dynamic Response of Unreinforced Masonry Buildings with Flexible Diaphragms," by A.C. Costley and D.P. Abrams, 10/10/96, (PB97-133573, MF-A03, A15).
- NCEER-96-0002 "State of the Art Review: Foundations and Retaining Structures," by I. Po Lam, to be published.
- NCEER-96-0003 "Ductility of Rectangular Reinforced Concrete Bridge Columns with Moderate Confinement," by N. Wehbe, M. Saiidi, D. Sanders and B. Douglas, 11/7/96, (PB97-133557, A06, MF-A02).
- NCEER-96-0004 "Proceedings of the Long-Span Bridge Seismic Research Workshop," edited by I.G. Buckle and I.M. Friedland, to be published.
- NCEER-96-0005 "Establish Representative Pier Types for Comprehensive Study: Eastern United States," by J. Kulicki and Z. Prucz, 5/28/96, (PB98-119217, A07, MF-A02).
- NCEER-96-0006 "Establish Representative Pier Types for Comprehensive Study: Western United States," by R. Imbsen, R.A. Schamber and T.A. Osterkamp, 5/28/96, (PB98-118607, A07, MF-A02).
- NCEER-96-0007 "Nonlinear Control Techniques for Dynamical Systems with Uncertain Parameters," by R.G. Ghanem and M.I. Bujakov, 5/27/96, (PB97-100259, A17, MF-A03).
- NCEER-96-0008 "Seismic Evaluation of a 30-Year Old Non-Ductile Highway Bridge Pier and Its Retrofit," by J.B. Mander, B. Mahmoodzadegan, S. Bhadra and S.S. Chen, 5/31/96, (PB97-110902, MF-A03, A10).
- NCEER-96-0009 "Seismic Performance of a Model Reinforced Concrete Bridge Pier Before and After Retrofit," by J.B. Mander, J.H. Kim and C.A. Ligozio, 5/31/96, (PB97-110910, MF-A02, A10).
- NCEER-96-0010 "IDARC2D Version 4.0: A Computer Program for the Inelastic Damage Analysis of Buildings," by R.E. Valles, A.M. Reinhorn, S.K. Kunnath, C. Li and A. Madan, 6/3/96, (PB97-100234, A17, MF-A03).
- NCEER-96-0011 "Estimation of the Economic Impact of Multiple Lifeline Disruption: Memphis Light, Gas and Water Division Case Study," by S.E. Chang, H.A. Seligson and R.T. Eguchi, 8/16/96, (PB97-133490, A11, MF-A03).
- NCEER-96-0012 "Proceedings from the Sixth Japan-U.S. Workshop on Earthquake Resistant Design of Lifeline Facilities and Countermeasures Against Soil Liquefaction, Edited by M. Hamada and T. O'Rourke, 9/11/96, (PB97-133581, A99, MF-A06).
- NCEER-96-0013 "Chemical Hazards, Mitigation and Preparedness in Areas of High Seismic Risk: A Methodology for Estimating the Risk of Post-Earthquake Hazardous Materials Release," by H.A. Seligson, R.T. Eguchi, K.J. Tierney and K. Richmond, 11/7/96, (PB97-133565, MF-A02, A08).
- NCEER-96-0014 "Response of Steel Bridge Bearings to Reversed Cyclic Loading," by J.B. Mander, D-K. Kim, S.S. Chen and G.J. Premus, 11/13/96, (PB97-140735, A12, MF-A03).
- NCEER-96-0015 "Highway Culvert Performance During Past Earthquakes," by T.L. Youd and C.J. Beckman, 11/25/96, (PB97-133532, A06, MF-A01).
- NCEER-97-0001 "Evaluation, Prevention and Mitigation of Pounding Effects in Building Structures," by R.E. Valles and A.M. Reinhorn, 2/20/97, (PB97-159552, A14, MF-A03).
- NCEER-97-0002 "Seismic Design Criteria for Bridges and Other Highway Structures," by C. Rojahn, R. Mayes, D.G. Anderson, J. Clark, J.H. Hom, R.V. Nutt and M.J. O'Rourke, 4/30/97, (PB97-194658, A06, MF-A03).

- NCEER-97-0003 "Proceedings of the U.S.-Italian Workshop on Seismic Evaluation and Retrofit," Edited by D.P. Abrams and G.M. Calvi, 3/19/97, (PB97-194666, A13, MF-A03).
- NCEER-97-0004 "Investigation of Seismic Response of Buildings with Linear and Nonlinear Fluid Viscous Dampers," by A.A. Seleemah and M.C. Constantinou, 5/21/97, (PB98-109002, A15, MF-A03).
- NCEER-97-0005 "Proceedings of the Workshop on Earthquake Engineering Frontiers in Transportation Facilities," edited by G.C. Lee and I.M. Friedland, 8/29/97, (PB98-128911, A25, MR-A04).
- NCEER-97-0006 "Cumulative Seismic Damage of Reinforced Concrete Bridge Piers," by S.K. Kunnath, A. El-Bahy, A. Taylor and W. Stone, 9/2/97, (PB98-108814, A11, MF-A03).
- NCEER-97-0007 "Structural Details to Accommodate Seismic Movements of Highway Bridges and Retaining Walls," by R.A. Imbsen, R.A. Schamber, E. Thorkildsen, A. Kartoum, B.T. Martin, T.N. Rosser and J.M. Kulicki, 9/3/97, (PB98-108996, A09, MF-A02).
- NCEER-97-0008 "A Method for Earthquake Motion-Damage Relationships with Application to Reinforced Concrete Frames," by A. Singhal and A.S. Kiremidjian, 9/10/97, (PB98-108988, A13, MF-A03).
- NCEER-97-0009 "Seismic Analysis and Design of Bridge Abutments Considering Sliding and Rotation," by K. Fishman and R. Richards, Jr., 9/15/97, (PB98-108897, A06, MF-A02).
- NCEER-97-0010 "Proceedings of the FHWA/NCEER Workshop on the National Representation of Seismic Ground Motion for New and Existing Highway Facilities," edited by I.M. Friedland, M.S. Power and R.L. Mayes, 9/22/97, (PB98-128903, A21, MF-A04).
- NCEER-97-0011 "Seismic Analysis for Design or Retrofit of Gravity Bridge Abutments," by K.L. Fishman, R. Richards, Jr. and R.C. Divito, 10/2/97, (PB98-128937, A08, MF-A02).
- NCEER-97-0012 "Evaluation of Simplified Methods of Analysis for Yielding Structures," by P. Tsopelas, M.C. Constantinou, C.A. Kircher and A.S. Whittaker, 10/31/97, (PB98-128929, A10, MF-A03).
- NCEER-97-0013 "Seismic Design of Bridge Columns Based on Control and Repairability of Damage," by C-T. Cheng and J.B. Mander, 12/8/97, (PB98-144249, A11, MF-A03).
- NCEER-97-0014 "Seismic Resistance of Bridge Piers Based on Damage Avoidance Design," by J.B. Mander and C-T. Cheng, 12/10/97, (PB98-144223, A09, MF-A02).
- NCEER-97-0015 "Seismic Response of Nominally Symmetric Systems with Strength Uncertainty," by S. Balopoulou and M. Grigoriu, 12/23/97, (PB98-153422, A11, MF-A03).
- NCEER-97-0016 "Evaluation of Seismic Retrofit Methods for Reinforced Concrete Bridge Columns," by T.J. Wipf, F.W. Klaiber and F.M. Russo, 12/28/97, (PB98-144215, A12, MF-A03).
- NCEER-97-0017 "Seismic Fragility of Existing Conventional Reinforced Concrete Highway Bridges," by C.L. Mullen and A.S. Cakmak, 12/30/97, (PB98-153406, A08, MF-A02).
- NCEER-97-0018 "Loss Assessment of Memphis Buildings," edited by D.P. Abrams and M. Shinozuka, 12/31/97, (PB98-144231, A13, MF-A03).
- NCEER-97-0019 "Seismic Evaluation of Frames with Infill Walls Using Quasi-static Experiments," by K.M. Mosalam, R.N. White and P. Gergely, 12/31/97, (PB98-153455, A07, MF-A02).
- NCEER-97-0020 "Seismic Evaluation of Frames with Infill Walls Using Pseudo-dynamic Experiments," by K.M. Mosalam, R.N. White and P. Gergely, 12/31/97, (PB98-153430, A07, MF-A02).
- NCEER-97-0021 "Computational Strategies for Frames with Infill Walls: Discrete and Smeared Crack Analyses and Seismic Fragility," by K.M. Mosalam, R.N. White and P. Gergely, 12/31/97, (PB98-153414, A10, MF-A02).

- NCEER-97-0022 "Proceedings of the NCEER Workshop on Evaluation of Liquefaction Resistance of Soils," edited by T.L. Youd and I.M. Idriss, 12/31/97, (PB98-155617, A15, MF-A03).
- MCEER-98-0001 "Extraction of Nonlinear Hysteretic Properties of Seismically Isolated Bridges from Quick-Release Field Tests," by Q. Chen, B.M. Douglas, E.M. Maragakis and I.G. Buckle, 5/26/98, (PB99-118838, A06, MF-A01).
- MCEER-98-0002 "Methodologies for Evaluating the Importance of Highway Bridges," by A. Thomas, S. Eshenaur and J. Kulicki, 5/29/98, (PB99-118846, A10, MF-A02).
- MCEER-98-0003 "Capacity Design of Bridge Piers and the Analysis of Overstrength," by J.B. Mander, A. Dutta and P. Goel, 6/1/98, (PB99-118853, A09, MF-A02).
- MCEER-98-0004 "Evaluation of Bridge Damage Data from the Loma Prieta and Northridge, California Earthquakes," by N. Basoz and A. Kiremidjian, 6/2/98, (PB99-118861, A15, MF-A03).
- MCEER-98-0005 "Screening Guide for Rapid Assessment of Liquefaction Hazard at Highway Bridge Sites," by T. L. Youd, 6/16/98, (PB99-118879, A06, not available on microfiche).
- MCEER-98-0006 "Structural Steel and Steel/Concrete Interface Details for Bridges," by P. Ritchie, N. Kaulh and J. Kulicki, 7/13/98, (PB99-118945, A06, MF-A01).
- MCEER-98-0007 "Capacity Design and Fatigue Analysis of Confined Concrete Columns," by A. Dutta and J.B. Mander, 7/14/98, (PB99-118960, A14, MF-A03).
- MCEER-98-0008 "Proceedings of the Workshop on Performance Criteria for Telecommunication Services Under Earthquake Conditions," edited by A.J. Schiff, 7/15/98, (PB99-118952, A08, MF-A02).
- MCEER-98-0009 "Fatigue Analysis of Unconfined Concrete Columns," by J.B. Mander, A. Dutta and J.H. Kim, 9/12/98, (PB99-123655, A10, MF-A02).
- MCEER-98-0010 "Centrifuge Modeling of Cyclic Lateral Response of Pile-Cap Systems and Seat-Type Abutments in Dry Sands," by A.D. Gadre and R. Dobry, 10/2/98, (PB99-123606, A13, MF-A03).
- MCEER-98-0011 "IDARC-BRIDGE: A Computational Platform for Seismic Damage Assessment of Bridge Structures," by A.M. Reinhorn, V. Simeonov, G. Mylonakis and Y. Reichman, 10/2/98, (PB99-162919, A15, MF-A03).
- MCEER-98-0012 "Experimental Investigation of the Dynamic Response of Two Bridges Before and After Retrofitting with Elastomeric Bearings," by D.A. Wendichansky, S.S. Chen and J.B. Mander, 10/2/98, (PB99-162927, A15, MF-A03).
- MCEER-98-0013 "Design Procedures for Hinge Restrainers and Hinge Sear Width for Multiple-Frame Bridges," by R. Des Roches and G.L. Fenves, 11/3/98, (PB99-140477, A13, MF-A03).
- MCEER-98-0014 "Response Modification Factors for Seismically Isolated Bridges," by M.C. Constantinou and J.K. Quarshie, 11/3/98, (PB99-140485, A14, MF-A03).
- MCEER-98-0015 "Proceedings of the U.S.-Italy Workshop on Seismic Protective Systems for Bridges," edited by I.M. Friedland and M.C. Constantinou, 11/3/98, (PB2000-101711, A22, MF-A04).
- MCEER-98-0016 "Appropriate Seismic Reliability for Critical Equipment Systems: Recommendations Based on Regional Analysis of Financial and Life Loss," by K. Porter, C. Scawthorn, C. Taylor and N. Blais, 11/10/98, (PB99-157265, A08, MF-A02).
- MCEER-98-0017 "Proceedings of the U.S. Japan Joint Seminar on Civil Infrastructure Systems Research," edited by M. Shinozuka and A. Rose, 11/12/98, (PB99-156713, A16, MF-A03).
- MCEER-98-0018 "Modeling of Pile Footings and Drilled Shafts for Seismic Design," by I. PoLam, M. Kapuskar and D. Chaudhuri, 12/21/98, (PB99-157257, A09, MF-A02).



- MCEER-99-0001 "Seismic Evaluation of a Masonry Infilled Reinforced Concrete Frame by Pseudodynamic Testing," by S.G. Buonopane and R.N. White, 2/16/99, (PB99-162851, A09, MF-A02).
- MCEER-99-0002 "Response History Analysis of Structures with Seismic Isolation and Energy Dissipation Systems: Verification Examples for Program SAP2000," by J. Scheller and M.C. Constantinou, 2/22/99, (PB99-162869, A08, MF-A02).
- MCEER-99-0003 "Experimental Study on the Seismic Design and Retrofit of Bridge Columns Including Axial Load Effects," by A. Dutta, T. Kokorina and J.B. Mander, 2/22/99, (PB99-162877, A09, MF-A02).
- MCEER-99-0004 "Experimental Study of Bridge Elastomeric and Other Isolation and Energy Dissipation Systems with Emphasis on Uplift Prevention and High Velocity Near-source Seismic Excitation," by A. Kasalanati and M. C. Constantinou, 2/26/99, (PB99-162885, A12, MF-A03).
- MCEER-99-0005 "Truss Modeling of Reinforced Concrete Shear-flexure Behavior," by J.H. Kim and J.B. Mander, 3/8/99, (PB99-163693, A12, MF-A03).
- MCEER-99-0006 "Experimental Investigation and Computational Modeling of Seismic Response of a 1:4 Scale Model Steel Structure with a Load Balancing Supplemental Damping System," by G. Pekcan, J.B. Mander and S.S. Chen, 4/2/99, (PB99-162893, A11, MF-A03).
- MCEER-99-0007 "Effect of Vertical Ground Motions on the Structural Response of Highway Bridges," by M.R. Button, C.J. Cronin and R.L. Mayes, 4/10/99, (PB2000-101411, A10, MF-A03).
- MCEER-99-0008 "Seismic Reliability Assessment of Critical Facilities: A Handbook, Supporting Documentation, and Model Code Provisions," by G.S. Johnson, R.E. Sheppard, M.D. Quilici, S.J. Eder and C.R. Scawthorn, 4/12/99, (PB2000-101701, A18, MF-A04).
- MCEER-99-0009 "Impact Assessment of Selected MCEER Highway Project Research on the Seismic Design of Highway Structures," by C. Rojahn, R. Mayes, D.G. Anderson, J.H. Clark, D'Appolonia Engineering, S. Gloyd and R.V. Nutt, 4/14/99, (PB99-162901, A10, MF-A02).
- MCEER-99-0010 "Site Factors and Site Categories in Seismic Codes," by R. Dobry, R. Ramos and M.S. Power, 7/19/99, (PB2000-101705, A08, MF-A02).
- MCEER-99-0011 "Restrainer Design Procedures for Multi-Span Simply-Supported Bridges," by M.J. Randall, M. Saiidi, E. Maragakis and T. Isakovic, 7/20/99, (PB2000-101702, A10, MF-A02).
- MCEER-99-0012 "Property Modification Factors for Seismic Isolation Bearings," by M.C. Constantinou, P. Tsopelas, A. Kasalanati and E. Wolff, 7/20/99, (PB2000-103387, A11, MF-A03).
- MCEER-99-0013 "Critical Seismic Issues for Existing Steel Bridges," by P. Ritchie, N. Kauh and J. Kulicki, 7/20/99, (PB2000-101697, A09, MF-A02).
- MCEER-99-0014 "Nonstructural Damage Database," by A. Kao, T.T. Soong and A. Vender, 7/24/99, (PB2000-101407, A06, MF-A01).
- MCEER-99-0015 "Guide to Remedial Measures for Liquefaction Mitigation at Existing Highway Bridge Sites," by H.G. Cooke and J. K. Mitchell, 7/26/99, (PB2000-101703, A11, MF-A03).
- MCEER-99-0016 "Proceedings of the MCEER Workshop on Ground Motion Methodologies for the Eastern United States," edited by N. Abrahamson and A. Becker, 8/11/99, (PB2000-103385, A07, MF-A02).
- MCEER-99-0017 "Quindío, Colombia Earthquake of January 25, 1999: Reconnaissance Report," by A.P. Asfura and P.J. Flores, 10/4/99, (PB2000-106893, A06, MF-A01).
- MCEER-99-0018 "Hysteretic Models for Cyclic Behavior of Deteriorating Inelastic Structures," by M.V. Sivaselvan and A.M. Reinhorn, 11/5/99, (PB2000-103386, A08, MF-A02).

- MCEER-99-0019 "Proceedings of the 7<sup>th</sup> U.S.- Japan Workshop on Earthquake Resistant Design of Lifeline Facilities and Countermeasures Against Soil Liquefaction," edited by T.D. O'Rourke, J.P. Bardet and M. Hamada, 11/19/99, (PB2000-103354, A99, MF-A06).
- MCEER-99-0020 "Development of Measurement Capability for Micro-Vibration Evaluations with Application to Chip Fabrication Facilities," by G.C. Lee, Z. Liang, J.W. Song, J.D. Shen and W.C. Liu, 12/1/99, (PB2000-105993, A08, MF-A02).
- MCEER-99-0021 "Design and Retrofit Methodology for Building Structures with Supplemental Energy Dissipating Systems," by G. Pekcan, J.B. Mander and S.S. Chen, 12/31/99, (PB2000-105994, A11, MF-A03).
- MCEER-00-0001 "The Marmara, Turkey Earthquake of August 17, 1999: Reconnaissance Report," edited by C. Scawthorn; with major contributions by M. Bruneau, R. Eguchi, T. Holzer, G. Johnson, J. Mander, J. Mitchell, W. Mitchell, A. Papageorgiou, C. Scaethorn, and G. Webb, 3/23/00, (PB2000-106200, A11, MF-A03).
- MCEER-00-0002 "Proceedings of the MCEER Workshop for Seismic Hazard Mitigation of Health Care Facilities," edited by G.C. Lee, M. Ettouney, M. Grigoriu, J. Hauer and J. Nigg, 3/29/00, (PB2000-106892, A08, MF-A02).
- MCEER-00-0003 "The Chi-Chi, Taiwan Earthquake of September 21, 1999: Reconnaissance Report," edited by G.C. Lee and C.H. Loh, with major contributions by G.C. Lee, M. Bruneau, I.G. Buckle, S.E. Chang, P.J. Flores, T.D. O'Rourke, M. Shinozuka, T.T. Soong, C-H. Loh, K-C. Chang, Z-J. Chen, J-S. Hwang, M-L. Lin, G-Y. Liu, K-C. Tsai, G.C. Yao and C-L. Yen, 4/30/00, (PB2001-100980, A10, MF-A02).
- MCEER-00-0004 "Seismic Retrofit of End-Sway Frames of Steel Deck-Truss Bridges with a Supplemental Tendon System: Experimental and Analytical Investigation," by G. Pekcan, J.B. Mander and S.S. Chen, 7/1/00, (PB2001-100982, A10, MF-A02).
- MCEER-00-0005 "Sliding Fragility of Unrestrained Equipment in Critical Facilities," by W.H. Chong and T.T. Soong, 7/5/00, (PB2001-100983, A08, MF-A02).
- MCEER-00-0006 "Seismic Response of Reinforced Concrete Bridge Pier Walls in the Weak Direction," by N. Abo-Shadi, M. Saiidi and D. Sanders, 7/17/00, (PB2001-100981, A17, MF-A03).
- MCEER-00-0007 "Low-Cycle Fatigue Behavior of Longitudinal Reinforcement in Reinforced Concrete Bridge Columns," by J. Brown and S.K. Kunnath, 7/23/00, (PB2001-104392, A08, MF-A02).
- MCEER-00-0008 "Soil Structure Interaction of Bridges for Seismic Analysis," I. PoLam and H. Law, 9/25/00, (PB2001-105397, A08, MF-A02).
- MCEER-00-0009 "Proceedings of the First MCEER Workshop on Mitigation of Earthquake Disaster by Advanced Technologies (MEDAT-1), edited by M. Shinozuka, D.J. Inman and T.D. O'Rourke, 11/10/00, (PB2001-105399, A14, MF-A03).
- MCEER-00-0010 "Development and Evaluation of Simplified Procedures for Analysis and Design of Buildings with Passive Energy Dissipation Systems, Revision 01," by O.M. Ramirez, M.C. Constantinou, C.A. Kircher, A.S. Whittaker, M.W. Johnson, J.D. Gomez and C. Chrysostomou, 11/16/01, (PB2001-105523, A23, MF-A04).
- MCEER-00-0011 "Dynamic Soil-Foundation-Structure Interaction Analyses of Large Caissons," by C-Y. Chang, C-M. Mok, Z-L. Wang, R. Settgast, F. Waggoner, M.A. Ketchum, H.M. Gonnermann and C-C. Chin, 12/30/00, (PB2001-104373, A07, MF-A02).
- MCEER-00-0012 "Experimental Evaluation of Seismic Performance of Bridge Restrainers," by A.G. Vlassis, E.M. Maragakis and M. Saiid Saiidi, 12/30/00, (PB2001-104354, A09, MF-A02).
- MCEER-00-0013 "Effect of Spatial Variation of Ground Motion on Highway Structures," by M. Shinozuka, V. Saxena and G. Deodatis, 12/31/00, (PB2001-108755, A13, MF-A03).
- MCEER-00-0014 "A Risk-Based Methodology for Assessing the Seismic Performance of Highway Systems," by S.D. Werner, C.E. Taylor, J.E. Moore, II, J.S. Walton and S. Cho, 12/31/00, (PB2001-108756, A14, MF-A03).

- MCEER-01-0001 “Experimental Investigation of P-Delta Effects to Collapse During Earthquakes,” by D. Vian and M. Bruneau, 6/25/01, (PB2002-100534, A17, MF-A03).
- MCEER-01-0002 “Proceedings of the Second MCEER Workshop on Mitigation of Earthquake Disaster by Advanced Technologies (MEDAT-2),” edited by M. Bruneau and D.J. Inman, 7/23/01, (PB2002-100434, A16, MF-A03).
- MCEER-01-0003 “Sensitivity Analysis of Dynamic Systems Subjected to Seismic Loads,” by C. Roth and M. Grigoriu, 9/18/01, (PB2003-100884, A12, MF-A03).
- MCEER-01-0004 “Overcoming Obstacles to Implementing Earthquake Hazard Mitigation Policies: Stage 1 Report,” by D.J. Alesch and W.J. Petak, 12/17/01, (PB2002-107949, A07, MF-A02).
- MCEER-01-0005 “Updating Real-Time Earthquake Loss Estimates: Methods, Problems and Insights,” by C.E. Taylor, S.E. Chang and R.T. Eguchi, 12/17/01, (PB2002-107948, A05, MF-A01).
- MCEER-01-0006 “Experimental Investigation and Retrofit of Steel Pile Foundations and Pile Bents Under Cyclic Lateral Loadings,” by A. Shama, J. Mander, B. Blabac and S. Chen, 12/31/01, (PB2002-107950, A13, MF-A03).
- MCEER-02-0001 “Assessment of Performance of Bolu Viaduct in the 1999 Duzce Earthquake in Turkey” by P.C. Roussis, M.C. Constantinou, M. Erdik, E. Durukal and M. Dicleli, 5/8/02, (PB2003-100883, A08, MF-A02).
- MCEER-02-0002 “Seismic Behavior of Rail Counterweight Systems of Elevators in Buildings,” by M.P. Singh, Rildova and L.E. Suarez, 5/27/02. (PB2003-100882, A11, MF-A03).
- MCEER-02-0003 “Development of Analysis and Design Procedures for Spread Footings,” by G. Mylonakis, G. Gazetas, S. Nikolaou and A. Chauncey, 10/02/02, (PB2004-101636, A13, MF-A03, CD-A13).
- MCEER-02-0004 “Bare-Earth Algorithms for Use with SAR and LIDAR Digital Elevation Models,” by C.K. Huyck, R.T. Eguchi and B. Houshmand, 10/16/02, (PB2004-101637, A07, CD-A07).
- MCEER-02-0005 “Review of Energy Dissipation of Compression Members in Concentrically Braced Frames,” by K.Lee and M. Bruneau, 10/18/02, (PB2004-101638, A10, CD-A10).
- MCEER-03-0001 “Experimental Investigation of Light-Gauge Steel Plate Shear Walls for the Seismic Retrofit of Buildings” by J. Berman and M. Bruneau, 5/2/03, (PB2004-101622, A10, MF-A03, CD-A10).
- MCEER-03-0002 “Statistical Analysis of Fragility Curves,” by M. Shinozuka, M.Q. Feng, H. Kim, T. Uzawa and T. Ueda, 6/16/03, (PB2004-101849, A09, CD-A09).
- MCEER-03-0003 “Proceedings of the Eighth U.S.-Japan Workshop on Earthquake Resistant Design of Lifeline Facilities and Countermeasures Against Liquefaction,” edited by M. Hamada, J.P. Bardet and T.D. O’Rourke, 6/30/03, (PB2004-104386, A99, CD-A99).
- MCEER-03-0004 “Proceedings of the PRC-US Workshop on Seismic Analysis and Design of Special Bridges,” edited by L.C. Fan and G.C. Lee, 7/15/03, (PB2004-104387, A14, CD-A14).
- MCEER-03-0005 “Urban Disaster Recovery: A Framework and Simulation Model,” by S.B. Miles and S.E. Chang, 7/25/03, (PB2004-104388, A07, CD-A07).
- MCEER-03-0006 “Behavior of Underground Piping Joints Due to Static and Dynamic Loading,” by R.D. Meis, M. Maragakis and R. Siddharthan, 11/17/03, (PB2005-102194, A13, MF-A03, CD-A00).
- MCEER-04-0001 “Experimental Study of Seismic Isolation Systems with Emphasis on Secondary System Response and Verification of Accuracy of Dynamic Response History Analysis Methods,” by E. Wolff and M. Constantinou, 1/16/04 (PB2005-102195, A99, MF-E08, CD-A00).
- MCEER-04-0002 “Tension, Compression and Cyclic Testing of Engineered Cementitious Composite Materials,” by K. Kesner and S.L. Billington, 3/1/04, (PB2005-102196, A08, CD-A08).

- MCEER-04-0003 “Cyclic Testing of Braces Laterally Restrained by Steel Studs to Enhance Performance During Earthquakes,” by O.C. Celik, J.W. Berman and M. Bruneau, 3/16/04, (PB2005-102197, A13, MF-A03, CD-A00).
- MCEER-04-0004 “Methodologies for Post Earthquake Building Damage Detection Using SAR and Optical Remote Sensing: Application to the August 17, 1999 Marmara, Turkey Earthquake,” by C.K. Huyck, B.J. Adams, S. Cho, R.T. Eguchi, B. Mansouri and B. Houshmand, 6/15/04, (PB2005-104888, A10, CD-A00).
- MCEER-04-0005 “Nonlinear Structural Analysis Towards Collapse Simulation: A Dynamical Systems Approach,” by M.V. Sivaselvan and A.M. Reinhorn, 6/16/04, (PB2005-104889, A11, MF-A03, CD-A00).
- MCEER-04-0006 “Proceedings of the Second PRC-US Workshop on Seismic Analysis and Design of Special Bridges,” edited by G.C. Lee and L.C. Fan, 6/25/04, (PB2005-104890, A16, CD-A00).
- MCEER-04-0007 “Seismic Vulnerability Evaluation of Axially Loaded Steel Built-up Laced Members,” by K. Lee and M. Bruneau, 6/30/04, (PB2005-104891, A16, CD-A00).
- MCEER-04-0008 “Evaluation of Accuracy of Simplified Methods of Analysis and Design of Buildings with Damping Systems for Near-Fault and for Soft-Soil Seismic Motions,” by E.A. Pavlou and M.C. Constantinou, 8/16/04, (PB2005-104892, A08, MF-A02, CD-A00).
- MCEER-04-0009 “Assessment of Geotechnical Issues in Acute Care Facilities in California,” by M. Lew, T.D. O’Rourke, R. Dobry and M. Koch, 9/15/04, (PB2005-104893, A08, CD-A00).
- MCEER-04-0010 “Scissor-Jack-Damper Energy Dissipation System,” by A.N. Sigaher-Boyle and M.C. Constantinou, 12/1/04 (PB2005-108221).
- MCEER-04-0011 “Seismic Retrofit of Bridge Steel Truss Piers Using a Controlled Rocking Approach,” by M. Pollino and M. Bruneau, 12/20/04 (PB2006-105795).
- MCEER-05-0001 “Experimental and Analytical Studies of Structures Seismically Isolated with an Uplift-Restraint Isolation System,” by P.C. Roussis and M.C. Constantinou, 1/10/05 (PB2005-108222).
- MCEER-05-0002 “A Versatile Experimentation Model for Study of Structures Near Collapse Applied to Seismic Evaluation of Irregular Structures,” by D. Kusumastuti, A.M. Reinhorn and A. Rutenberg, 3/31/05 (PB2006-101523).
- MCEER-05-0003 “Proceedings of the Third PRC-US Workshop on Seismic Analysis and Design of Special Bridges,” edited by L.C. Fan and G.C. Lee, 4/20/05, (PB2006-105796).
- MCEER-05-0004 “Approaches for the Seismic Retrofit of Braced Steel Bridge Piers and Proof-of-Concept Testing of an Eccentrically Braced Frame with Tubular Link,” by J.W. Berman and M. Bruneau, 4/21/05 (PB2006-101524).
- MCEER-05-0005 “Simulation of Strong Ground Motions for Seismic Fragility Evaluation of Nonstructural Components in Hospitals,” by A. Wanitkorkul and A. Filiatrault, 5/26/05 (PB2006-500027).
- MCEER-05-0006 “Seismic Safety in California Hospitals: Assessing an Attempt to Accelerate the Replacement or Seismic Retrofit of Older Hospital Facilities,” by D.J. Alesch, L.A. Arendt and W.J. Petak, 6/6/05 (PB2006-105794).
- MCEER-05-0007 “Development of Seismic Strengthening and Retrofit Strategies for Critical Facilities Using Engineered Cementitious Composite Materials,” by K. Kesner and S.L. Billington, 8/29/05 (PB2006-111701).
- MCEER-05-0008 “Experimental and Analytical Studies of Base Isolation Systems for Seismic Protection of Power Transformers,” by N. Murota, M.Q. Feng and G-Y. Liu, 9/30/05 (PB2006-111702).
- MCEER-05-0009 “3D-BASIS-ME-MB: Computer Program for Nonlinear Dynamic Analysis of Seismically Isolated Structures,” by P.C. Tsopelas, P.C. Roussis, M.C. Constantinou, R. Buchanan and A.M. Reinhorn, 10/3/05 (PB2006-111703).
- MCEER-05-0010 “Steel Plate Shear Walls for Seismic Design and Retrofit of Building Structures,” by D. Vian and M. Bruneau, 12/15/05 (PB2006-111704).

- MCEER-05-0011 "The Performance-Based Design Paradigm," by M.J. Astrella and A. Whittaker, 12/15/05 (PB2006-111705).
- MCEER-06-0001 "Seismic Fragility of Suspended Ceiling Systems," H. Badillo-Almaraz, A.S. Whittaker, A.M. Reinhorn and G.P. Cimellaro, 2/4/06 (PB2006-111706).
- MCEER-06-0002 "Multi-Dimensional Fragility of Structures," by G.P. Cimellaro, A.M. Reinhorn and M. Bruneau, 3/1/06 (PB2007-106974, A09, MF-A02, CD A00).
- MCEER-06-0003 "Built-Up Shear Links as Energy Dissipators for Seismic Protection of Bridges," by P. Dusicka, A.M. Itani and I.G. Buckle, 3/15/06 (PB2006-111708).
- MCEER-06-0004 "Analytical Investigation of the Structural Fuse Concept," by R.E. Vargas and M. Bruneau, 3/16/06 (PB2006-111709).
- MCEER-06-0005 "Experimental Investigation of the Structural Fuse Concept," by R.E. Vargas and M. Bruneau, 3/17/06 (PB2006-111710).
- MCEER-06-0006 "Further Development of Tubular Eccentrically Braced Frame Links for the Seismic Retrofit of Braced Steel Truss Bridge Piers," by J.W. Berman and M. Bruneau, 3/27/06 (PB2007-105147).
- MCEER-06-0007 "REDARS Validation Report," by S. Cho, C.K. Huyck, S. Ghosh and R.T. Eguchi, 8/8/06 (PB2007-106983).
- MCEER-06-0008 "Review of Current NDE Technologies for Post-Earthquake Assessment of Retrofitted Bridge Columns," by J.W. Song, Z. Liang and G.C. Lee, 8/21/06 (PB2007-106984).
- MCEER-06-0009 "Liquefaction Remediation in Silty Soils Using Dynamic Compaction and Stone Columns," by S. Thevanayagam, G.R. Martin, R. Nashed, T. Shenthan, T. Kanagalingam and N. Ecemis, 8/28/06 (PB2007-106985).
- MCEER-06-0010 "Conceptual Design and Experimental Investigation of Polymer Matrix Composite Infill Panels for Seismic Retrofitting," by W. Jung, M. Chiewanichakorn and A.J. Aref, 9/21/06 (PB2007-106986).
- MCEER-06-0011 "A Study of the Coupled Horizontal-Vertical Behavior of Elastomeric and Lead-Rubber Seismic Isolation Bearings," by G.P. Warn and A.S. Whittaker, 9/22/06 (PB2007-108679).
- MCEER-06-0012 "Proceedings of the Fourth PRC-US Workshop on Seismic Analysis and Design of Special Bridges: Advancing Bridge Technologies in Research, Design, Construction and Preservation," Edited by L.C. Fan, G.C. Lee and L. Ziang, 10/12/06 (PB2007-109042).
- MCEER-06-0013 "Cyclic Response and Low Cycle Fatigue Characteristics of Plate Steels," by P. Dusicka, A.M. Itani and I.G. Buckle, 11/1/06 06 (PB2007-106987).
- MCEER-06-0014 "Proceedings of the Second US-Taiwan Bridge Engineering Workshop," edited by W.P. Yen, J. Shen, J-Y. Chen and M. Wang, 11/15/06 (PB2008-500041).
- MCEER-06-0015 "User Manual and Technical Documentation for the REDARS<sup>TM</sup> Import Wizard," by S. Cho, S. Ghosh, C.K. Huyck and S.D. Werner, 11/30/06 (PB2007-114766).
- MCEER-06-0016 "Hazard Mitigation Strategy and Monitoring Technologies for Urban and Infrastructure Public Buildings: Proceedings of the China-US Workshops," edited by X.Y. Zhou, A.L. Zhang, G.C. Lee and M. Tong, 12/12/06 (PB2008-500018).
- MCEER-07-0001 "Static and Kinetic Coefficients of Friction for Rigid Blocks," by C. Kafali, S. Fathali, M. Grigoriu and A.S. Whittaker, 3/20/07 (PB2007-114767).
- MCEER-07-0002 "Hazard Mitigation Investment Decision Making: Organizational Response to Legislative Mandate," by L.A. Arendt, D.J. Alesch and W.J. Petak, 4/9/07 (PB2007-114768).
- MCEER-07-0003 "Seismic Behavior of Bidirectional-Resistant Ductile End Diaphragms with Unbonded Braces in Straight or Skewed Steel Bridges," by O. Celik and M. Bruneau, 4/11/07 (PB2008-105141).


- MCEER-07-0004 “Modeling Pile Behavior in Large Pile Groups Under Lateral Loading,” by A.M. Dodds and G.R. Martin, 4/16/07(PB2008-105142).
- MCEER-07-0005 “Experimental Investigation of Blast Performance of Seismically Resistant Concrete-Filled Steel Tube Bridge Piers,” by S. Fujikura, M. Bruneau and D. Lopez-Garcia, 4/20/07 (PB2008-105143).
- MCEER-07-0006 “Seismic Analysis of Conventional and Isolated Liquefied Natural Gas Tanks Using Mechanical Analogs,” by I.P. Christovasilis and A.S. Whittaker, 5/1/07.
- MCEER-07-0007 “Experimental Seismic Performance Evaluation of Isolation/Restraint Systems for Mechanical Equipment – Part 1: Heavy Equipment Study,” by S. Fathali and A. Filiatrault, 6/6/07 (PB2008-105144).
- MCEER-07-0008 “Seismic Vulnerability of Timber Bridges and Timber Substructures,” by A.A. Sharma, J.B. Mander, I.M. Friedland and D.R. Allicock, 6/7/07 (PB2008-105145).
- MCEER-07-0009 “Experimental and Analytical Study of the XY-Friction Pendulum (XY-FP) Bearing for Bridge Applications,” by C.C. Marin-Artieda, A.S. Whittaker and M.C. Constantinou, 6/7/07 (PB2008-105191).
- MCEER-07-0010 “Proceedings of the PRC-US Earthquake Engineering Forum for Young Researchers,” Edited by G.C. Lee and X.Z. Qi, 6/8/07.
- MCEER-07-0011 “Design Recommendations for Perforated Steel Plate Shear Walls,” by R. Purba and M. Bruneau, 6/18/07, (PB2008-105192).
- MCEER-07-0012 “Performance of Seismic Isolation Hardware Under Service and Seismic Loading,” by M.C. Constantinou, A.S. Whittaker, Y. Kalpakidis, D.M. Fenz and G.P. Warn, 8/27/07, (PB2008-105193).
- MCEER-07-0013 “Experimental Evaluation of the Seismic Performance of Hospital Piping Subassemblies,” by E.R. Goodwin, E. Maragakis and A.M. Itani, 9/4/07, (PB2008-105194).
- MCEER-07-0014 “A Simulation Model of Urban Disaster Recovery and Resilience: Implementation for the 1994 Northridge Earthquake,” by S. Miles and S.E. Chang, 9/7/07, (PB2008-106426).
- MCEER-07-0015 “Statistical and Mechanistic Fragility Analysis of Concrete Bridges,” by M. Shinozuka, S. Banerjee and S-H. Kim, 9/10/07, (PB2008-106427).
- MCEER-07-0016 “Three-Dimensional Modeling of Inelastic Buckling in Frame Structures,” by M. Schachter and AM. Reinhorn, 9/13/07, (PB2008-108125).
- MCEER-07-0017 “Modeling of Seismic Wave Scattering on Pile Groups and Caissons,” by I. Po Lam, H. Law and C.T. Yang, 9/17/07 (PB2008-108150).
- MCEER-07-0018 “Bridge Foundations: Modeling Large Pile Groups and Caissons for Seismic Design,” by I. Po Lam, H. Law and G.R. Martin (Coordinating Author), 12/1/07 (PB2008-111190).
- MCEER-07-0019 “Principles and Performance of Roller Seismic Isolation Bearings for Highway Bridges,” by G.C. Lee, Y.C. Ou, Z. Liang, T.C. Niu and J. Song, 12/10/07.
- MCEER-07-0020 “Centrifuge Modeling of Permeability and Pinning Reinforcement Effects on Pile Response to Lateral Spreading,” by L.L Gonzalez-Lagos, T. Abdoun and R. Dobry, 12/10/07 (PB2008-111191).
- MCEER-07-0021 “Damage to the Highway System from the Pisco, Perú Earthquake of August 15, 2007,” by J.S. O’Connor, L. Mesa and M. Nykamp, 12/10/07, (PB2008-108126).
- MCEER-07-0022 “Experimental Seismic Performance Evaluation of Isolation/Restraint Systems for Mechanical Equipment – Part 2: Light Equipment Study,” by S. Fathali and A. Filiatrault, 12/13/07 (PB2008-111192).
- MCEER-07-0023 “Fragility Considerations in Highway Bridge Design,” by M. Shinozuka, S. Banerjee and S.H. Kim, 12/14/07 (PB2008-111193).

- MCEER-07-0024 “Performance Estimates for Seismically Isolated Bridges,” by G.P. Warn and A.S. Whittaker, 12/30/07 (PB2008-112230).
- MCEER-08-0001 “Seismic Performance of Steel Girder Bridge Superstructures with Conventional Cross Frames,” by L.P. Carden, A.M. Itani and I.G. Buckle, 1/7/08, (PB2008-112231).
- MCEER-08-0002 “Seismic Performance of Steel Girder Bridge Superstructures with Ductile End Cross Frames with Seismic Isolators,” by L.P. Carden, A.M. Itani and I.G. Buckle, 1/7/08 (PB2008-112232).
- MCEER-08-0003 “Analytical and Experimental Investigation of a Controlled Rocking Approach for Seismic Protection of Bridge Steel Truss Piers,” by M. Pollino and M. Bruneau, 1/21/08 (PB2008-112233).
- MCEER-08-0004 “Linking Lifeline Infrastructure Performance and Community Disaster Resilience: Models and Multi-Stakeholder Processes,” by S.E. Chang, C. Pasion, K. Tatebe and R. Ahmad, 3/3/08 (PB2008-112234).
- MCEER-08-0005 “Modal Analysis of Generally Damped Linear Structures Subjected to Seismic Excitations,” by J. Song, Y-L. Chu, Z. Liang and G.C. Lee, 3/4/08 (PB2009-102311).
- MCEER-08-0006 “System Performance Under Multi-Hazard Environments,” by C. Kafali and M. Grigoriu, 3/4/08 (PB2008-112235).
- MCEER-08-0007 “Mechanical Behavior of Multi-Spherical Sliding Bearings,” by D.M. Fenz and M.C. Constantinou, 3/6/08 (PB2008-112236).
- MCEER-08-0008 “Post-Earthquake Restoration of the Los Angeles Water Supply System,” by T.H.P. Tabucchi and R.A. Davidson, 3/7/08 (PB2008-112237).
- MCEER-08-0009 “Fragility Analysis of Water Supply Systems,” by A. Jacobson and M. Grigoriu, 3/10/08 (PB2009-105545).
- MCEER-08-0010 “Experimental Investigation of Full-Scale Two-Story Steel Plate Shear Walls with Reduced Beam Section Connections,” by B. Qu, M. Bruneau, C-H. Lin and K-C. Tsai, 3/17/08.
- MCEER-08-0011 “Seismic Evaluation and Rehabilitation of Critical Components of Electrical Power Systems,” S. Ersoy, B. Feizi, A. Ashrafi and M. Ala Saadeghvaziri, 3/17/08 (PB2009-105546).
- MCEER-08-0012 “Seismic Behavior and Design of Boundary Frame Members of Steel Plate Shear Walls,” by B. Qu and M. Bruneau, 4/26/08.
- MCEER-08-0013 “Development and Appraisal of a Numerical Cyclic Loading Protocol for Quantifying Building System Performance,” by A. Filiatrault, A. Wanitkorkul and M. Constantinou, 4/27/08.
- MCEER-08-0014 “Structural and Nonstructural Earthquake Design: The Challenge of Integrating Specialty Areas in Designing Complex, Critical Facilities,” by W.J. Petak and D.J. Alesch, 4/30/08.
- MCEER-08-0015 “Seismic Performance Evaluation of Water Systems,” by Y. Wang and T.D. O’Rourke, 5/5/08.
- MCEER-08-0016 “Seismic Response Modeling of Water Supply Systems,” by P. Shi and T.D. O’Rourke, 5/5/08.
- MCEER-08-0017 “Numerical and Experimental Studies of Self-Centering Post-Tensioned Steel Frames,” by D. Wang and A. Filiatrault, 5/12/08.
- MCEER-08-0018 “Development, Implementation and Verification of Dynamic Analysis Models for Multi-Spherical Sliding Bearings,” by D.M. Fenz and M.C. Constantinou, 8/15/08.
- MCEER-08-0019 “Performance Assessment of Conventional and Base Isolated Nuclear Power Plants for Earthquake Blast Loadings,” by Y.N. Huang, A.S. Whittaker and N. Luco, 10/28/08.
- MCEER-08-0020 “Remote Sensing for Resilient Multi-Hazard Disaster Response – Volume I: Introduction to Damage Assessment Methodologies,” by B.J. Adams and R.T. Eguchi, 11/17/08.

- MCEER-08-0021 “Remote Sensing for Resilient Multi-Hazard Disaster Response – Volume II: Counting the Number of Collapsed Buildings Using an Object-Oriented Analysis: Case Study of the 2003 Bam Earthquake,” by L. Gusella, C.K. Huyck and B.J. Adams, 11/17/08.
- MCEER-08-0022 “Remote Sensing for Resilient Multi-Hazard Disaster Response – Volume III: Multi-Sensor Image Fusion Techniques for Robust Neighborhood-Scale Urban Damage Assessment,” by B.J. Adams and A. McMillan, 11/17/08.
- MCEER-08-0023 “Remote Sensing for Resilient Multi-Hazard Disaster Response – Volume IV: A Study of Multi-Temporal and Multi-Resolution SAR Imagery for Post-Katrina Flood Monitoring in New Orleans,” by A. McMillan, J.G. Morley, B.J. Adams and S. Chesworth, 11/17/08.
- MCEER-08-0024 “Remote Sensing for Resilient Multi-Hazard Disaster Response – Volume V: Integration of Remote Sensing Imagery and VIEWS™ Field Data for Post-Hurricane Charley Building Damage Assessment,” by J.A. Womble, K. Mehta and B.J. Adams, 11/17/08.
- MCEER-08-0025 “Building Inventory Compilation for Disaster Management: Application of Remote Sensing and Statistical Modeling,” by P. Sarabandi, A.S. Kiremidjian, R.T. Eguchi and B. J. Adams, 11/20/08.
- MCEER-08-0026 “New Experimental Capabilities and Loading Protocols for Seismic Qualification and Fragility Assessment of Nonstructural Systems,” by R. Retamales, G. Mosqueda, A. Filiatrault and A. Reinhorn, 11/24/08.
- MCEER-08-0027 “Effects of Heating and Load History on the Behavior of Lead-Rubber Bearings,” by I.V. Kalpakidis and M.C. Constantinou, 12/1/08.
- MCEER-08-0028 “Experimental and Analytical Investigation of Blast Performance of Seismically Resistant Bridge Piers,” by S.Fujikura and M. Bruneau, 12/8/08.








**EARTHQUAKE ENGINEERING TO EXTREME EVENTS**

University at Buffalo, The State University of New York  
Red Jacket Quadrangle ▪ Buffalo, New York 14261  
Phone: (716) 645-3391 ▪ Fax: (716) 645-3399  
E-mail: [mceer@buffalo.edu](mailto:mceer@buffalo.edu) ▪ WWW Site <http://mceer.buffalo.edu>



University at Buffalo *The State University of New York*

ISSN 1520-295X